THIRD AUSTRALIA – NEW ZEALAND CONFERENCE ON GEOMECHANICS

Wellington
May 12-16, 1980

Organised by
The New Zealand Geomechanics Society

Organisation Committee

CONVENOR

J. A. Webster
School of Architecture, Victoria University of Wellington.

FINANCE/NATIONAL COMMITTEE LIAISON

J. H. H. Galloway
Ministry of Works and Development, Wellington.

TECHNICAL PROGRAMME

M. J. Pender
Department of Civil Engineering, Auckland University.
G. Ramsay
Ministry of Works and Development, Wellington.

PUBLICITY

P. E. Salt
Ministry of Works and Development, Wellington.
T. J. Kayes
Tonkin and Taylor, Wellington.

SOCIAL PROGRAMME

P. Millar
Central Laboratories, Ministry of Works and Development, Lower Hutt.

Published by the New Zealand Institution of Engineers,
101 Molesworth Street, Wellington, New Zealand.

Printed by Bryce Francis Ltd, 11a Marion Street, Wellington.

PAPERS: VOLUME TWO

PAPERS: VOLUME ONE

Foundation Drainage Performance at Gordon Dam

S. GIUDICI
Section Engineer, Structures Section, Hydro-Electric Commission, Tasmania
R. H. W. BARNETT
Engineer-In-Charge, Safety of Dams Unit, Hydro-Electric Commission, Tasmania

SUMMARY In this paper, the drainage and piezometric systems of the 140 m high Gordon arch dam are briefly described. Experience in the operation of the relevant instrumentation, which included redrilling and duplication of a defective piezometer and extension of the coverage, is discussed with a view to improvements in the philosophy of the piezometric instrumentation of arch dams. The value of installing piezometers especially to monitor the efficiency of drainage systems is demonstrated. Use of a few key piezometers for interrogative and routine telemetering is explained.

The general picture of the distribution of interstitial fluid pressures in the foundation rock emerging from the results as the reservoir water level slowly rose is presented. Some comparisons are made of pore pressures observed with the corresponding values assumed in design calculations.

1 INTRODUCTION

Gordon Dam is a 140 m high, double curvature arch dam constructed on the Gordon River, in the south-west of Tasmania. Impoundment of water began in April 1974, the reservoir taking almost four years to reach a level close to full supply level at which it has remained sensibly constant for more than a year. (Fig. 4).

Provision was made during the design stage for monitoring the leakage flow through the foundation and for measuring of water pressures in selected areas of the abutments. Preliminary results were reported by Mitchell (1976). Five years of measurements now exist. This paper reports the findings, and discusses the behaviour of the drainage and piezometric system, including measures which were adopted to ensure that excessive pressure indications on one abutment were properly investigated.

2 DRAINAGE AND GROUTING SYSTEM

The dam is located in a narrow gorge of intensely folded rocks of Precambrian age. The rock sequence consists of fairly massively foliated quartzites containing thin interfoliated lenses of schistose chloritic and micaceous materials. Drill hole and adit investigation on the site revealed that the rock structure was generally very watertight, even where there was tectonic jointing. Water pressure testing in drill holes showed that water losses were confined to joints intersected by the drilling. The flow situation in the abutments could not therefore be considered homogeneous, and consequently the drainage and grouting system had to accord with the probability that most of the water which seeped through the rock around the dam would be confined to discrete joints.

Allen (1971) discusses the philosophy of drainage and grouting curtain location, and indicates the percolation pressure distributions which were used in the stability analysis. The positions of the drain and grout curtains are shown on Fig. 1, which also shows in diagrammatic form the distributions of pressure used for the stability analyses.

2.1 Drain Curtain

Drainage for the dam abutments was achieved by a series of adits about 30 m apart in elevation, oriented in the general direction implied in Fig.1. Fig. 2 shows the layout, with a series of 75 mm holes at 4 m spacing on the left abutment and 6 m on the right, drilled from one adit to the next below. In the area between the top-most adit and the crest of the dam, holes were drilled upwards in the same general plane as the holes below. Similarly, in the lowest adits, holes were drilled from the invert to levels below the dam. Around the base of the dam, a network of about 34 holes collared near the downstream toe was sunk to intersect known faults and joints. Advantage was taken of a second stage diversion opening in the dam, at foundation level near the right abutment, to drill a fan of holes underneath the dam. Water from these was piped to the downstream side when the opening was backfilled.

In contrast to the situation with gravity dams, drains in steep abutments such as exist at Gordon Dam can be made free draining from adit to adit. Within the plane of the adits the drill holes were generally oriented to intersect the principal joints, which, as mentioned above, would be the main water carriers.

In a typical adit, water entering from holes above is collected in a side drain and measured by V-notch weir before it is dropped to the adit next below. In the valley floor, a small concrete flume collects the drainage from the toe holes and a V-notch weir is again used to measure the leakage. Any strong individual leaks into a drainage adit can be monitored in addition to the measurement of total leakage.

2.2 Grout Curtain

Because of the position of the grout curtain in relation to the drainage curtain, drilling for the injection holes was done from upstream chambers at the ends of the drainage adits. Fans of holes were drilled giving a linked net covering the abutments effectively half the dam's height (locally) beyond the arch contact. In the valley floor, the grout curtain was vertical and drilled immediately upstream of the dam.

3 PIEZOMETERS

3.1 Piezometer arrangement

For monitoring pore pressures in the abutments, 31 piezometers were initially installed in the left abutment and 3 on the right. The preponderance of installations on the left abutment reflects the findings of the exploratory drilling and aditing, which revealed many more water bearing joints on the left than on the right. The object of the piezometer installation was to provide a quantitative basis for regular review of the effectiveness of the drainage system in controlling the pore pressures in the abutments. Piezometer location (shown in Fig. 3) was designed to give a spread of measurement sufficient to allow a comparison to be made between the measured and expected pressures. Carlson-type electrical resistance piezometers (supplied by Kyowa) were installed in drill holes, the stages of which were pressure-tested and lengthened until the water loss reached a value of 0.022 l/s/MPa in the stage. It was considered necessary to do this because of the general water-tightness, especially on the right abutment.

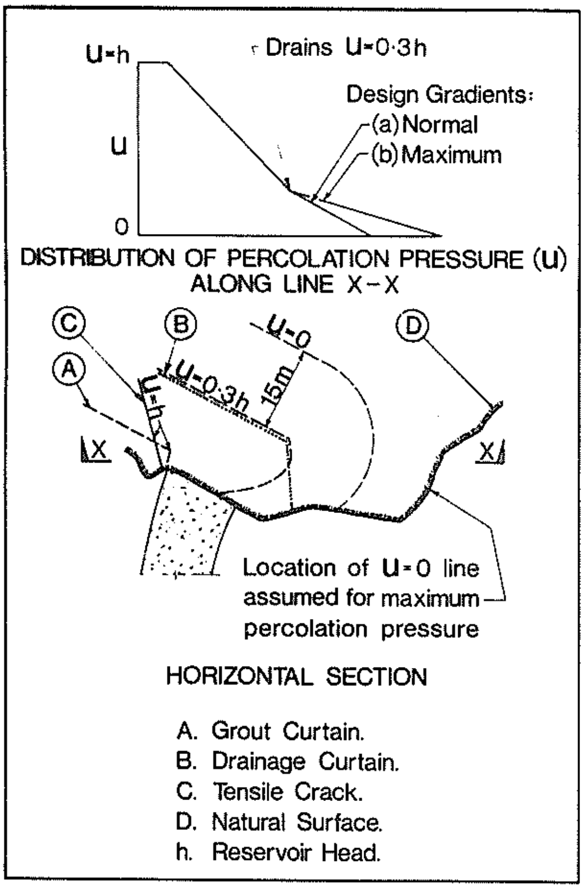

Figure 1 Design pore pressures (after Allen (1971))

3.2 Telemetering

Seven piezometer locations (six on the left, one on the right, shown ringed in Fig. 3) were chosen for remote monitoring, via a telemetry system, which also monitors twenty other instruments in the dam. It has been possible to telemeter for monitoring at very little cost, as a by-product of the remote control system for the nearby power station.

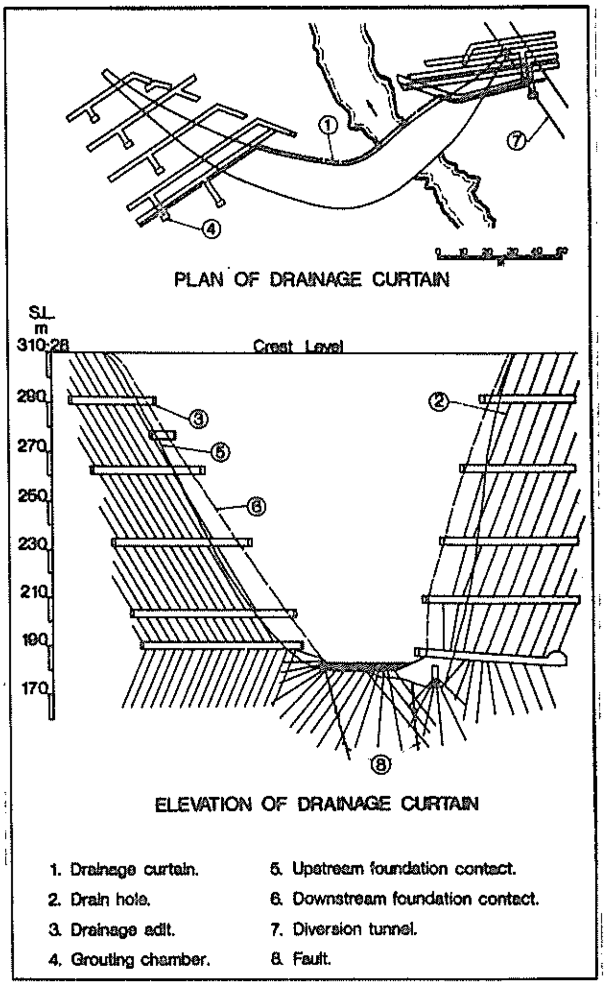

Figure 2 Drainage curtain layout

All the above instruments are continuously scanned and updated to a digital encoding unit near the top of the dam. This update is interrogated from Hobart automatically every thirty minutes, and transmitted to a display screen (in Hobart). The duty operator can call for a print-out at any time, day or night.

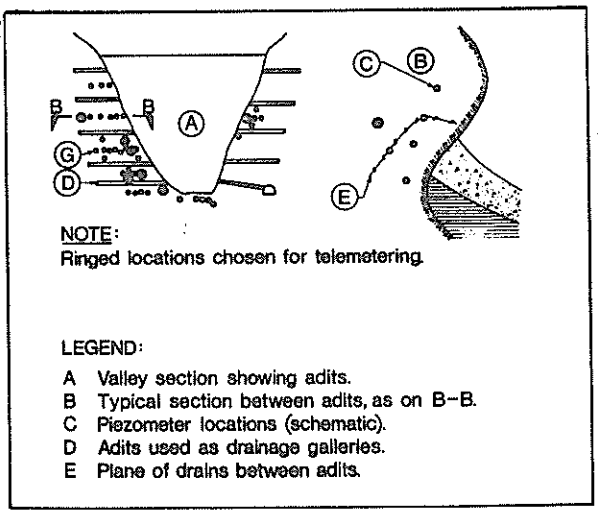

Figure 3 Piezometer location

4 PERFORMANCE

4.1 Leakage Measured

Fig. 4 gives a chronological picture of the leakage in various parts of the dam since filling of the reservoir began.

It can be seen that leakages have generally increased with lake level and stabilised at the attainment of Full Supply Level. It is also evident that the relative watertightness of each major section of the foundation can be assessed from information such as that presented in Fig. 4 and Fig. 7.

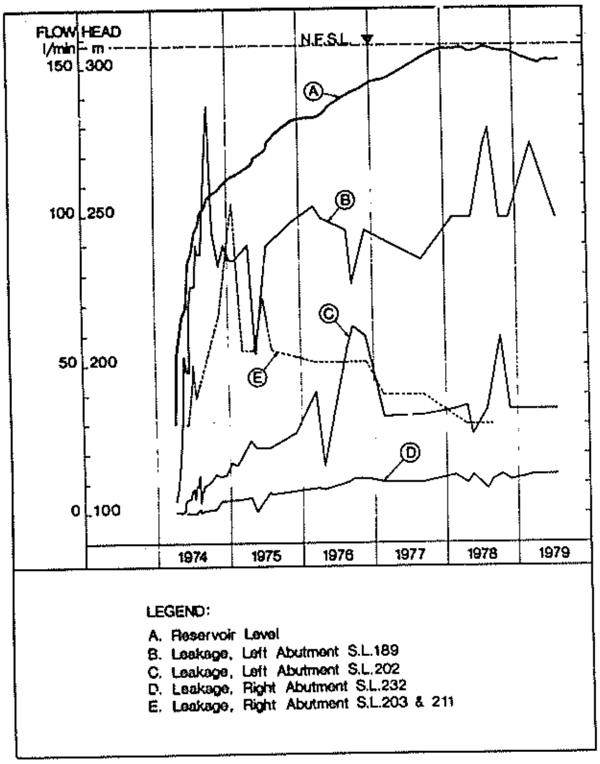

Figure 4 Typical leakage histories

4.2 Maintenance Problems

For the leakage results to have the same meaning in ensuing years as they do in the initial years of operation, it is necessary that a formal inspection procedure be utilized, which can, on a regular basis, give definitive reports about the state of maintenance of the system. We have instituted such a programme, and we find, for example, that even 75 mm vertical drain holes do become blocked occasionally, that V-notch weirs and their approaches need regular cleaning and that holes driven below the base of the dam become blocked. The sources of blockages were found to be as follows:

4.2.1 For the vertical drain holes, subsequent construction activity in the adits resulted in some construction materials finding their way into the holes. Also, displacement of some small rocks associated with joints crossed during drilling may be a contributory cause.

4.2.2 Some holes draining the base of the dam became clogged with calcium carbonate granules and encrustations. This was especially true of holes draining a known fault area which had been cement-grouted.

4.2.3 A gelatinous organic substance (of the nature of slime or yeast) formed at joints and shear zones carrying water. Growth seems more prolific in shear zones containing sand and rock chips, perhaps because of the greater surface area per unit volume of wetted rock. This made a thick (100 mm) covering over some surfaces and blocked V-notch weirs. Colour varies from red through brown to black depending presumably on the relative iron and manganese contents.

4.3 Remedies for the Blockages

4.3.1 For the vertical drain holes, jetting with water and rodding managed to clean them, and regular inspection makes sure that they are kept clean. It would be possible (as a last resort) to redrill or ream the holes from the galleries, because the adit size was made sufficiently large to allow a drilling rig to operate in them.

4.3.2 At the base of the dam, access for a drill rig was quite easy, by way of a haulage-way down the left abutment, but it was found that the percussion drilled holes could not, because of their winding nature, be redrilled. It was necessary to drill new holes to re-establish drainage paths which had been lost.

4.3.3 The rate of formation of the metalliferous slimes seems to be decreasing in recent years, but it is still necessary to remove them from a few locations where they reach the collector drains which run along the adit floors to the V-notches.

4.4 Piezometric Measurements

Of the 34 piezometers initially installed, 32 are still operational and 8 additional instruments (see 4.4.2 and 4.4.3) have been installed. Generally speaking, the pore pressure picture they indicate for the abutments and base is quite clear and confirms that the pore pressure assumptions made in design are on the safe side both in magnitude of pressure and in extent of foundation under such pressure (Fig. 7).

Several piezometers are purporting to record negative head. Assuming they have not developed faults this means the water table has dropped below them. Once suction is broken the piezometers can no longer follow the water table down.

4.4.1 Left abutment

Fig. 5 shows, for the left abutment, the pressures measured by three groups of piezometers as functions of time. One group is chosen near the bottom of the reservoir, one about a third from the bottom, and one about a third from the top. The labels A, B and C for each group refer to piezometer locations upstream of the drain curtain, at the drain curtain and downstream of the drain curtain respectively. Instruments at locations B and C show an essentially constant and low piezometric head, indicating that the drainage curtain is working and that high pressure water is not present downstream of it. Instruments A initially show a rise of pressure with the lake rise and then a generally constant pressure as the rate of rise of the lake has decreased. This accords with their position between the source of head and the drainage curtain. The pattern is similar to that of data presented by Casagrande (1961).

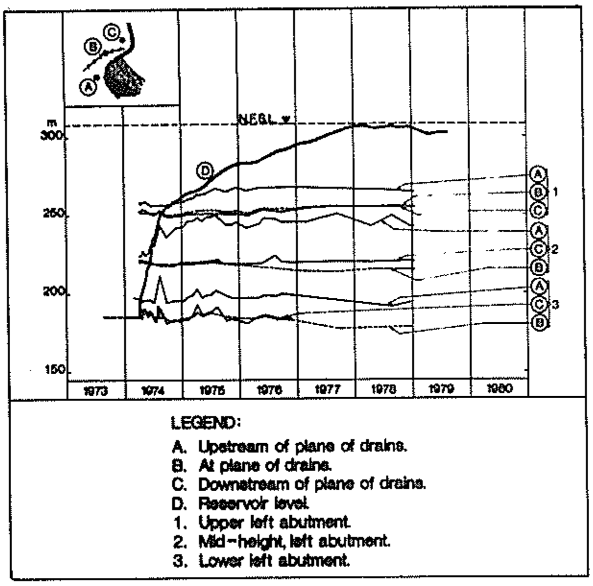

Figure 5 Typical L.A. piezometer records

4.4.2 Right abutment

For the right abutment, Fig. 6 shows a similar plot using the one set of piezometers initially installed, together with a replacement for a defective instrument.

At the drainage curtain, the piezometric head remained constant and low as the lake was rising, but at the instrument downstream of the curtain a pressure indication almost equal to that of the upstream instrument was consistently presented. Since there was no firm reason to disregard the instrument, and because the lack of instruments above and below it did not allow us corroborative evidence for or against the existence of a downstream pressure zone, we decided to drill some more holes into the zone in question. We could not be sure that a discrete joint was not carrying water past the drain curtain, or that water from above was not being trapped to the height implied.

During December 1976 and January 1977 eight diamond drill holes were placed in the right abutment, collared at the entrance to the drainage gallery at S.L. 231.70 m, where sufficient room for siting the drilling rig existed. Five of the holes were meant to augment the drainage, three being in the drain curtain plane and two approximately 10 m downstream of the drain curtain. Their orientation was chosen to intersect possible water bearing joints. The three remaining holes were positioned for installing piezometers to give a vertical coverage of about 35 m (between S.L. 225 m and 260 m) at a position 15 m downstream of the drain curtain.

Only two of the five drainage holes intercepted water sources. One of the three into the drain curtain leaked about 0.5 litre/minute, while one of the downstream holes had a "dripping" leakage too small to measure. Water from the first hole is consistent with supply to the area where high pressure was recorded.

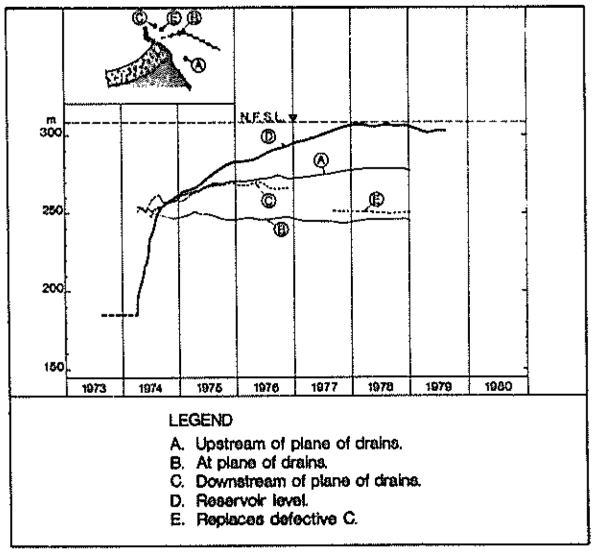

Figure 6 Right abutment piezometer data

The original piezometer registering the high downstream pressure became defective during drilling operations and this casts some doubt on the validity of its earlier record. Three piezometers were successfully installed and their readings (e.g. E on Fig. 6, which specifically replaces C) show that no high pressures have been recorded since.

4.4.3 Base of dam

The piezometers installed recently (1977) at the base of the dam are included in the general picture of Fig. 7. They monitor the effects of toe drains and faults in the river bed areas (and incidentally complement information from other sources such as rock deformation meters and V-notch weirs). Over their period of observation they have shown the same degree of stability as those plotted in Fig. 5.

4.4.4 Piezometric gradients

Information collected from the piezometers allows us to make some statements about the gradients of pressure, both in a horizontal section and between drainage adits, (see Figs. 7 and 8). A system of equipotentials can be constructed for a suitably chosen surface as an aid to interpolation between the piezometers.

The elevation in Fig. 7 is a projection on to a vertical plane of a curved and sloping section through either abutment and the base just behind the arch contact.

The piezometers are projected, in accordance with their positions in the flow path, on to contours of the surface at their respective installation levels (see plan view in Fig. 7). It can be seen that the drainage curtain is holding the piezometric head below the maximum limits assumed in design for abutment stability analyses. These limits are indicated in Fig. 1 and Fig. 7. Since there is no firm measure of the negative head near a negative reading piezometer, the equipotentials have been located as if such piezometers were reading zero excess pressure.

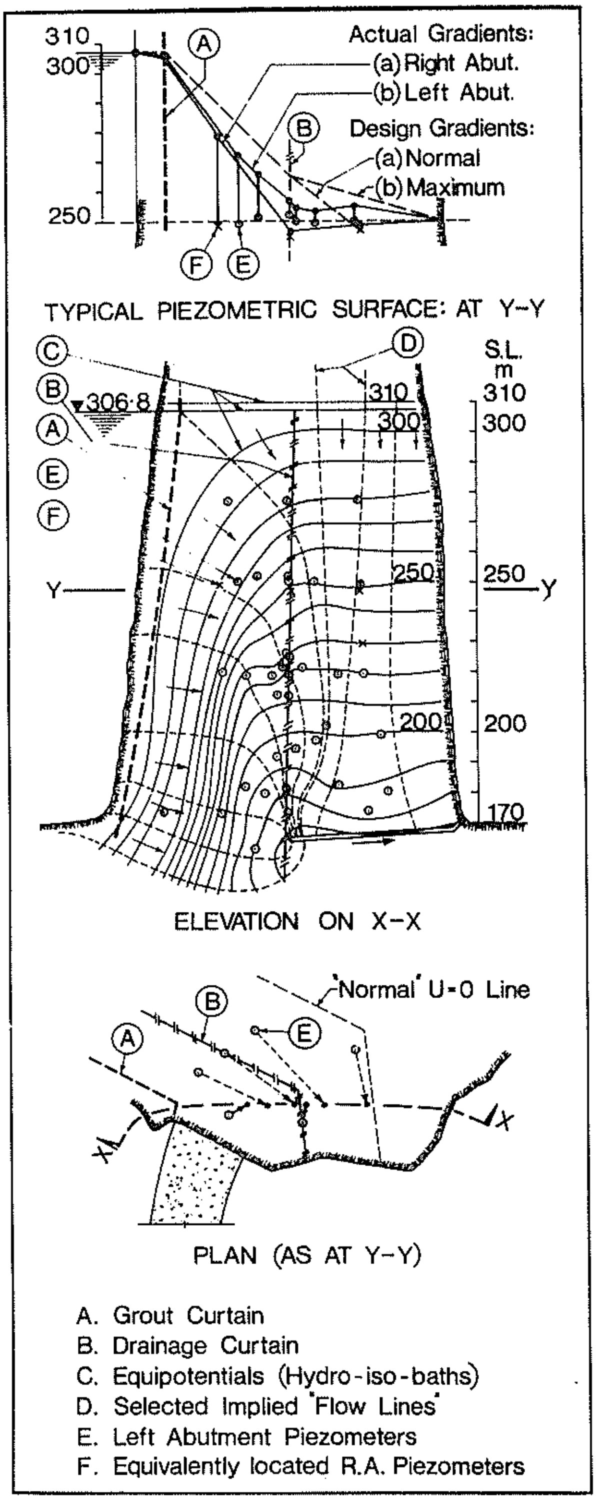

Figure 7 Record of all 40 piezometers, 29-8-78

The pattern of the dotted lines drawn at right angles to the equipotentials gives a general impression of the effect of the drainage curtain on abutment ground water movement.

Water represented as flowing down from above the lake surface level is from local run-off higher up on the abutment. The adits may be considered to be normal to the elevation on X-X, at the drainage curtain.

It would appear that the drainage and piezometer systems have intersected enough discrete joints in the otherwise impermeable rock mass to make such a representation realistic and useful.

There was some discussion at the design stage of an appropriate drain spacing. The observed values of pore pressure plotted in Fig. 8 as curve B (i.e. 0.041, 0.105, 0.043 MPa) are well below their "0.3 h" design equivalents (0.24, 0.26, 0.28 MPa). This indicates that the inter-drain pressures are adequately controlled with the chosen 4 m spacing for the left abutment, giving a fair margin for the effects of occasional blockages. The influence of the proximity to the adits is clearly shown.

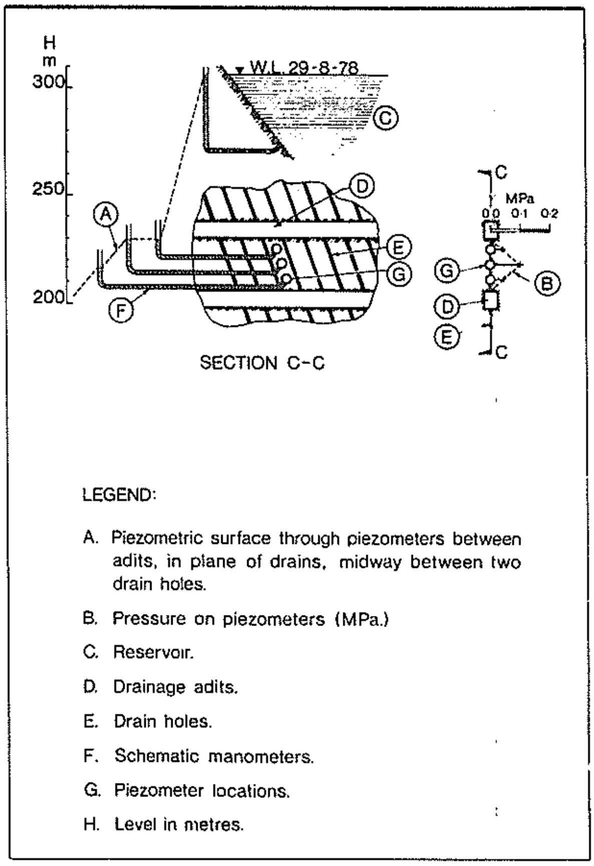

Figure 8 Pore pressures between drains

No similar piezometric check between right abutment drain holes, which are at about 5 m spacing measured perpendicular to the hole direction, is at present available. Because of a feeling of confidence in the right abutment stability which developed during the latter stages of design, even some piezometers appearing on 1974 revisions of the right abutment drawings were omitted.

5 CONCLUSIONS

Based on piezometer readings obtained to date, we conclude that the drainage system at Gordon Dam is effective. As Terzaghi has implied (Casagrande (1961)) we can never know how much leakage the grouting has prevented, but a grout curtain should prevent major piping.

Our experience at Gordon Dam vindicates the advice (ibid) that as well as a regular flow check on drainage facilities, a piezometric check must also be kept to ensure that a drop in flow rate is not accompanied by dangerous rises in pressure profiles.

Our maintenance programme has revealed that if one may have to clear or ream drain holes by drilling, then it is advisable for them to be diamond drill holes initially.

Piezometric measurements are important for indicating the current state of interstitial pressures in the foundations. Based on a regular flow of data, the plots can be used for making informed decisions about remedial action which might become necessary from time to time.

When designing piezometer installations for an arch dam, due regard must be given to the three-dimensional nature of the foundations, in order that anomalies in the readings might be assessed in the three dimensional context. This is the lesson to be learned from the drilling on the right abutment, which was done because of the absence of piezometers above and below the indicated high pressure location.

We believe that a tightly supervised inspection and maintenance programme with regular and comprehensive reporting is necessary for important hydraulic structures such as arch dams. Reliable records must be kept not only for total leakage, but for individual holes, adits, and so on. These should be included in the long-term record in order that a comprehensive picture of foundation pressures and percolations might be built up for any chosen time span.

6 ACKNOWLEDGEMENTS

The authors wish to thank Mr. J.R. Ashton, B.E., F.I.E. Aust., Commissioner of the Hydro-Electric Commission, for permission to publish this paper. Mr. W.R. Mitchell, B.E., F.I.E. Aust., is the Chief Civil Engineer. The assistance of other officers, in particular Mr. G. Clingeleffer who prepared the illustrations, is acknowledged.

7 REFERENCES

ALLEN, D.T. (1971). Abutment Stability Studies For The Gordon Arch Dam. Proc. First Aust.-N.Z. Conference on Geomechanics, Melbourne.

CASAGRANDE, A. (1961). Control of seepage through foundations and abutments of dams. Geotechnique, Vol. XI, No. 3, p. 161.

MITCHELL, W.R. (1976). The Gordon Arch Dam Drainage System, 12th I.C.O.L.D., Mexico. Discussion, Q45, Vol. IV, p. 268.

The Hazard of Lahars to the Tongariro Power Development, New Zealand

B. R. PATERSON
Engineering Geologist, Geological Survey, Department of Scientific and Industrial Rsearch, N.Z.

SUMMARY The Tongariro hydro-electric scheme intercepts a number of rivers which drain two active volcanoes and diverts them into rivers and natural lakes renowned for trout fishing. One of the active volcanoes, Ruapehu, is subject to unpredictable eruptions of its crater lake, during which lahars or volcanic mudflows are generated in several of the main valleys. As the chemical waters from the crater lake are toxic to fish, a lahar protection system was installed to prevent the spread of volcanic contamination into waters normally unaffected by these eruptions. This system also prevents volcanic debris from silting the power scheme waterways and reservoirs.

The lahar protection system was designed to cope with eruptions of the size that occurred in 1969, but proved to be inadequate for the 1975 eruption which was several times greater. Data obtained from the 1975 eruption have been utilized to upgrade the original lahar protection system and extend it into areas previously thought to be free from risk. The 1975 eruption also demonstrated the serious hazard of future eruptions to public safety as well as to the fisheries and the power scheme.

1 INTRODUCTION

The Tongariro hydro-electric power scheme is located in the centre of the North Island of New Zealand. It involves the interception and diversion of numerous streams and rivers into Lake Taupo through a complex system of intakes, dams, canals and tunnels.

Most of the streams intercepted rise on the slopes of three active volcanoes - Ruapehu, Ngauruhoe and Tongariro - each of which have erupted ash and lava in historic time. In addition Ruapehu has produced lahars or volcanic mudflows which are generated by the sudden release of highly acidic water from Crater Lake (Fig. 1), either by collapse of the crater wall (1953), or by eruption (1969 and 1975). The resulting floods of water and volcanic debris which travel down existing valleys pose a serious threat to power scheme installations as well as to public safety.

The lahar on 24 December 1953 swept away a railway bridge spanning the Whangaehu River, resulting in a train disaster with the loss of 151 lives (Healy 1954). Lahars on 22 June 1969 and 24 April 1975 damaged skifield installations on the upper slopes of Ruapehu and probably would have killed a number of people had the eruptions occurred when the skifield was crowded (Healy et al 1978). The 1975 eruption also flooded one of the power development tunnels where a group of tunnellers were lucky to escape with their lives.

Lahars are also capable of blocking power scheme waterways, causing siltation in reservoirs and damaging bridges. In addition, because several natural lakes and rivers utilized by the power scheme are important trout fisheries, accidental diversion of toxic lahar material could have a serious effect on fish life and the local tourist industry. A lahar protection system therefore has the dual purpose of protecting both the fisheries and the power scheme installations.

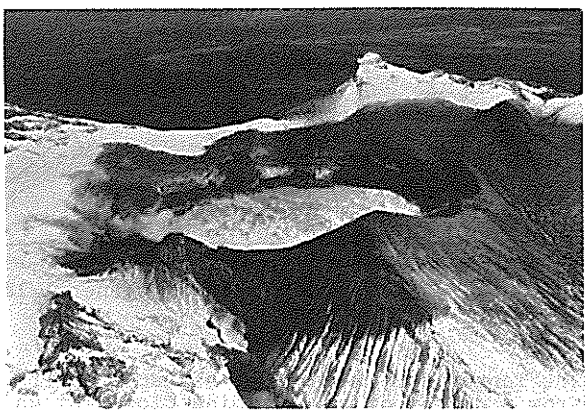

Fig. 1 Ruapehu Crater Lake after a minor eruption on April 27, 1975. Note the Whangaehu R outlet in lower centre.

In this paper the effects of the 1975 eruption on the power scheme are described, and data from major eruptions are utilized to delineate areas of greatest risk and devise an effective lahar protection system. The risk of similar future eruptions is assessed from previous recorded activity, and hydrological data is used to determine lahar velocities and volumes.

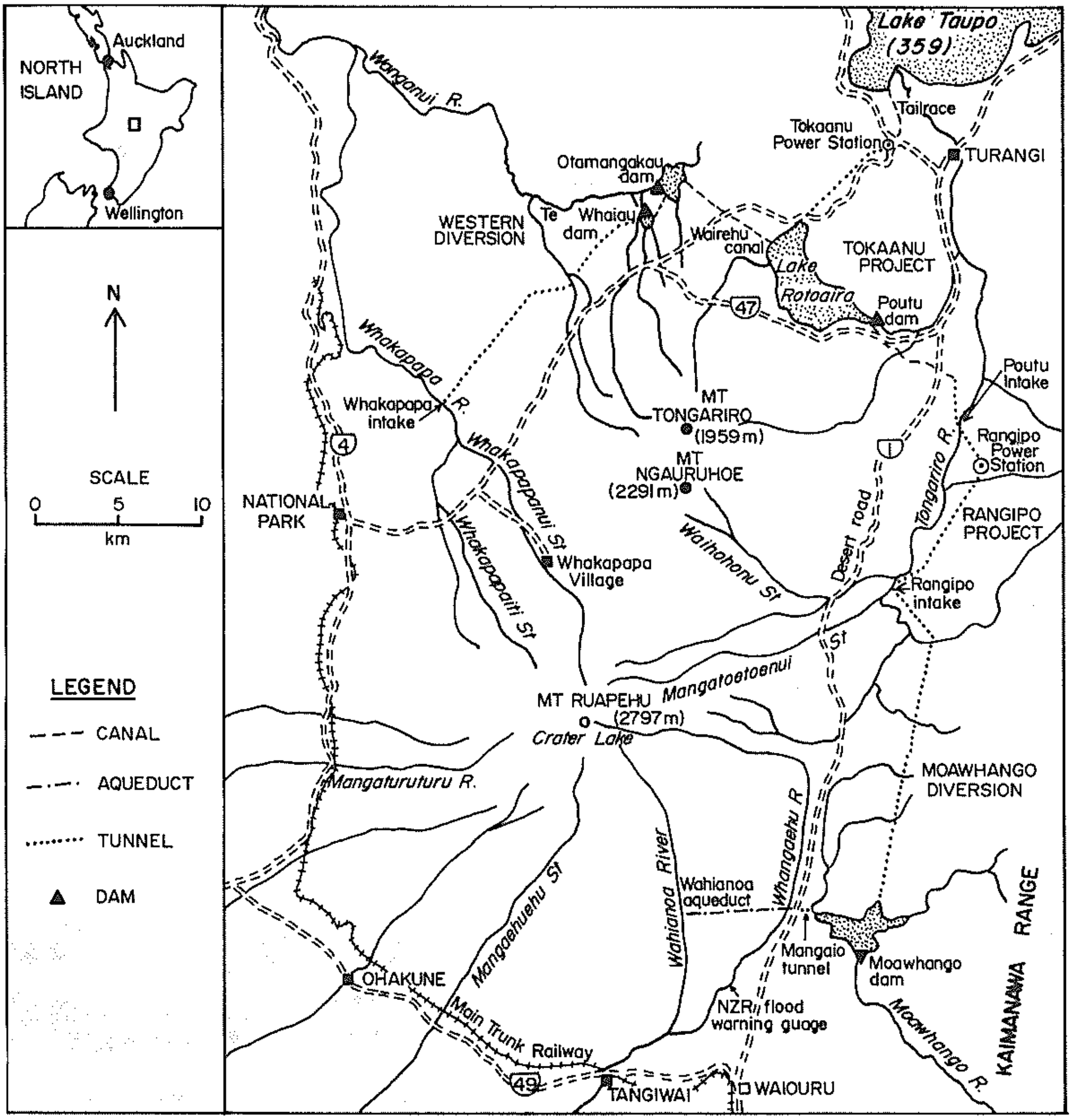

Fig. 2 Location and general layout of the Tongariro power scheme

2 TONGARIRO POWER SCHEME

The Tongariro power scheme collects water from a number of rivers which flow west and south from the volcanoes and diverts it northwards into Lake Taupo (Fig. 2). The water is utilized for power generation at the Rangipo (120 MW) and Tokaanu (200 MW) power stations, and in addition, the increased outflow from Lake Taupo raises the output from eight hydro-electric stations along the Waikato River (McCreight 1973).

The scheme can be subdivided into four sections as shown in Fig. 2. Because a large number of catchments are involved, environmental aspects required careful investigation to minimise possible harmful effects. Special provisions were incorporated into the design to preserve well known trout fisheries such as the Tongariro River and Lakes Rotoaira and Taupo. This entailed protection of important spawning streams and construction of special structures designed to prevent fish migration between catchments. Also the Whangaehu River which is the natural outlet of Ruapehu's crater lake was not incorporated in the power scheme because of the harmful effects the acid water would have on aquatic life. Because of the extent of these measures to protect the fisheries, it is logical that additional steps should be taken to prevent the spread of volcanic contamination between catchments during periodic lahar eruptions.

During investigation of the power scheme it was known that eruptions of lava and ash could be expected from Ruapehu and Ngauruhoe, but apart from minor siltation these were not considered to be a serious threat to the operation of the power scheme. It was recognized that lahars from Ruapehu were the greatest volcanic hazard to public safety in the area, but their threat to the power scheme was not realised until the eruption in 1969, after construction had commenced.

3 LAHARS FROM THE 1975 RUAPEHU ERUPTION

The main eruption of Ruapehu Crater Lake occurred on 24 April 1975 at 3:59 a.m. Heavy rain prevented any observation of the eruption. Ash deposits covered the summit area and fell in a narrow strip extending at least 115 km south-east of the volcano. At least 1.6×10^6 m^3 of Crater Lake water, lake floor deposits and blocks of hot rock were erupted onto the summit area, generating large lahars in several main valleys draining the volcano. The eruption resulted in an 8 m drop in lake level which represents 23% of the total lake volume of 7×10^6 m^3 from lake bathymetry. Details of the eruption are described by Nairn et al (1979).

On the upper slopes damage caused by the blast of the eruption and the impact of hot blocks of rock was limited to destruction of geophysical equipment and shelter huts. Most of the destruction was caused by lahars in the Whakapapa, Mangaturuturu and Whangaehu valleys and their main rivers downstream (Fig. 2).

3.1 Whakapapa Lahar

Lahars travelled down both tributaries of the Whakapapa River which meet 2.5 km upstream of the Whakapapa intake structure. In the headwaters, skifield installations and a refreshment kiosk were damaged, and further downstream within the Tongariro National Park two small suspension bridges were swept away. Near the Whakapapa Village a road bridge spanning the Whakapapanui River sustained slight damage when it was overtopped by the lahar.

At the Whakapapa intake, despite the installation of lahar detectors, a large volume of debris entered the tunnel and was deposited throughout its length. At the northern end of the tunnel, sediment and contaminated water flowed into the small Te Whaiau reservoir where it was spilled down the headwaters of the Wanganui River by emergency closure of the intake gate to the Wairehu canal (Fig. 2). This action averted the spread of contaminants into Lake Rotoaira and Lake Taupo but threatened the recently established fishery in Lakes Te Whaiau and Otamangakau.

Following the 1969 Ruapehu eruption when serious fish losses occurred in the Whakapapa and Wanganui Rivers, an investigation was carried out to determine the effects on fish life if contaminants from future eruptions were inadvertently diverted into Lakes Rotoaira and Taupo once the Western Diversions came into operation. Recommendations were made to install a lahar detector upstream of the Whakapapa intake to automatically close the tunnel gates before a lahar arrived, thereby preventing the spread of contamination (Paterson 1972). However because the conductivity probes were installed on the intake structure - not upstream as recommended - and a number of faults and deficiencies developed during the operation of the lahar protection system, a detailed study of the 1975 eruption was instigated with the view to upgrading the existing system.

3.2 Mangaturuturu Lahar

The lahar in the upper Mangaturuturu valley was highly erosive judging by the scouring of the valley floor, overtopping of spurs up to 8 m high, and the surging effects at river bends. Scouring and deposition altered the riverbed profile at the SH47 and main trunk railway bridges causing concern over the long term stability of these structures.

3.3 Whangaehu Lahar

The Whangaehu lahar was the largest from the eruption and was also highly erosive in the upper reaches of the valley. However, because of the remoteness of the area there was no property damage.

At the Wahianoa aqueduct the Whangaehu River changes from a wide floodplain upstream to a narrow incised valley. This constriction caused ponding of the lahar, and flooding of the aqueduct on either side of the river. The lahar flowed 0.6 km westwards along the aqueduct excavation to a stream-bed intake where it gained entry to the aqueduct pipeline below and filled it with debris over a length of 1.9 km.

Fig. 3 View looking west along Wahianoa aqueduct showing level of lahar, and flooded tunnel portal in foreground.

East of the river the lahar flooded the large aqueduct trench and buried the western portal of the Mangaio tunnel (Fig. 3). The material drained through the tunnel and emerged from the eastern portal where it flooded the portal establishment and spilled into the Mangaio Stream. The flow joined the Moawhango River upstream of the Moawhango dam and continued downstream where it eventually reached the Rangitikei River.

At the aqueduct a lahar warning system had been installed to protect workmen engaged in extending the pipeline beneath the Whangaehu River. The warning system was first installed in 1973 when high Crater lake temperatures were recorded, indicating a high risk of eruption and possible lahars in the Whangaehu valley. A fail-safe water level recorder was installed in the river upstream from the aqueduct which was designed to trigger an alarm at the construction site in the event of a lahar.

Although there were no eruptions during this period, the warning system was retained while construction continued in the western section of the Mangaio tunnel. When the 1975 eruption occurred the warning system was still in operation but had not been extended into the eastern tunnel section where tunnel work was being carried out at the time. Fortuitously the tunnellers were having a meal break outside when the lahar arrived and therefore escaped injury. Because there was no one working at the western end of the tunnel it is not known whether the warning system operated as planned.

Immediately downstream of the aqueduct the lahar completely filled the narrow river channel to approximately 6.5 m above normal river level, and overtopped the decking of a Bailey bridge. Approximately 5 km further downstream the New Zealand Railway Department had installed a flood warning device which is located in the river-bed 11 km upstream of the Tangiwai railway bridge. This structure was installed after the railway disaster in 1953 and consists of a robust concrete tower which houses a series of paired electrodes at staged heights (Fig. 4). It is linked by a land line to the Waiouru and Ohakune railway stations (located on either side of the Tangiwai railway bridge) where audible alarms are triggered in the event of a lahar, and a visual display indicates the height of the lahar. Approaching rail traffic is then delayed until the railway bridge is inspected and declared safe (pers. comm. L.I.D. Jamieson, N.Z. Railways Dept.).

The alarms were triggered in the railway stations 60 minutes after the 1975 eruption, and the visual display showed the lahar had reached level 4 on the 5 stage scale. Later inspection revealed that the lahar had overtopped the tower; by comparison the lahar from the 1969 eruption failed to reach level 1 on the same scale.

At Tangiwai both railway and SH49 bridges were undamaged by the lahar, but during the peak flow the road bridge - a recent concrete structure - vibrated alarmingly as large boulders carried in suspension hit the piers. A small wooden farm bridge spanning the Whangaehu River 6.5 km downstream from Tangiwai was swept away, and 10 km further downstream another bridge was overtopped and slightly damaged. In this area there were reports from residents living near the river of ground vibration similar to an earthquake during the peak flow.

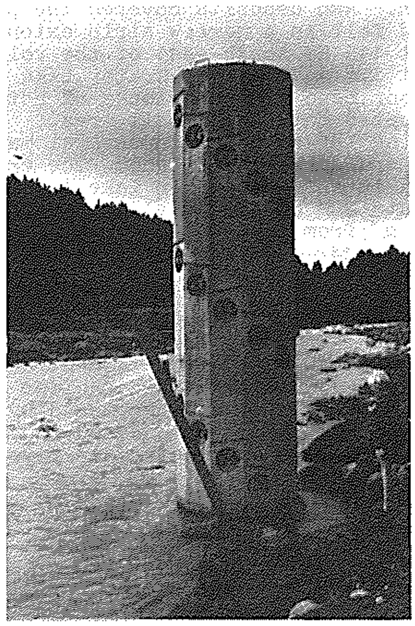

Fig. 4 N.Z. Railways Dept. lahar warning tower in the Whangaehu R.

4 LAHAR VELOCITIES AND VOLUMES

Automatic water level recorders registered the arrival times and stage heights of lahars from the 1969 and 1975 eruptions from which velocities and volumes were computed. Because the recorder sites are either near the base of the volcano or further downstream, no accurate hydrological data are available for the upper reaches where the velocities were greatest.

Lahars have a distinctive hydrograph peak which can be distinguished from those generated by rainfall (Fig. 5). Although it was raining when the 1975 eruption occurred, it was possible to differentiate the portions of the hydrographs attributed to rainfall and the lahars by analysis of rainfall data, and comparison with hydrographs of other rivers in the area unaffected by the eruption (Page and Paterson 1976).

The success of a lahar warning system relies on an adequate knowledge of the behaviour of lahars in different sections of the valleys. Calculated lahar velocities and volumes from recent Ruapehu eruptions are given in Table I. Lahar velocities depend on the nature and gradient of the channel as well as the viscosity and volume of the lahars. The highest average velocity recorded was

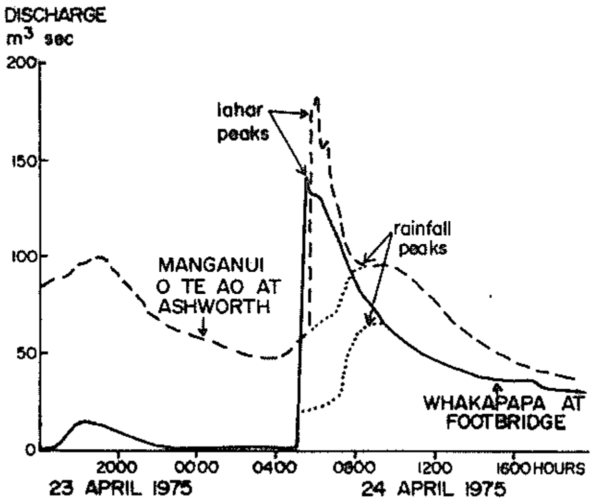

Fig. 5 Hydrographs of the 1975 lahars

8 m/sec for the first 22.1 km section of the Whangaehu lahar, although the actual velocities of the three main lahars in the first 5 km or so downstream from Crater Lake must have been considerably greater. The Whakapapanui lahar from the 1969 eruption was very viscous and achieved an average velocity of only 1.6 m/sec for the first 13.2 km (Healy et al 1978), whereas the Whakapapaiti lahar from the same eruption which was larger and less viscous had an average velocity of 4.0 m/sec for the first 27.9 km (Paterson 1972).

In the Whangaehu valley at Karioi (57.1 km downstream of Crater Lake) a water level recorder was operating during the period 30-10-62 to 5-1-72 during which numerous surges attributed to minor Crater Lake eruptions were recorded (Table I). The velocities of these flows were obtained by comparing the seismological record of Ruapehu (pers. comm. J.H. Latter, D.S.I.R. Geophysics Div.) with the hydrological record (pers. comm. C.E. Page, M.W.D. Hydrological Surveys). In general the velocities of these flows (0.9 - 3.2 m/sec) are considerably less than the 1975 lahar (5.6 m/sec). According to Healy (1954) the average velocity of the 1953 lahar between Crater Lake and Tangiwai was 5.2 m/sec compared with 6.4 m/sec for the 1975 lahar over the same reach.

Comparison of peak discharge levels near the Tangiwai road and railway bridges of the 1953 and 1975 Whangaehu lahars showed the former to be greater (Page and Paterson 1976). However judging by a 7.9 m drop in lake level in 1953 (Turner 1954), a total volume of 1.9 x 10^6 m^3 was released down the Whangaehu River which is only slightly larger than the volume of 1.8 x 10^6 m^3 calculated for the 1975 Whangaehu lahar. In 1953 the lake water was not released instantly (Turner 1954) which would have effectively lowered the peak discharge compared with that from an eruption. This factor was probably more than compensated for by debris accumulated during its passage downstream, whereas the 1975 lahar volume takes this factor into account.

Nairn et al (1979) recorded an 8 m drop in lake level following the 1975 eruption which indicates an apparent volume loss of 1.6 x 10^6 m^3. The latter is only about half the total lahar volume of 3.3 x 10^6 m^3 calculated from hydrological data, which suggests that the accumulation of debris from the river beds is a significant factor. This view is substantiated by the scouring of the river-beds in the headwaters, and

TABLE I

LAHAR VOLUMES AND VELOCITIES FROM RUAPEHU CRATER LAKE ERUPTIONS

Water-level recorder sites	Distance from Crater Lake (km)	Date of eruption	Lahar volume (m^3)	Lahar velocity (m/sec)	Average channel slope
Whakapapa at Footbridge N111/960859	24.9	22. 6.69 24. 4.75	117,000 900,000	4.0 4.1	1:13
Mangaturuturu at Ashworth N121/723621	40.2	22. 6.69 24. 4.75	24,000 600,000	1.9 4.9	1:17
Whangaehu at Karioi N131/965389	57.1	24. 7.66 26. 4.68 22. 6.69 8. 5.71 16. 5.71 16. 5.71 19. 5.71 21. 5.71 3. 7.71 4. 7.71 24. 4.75 2.11.77	1,000 729,000 67,000 41,000 72,000 58,000 18,000 9,000 5,000 19,000 1,800,000 130,000	0.9 2.4 2.6 2.9 2.8 2.3 1.6 2.0 5.6 3.2	1:29
Whangaehu at Kauangaroa N138/790874	169	24. 4.75	1,600,000	2.8	1:66

deposition of vast quantities of material in the lower reaches.

The apparent lake loss from the 1969 eruption was 0.5×10^6 m^3, and the total lahar volume calculated from hydrographs was only 0.2×10^6 m^3. The apparent reversal of volumes could be due to the high proportion of solid material erupted, and the thick coating of snow and ice on the summit area prior to the eruption (Healy et al 1978). Much of the solid material remained on the upper slopes, and melt water partly replenished the lake loss, both of which contribute to the discrepancy in volume calculations.

5 HAZARD OF FUTURE RUAPEHU ERUPTIONS

The volcanic activity of Ruapehu has been documented by Gregg (1960) for the period from the first eruption witnessed by Europeans in 1861 until 1959, and by Healy et al (1978) from 1959 to 1969. Eruptions since 1969 have been recorded by Nairn et al (1979).

Since 1861 numerous phreatic eruptions of Crater Lake have been recorded including at least 12 events that produced lahars in the Whangaehu valley. Only the three most explosive eruptions (1895, 1969 and 1975) ejected water and debris a sufficient distance from the crater to form lahars in the northwest catchments as well as in the Whangaehu valley. The 1895 eruption appears to have been the most violent event, but because the lake level was not checked until 26 days after the eruption (Gregg 1960) a direct comparison of lake loss with the 1975 eruption cannot be made. According to Allen (in Gregg 1960), during the 1895 eruption "the Wanganui River was discoloured down to the sea," the Whangaehu River" was for several days a river of mud" and the Mangatoetoenui Stream became "a mere sludge channel."

The total amount of material ejected onto the summit area is dependent on the magnitude and mechanism of the eruption although the distribution of the ejecta, and hence the size of lahars in any particular valley is strongly influenced by wind velocity and direction during the eruption. The snow conditions on the upper slopes will also effect the mobility and volume of the lahars; hence if the 1975 eruption had occurred during winter, more water would have passed down the Whakapapa valleys and damage may have been more severe.

Although volcanic activity of Ruapehu is continuously monitored from the Chateau seismological station and by regular inspections of Crater Lake, it is unlikely that eruptions will be able to be predicted in the foreseeable future. The greatest danger to lives is concentrated mainly on the upper slopes of Ruapehu, particularly during the skiing season, although some danger also exists on the lower slopes along the paths of lahars.

The hazard of lahars is well known in countries with active volcanoes, particularly in the circum-Pacific region. They are responsible for the greatest destruction of property of any other single volcanic process, and have caused the loss of thousands of lives during the past few centuries. A single eruption of Kelud volcano in Java in 1919 for example, caused massive destruction including the loss of 5500 lives when mudflows swept down the volcano following an explosive eruption beneath the crater lake (Bolt et al 1975).

Neall (1976a) reviewed the literature on lahars and included a classification based on their origins as well as a description of the most important lahars of each type that have occurred in historic times. Ruapehu was cited as a source of two types of lahar i.e. (a) an eruption through a crater lake, e.g. 1969 (b) collapse of a crater lake (non-eruptive), e.g. 1953. In a separate paper Neall (1976b) also discussed the hazard of lahars and referred to lahar protection measures adopted on several volcanoes including Ruapehu; the threat of lahars to the Tongariro power scheme was not mentioned however.

6 POSSIBLE EFFECTS OF FUTURE LAHARS ON THE POWER SCHEME

Future major eruptions of Crater Lake are almost certain to produce lahars in the Whangaehu, Mangaturuturu and Whakapapa valleys. During the 1975 eruption major lahars were restricted to these valleys although there was evidence of a flood flow 1.2 m above normal river level in the Wahianoa River (Nairn et al 1979). Small mudflows were reported in the headwaters of the Wahianoa, Mangaehuehu Rivers (Fig. 2), and water samples from these streams had a lower pH than normal indicating chemical contamination from the eruption. The Waihohonu Stream appeared to have been slightly contaminated, probably from ash fall as indicated by the acidity of a water sample collected the day of the eruption.

For several years after the 1975 eruption the Wahianoa Stream became slightly acidic during periods of summer thaw, when contaminants from the eruption were released from the ice into the headwaters (Paterson 1976a). A detailed investigation of the long term contamination was carried out by Carr (1978), who concluded that although the recorded pH levels were unlikely to be a danger to fish life, the surveillance of water quality should continue particularly after commissioning of the aqueduct.

Judging from Allen's description of the 1895 eruption and the contamination resulting from the 1975 eruption, the Mangatoetoenui Stream must be considered at risk from future major eruptions. There are no records of major lahars in the Wahianoa River although in the case of the 1895 eruption this may be due to lack of information. The headwaters of the Wahianoa River are closer to Crater Lake than the Mangatoetoenui headwaters. Hence, although a ridge approximately 50 m higher than the Summit Plateau separates the Crater Lake from the Wahianoa headwaters, the risk of lahars in both rivers is considered to be similar.

Since the 1975 eruption, construction of the Wahianoa aqueduct and Mangaio tunnel has been completed so that the only access for lahars to the Moawhango reservoir is through the aqueduct stream-bed intakes or the Mangaio tunnel access shaft. The latter has been built to a height above the level of the 1975 Whangaehu lahar, and embankments have been constructed on the west bank of the Whangaehu River to prevent lahars from flowing westwards along the aqueduct excavation. Therefore unless future lahars in the Whangaehu River are much larger than occurred in 1975, the only access for volcanic contaminants to the Moawhango reservoir is through the intake structure on the Wahianoa River.

The large volume of sulphurous water (pH = 1.2) forming Ruapehu's Crater Lake is the main threat to the power scheme and public safety. If the lake could be permanently drained the danger of future lahars would be eliminated. In a similar geological setting this was partially achieved in Java where drainage tunnels were driven through the crater wall of an active volcano and most of the lake water evacuated (Bolt et al 1975). A feasibility study of this method was suggested by Neall (1976b) and Paterson (1976b), but no action has been taken.

An early warning system to protect skiers on the upper slopes of Ruapehu has also been proposed (Hewson and Latter 1976). This system consists of a series of sensors designed to trigger alarms on the skifield immediately after an eruption. Although the prime purpose of this scheme is to save lives on the upper slopes of Ruapehu, if it is approved it could also act as an early warning system for the power scheme and communication routes. This would supplement rather than replace a power scheme lahar warning system, but it would provide extra time to execute emergency systems.

7 IMPROVEMENTS TO THE POWER SCHEME LAHAR WARNING SYSTEM

7.1 Western Diversions

The problems encountered in Western Diversions from the 1975 Whakapapa lahar would have been less serious had the Whakapapa tunnel gate been closed before the lahar arrived. The lahar would then have continued on its natural path down the Whakapapa River. To achieve this, paired conductivity probes are being shifted from the previous site at the Whakapapa intake and installed in the Whakapapaiti and Whakapapanui Rivers at the SH47 bridges 8 km and 6 km upstream of the intake structure (pers. comm. W. Strauss, Ministry of Energy, Electricity Div.) Provided the system functions as planned, this will give a minimum warning of 25 minutes (based on a lahar velocity of 4 m/sec) in which to close the gates before the arrival of a lahar.

Radio signals from one of each pair of probes are designed to activate an alarm in the Tokaanu power station, and the other to initiate emergency closure of the Whakapapa tunnel gate. The gate is designed to close completely from the parked position in a time of one and one-third minutes, and it will be capable of remote control from the Tokaanu control room as well as automatically by the probe, and manually at the intake structure (W. Strauss pers. comm.).

7.2 Moawhango Diversion and Rangipo Project

Prior to the 1975 eruption it was not considered necessary to have a lahar protection system for the Moawhango Diversion except to protect workmen during construction. Because of the risk of future lahars in the Wahianoa valley it is now proposed to install a lahar protection system, consisting of early warning devices which will operate an alarm in the Tokaanu power station and initiate automatic closure of a gate on the Wahianoa aqueduct. This should prevent contaminants from reaching the Moawhango reservoir.

The sites proposed for the detectors are in the headwaters of the Whangaehu River and at the Wahianoa intake. Because of the harsh climatic conditions, remoteness of the sites, and the variable pH of the water (particularly the Whangaehu River) it is proposed to use level sensing devices rather than conductivity probes. As there are no fish in the Whangaehu River the main threat is from lahars in the Wahianoa River. Hence it is not necessary to monitor small lahars in the Whangaehu River because minor eruptions would not affect the Wahianoa catchment.

A level sensing device on the Wahianoa River would not be capable of monitoring the long term contamination of the type that occurred after the 1975 eruption (Paterson 1976a and Carr 1978). If this level of contamination is unacceptable on the grounds that it could be harmful to fish life, a conductivity monitoring system will be necessary for the Wahianoa River either as a replacement or in addition to a level sensing device.

The Mangatoetoenui Stream could be affected by lahars during the operational life of the power scheme as proved by the 1895 and to a less extent the 1975 eruptions. The Waihohonu Stream is unlikely to be affected by lahars but could be temporarily contaminated by volcanic ash. Both streams are tributaries of the Tongariro River and once construction is completed they will be diverted through the Rangipo power scheme. As the water from these streams must travel either down the Tongariro River or be diverted through the Rangipo power station, it may be advisable to allow it to continue down the river because of possible harmful effects to power station equipment. In this case it would also be necessary to close the Poutu tunnel gates to prevent contaminated water from being diverted into Lake Rotoaira.

To date no system has been devised nor procedures established to perform these steps automatically. However, if an emergency procedure is formulated and accepted by the parties concerned, adequate protection of the Lake Rotoaira fishery could be accomplished by closing the Poutu tunnel gates by remote control as soon as the lahar alarm is activated in the Tokaanu power station. The resumption of diversion would then be delayed until a field inspection had ascertained the extent of the eruption.

8 CONCLUSIONS

Lahars formed by the eruption of Ruapehu's Crater Lake are the greatest volcanic risk to public safety and to the Tongariro power scheme. These large floods of highly acidic water and volcanic debris travel down existing valleys, and because of their high density and velocity are capable of damaging power installations and communication networks located along their paths. A popular skifield is located on the upper slopes of Ruapehu in the path of lahars which could result in serious loss of life if a major eruption occurred when the slopes were crowded. Also because of their chemical contamination lahars are a serious threat to fish life.

Since 1861 numerous phreatic eruptions of Crater Lake have been recorded, at least 12 of which generated lahars. To date methods of volcanic surveillance have failed to predict the two largest, most-recent eruptions and are unlikely to be successful in the foreseeable future.

During the 1975 eruption at least 23% of the total volume of Crater Lake was erupted, and it is possible that future eruptions could eject more than twice this volume; individual lahars could show an even greater increase in volume depending on wind conditions during the eruption.

Because the power scheme involves diversion of rivers prone to volcanic contamination, a lahar protection system is required which should operate effectively for all eruptions. Such a system has the dual purpose of restricting the spread of volcanic contaminants to important fisheries and protecting installations from damage and siltation.

Unless the serious threat of Ruapehu's lahars to public safety and property can be eliminated by draining Crater Lake, a co-ordinated effort should be made to devise a lahar protection system which will satisfy the requirements of all parties concerned.

9. ACKNOWLEDGEMENTS

For data included in this paper the author wishes to thank Mr W. Strauss, Ministry of Energy, Electricity Division, and Mr C.E. Page, Ministry of Works and Development, Hydrological Survey. The helpful assistance given by Mr S.A.L. Read and Mr S. Nathan is also acknowledged.

10 REFERENCES

BOLT, B.A., HORN, W.L., MACDONALD, G.A. and SCOTT, R.F. (1975). Geological hazards. Berlin, Springer-Verlag.

CARR, R.G. (1978). An investigation of contamination of the Wahianoa River, Tongariro Power Development. N.Z. Geol. Surv. Eng. Geol. Report EG300.

GREGG, D.R. (1960). The geology of the Tongariro Subdivision. N.Z. Geol. Surv. Bull. 40.

HEALY, J. (1954). Origin of flood and Ruapehu lahars in Tangiwai Railway Disaster, Report of Board of Inquiry. Government Printer, N.Z.

HEALY, J., LLOYD, E.F., RISHWORTH, D.E.H., WOOD, C.P., GLOVER, R.B. and DIBBLE, R.R. (1978). The eruption of Ruapehu, New Zealand, on 22 June 1969. N.Z. D.S.I.R. Bull. 224.

HEWSON, C.A.Y. and LATTER, J.H. (1976). Lahar warning system, Ruapehu. N.Z. D.S.I.R., Geophysics Division unpublished report.

McCREIGHT, P.T. (1973). Tongariro Power Development. N.Z. Engineering Vol. 28, No. 11, pp. 311-316.

NAIRN, I.A., WOOD, C.P. and HEWSON, C.A.Y. (1979). Phreatic eruptions of Ruapehu: April 1975. N.Z. J. Geol. & Geophys. Vol. 22, No. 2, pp. 155-173.

NEALL, V.E. (1976a). Lahars - global occurrence and annotated bibliography. Geol. Dept, Victoria Univ. of Wellington, N.Z. Publ. No. 5.

NEALL, V.E. (1976b). Lahars as major geological hazards. IAEG Bull. No. 14, pp. 233-240.

PAGE, C.E. and PATERSON, B.R. (1976). Lahars from the 1975 Mt Ruapehu eruption. Appendix I in N.Z. Geol. Surv. Eng. Geol. Report EG230.

PATERSON, B.R. (1972). The threat of volcanic pollutants to the fish of Lake Rotoaira. N.Z. Geol. Surv. Eng. Geol. Report EG137.

PATERSON, B.R. (1976a). Volcanic contamination of the Wahianoa River, Tongariro Power Development. N.Z. Geol. Surv. Eng. Geol. Report EG269.

PATERSON, B.R. (1976b). The effects of lahars from the 1975 April Mt Ruapehu eruption and the threat of future eruptions on Tongariro Power Development. N.Z. Geol. Surv. Eng. Geol. Report EG230.

TURNER, C.W.O. (1954). Progress of the flood in Tangiwai Railway Disaster, Report of Board of Inquiry. Government Printer, N.Z.

Geological Aspects of the Design and Construction of the Reservoir Inlet and Draw-off Channels, Sugarloaf Reservoir Project

W. M. REGAN
Senior Geologist, Coffey & Partners Pty Ltd, Melbourne (formerly Project Geologist, MMBW)
J. R. L. READ
Superintending Geologist, Melbourne & Metropolitan Board of Works

SUMMARY Large excavations for the inlet and draw-off channels of Sugarloaf Reservoir were open cut in a siltstone and sandstone sequence containing bedding plane seams with very low shear strengths. The construction of permanently stable faces in rock containing these seams dictated the design of the cut slopes to suit the geological structure at each site. Careful geological monitoring enabled the design to be kept under continual review during all construction stages.

1 INTRODUCTION

The Sugarloaf Reservoir Project, located 35 km north-east of Melbourne, Victoria, includes an off-river storage reservoir filled by pumping from an adjacent river and from an existing aqueduct. After comprehensive treatment the water will be distributed in the Melbourne Metropolitan district.

The Project is sited in folded Silurian-age sedimentary rocks. The nearest major fault is the Yarra Fault located 3 km east of the Project. There is no evidence of fault movement in the area since Pleistocene time and the region is seismically quiet.

Two large excavations have been constructed within the reservoir basin for discharge of water into the reservoir from an inlet tunnel and draw-off to an outlet tunnel. This paper describes how different designs were developed to suit the geology at each excavation site and how close monitoring during the early construction stages allowed the design of the draw-off channel to be modified.

The inlet channel was excavated between February and June, 1977, and the draw-off channel was excavated between May and November, 1978.

2 PROJECT DESCRIPTION

The Project layout is shown on Figures 1 and 2. Water will be abstracted from both the Maroondah Aqueduct and the Yarra River at Yering Gorge and pumped along a 1230 m long, 2.6 m diameter tunnel through the inlet channel into the reservoir.

The water will be impounded by an 85 m high, 1000 m long main dam and two saddle dams to form a reservoir having a live storage of 95 000 ML, covering 455 Ha. The main dam and the 28 m high, 520 m long saddle dam No. 1 are concrete-decked zoned rock fill structures. Saddle dam No. 2, which is 6 m high and 170 m long, is an earth and rock fill structure.

Water will be drawn from the reservoir through the draw-off channel and a 400 m long, 2.6 m diameter tunnel under the left abutment of the main dam. It will then be pumped up to a treatment plant, treated and stored in a 200 ML capacity clear-water reservoir before being discharged through a 2.1 m diameter gravity main to Melbourne.

3 GEOLOGICAL SETTING

The Project area geology is illustrated in Figure 2.

Broad, flat-topped ridges up to 90 m high are separated by creeks with side-slopes ranging between 10° and 30°.

The rock types comprise siltstone interlaminated with and grading into fine grained sandstone. Distinct beds of medium grained sandstone ranging from 100 up to 1000 mm thickness also occur. These rocks are locally intruded by igneous dykes.

The main regional structure is a broad syncline which plunges gently north (Fig. 2). The rock mass also contains many minor folds either as local anticlines and synclines with axes roughly parallel to the main synclinal axis or as monoclinal folds, many of which have axes oblique to the main axis.

The principal defects in the rock mass are joints parallel to bedding with other joints mostly grouped in two orthogonal sets normal to bedding. Sheared and crushed seams formed by Devonian and Tertiary-age folding and faulting typically occur almost parallel to the bedding, although some are parallel to the other joint sets. These crushed seams are generally less than 20 mm thick and in fresh rock contain mixtures of rock fragments,

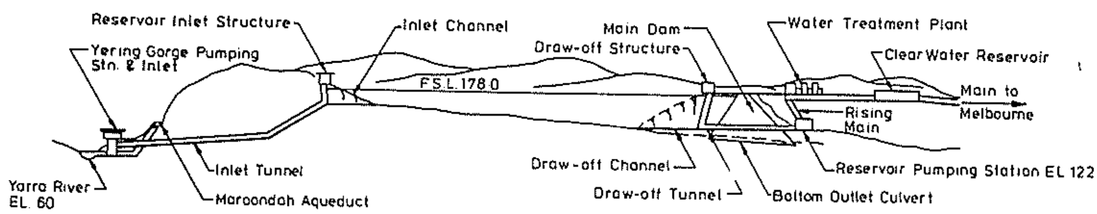

Figure 1 Schematic representation of project

silt and clay, and have soil properties (GP, GM and GC).

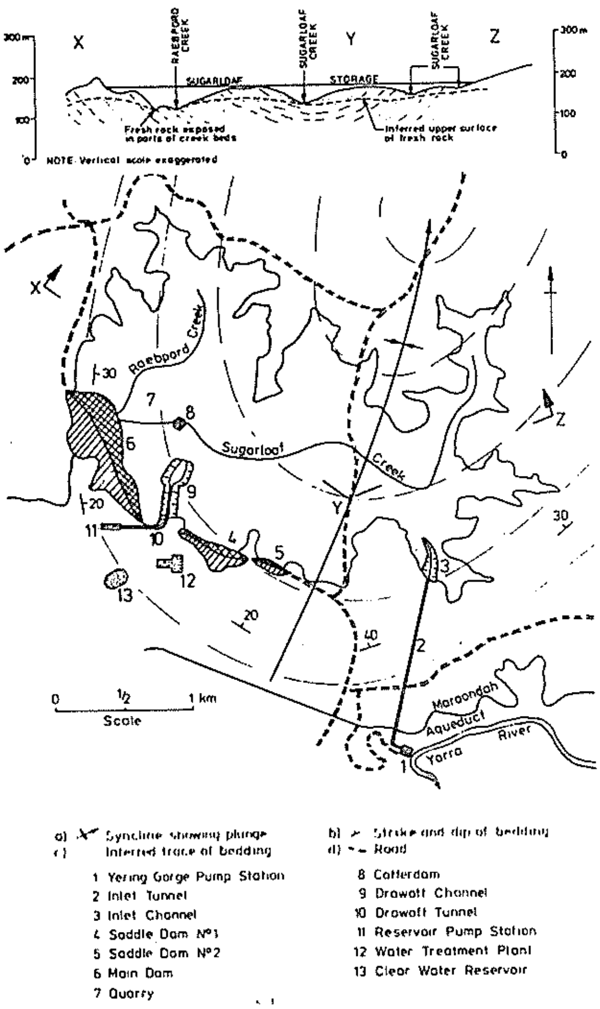

Figure 2 Project layout and geology

The rock mass has been subjected to the effects of weathering and erosion almost continuously since the end of the Devonian Period. As a consequence fresh rock is exposed only in the more deeply incised creeks and weathered zones of up to 70 m depth occur elsewhere. Above the fresh rock there is usually a gradational increase in the effect of weathering and, on the highest ridges, the joints and weathered rock substance are frequently limonite cemented.

Near-surface clay and gravelly infill seams occur where steeply dipping joints in the rock mass have opened due to mechanical weathering and down-slope movement. In the weathered rock extremely weathered seams occur along the bedding and other joints forming 10 to 30 mm thick seams of silty clay (CL). Some of these seams disappear within a few metres of the surface but many of them, particularly the extremely weathered seams along the bedding, persist and with depth grade into the crushed seams which are nearly parallel to the bedding (Fig. 3).

3.1 Strength of Extremely Weathered Seams

Laboratory direct shear tests were carried out on 15 to 20 mm thick samples of extremely weathered seam material taken from bedding planes at depths of 2 m to 10 m. The shallower samples were taken where the presence of open joints and infill seams indicated that downslope movement had taken place. Attempts were made to orientate the samples with respect to the direction of inferred past downslope movement. Some were sheared through the seam material and others along the soil-rock contact.

The range of peak and residual shear strengths obtained are shown in Figure 4. One of the tests showed no peak strength, i.e. the sample was already at residual strength, indicating that the sample had

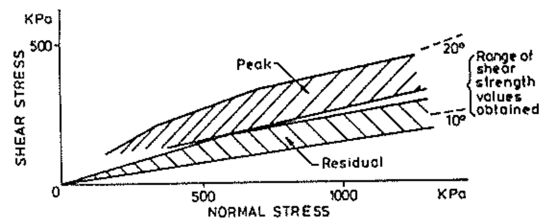

Figure 4 Shear strength of bedding plane seams

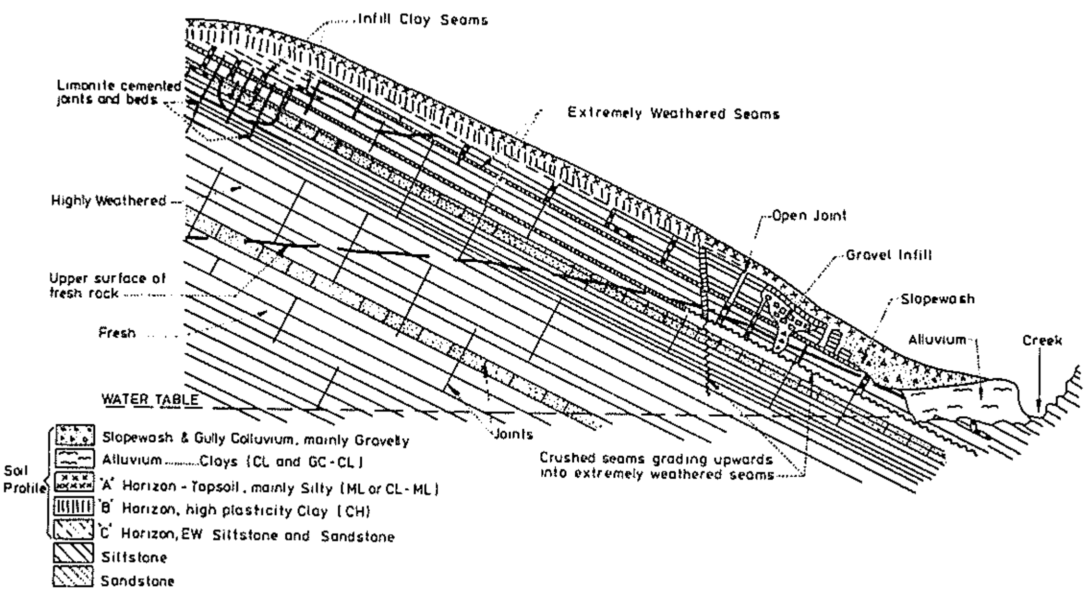

Figure 3 Soil and rock mass profile

been correctly orientated and sheared parallel to a pre-existing shear plane.

3.2 Groundwater

The rock mass permeabilities measured in the investigation boreholes were mostly in the low to very low ranges of less than 10 lugeons ($<10^{-6}$m/sec.). The groundwater table lies close to the bed of Sugarloaf Creek and the gradients beneath the higher ground are generally flat. Both the inlet and the draw-off channels are above the natural water table.

4 INLET CHANNEL

A control gate structure is inclined against and supported by the end wall of the inlet channel. This wall is 35 m high and 10 m wide at the channel invert (Fig. 5).

Site investigations, consisting of a bulldozer trench around the walls of the channel and a borehole in the deepest part of the channel, confirmed the site geology of interbedded siltstone and sandstone dipping 23° to 30° to the west. These rocks graded from highly weathered at the surface to slightly weathered in the deepest part of the channel and contained extremely weathered seams up to 50 mm thick along the bedding direction. Most joints were steeply dipping between 50° and 90°.

The channel was aligned with the end wall normal to the strike of bedding and an asymmetric shape was adopted (Fig. 5).

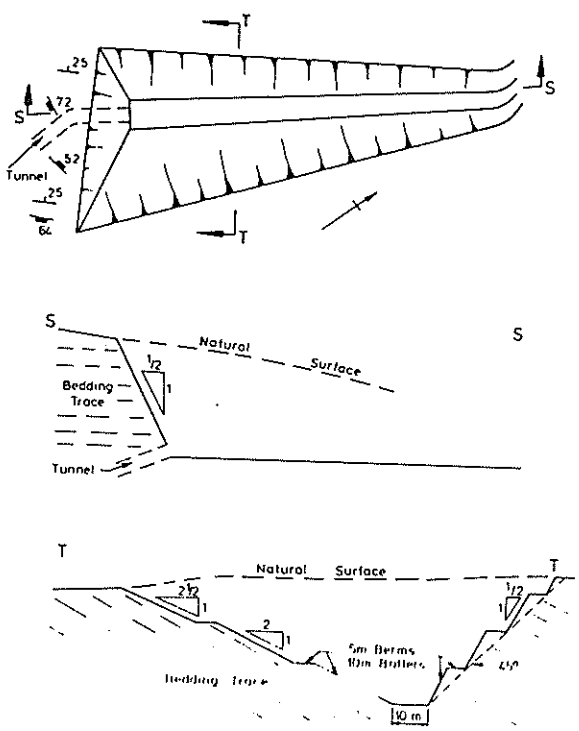

Figure 5 Inlet channel design details

4.1 End Wall

The end wall was cut at a slope of ½H : IV(63°) so that it would be stable with respect to the extremely weathered bedding plane seams and would not undercut the majority of the steeply dipping joints.

In addition the design allowed for the wall to be reinforced by 32 mm diameter mild steel deformed bars 5 m long, installed on a 2.5 m grid and inclined at a downward slope of 15° into the rock mass and grouted over their length.

The wall was first pre-split and then bulk excavation was carried out by ripping and dozing in 3 m vertical lifts. As each level was exposed the face was washed and geologically mapped to identify any seams or joints dipping out of the face which could require additional support or modification of the designed cut slope. Apart from some minor discontinuous seams and joints, which required the addition of local support, no such major defects were identified.

As the face was mapped the reinforcing bars were installed. Steel mesh was then pinned to the face and a 100 mm minimum thickness of a wet-mix shotcrete applied before the next lift was excavated. The shotcrete is intended to protect the weathered rock from fretting during the life of the reservoir. Drainage holes 2 m deep were drilled through the shotcrete to prevent hydrostatic forces from dislodging the shotcrete.

4.2 Dipslope Wall

The eastern wall of the channel was excavated parallel to the bedding planes (Fig. 5, Section TT). This was more economical than cutting a steeper face which would have required support to prevent sliding along the extremely weathered bedding plane seams. The design incorporated two 5 m wide berms and the face was geologically mapped as bulk excavation proceeded to ensure that the dip of the beds exposed was within the designed batter slopes of 2H : I V and 2½H : IV.

Except for a 25 m long meshed and shotcreted zone on the lowest batter, adjacent to the inlet structure, the dipslope wall was left unprotected.

4.3 Western Wall

For the western wall an overall slope of 45°, flatter than the majority of joints, was formed by cutting 10 m high batters inclined at ½H : IV, separated by 5 m wide berms (Fig. 5, Section TT).

The batters were pre-split and excavated with the end wall in 3 m vertical lifts. A 25 m long zone adjacent to the end wall was reinforced, meshed and shotcreted as for the end wall, but the remainder of the wall was left unprotected and unsupported. Geological mapping did not identify any areas requiring additional support.

5 DRAW-OFF CHANNEL

A control gate and trash rack structure incorporating shutters to permit water to be drawn off at any level is inclined against and supported by the end wall of the draw-off channel.

In the initial design the channel was to be located near the left abutment of the main dam in a gully to reduce the volume of excavation. However, this meant that one side wall would undercut a dipslope requiring either an excavation cut along the bedding, as in the inlet channel, or an extensive permanent support system. Neither option was economical so the possibility was examined of re-locating the channel along the axis of a nearby anticline which could result in a stable bedding orientation on both sides of the cutting.

After further investigation of the geometry of the anticline by bulldozer trenching and two boreholes, a 400 m long symmetrically shaped channel with a 65 m high end wall cut at ¼H : IV and side walls cut across bedding was adopted (Fig. 6). This arrangement gave a stable side wall situation with respect to the bedding planes. The joint pattern determined from the trenches showed that the principal joint sets were dipping at angles greater than 60° or, in the case of two sets (H and G, Fig. 6), in the range of 40° to 60°. Accordingly, the side wall slopes were designed at 45° overall. 10 m high, ½H : IV, batters separated by 5 m wide berms were originally selected but, after consideration of the height of cuts, 10 m high vertical batters separated by 10 m wide berms were adopted as a safety feature. Provision was made for fully grouted rock anchor support in case local areas of batter instability were encountered.

As the end wall undercut the gently plunging beds (Fig. 6, Section WW), additional measures were proposed to improve the stability of the face. The width of the channel was reduced within 75 m of the end wall by steepening the overall slope of the side wall from 45° to 57° in order to gain the maximum possible strength from arching effects and to reduce the size of any potential block or wedge failures. Presplitting followed by excavation in 3 m vertical lifts, patterned reinforcement with fully grouted 5 m long bars, and then meshing and shotcreting for protection were also proposed. In addition the reinforcing bars, mesh and shotcrete were extended to cover the steepened sections of the side walls.

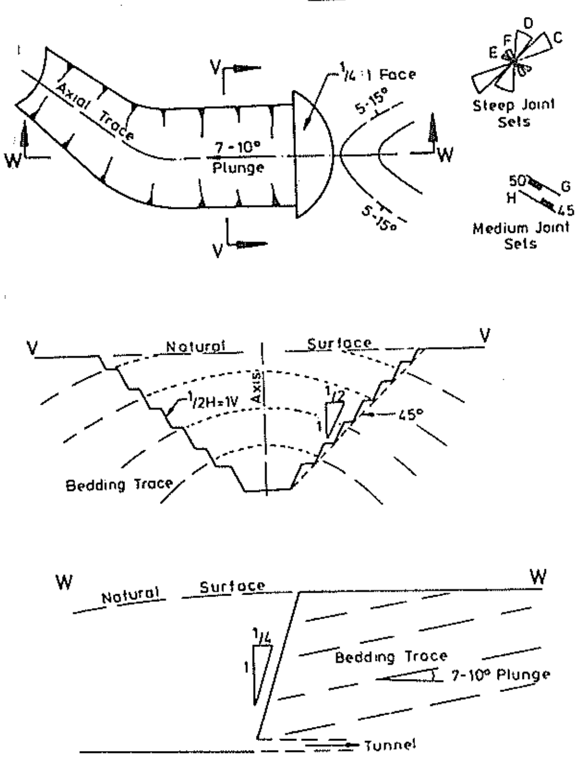

Figure 6 Design principle, draw-off channel

5.1 New Geological Data

During the construction of the main dam the Contractor exercised an option to widen and develop the northern end of the channel as a rockfill quarry. This action, together with the early completion of the draw-off tunnel to within 15 m of the channel portal, provided an opportunity to upgrade the geological model established during the investigation phase.

Geological mapping of the new exposures confirmed the overall geometry of the anticline and joint sets but revealed the moderately dipping joints of Set H (Fig. 6) to be more abundant and the steeper joint sets to be more continuous than envisaged. During quarry blasting it was also noted that slabs of rock were lifted. This new information was therefore used to re-assess the stability of the channel walls.

5.2 Side Wall Re-assessment

Two potential slip mechanisms were identified in the side walls of the channel. In the western wall blocks bounded by Sets H and D joints could fail and, in the eastern wall, blocks bounded by Sets G and D joints could fail (Fig. 7, Plan).

The potential size of the blocks depends on the overall side wall slope. Where the slope is 45° only partial berm failure would be likely (Fig. 7, Section XX), but where the overall slope is 57° complete slots could be formed for the full height of the channel (Fig. 7, Section YY).

Even though failures were possible in the steeper side wall sections adjacent to the end wall, it was decided not to flatten the overall slope in this area because :

- The probability of a failure occurring near the end wall was estimated to be only 10%.
- If necessary the potentially unstable blocks could be supported with rock anchors.
- Flattening the overall slope would increase the channel width thus reducing the end wall strength gained from arching effects and increasing the size of any potential block or wedge failure in the end wall.

5.3 End Wall Re-assessment

Two potential slip mechanisms were recognised in the end wall. They were (Fig. 7, Plan & Section ZZ).

- A thin, steep slab which could slide down along a Set G joint dipping 50°, pulling away from a Set E vertical joint and striking laterally against a Set D vertical joint. This is shown as the GD wedge.
- A series of blocks resting on bedding planes, triangular in plan. The triangular shape assumes failure back to joints of the two persistent near-vertical Sets C and E (or D). The size of the uppermost (wedge-shaped) block (1) is controlled by the outcrop of a bedding plane extending from the cutting face back to point P on the level surface. The other blocks (2) to (5) are triangular prisms and their sizes are limited by the levels at which their basal surfaces daylight in the cutting face.

5.4 Support Measures Adopted

5.4.1 Side walls

Systematic temporary or permanent support was judged to be unnecessary for side walls with an overall slope of 45°. However, the batters were geologically mapped as excavation proceeded. Any potentially unstable areas identified were either supported with fully grouted anchor bars or removed.

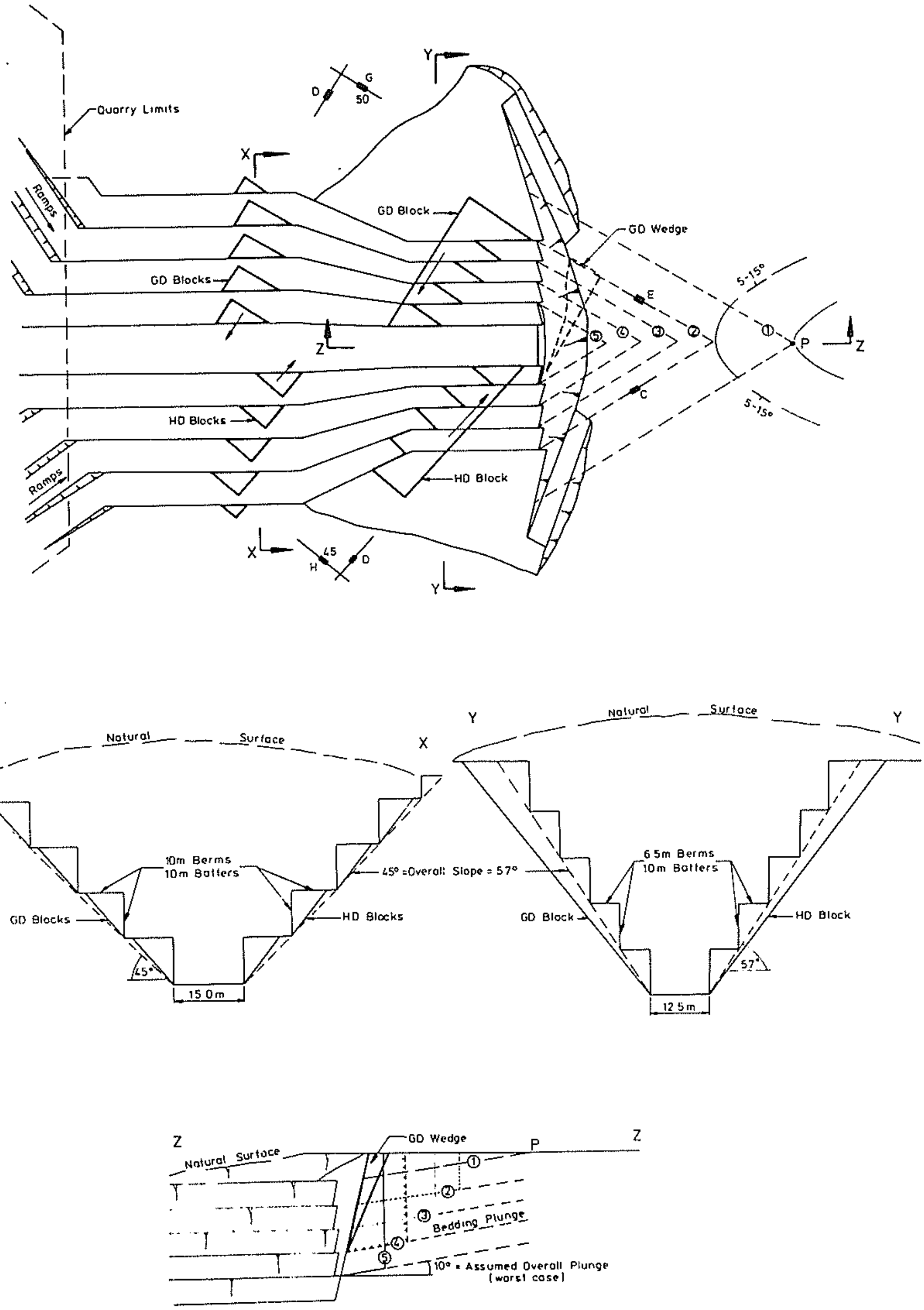

Figure 7 Draw-off channel as constructed

Within 40 m of the end wall the batters were pre-split in 10 m lifts but excavated in 3 m lifts. The walls were reinforced with 5 m long, fully grouted rock anchors installed at a downward slope of 10° on a patterned 2.5 m grid. Two metre long drainage holes were then drilled on a 2.5 m grid staggered between the rock anchors before the faces were meshed and protected with a 100 mm minimum thickness of wet-mixed shotcrete. The drainage holes were protected by plastic tubes which were removed after the shotcrete had been applied.

5.4.2 End wall

A vertical row of 10 m long, fully grouted rock anchors were first installed at 1.5 m spacings 1 m behind the end wall to prevent lifting and loosening of the rock mass. The face was then pre-split in 10 m lifts prior to any burden blasting within 50 m of the face. The last 10 m next to the face was shot with zero burden and excavated in 3 m lifts. Next, the face was reinforced with 38 mm high tensile cold worked bars 14 m long, installed at a downward slope of 15° on a 2.5 m horizontal by 3 m vertical grid and grouted over their length. Finally, 2 m long drainage holes, mesh and shotcrete were applied as for the adjacent side walls.

Both the end wall and the adjacent side walls were geologically mapped as they were excavated to check the geological model, and for any defects that might not be supported by the pattern of rock anchors. In the event no additional reinforcement was required in the end wall although some additional 5m anchors were required to support locally unstable areas in the side walls.

6 CONCLUSIONS

6.1

Large excavations can be successfully designed and constructed in interbedded sequences with unfavourable shear strength parameters provided :

- The geological model is carefully determined.
- An appropriate location and design recognising the limiting features of the geological model is adopted.
- All geological information obtained from construction monitoring is used to keep the geological model up to date so that the design can be kept under continual review.

6.2

The careful approach to excavation dictated by the use of vertical batters in large excavations is worth the effort. No rockfalls occurred during the construction period and a neat excavation with very little overbreak was obtained.

7 ACKNOWLEDGEMENT

The authors wish to thank the Melbourne and Metropolitan Board of Works for permission to publish this paper which is based on work executed on its behalf in connection with the design and construction of the Sugarloaf Reservoir Project.

Copeton Dam Spillway — Geological Investigations and Performance

D. J. THOMSON
Senior Engineering Geologist, Water Resources Commission, N.S.W.
R. C. WOODWARD
Engineering Geologist, Water Resources Commission, N.S.W.

SUMMARY The geological investigations undertaken in connection with the design and construction of Copeton Dam spillway are described, together with the factors influencing the spillway location and type of structure finally constructed. Following two minor discharges through the spillway extensive scour occurred in the discharge area, which necessitated additional geological and engineering investigations including stress measurements and resulted in remedial and additional construction work being performed at a total cost of \$1.3M. The fundamental cause of the problem was found to be the occurrence of high horizontal stresses of up to 20 MPa in the rock over this area. The mechanism of spillway scour here encountered is thought to be unique.

1 INTRODUCTION

Copeton Dam is a 113 metre high earth and rockfill structure on the Gwydir River near Inverell in northern New South Wales. The spillway is in a saddle through the right hand ridge some 500 metres from the dam, Fig. 1. Rockfill for the dam was obtained from a separate quarry located about one kilometre from the dam on the downstream left hand ridge system. Construction of the dam was commenced in 1968 and completed in 1976 using a three stage construction programme. (Douglas, 1979).

The spillway consists of a 156 metre wide concrete ogee crest supporting nine radial gates, each 13.01 metres high and 14.63 metres wide. The chute downstream of the control structure is lined for the first 55 metres and then passes through a 1 on 50 excavation to meet the natural surface. The design outflow capacity of the spillway is 14 800 m^3/s. The drop from the design flood level to the river bed downstream of the spillway is 130 metres with an average overall gradient of 1 on 4.

2 INVESTIGATIONS

Copeton Dam is located in an area of coarse grained porphyritic granite of Permian age which has been intruded by one main mass of fine grained granite and a number of smaller such bodies. Later intrusion by a series of dykes of basaltic composition of probable Tertiary age has occurred along a number of well defined orientations to produce a series of lineaments easily observable in aerial photographs, Fig. 1. The spillway is located in a saddle about 500 metres from the dam along the right hand ridge in predominantly coarse grained granite intersected by the Dingo lineament which crosses the saddle. The granite in the saddle is more deeply weathered than is generally the case in this area and these poorer foundation conditions for the structure were realised early in the investigations.

The spillway area was investigated by geological mapping, magnetic and electromagnetic geophysical surveys, trenching and diamond drilling of twenty five holes totalling 1297 metres in length together with borehole TV inspection of certain holes. Two of these holes were drilled downstream of the structure to test the rock conditions of the discharge area. These showed generally sound granite with moderately spaced joints and were not inspected using the borehole TV apparatus. The spillway design finally adopted is shown in Fig. 2, the concrete units and the gates being constructed under two separate contracts.

The location of spillway adopted was determined by the expected cost saving differential of a separate spillway and quarry over a spillway cum quarry, which tended to favour a minimum excavation spillway which was achieved at the location of the saddle. The quarry was located in the main mass of fine grained granite which had minimal overburden. The type of spillway was largely determined by the decision to use stage construction by the addition of gates. Due to the topography, alternative spillway locations considered required a spillway cum quarry arrangement or were not suitable for the addition of gates. The only viable alternative, a spillway cum quarry was at site B in the ridge to the right of the adopted spillway.

The spillway as designed was similar to the recently constructed new Wyangala Dam spillway, also situated on granitic rock, except that due to the topographic differences of the two sites, the head drop and gradient along the discharge path were considerably greater at the Copeton spillway. The spillway of the original Wyangala Dam (now replaced by a new dam with a new spillway) had one feature in common with the Copeton spillway in that it discharged into a natural gully and also experienced considerable scour (Thomson, 1967).

Some scour potential at the downstream end of the chute was realised and this was one factor favouring the use of nine gates rather than a lesser number. Flow velocities at the end of the chute for the maximum design discharge exceeded 15 m/s.

The spillway discharge area downstream of the excavation was generally covered by a significant depth of soil which greatly restricted geological mapping of this area. As the two exploratory holes drilled in the excavation cut area of the discharge channel had shown generally good quality granite, no effect was envisaged which would scour the downstream material to the extent necessary to significantly affect the granite in the excavation cut. Thus the stability of the spillway structure seemed assured. As no problem was anticipated, the normal spillway flows would be allowed to remove the soil and loose rock from this area.

The investigations of the lineaments in the spillway area revealed that the Dingo lineament consisted of a series of basaltic dykes and vertical weathered shear zones curving across the saddle area. To eliminate any possible scour of this lineament, the chute concrete and right hand training wall was extended to cover this feature. The Hardinge lineament was found to consist of one wide dolerite dyke together with associated faulting. The small gully into which the spillway discharged was not considered a major geological feature of this area in comparison with the adjacent lineaments.

3 CONSTRUCTION

Construction of the tunnel and the initial spillway excavation was carried out by day labour prior to the dam contract being let. The first indication of high stresses being present in the rock was noticed in the tunnel excavation where popping of the roof and floor of the tunnel occurred soon after driving commenced and continued for most of the length of the tunnel. It was considered at this stage to measure the stresses involved as an aid to solving this problem. This was never carried out firstly, as the construction problems were solved by altering the roof shape to a peak and bolting and meshing the roof region where the dangerous popping slabs occurred and secondly, the equipment to measure such stresses was not on hand nor readily available. As it was not considered that such stresses would in any way affect a relatively shallow surface excavation, and as popping failure was not observed in any of the subsequent surface excavations of the low and high level diversion cuts, spillway cut or the quarry excavation, no further consideration was given to the measurement of these stresses.

Although disced core in the investigation diamond drilling did occur for short sections in a few of the holes in the dam site area, it was not recognised at this time as being an indicator of active stress. After the occurrence of popping in the tunnel, further diamond cored holes were drilled into the roof of the tunnel which revealed highly disced cores whereas the earlier investigation holes in this area showed little or no such effects.

During the complete excavation of the spillway, detailed geological mapping of the excavated surface was carried out but this work did not disclose any new significant information beyond that already discovered during the investigation period.

The civil contract was completed in December 1973 and the spillway gate contract in March 1976.

4 PERFORMANCE

In January and February 1976 the first discharges from the Copeton spillway (maximum outflow 460 m^3/s) scoured a narrow (10 m wide) but unusually deep channel along the existing gully downstream of the concrete chute. (Carter, 1979). The scour produced by this comparatively small discharge showed several unusual and apparently related features including the occurrence of rockbursts in the floor of the scour channel and the great depth to which the downstream half of the channel had penetrated sound, unweathered granite. (Maximum depth below original natural surface 30 m, maximum penetration into unweathered granite 20 m).

The 1976 floods were passed through various combinations of the six right hand spillway gates while the three left hand gates were not opened. In addition to the main scour channel the floods also produced some minor undermining of backfill concrete at the downstream end of the spillway chute due to the removal of granite blocks bounded by weathered,

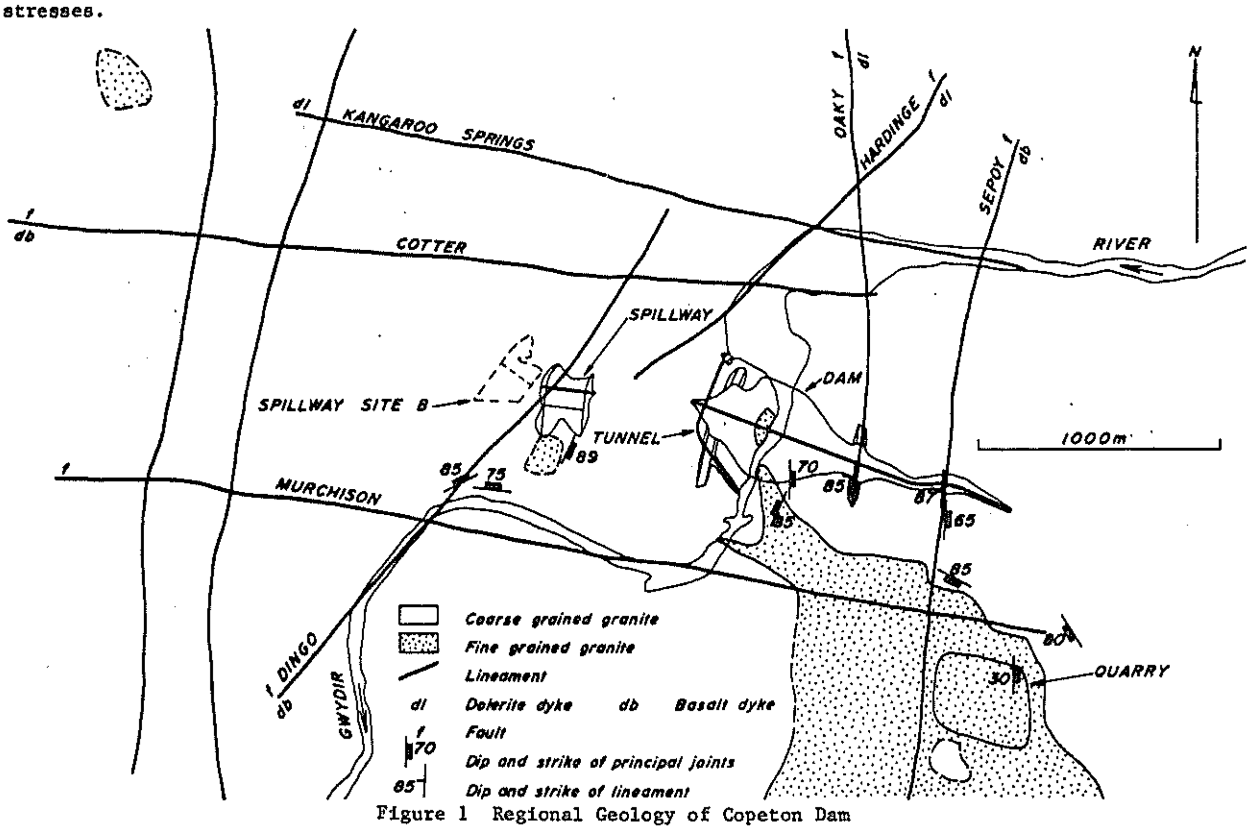

Figure 1 Regional Geology of Copeton Dam

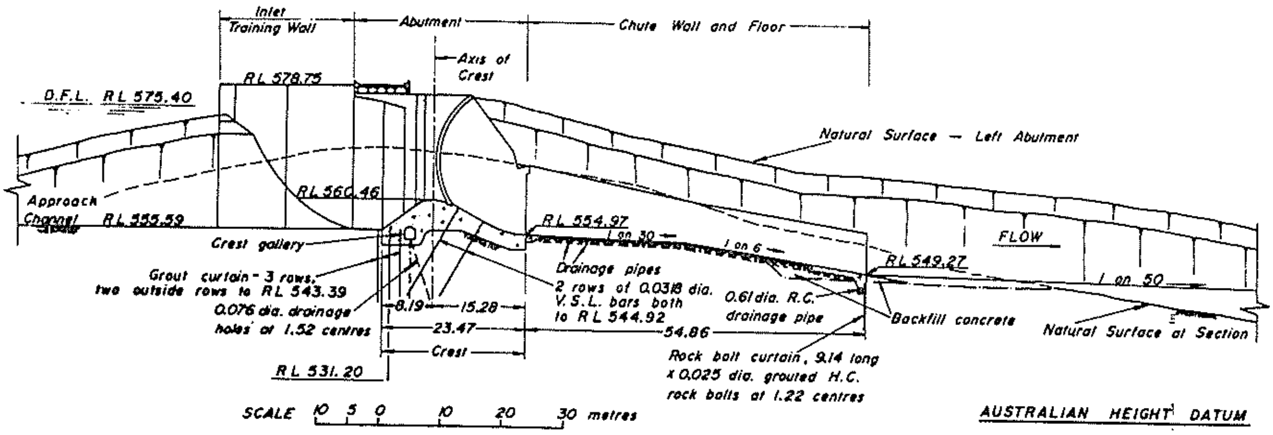

Figure 2 Adopted Spillway Design

erodible joints. The spillway structure itself sustained no damage during the 1976 floods.

For a long period following the cessation of the flood discharge the rock in the main scour channel showed significant deterioration due both to continued rock popping failure in the floor of the channel and also to the opening up on exposure of very extensive vertical, laumontite coated joints in the rock forming the walls of the scour channel.

The main scour channel appeared to owe its formation to a previously unrecorded mechanism of stress related scour (the removal of slabs of rock which had failed by upward buckling under high, horizontal in-situ stress). This scour mechanism had two unusual characteristics which indicated the need for some form of remedial works to ensure the future safe operation of the spillway.

Firstly the mechanism responsible for the formation of the main scour channel gave no indication of being self limiting. In a future major flood the deep scour channel could continue to migrate upstream towards the spillway structure and eventually be in a position to undermine the concrete chute. Secondly the removal of rock would continue for the duration of the flood. The unweathered granite in the floor of the scour channel had a high scour resistance before fracturing due to stress failure, but once failure occurred the rock slabs could be removed by even the smallest flow. The quantity of rock scoured by this mechanism during a flood event would thus depend more on the duration of the flood rather than on the peak discharge. This can be contrasted with the normal (not stress related) scour of resistant rock where the flow is capable of scouring rock for only a relatively short period at the peak of the flood. The quantity of rock removed under this normal scour mechanism depends mainly on the peak discharge and usually does not depend to any significant extent on the total duration of the discharge from the spillway.

The Copeton spillway is expected to operate on average once in three years with some discharges of up to six months duration. The combination of stress related scour with a major flood could thus present the possibility of serious damage to the spillway structure. The occurrence of this type of rock failure under stress in a spillway presents a situation quite different and much more serious than similar rock failure in a location not subject to the removal of failed rock by water flow. It is the removal of the failed rock which permits further continuing rock failure to occur without limit.

Geological investigations carried out following the 1976 floods consisted of the following:

- Surface stress measurements in the main scour channel and the adjacent spillway excavation. (Bowling and Woodward, 1979).
- Detailed geological mapping of the spillway excavation and the discharge area downstream of the excavation. (Fig. 3).
- Diamond core drilling in and adjacent to the main scour channel.

The spillway discharge area downstream of the concrete chute divided naturally into right and left hand areas separated by the central scour channel area.

Left Hand Area:

The left hand side of the spillway cut floor was still covered with construction rubble since the three left hand gates were not opened during the floods. The geological structure and hence the scour resistance of this area could not therefore be accurately assessed at this time.

It was not until after the testing of the secondary spillway following completion of the remedial works that it was possible to examine this area in detail. The rock floor on the left hand side of the spillway cut was then seen to be generally unweathered, massive granite with only a few, narrow zones of laumontite coated joints. Downstream of the excavation these joints become more frequent and these jointed zones eventually merge into the major zone of laumontite coated joints in the downstream half of the main scour channel.

Main Scour Channel Area:

The main scour channel commenced at the centre of the spillway near the end of the concrete chute and progressed downstream, becoming deeper as it did so, along an "en echelon" series of laumontite coated joints and faults. These joints strike slightly oblique to the channel and form its near-vertical side walls. The floor of the scour channel was located almost entirely in unweathered granite and consisted of stress relief fractures dipping downstream at 10° - 30° which were either pre-existing joints or fractures newly formed during the flood. The downstream half of the scour channel followed one major zone of laumontite coated joints and it was here that it attained its greatest depth with two

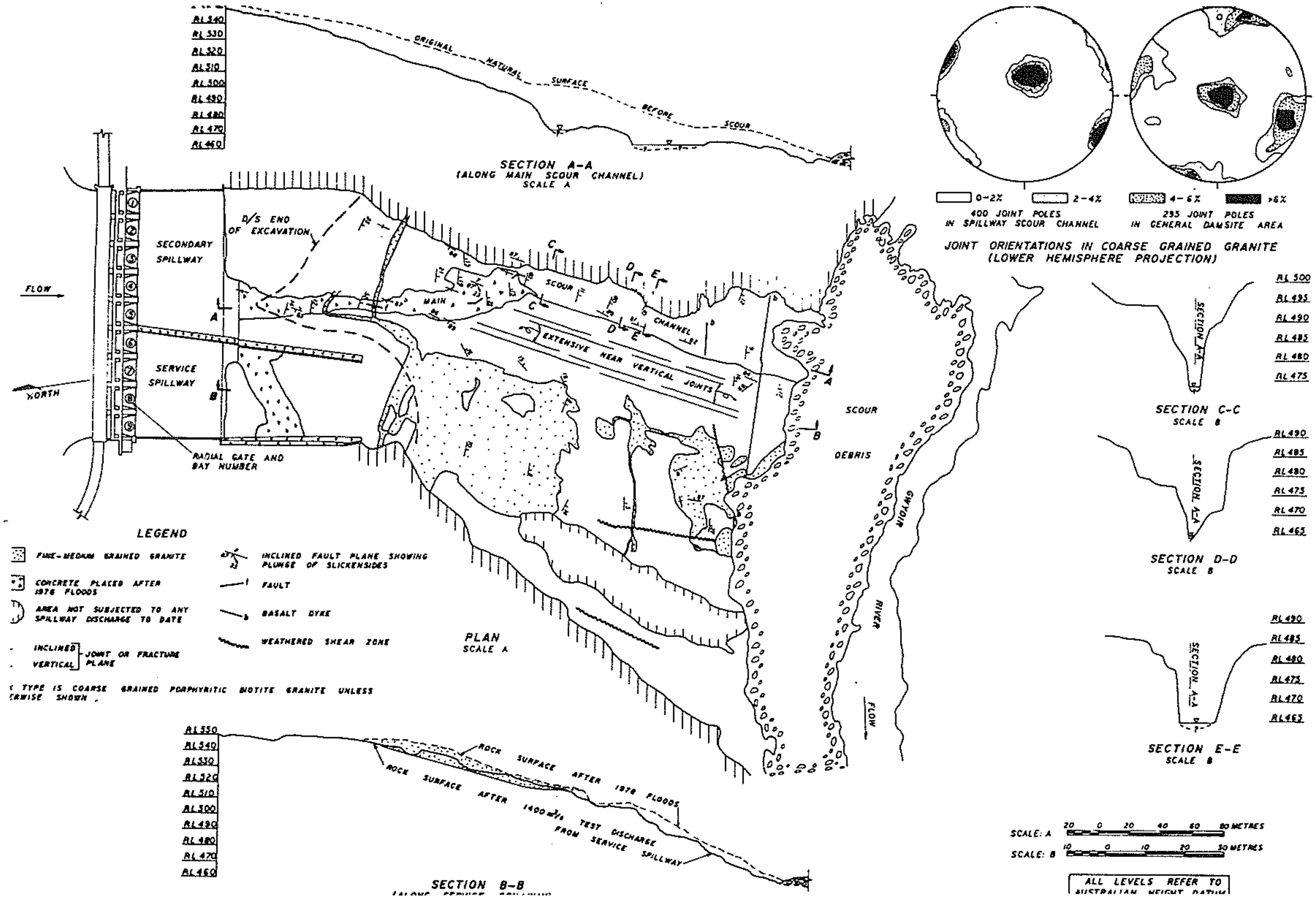

Figure 3 Copeton Spillway - Geological Plan and Sections.

scour holes up to 30 m deep below the original natural surface. There was every indication that future floods would cause these deep scour holes to migrate upstream towards the spillway chute.

Right Hand Area:

The right hand half of the spillway cut floor had suffered a certain amount of relatively minor scour controlled by weathered, erodible joints (not related to failure under stress). Generally however the granite on this side of the spillway cut was only sparsely jointed and appeared to have a high scour resistance. In particular the laumontite coated joints and faults so common in the main scour channel were almost entirely absent from this side of the spillway cut. Immediately downstream of the right hand half of the spillway cut a flat-lying sill-like body of fine grained granite outcroped. Diamond core drilling showed this fine grained granite to have a maximum thickness of about 10 m and to contain weathered, erodible joints as well as being generally more intensely jointed than the coarse grained granite within the cut immediately upstream.

5 REMEDIAL WORKS

The scheme of remedial works adopted consisted of constructing a training wall from the pier separating gates 5 and 6 so that the four right hand gates could be operated as a service spillway discharging up to 2800 m^3/s and the five left hand gates (including gates 4 and 5 which discharge directly into the scour channel) would then be operated only as an emergency secondary spillway (Fig. 3). The service spillway concept was feasible because of the very massive, sparsely jointed rock present on the right hand side of the spillway excavation. There was thus no possibility of a second scour channel developing which could migrate upstream into the service spillway area and undermine the right hand side of the spillway chute.

In addition to the construction of the training wall the following work was also carried out:

Concrete lining anchored to the rock of the upstream half of the scour channel floor to prevent scour on the rare occasions when it would be necessary to release water from the secondary spillway.

Concrete lining of the right hand wall of the spillway cut, downstream of the chute to protect numerous weathered and erodible joints exposed in the wall of the cut.

Extensive concrete lining of areas within the service spillway immediately downstream of the chute where weathered, erodible joints were exposed in the floor.

The training wall was constructed on massive granite to the right of the main scour channel and terminated about level with the downstream end of the right hand spillway cut wall thus stopping short of the fine grained granite sill just beyond the end of the spillway cut.

Under design flood conditions both sides of the training wall would be subject to water flow and to obtain a totally secure foundation for the wall it was necessary to site it well clear of the right hand wall of the main scour channel. This necessitated an alignment somewhat skewed to the right rather than one parallel to the spillway flow.

The construction of these remedial works commenced early in 1977 and was completed in January 1978. Since that time the remedial works have been tested up to the following maximum discharges by controlled releases:

Service Spillway	1400 m^3/s
Secondary Spillway	140 m^3/s

The flow duration at these maximum discharges was very short (1-2 hours). The general conclusions reached as a result of these tests are that the Service Spillway will be capable of safely discharging its designed capacity of 2800 m^3/s. Discharges from the Secondary Spillway are likely to cause further major scour downstream of the spillway without however endangering the safety of the spillway control structure. The probability of further scour and the possible requirement for further remedial work in this area is considered acceptable in view of the anticipated infrequent operation of the Secondary Spillway.

6 REVIEW OF ORIGINAL SPILLWAY DESIGN

The geological investigations carried out following the 1976 floods indicated that the factors responsible for the unusual scour were:

(i) the rock underlying the discharge gully was more jointed than the surrounding granite both by vertical, laumontite coated joints and faults and by near horizontal, pre-existing stress relief joints. The natural stress concentrating effect of the original gully profile probably meant that these pre-existing stress relief joints parallel to the topography were more intensely developed beneath the gully than elsewhere. In the near surface rock (about the upper 10 m) these joints were generally weathered and some were filled with erodible material.

(ii) the granite in the Copeton spillway area is carrying a virgin, horizontal, compressive stress in the range 15 - 20 MPa. Scour of the jointed rock in the gully produced a notch-like channel resulting in a concentration of this virgin stress which was then sufficiently high to cause the granite to fail by upward buckling (the rockbursts observed in the floor of the scour channel). The failure of the granite under high, horizontal compressive stress is believed to be the major factor responsible for the great depth to which the scour was able to penetrate the sound unweathered granite.

The failure of near surface rock under high stresses is unusual but several instances are recorded from various surface excavations around the world. However the occurrence of this phenomenon in a dam spillway leading to a major scour problem does not appear to have been previously reported.

The Copeton spillway, as originally constructed was closely based on the successful new Wyangala Dam spillway design. Both these spillways consist of a gated crest structure capable of handling the Probable Maximum Flood (of similar magnitude in both cases) with a short concrete chute which leads to an unlined channel excavated in granitic rock. Once the discharge leaves the spillway cut it flows over the natural surface to return to the river, no energy dissipation being provided in either case.

TABLE I

COMPARISON OF COPETON AND WYANGALA SPILLWAYS

Feature		Copeton	Wyangala
(A)	Width (m)	156.06	138.38
	Lined Length (m)	70.14	61.19
	Head drop (m) from design flood level to: - end of chute	26.13	22.77
	- river bed	130	77
(B)	Maximum discharge to date (m^3/s)	460	1 870
	Maximum Design Capacity (m^3/s)	14 800	14 700
*	Theoretical power of discharge per unit width at river bed level: - Maximum to date (kW/m)	3 700	9 800
	- Maximum discharge capacity (kW/m)	120 000	80 000
(C)	Topography of discharge area	Spillway discharges directly into a gully which runs from the spillway cut down to the river. Overall slope of discharge path from concrete chute 14 degrees. (1 on 4)	Spillway discharges over a broadly convex ridge which disperses flow. Overall slope of discharge path from concrete chute 4 degrees. (1 on 13)
	Geology of discharge path	Zones of vertical laumontite coated joints approximately parallel to flow. Concentrated flow in gully scoured a notch-like channel by erosion along these zones.	Significant geological structures normal to flow. One major shear zone dental concreted during construction.
	In-situ stress conditions	In-situ, horizontal compressive stress = 15-20 MPa. Stress concentration due to initial scour notch caused rock failure by upward buckling.	In-situ stress too low to cause rock failure.
(D)	Scour performance	Deep scour in unweathered granite underlying discharge gully.	No significant scour of unweathered rock.

* Theoretical value assuming no dispersion or concentration of flow downstream of the spillway cut and also no energy loss between reservoir and river bed below the spillway. Due to concentration of the flow in the downstream half of the main scour channel at Copeton, the actual maximum value to date could have been as high as 30,000 to 40,000 kW/m (assuming 1/2 - 3/4 total flow in channel).

This type of spillway design accepts the fact that a large amount of soil and weathered, near surface rock will be scoured from the natural surface downstream of the spillway cut and dumped in the river bed below the spillway. The basic assumption is however that this scour will be self-limiting, with non-erodible, scour resistant rock at a comparatively small depth below the natural surface and that once the scour reaches this depth a more or less stable situation will develop before there is any risk of damage to the spillway structure.

At Wyangala Dam this assumption has proved correct while at Copeton Dam this has not been the case, at least in the central gully area now occupied by the main scour channel. This does not mean however that the quality of the rock downstream of the Copeton spillway was significantly inferior to that assumed during the design of the spillway. The unweathered granite outside the zones of laumontite coated joints can only be described as excellent quality rock (joint spacings generally in excess of 3 m; R.Q.D. generally 90-100 per cent). Even within the zones of laumontite coated joints where joint spacings are generally in the range 0.1 m to over 1 m the majority of the rock would still be described as of good quality (R.Q.D. 75-90 per cent).

The design assumption of good quality rock in the Copeton spillway was therefore quite correct and it is necessary to look elsewhere for the cause of the unsatisfactory scour performance during the 1976 floods. The great similarity of the Wyangala and Copeton spillways from the geological, design and operational aspects suggested that the detailed comparison shown in Table I would be instructive.

The major factors whose combined effect was responsible for the Copeton scour and which were absent at the Wyangala spillway can be summarised as follows:

1. Spillway discharge flowed directly into an existing gully. The topography and geology of the gully area permitted the development of the initial, notch-like scour channel.

2. High in-situ, horizontal compressive stress in the near surface rock in the spillway area.

Having regard to the generally very good quality of the granite in the spillway area the absence of either one of the above factors would very probably have prevented the development of the major scour that did occur during the 1976 floods, the magnitude of which was accentuated by the high head, steep slope and concentration of flow in the discharge gully.

It is interesting to speculate whether a different location and/or design of spillway at Copeton Dam could have avoided the major, stress-related scour problem. Since alternative sites were never investigated in detail it is impossible to be certain but nevertheless it does appear to be a plausible speculation that a spillway of the same design at site B (about 150 m to the right of the existing spillway) may not have experienced the problems that did occur in the 1976 floods. The reasons for this belief are as follows:

A spillway at site B would have discharged eventually into the Dingo Lineament Gully and major scour would have occurred there but this gully would not have run directly upstream into the spillway cut and thus scour in the gully itself could not have posed a threat to the spillway structure. There is also a possibility that the in-situ stresses may not have been as high west of the Dingo Lineament as at the existing spillway site. Bowling and Woodward suggested a possible relationship between the stress field at Copeton Dam and the various faults (lineaments) in the area and there was some evidence that the stresses in the existing spillway area might be somewhat higher than elsewhere in the Copeton Dam area.

With regard to the possibility of providing a concrete chute over most of the discharge path it must be remembered that water flow over an irregular rock surface is aerated to a much greater extent than flow in a concrete lined chute. Had a long concrete lined chute been constructed at Copeton the lack of aeration during major flood discharges would have resulted in very high energy flows being directed onto the rock downstream of the chute with the possibility of major scour and also cavitation damage to the chute concrete.

The important role played by high in-situ rock stresses in the development of the Copeton scour indicates the desirability of establishing some guidelines as to what level of in-situ stress is likely to give rise to this type of problem.

According to Cook (1976) slabbing or buckling failure occurs when the stress actually being carried by the rock approaches a third to a half the uniaxial compressive strength. The actual stress in the rock depends on the virgin stress level and on the stress concentration factor, if any, which applies to the particular location in question.

Photoelastic model tests carried out by the Hydro-Electric Commission, Tasmania to interpret the results of the surface stress measurements in the Copeton spillway indicated that the maximum stress concentration factor likely to be encountered in the floor of a notch-like scour channel is about three.

From a knowledge of the virgin in-situ stress and the compressive strength of the rock it would then be possible to assess the probability of rock failure in the floor of any scour channel which might develop downstream of a partially lined spillway.

7 CONCLUSIONS

In view of the apparently unique nature of the stress related scour mechanism experienced in the Copeton spillway, it is not surprising that it was not anticipated during the design of the spillway.

The good quality of the granite in the Copeton area generally and the spillway site in particular did justify the type of spillway design adopted (partial lining with no energy dissipation). However, the Copeton spillway site had a high scour potential due principally to the high head and steep slope of the discharge path, even without the added factors of high in-situ rock stresses and unfavourably orientated geological structures.

Although at Copeton the high rock stresses were a major and probably a necessary casual factor in the scour which occurred, it can be said that generally it would be undesirable to site a high head spillway such that it will direct high energy discharges into an existing gully which continues directly into the spillway cut. In general a gully must be expected to be underlain by rock which is at least to some extent, less scour resistant than rock elsewhere where natural erosion processes have not created a topographic depression.

A spillway location which may be quite acceptable for spillways with low heads or infrequent operation may not be suitable for frequently operating high head spillways.

In the light of the Copeton experience it would be prudent to assess in-situ rock stress levels at any potential site for an unlined or partially lined spillway. Although sites where stresses are high enough to cause rock failure must be rare, nevertheless if such failure were to occur it could create a very serious situation for the safety of the spillway structure. In particular the possibility must be investigated of initial normal scour along an erodible geological feature creating a notch which then may concentrate the virgin stress by a factor of up to three. The Copeton scour clearly demonstrated that a major problem can develop even though the virgin stress itself is not high enough to cause rock failure.

8 ACKNOWLEDGMENTS

The authors wish to thank the Water Resources Commission of New South Wales for permission to publish this paper and Mr. K. Gordon, Senior Design Engineer and Mr. P. Carter, Design Engineer for reviewing the paper.

9 REFERENCES

BOWLING, A.J. and WOODWARD, R.C. (1979). An Investigation of Near Surface Rock Stresses at Copeton Damsite in New South Wales.
Australian Geomechanics Journal (in press).

CARTER, P.R. (1979). Copeton Dam Spillway Performance.
ANCOLD Bulletin. No. 53. pp. 14-19.

COOK, N.G.W. (1976). Methods of Acquiring and Utilising Geotechnical Data for the Design and Construction of Workings in Rock.
in Exploration for Rock Engineering.
Edt. Z.T. Bieniawski. A.A. Balkema. Cape Town.

DOUGLAS, A.W. (1979). Copeton Dam.
Institution of Engineers Australia Annual Conference, Perth, W.A. Event No. 506.2.

EAGLES, J.H. (1972). Copeton Dam Design.
ANCOLD Bulletin No. 36 pp. 34-46.

THOMSON, D.J. (1967). Geological Investigations for Wyangala Dam Spillway Site.
Aust. Civil Engineering Trans.
Vol. 9. No. 1 pp. 53-62.

Zonal Concept for Spatial Distribution of Fractures in Rock

N. R. P. BACZYNSKI
Post Graduate Student, University of Melbourne and CSIRO Division of Applied Geomechanics

SUMMARY Evaluation of the spatial distribution of fractures within the dolomitic shales at the Mount Isa Mine suggests that fractures tend to occur in zones. Computer modelling of fracture distributions indicates that the field mapping technique of single line sampling fails to provide sufficient data to fully characterize the rock mass. A simple data collection and model formulation concept is described that will enable the local variability within any rock mass to be assessed. The method permits the statistical evaluation of masses in terms of fracture intensities of each set that is likely to be associated with underground openings of any given shape and size. This information can then be extended to evaluate the variability in the mechanical properties of the rock surrounding underground openings.

1 INTRODUCTION

To a large extent, the physical and mechanical properties of rock masses are functions of the attitude, geometry and spatial distribution of faults, joints and other geological discontinuities within the mass.

Spatial distribution refers to the position of fracture plane centres within a given volume of rock. A literature survey indicates that very little information appears to have been published on this topic.

A number of writers have recognized the tendency for sets of fractures to occur in zones. However, most geotechnical analyses continue to be based on assumptions that the spatial distribution is random. It appears to be commonly presumed that the observed fracture clusters are purely a result of a random process.

Data collected at the Mount Isa Mine suggests that the observed spatial distribution of fractures at the mine cannot be explained in terms of the random model. The study indicates that it may be necessary to invoke a zonal model to satisfactorily account for the observed relationships within some rock masses.

2 GEOLOGICAL CONSIDERATIONS

2.1 Data Collection

Structural data requirements for engineering purposes and the necessary sampling procedures have been described in detail by a number of authors and will not be reiterated here. The most recent review of recommended techniques was released by the International Society for Rock Mechanics during 1978.

A commonly recommended field mapping procedure is the line sampling method, where all fractures crossing a continuous straight sample line are included in the data. The principal advantage of this technique is that it tends to yield unbiased results. Furthermore, it enables a direct comparison to be made between in situ mapping and orientated drill core data.

Between 1970 and 1974 most detailed structural data at Mount Isa Mine were collected by means of extensive line sampling of underground openings and logging of orientated drill cores, i.e. Baczynski (1974), Bridges (1975).

2.2 Orientation and Continuity of Fractures

Although orientation and continuity describe two very important properties of fracture planes, a detailed knowledge of these parameters is not required for purposes of the present discussion. It is sufficient to mention that field work at the mine suggests that the distribution of fracture trace lengths (as encountered along line samples) may be represented by a lognormal probability density function. However, evidence for this model is outside the scope of this paper.

2.3 Fracture Spacing

Investigations suggest that the spacing between adjacent fractures of each set (along line samples) may also be best described by means of a lognormal probability density function. A typical cumulative frequency plot on logarithmic probability paper is illustrated in Figure 1. The plot summarizes the spacing model for two of the fracture sets defined at the mine. The illustrated results are based on diamond drill core data and therefore the sample includes all fractures with continuities down to a lower limit of about 0.02m.

In general terms, the distributions highlight the observation that spacing between adjacent fractures is markedly skewed towards the smaller spacings in a manner such that the logarithm of the spacing variable is normally distributed. This suggests that fractures of a particular set are not evenly distributed within the rock mass, but tend to occur in clusters.

3 "RANDOM" SPATIAL MODEL

3.1 Assumptions Underlying Model Testing

The validity of the random model can be most readily tested with the aid of a simple computer prog-

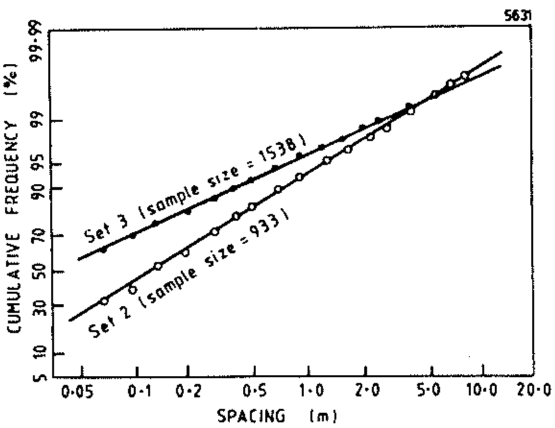

Figure 1. Cumulative Frequency Distribution for In Situ Spacing of Fractures.

ram based on the "Monte Carlo" method (Hammersley and Handscomb, 1964). The necessary input data for a fracture set to be simulated consists of:

(i) Average orientation of the fracture traces which is assigned to each member of the set,
(ii) Model for fracture trace continuity,
(iii) Mean spacing between fractures along line samples, and
(iv) A suitable model for the number of fractures or the total fracture trace length to be generated within the defined area.

The first three parameters may be determined from field data, whereas the fourth requires some consideration.

Assuming that the dimensions of the area selected for fracture trace generation are very large in comparison to the mean spacing between fractures, then on the average it would be expected that the spacing between fractures encountered along each and every hypothetical sample line transecting this area in a direction normal to the trace of the planes would approach the mean spacing for the set. On this premise, the total trace length of all fractures within the generation area may be simply derived by the formula:

$$\text{Total Trace length} = \frac{D_n}{S_m} \times D_p$$

where, D_n = Average dimension of the area in direction normal to fracture traces (parallel to line samples),

D_p = Average dimension of the area parallel to fracture traces, and

S_m = Mean spacing between fractures along line samples.

This estimate of the anticipated total trace length may be used to furnish the necessary fourth parameter.

The basic computer procedure adopted for generation of fracture traces within a defined area consisted of the following three iterative steps:

(i) Random generation of mid-point coordinates for fracture trace,
(ii) Statistical generation of trace length in accordance with a fracture continuity model, and
(iii) Determination of x- and y-coordinates for extremities of the fracture trace through the designated mid-point.

The iterative procedure is concluded when the cumulative trace length of the generated fractures equals or just exceeds the permissible total length. The coordinate data may then be output to a plotter. Furthermore, the fracture traces can be computer tested for intersection with selected sample lines and the spacing model may be derived.

3.2 Results of Model Testing

Figure 2 presents a typical fracture trace pattern generated on the basis of the random model. The most striking feature of this plot is the relatively homogeneous density of fractures over the entire area.

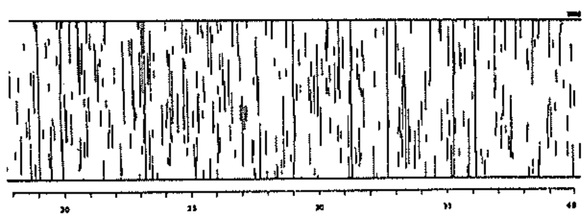

Figure 2. Typical Fracture Pattern Generated on Basis of a "Random" Spatial Distribution Model for Fracture Plane Centres.

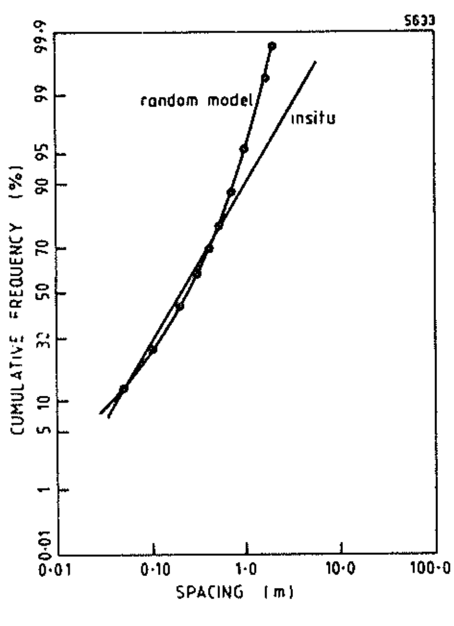

Figure 3. Cumulative Frequency Distribution for Spacing of Fractures Generated on Basis of "Random" Spatial Model.

The resulting cumulative frequency plot for the spacing between adjacent fractures is presented on logarithmic probability paper in Figure 3. It is apparent from this plot that the random spatial model fails to reproduce the lognormal spacing model observed at the mine.

4 "ZONAL" SPATIAL MODEL

4.1 Data Collection

In order to test the validity of this model, a mapping programme of continuous area traverses was undertaken at several locations in the mine. A simple and rapid procedure was adopted for mapping of underground openings.

After selected areas were photographed, a set of suitably enlarged, overlapping photographs were used as base maps to mark on the traces of all visible fractures in the walls of the openings. On completion of underground mapping, the data were transferred to non-distorted maps and fracture traces were assigned to sets on basis of their orientation. A separate transparent overlay was compiled for each set.

4.2 Data Analysis and Model Development

Each transparent overlay was sub-divided into unit areas, in the manner illustrated in Figure 4. For purposes of the analysis, "unit areas" were defined as an area equivalent to $1.0m^2$ in the direction normal to the average strike of the fracture set. This permitted the dimensions of unit areas to be adjusted according to the angular relationship between the strike of the set and the strike of underground openings, such that the "normalized" unit area remained the same or constant.

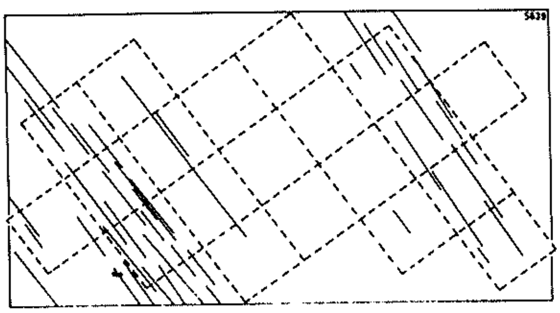

Figure 4. "Unit Area" Concept.

The total trace length of each set of fractures was determined within each unit area. The prime purpose of these analyses was to derive a model for the variability in the intensity of fracturing between unit areas (Figure 5), including determination of conditional probability density functions for the extent of fracture intensity "zones" in directions parallel (Figure 6) and normal to the average trace of a set.

To enable the 2-d model to be extrapolated into the third dimension, it was necessary to assume that each fracture plane continued for a unit distance into the third dimension, e.g., a 2-d unit area with an intensity of 8.0 linear metres of fracture traces was converted in the 3-d model to $8.0m^2$ per

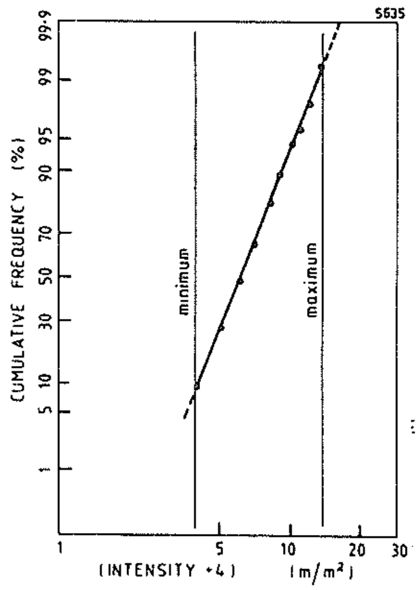

Figure 5. Cumulative Frequency Distribution for Intensity of a Fracture Set per Unit Area.

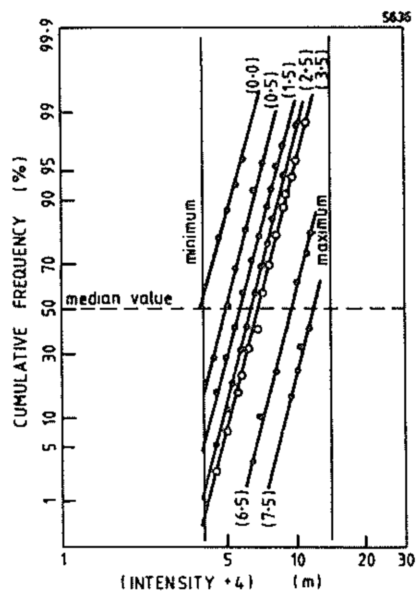

Figure 6. Cumulative Frequency Distribution for Intensity of a Fracture Set in a Unit Area Adjacent to a Unit Area with an Intensity Indicated by the Median Value, in the Direction Parallel to the Average Trace of fractures. (Conditional Probability Density Functions).

cubic metre unit domain. In short, this model assumes that for each fracture set, each unit volume of the rock mass is homogeneous for a metre in the direction parallel to the average strike of the set.

It is apparent that such assumptions would be very difficult to justify in situations where a relatively large dimension had been selected for unit areas or volumes. The smaller the dimensions, the more likely it is that the assumptions are valid. The dimensions of unit areas selected for the Mount Isa Mine study are approximately 2.5 times the mean spacing between fracture planes of the most common set and about 0.7 times their mean trace length.

4.3 Model Testing

4.3.1 Objectives of Tests

The prime purpose of the tests was to verify that the "zonal" model would yield the same mean fracture intensities per unit volume, as well as the lognormal spacing along line samples.

4.3.2 Testing Technique

The validity of the model was tested by comparing the above two parameters as generated by the computer modelling process with the prototype. A computer program developed by the author was used in the analysis. The basic principles underlying the program are indicated below.

(i) Selection of the desired dimensions for the test block and sub-division into unit volumes,

(ii) Assignment of fracture intensities to unit volumes in accordance with the statistical model determined for the set,

(iii) Generation and location of fracture planes within the test block until all designated local intensities within the test block are satisfied, and

(iv) Calculation of mean fracture set intensity per unit volume of the test block and generation of fracture plane patterns on selected planes "cut" through the block. Determination of spacing model for adjacent fracture traces along line traverses.

4.3.3 Results

On the basis of several hundred test blocks, each comprised of approximately 3500 unit volumes, that were generated for each fracture set, a reasonable correlation was achieved between the generated and in situ fracture intensity, as well as the spacing model for adjacent fractures along line samples.

The results for the fracture sets delineated in the dolomitic shales at the mine are summarized in Table I, which indicates the in situ and generated mean intensities per unit volume of the average test block.

Table I

Mean Intensity of Fractures per Unit Volume of Block

Fracture Set	In situ	Simulated
1	2.17	2.15
2	2.17	2.15
3	1.12	1.12
4	0.24	0.27
5	0.12	0.14
6	0.28	0.31
7	0.05	0.06
8	0.23	0.27
9	0.15	0.18
10	0.12	0.14

The typical fracture pattern generated with one set is illustrated in Figure 7 and the corresponding line sample spacing results are presented in Figure 8.

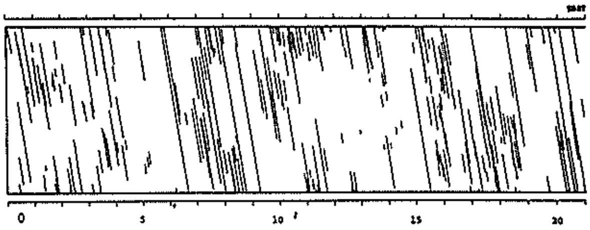

Figure 7. Typical Fracture Pattern Generated on Basis of a "Zonal" Spatial Distribution Model for Fracture Plane Centres.

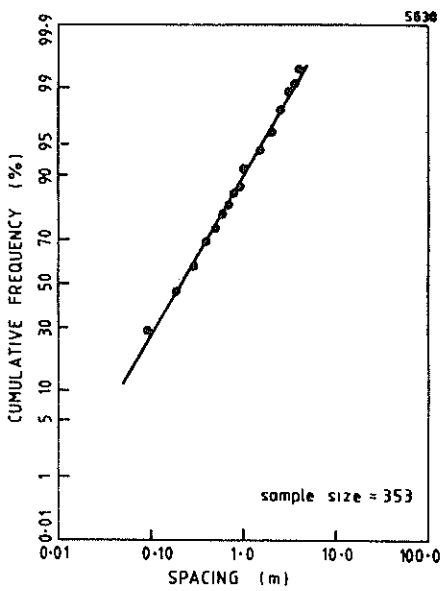

Figure 8. Cumulative Frequency Distribution for Spacing of Fractures Generated on Basis of a "Zonal" Spatial Model.

Figure 9 illustrates a typical pattern generated with the first six sets listed in Table I above. Rock mass variability and the contrast between low and high fracture intensity sub-domains are highlighted by this figure.

5 PRACTICAL APPLICATION OF ZONAL CONCEPT

The results indicate that fracture distributions generated on basis of the "zonal" concept are not only in accord with field evidence, but also they highlight to a greater extent the true variability within rock masses.

Provided that suitable sample areas exist, then the described principles of data collection can be applied to any rock mass, irrespective of the spatial distribution of fractures within them. Moreover, the additional data necessary for the development of a "zonal" model is not excessive, and the

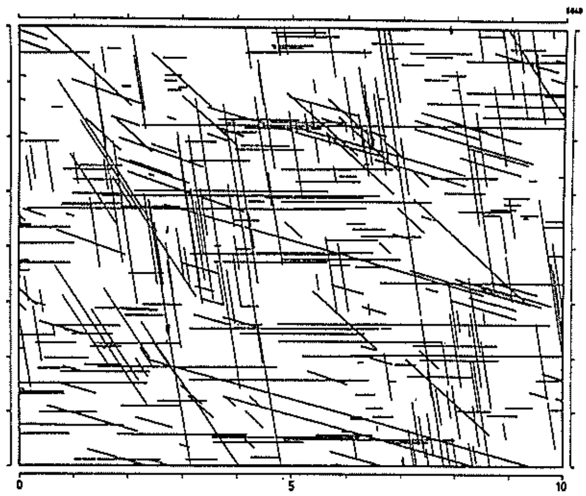

Figure 9. Typical Fracture Pattern Generated on Basis of a "Zonal" Spatial Distribution Model for Six Sets of Fracture Plane Centres.

investigation programme can be completed within a relatively short period of time. It should also be possible to derive similar models on the basis of orientated drill core data from two or more boreholes drilled parallel and within very close proximity to each other.

Once the field data have been analysed, the derived model may be utilized in its "rough" form, or alternatively it may be approximated by means of some standard statistical distribution such as the Gaussian or Poisson probability functions. However, care should be exercised to ensure that standard distributions are not always assumed even where these exhibit a poor degree of correlation with the "rough" distribution. An adequate sample size is necessary in all cases.

After formulation of the statistical model, it is then a routine matter to evaluate the variability in the average fracture intensity between rock mass blocks with any specified dimensions.

This information then yields a better understanding of the ground conditions that are likely to be encountered in the mass. For example, given the block dimensions, an iterative "Monte Carlo" method can be used to sample the population in order to evaluate the variability in modulus (provided that the normal and shear stiffness of fractures and intact rock are known), or to assess the likely range of various rock mass classification ratings (from which such parameters as stand-up time, support requirements, modulus, and others may be deduced).

6 CONCLUSIONS

The evidence presented suggests that the observed spatial distribution of fractures in at least one rock mass is not random. However, a zonal distribution appears to account for the lognormal model derived for spacing between adjacent fractures of the same set which transect straight line samples.

The spatial distribution of high intensity zones is assumed to be random for a defined volume of rock mass. On the other hand, the 2-d extent of zones in directions parallel and normal to the average orientation of fractures within them may be predicted statistically.

The zonal model approach offers a rapid and simple field method for the statistical evaluation of the rock mass in terms of fracture intensities of each set which is likely to be associated with underground openings of a defined shape and size. The model also provides a basis for the assessment of a number of rock mass parameters, including strength, modulus, stand-up time and others in terms of published rock mass classification systems.

In view of the fact that data collected purely on the basis of single line samples did not furnish all the necessary information for the 2-d or 3-d understanding of the spatial distribution of fractures in rock, the explicit use of this sampling technique should be reassessed. Consideration should be given to use of continuous area samples to supplement line sample data.

7 ACKNOWLEDGEMENTS

The study was undertaken as part of a post graduate project which is financially sponsored by Mount Isa Mines Limited. The writer also gratefully acknowledges the generous assistance provided by the CSIRO Division of Applied Geomechanics. The supervisory capacity of Mr. W.E. Bamford and Dr. J.R. Barrett during the course of this work are greatly appreciated. The text was reviewed by Mr. D.R. Miller of CSIRO.

8 REFERENCES

BACZYNSKI, N.R.P. (1974). Structure and Hanging Wall Stability in Lead Orebodies at the Mount Isa Mine. Thesis (M.Sc.), James Cook University of North Queensland.

BRIDGES, M.C. (1975). Presentation of Fracture Data for Rock Mechanics. Proc. Second Aust. N.Z. Conf. on Geomechanics, Brisbane, July 21-25, pp.144-148.

I.S.R.M. (1978). Suggested Methods for the Quantitative Description of Discontinuities in Rock Masses. Int. J. Rock Mech. Min. Sci. & Geomech. Abstr., Vol.15, No.6, pp.319-368.

HAMMERSLEY, J.M. and HANDSCOMB, D.C. (1964). Monte Carlo Methods. Methuen & Co. Ltd., London, 178p.

A Rational Approach to the Point Load Test

J. R. L. READ
Superintending Geologist, Melbourne & Metropolitan Board of Works
P. N. THORNTON
Senior Geologist, Melbourne & Metropolitan Board of Works
W. M. REGAN
Senior Geologist, Coffey & Partners Pty Ltd, Melbourne (formerly Project Geologist, MMBW)

SUMMARY Conversion factors correlating point load strength with uniaxial compressive strength are subject to errors. In addition, test results may be affected by sample anisotropy. Examples are given to show that provided these limitations are recognised the test can be successfully used to measure the strength of rock samples and classify rock.

1 INTRODUCTION

The point load test has been proposed as a quick, simple and accurate test to measure the strength of rock samples.

As originally described by Broch and Franklin (1972) and recently re-affirmed by Franklin (1977), the indirect tensile strength as measured by the point load test was postulated to be closely correlated with uniaxial compressive strength. A conversion of

	UCS =	24 x Is(50)
where	UCS =	Uniaxial Compressive Strength
and	Is(50) =	Point Load Strength Index for 50 mm Diameter Core

was proposed and was incorporated in the methods for determining the point load strength index suggested by the ISRM Committee on Laboratory Tests (1973).

It is our experience that the suggested conversion factor of 24 cannot be universally applied. Also, test results may be affected by sample anisotropy requiring modifications to the specified sample length to diameter ratio.

Although these aspects represent changes from the concept proposed by Broch and Franklin, once appreciated they need not limit the usefulness of the test. Examples of the variability of the conversion factor and examples of meaningful applications of the test in investigation and construction are described.

2 CONVERSION FACTORS

As more and more data from various sources becomes available, it is increasingly apparent that a value of 24 cannot be used as a universal conversion factor. For example, after studying 13 different rock types, Pells (1975) concluded that :

- For certain rock materials the UCS value that is predicted using the point load test and a conversion factor of 24 is sufficiently accurate for many engineering design and classification purposes (error less than 20%).

- There are certain rock materials, not identifiable visually, for which the point load test predicts UCS values that are significantly in error (error greater than 20%).

Because of these conclusions Pells recommended that whenever point load test results are used to predict uniaxial or triaxial rock material strengths, at least some conventional UCS test should be performed.

Work on rocks found in the Melbourne area support these conclusions and recommendation.

Two groups of results are presented comparing Is(50) and UCS results for sedimentary rocks and basalts exposed in and around Melbourne.

2.1 Sedimentary Rocks

Three types were tested: sandstone, siltstone and laminated siltstone. A minimum of 14 Is(50) and 8 UCS tests were carried out on each category tested.

TABLE I

DEFINITIONS OF WEATHERING AND ALTERATION

WEATHERING		
Extremely (EW)	:	Texture of the original rock still evident but rock substance exhibits soil properties, i.e., can be remoulded and classified according to the Unified Soils Classification.
Distinctly (DW)	:	Weathering is distinct in that there is either a colour change and/or a marked change in physical properties from fresh rock substance. The porosity may be greater or lesser than the original rock substance due to leaching or deposition of minerals.
Slightly (SW)	:	Rock substance partially stained or discoloured but strength properties essentially those of fresh rock substance.
Fresh (Fr)	:	Rock substance apparently unaffected.

ALTERATION OF BASALT

The rock substance shows a green-black or light blue colouration due to the formation of montmorillonite group minerals and vesicles become filled with clay minerals. There is usually some loss of strength compared with weathered rock.

The Is(50) results are based only on diametral tests. Cores which failed along bedding, cleavage

ROCK TYPE	SILTSTONE	SANDSTONE	LAMINATED SILTSTONE
WEATHERING	D DISTINCTLY WEATHERED	S SLIGHTLY WEATHERED	F FRESH
PROJECT	1	2	3

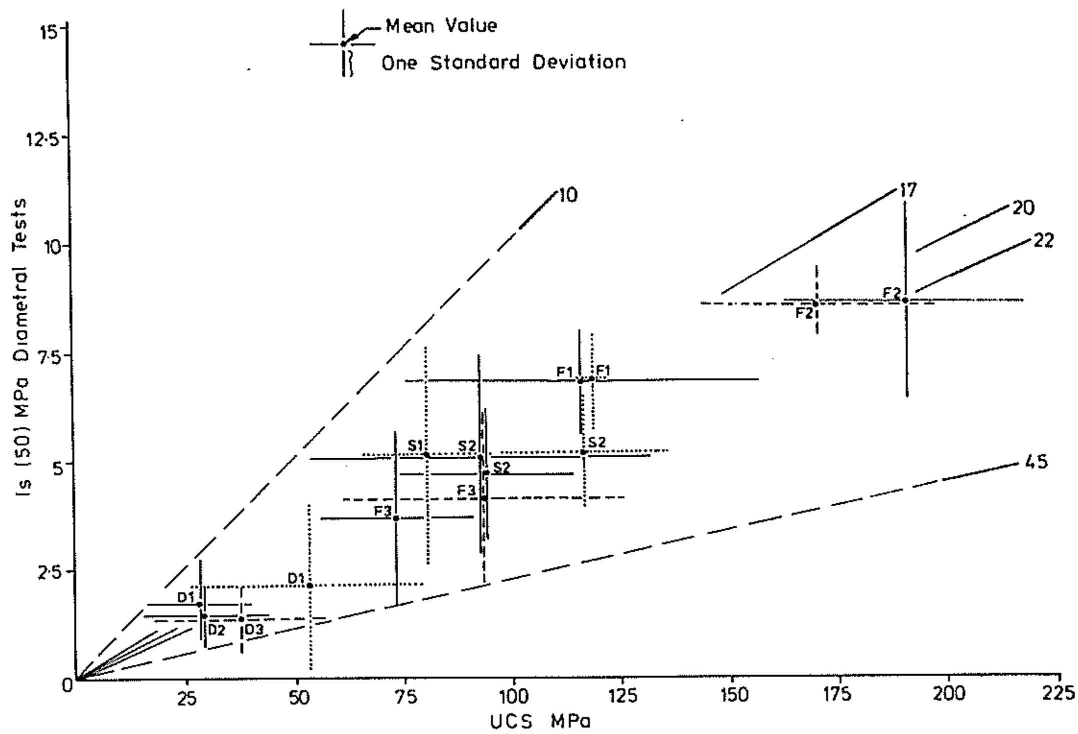

Figure 1 Test results, sedimentary rocks

or other obvious defects were discounted. The samples tested were subdivided on the basis of the project, rock type and degree of weathering as defined in Table I. The mean and standard deviation of the Is(50) and UCS results were then calculated and the comparison is plotted on Figure 1. Not every rock type and degree of weathering occurred at each project.

The line of best fit approximates a conversion factor of about 20 with a correlation co-efficient of 0.97. However, the results show a high degree of scatter, conversion factors ranging between 10 and 45. Within this range different lines of best fit can be recognised. For example, the line of best fit for distinctly weathered siltstone at Project Site 1, represented by Result D1, is about 17 and that for fresh siltstone at Project Site 2, represented by Result F2, is about 22.

2.2 Basalt

Basalt sampled from an area west of Melbourne was subdivided on the basis of degree of weathering and alteration as defined in Table 1. The results of 65 UCS and 304 Is(50) tests are summarised on Figure 2: the average number of UCS tests for each of the categories on Figure 2 was 7 and of Is(50) tests was 34.

From Figure 2 it is difficult to allocate a simple line of best fit passing through the origin although if there is one, it is obviously closer to 12 than 24. However, lines of best fit of 7.5, 11 and 16 can be allocated. On the basis of these lines the following general relationships can be recognised :

- Irrespective of the degree of weathering, the more vesicular the basalt the lower the conversion factor.
- If the basalt is altered the conversion factor increases to the next highest conversion factor.

In both of these cases the degree of alteration does not influence the relationship for the less vesicular basalt.

2.3 Errors

The ISRM suggested method states :

"Rocks to be classified are first divided into

		WEATHERING & ALTERATION		
		DW	SW	SW & ALTERED
VESICULARITY	>20%	A (7·5)	B (7·5)	C (11)
	10-20%	D (11)	E (11)	F (16)
	8-10%		G (16)	H (16)
	DENSE			I (16)

7·5 Suggested conversion factor for each set of results

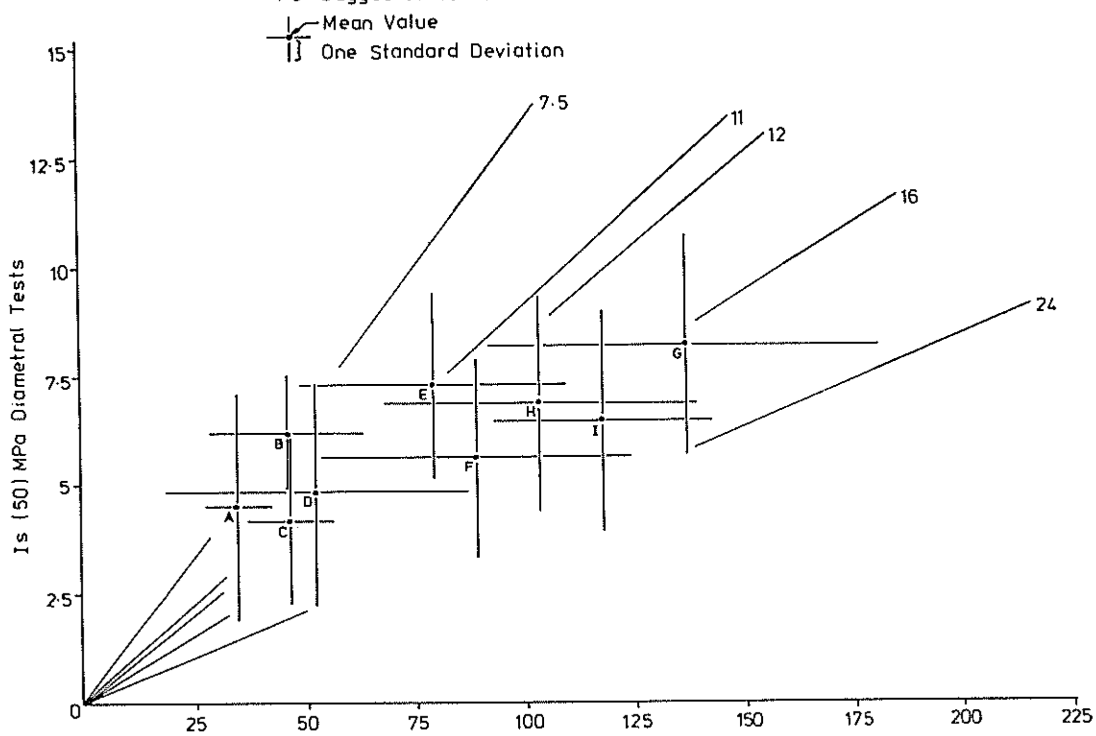

Figure 2 Test results, basalt

units, each of which is considered on the basis of preliminary inspection to have uniform strength.

One sample of rock containing sufficient material for the required number of test specimens is then selected from each unit."

During normal core logging the sample suggested by the ISRM will usually be much smaller than those represented on Figures 1 or 2. The errors involved in using a conversion factor on such small samples should be appreciated. For instance, Figure 3 shows the results obtained for dense, slightly weathered altered basalt. Using a conversion factor of 16 and the mean result of the 56 Is(50) tests for Group I (Fig. 2) the derived UCS value is 103 MPa, 12% under the actual mean UCS value of 118 MPa.

Also, if a smaller sample is considered the Is(50) value used may not be the mean but would tend to be within the range of 3.9 to 9 MPa, as shown on Figure 3. Using the conversion factor of 16 provides derived UCS values ranging from 62 to 144 MPa.

However, the actual range of UCS results determined by testing was from 93 to 143 MPa. Therefore, the derived values have underestimated the UCS by 33% in one case and overestimated it by 1% in the other.

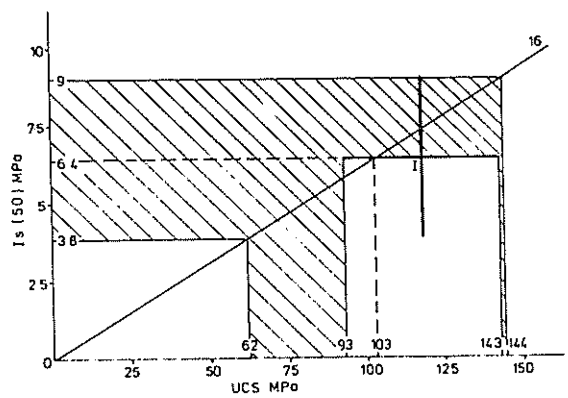

Figure 3 Example of conversion errors

The range of errors obviously vary from rock type to rock type. The example quoted is by no means unique and, in fact, there are many rock types in which the errors involved in conversion from Is(50) to UCS on a small sample (but acceptable within the guidelines suggested by the ISRM) are much larger.

2.4 Implications

The implication of the data presented above generate two conclusions :

- Errors in derived UCS values vary from rock type to rock type and can be significant.
- Because of the wide range of results that can be obtained, it is necessary to establish an appropriate conversion factor for particular rock types from particular areas by testing, especially if the derived UCS values are to be used in further calculations.

Together, these two conclusions suggest that it would in fact be preferable to base rock strength on either Is(50) or UCS results and not to relate the two tests. One is an indirect tensile test, and the other a compressive test. Whilst general comparisons may be made geological factors such as differences in composition and texture exist which make particular rock types behave differently in the two types of tests.

3 ANISOTROPY

As described above, only failure through the rock substance were used for the diametral Is(50) results presented above. This was necessary as it has been found that test results may be grossly affected by sample anisotropy. With bedded rocks, for example, failure may occur along bedding planes rather than through the rock substance. Pells (1975) found that it was impracticable to use diametral Is(50) results to derive UCS values for a highly anisotropic sandstone. We have had the same experience and have also found that when bedding is inclined at more than about 20° to the axis of a sample, it is difficult to perform a satisfactory test using the ratio specified for axial tests.

At one project site the dip of an interbedded sequence of siltstone and sandstone ranged from 10° to 70° but was mostly about 30°. Totally inconsistent diametral test results were obtained and the diametral test was discontinued. However, it was found that when axial tests were attempted at the specified length to diameter ratio of 1.1 the samples either rotated between the platens or broke off at the edges. After some experimentation, it was found that consistent results could be obtained when a ratio of 0.65 was used. This value was therefore adopted as the site standard.

4 APPLICATIONS

Criticisms of the point load test, based on experiences similar to those described above, have been voiced and doubts as to the usefulness of the test have been expressed.

We believe that many of the opinions are unnecessarily harsh. As with many other methods of investigation, geophysics for example, it is more a matter of being aware of the limitations of the test and ensuring that it is used only when and as appropriate.

Three inter-related examples involving the proving of rock durability, rippability assessment and rockfill control measures are presented to demonstrate how the point load test can be meaningfully and successfully applied. The examples are all from the project mentioned above, where a site standard of 0.65 was developed and adopted for axial tests on a sequence of interbedded and folded siltstone and sandstone. It involved the use of Is(50) results rather than derived UCS values.

4.1 Durability Testing

The point load test was one of several tests used to demonstrate the long term durability of fresh or slightly weathered siltstone which was regarded as a potential source of rockfill. The tests were carried out on samples taken from 90 year old spoil dumps as well as on samples taken from the potential quarry and exposed for 2 weeks after recovery from cored boreholes. The results from the spoil dumps averaged 5.1 MPa for slightly weathered siltstone which was slightly stronger than the average 4.6 MPa obtained for the 2 weeks old slightly weathered siltstone. In conjunction with the other tests, which included aggregate crushing tests and long term observational weathering tests, this result was taken as good proof of the long term durability of the fresh or slightly weathered siltstone when it was kept in a stable moisture environment away from the effects of sun, rain and frost.

4.2 Rippability

For any particular tractor and ripper arrangement used, the rippability of a rock mass will depend on the rock substance strength and the nature of the rock mass defects, including their strength, spacing, orientation and continuity.

Up to a certain substance strength the rock at the site usually broke readily through the substance regardless of the nature of the rock mass defects. Above this strength it was usually increasingly difficult to break the rock through the substance and ripping proceeded only if the rock mass was intersected by a suitable pattern of defects along which it could break up.

Ripping trials and production ripping with Caterpillar D7, D8, D9 and Komatsu D355A tractors were monitored and showed that the largest tractor could rip a distinctly weathered siltstone/sandstone rock mass with an average rock substance Is(50) of up to 2.5 MPa with little difficulty.

Above 2.5 MPa there was increasing substance resistance and rippability depended increasingly on the pattern and nature of the defects. Ripper penetration decreased from 500 mm at 3 MPa to 300 mm at 4.4 MPa, with fracture initiating along the defects and further breakdown occurring under the tracks. Over 4 MPa there was a reduction in the maximum particle size from 1000 to 300 mm. There was also a marked effect on the fines content with 50% minus 20 mm at 3 MPa reducing to 15% minus 20 mm at 4.4 MPa.

As a result of these observations it was possible to correlate the degree of weathering, Is(50) and rippability for the rock mass throughout the project site. As described below, this correlation was then used as the basis of a rock classification system used to control rockfill quality on the project.

4.3 Rockfill Quality Control

The degree of weathering and the Is(50) of the rock substance were combined with seismic velocity, rippability and visual appearance of the rock mass,

TABLE II

ROCK MASS CLASSIFICATION

GRADE	DEGREE OF WEATHERING OF SUBSTANCE	SUBSTANCE STRENGTH Is(50), MPa	SEISMIC VELOCITY m/sec.	ROCK MASS USUALLY RIPPABLE BY	APPEARANCE	EXCAVATED MATERIALS SUITABLE FOR
5	DW to EW	1.5	1000	D7	Brown, orange-brown reddish-brown	Unsuitable for random fill or rockfill
4	DW	1.5 to 2.5	1000 to 2200	D9	Dominantly brown with up to 50% light grey or grey-brown laminae	Random Fill, < 20% fines after compaction
3	DW to SW	2.5 to 4.0	2200 to 3000	D9 with favourable defect pattern	Dominantly dark to light grey with up to 50% grey-brown laminae	
2	SW	4 to 6	> 3000	Not rippable	Dark to light grey with up to 10% grey-brown laminae	Rockfill, < 10% fines after compaction
1	Fr	6	> 3000	Not rippable	Dark to light grey	

and the results of field embankment compaction trials to produce the rock classification shown on Table 2.

Quarry control measures were related to the end product in the embankment combined with a visual assessment and a point load test of the rock in each bench in the quarry. The Is(50) values indicated in Table II were used in the initial stages but, as more data became available, they were modified to fit a statistically derived minimum standard. This required that not less than 50% of each sample had an Is(50) of greater than 4 MPa and not more than 25% had an Is(50) less than 3 MPa. To check this at least 10 lumps of rock were sampled from a bench firing. Ten samples were cored normal to the bedding in each lump, trimmed to the site standard of 0.65 and then tested axially giving at least 100 results for statistical comparison with the required minimum standard.

Once the necessary procedures had been standardised, one person could carry out the complete test within a day.

5 CONCLUSIONS

The following conclusions are made :

- The point load test is a relatively quick, simple and inexpensive method of determining rock strength and classifying rocks.
- If a relationship between Is(50) and UCS is to be used it should be obtained by testing.
- The errors involved in deriving UCS values from Is(50) values may be significant. Certain of these errors are numerical. However, one test is an indirect tensile test and the other is a compressive test, and it may not be valid to make other than general comparisons.
- Anisotropy may seriously affect point load test results and may necessitate the adoption of a non-standard test specification.
- Despite the limitations imposed by the conclusions above, it is possible to successfully and meaningfully apply the point load test provided these limitations are realised and the test is not misapplied.

6 ACKNOWLEDGEMENT

The authors wish to thank the Melbourne and Metropolitan Board of Works for permission to use the results published in this paper. The opinions expressed are those of the authors.

7 REFERENCES

BROCH, E. & FRANKLIN, J.A. (1972). The Point-Load Strength Test. Int.J.Rock Mech.Min.Sci., Vol.9, pp 669-697.

FRANKLIN, J.A. (1977). Discussion of E. Hoek's paper "Rock mechanics laboratory testing in the context of a consulting engineering organisation". Int.J.Rock Mech.Min.Sci. & Geomech.Abstr. Vol.14, p 297.

INTERNATIONAL SOCIETY FOR ROCK MECHANICS (1973). Suggested Method for Determining the Point-Load Strength Index. ISRM Committee on Laboratory Tests, Document 1, pp 8-12.

PELLS, P.J.N. (1975). The use of the point load test in predicting the compressive strength of rock materials. Aust.Geomech.J.,Vol.G5, No.1, pp 54-56.

Physical Modelling of Sequential Slope Failure

M. DUNBAVAN
Post-doctoral Student, Division of Applied Geomechanics, CSIRO, Australia

SUMMARY A precis of the design considerations and testing results associated with the physical model study of the kinematics of a slope failure is given. The case investigated was a simple granular slope underlain by a thin weak cohesive stratum.

1 INTRODUCTION

The majority of analyses and numerical models associated with the investigation of slope stability are based on the concept that soil, or rock, behaves as a continuum. Although this approach is satisfactory for some soils, it has been shown that the response of granular materials may be more aptly described by discontinuum mechanics (e.g. Trollope, 1968). Because of the nature of granular materials, the stability analyses used for the design of slopes may not be relevant due to the invalidation of the assumptions inherent in the analyses. Furthermore, the importance of the slip mechanism and the physical constraints promoting its formation are generally disregarded in the slope stability calculations.

The study reported here was concerned with the definition of the kinematics of failure for a granular slope underlain by a thin weak stratum. Although the range of application for the results is relatively small, the situation is found in many surface mining operations. The development of a physical model for the study revealed several design characterstics and means for the interpretation of results which should be considered in all plane strain modelling.

2 FIELD EXAMPLES

The mechanism which resulted from the failure of a granular slope underlain by a weak layer was primarily of the two-wedge type. Figure 1 shows the general form of a failed slope, which is more distinct in cases where the transition between the slope and the weak layer is well defined; and the layer is thin in comparison with the height of the slope. Mining waste dumps have provided many excellent examples of the two-wedge mechanism with some being reported by Blight (1969) and Boyd *et al.* (1978), and it may be demonstrated that a two-wedge mechanism may have been present in the initial stages of the Aberfan disaster (vide Bishop *et al.* 1969). The formation of the two-wedge mechanism has been observed in embankments and natural slopes; however, the clearly defined nature of the landslips associated with mining waste dumps led to the concentration of research in that particular area.

With reference to Figure 1, some of the important features of the two-wedge slip in field cases are:

i) a relatively thin weak base layer;

ii) uniform movement along the base slip plane;

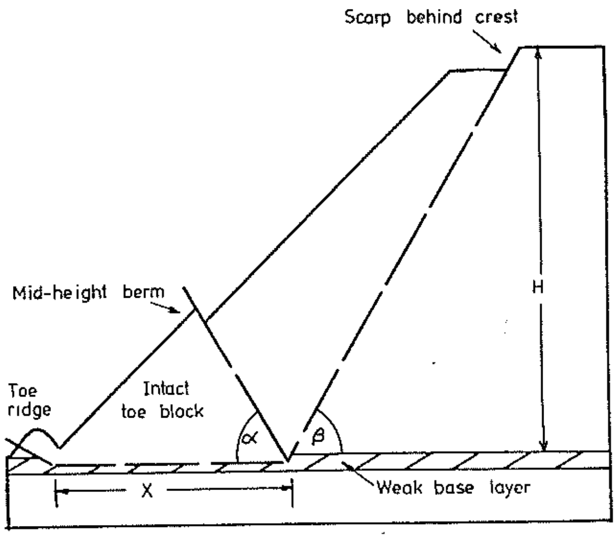

Figure 1 General slope failure profile

iii) intact condition of the toe block, and sometimes a rill of foundation material pushed up by the toe block;

iv) the appearance of a mid-height berm or a gentle S-shape of the slope face; and

v) formation of a slip scarp just behind the crest of the slope.

Thus, a successful physical model of the field situation would reflect the characteristics of the slope both before and after a slump. Many mining dump failures were of considerable lateral extent and could be properly considered as plane strain phenomena.

3 PHYSICAL MODEL FORMULATION

3.1 Purpose of Model

The research was based on the events which led to the formation of a two-wedge failure mechanism, rather than the response of a particular prototype. Therefore, the use of similitude was not critical, although some broad characteristics (outlined above) needed to be included in the response of the model. James (1971) discussed three classes of physical model from which the second class was chosen for this study. This approach required the detailed measurement and analysis of a small scale model as if it were a prototype, after which the analysis established to be most suitable for the situation was applied to a full scale prototype and the responses compared.

Because of the important role played by the two-wedge mechanism in the failure of the slope, the definition of the kinematics of that mechanism was the chief factor in the choice of model and subsequent design of the experimental apparatus. The use of a physical model in preference to a numerical model stemmed from the extreme difficulty in reproducing real material response and large scale movements; however, two models, one a block jointed finite element program (cf. Burman, 1971) and the other a dynamic relaxation program (cf. Cundall, 1971), were used for a qualitative comparison with field and physical model responses.

3.2 Details of Model

The model was at laboratory scale (in the order of 1 m long) and consisted of two dissimilar materials. The granular slope was constructed of a well graded, cohesionless, dry silica sand in a loose state with the face of the slope at the sand's angle of repose. This slope rested on a horizontal uniform layer of bentonite slurry, mixed to a moisture content of 900%. The dimensions of a typical model slope were:

Base length	1100 mm
Width	745 mm
Height	400 mm
Angle of repose	34^{o}
Sand density	1500 ± 20 kg m^{-3}
Bentonite thickness	5 - 30 mm.

Further information on material characteristics is given in a later section.

3.3 The Modelling Apparatus

It is not feasible to construct apparatus which does not have any effect on the materials used; however, there are certain design characteristics which may be incorporated in the design of the apparatus which will significantly reduce any adverse response. Deflections within the apparatus were limited to less than 1% of those expected to induce an "active" state in the sand under maximum loads (cf. Arthur and Roscoe, 1965); and the width to height ratio was 1.9, which would promote plane strain conditions (cf. Bransby and Smith, 1975). The effect of sidewall friction was minimised by the use of plate glass thoroughly cleaned with acetone before each test.

The bentonite was not strong enough to support the full thrust of the slope; therefore, a mechanical device along the sand-bentonite interface supported the slope and was retracted for the initiation of failure. This device tended to hasten the first few millimetres of movement, but an experiment which did not employ the base strengthening device showed that it did not affect the sequence of development or the characteristics of the failure mechanism. Figure 2 shows a schematic diagram of the strengthening device which was fixed beneath the floor of the sample enclosure.

4 MATERIAL CHARACTERISTICS

4.1 Modes of Testing

The description of the stress-deformation characteristics of loose sand is dependent on the

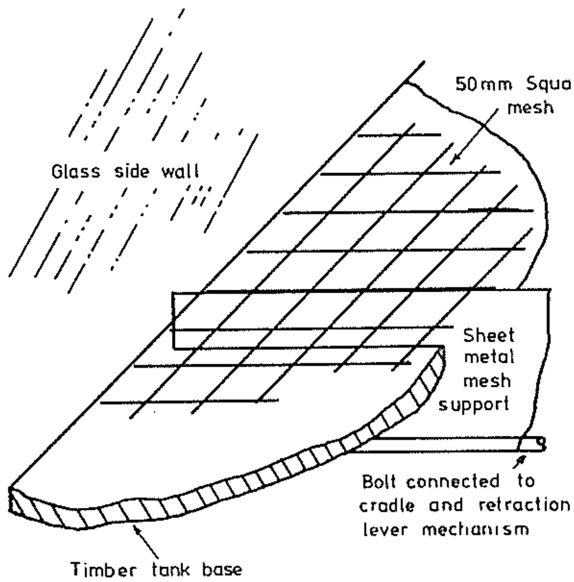

Figure 2 Strengthening device

type of test used. Thus, it was necessary to use plane strain tests at low confining pressures (less than 10 kPa) to record the response of sand as it might be observed in the model. Although the difference in strength (internal friction angle) between plane strain and triaxial tests on loose sand is very small, the deformational response in the test is significantly different, with the plane strain sample showing a much faster rise to peak strength and an increase in volume under axial compression (cf. Lee, 1970). Because of the possibility of some error in the data from the plane strain tests, a series of direct shear tests was carried out and the results were found to agree with the former tests. The bentonite was used in a state beyond its liquid limit (~600%) and behaved as a non-Newtonian fluid. The bentonite had a yield stress and was thixotropic; however, limited testing facilities permitted only an order of magnitude estimate of the yield stress to be made.

4.2 Interpretation of Tests Results

The sand's stress-deformation response in plane strain was compared with several continuum and particulate theories such as the Mohr-Coulomb criterion, Rowe's stress-dilatancy theory (Rowe, 1962), Parkin's particulate model (Parkin, 1965), and the Granta Gravel critical state model (Schofield and Wroth, 1968); however, none of these approaches proved satisfactory. The author found that the Freudenthal (extended von Mises) failure criterion fitted the observed stress response, but there were insufficient reliable test results available to extend this part of the research.

The study of the kinematics of failure led to the derivation of a deformational failure criterion which corresponded well with the octahedral stress characteristics measured during the plane strain tests. Figure 3 shows a generalised representation of this criterion which is summarised as:

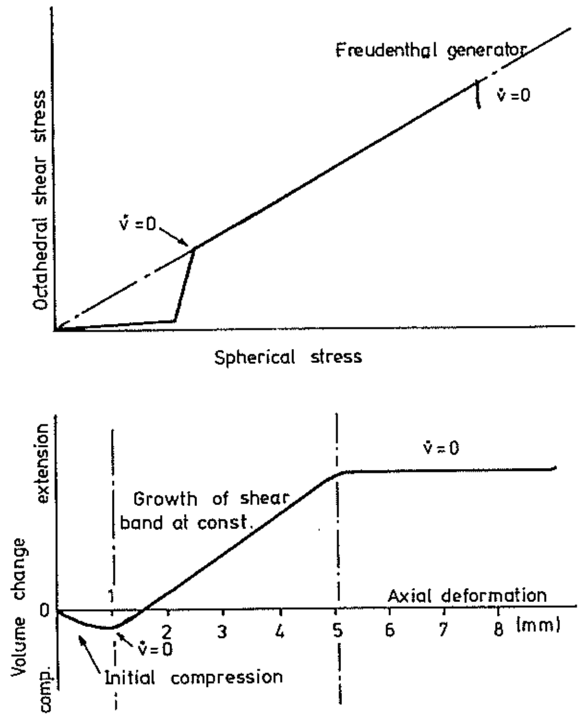

Figure 3 Deformational failure criterion

i) initial compression up to 1 mm movement;

ii) onset of failure when the rate of volume change becomes zero, followed by growth of the shear zone at constant dilatancy up to an axial deformation of 5 mm;

iii) cessation of growth of the shear zone with further slip taking place within the zone at practically zero dilation.

An estimation of the strength of the sand was made using a Mohr-Coulomb diagram in which the failure was defined along the observed slip plane rather than along the angle of maximum obliquity, and yielded 35^{o} and 33^{o} for peak and residual values respectively.

An extrusion rheometer was used to estimate the yield strength of the bentonite slurry and a value of .7 kPa was measured; however, the reliability of the value was low and should only be considered as an order of magnitude indicator. There was no measurement of the increase of the yield strength due to thixotropy, but the elapsed time between the placement of bentonite and the initiation of failure was kept at approximately 1½ hours in each of the experiments.

5 MODELLING RESULTS

5.1 Testing Programme

The major variable in the model was the thickness of the base layer, indicated in Section 3.2. A total of thirteen tests were carried out with at least two tests at each base thickness to ensure the repeatability of the results. Eight of the tests were recorded with a 16 mm Bolex movie camera and the resulting films were examined in detail for the qualitative description of the failure sequence. The remaining tests were recorded using a 35 mm single lens reflex camera with frames taken at varying time intervals and one of these sets was used for a quantitative examination of the model response. The measurements were made through a digitised Zeiss Stecometer with the data being punched onto paper tape and typed for a hard copy.

5.2 Sequence of Failure

Both qualitative and quantitative evidence was examined for the determination of the sequence of formation of the two-wedge failure mechanism. Figure 4 shows an idealised form of this sequence in four parts:

i) the simultaneous development of two slip planes - one through the weak layer and the second through the granular slope cutting the free surface just behind the crest; between the two planes is a broad shear zone dividing the front of the slope into toe and crest regions;

ii) movement of the two regions along their respective slip planes with the distortion in the shear zone tilting the lower half of the crest region away from the toe;

iii) formation of a third slip plane within the shear zone between the first two planes with no further shear distortion in that zone; and

iv) movement along the three slip planes with negligible volume change within the toe and crest regions.

The method of data collection and recording did not allow any further distinction in the initial stages of the failure sequence; however, it is the author's opinion that the first two slip planes form concurrently.

By observation of coloured sand lines in the model, the displacement at which the slip plane through the slope was first recognised was measured. The average of six values was 9 ± 2½ mm and the predicted displacement was 6.2 mm, using the author's deformational failure criterion (vide Section 4.2). An alternative prediction for the formation of the slip plane based on a failure strain gave the necessary displacement as 25 mm, which was more than twice the observed value.

5.3 Deformation of the Weak Layer

The characteristics of the slip planes in the granular slope were the main feature of the modelling results; however, the deformation patterns in the bentonite gave information which supported the definition of the sequence of failure. The slip plane through the bentonite formed close to the bottom of the layer with an abrupt termination at the point of intersection of the three slip planes which formed the mechanism. The weak layer beneath the immediate toe of the slope buckled in compression during the formation of the mechanism and did not push out a "passive" wedge, as might be expected. The horizontal displacement of the weak layer above the slip plane was constant along its length.

5.4 Characteristics of Mechanism

The characteristics of the slip mechanism in plane strain were not directly obtained from the photographs at the side wall due to the frictional

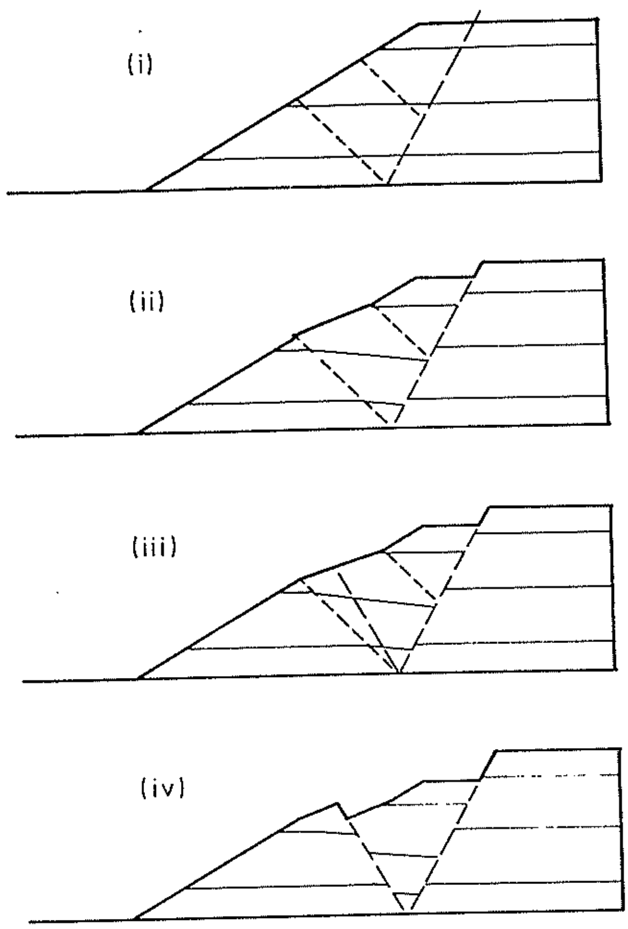

Figure 4 Failure sequence

effects; however, after corrections were applied, the values for the parameters defined in Figure 1 were:

$$\alpha = 75^\circ \pm 10^\circ$$
$$\beta = 56^\circ \pm 5^\circ$$
$$\frac{x}{H} = 1.15 \pm .1$$

Variation of the thickness of the weak layer (5-30 mm) did not alter the sequence of formation or the characteristics of the mechanism. The total displacement of the toe region varied non-linearly with the thickness of the layer and the relationship was:

$$s = 40\ (t^1 - 2) \qquad (1);$$

where s = total displacement (mm),
t^1 = $\log_2 t$,
t = layer thickness (mm).

6 FURTHER USE OF RESULTS

The next stage in the modelling process was to attempt to describe the observed results by a stability analysis or a numerical model. The scope of this paper does not allow further discussion on this matter, which may be pursued in Dunbavan (1979).

The basis of this modelling arrangement may produce more meaningful quantitative results with the use of large format cameras and different exposure techniques. It may be possible to place instruments within the model; however, great care would be required to ensure that the presence of the instruments did not influence the sequence of development of the mechanism.

7 CONCLUSIONS

The use of an idealised small scale physical model showed that a two-wedge mechanism, which had some similarity with field situations, developed in a discrete sequence of events. There was no evidence to support the relevance of progressive failure (by stress distribution) to the formation of the mechanism. Large scale movement of the toe region was dependent on the formation of the third slip plane; however, the visual recognition of a slip plane is related to the deformational response of the particular material in the slope. The deformation required to form particular slip planes does not alter the concept of the kinematics of failure being a discrete sequence of events.

The development and investigation of the model revealed that frictional edge effects may not be discounted; however, careful attention to the relationship between the displacements at the centre and the side walls of the model allowed these effects to be corrected. The response of the model was interpreted with the knowledge of the stress-deformation characteristic of the material, which had been established in plane strain tests at stress levels similar to those in the model. A review of some literature on plane strain and triaxial testing of loose sand showed that the stress-deformation response used in conjunction with a small scale model requires attention in the use of relevant constraints.

8 ACKNOWLEDGEMENT

This paper was based on a thesis presented by the author for a PhD degree at the James Cook University of North Queensland. The research was supervised by Professor D.H. Trollope and Dr. K.B. Wallace in the Department of Civil and Systems Engineering.

9 REFERENCES

ARTHUR, J.R.F. and ROSCOE, K.H. (1965). An examination of the edge effects in plane-strain model earth pressure tests. Proc. 6th Int. Conf. on Soil Mechanics and Foundation Engineering, Montreal, Vol. II, pp 363-367.

BISHOP, A.W., HUTCHINSON, J.N., PENMAN, A.D.M., and EVANS, H.E. (1969). Geotechnical Investigations into the causes and circumstances of the disaster of 21st October 1966. A Selection of Technical Reports submitted to the Aberfan Tribunal, Welsh Office; London HMSO.

BLIGHT, G.E. (1969). Foundation failures of four rockfill slopes. Jl. Soil Mech. and Found. Div., Proc. ASCE, Vol. 95 No. SM3, pp 743-767.

BOYD, G.L., KOMDEUR, W., and RICHARDS, B.G. (1978). Open strip pitwall instability at Goonyella Mine - causes and effects. Proc. 1978 Aust. IMM Conf., North Queensland.

BRANSBY, P.L. and SMITH, I.A.A. (1975). Side friction in model retaining-wall experiments. Jl. of Geot. Eng. Div., Proc. ASCE, Vol. 101 No. GT7, pp 615-632.

BURMAN, B.C. (1971). A numerical approach to the mechanics of discontinua. Thesis (Ph.D.), James Cook Univ. of Nth. Qld.

CUNDALL, P.A. (1971). The measurement and analysis of accelerations in rock slopes. Thesis (Ph.D.), Univ. of London.

DUNBAVAN, M. (1979). Sequential failure of Granular slopes. Thesis (Ph.D.) (subject to approval), James Cook Univ. of Nth. Qld.

JAMES, R.G. (1971). Some aspects of soil mechanics model testing. Proc. Roscoe Memorial Symposium, Cambridge. pp 417-440.

LEE, K.L. (1970). Comparison of plane strain and triaxial tests on sand. Jl. Soil Mech. and Found. Div., Proc. ASCE, Vol. 96 No. SM3 pp 901-923.

PARKIN, A.K. (1965). The application of discrete unit models to studies of the shear strength of granular materials. Thesis (Ph.D.), Univ. of Melbourne.

ROWE, P.W. (1962). The stress-dilatancy relation for static equilibrium of an assembly of particles in contact. Proc. of the Royal Society, London. Series A, Vol. 269, pp 500-527.

SCHOFIELD, A., and WROTH, P. (1968). Critical state soil mechanics. London, McGraw-Hill.

TROLLOPE, D.H. (1968). Rock mechanics in engineering practice. Chapter 9, London, John Wiley and Sons.

Assessing the Probability of Rapid Mass Movement

M. J. CROZIER
Senior Lecturer in Geography, Victoria University of Wellington
R. J. EYLES
Senior Lecturer in Geography, Victoria University of Wellington

SUMMARY Threshold conditions required to induce landsliding on Otago Peninsula and in Wellington City are identified by employing water balance calculations and antecedent rainfall indices to define the soil water status preceding each daily rainfall. These thresholds are used to compare terrain sensitivity and to assess the probability of landslide occurrence.

1 INTRODUCTION

While mass movement is one of the most important erosive processes on much of New Zealand's hill country, very little quantitative data is available; this is particularly true for the time of occurrence of mass movements because of the obvious difficulties of observing an extreme event which is discontinuous in both time and space. This paper, then, draws on information of variable quality compiled over a period of 12 years for three areas: Otago Peninsula, Wellington City and the Wairarapa.

As Selby (1979) has noted, 'nearly all examples of regional landsliding in recent years have occurred during individual storms or as a result of prolonged wet periods'. It is therefore reasonable to assume as a starting point that there is a rainfall threshold above which landslides will occur, and below which the input of rainfall to slopes is insufficient to trigger mass movements.

An examination of daily rainfall records shows that, instead of the presence of a distinct threshold, there is a wide range of rainfall values associated with landslide events. During 1974, landslides were reported to the Wellington City Corporation or in local newspapers on 20 individual days with rainfalls ranging from 3 to 88 mm. If the 20 December 1976 storm is included, Wellington City, since 1974, has experienced landslides on days with recorded rainfalls ranging from 3 to 236 mm. Similarly, landslide-triggering rainfalls on Otago Peninsula during 1977 and 1978 ranged from 6 to 57 mm. The 6 mm value was exceeded on no less than 79 days which were apparently free from slipping. It is therefore clear that no distinct threshold can be defined solely in terms of total rainfall on the day of landslide occurrence.

2 ANTECEDENT RAINFALL

The inability of daily rainfall amounts to define a consistent triggering threshold has been attributed in general terms to the variability of pre-existing soil moisture conditions. As direct measurements of soil moisture have only rarely been made immediately prior to a landslide event (e.g. Crozier, 1968) some other means of estimating antecedent conditions is generally required.

Of the four conventional methods of estimating antecedent moisture conditions: baseflow in rivers, well levels, climatic water balance and antecedent rainfall, the first two can be discounted because of insufficient regional data and their inability to reflect conditions in the uppermost metre of soil where most landsliding occurs. The climatic water balance and antecedent rainfall methods overcome both these problems, the latter having the advantage of being simple to calculate.

During dry conditions the amount of rainfall in a period preceding an event will give a general indication of soil moisture storage and during wet conditions will indicate in addition the amount of gravitational water in the soil system. If antecedent rainfall is sufficient to produce overland flow, a rare situation in temperate environments, antecedent rainfall values will over-estimate the amount of moisture in the soil. Inaccuracies will also occur as a result of variation in evapotranspiration rates throughout the year.

For these reasons and because of the unknown variability in soil and site properties throughout the areas studied, the amount of antecedent rainfall can be considered only as an index to antecedent soil moisture.

A measure of antecedent rainfall is used in Figure 1 in an attempt to define landslide triggering rainfall conditions for the Otago Peninsula during 1977 and 1978. Antecedent rainfall was determined for a 10 day period immediately prior to an event using the method outlined by Kohler and Linsley (1951).

$$Pa_o = KP_1 + K^2P_2 + \ldots.. K^nP_n \qquad (1)$$

where Pa_o is the antecedent daily rainfall for day 0,

and Pn is precipitation on the n'th day before day 0.

The value of 0.84 used for K is close to that used in hydrological studies in North America (Bruce and Clark, 1966) and has been chosen for its ability to delineate a threshold between landslide and non-landslide producing conditions. The K factor is decayed by an exponential function so that past rainfall exerts progressively less influence on the index as time elapses. Values derived from the equation should only be considered as an index as their power to depict actual soil moisture levels is unknown. The decay rate employed therefore represents only an approximation of outflow from the soil as a result of drainage and evaporation processes assumed to be operating at a constant rate throughout the year. The index does however, allow for greater absolute outflows with higher soil moisture levels, in recognition of the lower soil tensions and greater hydrostatic heads that prevail under such conditions.

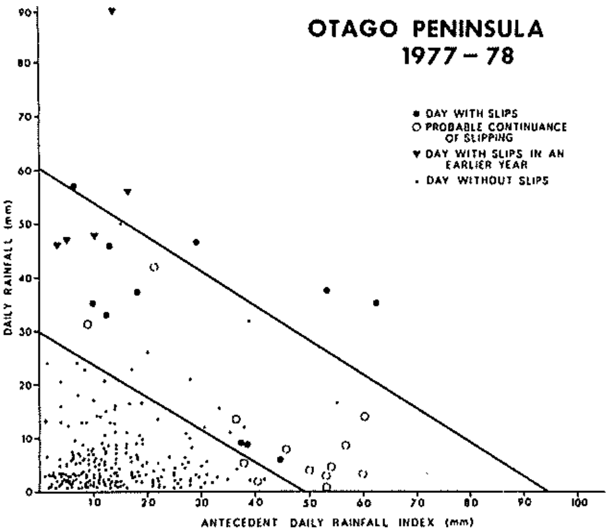

Figure 1 Landsliding episodes related to rainfall

Two principal envelope lines can be drawn on Figure 1 separating conditions with different probabilities of landsliding. As expected, the envelopes indicate that progressively smaller amounts of rainfall are able to trigger landslides as the antecedent rainfall index increases. The upper line is a well defined threshold indicating conditions which when exceeded invariably produced landslides during 1977 and 1978. The lower line represented the conditions above which there was some probability of slipping.

3 SOIL MOISTURE BALANCE

Antecedent conditions are more clearly defined in terms of soil moisture storage levels which depend, in addition to rainfall inputs, on loss of water to the atmosphere through evapotranspiration and the ability of the regolith to hold water. These factors are incorporated in a soil moisture balance model adapted by the New Zealand Meteorological Service from the theory of Penman (1948). Estimates of potential evapotranspiration are derived from mean temperature, vapour pressure, windspeed and sunshine hours, all of which are measured at official climatological stations. Available soil moisture capacity is defined as the amount of water that can be held in the top 76 cm of the regolith between tensions representing field capacity (the maximum moisture that can be held against gravity) and permanent wilting point (the level below which plant roots cannot extract water).

The model is used by the Meteorological Service to monitor soil moisture levels for pastoral and arable productivity, the 76 cm soil depth being an estimate of grass and crop rooting zones. This depth is, however, also appropriate for the shallow debris falls, slides, or flows which are the most common types of slope failure in New Zealand. While the soil moisture capacity of the top 76 cm varies considerably with soil type, a single value of 120 mm, an approximate mean of the values quoted by Gradwell (1974) for yellow brown and yellow grey earths in central and southern New Zealand, is adopted in this study. Deficit soil moisture storage (DS) is recorded in the water balance programme on every fifth day but its value on any one day can be readily derived by the equation:

$$DS_o = DS_1 - (P_o - PE_o) \qquad (2)$$

where DS_o is deficit storage on day 0,

DS_1 is deficit storage for the day before day 0,

P_o is precipitation on day 0,

PE_o is the potential evapotranspiration for day 0

The computer printout, giving soil moisture deficits at 5-day intervals, can be used together with daily rainfall values to plot graphs such as Figure 2. Zero on the soil moisture storage scale signifies field capacity, and a deficit of 120 mm implies that the regolith has dried out to wilting point; it is assumed that no further drying out takes place. When a rainfall event occurs of sufficient magnitude to recharge soil moisture storage to field capacity, any additional precipitation is termed 'excess' and is shown as a vertical line on the graph. Excess water generates positive pore water pressures which may trigger landsliding. 'Excess' rainfall is equivalent to 'runoff' in the Meteorological Service model and is printed out by the standard programme for each month. Daily 'excess' rainfall (EP) can be easily derived from the programme by the following equation:

$$EP_o = (P_o - PE_o) - DS_1 \qquad (3)$$

where EP_o is excess rainfall on day 0,

P_o is rainfall on day 0,

PE_o is potential evapotranspiration on day 0,

DS_1 is deficit storage on the day before day 0

The graph for Kelburn, 1974 (Figure 2), shows that the summer and autumn months of that year were dry with soil moisture deficit reaching 120 mm for a brief period in January and February. From mid-April to the end of October soil moisture storage was almost at, or above, field capacity. The year 1974 is the worst on record in terms of number of landslides experienced in Wellington City, with most of the estimated 2000 occurring on 29 May, 2 July and 8 October; the three days in which rainfall 'excess' reached 60 mm.

The model was applied to historic landsliding in Wellington City (Eyles, 1979) using newspaper reports to identify events. A reasonably consistent relationship was discovered, with daily rainfalls 50-55 mm or more in excess of soil field capacity triggering landsliding sufficiently serious to be reported by the news media. However, during 1974 several hundred mass movements in Wellington City occurred on days other than the three with high excess rainfalls. The model clearly, therefore, allows recognition of only the most serious events.

4 ANTECEDENT EXCESS RAINFALL

An assumption in the soil moisture balance model as

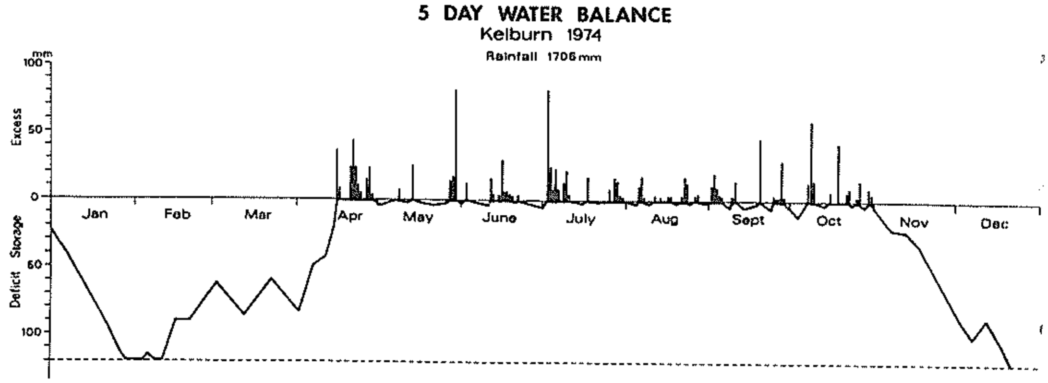

Figure 2 Soil moisture balance graph representing Wellington City, 1974

used above is that 'excess' rainfall drains through the top 76 cm of the regolith very rapidly, with no carry over of water above field capacity into the next day. While this may be valid for the steepest slopes and coarsest-textured greywacke regolith, it is not a realistic representation of the typical Wellington soil, much less of soils derived from finer-grained sedimentary rocks, typical of much of New Zealand's hill country.

Excess rainfall remaining in the soil in the form of gravitational water is likely to reduce slope resistance by diminishing soil cohesion or by developing positive porewater pressures. In many situations drainage will be sufficiently slow for gravitational water to exert an influence lasting over a number of days. In recognition of this factor, an antecedent excess rainfall index has been used in Figures 3 and 4 in an attempt to define more accurately landslide triggering conditions.

The antecedent excess rainfall index (EPa) is calculated by the equation:

$$EPa_0 = KEP_1 + K^2EP_2 \ldots + K^nEP_n \ldots \qquad (4)$$

where EPa_0 is the index for day 0,

EP_n is excess rainfall on the n'th day before day 0

For the same reasons used to establish the antecedent daily rainfall index, an exponential decay function employing a K factor of 0.84 over a 10 day period has been chosen for this index.

The antecedent excess daily rainfall index thus provides some measure of the overall soil water status when soil moisture is in excess of field capacity. At other times, the most appropriate measure of the soil water status is soil moisture storage, defined as deficit storage by the water balance model. Deficit storage and antecedent excess rainfall form a continuum representing the status of soil water existing immediately prior to any rainfall event. The soil water status defined in this way has been plotted on the abscissa in Figures 3 and 4 for the Otago Peninsula and Wellington City study areas.

In both lotalities, this approach has permitted the delineation of a single envelope which represents a distinct threshold separating landsliding conditions from non-landsliding conditions. The threshold lines for the two localities are nearly parallel and indicate a clear regional difference in susceptibility to landslide triggering conditions. For example, if both regions had reached a soil water status of 'antecedent excess rainfall' equalling 20 mm, the daily rainfall required to produce landslides in Wellington City would be 23 mm greater than the triggering rainfall on the Otago Peninsula.

The measures used in Figures 3 and 4 to define the water status of the soil have successfully explained landslide producing conditions for all but one event. This occurred in Wellington City in response to a 10 mm rainfall when antecedent excess rainfall had amounted to only 27 mm. Apart from local site factors, a possible explanation for this event might lie in the occurrence of an unusually high short-term rainfall intensity during the day concerned. This would facilitate a rapid build up of gravitational water which although only momentarily stored may be sufficient to induce instability. The development of temporary stores of gravitational water (perched water tables) can be enhanced not only by high rainfall intensities but also by the presence of relatively low permeability strata located within the regolith. The landslide event which occurred in response to a 91 mm daily rainfall (Figure 3) possibly reflects the presence of a low permeability stratum being located close to the soil surface and the consequent development of a perched water table during the rainstorm. This would account for the triggering of movement even though the daily rainfall appeared to be insufficient to bring soil moisture storage to full capacity. This illustrates that a soil moisture capacity of 120 mm is only an average figure based on assumed soil depth, and cannot be expected to adequately represent the variety of local conditions which exist throughout any region.

5 APPLICATIONS

The definition of threshold conditions for landsliding in different regions (Figure 5) can be used to rank the sensitivity of various terrain types to climatically induced slope instability. The 100% probability lines in Figure 5 indicate that the sensitivity of region B is greater than A which in turn is greater than C.

Sensitivity ranking alone, however, will only be a measure of relative susceptibility to landsliding under homogeneous climatic conditions. The ranking of regions on the basis of landslide susceptibility for land use planning purposes, therefore, generally requires an analysis of the regional climatic conditions. If the slip-triggering conditions represented by the threshold line can be

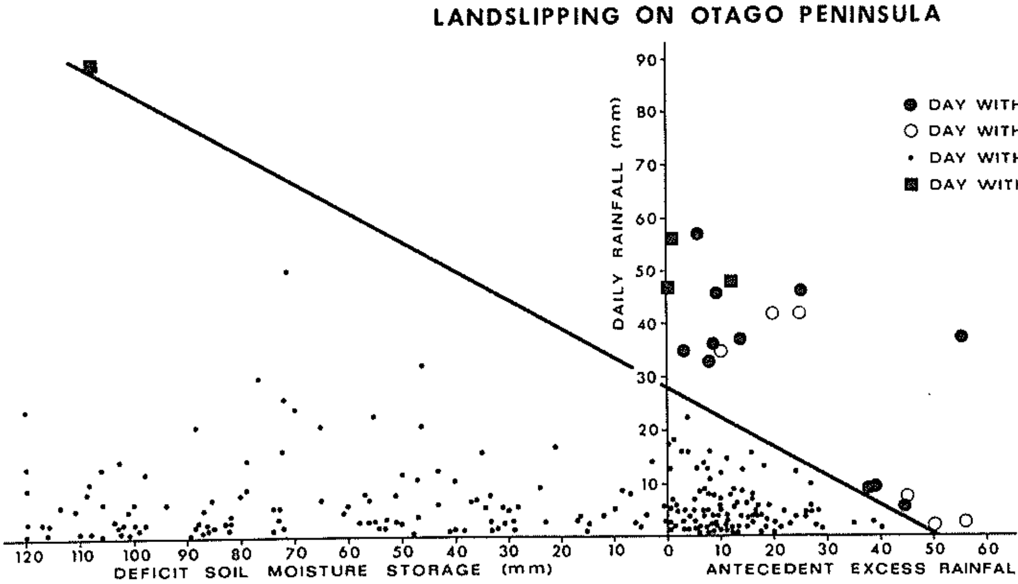

Figure 3 Days of landsliding in relation to daily rainfall and antecedent soil moisture status, Otago Peninsula

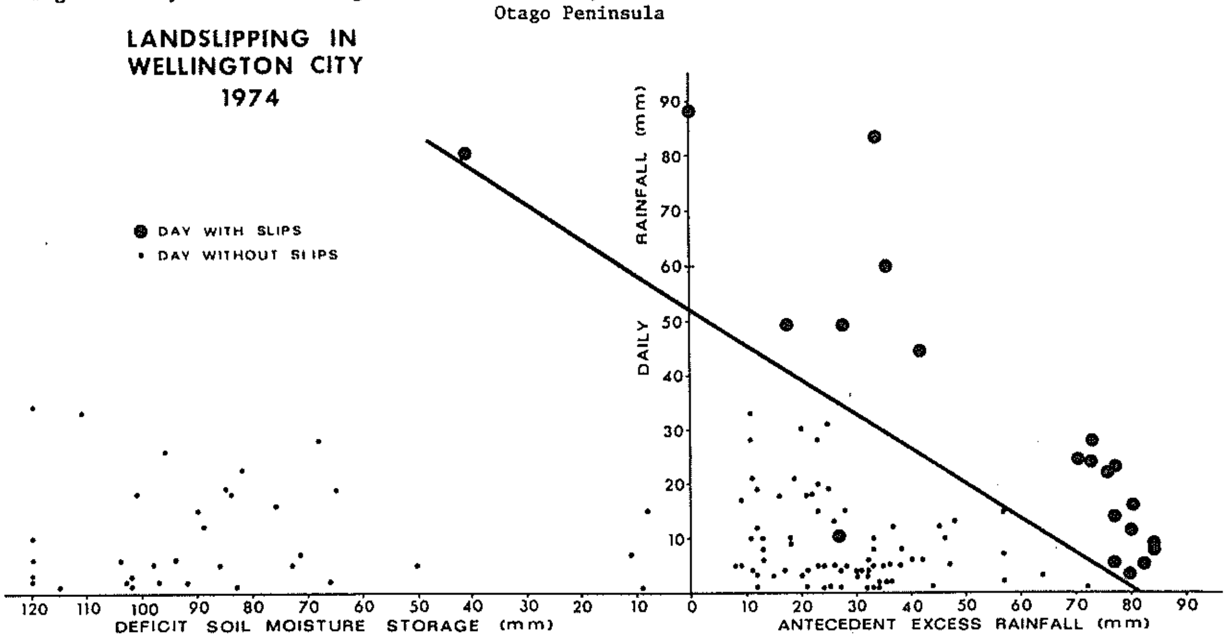

Figure 4 Days of landsliding in relation to daily rainfall and antecedent soil moisture status, Wellington City, 1974

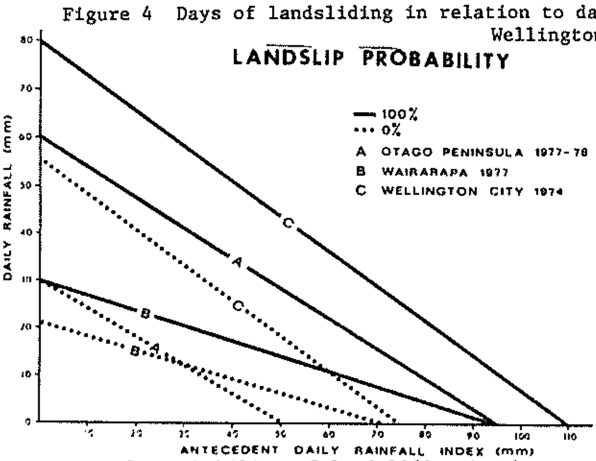

Figure 5 Probability of landsliding in three regions

assigned return periods on the basis of magnitude/ frequency analysis, then the susceptibility of each region can be ranked in terms of the probability of landslide triggering conditions being achieved within a finite time period. This represents an empirical approach to slope stability assessment which is not only less expensive than many other methods but most importantly recognizes the range of climatic induced stresses experienced in the field.

The other major application of this work is the provision of a procedure to quantitatively assess the likelihood of landsliding at any point in time. Assuming that regional landslide triggering thresholds have been established, the only calculation required is the updating of the antecedent daily rainfall index or the antecedent excess rainfall on a daily basis. From (1), for example, it is evident that:

$$Pa_0 = K(Pa_1 + P_1) \quad (5)$$

Where Pa_0 is the antecedent daily rainfall index for day 0,

Pa_1 is the antecedent precipitation for the day before,

and P_1 is precipitation for the day before

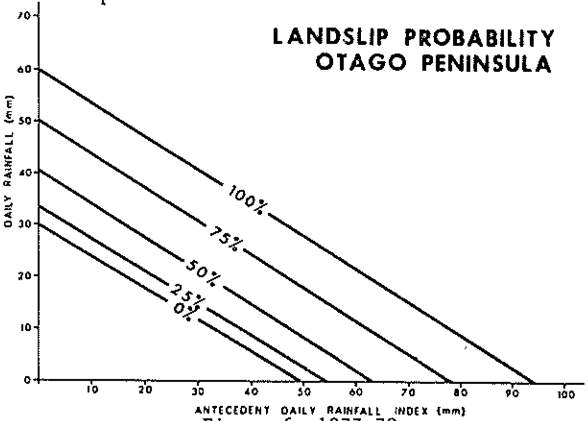

Figure 6 1977-78

Using the more readily calculated antecedent daily rainfall index as an example, the historical data can be presented in the form of a probability threshold diagram (Figure 6). Referring the updated index to the diagram, it can be seen that when a value of 54 mm is reached there is a 25% chance that the next rainfall will produce landsliding, at 64 mm a 50% chance, at 79 mm a 75% chance and at 95 mm a 100% chance. Although the index can be monitored in this way to reveal the onset of a critical soil water status, it is obvious that there is always a chance that a rainfall event of sufficient magnitude could trigger landsliding even when the index is less than 50 mm.

Information on current synoptic weather situation may complement the forewarning procedures outlined, as frontal and orographic induced rainfall is generally unable to produce landsliding on Otago Peninsula when the index is less than 20 mm. However, depressions, particularly tropical cyclones, may provide sufficient rainfall to cause slipping even when the soil moisture storage is in deficit.

ACKNOWLEDGEMENTS

The authors wish to thank the Otago Catchment Board, The Engineers Department, Wellington City Corporation and the New Zealand Meteorological Service for much of the data used in this paper.

REFERENCES

BRUCE, J.P. and CLARK, R.H. (1966). Introduction to Hydrometeorology, Pergamon Press.

CROZIER, M.J. (1968). Earthflows and related environmental factors of Eastern Otago. Jour. Hydrol. (NZ). Vol. 7, pp. 4-12.

EYLES, R.J. (1979). Slip-triggering rainfalls in Wellington City, New Zealand. N.Z. Jour. Sci. Vol. 22, pp. 117-21.

GRADWELL, M.W. (1974). The available water capacities of some southern and central zonal soils of New Zealand. N.Z. Jour. Agr. Res. Vol. 17, pp. 476-78.

KOHLER, M.A. and LINSLEY, R.K. (1951). Predicting the runoff from storm rainfall. U.S. Weather Bur. Res. Pap. 34.

LUMB, P. (1975). Slope failures in Hong Kong. Quart. Jour. Eng. Geol., Vol. 8, pp. 31-65.

PENMAN, H.L. (1948), Natural evaporation from open water, bare soil and grass. Proc. Roy. Soc. A., Vol. 193, pp. 120-45.

SELBY, M.J. (1979). Slope stability studies in New Zealand. Physical Hydrology. Ed Murray, D.L. and Ackroyd, P., New Zealand Hydrological Society.

The Geomechanics of Soil Conservation

J. G. HAWLEY
Scientist-in-Charge, Aokautere Science Centre, Ministry of Works & Development, N.Z.
P. G. LUCKMAN
Scientist, Aokautere Science Centre

ABSTRACT Current rates of soil loss, particularly from hill country pasture, are seen to be a major cause for concern. Five types of situation are described in which the application of geomechanics concepts and techniques can contribute towards reducing rates of loss of soil. These five types relate to engineering geological problems, slaking problems, strength problems, dispersion problems and infiltration problems.

1 INTRODUCTION

The disciplines represented in our geomechanics societies (soil mechanics, engineering geology and rock mechanics) have evolved, for the most part, in response to needs encountered in civil engineering. In such endeavours man adds a structure to or subtracts a volume of rock or soil from an area which usually has well defined limits. By contrast, soil conservators deal with land stability problems which extend over very wide areas of land and are not normally associated with any form of civil engineering endeavour.

While the membership lists of geomechanics societies are dominated by civil engineers and geologists, those of soil conservation societies are dominated by agricultural scientists.

In the long term good soil conservation is more essential for the survival of a civilisation than is good civil engineering. Evidence that this has been true in the past can be seen all around the Mediterranean where ruins of grand buildings and impressive civil engineering works (such as irrigation aqueducts) can be seen surrounded by unproductive land, much of it desert. These areas which once supported large and advanced civilisations have, since they lost their topsoil more than a thousand years ago, been able to support only small and often nomadic populations (Carter and Dale, 1974).

New Zealand's topsoil is being carried down to the sea today just as surely as was that of Mesopotamia two thousand years ago. The Manawatu river (which flows close to the Aokautere Science Centre) is not considered to be an unusually 'dirty' river and yet during a one year return period 'high flow' it carries almost half a million tonnes of sediment to the sea in one day (Manawatu Catchment Board, pers. comm.). This can be visualised as ten tonne truckloads of dry soil passing the river mouth every two seconds throughout the 24 hour period. (If the public were to see the operation as truckloads of dry soil instead of just as dirty water, the issue would immediately be the major concern of all environmentalists).

Scientists and engineers working in soil mechanics, engineering geology and rock mechanics can contribute towards finding ways of reducing the rate of loss of topsoil by:

1. Developing better understandings of the various processes which bring soil into the rivers,
2. Developing methods of slowing down these processes,
3. Identifying which situations are within man's abilities to influence and which are beyond his control,
4. Developing better methods of quantifying instability near sediment source areas so that accurate information can be obtained on the effectiveness, or otherwise, of soil conservation works.

In this brief review, five types of situation are described in which understandings developed in geomechanics disciplines are contributing to these challenges.

2 ENGINEERING GEOLOGICAL PROBLEMS

Engineering geologists are contributing to soil conservation in New Zealand by placing valuable geological perspectives on instability problems in many regions. Most of the value of this contribution at present is in the form of information on the age of mass movements. While in some cases it may be possible for man to stave off the natural processes of erosion, such "geological" erosion usually presents problems which are far too great to be arrested by artificial means.

Trending NNE to NE along the east coasts of the North Island and the northern South Island (Kaikoura) is a belt of rocks of predominantly Tertiary age which have been folded, faulted and uplifted by earth processes responsible for the appearance of the main mountain ranges in New Zealand. As in virtually all of New Zealand, uplift is continuing at the average rate of several millimetres per year, and here in the East Coast fold belt great masses of country have been brought into disequilibrium. The results are massive block and wedge glide failures along gently dipping bedding planes which are in the process of tilting by differential uplift.

A study, under contract to the National Water and Soil Conservation Organisation (NWASCO), has brought to light in a striking fashion the nature and extent of such instabilities in southern Hawkes Bay (Pettinga, 1980). Here, massive block glides occur in a Middle to Upper Miocene turbidite sequence (Fig. 1). One such glide occurs on a bedding plane lubricated by tectonically introduced montmorillonitic clays. Mass movement is facilitated by the presence of joints which form the headwall escarp-

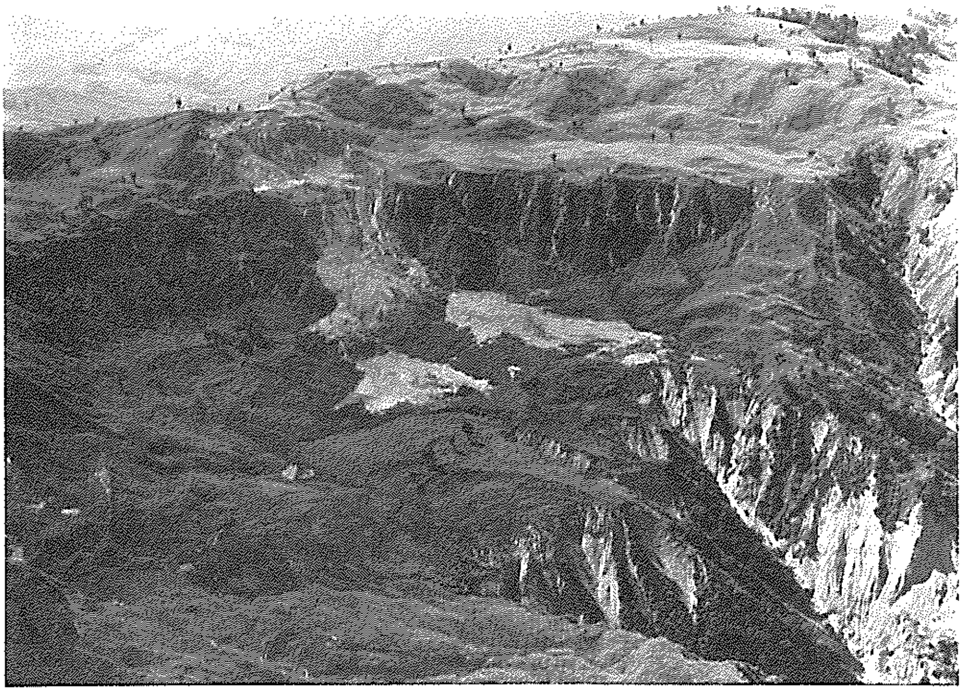

Figure 1 Block glide of sandstone over mudstone, lubricated by montmorillonitic clays, in middle Tertiary sequence, southern Hawkes Bay. (Photo: N.A. Trustrum)

ments and side shear planes. A similar study (also funded by NWASCO) in a less structurally complex area in the Rangitikei River valley has shown that block gliding of marine siltstone, again on montmorillonitic clay, commenced 11,000 - 20,000 years ago (and is occurring now) in response to doming of Upper Tertiary sediments by an upthrusting block of basement greywacke (Thompson, 1979).

Relatively superficial creeping earthflows, soil slips and debris flows can in many cases be prevented or stabilized, but geological mapping of the large failures shows them to be of such dimensions as to be probably unaffected by even the extreme soil conservation measure of reforestation. Further, this type of activity may in many cases be traced back more than a million years (e.g. Pettinga, 1980). While there has been considerable oscillation in both vegetative cover and groundwater conditions associated with the Pleistocene succession of Glacial and Interglacial periods, it seems certain that these deep seated movements are large scale tectonically controlled features.

With these understandings gained, soil conservation works can be designed more effectively and expediture focussed much more accurately than would have been possible without the geological studies.

3 SLAKING PROBLEMS

The relative importance of natural geological processes and the activities of man is sometimes obscure. This is true of earthflows which form a class of mass movement intermediate between soil creep and soil slip. In New Zealand usage, the term earthflow is generally reserved for creeping mass movements involving a well defined basal shear plane. Studies conducted at Aokautere Science Centre have shown that it is often practicable to measure rates of earthflow movement from aerial photographs, using trees as markers. Inclinometer records obtained to date have shown very small internal distortions.

Bentonitic mudstones of the East Coast fold belt, already weakened in many cases by extensive tectonization (shearing at depth), are particularly susceptible to the agents of mechanical weathering. The most severe of these is cyclic change in water content occurring near the surface. Most of the earthflow erosion in these mudstones is shallow, the planar failure surfaces being generally no more than a few metres deep.

Simple laboratory tests demonstrate that these bentonitic mudstones undergo substantial weakening when subjected to cyclic drying and wetting. Before these rocks are brought near the surface their condition is saturated. Shrinkage caused by subsequent drying sets up tensile and shear stresses which in places exceed the local strengths. Cracks form and the rock's integrity is destroyed. (On very steep slopes this process causes slabs of "shrunken" rock to fall off. Geologists call this exfoliation). The breakup of the rock on subsequent rewetting has been termed slaking and can be quite spectacular. High pore air pressures develop within the material as it is rewetted, and these literally burst the material apart. This process reduces the cohesion of the material. At the low total stress levels which prevail at depths of only a few metres the frictional resistance to shear failure is small so that the main factor governing failures is the magnitude of the cohesion. Flows develop as this cohesion is reduced by slaking.

The problem soil conservators face lies in determining the influence of land management (e.g. vegetation cover) on the rate of approach to

Figure 2 Sheep tracks can be the equivalent in pasture of the structural imperfections causing failure in engineering structures. (Photo: D.E.K. Miller)

failure of large areas of such swelling bentonitic mudstones. Field evidence would suggest that much earthflow erosion of this sort has been initiated or accelerated by removal of natural bush cover and subsequent conversion of the land to pasture. Just as infinitesimal imperfections in an aircraft structure can lead to failure so it has been noticed that surface features such as sheep tracks can form the sites of tension cracks which subsequently form the scarps of earthflows (Fig. 2).

Approaches to this problem involve artificial weathering of mudstone samples to determine relationships between shear strength and moisture content history. This area of research holds considerable promise as conclusions will indicate safe soil moisture fluctuations within hillsides and enable soil conservation measures to be designed accordingly.

4 STRENGTH PROBLEMS

One of the more important challenges facing soil conservators is the loss by soil slip of topsoil from hill country pastures (Fig. 3). In some parts of New Zealand this is so serious, and the exposed rocks so 'unfarmable' that pastoral farming may soon become uneconomic there.

The concept that soil strength can be considered as having two components, cohesion and internal friction, is now widely taught - in earth sciences, geography, and forestry courses as well as in soil mechanics and geology. The limitations of this concept are not so widely taught, and there is little appreciation that even 'soil strength' is a concept, not a real property of a soil for which there will be one correct value.

Engineers with experience on construction sites of sampling so carefully and testing so carefully that the results of their tests can be used with confidence in slope stability computations will need no persuading that in the rural scene such an approach is not sensible. The range of values of c' and ϕ' obtainable from samples taken at different depths, or a few tens of metres apart, when coupled with the uncertainties and errors accumulated in the sampling operation and the testing programme, is usually greater than that needed to span the gap between "very safe" and "bound to fail". On top of these sources of uncertainty is that associated with the choice of the type of strength test to be conducted and the choice of computational method.

Although in the rural situation ascribing numbers to c' and ϕ' is unlikely to be helpful, the concept

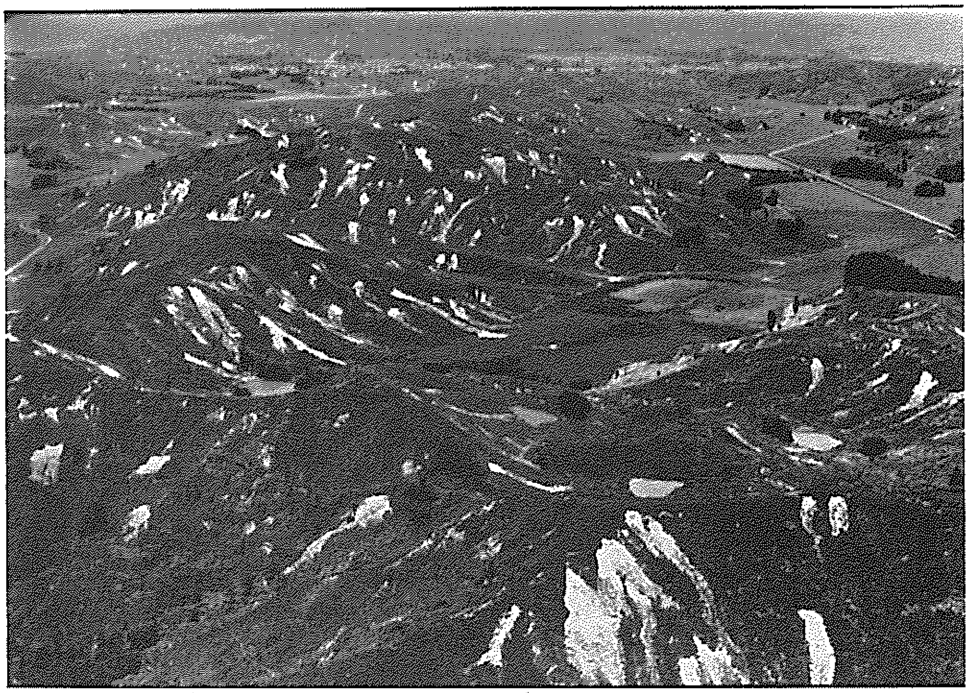

Figure 3 Widespread soil slip erosion in the Wairoa district. (Photo: N.A. Trustrum)

that the strength of the soil at failure may be regarded as having two components (cohesion and friction) is nevertheless a useful one, as is also an understanding of the effective stress principle.

The role of negative pore water pressures in maintaining slope stability is one which is not always given the attention it deserves. In rural hill country, the seasonal *rates* of development and decline of these negative pressures are probably the key factors determining stability. The negative pore water pressures associated with the concave water/air interfaces which form in the pores of unsaturated soils, give rise to very large increases in intergranular (effective) stresses, with associated large increases in (frictional) strength. However, even when negative as well as positive pore pressures are considered, conventional stability analyses using c' and ϕ' are of little relevance in soil conservation. This is not only because the scatter in values obtainable is so large, but more importantly because these concepts describe only the "at failure" situation.

What is needed, therefore, in those rural situations where lack of strength is the cause of soil loss, is a better understanding of the "pre failure" conditions - in particular, a better knowledge of *the development of failure conditions within the soil mass*. The proper question in the rural scene is not "what are the strengths of the soils?" but "How, and at what rates, do the strengths of the soils change?" These changes must include seasonal increases as well as decreases. Although a first stage in attempting to answer this second question could be represented by studies of the rates of changes of soil water pressures and suctions (as related to weather conditions, particularly rainfall) a useful understanding will probably not be gained unless the behaviour of the soil skeleton is considered as well. To model the pre-failure behaviour of soils, the school of soil mechanics developed at Cambridge University, known as Critical State soil mechanics, can be used (Schofield and Wroth, 1968). Early developments of this model were limited to normally consolidated and lightly overconsolidated soils (Roscoe and Burland, 1968). Pender (1978) extended this by developing a mathematical model which describes quantitatively the behaviour of overconsolidated soils, both lightly overconsolidated or "wet" soils, and heavily overconsolidated or "dry" soils.

Whereas, in civil engineering endeavours, soils are loaded by the addition of a structure, or the addition or subtraction (as in a cutting) of a mass of soil, in the rural pastureland scene the soil is loaded and unloaded by the weather and by plants - specifically by the imposition of soil water suctions. The drying out of the soil (which may be assisted by plants) leads to more sharply concave water/air interfaces linking soil particles. High negative pore water pressures develop tending to pull the particles closer together. These 'compressive' effective stresses tend to increase the dry density (and thereby the strength) of the soil. Conversely, in wet weather these water/air interfaces become less sharply concave and the compressive effective stresses are reduced. If the soil becomes saturated, positive pore water pressures develop and effective stresses are further reduced. It is an unfortunate accident of terminology that dry weather tends to move the soil into a state which is "wet" in the Cambridge sense, while wet weather tends to make the soil "dry", (Fig. 4).

Pender developed expressions for the recoverable and irrecoverable (elastic and plastic) components of volumetric strain, and an expression for shear strain - which is assumed to be all irrecoverable, i.e. elastic shear strain is assumed to be zero. These expressions apply to both the "wet" and the

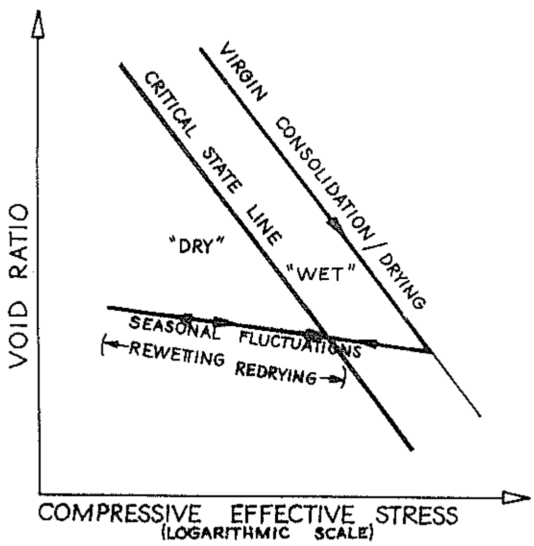

Figure 4 Soils tend to become "dry" of critical in wet weather and "wet" of critical in dry weather.

"dry" sides of the "critical state". The constants required to calibrate these expressions may be obtained from simple laboratory tests. Values for the variables however must be obtained from the field, because it is not practicable to reproduce the loading conditions, i.e. the weather (rain, wind, humidity and sunshine) in the laboratory, and it is the field rather than the laboratory behaviour which is of interest.

It is fortunate that reliable field data loggers are becoming more readily available at prices which will allow the duplication of measurement essential to this type of work. These may be used to record the daily and seasonal patterns of soil moisture stress, temperature and density. They may also record rainfall and sap flow rates in trees. The critical state theory promises to provide much of the framework needed for the interpretation of these field data.

Although the rate factor may be represented by groundwater flow rates, it is likely that the data will require extension of the critical state model to include the strain rate characteristics of the soil skeleton.

This work promises to provide soil conservators with improved understandings of the development of failure conditions within the soil mass, and how this development is affected by plants. This would then provide a more rational basis for choice and spacing of plants and the design of other soil conservation works (underdrains, graded banks, management practices etc) to suit particular climates and soils.

5 DISPERSION PROBLEMS

One of the more serious forms of erosion on New Zealand's hill country pasture is tunnel gully erosion. This occurs very commonly on loessial soils which are basically silts with a small clay fraction providing a limited amount of cohesion.

When initially deposited during Glacial times the loess consisted predominantly of fresh silt-sized particles derived usually from greywacke or schist. Since deposition however, weathering of the feldpars and other minerals in the loess has increased the content of both clay minerals and other particles of clay size. With the progressive warming and humidifying of the climate which followed the glacial period, the development of an appreciable clay fraction and the recent clearing of bush, these soils have developed a tendency to undergo cracking in response to desiccation. Rainwater can flow down the slope along the bases of these cracks which, if the soil is dispersive, tend to erode and link up to form tunnels. These tunnels grow in diameter until the ground above falls into them forming gullies. The critical soil property determining the rate at which this happens is the soil's dispersivity.

Clay particles have a net negative charge which is compensated for by an excess of cations (generally Ca^{2+}, Mg^{2+}, Na^{+}, K^{+}) in the soil water. There is a natural cation concentration gradient adjacent to the clay particles; as the distance from the clay particles increases the solution becomes more neutral. Adsorbed onto the clay particles is a "Stern layer" of hydrated cations. The thickness of this layer depends on the adsorbed cation species. Because there is still a negative charge on the clay particle despite the Stern layer, hydrated metal ions concentrate near the Stern layer in a diffuse outer layer. Movement of water through the soil water pores does not involve the adsorbed Stern layer or part of the diffuse outer layer. The thickness of the "double layer" thus affects the permeability of the soil because much of the soil water is not free to move and channel diameter is effectively reduced.

A typical illitic clay may have a water content of 50%. Most of this water will be "free" (not strongly bound to the mineral skeleton). However in many montmorillonitic clays, for example, extraction of the porewater may be very difficult. Certain clay minerals can immobilise a relatively large amount of water - the most common of these are halloysite and montmorillonite (e.g. Lambe and Whitman, 1979).

The thickness of the double layer of hydrated cations affects not only permeability but also soil structure and erodibility. Clay particles experience mutual repulsions and attractions - the repulsive forces arise from the negative charges on all clay particles while the attractive forces are Van der Waals forces which exist between all adjacent pieces of matter. The attractive Van der Waals forces are very short ranged however (decreasing in intensity with the eighth power of distance) and if the thickness of two double layers is greater than the range of these forces then the clay has a tendency to *disperse*: particles undergo a repulsion (Childs, 1969).

In the early 1960's many failures of small clay dams in Australia were shown to have been caused by dispersive clays (Aitchison, *et al*, 1965). A 1970-71 study sponsored by the U.S. Soil Conservation Service showed that similar failure of clay dams in the United States had been caused by piping of dispersive clay (Sherard, *et al*, 1972).

Dispersive soils are highly erodible. They erode by a process in which clay particles go into suspension individually. This may occur rapidly even in still water (Sherard, *et al*. 1976b). Erosion of a non-dispersive soil is quite different, requiring considerable velocity in the moving water to impart a critical shear stress to the soil surface (e.g. Wooding and Schafer, 1978).

Sherard and co-workers devised a simple "pinhole test" for identifying directly soils subject to erosion by dispersive piping (Sherard, *et al*, 1976a). In this test, distilled water flows through a hole 1.0mm in diameter in a sample of soil 25mm long. For dispersive clays the water becomes muddy and the hole rapidly erodes. For non-dispersive clays the water emerges clear and there is no erosion. Porewater dissolved salts, particularly the proportion of sodium relative to the other cations, is the main factor determining whether a clay is dispersive. Soils with high electrolyte content with high sodium are generally dispersive, while soils with a low content of dissolved salts in the soil water are non-dispersive in the pinhole test, even when the Na^+ content is high. Sherard, *et al*.(1976b) recommended that the pinhole test results always be used in association with tests of soil water salts.

The pinhole test, besides being useful for checking the dispersion characteristics of soils, may be used to check the effectiveness of different methods of inhibiting dispersion. Sherard, *et al*. (1976b) found that treatment of dispersive clays with small amounts of slaked lime converted the material without exception to a non-dispersive state. This can be attributed to the divalent Ca^{2+} ions replacing Na^+ ions in the double layer, reducing its thickness and hence promoting the effectiveness of the attractive Van der Waals forces.

Recent research funded by the National Water and Soil Conservation Organisation and reported elsewhere in this conference (Evans and Bell) has shown that the addition of small amounts of either phosphoric acid or lime to some New Zealand loessial soils reduces their tendency to undergo dispersive piping very substantially. This technique is unfortunately only practicable in the civil engineering situation - particularly backfilling around buried pipelines and treating roadside "water tables".

The treatment of tunnel gully-prone pastures with phosphoric acid or lime is not a practicable or economic proposition : the more traditional soil conservation techniques of grazing control and/or tree planting are still being studied and used. However the Sherard pinhole test is of use in this work; it allows the susceptibility of soil to dispersion to be assessed and conservation measures to be planned accordingly.

6 INFILTRATION RATE PROBLEMS

Changes in land use (typically from forest or scrub to pasture) usually lead to changes in the infiltration characteristics of soils (e.g. Pereira, 1973). In New Zealand this is most pronounced (and of serious concern) in the volcanic pumice soils of the central North Island.

In places where the land is still undeveloped (mostly covered in forest or scrub) there is little evidence of serious recent erosion. This contrasts with the situation in many areas which have been converted to pasture. Here, gullying occurs intermittently but often very suddenly and severely. Gullies up to tens of metres wide and several metres deep have been known to form in a matter of a few hours during heavy rain.

The obvious immediate interpretation of this gullying - that the grass-covered valley floors are less resistant to the scouring forces of overland flow than they were when covered with scrub/forest is not supported by close observation or by experiment. Close inspection of valleys within scrub covered catchments shows, in many cases, that no surface water flows in them, even during violent storms. Furthermore, experiments reported by Selby (1972) indicate that grass generally imparts better scour resistance to these soils then does scrub.

The alternative explanation, that conversion from forest or scrub to pasture has greatly increased the surface water flow in the valleys, is supported by direct measurements with infiltrometers, hydrological observation of stream flows and all of the circumstances of the gullying described here. Jackson (1973) reported a reduction of infiltration rate (as measured using ring infiltrometers) by a factor of 20 when the pasture was very heavily stocked.

Hydrological measurements of stream flows in undeveloped (native forest) pumice catchments (A. Dons, pers. comm.) support the view that, in the undeveloped state surface runoff is negligible even during major storms. The flow records for such streams show little evidence of rainstorms: evidently they are fed almost entirely by seepage of groundwater stored in the pumice soils. The streamflows in neighbouring developed catchments are comparatively sensitive to rainfall patterns (Fig. 5).

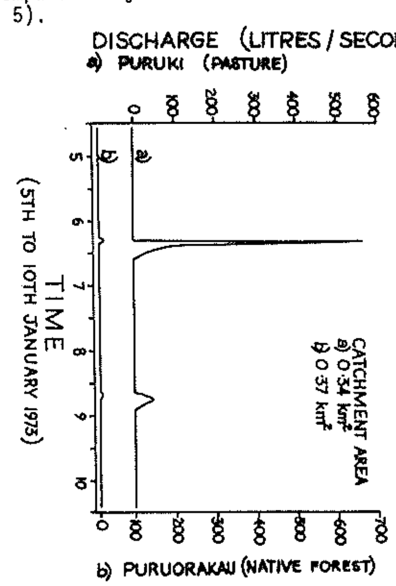

Figure 5 Changes in infiltration rate of pumice soils with changes in land use can dramatically affect runoff rates. Data from two NWASCO experimental catchments.

Experiments conducted by NWASCO at Moutere, Nelson (Luckman and Duncan, 1978) and comparisons between the hydrologic impact of different tree species (Swank and Miner, 1968) indicate that differences in rainfall interception capacity between developed and undeveloped catchments is sufficient to account for only part of the increase in runoff following development. Infiltrometer measurements have shown that infiltration rates of undeveloped pumice soils may be many times greater than maximum precipitation rates (Jackson, 1973) so it is through soil infiltration rates that we must approach the problem.

The spectacular reduction in infiltration rates consequent upon conversion from forest/scrub to pasture may be caused by:

i The formation of a more tightly packed (less permeable) surface layer, as a result of trampling by animals, or as a result of raindrop impact. Even low scrub or long grass would protect the soil from the impact of fast-falling raindrops. Overstocking would increase both of these effects.

ii The development of water repellency. A probable cause of water repellency in New Zealand pumice soils is fire. Savage (1975) found that fire-induced water repellency is deeper and more intense than any natural water repellency.

In studies of this problem the aim is to gain an understanding of the basic causes and then to quantify the various effects so that control measures may be designed. These measures will probably include the setting of upper limits on stock numbers, and establishing rules for stock and land management. These would be set to maintain infiltration rates at levels where the probability of gully formation during storms was acceptably low.

Because uniform stocking pressures are difficult to achieve, soils are artificially compacted in an experimental situation to densities which have been related to a range of stocking pressures. Areas compacted to different densities are then subjected to simulated rainfall, and infiltration and runoff rates can then be recorded.

Studies of this type call for the design of rainfall simulators. Because it is still not known what property of rainfall gives the best measure of its damaging effect, recently designed simulators represent attempts to model simultaneously the three quantities most likely to be relevant: intensity, velocity and dropsize. The design of compacting equipment, rainfall simulators and infiltrometers - as well as the interpretation of test results, all have very real geomechanics dimensions.

7 CONCLUSION

In this paper, brief indications have been given of some of the ways in which geomechanics concepts can be applied with advantage to soil conservation problems. There are of course many others. No mention has been made, for example, of the need for methodology for designing surface drainage and underdrainage schemes, for a stability analysis procedure applicable to the rural environment (and necessarily probabilistic), for understanding of the mechanisms of soil and rock creep, and for more soil testing which is conducted either *in situ* or under conditions which more nearly reproduce the *in situ* conditions.

It has been the intention here to alert scientists and engineers working in various geomechanics disciplines to a field of study whose importance is too often underestimated. It is to be hoped that our present civilisation can learn the lessons written in the history of past civilisations, and direct its energies and expertise to the more fundamental problems which conern us.

8 ACKNOWLEDGEMENTS

The authors wish to thank Mr J.C. van Amerongen for assistance with the section on infiltration problems and Dr N. Lambrechtsen for critically reading the manuscript.

9 REFERENCES

AITCHISON, G.D. and WOOD,G.C. (1965). Some interactions of compaction, permeability and post-construction deflocculation affecting the probability of piping failures in small dams. Proc. Sixth Int. Conf. Soil Mech. Fndn Eng. (Montreal), ISSMFE, Vol. II, p. 442.

CARTER, V.G. and DALE, T. (1974). Topsoil and civilisation, 2nd ed. University of Oklahoma. Press.

CHILDS, E.C. (1969). An introduction to the physical basis of soil water phenomena. Wiley - Interscience.

JACKSON, R.J. (1973). Catchment hydrology and some of its problems. Proc. Soil and Plant Symp. DSIR Inf. Series, No. 96, pp 73-80.

LAMBE, T.W. and WHITMAN, R.V. (1979). Soil Mechanics, S.I. Version. Wiley.

LUCKMAN, P.G. and DUNCAN, M.R. (1978). Hydrologic impact of afforestation with *Pinus radiata*. A progress report on an experiment in the Moutere Hills, Nelson. N.Z. Hydrol. Soc. Symp. (Wellington)

PENDER, M.J. (1978). A model for the behaviour of overconsolidated soil. Geotechnique Vol. 28, No. 1, pp 1-25.

PEREIRA, H.C. (1973). Land use and water resources. Cambridge University. Press.

PETTINGA, J.R. (1980). Geology and landslides of the eastern Te Aute district, southern Hawkes Bay. Ph.D. Thesis, University of Auckland.

ROSCOE, K.H. and BURLAND, J.B. (1968). On the generalised stress strain behaviour of wet clay. Engineering Plasticity. (ed. J. Heyman and F.A. Leckie) pp 535-609, Cambridge University. Press

SAVAGE, S.M. (1975). Occurrence and Phenomenon of natural and fire-induced water repellency. Special Publication, Soil Science Society of America, No. 7, pp 165-172.

SCHOFIELD, A.N. and WROTH, C.P. (1968). Critical state soil mechanics. McGraw-Hill.

SELBY, M.J. (1972). The relationship between land use and erosion in the central North Island, New Zealand. Jl Hydrology (NZ) Vol. 11, No. 2, pp 73-87.

SHERARD, J.L., DECKER, R.S., and RYKER, N.L. (1972). Piping in earth dams of dispersive clay. Proc. Specialty Conf. on the Performance of Earth and Earth-supported Structures, ASCE. Vol 1, pp 489-626

SHERARD, J.L., DUNNIGAN, L.P., DECKER, R.S. (1976a). Pinhole test for identifying dispersive soils. Jl Geotech. Eng. Div, Proc ASCE Vol 102, No.GT1, pp 69-85.

SHERARD, J.L., DUNNIGAN, L.P, DECKER, R.S. (1976b) Identification and nature of dispersive soil. Jl

Geotech. Eng. Div., Proc ASCE. Vol 102, No.GT4 pp 287-301.

SWANK, W.T. and MINER, W.H. (1968). Conversion of hardwood-covered watersheds to white pine reduces water yield. Water Resources Research, Vol. 4, pp 947-954

THOMPSON, R.C. (1979). Landsliding in soft rocks in the Utiku-Mangaweka area. 49th ANZAAS Conference (Auckland), Vol. 1, Section 3, p. 161 (Abstract only).

WOODING, R.A. and SCHAFER, G.J. (1978). Studies on erosion rates in soil. DSIR Applied Mathematics Division Report. No. 79.

Use of Movements in Determining the Stability of Natural Ground

J. M. O. HUGHES
Director, Situ Technology Inc, Vancouver (formerly Auckland University)
J. N. CLAPPERTON
Partner, Jackson Clapperton Goldschmidt & Partners, Auckland
P. R. GOLDSMITH
University of Auckland

1. INTRODUCTION

A recurring problem for Geotechnical engineers is the assessment of the stability of natural ground, either in its undisturbed state or after earth works such as cuts or fills have been constructed. Such assessments are generally far more difficult than the determination of the stability of "engineered" materials; for example, an earth fill dam, or an embankment constructed on a well chosen foundation. The material properties of such engineering works are usually well known. In addition, considerable effort is usually expended to ensure the fill material is placed in the desired manner. In contrast the material properties of a natural slope are exceedingly difficult to determine. Firstly a geological model of the site must be developed; then the in situ material parameters of the representative layers have to be determined.

In many cases the cost involved in such thorough investigations would be prohibitive, even if they could be done with confidence.

In the case of a well constructed dam or embankment, in which the strength properties of the soil are known, stability control is usually effected by measuring the pore pressures in the fill material and subsequently calculating the numerical value of the factor of safety. However, pore pressures, whilst having a major influence on the numerical value of the factor of safety, are very difficult to predict. In addition, unless the soil strength parameters are reliably known, total reliance on the measurement of pore pressures alone is of little use as they will not necessarily give a measure of incipient failure. The readings from three piezometers under an initially stable fill which was intentionally loaded to failure are shown in figure 1 (Lambe 1974). As the fill height increases the pore pressure increases almost linearly. From this figure alone there is no indication of approaching failure.

In circumstances where the soil properties are not accurately known, either because they are too difficult to assess or cannot be accurately evaluated, the measurement of soil movements are the most positive method of control. As in the case of the factor of safety based on insufficient data, such displacement measurements will not give a numerical measure of the stability of a slope, however, the displacements will indicate whether a slope is stable or not, at least over the period of time during which the measurements are taken.

What is perhaps not commonly recognised is that before visible signs of distress are noticed, (such as tension cracking), substantial movements could have occurred in the slope or embankment. Such movements prior to failure can be used to monitor the behaviour of natural materials.

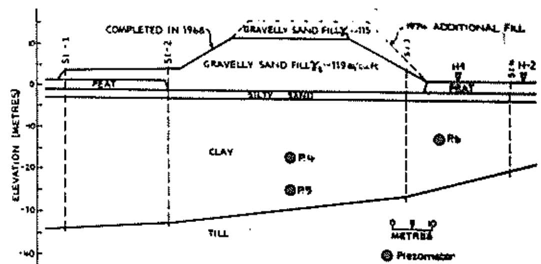

FIGURE 2(a)
CROSS SECTION AT STATION 265

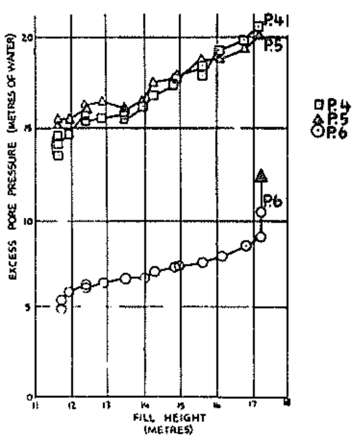

FIGURE 1 - Pore Pressure/Fill Height for an Embankment constructed to Failure (Lambe 1974)

2. STABILITY OF UNDISTURBED NATURAL SLOPES

Not all natural slopes are in an incipient state of failure. However, given the right changes in climatic conditions, such as prolonged periods of rain, the stability of many natural slopes becomes marginal. If a slope has moved substantially in the past, such old movements will usually be ascertained from a close inspection of the ground or be visible on aerial photographs.

If the slides are more recent it may be possible to observe a change in the land form by comparing the oldest available aerial photograph with the most recent. In New Zealand, the oldest aerial photographs are usually c. 1940. Old oblique photographs from library records, or even old maps, may be useful for this purpose.

Many cases are not, however, immediately apparent. Judgement may suggest to a geotechnical engineer that a slope has moved, however, when it moved and whether it is still moving are difficult questions to answer. It is in these instances of probably marginal stability, where accurate measurements of slope movements can be particularly valuable.

Often survey measurements taken on surface markers can be particularly useful. The results of such measurements taken by Messrs. Wood & Ptns. across a suspected unstable slope in the Auckland area are shown in figure 2. It is clear that significant movement has occurred over the period in which the measurements have been taken.

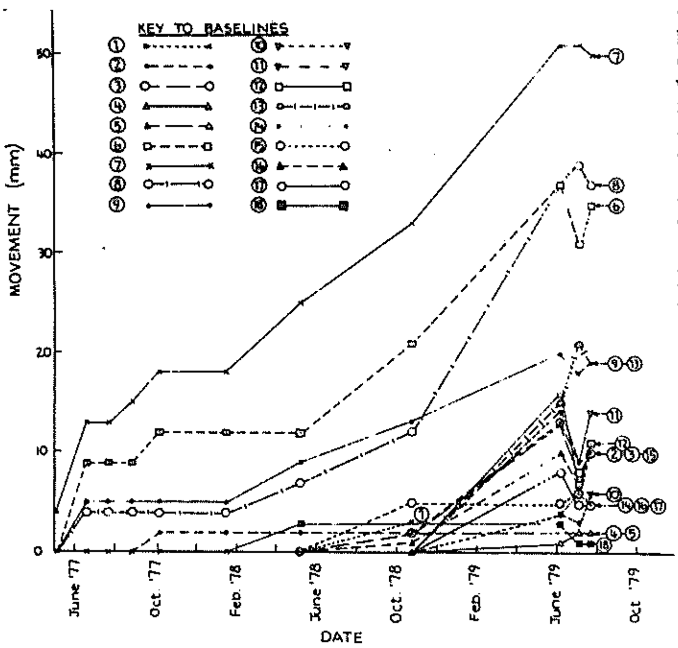

FIGURE 2 - Surface Movement/Time for a Cut in Natural Ground

Considerable care is required for the accurate determination of such surface movements, unless of course large movements have occurred. A further difficulty associated with surface measurements is the protection of markers from vandalism and plant and/or stock damage. In addition, if any effective remedial action is to be undertaken, the depth of the movement must also be determined.

Probably the first person to take particular note of the advantages of monitoring ground movements was S.D. Wilson, who developed the slope indicator in the mid 1950's (Wilson and Hancock, 1965). His instruments, or variations on them, are in current use all over the world. They are particularly useful in that they give a measure of both the ground surface movement and the deflection profile with depth, to an accuracy of a millimetre or so. From the deflection profile so obtained, the depth at which significant movement is occurring can be determined. Such instruments can detect movements at great depths, although 50 m is probably the usual maximum limit. In New Zealand these instruments are reasonably expensive and are not all that readily available. In commenting on N.Z. Ministry of Works experience with these instruments, Olsen (1976) observed that:
"The system is complex, sophisticated and extremely time consuming to install, operate and maintain ... It is only suitable where a real need has been established".

Probably because of these considerations, slope indicators are not used as freely as perhaps would be desirable.

For civil engineering works involving land subdivision for residential or commercial purposes, it is important to establish whether active ground movement is occurring, and whether such movement is sufficiently close to the surface to enable simple remedial measures to be undertaken. If it can be established that movement has occurred then this is usually sufficient evidence to require that either some remedial works are necessary or the site is unsuitable for building. If the movement is below about 5 m in depth, then the costs involved in attempting to improve the situation on the slip surface, (lowering the water table for example), are probably prohibitive and the site best not developed.

A simple device for assessing shallow ground movements has been developed by Goldsmith and Hughes (1977). This device is a very simple slope indicator designed to measure movement to a very limited depth of 6 m. Within this range of depth the displacements can be recorded with an accuracy of up to ± 1 mm; however, the total amount of movement able to be recorded is restricted to about 30 mm.

The authors have used this indicator for the assessment of land stability on a number of sites involving land subdivision.

The instrument is shown schematically in figure 3. The instrument liner is simply a length of PVC tube which is set into the ground. The end of the tube is sealed with a concrete plug. A rectangular aluminium bar (10 mm x 20 mm) is lowered down the tube and located in a pivot in a brass block in the centre of the concrete end plug. The bar is held in place by the pivot at the base and a slide which can be lowered on a wire down the bar. The slide keeps the bar a fixed distance away from the walls of the plastic tube. An initial borehole profile is obtained immediately after installation of the device. If the ground subsequently moves, the top of the bar will move relative to the top of the tube (figure 3b). If the relative movement of the top of the bar with respect to the top of the hole is measured with a steel rule or a dial gauge with the slider in successive positions down the bar, then the displacement profile of the borehole liner can be determined. Figure 4 shows the results of a series of observations on a proposed subdivision near Kamo in Whangarei. The soil underlying the site is Onerahi Chaos. From a visual examination of the site it was suspected that ground movement had occurred. There was however no evidence of substantial movements over the past 50 years either from aerial photographs or from local residents. The observations presented in figure 4 were taken across the start of the winter. Movements extending almost the full depth of the indicator

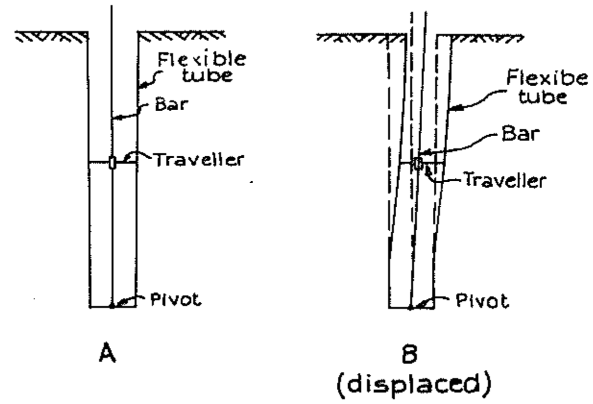

FIGURE 3 - Borehole Displacement Gauge

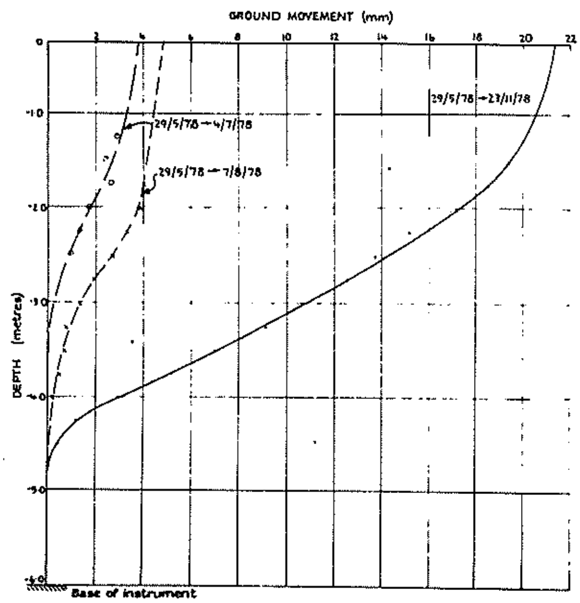

FIGURE 4 - Movement Profile/Time for Natural Height of Onerahi Chaos

are clearly shown. These movements do not appear to be confined to any particular zone. In this particular case it is difficult to envisage how this site could be stabilised without major geometric changes. A result of this nature is usually sufficient for the owner of the land to reconsider the intended development.

3. STABILITY OF EMBANKMENTS ON NATURAL SOILS

The material properties of the soil in an embankment are probably well known compared to those of the foundation material which may be difficult to assess. In such cases the movements in an embankment, founded on soft natural soils, are probably the key to monitoring their satisfactory performance.

Probably the simplest performance measurement is the lateral spread of the base of the fill. Such measurements are particularly sensitive indicators of an impending failure. The success of this approach is that these lateral movements can often be large and are therefore easy to monitor (up to a metre or more even on quite stable fills, Hughes 1969). Of particular significance however is that the rate of movement increases as failure is approached.

As a fill is being constructed, the foundation settles and spreads laterally as the load is increased. If the fill height and lateral spread are plotted against time they will have the form shown in figure 5. In this figure the spread increases as the height is increased. If the rate of spreading increases, such as beyond point C, then the fill could be in danger. If the engineer controlling the fill is immediately aware of this, the placing of the fill can be stopped, or if necessary, fill can easily be removed until the spreading stops.

If the pore pressures in the foundations are plotted against fill height, they will not show a corresponding increase in rate of change as incipient failure is approached.

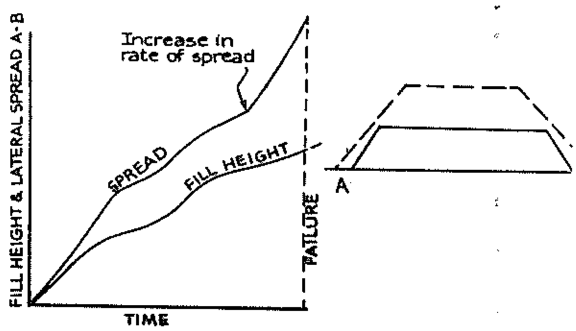

FIGURE 5 - Ideal Plot of Fill Height and Lateral Spread/Time for a Fill Which Fails

As indicated in figure 1, the pore pressure lines will usually break if the fill starts to spread. As a consequence, the peizometers will be rendered useless as a means of controlling stability.

The result of the lateral spread of a trial embankment at Kings Lynn, England, is shown in figure 6, (Wilkes 1972). The onset of failure is clearly indicated by the measurement of the lateral spread. Other than the fact that the piezometer ceased to function near failure, the pore pressure measurements were of little use.

The lateral spread of an embankment can be measured by conventional survey techniques in which the movement of markers placed near the toe of the fill are monitored. It has been the authors experience, however, that this method is not always satisfactory as the markers can get damaged. In addition, the method can be very time consuming and requiring much care. The installation of slope indicators at the toe of an embankment may also be used to give a measure of the lateral spread (Marsland and Powell, 1977).

A very simple technique, however, is to place a wire through the fill (Hughes 1969). This wire may be installed through a culvert if there is one, particularly if it is a flexible culvert; or can be placed through the fill inside a flexible plastic tube. If one end of the wire is fixed at one toe of the embankment, then the relative movement between the free end of the wire and a marker placed at that end, will give a measure of both the lateral spread and the settlement of the fill. This movement is very easy to measure and monitor by supervision personnel on the site.

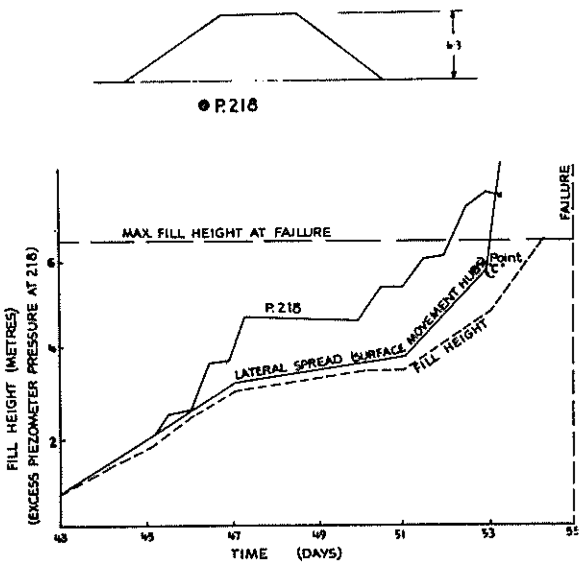

FIGURE 6 - Lateral Spread, Fill Height/Time for Trial Embankment at Kings Lynn (Wilkes 1972)

4. CONCLUSION

It is the authors opinion that ground movements in the soil are the most important single parameter for assessing either the stability of natural slopes, or the performance of a fill. This parameter is easy to measure and can be used to give a far greater appreciation of the behaviour of natural soils than the measurement of any other parameter, particularly in soils in which in situ properties are often difficult to obtain.

5. ACKNOWLEDGMENTS

The authors wish to gratefully acknowledge Messrs. Wood & Partners for the use of the surface marker results; and Mr. J. Cartwright, Chief Surveyor of the Lands and Surveys Department, Auckland, for permission to publish the results shown in figure 4.

6. REFERENCES

LAMBE, T.W. (1974), "Proceedings of the Foundation Deformation Prediction Symposium" Report No. FHWD-RD-75-515 US Dept. of Transportation

HUGHES, J.M.O. (1969), "Culvert Elongations in fills founded on Soft Clays", Canadian Geotechnical Journal VI, 2, 111-117

GOLDSMITH, P.R., HUGHES, J.M.O. (1977), "A borehole displacement gauge", Geotechnique Vol. 27, No. 2, June

WILSON, S.D. and HANCOCK, C.J. (1965), "Instrumentation for movements within Rockfill Dams", ASTM Spec. Tech. Publ. 392, pp. 115-130

OLSEN, A.J. (1976), "The Inclimometer Monitoring System", N.Z. Geomechanics News No. 13, Nov.

MARSLAND, A. and POWELL, J.J.M. (1977), "The Behaviour of a Trial Bank Constructed to Failure on Soft Alluvium of the River Thames", International Symposium on Soft Clay, Bangkok, Thailand, July

WILKES, P.F. (1972), "An Induced Failure at a Trial Embankment at Kings Lynn, Norfolk, England", Proc. ASCE Conf. on Perf. of Earth and Earth Supported Structures, Vol. 1, Pt. 1

Cryptic Landslides

P. M. JAMES
Engineering Geologist, Brisbane

SUMMARY The existance of a sub-group of landslides, dating from periods of low sea level and preserved today under a covering of either water or alluvium, is postulated. Examples of these cryptic landslides are given, together with some mention of their significance to civil engineering.

1 INTRODUCTION

The phenomenon of reactivation of Pleistocene landslides in terrestrial environments is well documented. Because of erosion, evidence of coastal landslips dating from the Pleistocene, in particular from periods of low sea level, is less available. Nonetheless, indications of past instability can sometimes be inferred today from retrogressive movements.

In the terrestrial environment, fossil landslip structures are now usually recognised in reconnaisance. Where these structures are preserved or partially preserved beneath water or recent sediments, they pose a problem of subterranean weakness of possible significance to civil engineering.

This paper is concerned with circumstantial and quantitative evidence pointing to the preservation of such cryptic structures, and with the environments in which they can be expected to occur.

2 GEOLOGICAL SETTING

The full sequence of sea level fluctuations throughout the Pleistocene has not been established in detail, but a number of sea level changes are known to have taken place, with the present level being possibly a relatively constant maximum (± a few metres) to which the sea has intermittently returned. The most recent low, -100m. approx., occurred around 25,000 to 20,000 yrs bp, and was followed by a fairly rapid rise back towards the present level which was attained perhaps in the last few thousand years.

Enormous fluviatile downcutting during the sea level lows can be inferred today, at least in tectonically stable regions, from the overdeepening of stream beds, e.g., the Brisbane River. Such overdeepening must have been accompanied by considerable landslip activity.

Subsequent sea level rises, in addition to reworking the Shelf sediments, would have

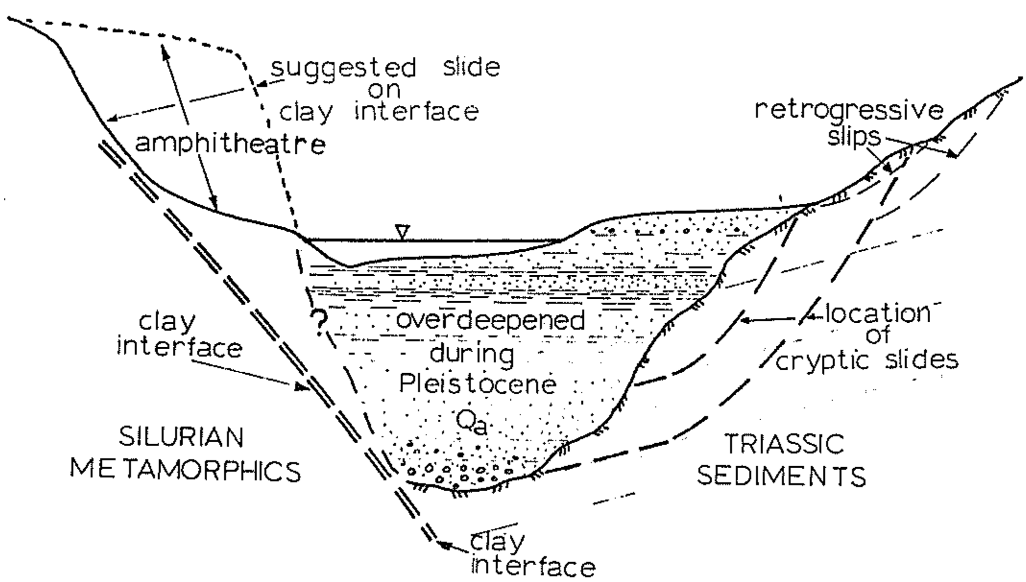

1. Brisbane River : typical overdeepened section considered conducive to past landslides

eroded the recently dissected shorelines, providing an environment for further landslip activity. Finally, fluviatile and estuarine sedimentation associated with the rises would have progressively stabilised and covered many of the slide zones then extant.

Examples are given to illustrate these points.

3 FLUVIATILE ENVIRONMENT

3.1 Brisbane River

The lower reaches of the Brisbane River contain some 30m. of recent bed sediments, Fig.1. The region is tectonically stable and if the present land surfaces are taken to be only slightly degraded versions of the pre-Pleistocene topography, then at the time of maximum downcutting the banks on either side of the river would have stood thirty or more metres higher than at present. Drawdown conditions after recent floods showed that these present banks are only quasi-stable in many places. It is therefore reasonable to assume that landslip activity along the higher banks, at the time of maximum downcutting, was fairly common.

The problem today is to delineate not only those zones where late Pleistocene slides might have occurred, but also where these slides might be preserved.

A special geological association occurs in the area and this was highlighted by a small slide (1970) which disrupted excavations for a road underpass in the city. The slide took place on the dipping junction of a Triassic sedimentary series unconformably overlying Silurian metamorphics. Both the formations are of moderatly hard rock, but flexural slip during folding had produced clay seams and mylonites along the interface. with very low, near residual strengths, James (1971).

2. Stereo views of two "amphi-theatres"

As for the road cutting today, so for the river in the past. In virtually all locations where the river intersects this dipping interface between these two strata, large amphi-theatre like depressions, with a microtopography suggestive of old slides, occur in the banks. Stereo air photos of two such features are shown in Fig.2.

The mechanism of failure may be inferred from Fig.1: the slides occurred around the time of maximum downcutting by the river and they owe their present stability to resedimentation.

It should be pointed out that no drilling to confirm or disprove the above proposition has been undertaken. Quantitative data is, however, available from the Canonvale site.

3.2 Canonvale Site

In 1973, the writer inspected a small seaboard site at Canonvale, N.Qld, proposed for development. The site contained a small conical hill of meta-volcanics, with side slopes that flattened out towards the base. No evidence of instability was noted on the steep elevated slopes. However, along the moderate and gentle colluvial slopes at the base of the hill, (11° to 12°) there were indications of down slope movements. The low relief, hummocky topography might be seen on the stereo view, Fig.3. The unusual factor here was that this "unstable" zone abutted against, and even appeared to continue beneath, the alluvial flats which were themselves at around high Spring tide level.

A number of trial pits were excavated. Those in the hummocky ground revealed shearing both in the colluvium and in the weathered rock, to depths of 2m. The orientation of the shearing confirmed the surface impression that the unstable zones continued below the level of the flat alluvium.

Undisturbed block samples of the shear zones and the intact colluvium were taken and tested under drained conditions in the shear box. In the shear zones a value of $\phi' = 13^{\circ}$ was obtained on first shear. Repeated shear tests gave $\phi'_r = 12^{\circ}$. Tests on the ambient clay gave a peak value of $\phi' = 20^{\circ}$. Thus, considerable movement along the shear zones is indicated.

Landsliding which continues below a flat ground surface requires some explanation. The implication here is that the instability must have been initiated prior to the existence of the alluvium, i.e., on an old land profile associated with a period of low sea level.

The existence of cryptic landsliding at this site was deduced from the retrogressive movements up-slope. It is, however, possible to conceive of situations where past landslip activity could be completely covered by Holocene alluvium or by water. Traditional site investigation methods would be fortunate indeed to pick up any evidence of such a situation, and while the existence of such cryptic structures might have little or no effect on small scale developments, the same could not be guaranteed in the case of large projects involving dams, bridge foundations, land reclamation schemes, etc.

4.1 Folkestone-Warren

The Folkestone Warren slips have been comprehensively investigated, most recently by Hutchinson, (1969). The oldest slips, still manifest, have been dated around 2,500 to 5,500 yrs bp, the earlier date corresponding to a sea level perhaps 7m. below the present.

The slips have occurred in the Gault Clay layer which divides the overlying Chalk from the underlying Lower Greensands. There is a small component of dip of these strata towards the east, about 1 in 100, and if conditions were taken back say 10,000 yr it is possible to conceive similar landslip activity in the Gault, occurring at a lower elevation, well to the east of the present site.

Thus, the slips at Folkestone-Warren could be merely the final stages of a much larger zone of instability from a time of lower sea level.

The extent to which shear zones in the Gault - or, for that matter, large masses of slide debris in the Chalk - might be preserved is, of course, highly conjectural.

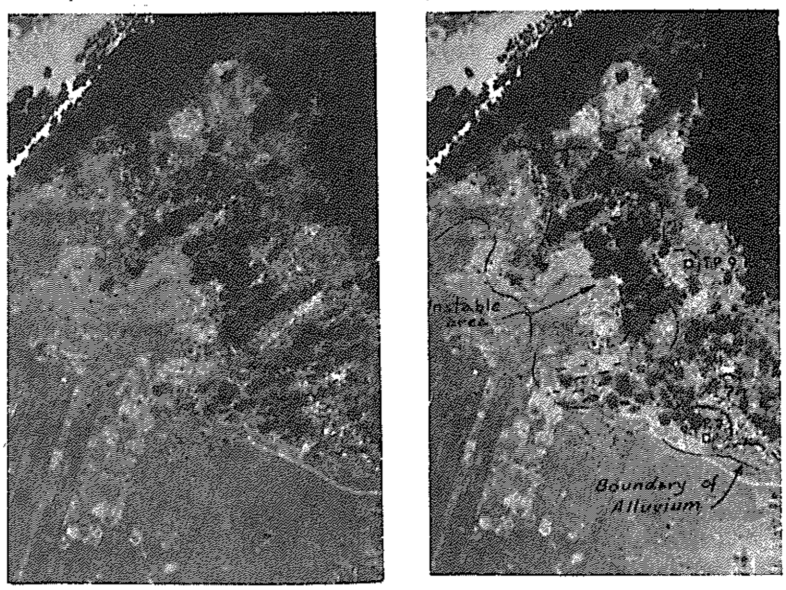

3. Stereo view of Canonvale site showing hummocky topography abutting against alluvium

4 MARINE ENVIRONMENT

In the marine environment, more complex processes are involved, as already briefly outlined. In certain sheltered environments, however, submarine features such as old river channels associated with low sea levels can be recognised in the submarine contours, today. Where these exist, the possibility of cryptic shear zones can not be fully discounted. A slight reinterpretation of two well known coastal slides is offered as a hypothetical model to suggest the presence of cryptic shear zones in the submarine environment.

4.2 Portuguese Bend, California, (1956)

The Portuguese Bend slide, Merriam (1960), occurred in the montmorillonitic Monterey Shales, after a relatively shallow trench was excavated along the toe area, near to the sea, Fig. 4. The slip was an obvious reactivation of an older slip, and the slip plane was recorded at several locations allowing, with surface evidence, an accurate plot. Merriam distinguished a lower slip (A) with a large associated retrogressive movement up slope (B).

If there is retrogression, the question arises as to its extent or, rather, as to its point of origin. If a slightly

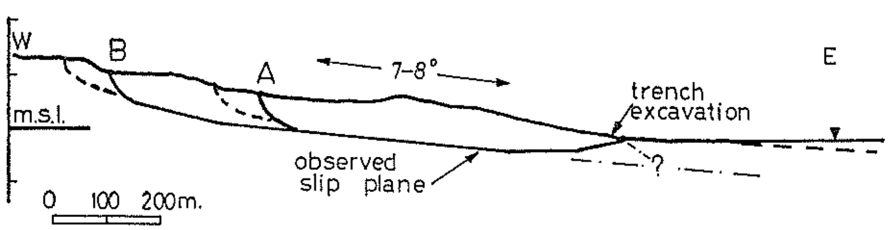

4. Portuguese Bend slide (1956)

lower sea level than the present is invoked, it is plausible to suggest that landslipping could have begun further down-slope than the present slip. In other words , the 1956 slip might not be merely the reactivation of a fossil slip of similar dimensions, but rather a recent manifestation of a retrogression originating somewhere out to sea.

5 CONCLUSIONS

In the past decade, there have been numerous instances where (terrestrial) slides have occurred in blatant contradiction to soil mechanics principles. The idea of Progressive Failure was put forward as an explanation in clays and clay shales. It is the writer's experience, however, that in the vast majority of cases the cause of failure could be attributed, not so much to true Progressive Failure, but to the presence of pre-existing shear planes in the ground. It is possible,then, that work in the future might also show a similar pattern for some unexpected submarine slides.

In this paper, largely circumstantial evidence has been proposed to show how late Pleistocene slip surfaces might be preserved under present day water or alluvium. Sufficient conditions for the development and preservation of these buried shear zones are: tectonically stable, fluviatile environments which have been subject to overdeepening during periods of low sea level; associated landsliding along the banks; subsequent stabilisation of the areas by water level rises and resedimentation.

Recognition of the conditions favouring the development of cryptic shear zones could be important for large scale civil engineering works. In many cases, surface indications, such as retrogressive slides, could be diagnostic, but this need not always be the case. For this reason, it is the writer's contention that any steep, subterranean, erosion features should be investigated with some care.

The probability of preservation of cryptic shear structures in the marine environment is low. Yet many stretches of the present day coastlines are the result of the "dynamic" erosion forces of the changing sea levels of the Pleistocene; certainly these sea level changes have caused much reworking of the sediments of the Continental Shelf. Under certain conditions, some preservation of slip structures is possible. In the location of submarine tunnels, pipeline routes, in the design of land reclamation schemes, consideration could profitably be given to the historical evolution of the present day submarine contours, in relation to the geology.

6 REFERENCES

HUTCHINSON J.N. (1969). A reconsideration of the coastal landlsides at Folkestone-Warren, Kent, in terms of effective srress. Geotechnique , 19 : 1 : 6 - 38.

JAMES P.M. (1971). The influence of structure on the behaviour of argillaceous sediments. Proc. 1st Aust. N.Z. Conf. on Geomechanics Melbourne.

MERRIAM R. (1960). Portuguese Bend landslide (California). Jnl Geology, Vol.68.

WEEKS A.G. (1969). The stability of natural slopes in S.E. England as affected by peri-glacial activity. Qtly Jnl Engin. Geol. 2 : 1 : 49 - 62.

Landslides in South Australia

J. SELBY
Supervising Geologist, Department of Mines and Energy, South Australia

SUMMARY Many South Australian landslides are due to mass movement of hillslope debris and have occurred during periods of intense rainfall. Earth flows, incorporating rotational movement, occur in Permian Sediments on the Fleurieu Peninsula and are due to the effects of land clearing. Massive rotational slumping, occurring in bedded rocks, has been recorded at several localities as have numerous rockslides in quarries, open cut mines, and road cuts.

1 INTRODUCTION

South Australia has the lowest average rainfall of any Australian State and a very subdued topography. Nevertheless mass movements (landslides) are widespread. Many of them are due to the results of changing land use and other human activity and have occurred within living memory, while some may have been the result of past seismic activity. Because of this the State Planning Authority requires geological inspection of slopes steeper than 15^{o} (1 on 4) before residential subdivision is permitted.

This paper summarises the main types of landslide which are known to have occurred and provides a guide to the recognition of situations where mass movements could occur in the future. The simple classification given in the Field Geologists Manual by Berkman (1976) has been used. Localities mentioned in the text are shown in Fig. 1.

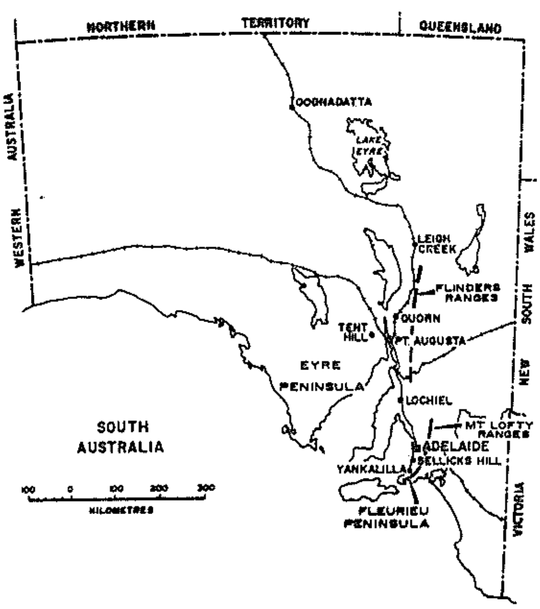

FIG. 1 Location Plan

2 MASS MOVEMENT OF SOIL

If the word 'soil' is used in its civil engineering sense it is apparent that most South Australian landslides are due to mass movement of this material. Several different modes of failure can be recognised:

2.1 Debris Slides

In the Flinders Ranges and Mt Lofty Ranges, which form a central spine to the most settled area of the State, debris slides ~~are fairly~~ common and have been described by Twidale (1968). Stream erosion has revealed that some of the lower slopes in these areas consist of several metres of hillslope debris (colluvium) consisting of poorly graded material of extremely variable grain size. A railway cutting along the Pichi Richi Pass near Quorn shows nearly 8 m of colluvium, ranging in size from silt to boulders, occurring as a thick layer on the floor of a narrow valley. Foundation investigations for a proposed water treatment works near Adelaide showed up to 10 m of heterogeneous hillslope debris in an area of suspected shallow bedrock. This caused a modification of the foundation design to incorporate a retaining wall tied in with rock anchors (Fig. 2).

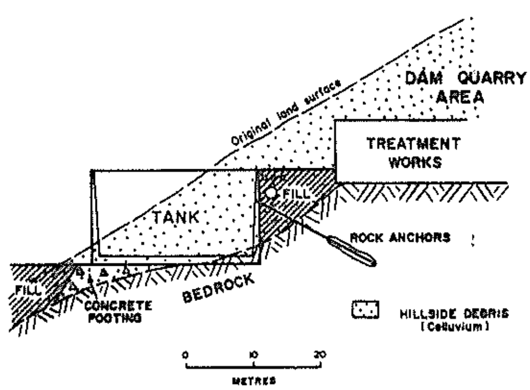

FIG. 2 Proposed water treatment works on Hillside debris.

Areas of debris material can often be recognised in the field and on air photographs by a characteristic hummocky terrain best seen under conditions of low incident light. On many lower hill slopes, the material has been temporarily impounded behind obstacles such as large boulders and trees to form terracettes. Evidence of hill creep can also be seen in inspection trenches which often show distortion of upper weathered rock layers indicating down-slope movement.

Most debris slides in South Australia appear to be stable unless disturbed by human activities such as changing land use or civil engineering works. The alignment of a dam near Adelaide had to be changed after slide debris began to move as a result of earthmoving operations and diversion of a stream to the toe of the slope. Every year in the hills around Adelaide many small debris slides are reported along road cuts during the heavier winter rain storms. In most cases permanent slope stabilisation would prove too expensive and the material is merely removed. One recent slide however required extensive treatment: In this case hillslide colluvium began to move after wetting caused by the combined effect of a leaking culvert and rising reservoir water at the toe of the slope. A seismic refraction survey showed several metres thickness of debris which was subsequently removed, replaced with rock fill, and the road section completely rebuilt. Examination of these debris slides shows that the bedrock surface forms the main sliding plane, particularly when lubricated by perched groundwater. Many of them occur on south west facing slopes - the direction of prevailing winter winds.

2.2 Earth Flows

These differ from debris slides in that failure takes place within a thick body of unconsolidated sediments (soils) and is accompanied by rotational movement. Failure depends on the strength and degree of saturation of the sediments and can occur rapidly and spontaneously without the agency of civil engineering works. Nevertheless those earthflows so far recognised in South Australia are believed to have been caused indirectly by man's activities (Twidale, 1976).

They occur mainly on Fleurieu Peninsula (Fig. 1) where Permian sand and clay occurs to a considerable thickness within buried valleys which frequently bear no relationship to the modern topography. They have been studied by Van Deur (1978) who located 33 earthflows on slopes ranging from 8 to 20^{o} in an area of approximately 100 km^{2} south of Yankalilla (Fig. 3). All of these slides apparently formed after European settlement but there has been a time lag between occupance and the majority of mass movements. This was acquired by slow physical and chemical changes in the soil, brought about by deforestation and a rising saline water table, gradually reducing its shear strength. The mechanism causing failure is not clearly understood but is no doubt related to rainfall and possibly, seismic activity.

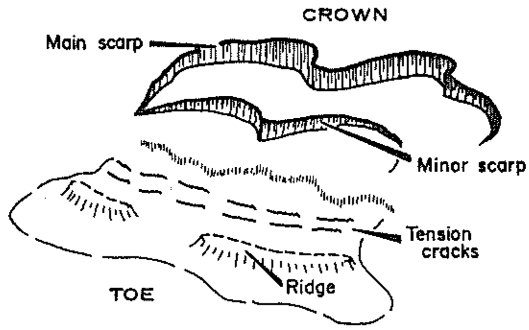

FIG. 3 Typical earthflow in Yankalilla area

2.3 The Adelaide area

A large number of cuts and excavations are opened up every year in Metropolitan Adelaide, chiefly in soil materials. The stiff to hard Pleistocene clay which underlies the City of Adelaide stands up well for short periods in dry conditions and a 10 m high unsupported face was described by Cox (1970) as being stable for three months on a 45^{o} batter. However, the effects of drying out make the material treacherous as it breaks up into coarse lumps which can collapse suddenly. A mantle of low density calcareous silt of wind blown origin (loess) is distributed as a shallow layer up to several metres thick over much of the Adelaide Region. When dry this material will stand vertically but collapses quickly when wetted.

Problems with saturated alluvium frequently occur on the outwash fans which underlie the eastern part of metropolitan Adelaide. On the coast 3-4 m deep dewatered sewer trenches have stood vertically without support in the silt, sand, and soft clay of the coastal estuarine deposits.

3 MASS MOVEMENT OF ROCK

The Flinders and Mt Lofty Ranges consist largely of well bedded and jointed sedimentary rocks which have been extensively folded and faulted. Alternating beds of quartzite, dolomite and shaly siltstone provide a wide range of materials of differing strengths and resistance to weathering. Mass movements in these materials may be divided into three types:

3.1 Rotational Slumping

Large masses of slumped rock material have been reported near Oodnadatta by Heath (1963). These can be up to 400 m long with an approximate volume of 3/4 million cubic metres. They occur in shales which form a steep escarpment 60 m high, and are the result of rotational movement caused by water saturation of joints and partings.(Fig.4). In each case the shale block is capped by a solid mass of duricrust which has protected the material from severe distortion and mechanical breakdown during slumping, so that the shale appears to dip steeply into the face of the escarpment. Similar features have been recognised from the Tent Hill area west of Port Augusta by Thomson (1965). Here large masses of quartzite, up to 150 m long, have slumped and travelled laterally on an underlying weaker shale formation (Fig. 5).

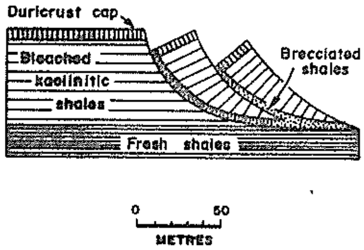

FIG. 4 Large scale rotational slumping near Oodnadatta.

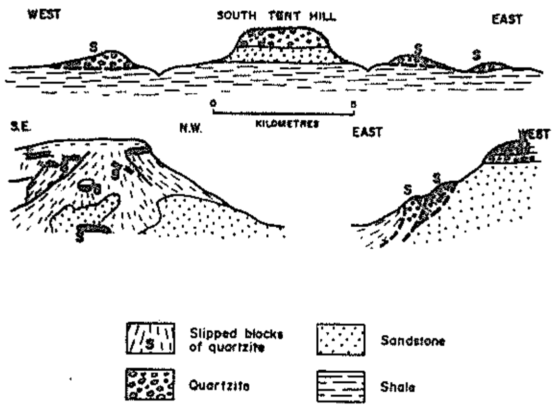

FIG. 5 Rotational slumping of Quartzite

The rock types described above are common in South Australia and, although these are the only cases so far documented, it is likely that other naturally occurring landslides of this type exist, possibly covered by scree debris, elsewhere in the Adelaide Hills and Flinders Ranges.

An example of incipient rotational slumping in shales underlying a coal seam occurred at Leigh Creek Coalfield and has been described by Townsend (1978). Removal of 50 m of overburden and the coal seam caused upward buckling of the underlying shales as a result of hydrostatic pressures and the weight of overburden dumps placed on the edge of the open cut (Fig. 6).

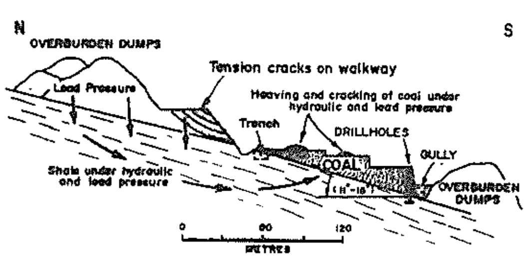

FIG. 6 Slope failure at Leigh Creek Coalfield

Remedial measures consisted of relieving hydraulic pressures in the shales by construction of a trench and a line of pressure relief wells at the toe of the slope.

3.2 Rockslides

A large number of rockslides caused by man's activities have occurred within the bedded rocks which form most of the hill country in South Australia. One of the most spectacular happened in 1974 at a dolomite quarry near Adelaide. A massive rockslide covering the whole of one face took place along a wedge failure direction formed by the intersection of the rock cleavage and a major joint set (Hazeldine, 1975). This slide happened over a period of days during a time of heavy winter rainfall and was due to excessively steep batter slopes which caused the wedge failure to daylight out of the quarry face. Remedial measures consisted of removing and regrading the entire face.

Another major rock slide occurred at an open cut iron ore mine on the Eyre Peninsula over a period of 11 days. Movement took place along a syncline whose axis plunged out of the face. It appears to have been initiated when a passive wedge of rock supporting the toe was broken by blasting.

An unusual rock slide having no direct cause has been reported from the Lochiel area by Twidale (1976). It took place on the sides of gently sloping hill (slope 16-21°) in 1974 after a period of heavy winter rain. Movement occurred within a quartzite formation dipping at the same angle and direction as the slope, possibly as a result of lubrication of thin clay seams within the quartzite by percolating rainfall. A detailed map of the slide, which involved about ¼ million tonnes of rock, is given in Fig. 7.

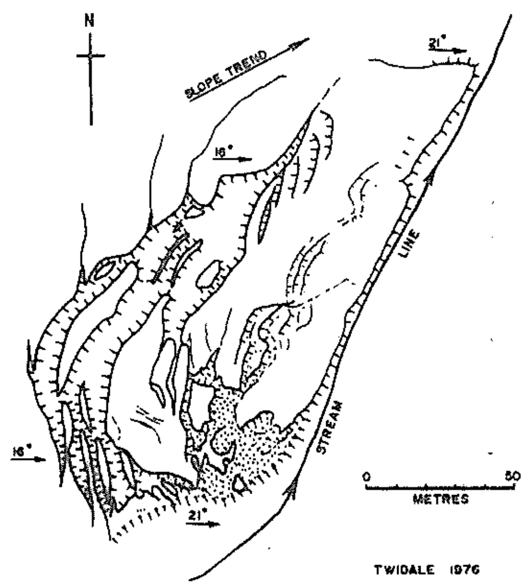

FIG. 7 Sketch map of the Lochiel Landslip.

Numerous examples of block and wedge rock slides are provided by road cuts in the Adelaide Hills. The Sellicks Hill road is probably the most spectacular of these where small movements are still occurring many years after construction. Other examples are given by Weber (1978).

3.3 Stability of valley sides

Site investigations for dam sites in the Mt Lofty Ranges have revealed that the valley sites can be potentially very unstable. The presence of sheet joints running parallel to the topography when combined with bedding or joint planes can cause large potentially unstable blocks which may not be revealed until site work has commenced (Fig. 8). It was the recognition of these features that caused a change in the design of Kangaroo Creek Dam from a concrete arch to a decked rockfill structure (Trudinger, 1973). During the investigations for Clarendon Dam in 1971 a 300 m long adit was constructed to evaluate the stability of a suspect abutment. Open sheets joints were also encountered in the abutments of Little Para Dam and these required careful evaluation and the installation of special drainage holes.

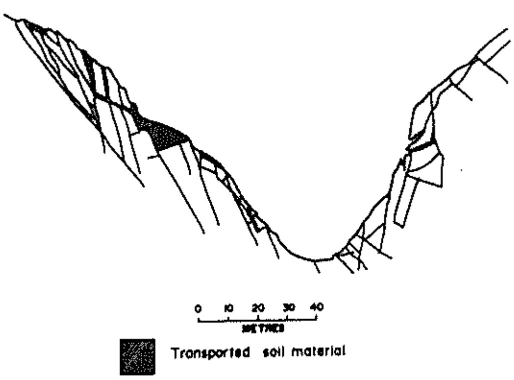

FIG. 8 Mechanical weathering of valley sides at Kangaroo Creek Dam.

4 CONCLUSIONS

Evaluation of potential slope instability is an important requirement of site investigations in South Australia. Even with careful investigation techniques, landslide situations may not become apparent until site works have commenced and it is important to cultivate a flexible approach to civil engineering construction.

5 REFERENCES

BERKMAN, D.A. (1976). Field geologists' Manual. Monograph 9, Austral. Inst. Min. Metall, Melbourne.

BOLT, B.A. and others (1978). Geological Hazards. Springer-Verlag.

COX, J.B. (1970). A Review of the geotechnical characteristics of the Soils in the Adelaide City area. Proc. Symp. Soils and Earth Structures in Arid climates, Adelaide. Inst. Engineering Aust.

HAZELDINE, R.K. (1975). The rock slope stability of the Riverview and Montacute aggregate Quarries S. Aust. Inst. Technology, School of Applied Geology, Grad. Dip. Thesis (unpublished).

HEATH, G.R. (1963). Large Scale slump structures south-east of Oodnadatta. Q. geol. Notes, geol. Surv. S. Aust., 7.

STEWART SHARPE, C.F. (1938). Landslides and Related Phenomena. Cooper Square Publishers Inc. New York.

THOMSON, B.P. (1965). Erosional features of the Tent Hill Formation. Q. geol. Notes, geol. Surv. S. Aust., 13.

TOWNSEND, I.J. (1978). Failure in overburden and coal, lode D, Leigh Creek. Q. geol. Notes, geol. Surv. S. Aust., 67.

TRUDINGER, J.P. (1973). Engineering Geology of the Kangaroo Creek Dam. Geol. Surv. S. Aust. Bull. 44.

TWIDALE, C.R. (1968). Geomorphology. Nelson, Melbourne.

TWIDALE, C.R. (1976). The origin of recently initiated exogenetic landforms, South Australia. Env. Geol. 1.

VAN DEUR, W.J. (1978). Earthflows in the Yankalilla area of South Australia. Trans. Roy. Soc. S. Aust. 102(6).

WEBER, B. (1978). Land Instability in the Adelaide Metropolitan area, 1978: Two case histories. Geol. Surv. S. Aust. Rpt. 78/128 (unpublished).

WILLIAMS, M. (1974). The Making of the South Australian Landscape. Academic Press.

The Evolution of a Risk-Zoning System for Landslide Areas in Tasmania, Australia

P. C. STEVENSON
Engineering Geology Section; Geological Survey of Tasmania
D. J. SLOANE
Engineering Geologist; Geological Survey of Tasmania

SUMMARY A man's house is his greatest material possession and to lose it is a personal disaster. The publication of reliable information of the expected risk from landslide damage can sometimes prevent this loss, and should be the task of geologists in the service of governments.

Estimates of risk, made by a process such as that to be described, should be published so that land use can be designed to avoid or minimise the landslide hazard. This hazard is comparable in personal impact to that due to flood, forest fire, earthquake, or cyclone. Estimates of risk can best be presented as zones on a topographic map.

The initial input to the risk zoning system is the topographic map which is divided into slope angle classes. The geological map can be interpreted to show the susceptibility to weathering, the formation of slip-prone talus, and the groundwater hydrology of various rock types. The combination of geology and slope classes can then be used to broadly indicate areas of possible instability.

The second stage is the direct approach where geological conditions are confirmed by field study and may be re-mapped at a suitable scale for the particular investigation. The morphology of the area is studied and mapped together with any features indicative of mass movement. Anomalous slope complexity is considered to be a major indicator of an unstable pre-history.

Detailed studies are made of selected critically unstable and stable areas using a similar methodology to the above with additional stratigraphical, geomechanical and hydrological information obtained from drilling. Stability analyses are calculated using the above information. This combined with all other information indicates the threshold slope angle for each rock type.

The result is a two tier zoning scheme of which one is descriptive and one proscriptive. The original descriptive system is of five classes of increasing landslip risk. This will shortly be altered to a simpler three class system. The proscriptive system is based on legislation and prohibits building or allows it to occur under a specific section of Building Regulations.

Some comments are made on the problems of administration.

1 INPUTS TO THE ZONING PROCESS

1.1 Topography

The topographic map is the first input to the zoning process. An examination of even 1:100 000 maps, contoured as ours are at 20 m intervals, can enable steeper areas to be recognised and marked for closer examination. Our current Tamar Valley Landslip Zone Maps are at a scale of 1:15 840 (Figure 1) and while extremely useful, inadequacies have become apparent as individual house lots are difficult to distinguish at this scale. Certain areas have been mapped at 1:2 500, an ideal scale for mapping small townships. The availability of suitable topographic maps is often the deciding factor and our existing maps are to be now remapped at a scale of 1:10 000 where the average city house lot will appear as 1.8 mm by 3.6 mm. In the absence of suitable topographic maps we have used aerial photographs enlarged to 1:5 000 and even produced our own oblique aerial photographs enlarged to a similar scale. The latter have proved very useful when mapping small landslip areas less than 3 km in extent.

Whatever suitable maps are chosen, slope angle classes are drawn on them. The choice of classes depends on the prevailing topography and geology and the scale and contour interval of the topographic map. Several methods have been used including paper templates and circular perspex templates extending over five contour intervals with each designed to represent the various slopes selected as the upper and lower bounds of each slope class. For aerial photographs slope angles are measured in the field by clinometer and the same slopes are used as standards for comparison on stereo-images. Another approach is to construct, using the methods of Miller (1961), square based pyramids having apparent sideslopes of predetermined angles. These are plotted on transparent film and viewed as a stereopair so as to form a model in space. This is laid over the photopair and direct comparisons made with unknown slopes. Where suitable computer facilities are available slope classes can be produced directly on the topographic map. This method is to be used in our next zoning investigation.

The initial result is therefore a series of slope angle classes drawn on a suitable base map. The ultimate and essential source of information is the landscape itself.

1.2 Geology

The second input to the zoning process is the geological map. We are fortunate in that good

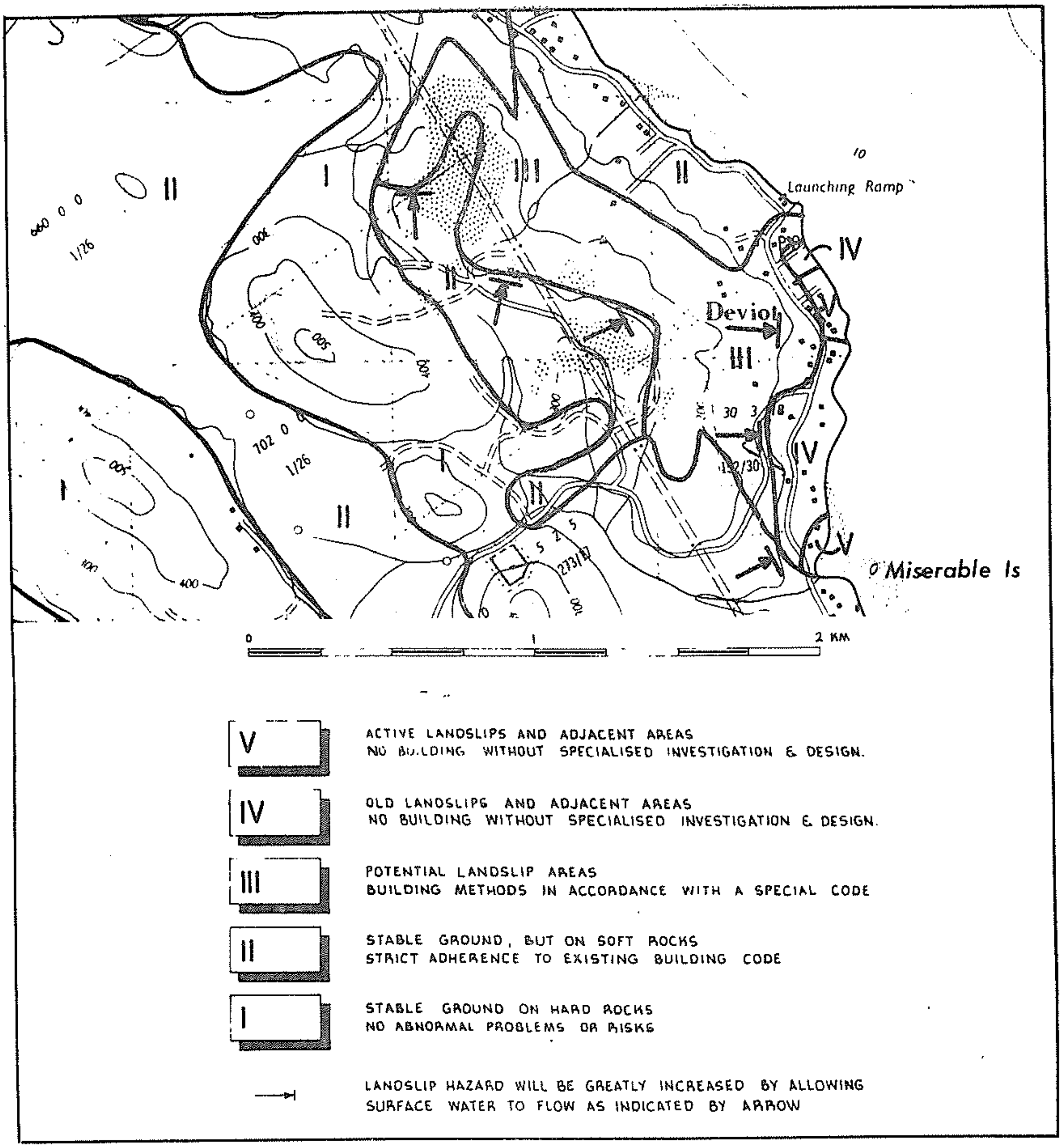

Figure 1 A section of the Batman Bridge sheet of the Tamar Valley landslip zone maps

1:50 000 geological maps exist of most of the areas we are required to investigate. However when zone mapping is conducted on a 1:10 000 scale or less then adjustments and additions are often required to be made to the geological base map. Where geological maps do not exist then this mapping is required as part of the geomorphological appreciation to be discussed later.

The geological map, if it does not already do so, must be interpreted in terms of rock types. Clays and weak shales will primarily suggest themselves as slip-prone materials but only field examination will determine this.

The harder rocks must also be considered as they may often function as loads at critical places on clay slopes, and more importantly as aquifers. The recognition of the influence of surface aquifers in producing instability in adjacent soft rocks was recognised by Denness (1972) as the reservoir principle and we have found this principle to be of the utmost importance where, as in our area, fresh fractured basalt overlies soft lacustrine sediments on steep slopes. The relationship between aquifers and their resulting springs, and the movement of colluvium in hillcreep must also be appreciated as occlusion of springs by mass movement may be a very potent agent of instability. The solid geology as indicated in most geological maps is therefore to be inspected for the presence of soft or softenable rocks and for aquifers capable of producing spring lines on or above steep slopes in these materials.

There is however, a considerable limitation to this simple approach. The colluvial materials on the slopes are probably critical in determining slope stability and are not usually represented on a geological map. Here a direct method has to be used, that of inspecting the slopes on each rock type in the field and determining the colluvium thickness, expected variation, and general nature. This process can be treated qualitatively at this stage but will need to be pursued in detail when the morphology is dealt with. Recent geological mapping has changed in that surficial deposits are now often differentiated, consequently improving their usefulness.

The geological map does not recognise the state of weathering of the rocks. This factor may drastically alter the whole nature of the rock and consequently affect its stability potential.

At this point the information obtained from the topographic map with slope classes and the geological map can be combined. This will indicate areas that may be unstable or potentially unstable. These areas will require more detailed inspection at the next stage in the zoning process which involves direct field observation.

1.3 Morphology

The geomorphic mapping process relies on field observation and the recognition of slope features associated with mass movement.

Some consideration of slope classes has already been made. The angles which are used as the class limits are chosen after an examination of active failures. An inspection of several recent failures in what appears to be the same geology will generally indicate a lower limiting angle. With so many factors influencing the stability of slopes, it might be thought that the slope angle is too simple a criterion to use, but an extended area of similar materials, where several failures can be compared has, in our experience, generally indicated a lower bound to the failing slope angle. This we have called the critical angle or threshold slope angle for the prevailing geology.

Where the geology changes, the critical angle will change also. Our areas show a variety of critical angles, for example in Tertiary lake sediments 7° is taken, while on weathered basalt soils 14° is used. It would be illusory to depend too much on these exact angles but the whole process of zoning is an approach to an ideal and the establishment of critical angles is a step on the way.

Slope segments are mapped in the field by outlining breaks of slope and slope angle measurements are taken by inclinometer. Comparisons may then be made between observed slope angles and the threshold slope angle. Slope mapping forms the basis of the geomorphic map. Features from the slope map which may indicate active or previous mass movement include arcuate scarps which may have become vegetated or subdued by erosion, benching of slope profiles often with backsloping areas, and unusual convexities or concavities of slope regions. Slope complexity has been used by us as indicative of the mass movement history of a slope region when compared with much simpler slopes profiles in adjacent areas on the same hillslopes.

The next stage of our geomorphic appreciation is directed to the surface drainage features. The textbook examples of drainage patterns are not uncommonly seen to be represented in the field, but in mass movement areas disruption of drainage is a marked characteristic. The scale on which this occurs is often not large enough to appear significant on a 1:100 000 topographic map, but on photos or in the field it is usually obvious. Simple stream flow patterns diverted by debris tongues, ponds behind rotated blocks, and the subsequent drainage along rather than across the contours of the original slope, seepages, hillside swamps with no outlet, small valleys containing paired streams, and many other anomalies in the surface hydrology can point to movement. Other features to be mapped include anomalous leaning or kinked trees and the universally present but ill-defined 'hummocky ground'.

All these features have been exhaustively described by others and Pulinowa et.al.(1977) have produced an atlas of symbols to represent the whole of the morphology. To these natural features may be added the stretching of fences, cracks in roads, walls, and pipes, the tilting, distortion and final destruction of buildings. All must be recorded on the geomorphic map.

At this stage the three major inputs will contribute to a map which will indicate active and inactive areas of mass movement. Features associated with such phenomena will be apparent and areas similar in slope, geology etc. can be outlined as regions of potential instability where caution may be required when landuse decisions are to be made.

1.4 The Age Problem

The problem of dating a particular landslip feature is perhaps the most difficult part of the zoning process. Underestimation of the age of a disrupted slope may lead us into conservatism so that even Pleistocene slope failures which may be perfectly stable under present conditions are considered unstable. The question that arises is what is the age of the disturbance? It is a question of real significance because any zoning scheme must be based on the realisation that it operates in a time scale short by geological standards, but long in comparison to the occupancy of a house. A period of fifty years is a convenient yardstick, almost a lifetime, long for a house of light modern construction, long enough to see several generations of active engineering geologists and to see dramatic changes in investigation technique. It is all the more reason for zoning to be placed on a practicable and defensible methodology for it is going to influence urban land use beyond the foreseeable future.

Dating old mass movements is difficult but where possible we can attempt to predict how soon the mass movement cycle will be repeated. The work of Hutchinson (in Skempton and Hutchinson, 1976) shows that in well placed cases dates can be found for old movements, but in Australia with less than two hundred years of recorded history the problem is doubly difficult. Currently active movements can be readily observed and the value of photographs, measurements and descriptions is important as features rapidly become indistinct either by natural erosion or deliberate concealment.

Mass movement is also part of the response of geology to climate so that climatic variation studies both in the long and in the short term are of some use. Rainfall variations are influential in controlling pore pressures in fissured clays and the monitoring of piezometers through several years has revealed some unexpected and significant behaviour in relation to landslide movements (Knights and Matthews, 1976). Rainfall records can usefully be reviewed against historical accounts, although correlations based on newspaper articles have not been very successful. Beyond rainfall records, recent advances in Holocene climatology may enable the truly fossil movements of the end of the last glacial stages and beyond to be separated out. In our case the sheer size of what we believe to have been Pleistocene failures compared with modern failures, together with the anomalous relation to what are now permeable sediments, enable us to distinguish them with some confidence.

The problem of the role of vegetation in controlling stability is still with us. It cannot really be regarded as established that vegetation invariably increases stability. It depends too much on what vegetation, what climate, and what kind of slopes are involved.

A consideration of the age of a landslip movement is therefore important in our decision making process when trying to ascertain if these areas are currently stable and are likely to remain stable within the life of the landslip zoning system.

1.5 Detailed Studies

We must now turn to the crux of the zoning problem where we see landslides in action. Working in this field where potential failures or long term stability are everyday concepts, the sight of a slope actually undergoing failure is a sobering experience. When the slope is actually failing, it is possible to say that the factor of safety is less than unity, that the many conditions for failure are satisfied, that doubts are removed and, however the process works, it is doing so here and now. A failure provides an example of the process that is of great value for it is then possible to investigate a real example, not a scenario or a potential situation.

The methodology is the same as in a regional analysis. The topography of the slide and its immediate surroundings, and the geological setting must be discovered. The materials present must be examined and sampled by drilling, and the soil parameters and water conditions determined. The changes in time in water conditions, particularly of pore pressures must be recorded. The variability of these is of particular importance in analysis.

With this sum of information we must proceed to set up an analysis of the failure so that the limits of the input parameters may be found and to check for realism. Classical analysis after Bishops simplified method, or for shallow slab failure, after Skempton and De Lory is known to be incapable of coping with the real world facts of progressive failure or long term stability. Many other formulations are current but none show any advantages in the real world, and stability analysis must be recognised for what it is, a simplified mathematical model of the failure process to be considered as another tool useful in the assessment of stability but no more credible for its numerical appearance.

Stable areas where no sign of past movements can be distinguished and dormant areas where past movement is known or suspected must also be subjected to analysis. The determination by back analysis of acceptable values of input parameters must be made as a parallel to the work in active areas. The stability of the stable areas as well as the failure of the active areas must be confirmed by analysis.

The empirical methods outlined by Stevenson (1977) have some relevance here for they enable the relative stability of an area to be estimated in relation to the analysed areas. Analysis cannot be used in a great number of locations for reasons of cost and effort, but if it can be used in the more critical places, then other similar locations can be estimated with perhaps only a minimum of groundwater information.

2. THE ZONING SCHEME

We have now accumulated a great deal of information on the area to be zoned, and we must now turn to the task of synthesis. The zoning scheme can be considered as land use planning with respect to a geological hazard that is the risk of landslip movement.

Zoning has always been conceived in our minds as a control on the development of dwelling houses. Any larger structures are not generally built or owned by individuals on their own financial resources, and the impact of damage is borne corporately. In most countries landslides are not an insurable risk and every possible precaution must be taken to avoid damage as the cost falls heavily on individual owners. In those countries where some corporate risk is borne, this does not relieve the cost but only spreads the impact.

Larger structures, public buildings, installations, road and rail routes all carry with them the assumption that adequate investigation has been made in the course of which the landslide risk has been recognised and minimised either by design or relocation. If the assumption is invalid then damage may result, but it will be borne by the community at large and not by an individual.

2.1 Descriptive Zones

In this State a two-tier zoning scheme has evolved. The lower tier is descriptive, and until recently consisted of the following classes:

I Stable ground on hard rocks.

II Stable ground on soft rocks.

III Potential landslip areas.

IV Old landslips and adjacent areas.

V Active landslips and adjacent areas.

This system attempts to represent the geological truth as far as this can be known, in terms that any reasonable person can understand. The zones are advisory, are published in easily obtainable, cheap maps and are circulated to local councils and other interested government departments.

Zone I is, in our areas, normally on dolerite, basalt or sandstone, weathering is no more than moderate, and the soil cover is not normally greater than 1.5 m. It is essentially a zone where clay failures cannot exist and slope failures of other kinds are vanishingly small under the impact of urban housing. One cannot rule out the exceptional occurrence which may be brought about by a previously unknown phenomenon or incompetent building methods.

Zone II is those areas where clay and deep soil capable of slope failure exist, but slope angles are less than the minimum observed failure slope. These areas are often subject to a swelling soil problem, but this is not directly relevant.

Zone III is those areas where both sufficient slope and failure-prone materials are present, but where no failures are known to have taken place. Presumably the groundwater conditions are not such as to bring about failure, but the possibility exists that a change in conditions caused by development could precipitate instability.

Zone IV is those areas where sufficient evidence exists of past instability to warrant an assumption of reactivition, and those areas adjacent which such reactivition could endanger.

Zone V is those areas where measureable movement is taking place and those areas which could be endangered.

In the light of the analysis that has been described boundaries must be drawn on the zone map, on the strength of the topographic, geologic, and morphologic findings and with the assistance of the stability analyses, but without reference to existing man-made structures.

The Tamar Valley Region of northern Tasmania has been mapped as a series of 1:15 840 maps using the above five descriptive zones. This system is now to be simplified to a three zone system designed for ease of use by the public, local authorities and government institutions. The new three zone system is more proscriptive in nature and the zone definitions are broadly based on whether development may proceed without restrictions, may proceed with some restrictions or may not proceed at all. The three zones will be:-

1 Green Zone. Areas where no undue risk is recognised and building and development may take place under the normal control of councils under the Building Regulations.

2 Yellow Zone. Areas where doubts exist as to the stability of the area and a more or less detailed investigation is required before building can take place. Some or all of the terms of the special regulations for landslide areas (Building Regulations Part IV, Division 5, 1978) would apply, the impact of these depending on the results of the investigation.

3 Red Zone. Areas where active movement is occurring and building is prohibited.

In this three zone system the Green Zone would closely correspond to Zone I and II of the original system, the Yellow Zone would closely correspond to Zone III and some of Zone IV and the Red Zone would be similar to part of Zone III and Zone IV and all of Zone V. These zones can be defined descriptively for the benefit of interested authorities and persons.

In summary the lower tier, descriptive zone system is used to persuade the public, local councils and government authorities of the danger and risk of the landslide hazard.

2.2 Proscriptive Zones

The second tier of zones is brought into use when advice is no longer enough and compulsion becomes necessary. The zones are proscriptive, and are proclaimed under the State's Local Government Act (1974).

Legal sanctions sometimes become necessary when settlements have existed before the recognition of the extent and seriousness of the landslide risk. In this case, the risk must be made plain to the owners of houses in the area so that they may be able to take prudent precautions such as the maintenance of drainage or the avoidance of deep earthworks on steep slopes, and as a warning to intending purchasers.

It may also happen that entrepreneurs have committed themselves to the construction of housing before the recognition of the risk. They will of course wish to lose as little of their investment as possible, and the zones inform them of the constraints on building.

The proscriptive zones are known as A and B landslip zones under the Act. In an 'A' zone all building is prohibited with some minor exceptions. In a 'B' zone, buildings are controlled in respect of size, siting, drainage, earthworks and the removal of trees. Restrictions are included as Part IV, Division 5 of the Tasmanian Building Regulations (1978).

The problems that arise when landslip risks are first recognised are unavoidable. We have previously generally been consulted after the problem has occurred rather than during the initial development of potentially unstable areas. Local councils and Government authorities have now become more aware of the problem and little development of potentially unstable areas can now occur without inspection by the Tasmanian Department of Mines.

The relationship between the zones of the I-V scale of descriptive zones and the A and B proscriptive zones has evolved through usage, and introduces a useful degree of flexibility into the system. Originally, B, the zone where limited building could take place, was taken as equivalent to III and A as equivalent to IV and V. As the whole problem has been investigated and our confidence has increased, a partial relaxation has been made in zone IV. The term 'old landslips' has always included structures of a range of ages. The oldest of these, probably originated under different climatic conditions and are now quite stable, and so can be released for controlled building. Different parts of old structures also vary in their potential for failure. The heel area is often quite stable, while the over-steepened toe zone may still show parasitic modern failures.

Another advantage of the two-tier system of zoning is that amendments to the descriptive zones are easily introduced as they arise from detailed investigations, while proscriptive zones require a statutory process. In practice, even the first kind of amendment has not been very common, and the original descriptive zones have proved to be a good general guide.

Any recommendation for the proclamation of Landslip Areas under Section 431A of the Local Government Act No. 2, 1973 would necessitate a transformation of the Green-Yellow-Red zones into 'A' and 'B' areas in the same way as has occurred previously with the five zone system. Broadly Yellow areas would become 'B' landslip areas and Red areas would become 'A' landslip areas, not automatically but after specific investigation and recommendation by the Tasmanian Department of Mines.

2.3 Problems of Administration

The administrative procedures have not functioned well. Little guidance can be offered in this respect as the political climate and that of public opinion, and indeed the whole physical circumstances surrounding the social impact of the landslide process are likely to be quite different in another society.

Briefly, the proclamation process is initiated by the geologists working on the landslide survey. They become aware of damage or the risk of damage and of the possibility of social loss. The geological and morphological circumstances are closely examined, and if time permits, some subsurface work is done, mainly to establish material properties and water conditions. A recommendation is then made by the departmental director, and is passed to the local authority (council) of the area concerned, which has the responsibility of informing all landowners that zoning has been recommended, and calling for objections.

The whole confrontation has culminated in the past in an Objectors Meeting, where objectors are able to meet the geologists. These meetings, surprisingly, are often able to calm the worst fears of some objectors, and to explain the logic of the recommendation to those affected. While not a pleasant experience for the geologists, it is an interesting and useful one, both in appreciating the effect of the investigation and in conveying difficult scientific and technical concepts to an interested and unsympathetic section of the public.

The inability of the council to identify and inform every involved landowner has proved to be the greatest stumbling block, especially when proclamations have to be made in already built-up areas. This process has tkane more than two years, and in one case has had to be abandoned. A simpler and perhaps less scrupulous process may have to be adopted.

The impact of a proclamation depends on the state of development. Where little or no work has been done on the ground by the developers, and the land is still rural, the effect is simply to prevent or restrict building. In 'B' areas, where restrictions apply, some discussion takes place on the exact details of what may be built where, and how adequate stability may be achieved. These discussions are a fertile source of ideas for construction methods, and some progress has been made in using 'B' areas wisely and well.

Where a developed township is proclaimed, the main effect is on new building, which is either prohibited, resulting in open spaces being left or is again restricted. Proclaimed areas in towns are usually those where some destruction of houses has taken place and the open spaces are readily accepted, and become parks or lesser amenity areas. Proclamation in areas of damage is easily achieved as little persuasion of its necessity is required. In areas of potential instability, the whole process of conviction must be worked through and is only ever partially successful.

The loss of land value is probably the greatest complaint aimed at the zoner. His reply generally takes the form that he is merely restoring to the land the correct value that was previously overestimated in error. To the charge of arrogance in presuming to do so, he can only reply that the care he has taken is demonstrably greater than that used in the first place when 'market forces' operated. We are not aware of any systematic studies that have been made of changes of value in the market as a result of landslide zoning, although valuations for taxation purposes have been altered on an 'ad hoc' basis.

Generally the descriptive five zone maps have proved useful in the majority of areas where little or no development has occurred. The local councils and government authorities may use these to control the development of these areas by acting on the advice of the Tasmanian Department of Mines without the need for proscriptive zone proclamation. The proposed new three zone proscriptive maps will work in the same way as the previous system but will be easier for the public, local councils and government authorities to interpret.

3 CONCLUSIONS

This paper has outlined the methodology behind the development of a descriptive and proscriptive landslip zoning system currently in use in the State of Tasmania, Australia. A new three zone descriptive system that has evolved from experience with the previous system and which is to be used in the future, has also been discussed.

The implementation of the zoning process is to constitute a warning to those who seek to use the land that instability is, or may be, present. If it is, let them beware. If it may be, then the use and value of the land may be protected by prudent precautions. Forewarned is forearmed.

If warnings fail, are inaccurate, or come too late, loss can result, and can be protracted and devastating both materially and spiritually for the individuals and families affected. Only those who have suffered such a disaster can appreciate the effect of it.

Landslides are unique among natural disasters in that they are uninsurable. Why this should be so may be related to their comparative rarity, their usually small area of impact, and their often slow and unspectacular behaviour. Floods, fires, earthquakes, cyclones and tsunamis, none fulfil these three conditions, and so have attracted public attention and consequent sympathy for their victims.

Landslides have been regarded as 'acts of God', a lawyers term implying a blind unpredictability. This paper attempts to show how a system has been evolved to establish landslide zones, and so predict as far as is presently possible the risks of this disaster. The establishment of insurance should now be possible.

4 ACKNOWLEDGEMENTS

We wish to acknowledge the work of our colleagues of the Tasmanian Geological Survey and the benefit of discussions with them, from which this system of zoning has evolved during the last ten years.

This paper is published with the permission of the Director of Mines, Tasmania.

5 REFERENCES

DENNESS, B. (1972). The reservoir principle of mass movement. Rep.Inst.Geol.Sci. Vol.72, No.7.

KNIGHTS, C.J. and MATTHEWS, W.L. (1976). A Landslip study in Tertiary sediments, northern Tasmania. Bull.Int.Ass.Engng.Geol. 14:p.p. 17-22.

MILLER, V.C. (1961). Photogeology. McGraw-Hill : New York : p.p. 48-50.

PULINOWA, M.A., PAWLAK, W. and WOROPAJEW, E. (1977). A contribution to the problem of morphogenetical principles of landslide mapping. Bull.Int.Ass.Engng. Geol. 16:p.p. 56-62.

SKEMPTON, A. and HUTCHINSON, J.N. (1976). A discussion on valley slopes and cliffs in southern England. Proc.Roy.Soc. A283:p.p. 557-604.

STEVENSON, P.C. (1977). An empirical method for the evaluation of relative landslip risk. Bull. Int.Ass.Engng.Geol. 16:p.p. 69-72.

TASMANIA (1974). Local Government Act (No.2) 1973. Acts - 71(96):p.p. 915-919.

TASMANIA (1978). Building Regulations 1978. Stat. Rules 1978 No. 135.

A Classification of Weathered Foliated Rocks for Use in Slope Stability Problems

RODOLFO T. SANCIO
Associate Professor, Universidad Simon Bolivar, Caracas, Venezuela
IAN BROWN
Post Graduate Student, University of California, Berkeley

1 INTRODUCTION

A universal classification system for use in rock engineering is an ideal sought by numerous workers. The objective of such a classification is to group the wide variety of rocks in a few categories to allow a prediction of their engineering behaviour. Although various restricted classification systems are used, as far as we know there is no universal classification.

Classification systems have been developed that are related to specific engineering problems such as tunnel design (e.g. Terzaghi, 1946, Deere et al., 1967, Bieniawski, 1975, Barton et al., 1974). Of the few classification systems that have been proposed for use in rock slope engineering, Goodman and Duncans' (1971) is considered to be most useful. Classification systems which are based on the final morphology of a slope rather than the mechanisms involved in failure have limited application in slope design.

This paper describes a simplified classification system for use in the design of cut slopes in foliated rocks. Rock weathering, which influences all rock engineering carried out near the ground surface, is given special consideration. The classification has been used in the design of slopes in the Caracas (Venezuela) area, for the design of low cut slopes which are not normally subjected to a geotechnical investigation and analysis. Such slopes are commonly found in housing subdivisions and along transportation routes.

2 A REVIEW OF ROCK CLASSIFICATIONS

A common area of debate in the earth sciences literature is that of the boundary between rock and soil. In the field of slope engineering, different behaviours have made it necessary to differentiate between rock, weathered rock, and soil.

The American Geological Institute (1957) considered rock to be 'any consolidated or coherent and relatively hard, naturally formed mass of mineral matter'. The practice of defining rock in some other manner to facilitate a particular project is considered misleading and unnecessary, as rock is the same regardless of the nature of the study.

The classical rock names used by geologists can serve a useful purpose for the geotechnical engineer. Names are based on mineral composition and texture, which in turn influence the physical properties of the rock. Terms such as granite, limestone and schist immediately convey to a geotechnical engineer an impression of a material that has a predictable range of behaviours. Such rock classes are easily mapped, thus providing the geometric framework for the material that the engineer will have to work with.

The genetic classification of rocks into the categories of igneous, metamorphic, and sedimentary has been widely used for engineering purposes. The predominant feature of metamorphic rock is a foliation due to coplanar platy minerals such as mica, causing strong anisotropy and surfaces of weakness within the scale of a specimen. These small scale structures and oriented minerals strongly influence rock behaviour.

Soil, according to the American Geological Institute (1957) is 'that earth material which has been so modified and acted upon by physical, chemical and biological agents that it will support rooted plants'. Other terms which are sometimes used for this material, such as saprolite and regolith, only tend to complicate the terminology. Unlike rocks, soil genetic classifications seem to be much less adaptable to the needs of engineering. This was undoubtedly why geotechnical engineers devised a unified classification of soils (U.S. Bureau of Reclamation, 1960).

Various general engineering classifications of rocks can be found in the literature. Some are based on the properties of small rock specimens (e.g. Coates, 1964, Deere et al., 1967) and others considered the properties of the rock mass (e.g. John, 1962, Muller and Hoffman, 1970). These classifications have been used in different ways, but in most cases it has been found that their application to design in rock is limited. Relatively sophisticated rock classifications have been devised, especially for use in tunnel design. It is our impression that these classifications are being used with little regard for their inherent limitations, and in some cases are applied to different design problems than were originally intended. There is the danger that people who do not understand geological materials may use a 'cookbook' approach to rock engineering.

3 ROCK WEATHERING

Rock weathering effects are greatest near the ground surface, with a wide transition between material commonly described as rock, and that commonly described as soil. When undertaking near-surface construction in rock, the weathered nature of the rock strongly influences its behaviour. In tropical and subtropical areas with warm temperatures and high annual rainfall, the depth of weathered rock may be considerable, sometimes greater than 30 m.

Much research has been devoted to weathering of rock and its constituent minerals, and a useful weathering classification proposed by Saunders and Fookes (1970) has been widely adopted. In their classification of rock weathering, they distinguished five categories in the range from slightly weathered rock to residual soil.

In a cut slope, the physical properties of the rock may vary with depth reflecting the weathering profile. Also the physical properties may change with time following excavation of the cut slope. This is due to acceleration of weathering caused by changes in the groundwater level, and hydrolysis combined with repeated leaching with fresh rain water.

Deere and Patton (1971) reviewed the weathering profiles for igneous and metamorphic rocks as defined by various workers. Some of the criteria that they used to define weathered rock can be misleading. For instance, R.Q.D. (Rock Quality Designation, Deere et al., 1967) should not be used to distinguish different weathering zones; low R.Q.D. may be due to natural rock discontinuities rather than disaggregation following weathering. Permeability is also not a reliable index for weathering as soils and unweathered rocks can show a great range in permeabilities.

4 A CLASSIFICATION FOR WEATHERED FOLIATED ROCKS

A suitable rock weathering classification is one which follows a logical sequence, uses familiar terminology, and is relatively simple to use. Each horizon of the weathering profile should describe a rock mass with characteristic features, allowing the estimation of common and/or extreme indices obtained from site investigations that are normally part of a slope stability study (surface mapping, petrological identification, and drilling). Provided there are no major lithological or structural changes in the area of the project, each weathering horizon should be so defined as to allow its study as a unit. Common physical properties can then be assigned based on testing, previous experience, or preferably by back-calculations.

The classification outlined in this paper is intended to be applicable to foliated rocks, which are often subject to chemical weathering due to a high feldspar content. The classification consists of two parts. The first considers the weathered nature of the rock (Table I) and is based mainly on the work of Saunders and Fookes (1970). Their division of weathered rock into highly, moderately, and slightly weathered has not been followed because from our experience in Venezuela and New

TABLE I

ENGINEERING CLASSIFICATION OF WEATHERING PROFILE FOR FOLIATED ROCKS

Term	Abbreviation	Description	Behaviour in Slopes**
	T S	Top soil with roots and organic material (humus).	
Residual Soil	R S	The rock is discoloured and is completely changed to soil with the original fabric completely destroyed. Rich in clay sized minerals, leached in its original soluble constituents. Characteristically rich in iron aluminum oxides and hydroxides, and silica. Parent material may be indicated by isolated fragments. Inherited structures, if any, do not modify the mechanical behaviour of the soil mass.	Ravelling and slumping materials.
Completely Weathered or Decomposed Rock	D R	The rock is discoloured and is apparently changed to a soil, but the original fabric and structure are mainly preserved. Minerals are dull, feldspar is mostly converted to clay, and other minerals, except quartz, are altered. Although the matrix is partially disrupted and the rock may crumble under the pressure of the fingers, its behaviour depends on some of the parent rock features (i.e. fabric or structure)	Typically slumping rock with part of the failure surface controlled by fabric or structure.

Continue Table I

(Engineering Classification of Weathering Profile for Foliated Rocks)

Term	Abbreviation	Description	Behaviour in Slopes**
Weathered Rock	W R	The rock is discoloured; discontinuities may be open and the alteration penetrates deeply inwards. The material near the discontinuities may be completely weathered, and the rock material may be weaker than the fresh rock.	Typically foliated rock, but slabby, buttressed and blocky rock behaviour also possible due to heterogeneity and joints. Shear strength mainly determined by the decomposed rock along discontinuities Failure surface mainly controlled by fabric and structure.
Fresh Unweathered Rock	F R	The rock may be slightly discoloured; discontinuities may be open and have slightly discoloured surfaces; the rock material is not, as determined in the field, weaker than the truly fresh rock	Typically sheeted, slabby, buttressed and blocky rock behaviour. Shear strength controlled by the discontinuities and the matrix of the fresh rock. Failure surface is controlled by fabric and structure.

**Designations according to Table II

Zealand, little relevant difference in slope behaviour is expected from variations within the group of weathered rock. The weathering classification is then used in conjunction with a classification of rock masses for surface excavations proposed by Goodman and Duncan (1971), (Table II).

5 CASE HISTORY

During 1971 and 1972, an extensive study was made of a suburb in Caracas that contained many landslides (Sancio and Mejia, 1972). Landslides that occurred in the period 1961 to 1971 had caused 54 deaths and left more than 4000 people homeless. The area investigated covered about 365 hectares, and included 3 kilometres of the freeway that connects Caracas with its seaport and airport. The majority of landslides occurred in areas where the rock was predominantly calcareous schist. Its behaviour was of type 4 and 5 (ravelling and slumping rock) as described in Table II.

Initially an attempt was made to subdivide the

TABLE II

CLASSIFICATION OF ROCK MASSES FOR SURFACE EXCAVATIONS
(after Goodman and Duncan, 1971)

	Type	Description	Attributes
1.	Strong homogeneous rock	Rock comparable in strength to concrete and free from discontinuities or chemical defects.	Stable vertical slopes of great height.
2.	Weak homogeneous rock	Rock much weaker than concrete, free from discontinuities or chemical defects.	Safe angle depends on height. It can be determined by soil mechanics techniques.

Continue Table II

(Classification of Rock Masses for Surface Excavations)

	Type	Description	Attributes
3.	Terraced rock	Horizontal beds varying from strong to weak forming a heterogeneous mass. Free from discontinuities or chemical defects.	Safe angle varies from point to point. Groundwater regime can be significant. Soft seams can control overall strength.
4.	Ravelling rock	Rock free from defects but susceptible to break up by weathering. Columnar jointed rock, friable sandstones and conglomerates, closely fractured shales.	Base of slope covered with running material. Benches and walls necessary for protection.
5.	Slumping rock	Altered or clay rich rock with very low strength: major fault zones; montmorillonitic compaction shales; hydrothermally altered zones; highly weathered zones.	Retaining walls, gabions or rock blankets and horizontal drains required. Frequent maintenance necessary.
6.	Sheeted rock	Hard, strong rock with planar weaknesses roughly parallel to natural slopes; commonly granitic rocks.	Drainage of sheet joints essential if natural slope is steeper than about 30°. Rock bolts can be used to tie sheets together.
7.	Slabby rock	Hard rock with one strongly developed set of discontinuities which control the strength of the mass. Typically, silty shales and shaly limestone.	Support may be required if slabs daylight and are inclined more steeply than friction angle Ø. Ø determined from direct shear tests and field observations.
8.	Buttressed rock	Hard rock with two sets of weakness planes which dominate the rock mass strength. Line of intersection of weakness planes delimits buttresses.	Benches or possibly retaining walls necessary. to hold blocks if line of intersection is steeper than about 30° and undercut by slope.
9.	Blocky rock	Hard rock with 3 or more sets of weakness planes which dominate the rock mass behaviour; typically, quartzite limestone, jointed granites.	Benches necessary to accumulate fallen rock. Wire mesh and gunite may be necessary to prevent rock falls, especially if joints are very weak. Rock bolts on pattern can be used.
10.	Foliated rock	Foliation planes, usually steeply dripping, control rock mass behaviour; mica schists, phyllites and slates.	Creep leading to slump-like slides may occur as leaves of rock gradually deform. Particularly severe where rock is highly weathered or foliation is controlled by mica.

weathered rock according to the classification of Saunders and Fookes (1970), however the subjective nature of the classification caused some difficulties. The degree of weathering and the physical condition of the rock were determined by comparing the description of the material with index properties and drilling characteristics (Table III) and the subsoil profile was subdivided according to the nomenclature and criteria outlined in Tables I and II.

TABLE III

ESTIMATION OF ROCK QUALITY BASED ON DATA OBTAINED FROM STANDARD EXPLORATION DRILLING

Term	Abbreviation	Index Properties and Drilling Behaviour
Soft rock	XRsx	Not recoverable by drilling[1] The split spoon penetrates at at least 10 cm with fewer than 100 blows[2]
Hard Rock	XRhx	Can be continuously drilled only with a diamond bit.
Fractured Rock	XRxf	R.Q.D. < 100%
Sound Rock	XRxs	R.Q.D. = 100%

[1] NW-size bit, double barrel
[2] SPT (Standard Penetration Test) procedure

Notes
In the abbreviations, X stands for either W (Weathered), or F (Fresh), or D (Decomposed). In the categories of Soft Rock and Hard Rock, x represents either f (fractured) or s (sound). In the categories of Fractured Rock and Sound Rock, x represents either s (soft) or h (hard). Decomposed rock is normally soft and fractured, hence the letters s and f are not used with this abbreviation.

It was found that the area most affected by landslides could be subdivided into three major units:
a) Decomposed rock (DR) and weathered, soft, fractured rock (WRsf)
b) Weathered, hard, fractured rock (WRhf)
c) Weathered, hard, sound rock (WRhs) and fresh rock (FR)

Material parameters were deduced from back calculation of landslides, and from field shear tests (Table IV). Back calculations with standard slope stability analyses do not take into account the position and depth of tension cracks observed in the upper part of the slope. Therefore, a new approach to slope stability analysis was used, which makes use of the tensile strength of the rock (Sancio and Goodman, 1979).

TABLE IV

MATERIAL PARAMETERS FOR WEATHERED FOLIATED ROCK, CARACAS

Rock Mass Description	Unit weight ($kN\ m^{-3}$)	Angle of friction	Cohesion (kPa)
DR, WRsf	20,6	28°	9,8
WRhf	22,6	32°	10,2
WRhs, FR	24,5	32°	49,0

6 CONCLUSIONS

With the rock classifications presently available, we consider that sound engineering judgements based on considerable experience is required if they are to be used without any difficulties. For a classification of rock for engineering purposes to be useful, it must have a restricted function.

A functional, simplified classification system which has been used in the design of slopes in weathered foliated rocks is introduced in this paper. The authors have taken advantage of previous experience and used terminology familiar to both geologists and engineers.

Using the classification system, rock types shown in maps and cross sections can be labelled as indicated in Table III, using data easily obtainable from routine site investigations. Once the major rock categories are identified, strength testing and back-calculations of previous landslides can give, for each rock category, the parameters necessary for slope design. In slope engineering, these data will include the angle of friction, the cohesion, and the unit weight. Use of this classification together with simple testing and back calculations can lead to a considerable reduction in cut slope stability problems.

7 ACKNOWLEDGMENTS

The authors are grateful to the National Council for Scientific and Technological Investigations (COINCIT) of Venezuela, for their contribution to the preparation of this paper. Ian Brown has been supported by a National Research Advisory Council Fellowship while on leave from Department of Scientic and Industrial Research, Wellington.

8 REFERENCES

AMERICAN GEOLOGICAL INSTITUTE (1957). Dictionary of Geological Terms. New York, Dolphin Books.

BARTON, N.; LIEN, R.; LUNDE, J. (1974). Engineering classification of rock masses for the design of tunnel support. Rock Mechanics, Vol. 6, pp 189-236.

BIENIAWSKI, Z.T. (1975). Case studies: prediction of rock mass behaviour by the geomechanics classification. Proceedings of 2nd Australia - New Zealand Geomechanics Conference, Brisbane, pp 36-41.

COATES, D.F. (1964). Classification of rocks for rock mechanics. International Journal of Rock Mechanics and Mining Sciences, Vol. 1, pp 421-429.

DEERE, D.; HENDRON, A.J.; BARTON, F.; CORDING, E.J. (1967). Design of surface and near surface construction in rock. Proceedings of 8th Symposium on Rock Mechanics, Minnesota, pp 238-302.

DEERE, D.; PATTON, F. (1971). Slope stability in residual soils. Proceedings of Fourth Panamerican Conference on Soil Mechanics and Foundation Engineering, Puerto Rico, pp 87-170.

GOODMAN, R.E.; DUNCAN, J.M. (1971). The role of structure and solid mechanics in the design of surface and underground excavation in rock. Proceedings of the Conference on Structure, Solid Mechanics and Engineering Design, Part 2, pp 1379-1404.

JOHN, K.W. (1962). An approach to rock mechanics. Journal of the Soil Mechanics and Foundation Division, American Society of Civil Engineers, Vol. 88, pp 1-30.

MULLER, L.; HOFFMAN, H. (1970). Selection, compilation, and assessment of geological data for the slope problem. Proceedings of Symposium on Planning Open Pit Mines, Johannesburg.

SANCIO, R.T.; GOODMAN, R.E. (1979). Analysis of the stability of slopes in weathered rocks. Proceedings of the 4th International Society for Rock Mechanics Congress, Montreux.

SANCIO, R.T.; MEJIA, T.M. (1972). Informe geotecnico de los barrios Gramoven. Geodinamica S.R.L., Contract No. 13619 M.O.P., Vol. 1.

SAUNDERS, M.K.; FOOKES, P.G. (1970). A review of the relationship of rock weathering and climate and its significance to foundation engineering. Engineering Geology, Vol. 4, pp 289-325.

TERZAGHI, K. (1946). Introduction to tunnel geology. Rock Tunnelling with Steel Supports, (Proctor and White, eds), Commercial Shearing and Stamping Company, Youngstown, Ohio.

U.S. BUREAU OF RECLAMATION (1960). Earth Manual. U.S. Government Printing Office, Washington.

The Deterioration of a Dolerite Escarpment

P. C. STEVENSON
Engineering Geology Section, Tasmanian Geological Survey, Hobart

SUMMARY A dolerite escarpment above a mountain road near Hobart may pose a threat to tourist traffic, and a study has been made of several modes of deterioration. Relaxation, weathering and slow movement of dolerite columns leads to several kinds of instability, some of which can be dangerous. One phenomenon, the hinge block is of particular interest as its origin is obscure, but it does not present any danger.

1 THE IMMEDIATE AND BROADER PURPOSES OF THE STUDY

The writer is a geologist concerned with the geology of urban areas in Tasmania. This State has some pretensions as a tourist area, and Mt Wellington, the large mountain very close to Hobart is on the route of many tours by car and bus. The road to the summit passes diagonally across the mountain face as seen from Hobart, and close under the high cliffs just beneath the Pinnacle. In discussion with officers of the Hobart City Council, the question of rock-falls blocking the road and of the safety of traffic arose. The immediate aim of the study has been to examine the erosion processes operating on the mountain face, their nature, range, velocity and controls, so as to be able to form some idea of the hazard and risk. The broader purpose is to study the erosion processes of dolerite escarpments in general (and Tasmania has some 1 000 km of them) and perhaps shed some light on more complex hard rock escarpment failure. Little indeed has been written on the subject, and it is hard to find much outside general textbook accounts. Fairbridge (1968) gives some references but it is plain that the details of the mechanism from undisturbed rock to talus slope are largely unknown. Accounts mention isolated processes such as ice-wedging or the influence of water pressures, but the discrete stages in the process are not well known and in particular cases the rate of processes is usually guessed. Terzaghi (1967) gives an account of rock and rock joints, but is mainly interested in the stability afforded by cohesive and frictional properties and its maintenance rather than deterioration. Indeed he specifically says that his paper does not cover "rock slopes in (an) advanced stage of development". Yet this is the normal stage of a rock escarpment. New scarps are rare. Price and Knill (1967) is a detailed account of a particular investigation with a useful blend of geology and engineering, but is not much concerned with time-dependent mechanisms of deterioration. de Freitas and Watters (1973) deal with toppling failure and give some interesting examples, but do not deal with rock slope failure in general. Rock slopes in Tasmania have been dealt with by Hale (1957) who deals particularly with weathering and toppling is closely studied by Caine (1979).

2 THE DOLERITE SILL

Any visitor to Hobart immediately becomes familiar with Mt Wellington. The summit of the 1 270 m mountain is only 7 km from the city centre and it forms an impressive backdrop to the city.

The dolerite sill lies sub-horizontally on the top of the mountain more or less conformably on Triassic sandstones and fine Permian quartz mudstones (Leaman 1976). The sill is about 210 m thick and the upper part, judging from the mineralogy and crystallinity is missing. It was perhaps 300 m thick originally.

The dolerite is of tholeiitic basalt magma composition and is a complex intrusion, much faulted in the Hobart area (Leaman 1974). The mass capping Mt Wellington is however almost a simple slab and is thought to be distant about 5 or 6 km from each of three feeders.

The most prominent feature of the escarpment face overlooking Hobart is the Organ Pipes, a face formed of dolerite columns 100 - 200 m high, but even the less prominent parts of the face are columnar also. The rock being almost constant in composition, with little gross variation even in grain size and a consistent columnar jointing makes it a good subject for a study of erosional deterioration.

3 STAGES OF DETERIORATION

A full account of the deterioration process must encompass every stage from the erosional uncovering of the dolerite slab from its sandstone roof-rock right through to the development, weathering and final disposal of the taluses. This ideal is not possible here and this paper should be regarded as a preliminary attempt to examine some of the questions raised by this very large phenomenon. Three in situ stages will be described, corresponding to the degree of confinement of the rock columns. The slab stage shows three-dimensional confinement with more or less retention of elastic stresses. The screen stage shows rows of columns standing free of the main mass, and the pillar stage shows remaining columns standing free of each other. Each stage has characteristic features which pose fascinating questions.

The intact slab was intruded into its Triassic sandstone-mudstone host rock in early Jurassic times (Leaman 1974) without catastrophic distortion, although some undoubtedly contemporaneous faulting occurred. No erosion can take place without uplift and this took place to expose the edge of the slab, on one of the many faults mapped in the Hobart area. No trace of this first cause of the escarpment now

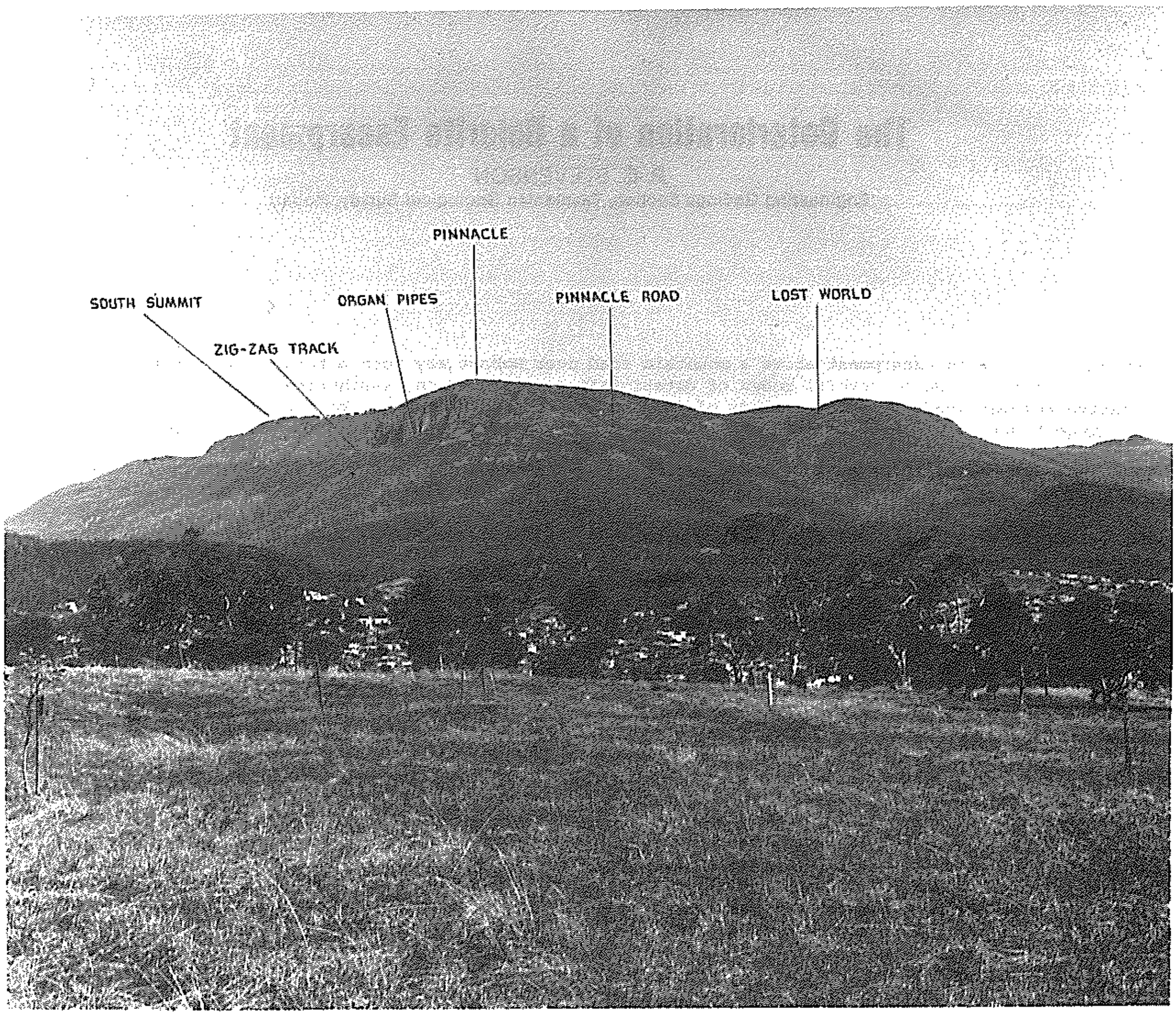

Figure 1 Mt Wellington seen from Hobart Domain. Localities mentioned in the text are indicated.

remains, and we can only consider the erosion as a continuing process. We can deduce that the uplifted slab retained its sedimentary cover for some time, but this was removed by erosion as were some scores of metres of the dolerite and the erosion process then took roughly the form we see in operation today.

3.1 The Role of Relaxation

We would expect the slab to contain some in situ stress. A major part, that arising from its thermal origin, would be lost in the development of the columnar joints but it appears to retain considerable tectonic as well as lithostatic stresses (A.J. Bowling, pers. comm.). Such results as exist parallel closely the work of Lee (1978) on the Niagara escarpment. The formation of a scarp face allows stresses to dissipate locally and this may be shown by seismic traverses observed on top of the mountain normal to the scarp face. These show that a higher velocity zone may be detected becoming shallower as one moves away from the scarp.

The relaxed edge of the slab is attacked by processes to be described in the next section, but the top surface is also attacked by weathering down the lines of weakness created by the thermal columnar joints. The rock is not chemically very stable and in the presence of water easily weathers it to a reddish (or in reducing conditions) a greenish clay. This material is fairly impermeable and expansive, and readily blocks the joints, so that weathering penetration is limited vertically to a few metres where columns are well confined. Clay mineralogy is variable (see Hale 1957) but kaolin and montmorillonite are usually present, the latter particularly in ill-drained situations (W.L. Matthews, pers. comm.).

The simple picture of a relaxing slab edge is confused by the great variety of resulting effects, but two localities may be described to illustrate it. The back face of the Lost World (Fig. 1 and Fig. 2(a)) consists of a row of columns 1 - 2 m across and standing about 30 m high.

In many places this now stands a metre or so clear of the main slab behind so that a chasm is formed 30 m or so deep and often bridged by fallen blocks. It is difficult to see how this chasm can form except by slight outward toppling of the screen or by bodily translation outward. Time and again one

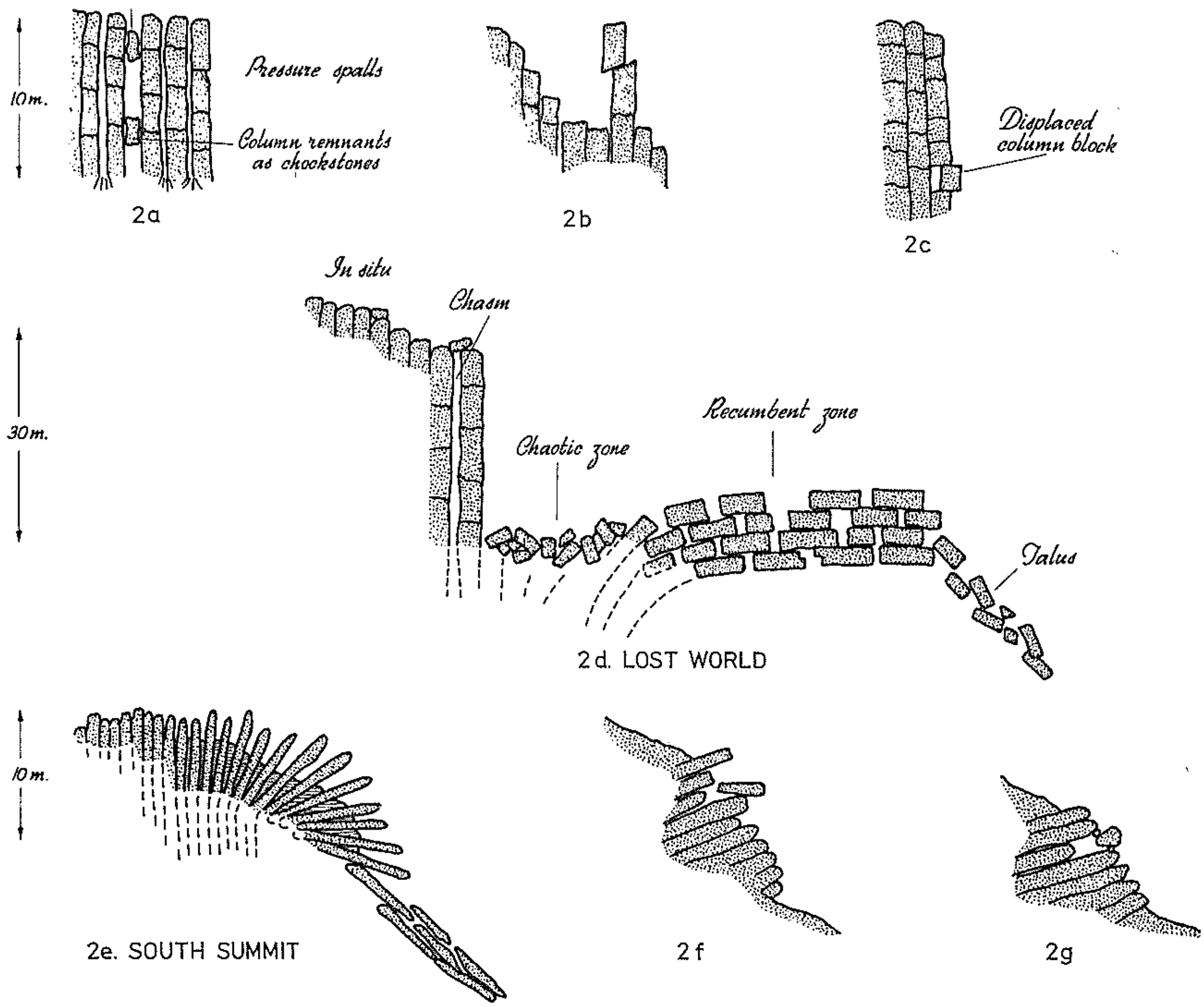

Figure 2 Features of dolerite escarpment deterioration

is confronted by dilemmas of this kind where no reasonable explanation seems possible and one has to choose the least unreasonable one. In this case the toppling explanation seems possible and we shall return to it. The second localities where one may see the effect of slab-edge relaxation are those mountain slopes to the north and south of the Zig-zag Track where vertical columns stand in turreted formations, apparently becoming more and more isolated from one another. It is not clear whether this increasing isolation is all caused by lateral movement of columns or partly by the weathering process described in the next section.

3.2 The Role of Weathering

The impact of weathering on the top of the slab has been mentioned. Decreasing confinement means that more faces are exposed to weather. Two modes of weathering are evident on the dolerite of the mountain. These might be called the high- and low-exposure modes. The first is seen on rock faces well-exposed to the rain, snow, wind, and frost of the alpine climate. The surface of the rock turns brown and becomes very rough from the evident etching-out of more vulnerable minerals. A skin of brown oxidised and hydrated rock forms up to 20 mm thick but normally much thinner. A dimensional change occurs in this skin so that it readily spalls off, exposing unweathered blue dolerite beneath. Measurements with a Schmidt hammer show that a reduction in strength also occurs. The shed spalls collect at the foot of the surfaces, breaking up into a gritty crystal sand which soon disintegrates into clay soil. The spalling process is obviously a rapid one, as spalls may be seen lying on vegetation, and the fresh blue dolerite soon becomes brown. The process is a potent one in geological and even shorter time scales and results in thinning columns. It is of interest that the spalling phenomenon is not obvious on the rocks at Mt Wellington Pinnacle and only becomes common at distances of about a kilometre from it. The reason seems to be that the Pinnacle rocks are climbed on by a great number of visitors and the fragile spalls never grow to any size before being broken off.

The clay soils produced from the disintegrating spalls and from the rain-washing of weathering rock faces accumulate round the bases of columns and faces and become insinuated into the opening joints below. This is the low-exposure weathering situation. High exposure implies large and rapid temperature and moisture variations wind and rain splash, free access of air, sun and frost.

Low exposure implies fairly constant temperature high and constant moisture, water and snow ponding, and protection from frost and sun with rock faces mantled in clay and vegetation. In such conditions the proportion of montmorillonite increases and expansion and contraction of clay becomes important.

When weathering and relaxation act on screens or rows of columns the spaces between them increase from about 1 mm to perhaps as much as a metre. This appears to be brought about by lateral translation of the columns but probably to a greater extent by column thinning. At 1 mm per year the column will be drastically modified, so that individual columns may drop out of their row. Evidence that this has happened is provided by those cases illustrated in Figure 2(a) where column sections are left suspended as chock-stones while the remainder has disappeared. The increasing instability of the remaining columns enables them to grip the chock-stones firmly.

When columns become isolated either on top of the slab as tor-like masses, or on the slopes as castellated areas, the effect of high exposure weathering is fully felt. The thinning-down columns become increasingly unstable as their aspect ratio increases. Angular faces become increasingly attacked and therefore more rounded and the articulating joints of each column become rounded also. The rainwash is carried down each column and readily enters sub-horizontal joints providing a clay pad in the joint. Increasing instability produces slight toppling and the increase of pressure on the side of the column towards which it is moving spalls off a part of the corner (Fig. 2(a)).

The clay pad in an articulating joint may aid what appears to be a slow creep process on inclined joints when the upper part of a column becomes increasingly eccentric on the lower part (Fig. 2(b)). The reality of high-stress accelerated weathering in this situation is an unanswered question. The situation illustrated in Figure 2(c) is not unique and if it were not for the sizes of blocks involved one might suspect the hand of the practical joker.

Weathering, the resulting thinning and loss of confinement and the failure of joint surfaces will finally bring about the fall of individual columns, triggered perhaps by snow loading, wind, the swelling of clay in joints or growing vegatation. These processes are understandable and the probability of failure of columns could be mapped. But this course to failure is not universal and at least two other processes are illustrated on a large scale on Mt Wellington.

4 HINGE BLOCKS

The area known as the Lost World illustrates the feature named a hinge block by Prof. J.L. Davies. The essential elements are as shown in Figure 2(d). The in situ slab and the free standing screen have already been mentioned. Below this 30 m high face lies a jumbled mass of column sections, the chaotic zone, and outward again the recumbent zone, where 30 - 40 m of disarticulated but still easily matched columns lie almost horizontally in a stack at least five high. It is as if a section of the scarp face about 120 m long had fallen outward but had miraculously remained almost intact. Towards the scree slope the columns tilt over and fall to become incorporated in the random tumble of blocks.

How does it happen?

Could the columns actually be in situ? The orientation of columns is generally accepted to be the result of the heat-flow during cooling, so that columns form normal to isotherms. This could hardly be the case at the Lost World for it would imply a sharp discontinuity in the heat flow. Horizontal and vertical columns exist alongside each other at the sides of the structure. Neither does it seem possible that the fall was catastrophic. Any rock fall involving a mass of columns five deep, falling fifty metres and rotating through a right angle could hardly fall so as to retain mutual relationships. The block glide process could deal with this mass, but could not produce the rotation.

We do not see any process operating today which could form the hinge block, unless it were very slow, too slow to be deduced or detected by observation. We must look for a powerful but slow agent not presently active and an obvious one is the harsh climate of the last glacial maximum. This may be assumed to have produced thick though not necessarily permanent mantles of snow and ice particularly on the lee sides of mountain tops. Ice consolidating around barely stable groups of columns could have cemented them together and not only caused them to topple but also cushioned their fall. The columns would have bent over and been lowered into their present position to be subsequently freed from their jacket of ice. If this picture is true then the presence of more inclined columns and possibly talus under the chaotic zone would confirm it.

The Lost World is an excellent and well exposed example but recumbent columns are common elsewhere on the mountain face. Above the Zig-zag Track they are very common and exist in hundreds, inclined at about 10° into the face. There the upper surface is not clearly exposed, being mantled in blocks and soil from above. Nevertheless the column ends project from the slope and climbing amongst them reveals the same disarticulated but still recognisable columnar mass. In this location too, no vertical back face is apparent, as if the chaotic zone had expanded to fill the void and mantle the whole structure.

5 TILTING

The South Summit of Mt Wellington shows another process of deterioration, illustrated in Figure 2(e). The nature of weathering and the production of clay soils has been mentioned. Where vertical columns become thinned down the resulting clay may accumulate round column bases so that each becomes clay-socketed. In these low-exposure conditions the column bases may be strongly attacked. When toppling finally supervenes, columns can move individually but are restrained by the clay socket, and by interference of the column roots in the clay matrix. Seasonal wetting and drying of the clay enables periodic movement to take place and the result is the slow-motion falling illustrated. An abundance of long thin columns provides ample space for the clay bed to form and control the process.

Soils, both as expansive clays and as hosts for vegetation appear to be important in many parts of the deterioration process. When a spring thus occurs after snowfall, a soil scar is apparent under almost every rock on soil mantled slopes. Its appearance is as if the soil and vegetation had moved 20 or 30 mm down slope leaving a bare soil rim below every rock. The reality of this movement has yet to be demonstrated.

6 PERCHED AND TRAPPED BLOCKS

Of the many peculiar items of dolerite escarpment deterioration, two others deserve mention. Rocking boulders are quite common in other rock terrains, particularly granites, and one is illustrated, from east of the Pinnacle in Figure 2(f). The other item is shown in Figure 2(g). This 8 m^3 boulder is trapped between two projecting recumbent columns and is retained by two hand-sized chocks, one on each side. Were it not for the size and precarious position of this rock and the sheer difficulty and danger of making this arrangement one might again suspect a practical joker. As it is, the explanation offered for both these items is a more prosaic one, where boulders becoming buried either in ice or soil are subsequently exhumed by melting or rainwash and the random contacts made while buried become temporary supports for a few.

7 CONCLUSIONS

From the descriptive work that has been done, it will be obvious that the aim of estimating risk of danger from rock fall is still far off. Nevertheless, if these are the sorts of mechanisms that operate they could perhaps be arranged in order of hazard. Perched and trapped blocks though unsafe are not usually large. Thinning, isolated columns constitute a much greater mass, and although they fall with less frequency are many times greater in number. Clay socketed columns and hinge blocks though interesting in their geomorphic implications are not an appreciable danger.

Such an ordering, combined with a locality map and a fall track map as has been used by D.G. Price (pers. comm.) would be a further stage on the way to a practicable risk estimate. In spite of the spectacularly precarious appearance of many blocks on the mountain, risks to persons and vehicles do not appear to be great, possibly because the rolling range of column sections is not as great as might be expected because of their elongated shape. The investigation is however too incomplete for complacency and work will continue.

8 ACKNOWLEDGEMENTS

I wish to acknowledge the help and the benefits of discussions with the many colleagues who have accompanied me on Mt Wellington. This paper is published with the permission of the Director of Mines, Tasmania.

9 REFERENCES

CAINE, N. (1979). The origin of large scale dolerite topples in the Ben Lomond National Park. Rept. to National Parks and Wildlife Service, Tasmania.

de FREITAS, M.H. and WALTERS, R.J. (1973). Some field examples of toppling failure. Geotechnique Vol. 23, No. 4, pp 495-514.

FAIRBRIDGE (1968) ed. The Encyclopedia of Geomorphology 1st ed. New York. Reinhold Corp.

HALE, G.E. (1957). Some aspects of jointing and decomposition in Tasmanian dolerites. Dolerite - a symposium University of Tasmania pp 184-196.

LEAMAN, D.E. (1974). Form, mechanism and control of dolerite intrusion near Hobart Tasmania. Journ. Geol.Soc.Aust. Vol. 22 part 2 pp 175-186.

LEAMAN, D.E. (1976). Geological survey explanatory report, Hobart Zone 7 Sheet 82 50,000 series Dept. of Mines, Tasmania.

LEE, C.F. (1978). Stress relief and cliff stability at a power station near Niagara Falls. Engineering Geology Vol. 12 No. 2 pp 193-204.

PRICE, D.G. and KNILL, J.L. (1967). The engineering geology of Edinburgh Castle Rock. Geotechnique Vol. 17 pp 411-432.

TERZAGHI, K. (1962). Stability of steep slopes in hard unweathered rock. Geotechnique Vol. 12 No. 4 pp 251-270.

Determination of Mass Moduli for Slope Design

B. A. CHAPPELL
Head Department of Geomechanics and Materials, Snowy Mountains Engineering Corporation
R. MAURICE
Civil Engineer, Department of Geomechanics and Materials, Snowy Mountains Engineering Corporation

SUMMARY Classification of rock masses is correlated with in situ moduli measured from jacking tests and theoretically derived moduli using composite elastic theory. A means of improving the in situ moduli by rock bolting is then considered. In order to assess the effectiveness of the remedial measure pseudo elastic theory is used to analyse the specific problem of slope stability. The results of the moduli changes due to rock bolts are checked by in situ jacking tests.

1 INTRODUCTION

This paper deals with the stability of soft-hard rock slopes where systems of joints and faults control the behaviour of the slopes. If the material is a soil or soft rock the various plastic design approaches varying from the Swedish Slip Circle to Janbo's wedge analysis are generally used. If the material is a hard intact rock an elastic design approach is used. In turn, if the material is neither plastic nor elastic in its deformational response, an elastic plastic analysis or pseudo plastic or pseudo elastic approach is used. When these latter methods are used the definition and determination of deformation moduli require careful consideration. Namely because in the deformational process the mechanisms of slip and rotation occur between and across the joint and fault systems. However, when stress or load gradients are minimal, Chappell (7), these latter mechanisms are also minimal and the representation of the jointed rock mass as a composite material in pseudo elastic theory is valid.

It is generally recognized that the deformational moduli obtained from relatively small intact rock samples are very much different to the deformational moduli of the jointed rock mass from which the intact rock samples are retrieved. Consequently, in situ testing techniques developed to measure the mass deformational moduli, are an important and essential part of the investigation program. In order to determine the moduli defining the constitutive relation some assumption or coefficient is applied to the measuring instrument, be it a flat jack, dilatometer, or plate bearing device. This coefficient is required in that it defines the boundary conditions and when used in conjunction with the elastic moduli gives the stress distribution. In a continuous or discontinuous material the constitutive relation is defined by the elastic modulus or pseudo elastic modulus. Consequently these moduli are very much dependent on the boundary interactions, and if the boundary conditions are ill defined and the mechanism causing deformation undefined then the evaluated coefficient of the measuring instrument is suspect.

Here the deformational response of the rock slopes is neither elastic nor plastic. With these aspects in mind a simple field test is devised to measure the deformational moduli of the jointed and faulted rock masses which have zones of hard and soft intact rock. Many of the slopes excavated in this material had failed and others were still to be excavated. Remedial measures to ensure the stability of existing and future slopes required careful assessment and design. A comparison of the measured moduli before and after slope stabilisation was the control criterion used to measure the effectiveness of the remedial measures and confirm the design process.

The rock material where the in situ moduli were measured was classified and collated with the various geological structural zones. From this the designed remedial rock bolt patterns for specific rock mass classes were allocated and documented. Consequently, the rock mass type encountered in the field was easily classified and the appropriate slope treatment defined.

2 SLOPE DESCRIPTION

2.1 Material Types

The geology of the site is not reported in detail here but the general characteristics of the material and profile of the slopes are given.

Because of the complexity of the geology and material in which the slopes are excavated it is important to classify the different rock zones encountered. An important addition of the classification used here was the measurement of the deformational response. From this the required remedial measures in the form of rock bolt patterns were determined by using a pseudo elastic design process. Three classification systems were considered namely those described by Barton et al (2) Bieniawski (3) and Wickham (4). Of these Bieniawski's RMR, rock mass rating, was used to define and assess the behaviour of the structural rock zones related to the excavated slopes.

The area in which the slopes were excavated is Jurassic in age and is highly crushed and contorted. Low grade pressure and temperature metamorphism occurs which causes a wide variation in the material types and fault-joint systems. The resultant materials are derived from sandstones and basalts giving quartzitic sandstone, greenstone, jasper and calcite. Superimposed on these metamorphosed material types are the geological structural features and resultant gouge material. The gouge is a breccia and mylonite material with seams of calcite, chlorite, kaolinite and montmorillonite being quite common.

When classifying both the material and structural zones (1), the rock mass is defined on a rating scale of class 1, 2, 3, 4 or 5 which in descriptive terms is excellent, very good, good, bad and very bad respectively. The slopes considered here were excavated in rock masses defined as class 4 and 5 with some class 3 in the upper regions of the slope. The heights of the slopes varied from 50 m to 130 m.

2.2 Material and Slope Profile

In many situations in practice the rock profile is generally such that the strength and deformational characteristics of the rock mass improve with depth. This is accepted as being consistent with the weathering profile and stress environment generally encountered. Here, however, there is a general improvement to a depth of about 30 m and then below this depth the strength and deformational characteristics markedly decrease with an increase in depth.

This means that as the depth of excavation is increased the toe of what was a stable slope becomes softer and deforms more readily. Though the toe of the slope does not necessarily fail, excessive deformation occurs. This excessive deformation causes the loosening of the joint and fault system in the stiffer upper regions of the slope and this in turn causes unravelling and local wedge failures. From this general slope failure ensues. A typical excavation profile is depicted in Figure 1.

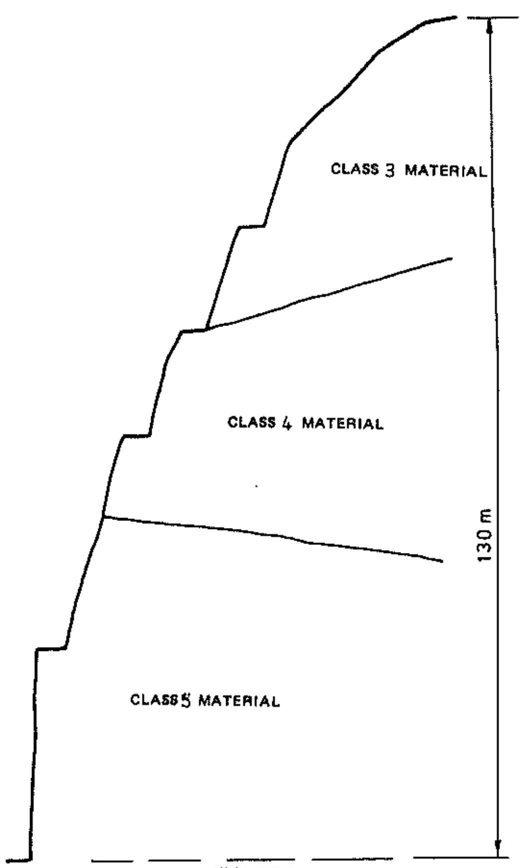

FIGURE 1

TYPICAL SECTION OF SLOPE

In order to prevent a recurrence of these events some means of reducing the deformational response especially in the region of the toe is required. Rock bolts which impose a confining stress and kinematic restraint on the rock mass not only reduces the deformational response but also markedly increases the strength of the rock mass. Though deformation and strength are inextricably related it is felt especially in a discontinuous material that an understanding of the deformation process must be acquired before the strength can be defined.

With these aspects in mind a series of ungrouted rock bolt plate bearing type tests are devised and performed where the deformational response of the loosened and then prestressed rock mass is measured.

It should be noted that the prestressed and then subsequently grouted bolt serves in the main two functions. As an active prestressed bolt the normal forces across the joint sets are increased and consequently the magnitude of the deformational modulus is increased. In addition as the depth of excavation is increased the magnitude of deformation of the rock mass is inhibited by the passive interaction of the grouted bolt within the jointed rock mass.

3 MODULI DETERMINATION

3.1 Deformational Moduli

In order to perform a pseudo-elastic plastic analysis knowledge of the deformational response and strength parameters is required. The deformational response is given in terms of a constitutive relation. Smart (5) and Singh (6) and others consider the discontinuous rock material as a multiphase composite material. Deformational mass moduli are evaluated using elastic multi-phase continuous models. These approaches are fraught with many dubious assumptions (7) especially if the mechanisms of slip and rotation are occurring. By using the criteria of compatibility and equilibrium Hill (8) shows that the upper and lower bounds of deformational moduli for an elastic multi-phase continuum are obtained. In turn by measuring the mass moduli in situ plus composing the mass composite moduli from component parts and then comparing these results with the upper and lower evaluated bounds an appreciation of discontinua is obtained. This latter approach is valid when the mechanisms of slip and rotation are absent and this is so if the stress or load gradients are small.

By knowing the separate deformational response of the two phases making up the jointed rock mass namely the intact rock and joint material the mass deformational modulus is compiled (9). These material characteristics related to deformational response and strength were determined by standard laboratory techniques. While performing the joint tests both normal and shear stiffnesses are also measured. In addition to the above information the core retrieved from the rock bolt moduli test holes was classified.

The in situ deformational response of the jointed rock mass was measured by noting the movements of both the anchor and face plate of a loaded hollow rock bolt. This allowed the determination of the deformational modulus of both the destressed surface rock and inner confined rock mass. The difference between the magnitude of these two moduli gives the effect of the stress environment in a jointed rock on the deformational response. Initially, as the rock mass making up the slope is unloaded and as there is no surrounding rock bolt which pre-loads or kinematically constrains the contiguous rock mass, the mass deformational response relates to an unloaded rock mass. After determining the unloaded deformational response the region was preloaded by loading a nearby rockbolt and the deformational response at the same location was repeated. This gives the decrease in deformational response due to the active preloading across the joint systems. It does not measure the kinematic passive constraint inhibiting dilation of the rock mass as further deformation of the rock mass occurs.

3.2 Joint Moduli

Using the Hoek direct shear box machine the apparent cohesion and friction angle of the joints were measured. In addition to this the shear stiffness was determined. Tables 1 and 2 show the results of the intact and joint properties plus stiffnesses for the joint system.

Sample No.	Intact Modulus Ei GPa	Apparent Poisson's Ratio	Unconfined Comp. Str. MPa	Description
IC–1	55.6	0.32	75.7	Greenstone
IC–2	38.0	0.23	85.6	Greenstone
3C–1	84.0	0.28	87.5	Greenstone
4C	49.3	0.29	74.5	Greenstone
6C	71.0	0.19	15.5	Greenstone
8C	23.0	0.51	38.2	Jasper
9C	13.0	0.98	10.0	Jasper
2C–2	32.1	0.24	55.0	Quartzite
3C2	55.5	0.21	64.5	Quartzite

TABLE 1
Intact Rock Properties

Test No.	Description	Location	Normal Stress MPa	Residual Angle of Fric	Normal Stiffness MPa/mm	Shear Stiffness MPa/mm
1	Greenstone on Greenstone	South side	8.0	35	3.86	2.7
2.	Greenstone with Chlorite infill	South side	4.76	19	2.44	0.84
3	Chlorite on Chlorite	South side	2.0	19	2.7	0.93
4	Jasper on Jasper	South side	3.7	29	0.83	0.46
5	Chlorite on Chlorite	South side	2.9	17	5.56	1.7
6	Greenstone on Greenstone	North side	1.9	19	2.45	0.75
7	Greenstone on Jasper	North corner	4.62	12	5.6	1.2
8	Jasper on Jasper	Centre	3.33	26	3.03	1.48

TABLE 2
Joint Properties

3.3 Combined Moduli

When combining the component parts of multi-phase material by composite elastic theory an important assumption is that normal loads do not induce shear forces. This does not apply in a jointed material where the joints are in any way staggered, (7). This however, is not significant if the mechanisms of slip and rotation do not occur.

The formula used for determining the upper and lower bound deformational moduli are evaluated from (7),

$$E_{v\,upper} = E_1V_1 + E_2V_2 + \cdots \quad (1)$$

$$\frac{1}{E_{v\,lower}} = \frac{V_1}{E_1} + \frac{V_2}{E_2} + \cdots \quad (2)$$

E_v upper and E_v lower are the upper and lower bound composite moduli,
E_1, E_2, etc. are the component moduli of phases 1, 2, etc.
V_1, V_2, etc. are the percentage volumes of phases 1, 2, etc. in relation to the total volume considered.

Upper and lower bound moduli are given in Table 3 for the various frequencies of joints per metre thickness of material.

3.4 In situ field moduli

There are a number of ways of determining the deformational response in a discontinuous rock mass. It is difficult, however, to achieve consistent or repeatable values of deformational response from the various methods generally used (10), (11), (12). From experience gained measuring the deformational response with devices such as flat jacks, plate bearing, overcoring, extensometers and pressuremeters it was decided to use a rock bolt type plate bearing test, or often termed the jacking test.

The test performed here used a hollow rock bolt anchored from 3 m to 9 m into the rock mass, Figure 2. Using an oil jack the rock bolt is loaded and the deformations of both the bearing face plate and anchored extension rod are measured, Figure 3. From this the deformation of the rock loaded between the face plate and anchor is known. Initially, difficulty was experienced in achieving adequate anchorage in the class 4 and 5 rock. This was overcome by creating a cavity at the anchor end with a small quantity of explosive using a detonator. Good anchorage was achieved and the size of anchorage was determined by measuring the quantity of grout used for anchorage and the depth of drill hole before and after grouting the anchor.

Intact Material Type	Intact Mod. GPa	Joint Type	Int Thick mm	Int Mod. MPa	1 Joint/m Eupp	1 Joint/m Elow	1 Joint/m Eu/El	5 Joints/m Eupp	5 Joints/m Elow	5 Joints/m Eu/El	10 Joints/m Eupp	10 Joints/m Elow	10 Joints/m Eu/El
Greenstone	60	Greenstone	2.5	8	59.85	3.04	19.7	59.25	0.63	93.3	58.5	0.32	184
Greenstone	60	Chlorite	5	3	59.7	0.59	100	58.5	0.12	488	57.0	0.06	950
Greenstone	60	Jasper	10	0.5	59.4	0.05	1 188	57	0.01	5 700	54.0	0.005	10 800
Jasper	18	Greenstone	2.5	8	17.96	2.72	6.6	17.78	0.62	28.8	17.55	0.315	56
Jasper	18	Chlorite	5	3	17.91	0.58	30.8	17.55	0.12	147	17.1	0.06	286
Jasper	18	Jasper	10	0.5	17.82	0.05	356	17.1	0.01	1 710	16.2	0.005	3 240

TABLE 3
Ratios of Upper & Lower Bound Moduli

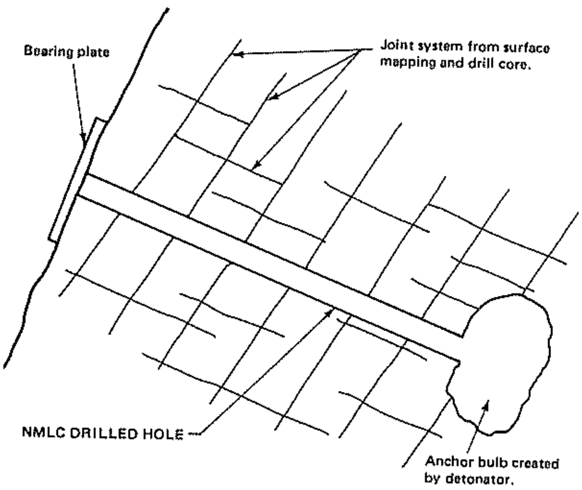

FIGURE 2

TYPICAL STRUCTURAL MODEL DETERMINED TO MEASURE IN SITU DEFORMATION MODULUS

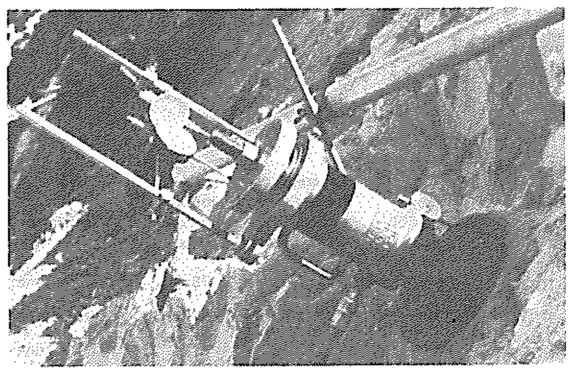

FIGURE 3

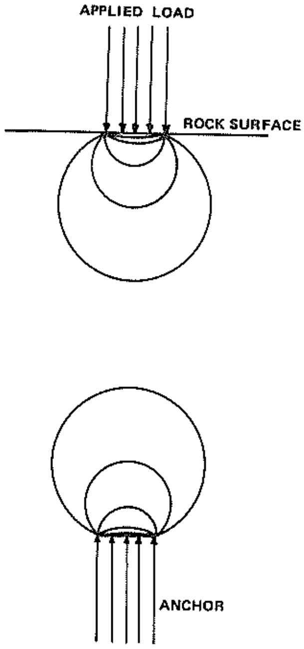

FIGURE 4
CONTINUOUS STRESS DISTRIBUTION

The load distribution between the face plate and anchor is largely conjectural. However because the stress distribution for a continuous material is as shown in Figure 4 and the stress distribution for a discontinuous material is as shown in Figure 5, the stress distribution between the plate and the anchor is assumed to be uniform. Assuming the stress distribution as given in Figure 5 depicting the results of the geological and computer model and the in situ deformational response Figure 6 the mass deformational response is evaluated. This gives the deformational modulus which is the constitutive parameter used to relate load and deformation, Table 4.

Table 4 also gives the modulus of the same material measured from the same rock bolt after loading the material with a nearby rock bolt. The nearby rock bolt is located within a radius of 1/2 the length of the initial rock bolt, and is also equal to the length of the initial rock bolt.

Moduli determined from the deformation of the face plate and anchor are also given in Table 4. These values of moduli show the effects of destressing the surface or skin of the slopes and the increase of moduli due to the confining or stressing effects of the inner rock mass. When determining the surface or skin moduli the elastic theory formula

$$E_v = \frac{P(1-\nu^2)}{2\rho a}$$

was used, where E_v is the deformational modulus P is the applied force applied to a rigid punch, ν is Poisson's ratio, ρ is the measured displacement of the rigid punch of radius a.

Bore Hole No.	Hole Diameter mm	Length m	Face Plate Modulus GPa	Absolute Modulus GPa	Reinforced Modulus GPa
1	75	6.96	0.25	6.26	
2	45	1.9	0.38	3.68	
3	45	1.58	0.15	1.62	
4	45	2.43	0.98	1.82	
5	75	6.96	0.16	5.13	
6	45	1.8	0.2	3.01	
7	45	1.88	0.67	3.15	11.3
8	75	6.34	0.16	7.43	
9	45	1.35	0.08	0.53	3.15
10	45	2.14	0.07	0.66	
11	75	8.0	0.45	12.7	
12	45	1.65	0.35	2.1	5.47

TABLE 4
In Situ Measured Moduli

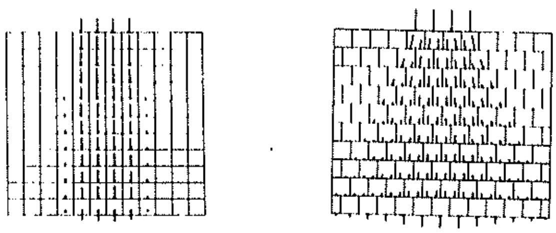

LOAD DISTRIBUTION
FIGURE 5

3.5 Pseudo Elastic Analysis

Table 4 shows that there is difference between the surface moduli and anchor moduli due to the effects of joint constraints and confining stresses. The rock mass deformational modulus increases with depth from the surface of the excavation. In order to account for this the absolute deformations measured between the face plate and anchor are used to evaluate the rock mass deformational moduli. This value to the measured depth namely 6 m is used for the skin value of the slope stability analysis while the deformation of the anchor is used to determine the modulus of the inner rock mass. From these moduli the analysis of the slopes were performed using a pseudo elastic finite element program. The result of this was that tensile or much reduced compressive stress zones which were generated in the upper regions of the slope were eliminated after the remedial rock bolts were applied to the toe regions of the slopes.

By increasing the magnitude of skin moduli the tensile stress zones were eliminated in the upper destressed regions of the slope. The two main modes of decreasing the deformational response of a rock mass are by grouting and/or prestressing with anchors or rock bolts. In this particular instance grouting would not be effective in that the joints were infilled with gouge which would prevent the penetration of grout and much of the excavation had already been performed. Of consequence rock bolting was used to improve the deformational characteristics of the slopes. The situation considered here is that the rock mass without the rock bolts generally expands as the excavation is created and the loads redistribute. By using rock bolts, slip and rotation

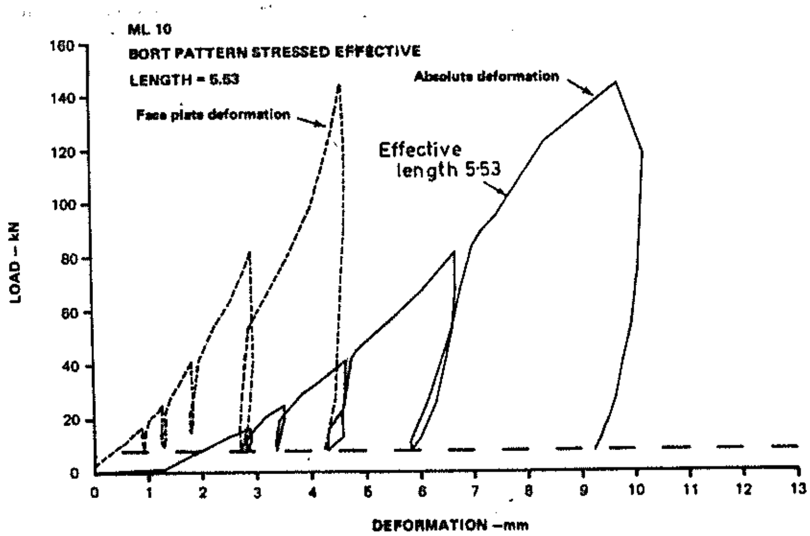

FIGURE 6
MEASUREMENT OF BEARING PLATE
AND ANCHOR DEFORMATIONS

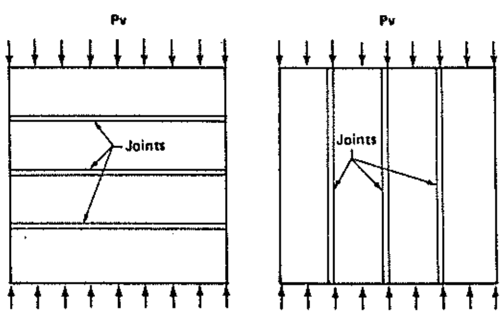

FIGURE 7

JOINT SETS ORIENTATED PERPENDICULAR
AND PARALLEL TO IMPOSED LOADS

of the joint and fault sets is inhibited and as these mechanism of slip and rotation are the main processes of loosening and causing the consequent loss of rock mass strength the value of the rock bolt is evident. Besides this, however, the rock bolts also increase the normal loads across the joint system. This increases the stiffness of the joint which in turn increases the deformational modulus of the rock mass. With these aspects in mind the measured in situ moduli were used in a pseudo elastic plastic analysis. Where any zones of tensile or small compressive stresses occurred, the rock mass was pre-loaded with patterns of rock bolts so placed that zones of doubtful stress conditions were eliminated.

With the above approach the soft toe areas were pre and post stressed and the upper regions of the slope consequently stabilised. A very difficult and precarious condition is stabilised by measuring in the field the mass rock moduli before and after loading with rock bolts.

By combining the intact modulus of the parent rock and the modulus of the joint the upper and lower bound moduli are determined. A simplistic picture of the effect on these bound moduli caused by the orientation of the joint system relative to the direction of imposed load is given in Figure7&8. When the joints are perpendicular to the direction of the load a lower bound value of modulus is obtained when

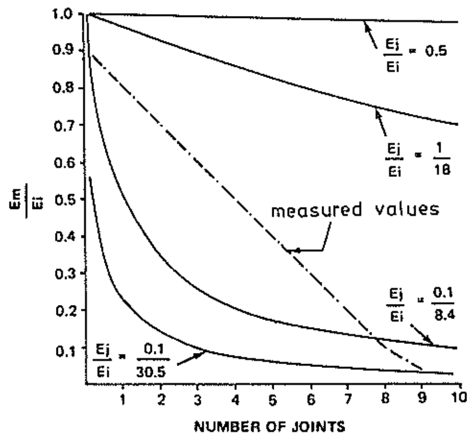

FIGURE 8

parallel an upper bound value results. This introduces an anisotropy into the material which is characterised by the orientation of the joints and their physical properties, Table 3. It is evident that here the intact rock controls the upper bound modulus and the joints control the lower bound modulus. Therefore if the intact rock is soft the upper bound modulus would be low in magnitude and have a high classification value depicting bad rock mass even if the mass had no joints. On the other hand if the intact rock were hard but had numerous soft joints the rock mass would still have a high classification rating and be considered bad. It is therefore evident that joint properties and the associated orientation relative to the imposed loads has an important effect on the rock mass classification and the consequent deformational response.

The measured in situ rock bolt mass moduli varied from 0.53 GPa to 30 GPa. This was collated with the rock mass classification defined below.

Class	3	4	5
Modulus	≥ 10 GPa	< 10 GPa but ≥ 1 GPa	< 1 GPa

The moduli measured before and after rock bolting showed that the bolts in effect increased the classification rating of the rock mass. A characteristic not investigated here but nevertheless important is that the rock bolt inhibits loosening of the rock mass thus preventing load redistributions and dilation. This increases the strength characteristics of the rock mass.

Table 5 shows the percentage reduction of the deformational response of the intact rock modulus caused by the joint-fault systems, John (13). The intact moduli of the Greenstone and Jasper were taken as 60 and 18 GPa respectively and the measured mass moduli are those related to the classified rock mass.

By comparing Tables 3 and 4 it is seen that the measured in situ mass moduli lie within the upper and lower bounds of the evaluated moduli. The effects of the rock bolts on the mass deformational response is to improve the rock mass classification by at least one class and in some cases two. That is if the rock mass was class 5 before installing the rock bolts it is improved to at least a class 4 and in some cases a class 3.

4 CONCLUSIONS

When the mechanisms of slip and rotation in a jointed rock mass are not part of the deformational process, the rock mass is considered a composite elastic material. From this the pseudo elastic theory is used to analyse the stability of the rock slopes. In order to perform the analysis the constitutive relation between load and deformation is required. In situ field jacking tests using hollow anchored rock bolts are found suitable for determining the deformational modulus of the rock mass. A geological model of the rock material making up the jacking test zone, is constructed and this coupled with the results of the in situ deformational response give the required deformational muduli required for the pseudo elastic analysis.

Laboratory tests are performed on the NMLC core retrieved from the holes drilled for the jacking tests. Standard laboratory testing give the moduli of the intact rock material and stiffnesses of the joint-fault sets. The results of the testing are incorporated in the geological structural model to determine the in situ pseudo elastic moduli or used in composite elastic theory to give the upper and lower bound moduli of the rock mass.

Using an appropriate classification system the rock zones are classified; which in this instance are class 3, 4, and 5 being fair, bad and very bad rock masses respectively. The deformational moduli associated with these rock zones are carefully correlated. This means that when encountering a rock of a specific class the appropriate rock bolt patterns and remedial measures are applied.

The possibility of connecting the classification system with design by measuring the concomitant deformational moduli has wider aspects than those reported here. The quantification of classification with design has great potential in documentation of both specifications and contracts associated with earth material.

TABLE 5

	Rock Mass Class (Classification) 3	4	5
Greenstone % Modulus reduction	<16.7	>16.7 but < 1.7	> 1.7
Jasper % Modulus reduction	<55.6	>55.6 but <5.6	> 5.6

5 ACKNOWLEDGEMENTS

The work presented here involved many personnel employed in the Geomechanics and Materials Branch at SMEC especially Mr Dankers and Huggett and thanks is extended to all who helped. The authors also wish to thank the management of SMEC for permission to publish this work.

6 REFERENCES

(1)
CHAPPELL, B.A., Classification of Rock Mass related to foundations. Paper submitted to International Conf. on Structural Foundations on Rock, 1980.

(2)
BARTON, N., LIEN, R. and LUNDE, J., Engineering Classification of rock masses for the design of tunnel support. Rock Mechanics, Vol. 6, No. 4, pp 189-236 (1974).

(3)
BIENIAWSKI, Z.T., Rock mass classification in rock engineering. Proceedings of the Symposium on Exploration for Rock Engineering. Johannesburg, pub. Balkemma, Cape Town, Vol. 1, pp 97-106. (Nov. 1976).

(4)
WICKHAM, G.E., TIEDEMANN, H.R., and SKINNER, E.H., Ground support prediction model (RSR concept). Proc. 1st Rapid Transit and Tunnelling Conference, AIME, New York, pp 43-64 (1972).

(5)
SMART, P., Strength of weathered rock. Int. J. Rock Mech. Min. Sci. 7, 371-389 (1970).

(6)
SINGH, B., Continuous characterization of jointed rock masses. Part 1 - The constitutive equations. Int. J. Rock Mech. Min. Sci. 10, 331-335 (1973).

(7)
CHAPPELL, B.A., Component Characteristics of Jointed Rock Masses. Int. J. Rock Mech. Min. Sci. & Geomech. Abstr. Vol. 12., pp 87-92 (1975).

(8)
HILL, R., The elastic behaviour of a crystalline aggregate. Proc. Phys. Soc. Lond. A65, pp 349-354, 1952.

(9)
CHAPPELL, B.A. Design parameters for Aberdeen tunnel, Hong Kong. Proceedings of the Symposium on Exploration for Rock Engineering, Johannesberg., pub. Balkemma, Cape Town, Vol. 1, pp 181-188 (1976).

(10)
CHAPPELL, B.A. Deformational Response in Discontinua. Paper accepted for pub. in the Int. J. Rock. Mech. Min. Sci. (1979).

(11)
CHAPPELL, B.A., Load Distribution and Redistribution in Discontinua. Paper accepted for pub. in the Int. J. Rock. Mech. Min. Sci. (1979).

(12)
BIENIAWSKI, Z.T., Determining Rock Mass Deformability Experience from Case Histories. Int. J. Rock. Mech. Min. Sci. & Geomech. Abstra. Vol. 15. 237-247 (1978).

(13)
JOHN, K.W., Civil Engineering Approach to Evaluate Strength and Deformability of Regular Jointed Rock. Rock Mechanics Theory and Practice. Eleventh Symp. on Rock Mech. B erkeley, pp 69-80 (1969).

Stability Charts for Simple Earth Slopes allowing for Tension Cracks

B. F. COUSINS
Senior Lecturer in Civil Engineering, University of Tasmania

SUMMARY In a previous paper by the author (Cousins, 1978) stability charts were presented for simple earth slopes ignoring tension cracks. Tension cracks are usually the first sign of impending failure in cohesive soils and therefore should be taken into account. In this paper the effect of tension cracks both dry and filled with water is investigated. Stability charts are presented for toe circles with no water in the tension crack and for a homogeneous pore pressure ratio r_u = 0, 0.25 and 0.5. A chart is also given for pore pressure ratio r_u = 0 with the tension crack filled with water. The charts have been constructed assuming the worst possible location and depth of the tension crack. As such they represent a lower bound for the safety factor. The maximum reduction in safety factor of 40% was found for slope angle $\alpha = 60^\circ$ and dimensionless parameter $\lambda_{c\phi} = 20$ with the tension crack filled with water. For most cases the reduction was much less than this.

1 INTRODUCTION

Most charts for investigating the stability of simple homogeneous slopes do not allow for tension cracks. See, for example, Bishop and Morgenstern (1960), Spencer (1967), Janbu (1967) and Cousins (1978). One exception is Hoek and Bray's (1977) charts. Hoek and Bray locate the tension crack so that the safety factor for the slope is a minimum for the slope geometry and groundwater conditions considered. The charts do not give the depth of tension crack used. Also their method for dealing with pore pressure is different from most other charts. In this paper pore pressure will be taken into account by assuming a homogeneous pore pressure ratio, r_u.

There is much conjecture on what value to take for the tensile crack depth in cohesive soils (Chowdhury 1978). An expression often used is

$$z_c = \frac{2c}{\gamma} \tan\left(\frac{\pi}{4} + \frac{\phi}{2}\right) \qquad (1)$$

where c and ϕ apply to total stresses. In any case this type of expression cannot conveniently be used in a non-dimensional treatment of slope stability.

A better approach is to assume that the tension crack depth and location are chosen to give the lowest possible safety factor. In this paper the tension crack depth is made non dimensional by dividing by the height of the slope. The depth of the tension crack has been limited to half the height of the slope as suggested by Terzaghi (1943).

Slope failure often occurs during heavy rainfalls. This suggests that tension cracks if present may become partially filled with water which acts as a trigger to failure. The efeect of water in tension cracks is allowed for in this paper by assuming that the tension crack is filled with water having a unit weight equal to half that of the bulk unit weight of the soil. This assumption is necessary to make the effect non dimensional.

In the past it has been suggested (Terzaghi, 1943) that the effect of tension cracks can be allowed for by reducing the cohesive strength. This paper will eliminate the need for such assumptions.

2 NOTATION

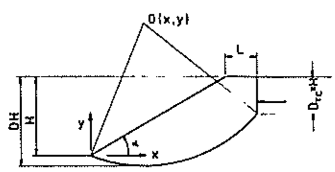

Figure 1 Notation for simple slope

c' = cohesion strength based on effective stresses
c'_m = mobilized cohesion stress
D = depth factor
D_{TC} = tension crack depth factor
F = factor of safety
H = height of slope
L = distance from crest of slope to tension crack
N_F = $F\gamma H/c'$ = $\gamma H/c'_m$ = stability number
r_u = pore pressure ratio
α = slope angle in degrees
γ = bulk unit weight of soil
$\lambda_{c\phi}$ = $\gamma H \tan\phi'/c'$ = dimensionless parameter
ϕ' = internal friction angle based on effective stresses
ϕ'_m = mobilized friction angle.

3 LIMIT EQUILIBRIUM METHOD USED

The method of analysis used in this investigation is simply an extension of the method used in a previous paper (Cousins 1978). The pattern search method of optimization (Adley and Dempster, 1974) is used to find the minimum value for the stability number, N_F for a given slope angle α, pore pressure ratio r_u, and mobilized friction angle ϕ'_m. Figure 2 gives a simplified flow chart of how the stability number N_F is determined for a given value of the dimensionless parameter, $\lambda_{c\phi}$. However, the pattern search method did not always work for reasons discussed later.

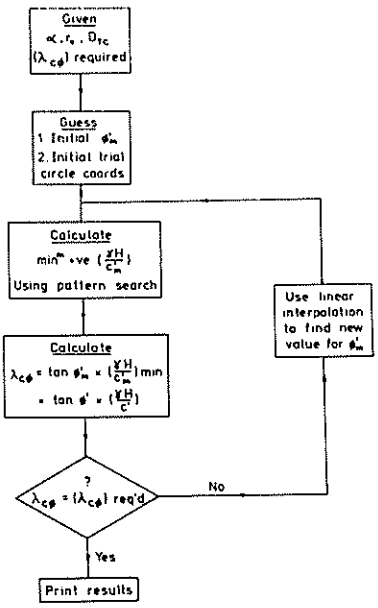

Figure 2 Flow chart for determination of stability number N_F

4 LOCATION OF TENSION CRACK

Trial slip circles are defined in this investigation by fixing circle centres and specifying a depth factor D or a common point. The location of a tension crack of a given depth is then automatically fixed. It is located at the highest point on the slope where the height between the ground surface and the failure arc is equal to the required tension crack depth. See Figure 1. It is possible for the height between the ground surface and the failure arc to be less than the required tension crack depth along the whole length of the arc. In this case the trial circle is not allowed.

The computer program allows the tension crack to progress down the slope face if this is geometrically possible. However, it is not possible in a homogeneous soil with a uniform pore pressure ratio distribution for the exit point of the critical circle to progress down the slope face. This applies whether the tension crack is filled with water or not. The reason for this is quite simple. Suppose the tension crack for the critical circle is located on the slope face. The height of the slope could then be increased indefinitely without altering the critical circle since the forces acting on the critical circle mass would be unchanged. Clearly the supposition is unrealistic. This is verified in all cases by the computer results.

5 OPTIMIZATION PROBLEMS

A typical contour map for N_F is given in Figure 3. It shows the critical circle with its tension crack on the crest of the slope. It also illustrates one of the problems of the investigation. The location of the centre of the critical circle is close to the non permissible boundary. In fact for higher values of slope angle α and $\lambda_{c\phi}$ the centre of the critical circle lies on the non permissible boundary.

6 VARIATION OF STABILITY NUMBER WITH TENSION CRACK DEPTH

Plots of normalized stability number N_F against tension crack depth factor for toe circles are given in Figures 4 and 5 for slope angles of 20° and 45° and a range of $\lambda_{c\phi}$ values.

For the case of no water in the tension crack all the curves show an initial decrease in the stability number N_F followed by an increase. Clearly the $\phi = 0$ value gives the greatest reduction in stability number for both slope angles, the extent of the reduction increasing as the slope angle increases. The maximum reduction of 14% occurs when the slope angle $\alpha = 60^\circ$ and $\phi = 0$. It must be remembered that these results apply to toe circles. A reduction of 10% occurs for the depth factor D = 1 case for $\alpha = 20^\circ$. For $\alpha = 45^\circ$ the toe circles have a depth factor D almost equal to 1. The graphs clearly indicate that a particular tension crack depth such as that given by equation (1) will give a stability number higher or lower than the no tension crack case depending on the relative values of the parameters involved.

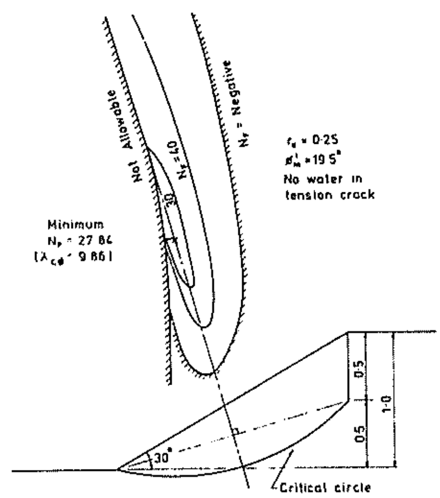

Figure 3 Typical contour map for stability number N_F

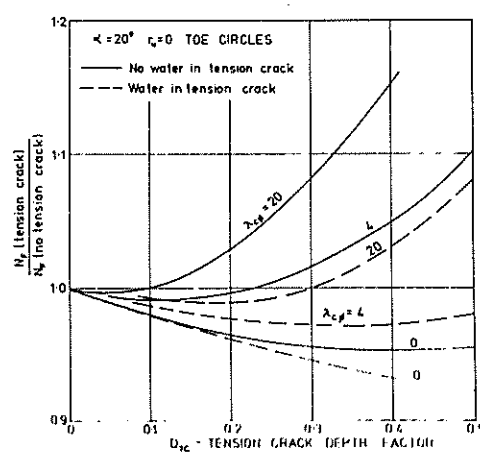

Figure 4 Variation of stability number N_F with tension crack depth, $\alpha = 20^\circ$

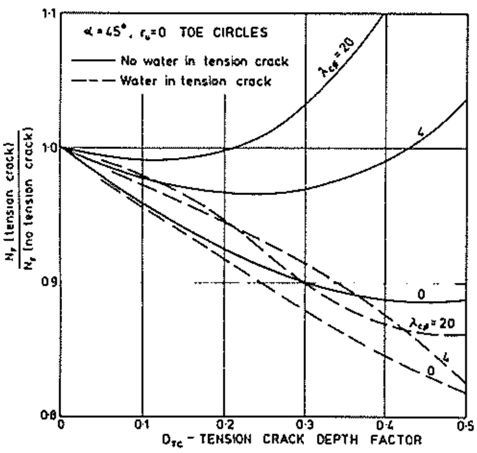

Figure 5 Variation of stability number N_F with tension crack depth, $\alpha = 45^o$

When the tension crack is filled with water the decrease in stability number N_F is higher than the no water case. The minimum also occurs at a higher tension crack depth factor. For the lower values of $\lambda_{c\phi}$ the stability number N_F is still decreasing at a tension crack depth factor D_{TC} equal to the cut off value of 0.5. The maximum reduction of 40% in stability number N_F occurs when the slope angle $\alpha = 60^o$.

7 STABILITY CHARTS FOR TOE CIRCLES

Clearly the number of charts would be too numerous if sets were given for a range of constant tension crack depth factors. It is more sensible to give charts based on a minimum stability factor N_F obtained by allowing the tension crack depth to vary. The program was modified to allow the tension crack depth factor corresponding to the minimum stability number to be determined. The required tension crack depth factor, D_{TC} was obtained to an accuracy of ± 0.01H.

Figures 6-8 give the minimum stability number N_F for the no water in the tension crack case for values of the pore pressure ratio = 0, 0.25 and 0.5 respectively. It should be noted that these charts have the same format as that given by Cousins, (1978). However, the slope angle α has been increased to a maximum of 60°. This is possible because the presence of a tension crack eliminates the inter granular tension around the failure arc for the higher slope angles and pore pressure ratios. Even so the slope angle in Figure 8 has been limited to 50° because of problems associated with the stress distribution around the failure arc. The concept of a pore pressure ratio is more relevant for the lower slope angles. For high slope angles and high values of $\lambda_{c\phi}$ the critical circle is quite superficial thus making it difficult to estimate a reasonable value for the average pore pressure ratio.

Curves are also given in Figures 6-8 which allow the critical tension crack depth factor D_{TC}, the toe circle depth factor D, and the mobilized friction angle ϕ'_m to be determined. In all cases examined the critical tension crack depth factor D_{TC} is greater than 0. However, the difference in stability number N_F is not significant for higher values of $\lambda_{c\phi}$ if the slope angle α is less than 20°. The upper limit for D_{TC} of 0.5 is just reached when the slope angle equals 60°.

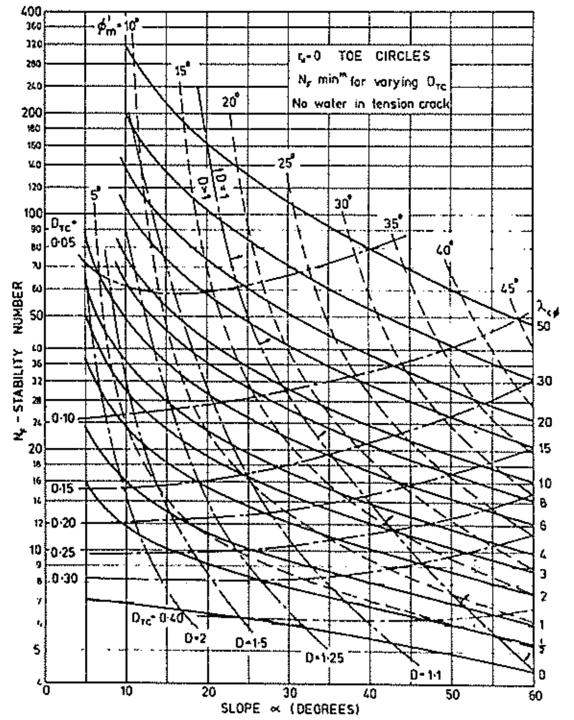

Figure 6 Stability number N_F for no water in tension crack, $r_u = 0$

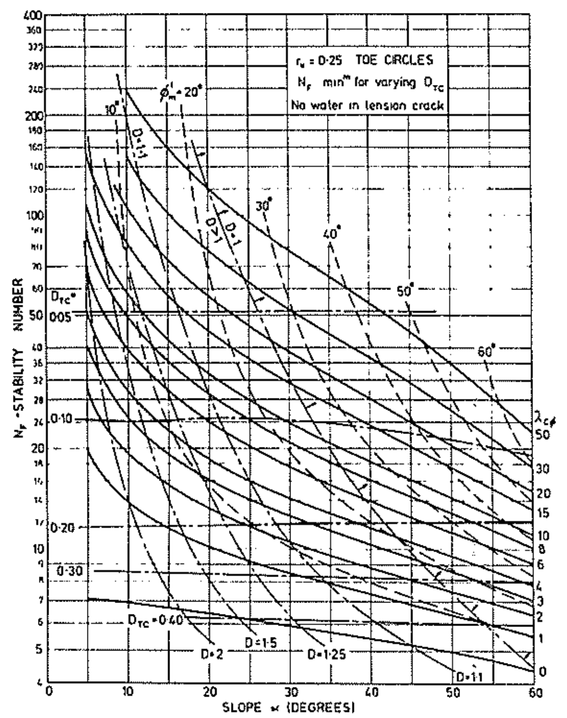

Figure 7 Stability number N_F for no water in tension crack, $r_u = 0.25$

Figure 9 gives the stability chart for $r_u = 0$ when the tension crack is filled with water. In this case the upper limit for D_{TC} of 0.5 is reached at low values of slope angle, α. A comparison with Figure 6 indicates that the importance of water in the tension crack increases with slope angle, α.

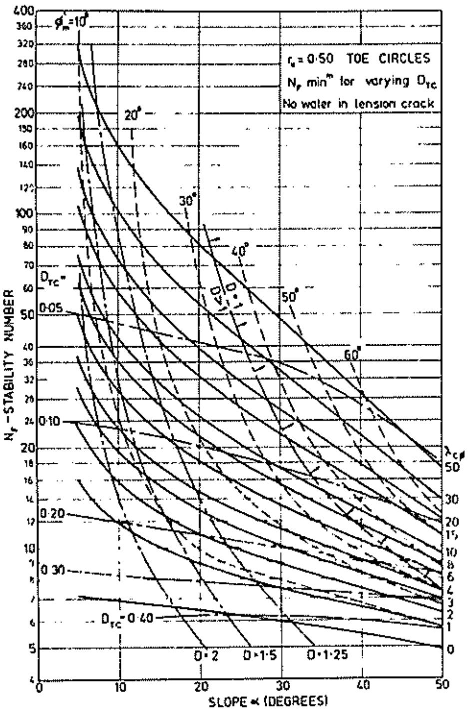

Figure 8 Stability number N_F for no water in tension crack, r_u = 0.5

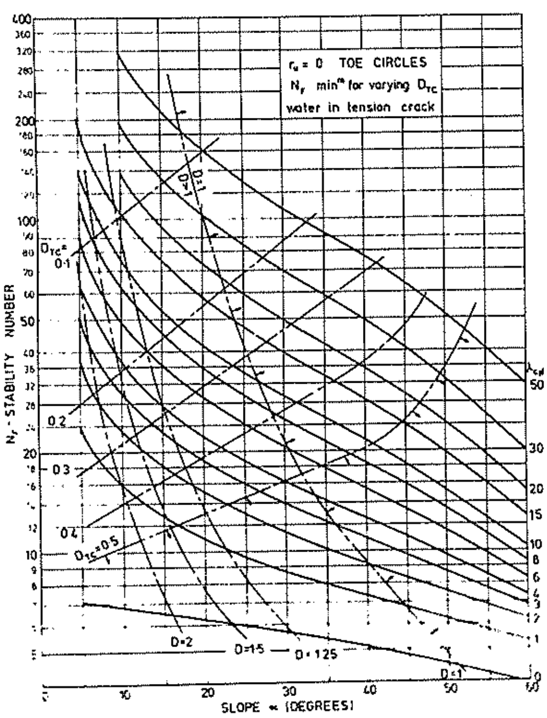

Figure 9 Stability number N_F for water in tension crack, r_u = 0

The location of the critical tension crack is given in Figures 10 and 11 for the no water in the tension crack case and the water in the tension crack case respectively. In Figure 10 the exit point of the critical circle for the no tension crack case is also given to aid comparison. Allowing for tension cracks causes the exit point on the crest of the slope to move closer to the slope face as expected. For higher values of slope angle the critical tension crack is located approximately half way between the crest point and the exit point for the no tension crack case. Figure 11 indicates that the critical tension crack moves even closer to the crest if the tension crack is filled with water. For slope angles $\alpha > 25^o$ and $\lambda_{c\phi} > 3$ the critical tension crack is actually located at the crest.

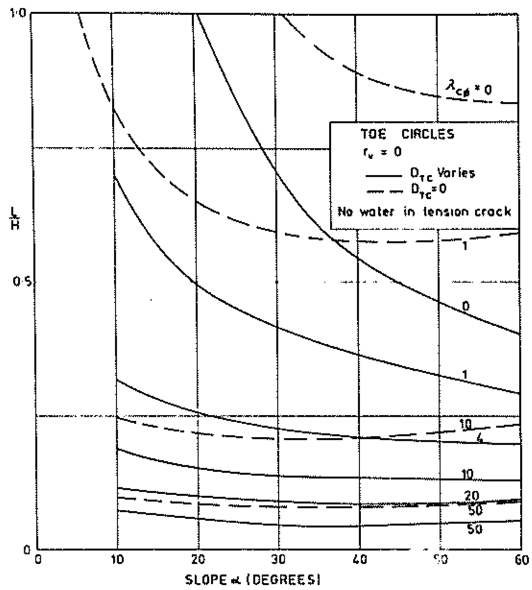

Figure 10 Values of L/H for no water in tension crack

8 EXAMPLE

Find the safety factor with and without allowing for tension cracks for a simple slope. The relevant parameters are: H = 20m; γ = 20 kN/m^3;
c' = 80 k Pa; ϕ' = 11.3^o; r_u = 0.
Thus $c'/\gamma H$ = 0.20 and $\lambda_{c\phi} = \gamma x H \tan\phi'/c'$ = 1.00.
No water in tension crack case:
Figure 6 gives N_F = 8.7, thus F = 8.7 x $c'/\gamma H$ = 1.74.
Also D = 1.09, D_{TC} = 0.29.
Water in tension crack case:
Figure 9 gives N_F = 7.9, thus F = 1.58.
In this case D = 1.1, D_{TC} = 0.50.
No tension crack case:
The author's previous charts (Cousins, 1978) gives N_F = 9.15, thus F = 1.83 and D = 1.09.
For this example allowing for the worst possible condition gives a reduction of 14% in the safety factor over the no tension crack case.

9 CONCLUSIONS

1 Assuming the most severe combination of location and depth of tension crack gives a maximum reduction of 20% over the no tension crack case for values of slope angle less than 45^o.

2 The stability number N_F for a particular tension

crack depth may be higher or lower than for the no tension crack case. However, the minimum stability number is always reduced if the tension crack depth is allowed to vary.

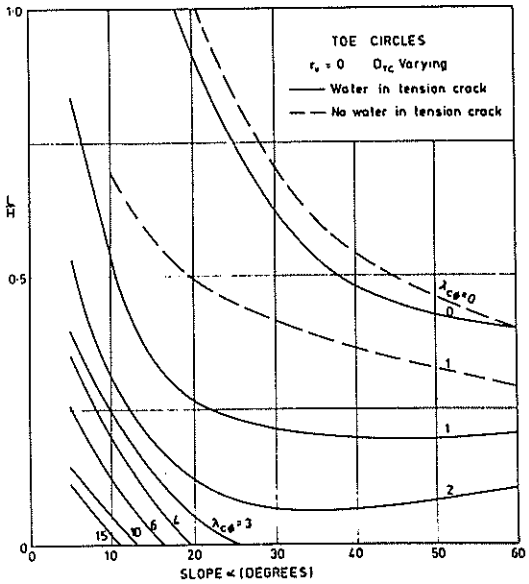

Figure 11 Values of L/H for water in tension crack

3 The location of the critical tension crack is quite close to the crest of the slope for the no water in the tension crack case and even closer if the tension crack is filled with water. For slope angles $\alpha > 25^{o}$ and $\lambda_{c\phi} > 3$ the critical tension crack is located at the crest if the crack is filled with water.

4 The restrictions placed on Janbu's (1967) method for allowing for the pore pressure ratio given in a previous paper (Cousins 1978) are still applicable when tension cracks are allowed for.

10 REFERENCES

ADLEY, P.R. and DEMPSTER, M.A.H. (1974). Introduction to optimization Methods. London, Chapman and Hall.

BISHOP, A.W. and MORGENSTERN, N.R. (1960). Stability Coefficients for Earth Slopes. Geotechnique, Vol. 10, No. 4, pp 129-147.

CHOWDHURY, R.N. (1978). Slope Analysis. Amsterdam, Elsevier Scientific Publishing Company.

COUSINS, B.F. (1978). Stability Charts for Simple Earth Slopes. Journal of the Geotechnical Engineering Division, ASCE Vol 104, No. GT2, Proc. Paper 13572.

HOEK, E. and BRAY, J.W. (1977). Rock Slope Engineering. London, Institution of Mining and Metallurgy.

JANBU, N. (1967). Discussion of Paper - Dimensionless Parameters for Homogeneous Earth Slopes by Bell, J.M., Journal of the Soil Mechanics and Foundations Division, ASCE. Vol. 93, No. SM6. pp 367-374.

SPENCER, E. (1967). A Method of Analysis of the Stability of Embankments Assuming parallel Inter-Slice Forces. Geotechnique, Vol. 17, No. 1, pp. 11-26.

TERZAGHI, K. (1943). Theoretical Soil Mechanics. New York, McGraw Hill.

Stabilisation of a Mudstone Derived Colluvium Slope

G. RAMSAY
Design Engineer, Ministry of Works and Development, Wellington, N.Z.

SUMMARY

The design and effectiveness of drainage measures installed to stabilise a colluvium slope are reviewed in terms of observations made during construction. The difficulties in determining complex subsurface geometry and in situ permeabilities with reasonable predesign investigations are highlighted. The benefits of reassessment of the design on the on the basis of additional information obtained during construction are illustrated.

1 INTRODUCTION

Replacement of the Poro-o-Tarao railway tunnel in the centre of the North Island of New Zealand involved establishment of a portal in an area of known slope instability.

The geology in the area includes mudstones and siltstones of the Mahoenui Group, locally known as 'papa' (Borrie and Riddolls (1980)). Slope stability problems are common in the area, some being attributed to movement of colluvium, possibly formed by rotational slumps, on underlying intact mudstone. The New Zealand Railways have had a number of stability problems in the area. Aerial photographs of the area around the proposed portal show evidence of recent slope movement and local residents have reported slope failures in the general area over the last fifty years.

Investigations and design studies reported by Parton (1974) indicated that acceptable slope stability could be achieved by installing drainage measures to lower ground water and by constructing a portal structure to minimise slope excavation.

This paper discusses additional subsurface information obtained during construction, and the revised slope model deduced from this information. The effectiveness of the drainage measures is reviewed in terms of recorded piezometer readings and drain discharges.

Modifications to the original design slope contours were made following a reanalysis of the slope stability using the revised slope model.

2 NOTATION

C' Effective cohesion (kPa)

ϕ' Effective angle of internal friction

γ Soil Weight Density (tonne/m^3)

B Pore pressure coefficient

α Angle of inclination of sliding surface

H Depth of sliding block

H_w Height of water table above failure surface

3 ORIGINAL DESIGN AND INVESTIGATION

Pre-design investigations involving 15 boreholes and seven 1 m diameter shafts indicated a stiff dark grey silt/clay colluvium containing mudstone fragments overlying hard grey mudstone bedrock. The interface was characterised in some cases by a zone of highly fractured mudstone with considerable water inflows. In some shafts a thin layer of highly plastic clay was observed between the mudstone and the colluvium. Interpretation of core from the small diameter (NX) holes was difficult due to drilling disturbance in the mudstone, and a clear picture of conditions was only obtained after the shafts were sunk and logged.

Design studies were based on the inferred colluvium-mudstone interface location and utilised effective residual shear strength parameters for the colluvium. Pore pressures measured by vibrating wire piezometers installed in the exploratory shafts were used. The analysis reported by Parton (1974) gave stability factors of safety in the range .9 - 1.1 for the known marginally stable preconstruction condition. It was shown that the only feasible method of achieving adequate factors of safety after excavation of the slope for the tunnel portal was to construct a portal approach structure and to install drainage to lower the water table slope to within 2 m of the interface, (as compared with the then existing 8 m level). The drainage was intended to lower ground water levels to an acceptable level prior to final slope excavation. The analysis showed a minimum improvement over existing factors of safety of 50% for static cases and 25% for seismic loading.

To dewater the slope a curtain of .6 m diameter sand drains, spaced at 2 centres and discharging into a 300 m long drainage drive located below the interface was proposed. The drain size and spacing were determined on the basis of permeability values calculated from recharge in the exploratory shafts. In addition to the subsurface drainage the design provided for reducing surface infiltration by the draining of surface swampy areas, lining of water courses and by afforestation.

Locations of the drainage drive, sand drains and portal structure are shown on Figure 1.

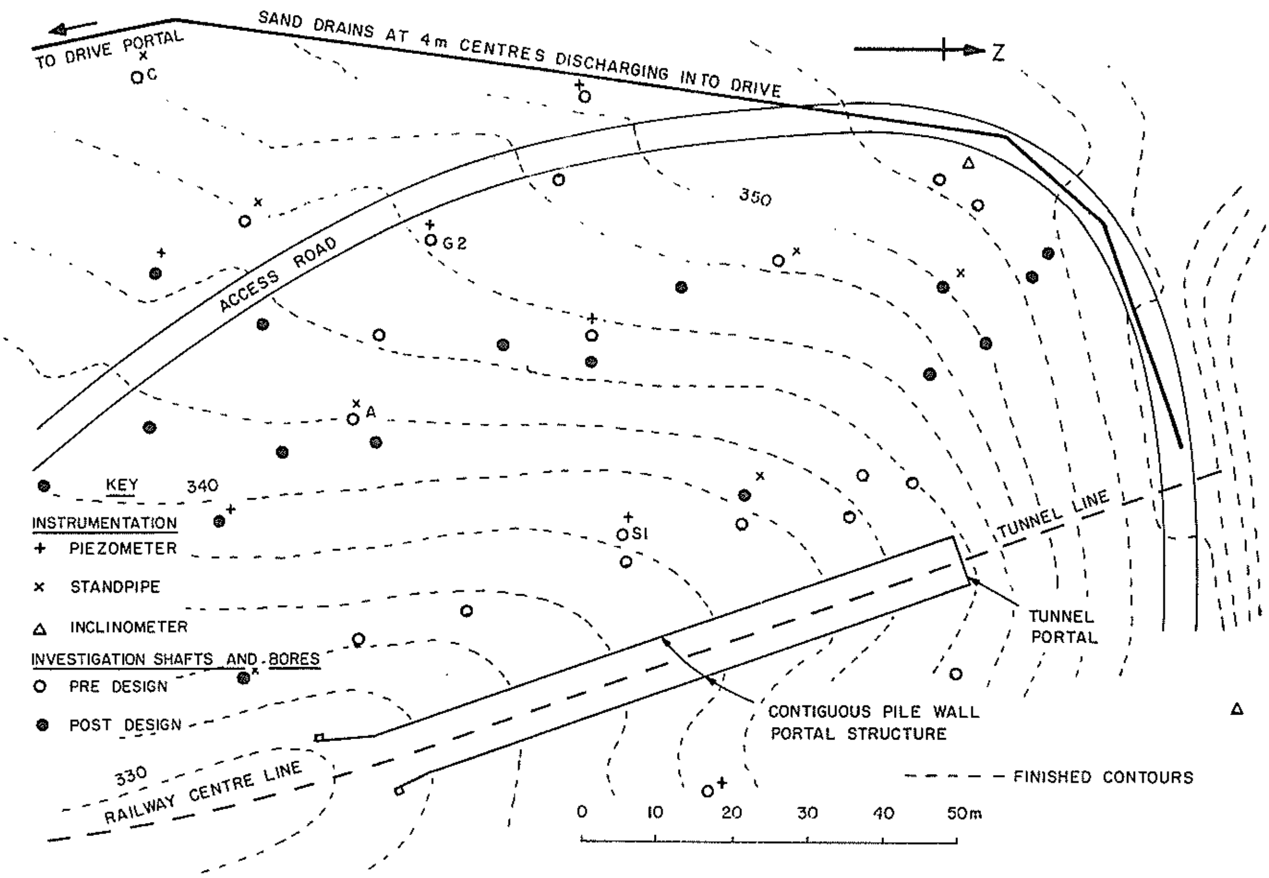

FIG. 1 LAYOUT OF SOUTH PORTAL PORO-O-TARAO TUNNEL

4 CONSTRUCTION SEQUENCE

The sequence of major construction activities is shown on Figure 2. Prior to 1976 minor works aimed at improving surface runoff were carried out. These included the diversion of streams crossing the slope into channels lined with a butyl rubber membrane overlain by concrete 'gobi blocks', and the draining and recontouring of some swampy areas.

To enable the drainage system to have the maximum effect on water levels prior to final excavation, the slope was excavated in two stages. The first stage excavation removed the minimum amount of material necessary to allow access for construction of the portal structure.

Because of delays incurred in constructing the drainage drive and sand drains, supplementary drainage measures, including inclined drains and pump shafts, were installed to accelerate slope dewatering.

The second stage excavation was delayed until the drainage measures had been installed and the analysis described in Section 7 had been made.

Minor surface slumps occurred during or shortly after both excavation stages. Remedial treatment of these slumps included removal of the slump material, local flattening of slopes and drainage by inclined under drains.

5 SITE INSTRUMENTATION

5.1 General

Instrumentation was installed in the portal area to perform three distinct functions:

(a) To provide piezometric data for back analysis of the known marginally stable preconstruction condition.

(b) To monitor the effect of the drainage measures installed.

(c) To detect any slope movements prior, during and after construction.

During the construction period additional piezometer stations were installed as the complexity of the subsurface conditions became apparent and addition stations appeared warranted.

The locations of the instrumentation stations are shown in Figure 1.

5.2 Piezometric Survey

In situ pore water pressures have been monitored by Geonor M600 vibrating wire piezometers and by conventional standpipes fitted with a porous tip located in a sealed length of borehole or shaft. Of the nine Geonor instruments installed two have been abandoned after reading faults developed. Tests carried out on Geonor piezometers held in stock indicated that the devices are temperature

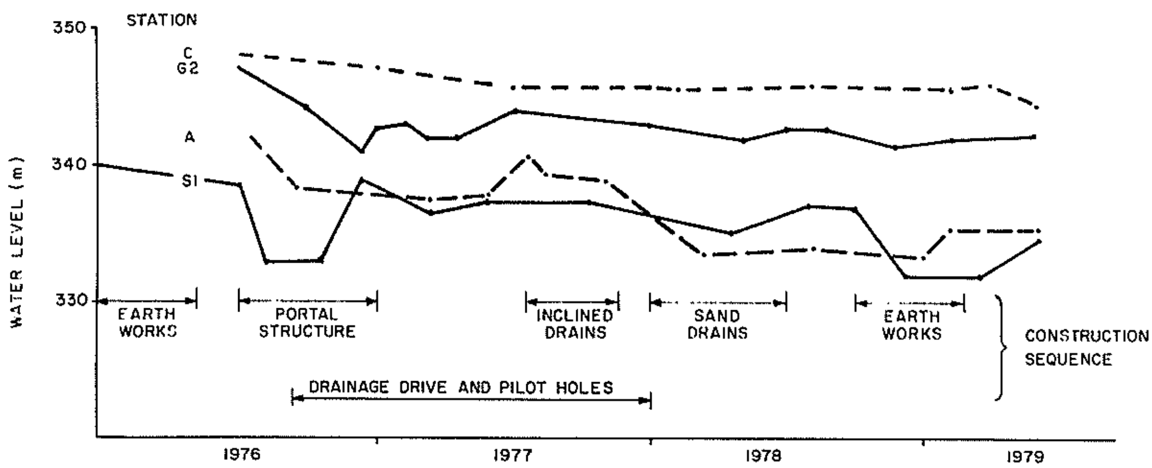

FIG. 2 SELECTED WATER LEVEL RECORDS

sensitive, the indicated pressure varying by .75 - 3 kPa per ^{0}C. The installed piezometers had been calibrated at 21^{0}C while measured groundwater temperatures ranged from 12 to 14^{0}C. As a result the accuracy of the absolute pressures indicated by the installed piezometers was questionable and conventional standpipes were installed adjacent to the piezometers to allow the latter to be field calibrated.

This emphasised the need for exhaustive pre-installation calibration of in situ measurement devices and the desirability of means of in situ recalibration. It is understood that Geonor piezometers are now supplied with temperature correction data and models permitting field calibrations are available.

5.3 Slope Movement Monitoring

Five borehole inclinometer tubes were installed in and adjacent to the area of construction activity. No significant movements have been detected from the inclinometer readings.

6 EFFECTIVENESS OF SLOPE DEWATERING

6.1 General

Daily rainfall records were kept and piezometers and drain discharges read at regular intervals. After major construction activities the frequency of readings was increased until readings had stabilised at new equilibrium values.

6.2 Piezometer Readings

The vibrating wire piezometers and standpipes tips are sealed into boreholes near the level of the colluvium/mudstone interface and record the ground water pressures at that level. Figure 2 shows the variation of recorded pressures at four stations selected from the fourteen installed.

Factors which were expected to influence the water pressures were the drainage measures installed, the unloading of the slope by excavation and seasonal rainfall variations. The time of occurrence of the major construction activities is shown in Figure 2.

Standpipe C which is located outside the area excavated has shown a steady but significant decrease in water pressure since installation. This reduction may result from the effects of surface drainage measures reducing rainfall infiltration.

Stations S1 and G2 located in an area where the interface forms a gully have shown apparent seasonal variations and major reductions related to construction activities and in particular slope excavation. The temporary drop of 6 metres in water level at station S1 in 1976 is associated with successful dewatering of the shafts for the portal structure by the use of adjacent pump shafts.

6.3 Drain Discharges

Discharges from individual included drains, vertical sand drains and pump shafts were monitored. In most cases the discharges increased significantly after periods of heavy rainfall. Figure 3 shows the variations of the total sand drain curtain discharge with time and Figure 4 gives individual sand drain discharge on two occasions.

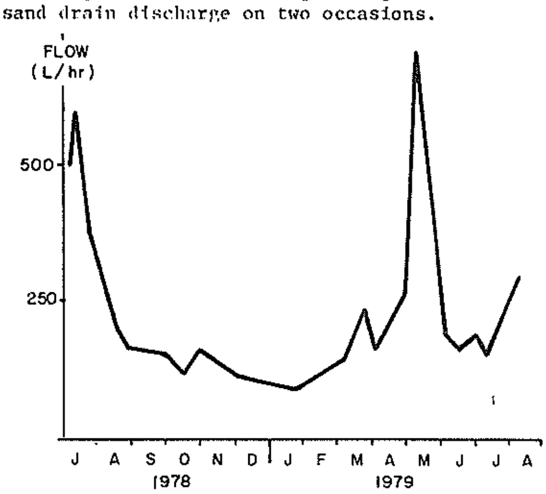

FIG. 3 TOTAL DISCHARGE FROM SAND DRAINS

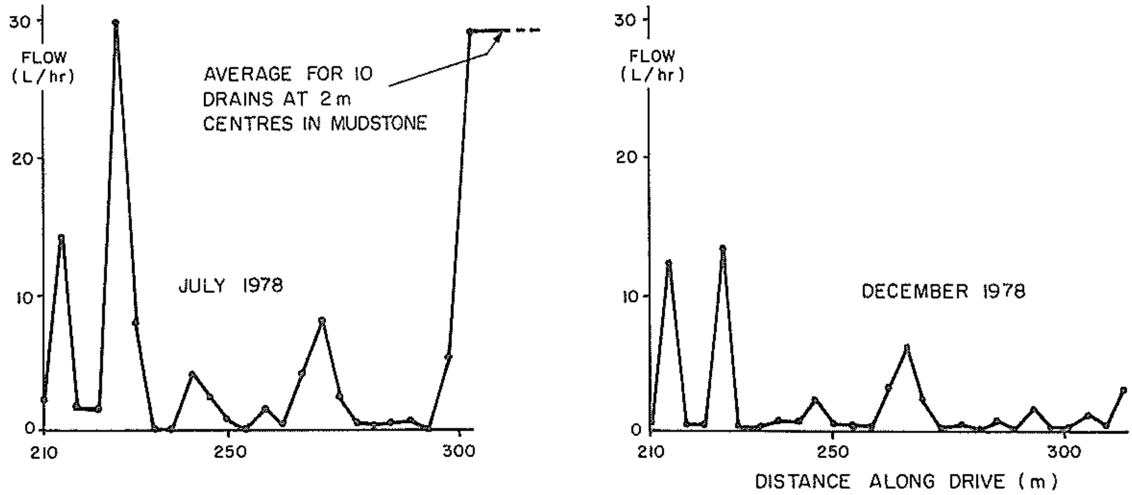

FIG. 4 INDIVIDUAL SAND DRAIN DISCHARGES

Discharges from inclined drains showed similar variations in discharge between closely spaced drains and similar peaks associated with periods of rain. Five pump shafts installed to accelerate slope dewatering were unsuccessful and required only periodic baling, being essentially dry holes.

6.4 Effectiveness of Drainage Measures

The spacing and size of the sand drains were determined using a coefficient of permeability obtained from analysis of recharge rates in exploratory shafts. The value obtained (4×10^{-6} m/sec) was considered as an average between the high "permeability" of the blocky zones observed in the mudstone and the low permeability of the colluvium (2.5×10^{-9} m/sec) as inferred from consolidometer tests and empirical grading/permeability relationships.

The variation in the sand drain discharges suggests that the blocky zones may be localised and that in most of the drains a considerably lower coefficient of permeability would be appropriate.

Observations suggest that the sand drains exhibiting the high flows providing the peaks in Figure 3 have very variable discharge. It is possible that these drains intersect blocky zones and are intercepting recharge water entering the slope through the high permeability blocky zones.

The base discharge from the drainage drive of approximately 100 litres/hour is possibly an indication of the water being removed by the sand drains acting in their designed function as draw down wells. The recorded base discharge is approximately one fifth of the design estimated discharge for the pre-construction water table.

Despite the fact that drainage measures are removing significant volumes of subsurface water, reductions in water pressure due to the major drainage curtain system are not obvious. That drainage measures can reduce in situ water pressures is evidenced by the temporary lowering of water levels at station S1. Similarly at standpipe A a permanent water level lowering of 2.2 metres occurred after an inclined drain passing close to the station discharged 62,000 litres in 3 months.

6.5 Conclusions

The dilemma faced in assessing the causes and permanence of recorded reductions in the water pressures revolves around whether the reductions result from the removal of water by the drains or from reduction in porewater pressure due to the slope excavation. It is likely that the time for the drainage measures to become effective and for unloading induced pore pressure reductions to dissipate will be similarly affected by variations in permeability.

It is possible that the localised drainage of blocky zones in the mudstone beneath and near the inferred failure surface has a significant though non quantifiable affect on water pressures at the interface. Thus the sand drains may be effective in reducing water pressures at the interface even though they may be relatively ineffective in their design function as draw down wells to dewater the colluvium.

The variation of permeability within the slope suggests that the use of published methods for computing the effects of inclined drains (Kenney et al (1977)) and other drainage measures (Mansur and Kaufmann (1962)) may be unsuitable. Such methods may lead to incorrect and possibly non conservative estimates of the time required for drainage measures to lower a water table.

7 REANALYSIS OF SLOPE

7.1 General

As construction proceeded a considerable amount of additional subsurface data was accumulated and, as intended by the designer, the design was reviewed in the light of this information.

7.2 Mudstone Colluvium Interface Profile

Excavation of the bored piles for the portal structure and drilling of the sand drains provided accurate interface levels at the top and bottom of the slope excavation area. In addition to the predesign investigation bores and shafts 24 small diameter bores and six 1 m shafts were drilled and logged during construction. The interface was also

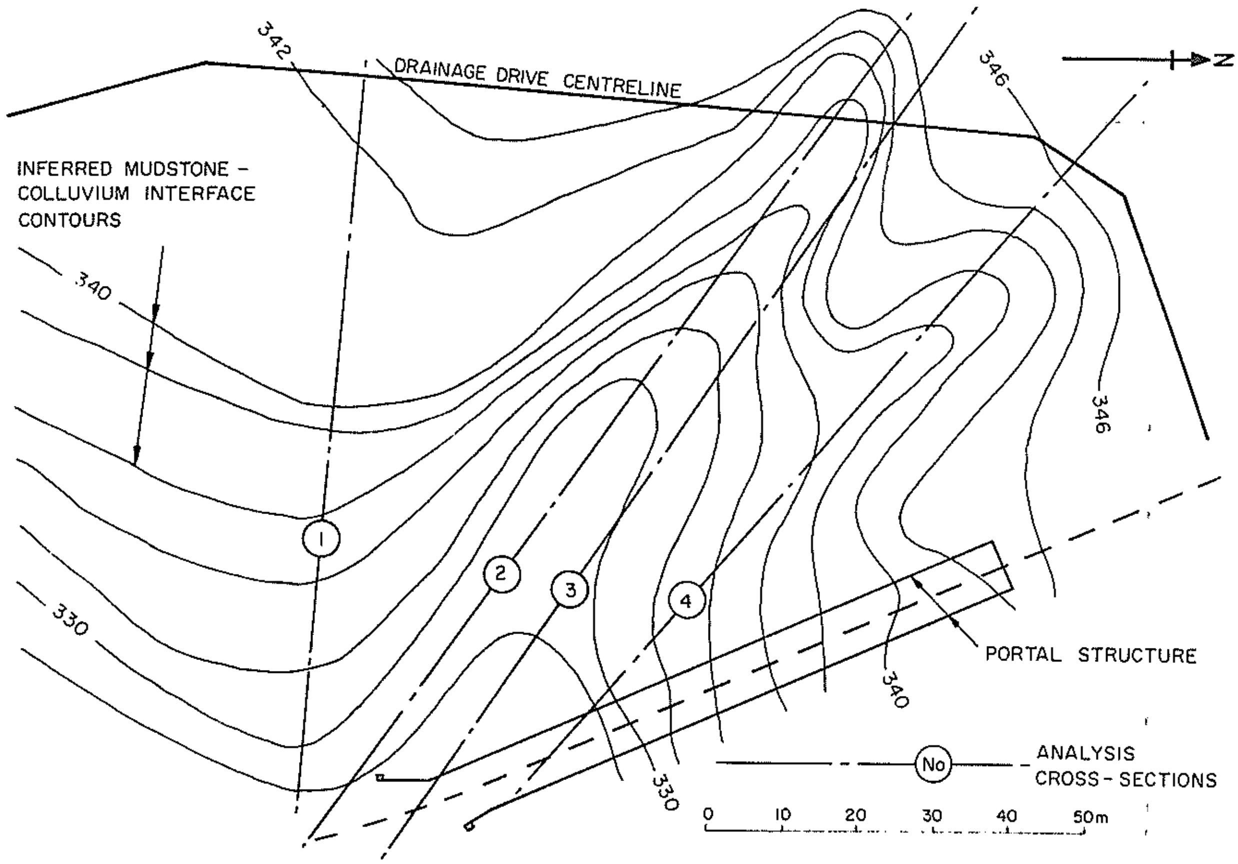

FIG. 5 CONTOURS ON MUDSTONE COLLUVIUM INTERFACE

surface exposed north of the portal structure during the first stage excavation. Figure 5 shows an inferred contour plan of the interface produced from data available at a late stage in construction. A total of 90 spot levels were available and of these 12 are not in agreement with the contours as drawn. It is possible that some of these may indicate further gullies in the interface which could only be confirmed by further extensive drilling. In other cases the discrepancies may result from difficulty in detecting the interface using disturbed NX core.

It is apparent that the interface is complex, gullied, and could not be realistically defined with reasonable pre-design investigations. In this case, the designer had 22 spot levels available of which 4 are possibly inaccurate and misleading for the reasons given above.

Further, design cross-sections derived on the assumption of a reasonably planar interface would provide an inaccurate model. The cross-sections analysed in the original design incorporated soil profiles from boreholes off set up to 30 m from the cross-sections. Some of the cross-sections did not show gullies in the interface apparent in Figure 5.

7.3 Piezometric Data

Even with piezometric data available at fourteen locations in the area it was difficult to obtain a clear model of the water table shape. It appears that the water table may be lower in areas above gullies in the interface, although the water pressure at the interface was higher in these areas due to the greater depth of the interface.

Just as definition of the complex interface geometry is not possible without a large number of spot levels, it is also likely that a considerable (and excessive) number of piezometer stations would be required to determine the distribution of water pressures in the slope.

7.4 Reasons for Full Reanalysis

The colluvium interface geometry discussed in sub section 6.2 was significantly different from that assumed at the time of design. It therefore did not appear appropriate to simply repeat the analysis of the design cross-sections with the as measured water pressures.

To assess the likely effects of the changed interface model a crude sensitivity analysis was made using an infinite slope model.

The effects of varying the inclination of the sliding surface and the ratio of the height of the water table and the height of soil above the sliding surface were examined. The results are presented in Figure 6.

The revised interface model had a locally steeper interface and locally reduced colluvium thickness compared with the original design model. Examination

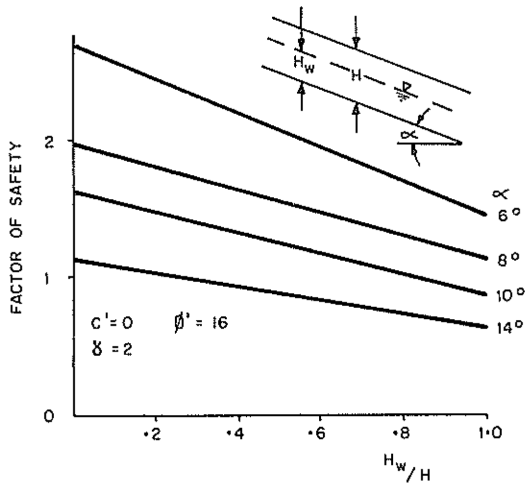

FIG. 6 STABILITY OF INFINITE SLOPE

of Figure 6 suggested that if the original design slope profile was retained the stability factors of safety might be unacceptably low. Accordingly a full reanalysis was undertaken.

7.5 Reanalysis

Seven cross-sections were examined for short and long term stability. Non circular failure surfaces following the interface were examined using the method of Janbu (1973) and a computer program with a search routine was used to determine critical circular failure surfaces within the colluvium. The locations of four typical cross-sections are shown on Figure 5.

For the short term case, the measured piezometric pressures were used, with residual shear strength parameters ($\phi' = 16^0$) being assumed within 1 m of the presheared colluvium interface and peak strength parameters ($\phi' = 33^0$) elsewhere. For the long term case a water table 2 m above the interface was assumed with residual strength parameters throughout the colluvium.

The results of the analysis indicated that the final factors of safety for the as designed slope would be of the order of 1.2 - 1.3 on critical sections compared with 1.5 as calculated on the basis of the information available to the original designer.

LINE	CONTOURS	FAILURE MODE	WATER TABLE	F.S
1	As designed	Circular	Existing	1.1
2	As designed	Circular	Final	1.3
3	Revised	Circular	Existing	2.3
4	Revised	Circular	Final	1.5
5	As designed	Non circular	Existing	.95
6	As designed	Non circular	Final	1.3
7	Revised	Non circular	Existing	1.5
8	Revised	Non circular	Final	1.6

Table 1 : Factors of Safety for Cross-section 3

Analysis showed that extending the portal structure by 15 m and thereby reducing the slope excavation above the portal structure resulted in more acceptable factors of safety. Results for analysis on cross-section 3 (shown on Figure 3) are presented in Table 1, the critical failure surfaces for the as designed and proposed modified surface contours being shown on Figure 7.

Table 1 indicates that with the as measured water table a slope cut to the as designed contours would fail. However in practice the pore water pressures in the slope would be reduced as a result of the unloading associated with slope excavation. For a Skempton (1954) pore pressure coefficient B of 1.0 the immediate post excavation pore pressures would be approximately equivalent to the assumed long term lowered water table and thus the immediate stability would approximate the long term stability.

The circular failure surfaces were analysed to confirm that the non circular failure surface following the interface was the critical case. For the short term (existing water table) cases the circular surfaces are non critical. However for the long term (final water table) cases the circular surfaces are shown as being critical. Because these circular surfaces do not follow a pre-existing failure surface the use of residual strength parameters is unwarranted (Morgenstern (1977)) and the values in Table 1 are overconservative.

As shown in Figure 7 the critical circular failure surfaces are different for the short and long term cases.

7.6 Three Dimensional Stability Analysis

The use of two dimensional (2D) analysis for an apparent three dimensional (3D) situation appeared questionable. While some solutions for 3D failure surfaces have been published these did not suit the geometry or allow for the effects of water pressure. Therefore a solution for a trough shaped section failing in an infinite slope was derived. Normal forces on the side surfaces were derived by resolving vertical and at rest horizontal (Ko) stresses acting in the soil. The solution was expressed as a ratio of the factor of safety for the wedge (F_3) and the factor of safety for a 2D slice through the centre of the wedge (F_2).

Typical results for a cohesionless material are presented in Figure 8. For the case under consideration the variation between the 2D and 3D factor of safety is not significant.

These results vary from those of Hovland (1977) who considered wedge failures without considering the effects of at rest horizontal stresses and obtained considerably lower factors of safety for the 3D case. These may be appropriate for failure of a jointed rock mass but are in the author's opinion overconservative for an intact soil mass. Considerable increases in the factor of safety for the 3D wedge case are obtained for purely cohesive materials (Baligh and Azzouz (1975)).

7.7 Design Modifications

As a result of the reanalysis the portal structure was extended by 15 metres and the extent of the second stage excavation was reduced.

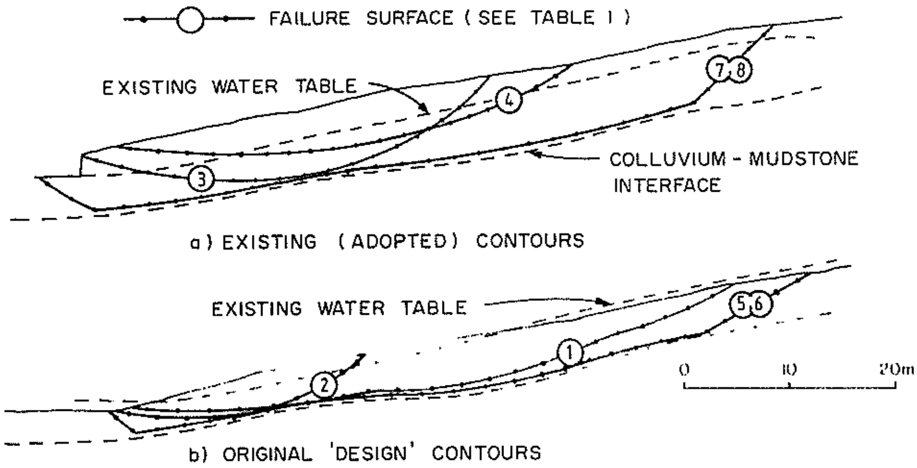

FIG. 7 CRITICAL SURFACES ON SECTION 3

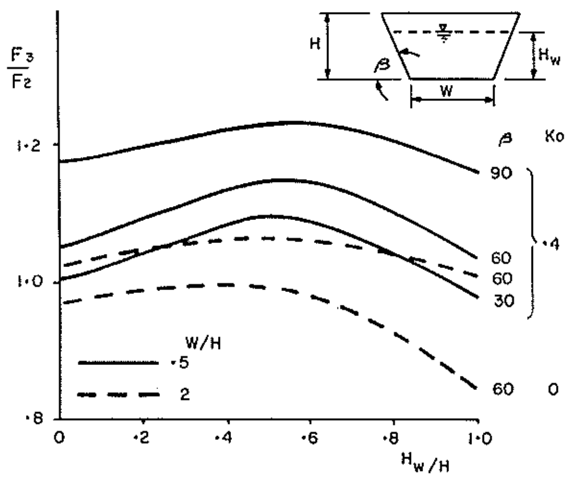

FIG. 8 RATIO OF F.S. FOR INFINITE SLOPE (F_2) AND F.S. FOR INFINITE WEDGE (F_3)

In addition a pattern of inclined drains are to be installed from within the portal structure. It is hoped that some of these will intersect blocky zones near the interface and in particular in interface gully areas where water pressures still appear to be high.

8 CONCLUSIONS

The case history reported illustrates the need in slope stabilisation exercises for the designer to review and where necessary modify the original design in the light of additional subsurface and instrumentation data gathered during construction.

Information gained from extensive drilling and shaft excavation carried out during construction suggests a complex gullied mudstone/colluvium interface which could not have been defined with reasonable pre-design investigations. Positive identification of the interface in small diameter (NX) core was difficult due to drilling disturbance in the mudstone. Down hole logging of 1 m shafts provided the only accurate method for locating the interface.

Piezometer readings suggest a complex ground water regime with depressions in the water table surface corresponding to gullies in the interface. While significant reductions in water levels occurred during construction, it was not possible to accurately assess to what extent these resulted from the influence of the drainage measures or from reductions in pore water pressure due to the unloading associated with slope excavation.

Discharges from closely spaced subsurface drains varied considerably and it is suggested that the drain discharge depends largely on whether or not a zone of blocky mudstone below the interface is intersected. It does not appear possible to predict or pre-determine the location of such zones. The colluvium, intact mudstone and blocky mudstone have significantly different permeabilities and the applicability of available solutions for computing drain discharge is doubtful due to the difficulty in assigning a suitable permeability value.

Reanalysis of the slope using the additional information collected during construction indicated a need for some modifications to details in the original design.

While the drainage measures adopted are removing significant quantities of water from the slope it may be some years before the stability of the slope becomes dependent on the effectiveness of the drainage measures. Long term maintenance and monitoring of the drainage measures is therefore essential.

9 ACKNOWLEDGEMENTS

The author acknowledges the permission of the Commissioner of Works to publish this paper, and wishes to thank I.M. Parton and G. Borrie for their useful comments.

10 REFERENCES

BALIGH, M.M. and AZZOUZ, A.S. (1975). End Effects on Stability of Cohesive Slopes, Proc A S C E, Vol. 101, No. GT11, pp 1105-1117.

BORRIE, G.W. and RIDDOLLS, B.W. (1980). Engineering Geological Investigations in Soft Rock Terrain, Poro-o-Tarao Tunnel, New Zealand. 3rd Aust. - NZ Geomechanics Conference, Wellington, New Zealand.

HOVLAND, H.J. (1977). Three Dimensional Slope Stability Analysis Method, Proc A S C E, Vol. 103, No. GT9, pp 971-986.

JANBU, N. (1973). Slope Stability Computations, Embankment Dam Engineering, Casagrande Volume, ed. by R.C. Hirschfield and S.J. Poulos.

DENNEY, T.C., PARZIN, M. and CHOI, W.S. (1977). Design of Horizontal Drains for Soil Slopes. Proc A S C E, Vol. 103, No. GT11, pp 1311-1323.

MANSUR, C.I. and KAUFMAN, R.I. (1962). Dewatering Chap. 3 of Foundation Engineering, ed. by Leonards. McGraw-Hill, publishers.

MORGENSTERN, N. (1977). Slopes and Excavations in Heavily Over Consolidated Clays. Proc 9 Int. Conf. Soil Mech. and Found. Eng., Tokyo, pp 567-581.

PARTON, I.M. (1974). Assessment of Slope Stability at Poro-o-Tarao Tunnel South Portal. Proc Symp. on Stability of Slopes in Natural Ground, NZ Geomechanics Soc., Nelson.

SKEMPTON, A.W. (1954). The Pore Pressure Coefficients A and B, Geotechnique, Vol. 4, pp 143-147.

Stability of Cut Slopes in a Pumice Soil Deposit with Particular Reference to Tensile Failure

T. YAMANOUCHI
Professor of Civil Engineering, Kyushu University, Japan
K. GOTOH
Associate Professor of Civil Engineering, Kyushu University, Japan
H. MURATA
Associate Professor of Civil Engineering, Kagoshima Technical College, Japan

SUMMARY The properties of a pumice soil called *Shirasu* distributed especially in southern Kyushu of Japan are varied from those of granular soil to those of weak rock in its undisturbed state. In dealing with its cut-off slopes, the tensile failure is unavoidable in the traditional vertical slopes. This paper reports with regard to the problem of tensile failure causing in the cut-off *Shirasu* slopes, dividing into three parts; (1) the identification and classification of the undisturbed *Shirasu* applying a practical measure called soil hardness, (2) strength and elastic constants of the undisturbed specimens in the triaxial compression tests, and (3) stability analyses of the cut-off *Shirasu* slopes of a few kinds of slope angles not only at the ordinary time but also at the time of earthquake, using the finite element method and the seismic coefficient method jointly. The third part indicates where the tensile failure arises in the slopes, and the result proved the superiority of Kyushu Transverse Expressway in which the gentle cut-off slope of 45 degrees was for the first time adopted in the *Shirasu*-distributed area. The gulley erosion is there prevented by means of scrupulous drainage arrangements.

1 INTRODUCTION

The properties of a pumice soil called *Shirasu* distributed in certain areas in Japan are varied from those of granular soil to those of weak rock in its undisturbed state, and there are known no cases of rotational shear-slide failure occurring to cut slopes in usual soil deposits. *Shirasu* may be classified as a soil similar to the yellow-brown pumice soil distributed in North Island of New Zealand. In dealing with these cut-off slopes, two kinds of problems have to be faced; one is the gulley erosion resulted from heavy rainfalls and the other is tensile failure that is unavoidable in the traditional steep cut-off slopes. The gulley erosion is, however, prevented now by means of careful drainage works, but there is much to be made clear about the problem of tensile failure.

The authors made an analytical study on the cut-off slopes of *Shirasu* using the finite element method and from the viewpoint of tensile failure, exclusively on the statical condition (Yamanouchi et al, 1975). They have also published a study on the failure mechanism of the undisturbed samples of *Shirasu* where the rock mechanics approach was applied (Yamanouchi and Murata, 1979).

This paper consists of three parts and the first part deals with the identification and classification of the original *Shirasu* ground according to the soil hardness, giving the result of statistical analysis with the analysis of principal components as its main point. In the second part, strength constants of the undisturbed *Shirasu* specimen are considered in relation with the tensile strength and the hardness. In the third part, the stress condition of slope, either at the ordinary time or at the earthquake time, is analysed to compare the value of slope angle with the occurrence and the magnitude of tensile stress, and at the same time, the significance of the result thereby in the actual damage is discussed. Incidentally, in carrying out the analysis the finite element method and the seismic coefficient method are jointly used by regarding the original *Shirasu* ground bearing a slope as an isotropic and linearly elastic body.

2 IDENTIFICATION AND CLASSIFICATION OF UNDISTURBED *SHIRASU*

2.1 Object of Identification and Classification, and Definition of Hardness

Since engineering properties of the original *Shirasu* ground are not homogeneous, being considerably varied according to its state, careful consideration should be paid to the above-mentioned difference in the properties in the project of slope angle, the slope protection work and the drainage arrangements of cut-off slopes. For that purpose, the identification and classification were carried out depending upon the hardness by means of Yamanaka's soil penetrometer (Yamanaka and Matsuo, 1962) which renders a measurement comparatively easy in detecting the mechanical properties of *Shirasu* at the fields.

According to Yamanaka (1965), the hardness is defined as the force required for the material of greater hardness to penetrate into the inner part of soil against the welded bonds among particles. In this case, the authors will define the value measured by Yamanaka's soil hardness-meter, where a spring that contracts 40 mm precisely against the load of 78.45 N is used as the hardness of *Shirasu*. This hardness of soil is obtained by reading the resistance required for driving a part of the cone, 40 mm long, 18 mm in bottom diameter and 12°40' in vertical angle, into the soil by checking the contraction length of spring.

2.2 Determination of Boundary Hardness by Statistical Analysis

To identify and classify the original *Shirasu* ground, the authors have to determine first the boundary hardnesses which are to be the indication of classification. The principal component analysis was carried out at first, based on the data obtained from the field investigation, followed by the identification and classification based on the hardness from the result. Then the frequency distribution was examined by χ^2-test to see whether it would assume a normal distribution, the significance of

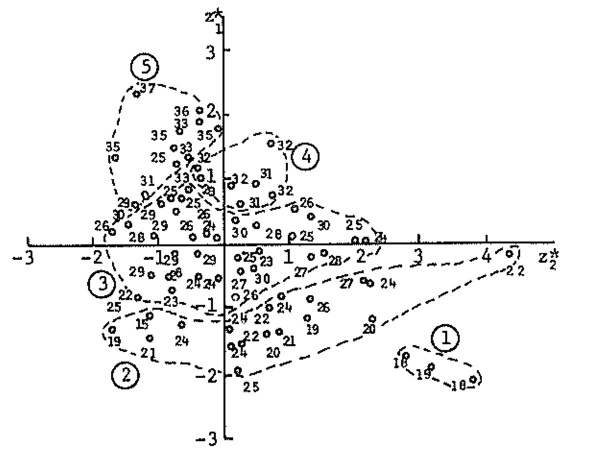

Figure 1 Group classification based on principal component analysis

group classification is confirmed by undergoing F-test and t-test. Boundary hardness will be determined later on by the average and the standard deviation of hardness of each group already classified respectively. The data of investigation used here have been collected from 84 sites in the *Shirasu*-distributed area of Kagoshima Prefecture by Kyushu Engineering Office, Kyushu Construction Bureau, Ministry of Public Works.

Figure 1 shows the result obtained through the principal component analysis by using 5 variables of moisture content ratio, specific gravity of particle, void ratio, coefficient of uniformity and hardness. The ordinate and the abscissa in the figure represent the first principal component and the secondary one respectively, both of which are the values already normarized. The numerical values fixed to each point signify the hardness (mm), and this hardness makes it possible to devide each point in the figure into 5 groups, as shown by a broken line. In order to check whether or not the frequency distribution of the hardness belonging to each group is normal one, the authors evaluated theoretical frequency distribution based on the average of measured values and the standard deviation and carried out the test. As the result, the hardness distribution of each group was found out to be in a good accordance with that of theoretical frequency. When the significance of individual group classification was examined by F-test and t-test, therefore, it was confirmed that 5 groups fall under other population respectively. Accordingly, it is possible, if we take (average hardness $\pm$ standard deviation) to distinguish *Shirasu* thus classified into 5 categories according to the hardness, to consider that the first group lies within the range of 17.8 to 18.8, the second group 19.5 to 25.1, the third group 25.0 to 29.6, the fourth group 29.9 to 32.1 and the fifth group 32.5 to 35.9 and that the boundary hardness of each group is 20, 25, 30 and 33.

From the result of analysis made so far *Shirasu* may be classified into 5 groups of one with the hardness below 20 mm, one between 20 to 25 mm, one between 25 to 30 mm, one between 30 to 33 mm and one above 33 mm, and each group will be assumed as equivalent to its conventional name respectively, namely, very soft *Shirasu*, soft *Shirasu*, semi-hard *Shirasu*, hard *Shirasu* and welded tuff.

3 STRENGTH CONSTANTS OF UNDISTURBED *SHIRASU* SPECIMEN

3.1 Relation between Tensile Strength and Hardness

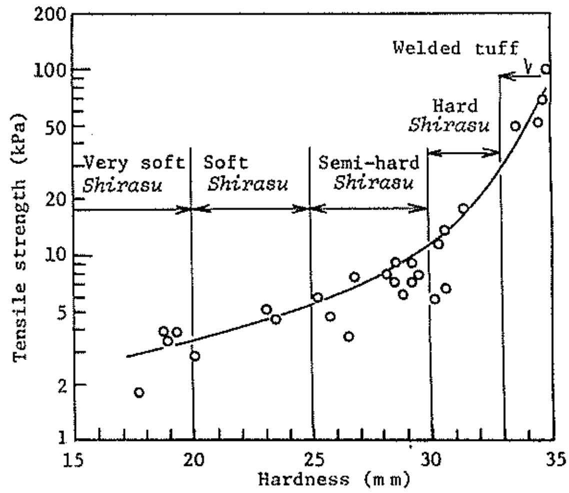

Figure 2 Relation between tensile strength and hardness of *Shirasu*

Undisturbed samples taken from the fields by using a specially devised cutter are characterized by the fact that it bears tensile strength resulted from the geological welding effect. This tensile strength can be measured simply by means of the splitting tensile test from the following equation (Akazawa, 1943)

$$\sigma_t = \frac{2P}{\pi d l} \qquad (1)$$

where, σ_t: splitting tensile strength, P: compression load, d: diameter of sample, l: thickness of sample. Incidentally, the fact that the splitting tensile strength of undisturbed *Shirasu* becomes nearly equivalent to the uniaxial tensile strength has already been confirmed (Murata and Yamanouchi, 1977). Figure 2 shows the relation between the splitting tensile strength of undisturbed *Shirasu* and the soil hardness measured at the same field as the place where the undisturbed specimen is sampled. As expected from the figure, it is obvious that the higher hardness index number rises, the higher tensile strength goes up. Also, the higher the hardness is, the larger unit weight grows, and therefore, the hard *Shirasu* is estimated to possess properties most resembled to soft rock. In southern Kyushu, therefore, there was a customary practice to build the cut-off *Shirasu* slope almost perpendicular as the countermeasure to protect the cut surface from water flow in that rainy district, though no measure were taken yet about the mechanical stability. The tensile strength of very soft *Shirasu* is extremely small, to a degree almost negligible, it seems, but when compared with disturbed samples, the effect from a welding effect is not to be overlooked.

3.2 Relation between Tensile Strength and Constants

Elastic constants and shear strength constants can be evaluated by carrying out the triaxial compressive test, using the undisturbed samples taken from the fields by using the specially devised cutter. The characteristics of the sress-strain curve obtained from the test are; i) the relation of stress with volumetric strain decreases linearly in the initial stress stage, followed by the occurrence of rapid dilatancy, ii) the difference between the maximum axial stress and the residual deviator stress is large. Since the Griffith failure criterion is applicable to the stress limit of the former, *Shirasu* may be assumed as an elastic body in the above stress zone. At this time of elastic limit, the relation between Young's modulus E_e in the case

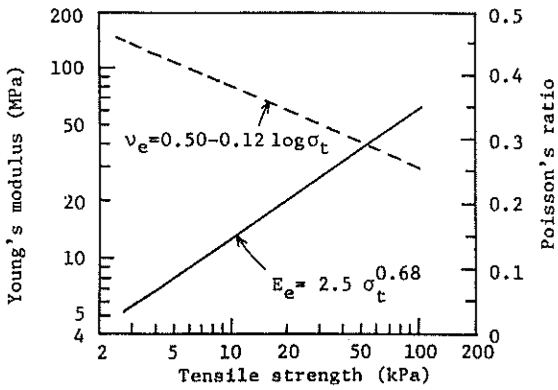

Figure 3 Relation between Young's modulus, Poisson's ratio and tensile strength

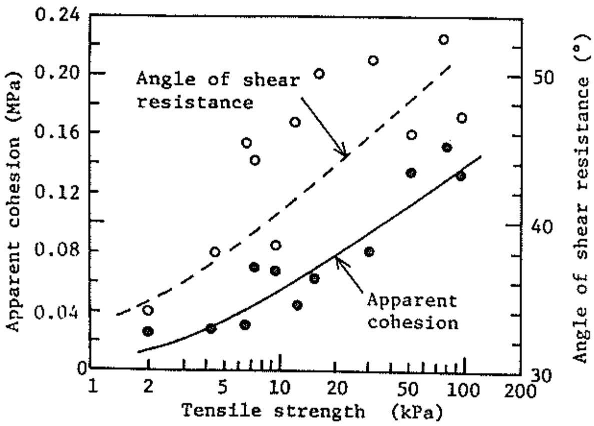

Figure 4 Relation between apparent cohesion, angle of shear resistance and tensile strength

when the confining pressure is zero and Poisson's ratio ν_e and tensile strength may be expressed by the following equation, as seen by Figure 3 (Yamanouchi and Murata, 1979).

$$E_e = 2.5\,\sigma_t^{0.68} \tag{2}$$

$$\nu_e = 0.50 - 0.12\log\sigma_t \tag{3}$$

As stated above, undisturbed samples have an elastic domain in their initial deformation zone, but ultimately they cause shear slide failure in the same way as the disturbed *Shirasu*, resulting in shear failure. That point of time falls on that of the maximum axial stress, and under this stress condition, the modified Griffith failure criterion is applicable.

In Figure 4 are given the relation between apparent cohesion c_f and angle of shear resistance ϕ_f, which have been evaluated from the failure envelop of Mohr-Coulomb under the maximum deviator stress condition with tensile strength. The Mohr-Coulomb failure envelop of the undisturbed *Shirasu* changes to a curve with the cohesion, and the value has stopped below 0.2 MPa. Since the apparent cohesion and the angle of shear resistance, evaluated from the Mohr-Coulomb failure envelop under the condition of residual deviator stress, are almost constant independently of the tensile strength and nearly agree with the values of them when the very soft *Shirasu* gives the maximum axial stress, a rapid growth of c_f and ϕ_f with the increase of tensile strength is understood as mainly resulted from the welding effect of undisturbed *Shirasu*.

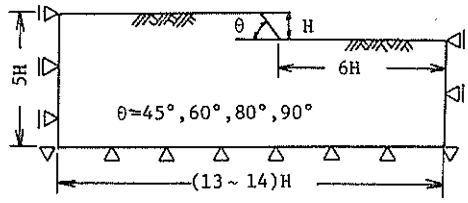

Figure 5 Analysis domain and boundary conditions for pseudo-dynamic F.E.M. analysis of cut-off *Shirasu* slope

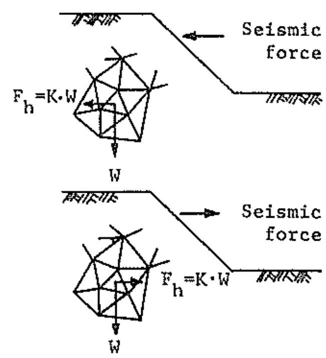

Figure 6 Key figure for seismic coefficient method

4 STABILITY ANALYSES OF CUT-OFF *SHIRASU* SLOPES

4.1 Computing Method

The analysis domain for the finite element method is given, as shown in Figure 5. As the object of the present analysis is laid in grasping of the slope behavior, it is planned in a way that the effect from sides as well as lower boundary may be prevented as much as possible. As for boundary conditions, the horizontal displacement is restricted against lateral boundary and for the lower boundary the condition of perfect fix is given.

Concerning the elastic constant, here is used the value of static condition as it is, even for the pseudo-seismic analysis, because there is hardly any dynamic value to be obtained, excepting the observed value by Omote et al (1973), nor is the result of observation made by Omote et al satisfactory enough. The tensile strength of each *Shirasu* material, elastic constant and shear strength constants to be used for analysis are given in Table I.

The key figure of the seismic coefficient method is shown in Figure 6. As seen in the figure, each

TABLE I STRENGTH CONSTANTS USED FOR ANALYSES

Kinds of *Shirasu*	Soft *Shirasu*	Semi-hard *Shirasu*	Hard *Shirasu*
Tensile strength σ_t (kPa)	5	8	22
Apparent unit weight γ_t (kN/m^3)	12.7	13.7	15.0
Young's modulus E_e (MPa)	8	11	22
Poisson's ratio ν_e	0.41	0.38	0.33
Apparent cohesion c_f (kPa)	30	42	80
Angle of shear resistance ϕ_f (°)	38	41	45

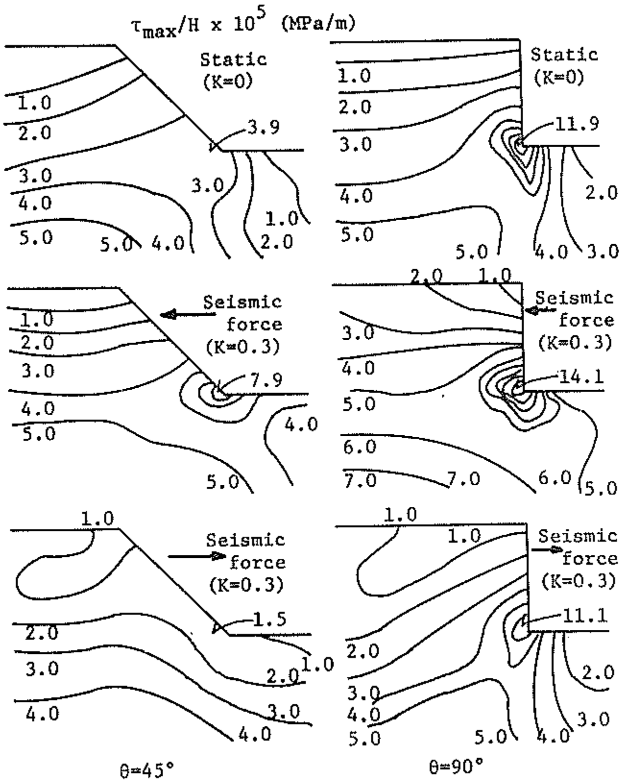

Figure 7 Maximum shear stress contours in case of semi-hard *Shirasu*

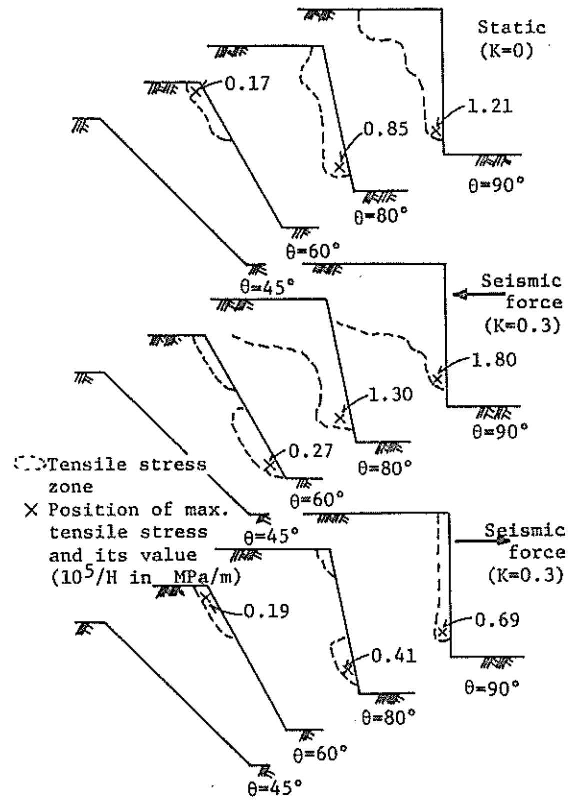

Figure 8 Relation between magnitude of tensile stress zone and slope angle in case of semi-hard *Shirasu*

element is subject to horizontal force, which is obtained by multiplying by the horizontal seismic coefficient K besides its own weight. In the case the finite element method is used, the horizontal seismic force can be taken optionally for it, but it was assumed here for simplicity that all elements are constant, and the value K = 0.3 which was estimated at the time of 1968 Ebino earthquake (Research Committee on *Shirasu*, Japanese Society of SM and FE, 1968) was adopted. Furthermore, as shown in the figure, there are two ways of input method in the seismic force acting upon the slope. One is the case when the seismic force goes toward the inside of the slope and the other is the case when it goes out of the slope, and the direction of the horizontal force acting upon each element agrees with that of this seismic force.

4.2 Distribution of Maximum Shear Stress

In Figure 7, the maximum shear stress is traced after equivalent points on the slope where the slope angle of semi-hard *Shirasu* is either 45° or 90° respectively. As plain from the figure, the maximum shear stress at the part near the toe is smaller than its static condition when the earthquake force acts in the outward direction of the slope, but it gets larger when the force acts in the incoming direction. And on the gentle slope of θ = 45°, there appears conspicuously such a concentration of the maximum shear stress on the toe as that seldom seen under a static condition. The magnitude of it is, however, far smaller than the steep slope of θ = 90°, and not only under static condition but also at the time of earthquake the danger of shear failure in the neighborhood of the slope toe is presumably higher on the slope of a steep slope.

4.3 Tensile Stress Zone and Its Magnitude

According to the result of analysis, while the major principal stress of each element is on the side of compression, the minor principal stress turns to the direction vertical to the slope, inclining to the compression side in case of gentle slope, but showing the tensile side in case of steep slope. Figure 8 shows tensile stress zone and its maximum value concerning semi-hard *Shirasu*. What is to be pointed out as a remarkable characteristics in the figure is that, on a gentle slope of θ = 45°, there occurs no tensile stress even at the time of earthquake, just as in case of static condition. In case of the slope of θ = 60°, there is merely the occurrence of tensile stress only on the slope shoulder, similarly as in case of static condition, with respect to the earthquake force going out of the slope, but for the earthquake force coming into the slope the domain of tensile stress is seen to spread almost entirely over the slope, showing the maximum value at the slope toe. As it comes to the steep slopes of θ = 80° and 90°, the tensile stress is seen to spread wider than that in case of static condition, not only the entire surface of the slope but also down to the depth of the slope, especially when earthquake force acts in the direction entering the slope.

Figure 9 shows the relation between the magnitude of tensile stress at the part of slope toe and slope shoulder and slope angle. There the value at the time of earthquake is recorded in the case when earthquake force enters the slope. As easily understood from the figure, the tendency of tensile stress at the time of earthquake is the same as that under the static condition, where the tensile stress at slope shoulder slightly increases with the increase of slope angle, whereas the tensile stress at the slope toe increases remarkably with the increase of the slope angle. And the value is then much larger than that under a static

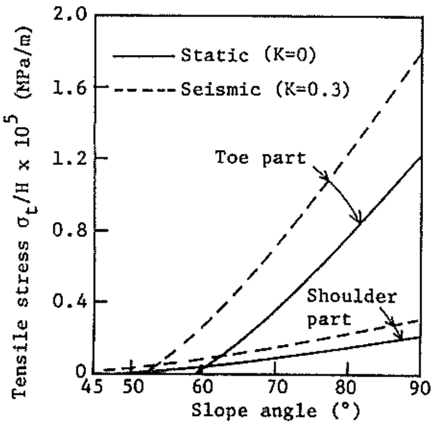

Figure 9 Relation between magnitude of tensile stress and slope angle in case of semi-hard *Shirasu*

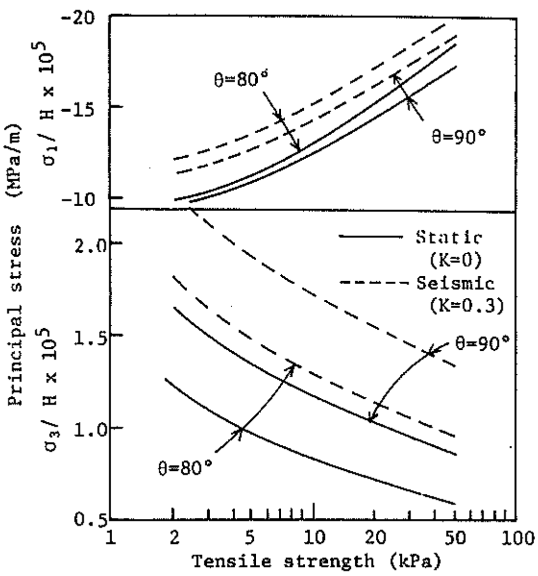

Figure 10 Relation between magnitudes of principal stresses at the toe part and tensile strength

condition. Tensile failure of the slope at the time of earthquake is, therefore, hardly possible to occur at a gentle slope, but in case of a steep slope the said danger is presumed to be greater at the toe part, under a static condition.

Figure 10 shows the relation of major principal stress and minor principal stress (tensile stress) at the slope toe in the steep slope with the tensile strength borne by *Shirasu*. It is obvious that the minor principal stress (tensile stress) which acts in the direction almost normal to the slope is larger when the tensile strength is smaller. As clearly seen from this, the major principal stress (compressive stress) gives a fairly large value and acts upon the slope in almost parallel direction, the circumstances readily lead to cause tensile failure in case of steep slope.

4.4 Relation between Local Tensile Failure and Local Shear Failure

When the height of a slope, where the maximum tensile stress occurring in the slope becomes equal to the tensile strength borne by *Shirasu*, is defined as non-cracking critical height H_{ct}, H_{ct} may be

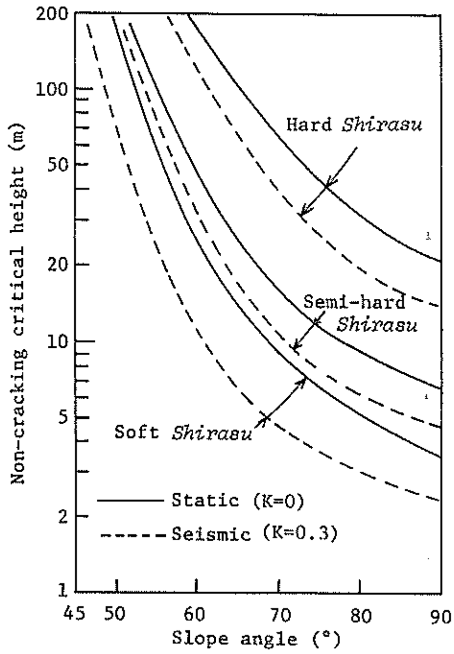

Figure 11 Relation between non-cracking critical height and slope angle

evaluated by the following equation.

$$H_{ct} = \sigma_t \,/\, \sigma_{td.max} \tag{4}$$

Where, σ_t: the tensile strength possessed by *Shirasu*, $\sigma_{td.max}$: maximum tensile stress occurring in the slope. Hence, so-called non-cracking critical height signifies that it is a certain element in the slope, representing slope height at the time when there occurs tensile failure locally, and it is important for investigating the stability of slope. By giving light to the relation between this non-cracking critical height and the slope angle of the slope with respect to three kinds of *Shirasu*, we can disclose the following facts, as shown in Figure 11.

First of all, let us pay attention to the kinds of *Shirasu*. While with hard *Shirasu* it is found in non-cracking state on the slope as high as some 20m, even when it is a steep slope above θ = 80°, with semi-hard and soft *Shirasu* of small tensile strength, non-cracking critical height considerably decreases. In case of θ = 60°, there is expected tensile failure on the slope shoulder, but the non-cracking critical height of hard *Shirasu* and semi-hard *Shirasu* arises above 50 m, and there is no danger of failure. At the time of earthquake, the non-cracking critical height of three kinds of *Shirasu* decreases further compared with that of static case. By the way, since the non-cracking critical height in the case when earthquake force acts in the direction going out of the slope arises higher than that of static case, it is left out of the figure.

With the elements in a slope, as it is sometimes expected that there might occur local shear failure, we have to investigate superfluity level S_L which is detected vertical to the Mohr-Coulomb failure envelop of shear stress of each element. S_L will be given by the following equation, referring to Figure 12.

$$S_L = \frac{(\sigma_1 - \sigma_3)/2}{(\sigma_1 + \sigma_3)/2 \cdot \sin\phi_f + c_f \cos\phi_f} \tag{5}$$

Where, σ_1, σ_3: major principal stress and minor

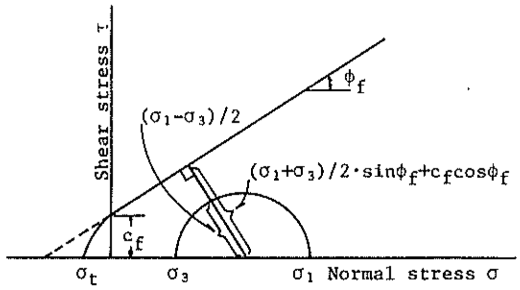

Figure 12 Illustrative figure for superfluity level S_L against shear failure

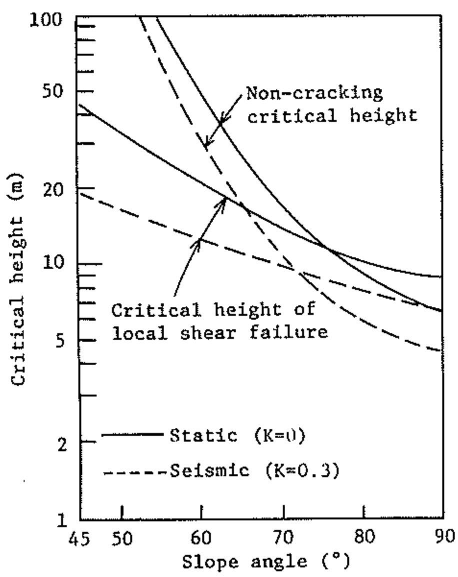

Figure 13 Relation between two kinds of critical heights and slope angle in case of semi-hard *Shirasu*

principal stress respectively, c_f, ϕ_f: the apparent cohesion and angle of shear resistance.

It is possible, therefore, to define the slope height where elements $\sigma_{td} < \sigma_t$ as well as $S_L > 1$ have appeared in the slope as the slope height H_{cs} at which local shear failure takes place. Figure 13 shows the relation between critical height H_{ct}, H_{cs} of each semi-hard *Shirasu* and slope angle of the slope. As seen from the figure, H_{ct} is larger than H_{cs} in case of $\theta \leq 75°$ to be inverse in case of $\theta \geq 75°$, whether it is under a static condition or at the time of earthquake. Such a tendency remains the same either with hard *Shirasu* or with soft *Shirasu*. It is therefore evident in case of a steep slope that the local tensile failure at the slope toe plays a dominant part in the failure of slope. Also, with the slope of $\theta = 60°$, it is presumed that tensile failure has endangered the stability of the slope before the occurrence of a complete shear failure. Moreover, on the slope of $\theta = 45°$, where there has taken place local shear failure with H = 45 m (static condition) and H = 20 m (earthquake time condition), the domain is confined only to the surface of the slope, nor there has occurred any local tensile failure, we can safely judge that it is mechanically stable.

Again as the countermeasure against tensile failure on the slope, the authors have made it known that cutting of shoulder part or some retaining works at the toe part are effective (Yamanouchi et al, 1975).

5 CONCLUSIONS

Considerations made so far are on the stability of the slope, which was worked out by the application of the engineering classification of undisturbed *Shirasu* and the finite element method as well as the seismic coefficient method to each kind of the original *Shirasu* ground bearing cut-off slopes. The result obtained will be summarized as follows.

(1) The original ground *Shirasu* may be classified into four categories according to its hardness.
(2) The maximum shear stress is conspicuously concentrated on the slope toe, more in case of steep slope than in the gentle slope, and its degree is higher at the time of earthquake and in case of soft *Shirasu*.
(3) While tensile stress at each part of the slope, except at the toe, increases only slightly when the slope angle is larger than about 60°, the tensile stress at the slope toe increases with the increase of slope angle, and its value is larger at the time of earthquake and in case of soft *Shirasu* than under the static condition.
(4) With the slope of the slope angle larger than 75°, the local tensile failure surpasses the local shear failure at the toe, and the tensile failure of the slope is predominant. On the other hand, non-cracking critical height decreases considerably at the time of earthquake.

6 ACKNOWLEDGEMENTS

The data used for the statistical analysis, for the purpose of identification and classification of the undisturbed *Shirasu*, are indebted to Kyushu Engineering Office, Kyushu Construction Bureau, Ministry of Public Works, and the authors wish to express their gratitude for the cooperation.

7 REFERENCES

AKAZAWA, T. (1943). The new method to obtain the internal stress due to the compression on concretes. J. Japan Society of Civ. Engs., Vol. 29, No. 11, pp 777-787 (in Japanese).
MURATA, H. and YAMANOUCHI, T. (1977). Factors affecting the strength characteristics of the undisturbed *Shirasu*. J. Japanese Society of Soil Mech. and Found. Engg., Vol. 17, No. 3, pp 81-91 (in Japanese).
Omote, S. et al (1973). Dynamic characteristics of Kajiki *Shirasu* ground. Proc. Tenth Symp. Natural Disaster Sciences, pp 267-268 (in Japanese).
RESEARCH COMMITTEE ON *SHIRASU*, JAPANESE SOCIETY OF SOIL MECH. AND FOUND. ENGG. (1968). 1968 Ebino earthquake and geomechanical damages. Tsuchi-to-Kiso, Japanese Society of Soil Mech. and Found. Engg., Vol. 16, No. 9, pp 47-59 (in Japanese).
YAMANAKA, K. and MATSUO, K. (1962). A study of soil hardness (1st Report), Relation between hardness and moisture content on soils. J. Science of Soil and Manure, Japan, Vol. 33, No. 7, pp 343-347 (in Japanese).
YAMANAKA, K. (1965). Measurement method of soil consistency, determination of bond, crushing degree and hardness. Soil Physical Conditions and Plant Growth, Japan, No. 11 and 12, pp 1-8 (in Japanese).
YAMANOUCHI, T., GOTOH, K. and MURATA, H. (1975). Stability of cut slopes of *Shirasu*. Proc. Fifth Asian Reg. Conf. Soil Mech. and Found. Engg., Bangalore, Vol. 1, pp 45-49.
YAMANOUCHI, T. and MURATA, H. (1979). Failure mechanism of the undisturbed samples of a pumice flow soil "*Shirasu*". Proc. Sixth Asian Reg. Conf. Soil Mech. and Found. Engg., Singapore, Vol. 1, pp 107-110.

The Application of a Critical State Soil Model to Cyclic Triaxial Tests

J. P. CARTER
Lecturer, Department of Civil Engineering, University of Queensland, Brisbane
J. R. BOOKER
Department of Civil Engineering, University of Sydney
C. P. WROTH
Professor of Engineering Science, University of Oxford, United Kingdom

SUMMARY Recently, several sophisticated constitutive models have been proposed to predict the behaviour of soils under cyclic loading. In this paper the concepts of the critical state soil mechanics have been used to develop a simple model which predicts many aspects of clays under repeated loading.

1 INTRODUCTION

An understanding of the behaviour of soils under cyclic loading is important in the fields of earthquake, offshore and highway engineering. The properties of sands under cyclic loading have been studied extensively (Seed and Lee, 1966; Seed, 1979) and engineering theories developed for particular classes of problems(Martin et al ,1970). More recently data pertinent to cyclic loading of clay have been collected (Taylor et al, 1965, 1969; Andersen, 1975, 1976; Van Eekelen and Potts, 1978). Although the conclusions of these tests are not unanimous, several facts emerge. The most important of these is that under undrained loading excess pore pressures are generated and if cyclic loading is continued for a sufficiently long time a failure or critical state condition may be reached.

There have been several attempts at modelling this behaviour mathematically (Mróz et al 1979; Prévost, 1977). These models are complex involving multiple yield surfaces and both kinematic and isotropic hardening and involve the specification of a number of parameters which may be difficult to determine in practice. A less complicated model, which is potentially applicable to cyclic loading, has been suggested by Pender (1977, 1978).

In this paper the concepts of critical state soil mechanics have been extended to provide a description of the response of clay under cyclic loading. Only one additional parameter, which can be determined from the number of cycles to failure in an undrained cyclic triaxial test, is required.

2 THEORETICAL DEVELOPMENT

2.1 Modified Cam Clay

In the interest of clarity the essential features of the modified Cam-clay model are described. Attention is restricted to triaxial conditions where it assumed that the state of effective stress may be completely described by the quantities $p' = \frac{1}{3}(\sigma_z' + 2\sigma_r')$ and $q = \sigma_z' - \sigma_r' = \sigma_z - \sigma_r$, where σ_z', σ_r', σ_z, σ_r are the axial and radial components of effective and total stress respectively. The symbol u will be used to represent excess pore pressure. The convenient measures of strain are the volume strain, $v = \varepsilon_1 + 2\varepsilon_3$ and a measure of the octahedral strain, $\varepsilon = \frac{2}{3}(\varepsilon_1 - \varepsilon_3)$; where ε_1, and ε_3 are major and minor principal strains respectively.

The modified Cam-clay model requires the specification of five parameters, values of which may be readily obtained from standard oedometer and triaxial compression tests. These parameters are :

- λ the gradient of the normal consolidation line in e-$\ell n\ p'$ space,
- κ the gradient of the swelling and recompression line in e-$\ell n\ p'$ space
- e_{cs} a value of voids ratio which locates the consolidation lines in e-$\ell n\ p'$ space, conveniently taken as the value of e at unit p' on the critical state line,
- M the value of the stress ratio q/p' at the critical state condition; M is related to ϕ', the angle of friction obtained in triaxial compression tests, by $M = 6 \sin\phi'/(3-\sin\phi')$
- G the elastic shear modulus.

For states of stress within the current yield surface the soil responds elastically and the incremental effective stress-strain law may be written as

$$\begin{Bmatrix} dp' \\ dq \end{Bmatrix} = \begin{bmatrix} K & 0 \\ 0 & 3G \end{bmatrix} \cdot \begin{Bmatrix} dv \\ d\varepsilon \end{Bmatrix} \qquad (1)$$

where $K = (1+e)p'/\kappa$ is the bulk modulus and the shear modulus G is constant.

Yielding of the material occurs whenever the stresses satisfy the following criterion

$$q^2 - M^2\{p'(p_c' - p')\} = 0 \qquad (2)$$

where p_c' is a hardening parameter - analogous to a preconsolidation pressure - which defines the non-zero intersection of the current elliptical yield locus and the p' axis in effective stress space - see Figure 1. Plastic flow is determined by an associated flow rule and the permanent volume strain dv^p is related to the change in the hardening parameter p_c' as follows

$$dv^p = \left(\frac{\lambda-\kappa}{1+e}\right)\frac{dp_c'}{p_c'} \qquad (3)$$

Types of loading can be categorised in terms of a variable p_y', defined as

$$p_y' = p' + q^2/(Mp') \qquad (4)$$

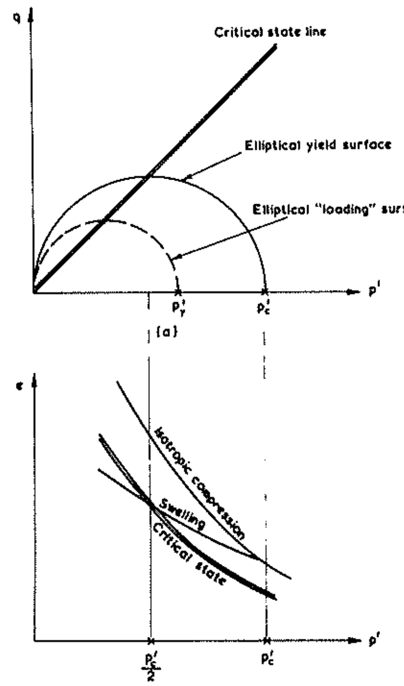

Figure 1 Some aspects of the modified Cam-clay model for triaxial conditions

Equation (4) is also the locus of an ellipse, in p'-q space, which passes through the current stress point and the origin, and is centred on the p' axis, i.e. it has the same shape as the yield locus - see Figure 2. This variable p_y' is the (non-zero) value of p' at which the ellipse cuts the p'-axis and is a convenient way of comparing the current stress state with the current yield locus represented by p_c'.

The material is elastic whenever $p_y' < p_c'$ and during the elastic deformation

$$dp_c'/p_c' = 0 \qquad (5)$$

The material behaves plastically whenever $p_y' = p_c'$ and three conditions can be identified. These are (a) the material hardens whenever $dp_y' = dp_c' > 0$, (b) the material softens whenever $dp_y' = dp_c' < 0$, and (c) 'neutral loading', when the yield locus does not change while plastic behaviour occurs, $dp_y' = dp_c' = 0$. Condition (a) requires $p' > p_c'/2$, i.e. the material is said to be 'wet' of critical, and (b) requires $p' < p_c'/2$, i.e. the material is said to 'dry' of critical.

During plastic behaviour the yield locus changes according to the law

$$dp_c'/p_c' = dp_y'/p_y' \qquad (6)$$

The incremental stress-strain relation during yielding may be shown to be

$$\begin{pmatrix} dv \\ d\varepsilon \end{pmatrix} = \begin{bmatrix} C_{11} & C_{12} \\ C_{21} & C_{22} \end{bmatrix} \cdot \begin{pmatrix} dp' \\ dq \end{pmatrix} \qquad (7)$$

where the compliance coefficients are given by

$$C_{11} = \left(\frac{\lambda-\kappa}{1+e}\right)\frac{a}{p'} + \left(\frac{\kappa}{1+e}\right)\frac{1}{p'}$$

$$C_{12} = C_{21} = \left(\frac{\lambda-\kappa}{1+e}\right)\left(\frac{1-a}{p'}\right)$$

$$C_{22} = \left(\frac{\lambda-\kappa}{1+e}\right)\frac{b}{p'} + \frac{1}{3G}$$

and

$$a = (M^2-\eta^2)/(M^2+\eta^2), \quad b = 4\eta^2/(M^4-\eta^4),$$

$$\eta = \text{the stress ratio } q/p'$$

As would be expected, (7) breaks down when the soil reaches the critical state condition $\eta = M$.

2.2 A Model for Cyclic Loading

The modified Cam-clay model has been shown to match well the observed behaviour of insensitive clays subjected to monotonic loading for which the stress level increases. However, the predictions are not as satisfactory when the soil undergoes repeated loading.

When saturated clay is unloaded and then reloaded it is found that permanent strains occur earlier than predicted by the modified Cam-clay model. One way of interpreting this real behaviour is to assume that the position and perhaps the shape of the yield surface have been affected in some way by the elastic unloading.

For the sake of simplicity in developing a new model it is assumed that the form of the yield surface is unchanged but that its size has been reduced in an isotropic manner by the elastic unloading. This can only mean that the hardening parameter p_c' has been reduced by the unloading process. In order to specify how this reduction occurs a relation is proposed between the hardening parameter p_c' and the loading parameter p_y'. In view of (5) it seems reasonable to postulate that when the material is elastic ($p_y' < p_c'$) and when $dp_y' < 0$, the following relation holds

$$dp_c'/p_c' = \theta\, dp_y'/p_y' \qquad (8)$$

If θ takes a value of unity, then the yield surface would shrink back in such a way that the stress state always lay on it. It is to be expected that the yield surface will recede only a fraction of this amount and the values of θ will tend to be quite small. If, however, the material is elastic, but $dp_y' > 0$, it is postulated that the current yield surface is not changed, i.e.

$$dp_c'/p_c' = 0 \qquad (9)$$

The distinction between these types of behaviour is shown schematically in Figure 2.

It has been shown elsewhere that θ may be regarded as an OCR degradation parameter (Carter et al, 1980). A consequence of introducing this degradation parameter θ into the model is that repeated loading under fully drained conditions will result in a continued densification of the soil sample. In modified Cam-clay, for which θ = 0, no such densification will occur. Some predictions of the new model for undrained loading under triaxial test conditions are now discussed.

3 PREDICTION OF THE BEHAVIOUR OF NORMALLY CONSOLIDATED CLAY

In order to illustrate the behaviour predicted by this model one set of values for the conventional Cam-clay parameters has been selected. These are

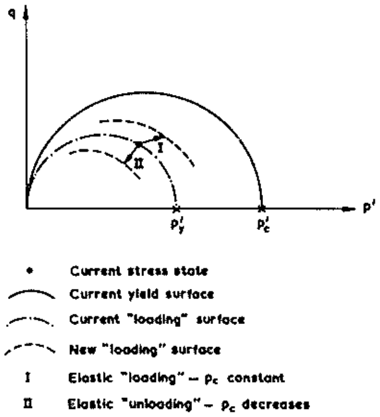

Figure 2 The yield surface and the "loading" surface in p'-q space

λ = 0.25, κ = 0.05, M = 1.2, G = 200 c_{uo}, where c_{uo} is the initial value of undrained strength predicted by the modified Cam-clay model. For all calculations in which the soil is initially in a normally consolidated state, the initial voids ratio is taken as e_0 = 0.6.

3.1 Undrained Stress Controlled Loading

Calculations have been performed for the case of cyclic axial load at constant cell pressure in the triaxial test. In each case loading is applied so that the deviator stress q is varied continuously between limits of 0 and q_c, i.e. one way compression loading where $\sigma_z \geqslant \sigma_r$ with σ_r constant.

Typical results for calculations with θ = 0.1 and q_c = 1.5c_{uo} are shown in Figure 3. The effective stress path, plotted in p'-q space, is shown in Figure 3(a). In the first half of the first cycle the yield surface expands, i.e. the material work hardens, and the stress path is identical to that predicted by modified Cam-clay. During the second half of the first cycle the soil is unloaded (q decreasing) and it responds elastically. As no drainage occurs there is no change in p', however, the value of p_c' will have decreased according to (8), i.e. the yield surface will have contracted slightly. On reloading in the second cycle the material behaves elastically until the stress point reaches the yield locus again*, therafter the material yields, the yield surface expands, further plastic deformations occur, the stress state migrates toward the critical state condition and additional excess pore pressure is generated. This sequence is repeated at each additional load cycle and ultimately, if this process is continued, a critical state condition is reached. In every cycle there is yielding and associated permanent strains and, in particular, during any cycle there is an increment of permanent volume strain. Because the deformation occurs at constant volume there must be a corresponding elastic volume increase and this implies a decrease in mean effective stress, i.e. an increase in pore pressure. The accumulation of excess pore pressure with each cycle is plotted against mean effective stress in Figure 3(c) and against shear strain in Figure 3(d). The relation between deviator stress and shear strain is also shown in Figure 3 (b).

For this material, which has θ = 0.1, failure occurs on the loading portion (q increasing) of the 12th cycle. In general the number of cycles to failure N_f will be dependent not only on the value

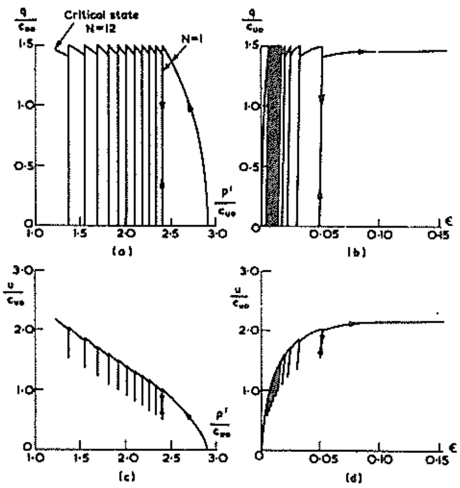

Figure 3 Predictions for a one-way, stress controlled, undrained triaxial test: OCR = 1, θ = 0.1

of θ but also on the cyclic load level q_c. Results are presented in Figure 4 for a number of values of θ and a range of different load levels. It can be seen that for a given material, i.e., a particular value of θ, the number of cycles to failure increases as the amplitude of loading is decreased. For a given amplitude of loading the number of cycles to failure decreases as θ increases. This is as expected since a larger value of θ implies a greater contraction of the yield surface with elastic "unloading". Consequently there are greater permanent volume strains and greater excess pore pressures generated per cycle and thus the material will reach critical state after fewer cycles.

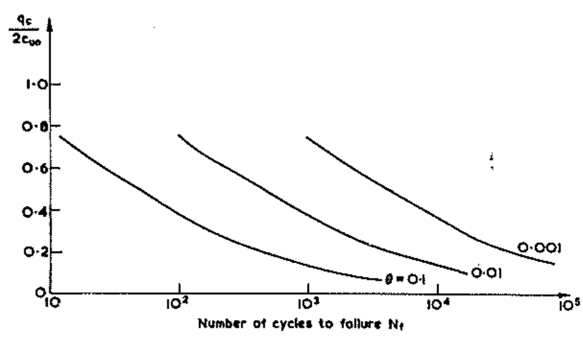

Figure 4 Variation of the number of cycles to failure with cyclic stress amplitude q_c, in a one-way, stress controlled, undrained, triaxial test: OCR = 1

Another important feature predicted by this model is indicated in Figure 5 where the ratio of the undrained shear strength c_u, measured immediately after the "Nth" cycle, to the original undrained strength c_{uo}, measured before cycling, is plotted against the ratio N/N_f. The results show a continual reduction in the undrained shear strength for soils subjected to repeated increments of

* In modified Cam-clay the yield surface will have remained fixed during the unloading and elastic behaviour would be predicted for all subsequent cycles and there would be no further increase in pore pressure.

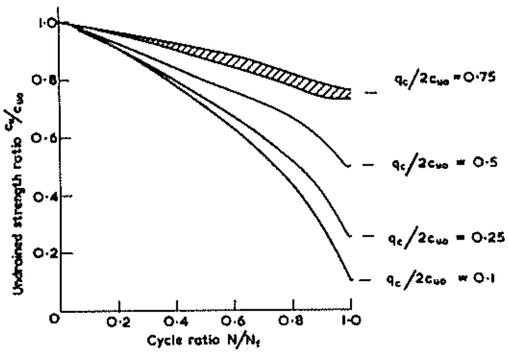

Figure 5 Effect of cyclic stress amplitude q_c on the change in undrained strength

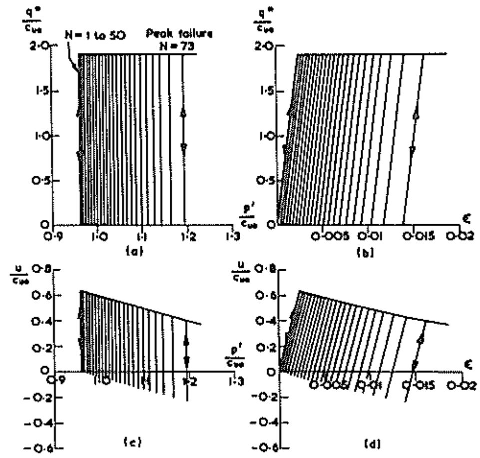

Figure 6 Predictions for a one-way, stress controlled, undrained, triaxial test: OCR = 4, θ = 0.001, G = 200 c_{uo}

deviator stress. Each of the curves of Figure 5 corresponds to a different amplitude of cyclic deviator stress and results for materials with θ in the range $0.001 \leq \theta \leq 0.1$ appear to lie on either a unique curve or in a narrow region as shown. When the soil reaches failure after N_f cycles the final undrained shear strength is equal to one half of the amplitude q_c of the cyclic deviator stress. This effect of a reduction in strength after cyclic loading with increasing number of cycles has been observed in tests on many clays (e.g. Taylor and Bacchus, 1969; Andersen, 1975, 1976).

4 PREDICTIONS OF THE BEHAVIOUR OF OVERCONSOLIDATED CLAY

The behaviour of an initially overconsolidated sample when subjected to repeated loading may be contrasted to that of an initially normally consolidated soil. In Figure 6 results are presented for a material with θ = 0.001 which has been initially isotropically consolidated to an effective stress of $3.85c_{uo}$ and has then been allowed to swell to a mean effective stress equal to 0.961 c_{uo}, so that the conventional overconsolidation ratio is equal to 4. The soil has then been subjected to a continuous variation of deviator stress between the limits $0 \leq q \leq q_c$, where $q_c = 1.9c_{uo}$, under undrained conditions. All stress levels quoted here have been expressed as multiples of the undrained strength c_{uo}, which is the value after swelling to an OCR of 4 but prior to cyclic loading.

The initial swelling and the period when q decreases in each cycle constitute elastic "unloading" as defined above, i.e. p'_y decreasing. During each of these unloading events the yield surface contracts until eventually the stress point contacts the yield surface. Thereafter, there will be periods of plastic loading in each cycle. In this particular example the first plastic strains were observed in the 51st cycle. Thus during the first 50 cycles the material responds entirely elastically; there are no permanent strains and the excess pore pressure oscillates between 0 and $\frac{1}{3}$ q_c. After 51 cycles, permanent strains occur and in this particular case the material dilates and plastically softens because the stress state is on the "dry" side of critical. Since the deformation is occurring at constant volume the increase in plastic volume strain must be compensated by a decrease in elastic volume strain, i.e. the stress state migrates towards critical state and the pore pressure decreases. In common with modified Cam-clay the cyclic model predicts a peak strength in a stress defined test under certain circumstances; hence failure may occur either by the stress state reaching critical state or by reaching this peak undrained strength, whichever occurs first. In samples which are initially highly overconsolidated, such as the one considered here, peak failure is likely to occur. In contrast, soils which are slightly overconsolidated, i.e. on the "wet" side of critical, will, after sufficient cycles, behave in the manner of initially normally consolidated soils. It is also a feature of this model that all initially overconsolidated soils will eventually respond to cyclic loading in the same manner as an initially normally consolidated soil, as long as the deviator stress q is never greater than M times p'.

4.1 The Effect of Initial OCR on Cyclic Behaviour

Calculations have been performed for a number of ideal soils with different values of θ but all having the same conventional overconsolidation ratio of 4.

Figure 7 shows the prediction of the number of cycles to failure N_f in a one way stress controlled test plotted against the magnitude of the applied deviator stress q_c. Curves have been plotted for three different materials corresponding to θ = 0.001, 0.01 and 0.1. The trend is the same as that for normally consolidated soils, i.e. the number of cycles to failure increases as q_c decreases and as θ decreases. Broken curves have also been plotted in Figure 7 for soils with OCR = 1 and the same values of θ. A comparison of the three pairs of curves shows that the number of cycles to failure is also a function of the initial overconsolidation ratio of any soil. The model predicts that overconsolidated soils fail sooner, i.e. in fewer cycles, in repeated load tests than do normally consolidated samples of the same soil. This prediction is in agreement with the trends shown in laboratory tests on Drammen clay (e.g. Andersen, 1975).

5 COMPARISON OF PREDICTIONS WITH EXPERIMENTAL RESULTS

5.1 Tests of Taylor and Bacchus

Taylor and Bacchus (1969) reported the results of cyclic triaxial tests in which one hundred sinusoidal strain-controlled cycles were applied to artificially prepared saturated clay samples. The significant effect on normally consolidated clay was to reduce the mean effective stress p' by an amount which depended on the applied strain

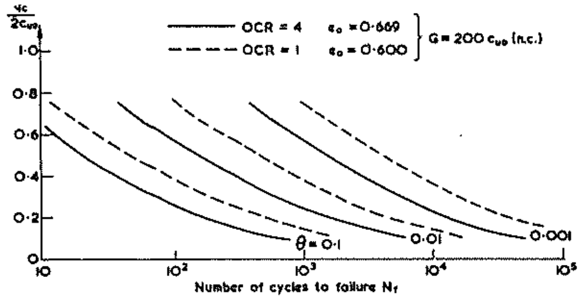

Figure 7 Effect of initial OCR on the number of cycles to failure in a one-way, stress controlled, undrained triaxial test

amplitude. The results of one of these tests in which the initial OCR = 1, e_o = 0.962 and p_o' = 64 lbf/in^2, are plotted in Figure 8 for the case where the strain was varied continuously in the range $-0.003 \leqslant \varepsilon \leqslant 0.003$. Also shown on this plot are some predictions made using the new model. Values selected for the model parameters are λ = 0.132, κ = 0.021, M = 1.5, G = 5000 and 2500 lbf/in^2 and θ = 0.03. It can be seen that the predictions in these strain-controlled tests are very dependent on the value selected for the elastic shear modulus G. In both predictions the rate of decrease in p' is overpredicted in the latter stages of both tests and possible reasons for this behaviour are discussed below. Nevertheless, the model predicts the correct trend in this type of cyclic test.

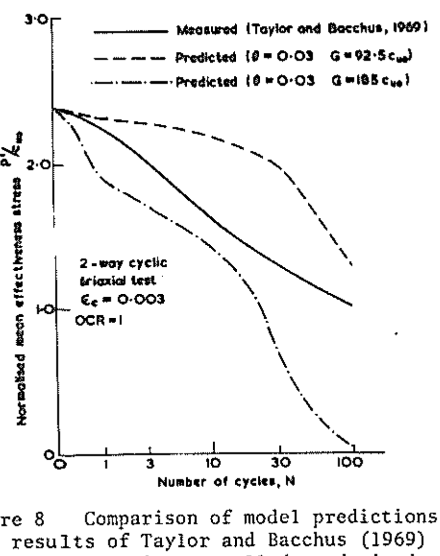

Figure 8 Comparison of model predictions with test results of Taylor and Bacchus (1969) for a two-way strain controlled, undrained, triaxial test

Test results reported by Tayler and Bacchus, and predictions made using the cyclic model are shown in Figure 9 for the case of a monotonic triaxial compression test under undrained conditions. It can be seen, that although the predictions for the ultimate deviator stress are very accurate, the predicted shear stress-strain responses are both too stiff prior to failure. These predictions for monotonic loading, which are the same as would be provided by the modified Cam-clay model, do not show enough plastic shear strain and in fact over-predict the plastic volume strain. As a result a given drop in p' (or increase in u) is predicted in a cyclic test in fewer cycles than is observed. Both static and cyclic tests suggest that the

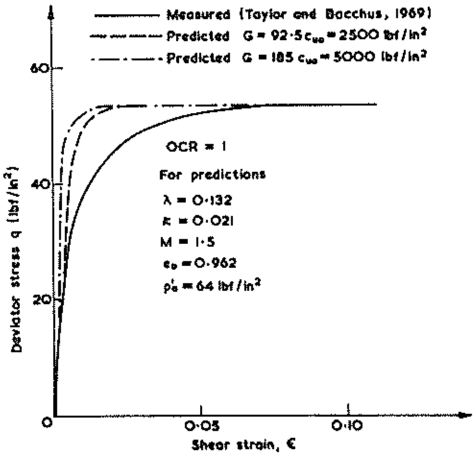

Figure 9 Comparison of model prediction with test results of Taylor and Bacchus (1969) for an undrained, monotonic, triaxial compression test.

elliptical yield locus used in the model (which is identical to the plastic potential because of an associated flow rule) is not an accurate representation of the actual behaviour. Better predictions might be obtained, for this particular material if some other shape is used for a yield locus; one in which plastic shear strains are greater at lower values of deviator stress q, than predicted by the ellipse. A shape like the original Cam-clay yield locus might be better as long as the singularity at the isotropic axis is removed.

6 CONCLUSIONS

A soil model, capable of predicting many of the observed features of the behaviour of clay when subjected to repeated loading, has been presented. The model possesses most of the characteristics of the former critical state models but with a simple, yet important modification. This involves a specified contraction of the yield surface as the soil sample is unloaded (with the definition of unloading as given above). With the introduction of this modification an additional parameter must also be defined. A value for this parameter may be determined, in a straight forward manner, from a laboratory triaxial test involving repeated, undrained loading. For example, if the number of cycles to failure N_f is measured and the cyclic deviator stress q_c is known, the parametric results, such as those presented in Figure 4, may be used to infer a value for θ.

It should be emphasised that the model described in this paper cannot be expected to reproduce accurately all features of the behaviour of a real clay under monotonic and cyclic loading. Indeed, it is believed that no mathematical model, that can be used sensibly and economically for design calculations, is likely to achieve this modest aim. The philosophy behind this work has been the need to develop as simple a family of models as possible that reproduce qualitatively the salient features of cyclic behaviour of soils, and that are expressed in terms of soil parameters that have physical meaning and which can be easily measured in conventional laboratory tests.

7 ACKNOWLEDGEMENTS

The authors wish to acknowledge that this work was produced on a British Science Research Council contract with the University of Cambridge, which provided financial support for J.P. Carter as a research assistant and support for J.R. Booker as a visitor.

8 REFERENCES

ANDERSEN, K.H. (1975). "Research project, repeated loading on clay - Summary and interpretation of test results". Norwegian Geotechnical Institute Report No. 74037-9, Oslo.

ANDERSEN, K.H. (1976). "Behaviour of clay subjected to undrained cyclic loading". Proc. BOSS Conf., NGI, pp 392-403.

CARTER, J.P., BOOKER, J.R. and WROTH, C.P. (1979). "A critical state soil model for cyclic loading". Proc.Int.Symp. on Soils under Cyclic and Transient Loading, Swansea, Jan. 1980.

EEKELEN, H.A.M. VAN and POTTS, D.M. (1978). "The behaviour of Drammen clay under cyclic loading". Géotechnique, Vol. 28, No. 2, pp 173-196.

MARTIN, G.R., FINN, W.D.L. and SEED, H.B. (1974) "Fundamentals of liquefaction under cyclic loading". University of British Columbia. Dept. of Civil Engineering, Soil. Mech. Series No. 23.

MROZ, Z., NORRIS, V.A. and ZIENKIEWICZ, O.C. (1979). "Application of an anistropic hardening model in the analysis of elasto-plastic deformation". Géotechnique, Vol. 29, No. 1, pp 1-34.

PENDER, M.J. (1977). "Modelling soil behaviour under cyclic loading". Proc. 9th Int. Conf. Soil Mech. Found. Engng., Tokyo, Vol. 2, pp 325-331.

PENDER, M.J. (1978). "A model for the behaviour of over-consolidated clay". Géotechnique, Vol. 28, No. 1, pp -125.

PREVOST, J.H. (1977). "Mathematical modelling of monotonic and cyclic undrained clay behaviour". Int. J. Numerical Analytical Methods in Geomechanics, Vol. 1, pp 195-216.

ROSCOE, K.H. and BURLAND, J.B. (1968). "On the generalised stress-strain behaviour of 'wet' clay" in Engineering Plasticity, (Ed, J. Heyman and F. A. Leckie). Cambridge University Press, pp 535-609.

SCHOFIELD, A.N. and WROTH, C.P. (1968). "Critical State Soil Mechanics". McGraw-Hill, London

SEED, H.B. (1979). Nineteenth Rankine Lecture, Géotechnique, Vol.19, No.3, pp 213-263.

SEED, H.B. and LEE, K.H. (1966). "Liquefaction of saturated sands during cyclic loading". J. Soil Mech. Found. Divn., ASCE, Vol. 92, No. SM6, pp 105-134.

SEED, H.B., MARTIN, P.P. and LYSMER, J. (1975). "The generation and dissipation of pore water pressures during soil liquefaction". Earthquake Engineering Research Centre. Report No. EERC 75-26, University of California, Berkeley.

TAYLOR, P.W. and BACCHUS, D.R. (1969). "Dynamic cyclic strain tests on a clay". Proc. 7th Int. Conf. Soil Mechs. Found. Engng., Mexico, Vol. 1, pp 401-409.

TAYLOR, P.W. and HUGHES, J.M.O. (1965). "Dynamic properties of foundation subsoils as determined from laboratory tests". 3rd World Conf. Earthquake Engng., Vol. 1, pp 196-211.

Elastic Behavior of Normally Consolidated Clay

S. OHMAKI
National Research Institute of Fisheries Engineering, Hiratsuka, Japan

1 INTRODUCTION

In general, soil exhibits an irreversible stress-strain behavior and a hysteresis loop in the loading-unloading-reloading process. Such characteristics are shown in both volumetric and shearing strains. Therefore, in order to take such phenomenon into account when formulating the stress-strain relationship, it is neccesary to study the behavior of soil after yielding, as well as during the yielding process.

Some investigators have pointed out that there might be two modes of soil yielding, i.e., volumetric change and shearing deformation. They have suggested that these characteristics should be taken into account in formulating a stress-strain relationship (Poorooshasb, 1966, Tatsuoka and Ishihara, 1974, Nishi and Esashi, 1978, Vermeer, 1978, Ohmaki, 1979).

Accordingly, it is assumed in this paper that elastic as well as plastic strains can each be divided into two components one of which is caused by changes in the stress ratio and the other by changes in the mean effective stress. In order to clarify the properties of these two components of elastic strain, two kinds of loading-unloading-reloading tests were carried out. One was a cyclic test of stress ratio, in which the mean effective stress was kept constant and the other was a cyclic test for mean effective stress, in which the stress ratio was kept constant. Results of experiments in which the stress ratio was decreased and the mean effective stress was increased simultaneously are also shown. Based upon these experimental results, a simple, empirical law for stress-strain behavior under axisymmetric conditions is proposed.

2 PROCEDURE USED TO ANALYZE EXPERIMENTAL RESULTS

Results of drained shear tests on clay, performed under triaxial compression and extension conditions, are examined here. In the analysis, the following parameters are used:

$$p = \frac{1}{3}(\sigma_a' + 2\sigma_r'),\ q_a = \sigma_a' - \sigma_r',\ \eta_a = \frac{q_a}{p},$$

$$v = \varepsilon_{axial} + 2\varepsilon_{rad},\ \varepsilon_a = \frac{2}{3}(\varepsilon_{axial} - \varepsilon_{rad}),$$

where, σ_a' and σ_r' denote axial and radial effective principal stresses, and ε_{axial} and ε_{rad} denote strains in axial and radial directions, respectively, of the cylindrical specimen.

Now, we express the increments, dv, of volumetric strain and $d\varepsilon_a$ of deviatoric strain as follows:

$$dv = dv^e + dv^p = dv^e_\eta + dv^e_p + dv^p_\eta + dv^p_p, \quad (1)$$

$$d\varepsilon_a = (d\varepsilon_a)^e + (d\varepsilon_a)^p$$
$$= (d\varepsilon_a)^e_\eta + (d\varepsilon_a)^e_p + (d\varepsilon_a)^p_\eta + (d\varepsilon_a)^p_p, \quad (2)$$

where superscripts e and p denote elastic and plastic components, respectively. Strain increments with subscripts η and p will be called the η-component and p-component of the strain. Experimentally, we obtain the η-component of the volumetric and deviatoric strain increments from triaxial tests in which the stress ratio is increased or decreased while p is kept constant. The p-component of these increments is obtained from tests in which mean effective stress is increased or decreased while the stress ratio is kept constant. In tests where p and η_a change simultaneously, the strain increment obtained is the sum of each component, as expressed in eqs. (1) and (2).

In this paper, we consider only results of experiments in which the stress ratio $|\eta_a|$ is decreased. Thus the η-components of plastic strain increments, dv^p_η and $d\varepsilon^p_\eta$, in equations (1) and (2) drop out and these equations can be rewritten as follows:

$$dv = dv^e_\eta + dv^e_p + dv^p_p \quad (3)$$

$$d\varepsilon_a = (d\varepsilon_a)^e_\eta + (d\varepsilon_a)^e_p + (d\varepsilon_a)^p_p \quad (4)$$

When (-de) is used to denote a decrement of the void ratio, the following relationship is obtained:

$$(-de) = (1 + e)\, dv \quad (5)$$

3 SAMPLES AND TEST PROCEDURES

The gray silty clay which was used in this study was taken from Fujinomori, in the southern part of Kyoto Prefecture, Japan. Its liquid limit is 43.6 % and plastic limit 26.1 %. The texture of this soil is as follows: clay 17.5 %, silt 50.8 % and sand 31.7 %. The specific gravity is 2.648. The sample used in the experiment was remoulded and reconsolidated. Details of the sample preparation are described in another paper (Ohmaki, 1979). Samples were trimmed to cylindrical specimens 35 mm in diameter and 79 mm in height. They were placed in a triaxial cell and covered with rubber membranes. For consolidation and shearing, samples were placed on a pedestal and converted to porous stone by draining through filter paper. Frictionless end platens were used which were covered with rubber membranes, lubricated with silicone grease. During the tests, the volume of water expelled from the specimen was measured with a burette and the displacement at the top of the specimen was measured with a dial gauge, through the loading piston. All the tests were performed under controlled stress conditions in a temperature controlled room set at 20 ± 0.5 °C.

4 EXPERIMENTAL RESULTS

4.1 Results of constant p tests

Figure 1 shows results of the loading-unloading-reloading tests for stress ratio, η_a , performed under triaxial compression and extension, with p held constant (= 2 kgf/cm^2). The relationship between η_a and ε_a is shown in Figure 1(a). It is evident in this figure that the hysteresis loop is small if the amplitude of the shear stress ratio is small. Figure 1(b) shows the relationship between volumetric strain, v , and stress ratio, η_a . In this figure it can be seen that, when the amplitude of η_a is small, the specimen always contracts in both unloading and reloading under triaxial compression and extension. On the other hand, where the amplitude of η_a is large, the soil specimen tends to dilate.

Next, results of simple unloading tests for η_a with p kept constant are shown. The stress paths used are shown in Figure 2. Soil specimen were consolidated isotropically by increasing the value of p in steps, 0.5, 1.0, 2.0 and 4.0 kgf/cm^2, at two day intervals. Then, after the specimen was sheared to the stress ratio η_{ai} with p kept constant, the shear stress was reduced step by step, as shown in Figure 2. The

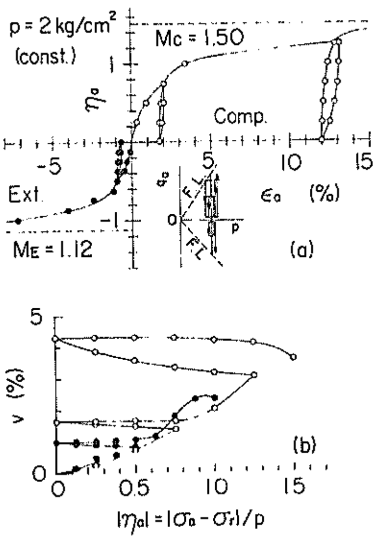

Figure 1 Cyclic shear test results with p kept constant

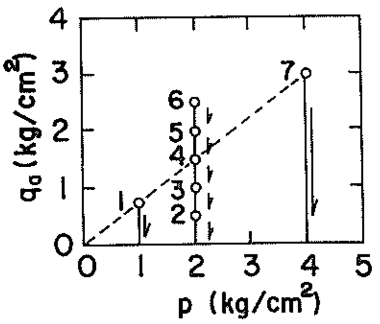

Figure 2 Stress paths of unloading tests with p kept constant

specimen was both loaded and unloaded in steps, separated by one day intervals. These steps are indicated by plots in Figures 3 and 4. For tests where p equals 2 kgf/cm^2, 0.25, 0.50, 0.75, 1.00 and 1.25 were taken as values of η_{ai} . However, for tests where p equals 1.0 and 4.0 kgf/cm^2, a η_{ai} value of 0.75 was used. Test results are shown in Figure 3. It is apparent in Figure 3(a) that $\eta_a \sim \varepsilon_a$ curves are parallel to each other irrespective of η_{ai} . It is also apparent in Figures 3(b) and (c) that $v \sim \eta_a$ curves as well as $(-\delta e) \sim \eta_a$ curves are parallel irrespective of η_{ai} . Figure 4 shows the results of unloading tests for η_{ai} equal to 0.75 with p kept constant (= 1.0, 2.0 and 4.0 kgf/cm^2). In Figure 4(a) the $\eta_a \sim \varepsilon_a$ curves are parallel to each other during unloading, although during loading they are fairly different, depending on the value of p. In Figure 4(b) the $\eta_a \sim v$ curves are also parallel to each other during unloading.

Now, we have seen from the unloading and reloading tests under constant p, that $\eta_a \sim \varepsilon_a$ curves under this condition are parallel to each other and that $\eta_a \sim v$ curves are independent of p. These properties are idealized in Figure 5. That is, we assume that the relationship between normalized stress ratio $|\eta_a/M|$ and $|\varepsilon_a|$ during unloading and reloading under constant p, where M is the stress ratio $|\eta_a|$ at failure, can be expressed as a straight line with a slope of G. Another idealized relationship is shown in Figure 5(b), in which it is likewise assumed that the relationship between v and $|\eta_a/M|$ can be expressed as a straight line with a slope of ± d and that the specimen always contracts under the conditions described above.

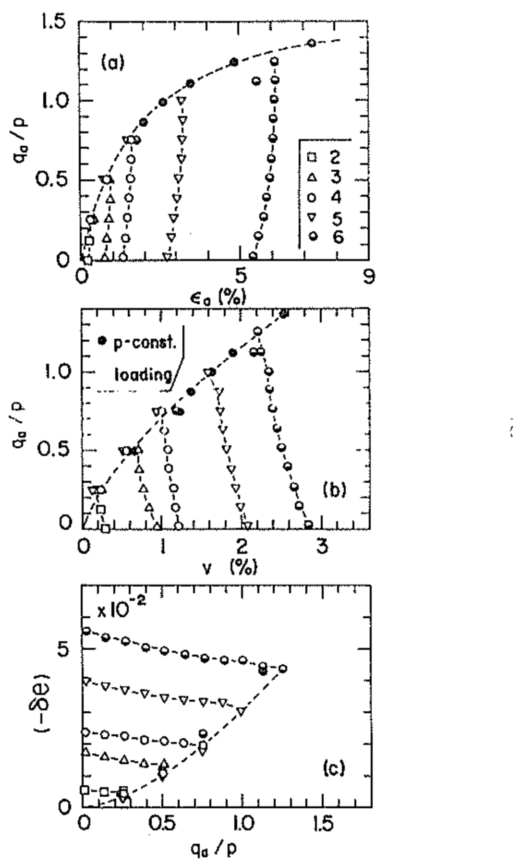

Figure 3 Unloading test results with p kept constant (p = 2 kgf/cm^2)

As a results of these assumptions, strain increments under the above conditions are expressed as follows.

$$dv^e_\eta = \frac{d}{M}\,|d\eta_a| \qquad (6)$$

$$(d\varepsilon_a)^e_\eta = \frac{G}{M}\,d\eta_a \qquad (7)$$

It is reasonable in these equations that M take the value corresponding to triaxial compression or extension. An expression similar to equation (6) is used by Karube and Kurihara (1966).

4.2 Results of the constant η_a tests

Next we show the results of tests in which mean effective principal stress was loaded, unloaded and reloaded while keeping the stress ratio constant (constant η_a). Figure 6 shows the stress paths used

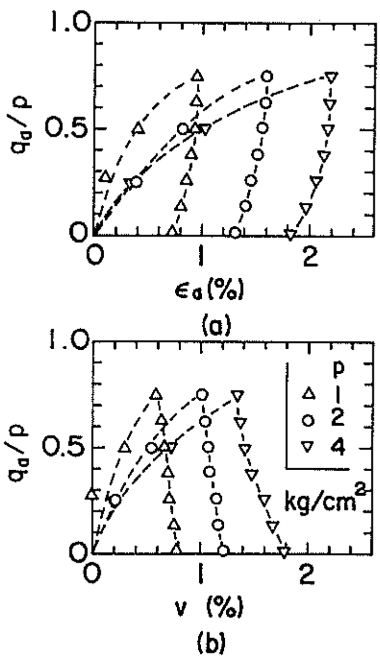

Figure 4 Unloading test results with p kept constant (η_{ai} = 0.75)

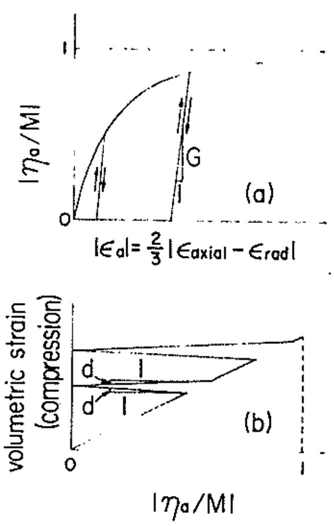

Figure 5 A stress-strain model of soil during shear with p kept constant

in these tests. Tests were carried out as follows: After the specimens were consolidated isotropically at p equal to 0.5 kgf/cm² for one day, they were sheared under triaxial compression and extension to the stress ratio η_{ai} , while p was kept constant. Then, p, the mean effective stress, was increased, decreased and again increased, while η_a was kept constant (= η_{ai}). This was done in steps, indicated in Figure 6, separated by one day intervals.

In Figure 7, (-δe) ∿ log p data from these tests are plotted. For these tests the (-δe) ∿ log p curves for swelling and recompression are parallel to each other and independent of η_{ai} . Therefore we can say

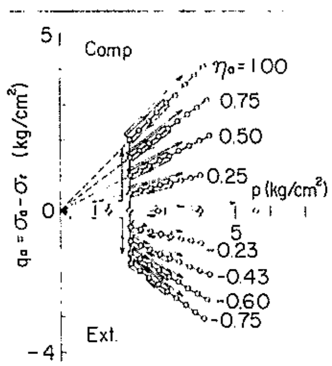

Figure 6 Stress paths of cyclic tests of p

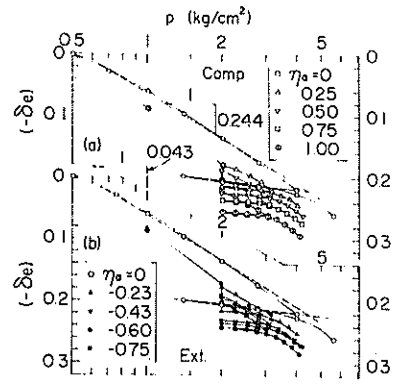

Figure 7 e ∿ log p plots of cyclic tests of p

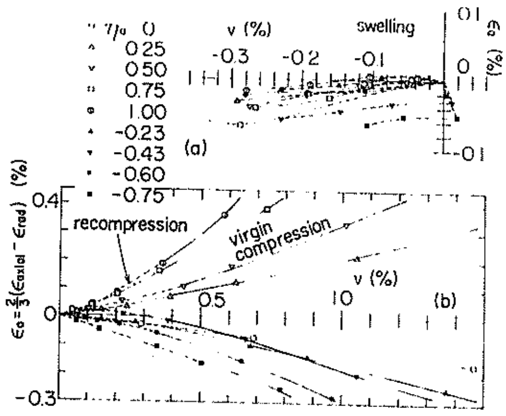

Figure 8 ε_a ∿ v relations during (a) swelling, (b) recompression with stress ratio kept constant that the slope of these curves is equal to the swelling index, Cs (= 0.043), of the isotropic swelling test. Here we take 0.244 as the value of the compression index, Cc , from the virgin consolidation curve in this figure. The relationships between ε_a and v during the swelling and recompression parts of these tests are shown in Figure 8 (a) and (b), respectively. It is apparent in Figure 8(a) that ε_a is negligibly small compared with v , and it tends to decrease slightly as v decreases. Since this tendency appeared in the test performed under isotropic stress conditions, it is considered to be due to anisotropy inherent in the specimen. Figure 8(b) shows relationships between ε_a and v during recompression. Dashed portions of curves denote regions of overconsolidaton and solid portions denote normal consolidation. It can be seen in this figure that slopes of $\varepsilon_a \sim v$ curves increase gradually as η_{ai} increases and that curves are convex towards the v-axis. That is,

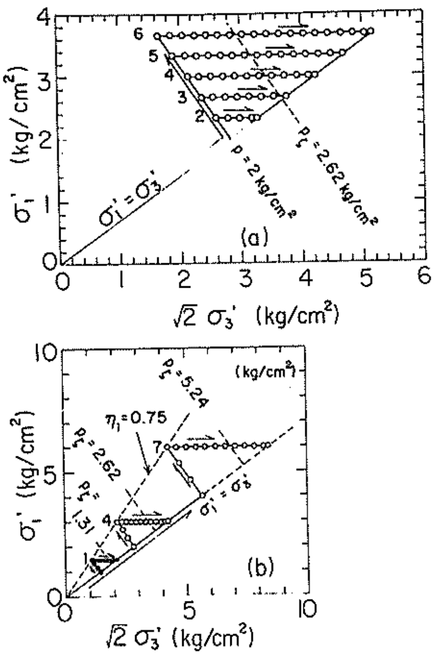

Figure 9 Stress paths of the unloading tests with σ_a' kept constant

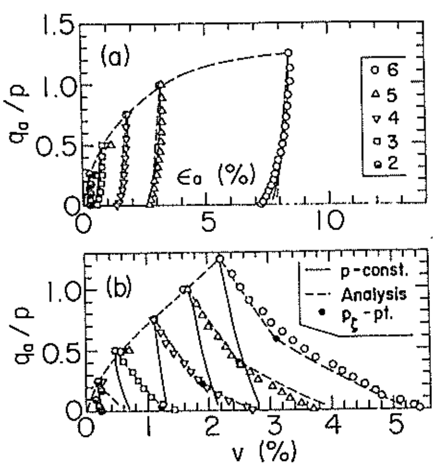

Figure 10 Comparison between experimental and analytical results of constant σ_a' tests (p = 2 kgf/cm²)

deformation of the specimen is not isotropic. Using the results of the swelling tests, we can express the strain increments, dv_p^e , and $(d\varepsilon_a)_p^e$, as follows:

$$dv_p^e = \frac{\kappa}{1+e}\frac{dp}{p} , \tag{8}$$

$$(d\varepsilon_a)_p^e = 0 , \tag{9}$$

where κ = 0.434 Cs .

4.3 Results of tests in which $dp > 0$ and $d\eta_a < 0$

Here we present results of tests carried out along stress paths where $dp > 0$ and $d\eta_a < 0$. Two kinds of experiments were conducted, which we will call series 1 and series 2 tests.

First we will describe the results of series 1 tests, in which each specimen was sheared to stress ratio η_{ai} while p was held constant, after being isotropically consolidated to the mean effective stress, p_i . Then, radial stress was increased and therefore stress ratio η_a was decreased while axial stress was kept constant. Each experiment was proceeded in steps, as indicated (by small circles) in Figure 9, separated by one day intervals. Initial stress values in these unloading tests correspond to those shown in Figure 2.

Figure 10 shows results of tests in which the value of η_{ai} was varied while p_i was kept constant (= 2 kgf/cm²). Figure 11 shows results of tests in which p_i was varied, while η_{ai} was held constant (= 0.75). In these figures, the stress-strain curves for the unloading tests in which p was held constant (Figures 3 and 4) are represented by solid lines. The initial unloading points of these curves coincides with those of the corresponding tests indicated by plots in this figure. Also in these figures, analytical curves to be described later are represented by dashed lines. In Figures 10(b) and 11(b), $\eta_a \sim v$ curves are quite similar to each other and independent of η_{ai} and p_i .

Next, we examine the results of series 2 tests. Figure 12 shows the stress paths used. Tests were

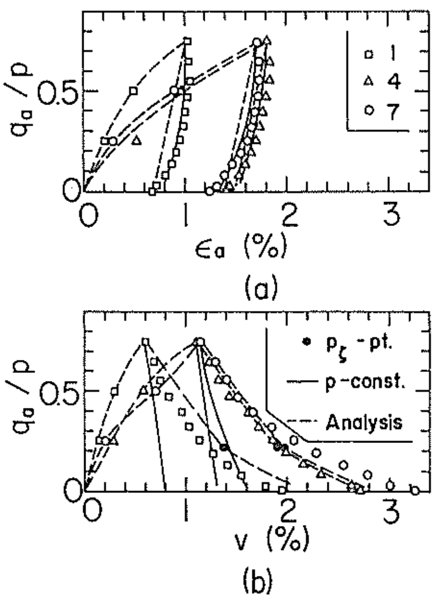

Figure 11 Comparison between experimental and analytical results of constant σ_a' tests (η_{ai} = 0.75)

performed in the same manner as in series 1. The stress conditions at initial unloading points for all tests were: $p_i = 2$ kgf/cm^2 and $\eta_{ai} = 0.75$.

In Figure 13 results of each test are plotted. The dashed lines are analytical curves (described below). It is apparent in Figure 13(a) that the $\eta_a \sim \varepsilon_a$ relationships for these tests are almost identical, irrespective of stress paths.

5 ANALYTICAL RESULTS

We have already shown that the $\eta_a \sim \varepsilon_a$ relationships during unloading are almost identical to the results of tests in which p was kept constant (Figures 10(a), 11(a) and 13(a)). Similar results have already been shown by Balasubramaniam (1975). Taking these facts into account, the following equation can be reasonably assumed in equation (4) when $|\eta_a|$ is decreased.

$$(d\varepsilon_a)^p_p = 0 \tag{10}$$

Next we examine the volumetric behavior of soil specimens. Figures 14 and 15 show the relationship between $\{(-\delta e) - (-\delta e)_\eta\}$ and $(-\delta e)_p$, where $(-\delta e)_\eta$ represents a decrease in the void ratio from the initial unloading point of the corresponding constant p test, and $(-\delta e)_p$ also represents a decrease in the void ratio, calculated as follows:

$$(-\delta e)_p = \lambda \ln \frac{p}{p_i} \tag{11}$$

In this calculation $\lambda \doteq 0.434$ Cc and Cc denotes the compression index. From Figure 7, we know Cc is

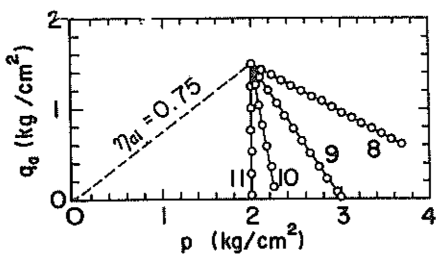

Figure 12 Stress paths of the unloading tests of series 2

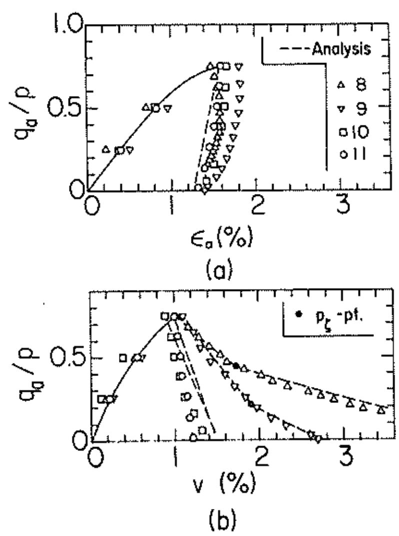

Figure 13 Comparison between experimental and analytical results (series 2)

equal to 0.244. In Figure 14 the data points which all lie clearly below the dashed line with a slope of one, have been approximated by two straight lines. Here we denote the value of $\{(-\delta e) - (-\delta e)_\eta\}$ at the point where the two lines intersect by Δe_0. Figure 16 shows this relationship schematically in an e_p $\{= e - (-\delta e)_\eta\} \sim \ln p$ plane. It is clear from this figure that when η_a is decreased and p is simultaneously increased, after the specimen is sheared under constant p ($= p_i$), the void ratio e_p is decreased by Δe_0 along a line of slope ζ ($< \lambda$), and then along a line which has a slope equal to λ. This phenomenon is a sort of p_c-effect, resulting from a sudden change of stress paths.

For the portion of the line where $\{(-\delta e) - (-\delta e)_\eta\} < \Delta e_0$ we denote the slope by i, and obtain the relationship, $\zeta = i \cdot \lambda$. If p_ζ denotes the value of p at the point where the two lines in Figure 16

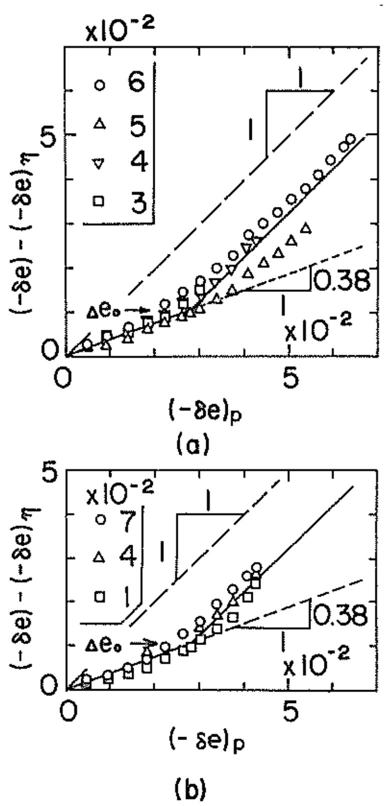

Figure 14 $\{(-\delta e) - (-\delta e)_\eta\} \sim (-\delta e)_p$ plots (series 1)

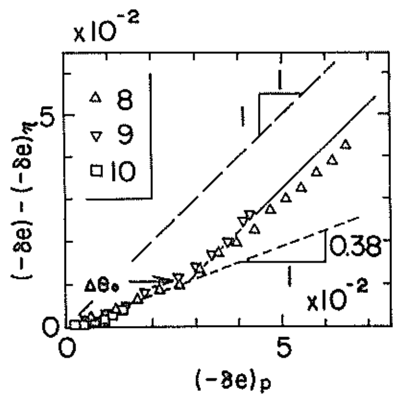

Figure 15 $\{(-\delta e) - (-\delta e)_\eta\} \sim (-\delta e)_p$ plots (series 2)

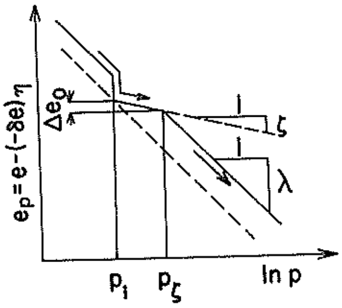

Figure 16 A relation between e_p and ln p

intersect, we obtain the following equation.

$$\Delta e_0 = \zeta \ln \frac{p_\zeta}{p_i} \qquad (12)$$

It is reasonable to assume from equation (12) that p_ζ/p_i is constant since it is clear in Figures 14 and 15 that Δe_0 and i are almost constant, irrespective of p_i and η_{ai} . Thus, when $(-\delta e)_p \leq \Delta e_0$,

$$dv_p^p = \frac{\zeta - \kappa}{1 + e} \frac{dp}{p} , \qquad (13)$$

and when $(-\delta e)_p > \Delta e_0$, dv_p^p can be expressed as:

$$dv_p^p = \frac{\lambda - \kappa}{1 + e} \frac{dp}{p} , \qquad (14)$$

From Figures 14 and 15, we obtain the following.

$$\Delta e_0 = 0.0106, \quad p_\zeta/p_i = 1.31, \quad \zeta = 0.040$$

In Figure 9 the constant, $p = p_\zeta = 1.31\, p_i$, is expressed by the dashed line. It is clear in this figure that most or all of the unloading process does not reach p_ζ when η_{ai} is small. As a result, the following relationships are obtained from tests with stress paths treated in this paper ($dp \geq 0$, $d\eta_a \leq 0$).

$$d\varepsilon_a = (d\varepsilon_a)^e_\eta = \frac{G}{M}\, d\eta_a \qquad (15)$$

$$dv = \frac{d}{M}\, |d\eta_a| + \frac{\zeta \text{ (or } \lambda)}{1 + e} \frac{dp}{p} \qquad (16)$$

Analytical results represented by the dashed curves in Figure 10, 11 and 13 were calculated using equations (15) and (16). Values of parameters used in these calculations are shown in Table 1. In Figures 10, 11 and 13, points corresponding to the points of intersection of the two lines in Figure 16 are shown as p_ζ points. Reasonable agreement was obtained between experimental and analytical results.

6 CONCLUSIONS

In this paper the elastic strain of soil is assumed to consist of two components, one caused by changes in stress ratio and the other by changes in mean effective stress. These components of elastic strain were studied by conducting by triaxial drained tests with various stress paths. From these tests the following conclusions were reached.

1) From the loading-unloading-reloading tests in

Table 1
Values of parameters used in the analysis

λ	0.106	Δe_0	0.0106
Mc	1.50	d	0.0067
ζ	0.040	G	0.0065

which the stress ratio was varied while the mean effective stress was kept constant, $\eta_a/M \sim \varepsilon_a$ curve has the same slope during unloading as during reloading. The slope of the $\eta_a/M \sim \varepsilon_a$ curve under triaxial compression is almost equal to that of the same curve under triaxial extension. On the other hand, for volumetric strain, we observed irreversible behavior.

2) During unloading and reloading of p with η_a kept constant, e ∿ log p curves exhibited nearly the same slope irrespective of η_a . Changes in deviatoric strain during swelling, while η_a is kept constant, are negligible. However, in reloading, the distortional strain increases gradually as p increases.

3) When the stress ratio is decreased and the mean effective stress is increased, the soil specimen shows the so-called p_ζ-effect in the relationship between e_p {$= e - (-\delta\hat{e})_\eta$} and ln p. In these tests the $\eta_a \sim \varepsilon_a$ curves did not appear to be influenced by the effective stress paths.

7 ACKNOWLEDGMENT

The research described in this paper was carried out under supervision of Prof. T. Shibata of Kyoto University. Experimental work was carried out by Technical Official H. Shimizu under the author's supervision in Kyoto University. The author expresses his sincere acknowledgment to them.

8 REFERENCES

Balasubramaniam, A.S. (1975). Stress-strain behaviour of a saturated clay for state below the state boundary surface. Soils and Foundations, Vol. 15, No. 3, pp 13-26.

Karube, D. and Kurihara, N. (1966). On the dilatancy and shear strength of remoulded clay. Proc. JSCE, No. 135, pp 10-24.

Nishi,K. and Esashi, Y. (1978). Stress-strain relationships of sand based on elastoplasticity theory. Proc. JSCE, No. 280, pp 111-122.

Ohmaki, S. (1979). A mechanical model for the stress-strain behaviour of normally consolidated cohesive soil. Soils and Foundations, Vol. 19, No. 3, pp 29-44.

Poorooshasb, H.B., Holubec, I. and Sherbourne, A.N. (1966). Yielding and flow of sand in triaxial compression, Part 1. Can. Geotech. Journ., Vol. 3, No. 4, pp 179-190.

Tatsuoka, F. and Ishihara, K. (1974). Yielding of sand in triaxial compression. Soils and Foundations, Vol. 14, No. 2, pp 63-76.

Vermeer, P.A. (1978). A double hardening model for sand. Geotech., Vol. 28, pp 413-433.

Acceleration Waves in a Granular Medium with Critical State

R. O. DAVIS
Department of Civil Engineering, University of Canterbury
J. B. BERRILL
Department of Civil Engineering, University of Canterbury

SUMMARY: Propagation of acceleration waves in three different rate-type constitutive models for granular media is investigated. Each of the models possesses a critical state, but in regard to other constitutive assumptions they appear to be considerably different. Nevertheless, we find similarities in the speeds of propagation of acceleration waves. All three models yield the same speed for transverse waves, both for loading and unloading processes. Birefringence of transverse waves occurs in all but very special initial stress regimes. Longitudinal wave speeds differ for the three models for loading processes, but are similar for unloading processes. Longitudinal wave speeds need not exceed transverse wave speeds but longitudinal waves exhibit material attenuation.

1. INTRODUCTION

Accurate characterization of the stress-strain response of soils and other granular media continues to pose a serious problem in the development of analytic theories and engineering solutions to questions involving foundations and earthworks. The non-linear, hysteretic, and dilatant nature of real soil is, at best, very difficult to model mathematically. Perhaps the most noteworthy work in this field is that performed at Cambridge University under the general heading of critical state theories. From a qualitative standpoint, at least, the critical state concept appears to account for most of the commonly observed response characteristics of real soils. One of the more convenient ways to employ the critical state concept is in a rate-type constitutive model. Rate-type descriptions differ from conventional plasticity descriptions in that the material response is entirely smooth and computational efficiency is greatly enhanced. For these and other reasons, the rate-type approach to soil modelling has gained wide spread acceptance, and a large number of models have been put forward.

Unfortunately, proliferation of material models is not always accompanied by analysis and comparison. This seems to be true for the critical state family of models (with the noteworthy exception of the recent paper by Gudehus, 1979). In the present paper, we attempt to compare three recent rate-type theories (Romano, 1974; Davis and Mullenger 1978 and 1979) by analysing their propagation characteristics for acceleration waves. We find that the models, while apparently quite different, yield many similar results, especially for the case of transverse waves.

In section 2 we briefly summarize each of the three models. Section 3 considers the general propagation condition and acoustic tensor for rate-type materials. Sections 4 and 5 consider transverse waves and longitudinal waves, respectively, in each of the three models. We use direct tensor notation where appropriate.

2. CONSTITUTIVE EQUATIONS

The constitutive equation for a rate-type material has the general form (Truesdell and Noll, 1965)

$$\overset{\circ}{\underset{\sim}{T}} = \underset{\sim}{G}\,(\underset{\sim}{T},\ \rho,\ \underset{\sim}{D}) \qquad (1)$$

where G is an isotropic tensor function whose arguments are the stress tensor T, the mass density ρ, and the rate of deformation tensor D. The left hand side of (1) is the co-rotational stress rate

$$\overset{\circ}{\underset{\sim}{T}} = \dot{\underset{\sim}{T}} - \underset{\sim}{W}\,\underset{\sim}{T} + \underset{\sim}{T}\,\underset{\sim}{W} \qquad (2)$$

where W is the spin tensor and the superposed dot implies differentiation with respect to time. If the function G is assumed to be linear in D and polynomial in T, then the most general form of (1)

$$\begin{aligned}\overset{\circ}{\underset{\sim}{T}} = &(g_1 \operatorname{tr} \underset{\sim}{D} + g_2 \operatorname{tr} \underset{\sim}{T}\,\underset{\sim}{D} + g_3 \operatorname{tr} \underset{\sim}{T}^2\underset{\sim}{D})\ \underset{\sim}{1}\\ &+ (g_4 \operatorname{tr} \underset{\sim}{D} + g_5 \operatorname{tr} \underset{\sim}{T}\,\underset{\sim}{D} + g_6 \operatorname{tr} \underset{\sim}{T}^2\underset{\sim}{D})\ \underset{\sim}{T}\\ &+ (g_7 \operatorname{tr} \underset{\sim}{D} + g_8 \operatorname{tr} \underset{\sim}{T}\,\underset{\sim}{D} + g_9 \operatorname{tr} \underset{\sim}{T}^2\underset{\sim}{D})\ \underset{\sim}{T}^2\\ &+ g_{10}\,\underset{\sim}{D} + g_{11}\,(\underset{\sim}{D}\,\underset{\sim}{T} + \underset{\sim}{T}\,\underset{\sim}{D})\\ &+ g_{12}\,(\underset{\sim}{D}\,\underset{\sim}{T}^2 + \underset{\sim}{T}^2\underset{\sim}{D})\end{aligned} \qquad (3)$$

where the coefficients g_1, ..., g_{12} are functions of the invariants of T and density ρ. We consider only the special case of (3) where

$$g_3 = g_6 = g_7 = g_8 = g_9 = g_{11} = g_{12} = 0$$

Thus the general material constitutive relation and starting point for each of the three special models is

$$\begin{aligned}\overset{\circ}{\underset{\sim}{T}} = &(g_1 \operatorname{tr} \underset{\sim}{D} + g_2 \operatorname{tr} \underset{\sim}{T}\,\underset{\sim}{D})\ \underset{\sim}{1}\\ &+ (g_4 \operatorname{tr} \underset{\sim}{D} + g_5 \operatorname{tr} \underset{\sim}{T}\,\underset{\sim}{D})\ \underset{\sim}{T} + g_{10}\,\underset{\sim}{D}\end{aligned} \qquad (4)$$

All quantities here refer to the skeleton of solid particles of the granular medium. If a pore fluid is present, then the stress tensor $\underset{\sim}{T}$ is the effective stress. The density ρ represents the mass of solid particles per unit volume.

Introducing the mean stress p and stress deviator tensor $\underset{\sim}{T}^*$

$$p = -\frac{1}{3}\,\mathrm{tr}\,\underset{\sim}{T},\quad \underset{\sim}{T}^* = \underset{\sim}{T} + p\,\underset{\sim}{1} \tag{5}$$

(4) can be decomposed into two equations describing spherical and deviatoric response

$$\begin{aligned}\dot{p} &= -(g_1 - g_2 p - g_4 p + g_5 p^2 + \tfrac{1}{3} g_{10})\ \mathrm{tr}\,\underset{\sim}{D}\\ &\quad -(g_2 - g_5 p)\ \mathrm{tr}\,\underset{\sim}{T}^*\underset{\sim}{D}^*\\ \frac{1}{2}(\dot{q}^2) &= (g_{10} + g_5 q^2)\ \mathrm{tr}\,\underset{\sim}{T}^*\underset{\sim}{D}^*\\ &\quad + (g_4 - g_5 p)\, q^2\ \mathrm{tr}\,\underset{\sim}{D}\end{aligned} \tag{6}$$

where q denotes the square root of the second invariant of $\underset{\sim}{T}^*$

$$q^2 = \mathrm{tr}\,\underset{\sim}{T}^*\underset{\sim}{T}^* \tag{7}$$

and $\underset{\sim}{D}^*$ is the deviatoric rate of deformation tensor

$$\underset{\sim}{D}^* = \underset{\sim}{D} - \frac{1}{3}(\mathrm{tr}\,\underset{\sim}{D})\,\underset{\sim}{1} \tag{8}$$

The three constitutive models we consider below, differ in their motivation for, and ultimate choice of, the five response coefficients g_1, g_2, g_4, g_5, and g_{10}. All, however, are guided by the critical state concept which assumes the existence of a unique critical mean stress, denoted p_c, which is only a function of the density ρ. The function $p_c = p_c(\rho)$ is called the critical state pressure. In addition, each model employs a Drucker-Prager failure criterion of the form

$$q \le Mp \tag{9}$$

where M is a dimensionless material constant. If $p = p_c$ and $q = Mp$, then the material is said to be at the critical state and it is assumed that plastic flow may occur without change in volume. Each model employs the basic assumption that the constitutive coefficients may differ in loading and unloading processes. Generally, loading is assumed to occur when the rate of working of the stress is positive. In the three subsections below, we summarize the choice of constitutive coefficients for each of the models.

2.1 The Model of Romano (1974)

For loading processes, Romano made the following constitutive assumptions

$$\begin{aligned}g_1 + \tfrac{1}{3} g_{10} - g_2 p &= \Gamma(p,\rho)\\ g_2 &= -\frac{2\mu p}{M^2 p_c^2} - \frac{(q - Mp)\,|Mp_c - Mp|}{b}\\ g_4 &= -\frac{2\mu p}{M^2 p_c^2}\\ g_5 &= -\frac{2\mu}{M^2 p_c^2}\\ g_{10} &= -2\mu\end{aligned} \tag{10}$$

Here μ represents the initial or small strain shear modulus of the granular medium, b is a material constant with dimensions of $(\text{stress})^2$, and Γ is a complex function of mean stress and density which plays the role of the tangent bulk modulus of the medium. For unloading processes, Romano set

$$\begin{aligned}g_1 + \tfrac{1}{3} g_{10} &= \Gamma_u(p,\rho)\\ g_2 = g_4 &= g_5 = 0\\ g_{10} &= 2\mu\end{aligned} \tag{11}$$

where $\Gamma_u \ge \Gamma$ is the unloading bulk modulus. The exact forms of the functions Γ and Γ_u were chosen to represent typical void ratio-mean stress response of soil. Since the functions are complex and add nothing to the present discussion, we omit them here and refer to Romano's original paper. The initial shear modulus μ was assumed to depend upon the soil density. Its precise form may also be found in Romano's paper.

2.2 The Model of Davis and Mullenger (1978)

Davis and Mullenger (1978) made the following constitutive assumptions for loading processes

$$\begin{aligned}g_1 + \tfrac{1}{3} g_{10} - g_2 p &= \Gamma(p,\rho)\\ g_2 &= -\frac{2\mu}{M^2 p}\\ g_4 &= -\left(\frac{\rho_c}{\rho}\right)^{\gamma}\frac{2\mu}{M^2 p}\\ g_5 &= -\left(\frac{\rho_c}{\rho}\right)^{\gamma}\frac{2\mu}{M^2 p^2}\\ g_{10} &= 2\mu\end{aligned} \tag{12}$$

where μ is the initial shear modulus, γ is a constant, $\rho_c = \rho_c(p)$ called the critical density, is the inverted form of the critical state pressure function $p_c = p_c(\rho)$, and Γ is the tangent bulk modulus. For unloading processes, the following assumptions were made

$$\begin{aligned}g_1 + \tfrac{1}{3} g_{10} - g_2 p &= \Gamma_u(p,\rho)\\ g_2 &= -\beta\,\frac{2\mu}{M^2 p}\\ g_4 &= -\beta\left(\frac{\rho_c}{\rho}\right)^{\gamma}\frac{2\mu}{M^2 p}\\ g_5 &= -\beta\left(\frac{\rho_c}{\rho}\right)^{\gamma}\frac{2\mu}{M^2 p^2}\\ g_{10} &= 2\mu\end{aligned} \tag{13}$$

where $\Gamma_u \ge \Gamma$ is the unloading bulk modulus and $\beta \le 0$ is a constant. The precise forms of the functions Γ and Γ_μ in (12) and (13) are different from those in (10) and (11), but the two functions play the same role in the respective models. Davis and Mullenger assumed μ to depend upon p rather than ρ, but again, the fundamental role of the function is the same for both models.

Precise forms of Γ and Γ_u (with slightly different notation) and of μ may be found in Davis and Mullenger's paper (1978).

2.3 The Model of Davis and Mullenger (1979)

The impression that the above two models, as well as others of the same genre, were unnecessarily complex led Davis and Mullenger to suggest a second simplified rate-type description for soil. The constitutive coefficients for this model, for loading processes, were

$$\begin{aligned} g_1 &= -\frac{2}{3}\mu \\ g_2 = g_4 &= -\frac{2\mu p}{M^2 p_c^2} \\ g_5 &= -\frac{2\mu}{M^2 p_c^2} \\ g_{10} &= 2\mu \end{aligned} \tag{14}$$

and for unloading processes

$$\begin{aligned} g_1 &= 2\mu\left(\frac{1}{M^2} - \frac{1}{3}\right) \\ g_2 = g_4 = g_5 &= 0 \\ g_{10} &= 2\mu \end{aligned} \tag{15}$$

Comparison of (14) and (15) with the preceeding two models reveals considerable simplification. No special material parameters such as b or γ are present, and no bulk modulus function is required (although a bulk modulus is implied as we discuss below). The small strain modulus μ was assumed to be a function of density.

3. ACCELERATION WAVES

The term acceleration wave refers to the propagation of discontinuities in acceleration and the spatial derivatives of the stress tensor. While stress and velocity remain continuous, their derivatives may suffer discontinuous jumps in crossing singular surfaces within the material. The propagation condition for a rate-type material is

$$\underset{\sim}{Q}(\underset{\sim}{n})\,\underset{\sim}{a} = \rho U^2 \underset{\sim}{a} \tag{16}$$

where $\underset{\sim}{a}$ is the amplitude, U is the speed of propagation, and $\underset{\sim}{Q}$ is the acoustic tensor which depends upon the unit normal to the wave front $\underset{\sim}{n}$. Principal waves result when the vector $\underset{\sim}{n}$ is aligned with one of the three principal directions of stress. Let us assume the co-ordinate frame aligns with the principal directions of stress so that

$$[T] = \begin{bmatrix} \sigma_1 & 0 & 0 \\ 0 & \sigma_2 & 0 \\ 0 & 0 & \sigma_3 \end{bmatrix} \tag{17}$$

where σ_1, σ_2, and σ_3 are the principal stresses. No ordering of magnitude among σ_1, σ_2, and σ_3 is implied here. If we now consider the case of a wave front with unit normal $n = (1, 0, 0)$, then the wave is a principal wave, and the acoustic tensor corresponding to the constitutive relation (4) follows as a special case of the hypo-elastic accoustic tensor derived by Truesdell (1963).

$$\underset{\sim}{Q}(\underset{\sim}{n}) = (g_1 + \frac{1}{2}g_{10} + g_2\sigma_1 + g_4\sigma_1 + g_5\sigma_1^2)\,\underset{\sim}{n}\otimes\underset{\sim}{n} + \frac{1}{2}(g_{10} + \sigma_1)\,\underset{\sim}{1} - \frac{1}{2}\underset{\sim}{T} \tag{18}$$

where $n \otimes n$ represents the tensor product of $\underset{\sim}{n}$ with itself. The speed of propagation now follows from (16) by taking a to be a unit vector aligned with n (for longitudinal waves) or perpendicular to n (for transverse waves). Thus, letting U_{11} denote the longitudinal wave speed, we have

$$\rho U_{11}^2 = g_1 + g_{10} + (g_2 + g_4)\sigma_1 + g_5\sigma_1^2 \tag{19}$$

Similarly, letting U_{12} and U_{13} denote speeds of the two transverse waves, polarized in the 2 and 3 directions,

$$\begin{aligned} \rho U_{12}^2 &= \frac{1}{2}(\sigma_1 - \sigma_2) + \frac{1}{2}g_{10} \\ \rho U_{13}^2 &= \frac{1}{2}(\sigma_1 - \sigma_3) + \frac{1}{2}g_{10} \end{aligned} \tag{20}$$

We will consider the cases of longitudinal and transverse waves separately, beginning with transverse waves because they are simpler.

4. TRANSVERSE WAVES

In all of the equations (10), (11), (12), (13), (14), and (15) the coefficient g_{10} has the value 2μ. Thus, for all three models, in both loading and unloading processes, the speeds of propagation of transverse waves will be

$$\begin{aligned} \rho U_{12}^2 &= \frac{1}{2}(\sigma_1 - \sigma_2) + \mu \\ \rho U_{13}^2 &= \frac{1}{2}(\sigma_1 - \sigma_3) + \mu \end{aligned} \tag{21}$$

Thus the only difference between the three models lies in the exact functional form chosen for μ. Moreover, we see that both loading and unloading transverse waves propagate with the same speed implying that such waves will not exhibit material attenuation. Subtracting equations (21) yields

$$\rho(U_{12}^2 - U_{13}^2) = \frac{1}{2}(\sigma_3 - \sigma_2) \tag{22}$$

exhibiting the fact that transverse waves polarized in different directions will not, in general, propagate with the same speeds. Thus all three models possess the property of acoustic birefringence.

5. LONGITUDINAL WAVES

We shall consider only the special case of biaxial stress, where $\sigma_2 = \sigma_3$. First consider unloading processes. For the model of Romano, using (11) in (19) gives

$$\rho U_{11}^2 = \Gamma_u + \frac{4}{3}\mu \tag{23}$$

For Davis and Mullenger (1978), use of (13) in (19) gives

$$\rho U_{11}^2 = \Gamma_u + \frac{4}{3}\mu - \beta\sqrt{\frac{2}{3}}\,\frac{2\mu q}{M^2 p^2}\,[p + \left(\frac{\rho_c}{\rho}\right)^{\gamma}\sigma_1] \tag{24}$$

where the relationship $p + \sigma_1 = \sqrt{\frac{2}{3}}\, q$ has been used. For Davis and Mullenger (1979), use of (15) in (19) gives

$$\rho\, U_{11}{}^2 = \Gamma_u + \frac{4}{3}\mu \tag{25}$$

where we have taken Γ_u to be

$$\Gamma_u = \frac{2\mu}{M^2} \tag{26}$$

Comparing (23), (24), and (25) we find several similarities. If β in (24) is set equal to zero, (23) results. Thus, for one particular choice of material parameter, the models of Romano and Davis and Mullenger (1978) are equivalent. In (25), we have used the implied value for the bulk modulus given by (26). With this interpretation, the simplified model of Davis and Mullenger (1979) is equivalent to that of Romano. In fact, the two models do not yield exactly the same unloading wave speeds, since Romano's functional form for Γ_u is different from (26). Nevertheless, the two models are qualitatively equivalent. For the case where β is different from zero, (24) may give a propagation speed considerably different from (23) or (25).

Next, consider loading processes. For Romano, use of (10) in (19) gives

$$\rho\, U_{11}{}^2 = \Gamma + \frac{4}{3}\mu - \frac{4\mu q^2}{3MP_c{}^2} - \sqrt{\frac{2}{3}}\,\frac{Mq}{b}\,(q - Mp)\,|p_c - p| \tag{27}$$

For Davis and Mullenger (1978), use of (12) in (19) gives

$$\rho\, U_{11}{}^2 = \Gamma + \frac{4}{3}\mu - \sqrt{\frac{2}{3}}\,\frac{2\mu q}{M^2 p^2}\,[p + \left(\frac{\rho_c}{\rho}\right)^{\gamma} \sigma_1] \tag{28}$$

And for Davis and Mullenger (1979), use of (14) in (19) gives

$$\rho\, U_{11}{}^2 = \Gamma + \frac{4}{3}\mu - \frac{2\mu}{M^2 p_c{}^2}\,(p_c + \sigma_1)^2 \tag{29}$$

In (27), (28), and (29) we have again used the fact that $p + \sigma_1 = \sqrt{\frac{2}{3}}\, q$, and in (29) we have set Γ equal to $2\mu/M^2$, the implied bulk modulus for the simplified model.

There are several conclusions that may be drawn from inspection of (27), (28), and (29). First, comparing the loading velocities with their counterparts for unloading given by (23), (24), and (25), it is evident that loading and unloading longitudinal waves will generally propagate with different speeds. Closer inspection shows that loading waves will always propagate either slower or at the same velocity as unloading waves. In the special case where the stress is isotropic (i.e. $\sigma_1 = \sigma_2 = \sigma_3$), (27) and (28) will agree with (23) and (24) provided Γ and Γ_u are identical. In all other cases, the loading wave will propagate more slowly. Thus, in general, longitudinal waves in all three models will exhibit material attenuation.

Next note that the term

$$\sqrt{\frac{2}{3}}\,\frac{Mq}{b}\,(q - Mp)\,|p_c - p|$$

in (27) will generally be much smaller than the other terms in that equation. This occurs because the magnitudes of the stresses p and q will be much less than the modulii Γ and μ. Also, Romano's suggested value for the parameter b is quite large. Thus, if we ignore the last term in (27) we see that all three models have roughly similar forms for the speed of propagation of loading waves. This similarity becomes striking for the special case where $p = p_c$. For this case $\rho_c = \rho$, and all three equations reduce to

$$\rho\, U_{11}{}^2 = \Gamma + \frac{4}{3}\mu - \frac{4}{3}\,\frac{\mu q^2}{M^2 p_c{}^2} \tag{30}$$

Pursuing the same vein, if the material is at the critical state, then $q = Mp_c$ and (30) becomes simply

$$\rho\, U_{11}{}^2 = \Gamma \tag{31}$$

for all three models.

Finally, we note that there is no assurance in any of the three models that longitudinal waves will propagate faster than transverse waves. Whether this will be so or not depends entirely upon the exact choice of material parameters. This fact might be employed as a constraint on the choice of material parameters in the use of any of the models.

6. CONCLUSIONS

Our comments above seek to compare and perhaps clarify the three constitutive models, but not to criticise one or favour another. In fact, from the standpoint of wave propagation, all three appear to be surprisingly similar. Whether this similarity extends to other conditions of stress or deformation is not clear. Nevertheless, wave mechanics has been one of the primary tools for investigation of material behaviour, both experimentally and analytically, for more than a century. Fundamental differences are emphasized and similarities are easily placed in perspective.

7. REFERENCES

DAVIS, R.O. and MULLENGER, G. (1978). A rate-type constitutive model for soil with a critical state. Int. J. Numer. Anal. Methods Geomech. Vol. 2, pp. 255-282.

DAVIS, R.O. and MULLENGER, G. (1979). A simple rate-type constitutive representation for granular media. Proc. Third Int. Conf. Numerical Methods in Geomechanics, Aachen, pp. 415-421.

GUDEHUS, G. (1979). A comparison of some constitutive laws for soils under radially symmetric loading and unloading. Proc. Third Int. Conf. Numerical Methods in Geomechanics, Aachen, (to appear in Vol. 4).

ROMANO, M. (1974). A continuum theory for granular media with a critical state. Arch. Mech., Vol. 26, pp. 1011-1028.

TRUESDELL, C. (1963). Remarks on hypo-elasticity. J. Res. National Bureau of Standards, Vol. 67B, pp. 141-144.

TRUESDELL, C. and NOLL, W. (1965). The non-linear field theories of mechanics. In S. Flugge (ed.) Handbuch der Physik, Vol. III/3, Berlin, Springer-Verlag.

Application of Various Rock Mass Classifications to Unsupported Openings at Mount Isa, Queensland: A Case Study

N. R. P. BACZYNSKI
Post Graduate Student, University of Melbourne and CSIRO Division of Applied Geomechanics

SUMMARY: A number of published rock mass classification systems are applied to the assessment of unsupported openings within the dolomitic shales at the Mount Isa Mine. A statistical model for local variability in the intensity of fracturing within the shales serves as a basis for the structural data input. Results of the analysis are presented and limitations of the classification systems are discussed. Possible improvements in the systems are suggested. Past mining experience at the mine indicates that the classification systems yield conservative estimates for some rock mass parameters.

1. INTRODUCTION

One of the principal objectives of rock engineering is the estimate of the immediate and long-term stability of structures that are excavated in rock masses. This necessitates a quantitative evaluation of those physical and mechanical properties of rock masses which govern their strength and deformation characteristics.

The need for a relatively simple rock mass classification for practical engineering purposes has been long recognised and numerous proposals have been made over the last 40-50 years.

Ideally, a classification system suitable for mining of unsupported, open stopes should yield information on the permissible dimensions for such openings, strength of the rock mass to enable pillar design, modulus of the mass to permit prediction and interpretation of observed displacements during mining, and information for estimates of the effect of stress changes on each of the above parameters. This information is necessary for the optimum design of stopes that are to be extracted at progressively deeper levels within mines.

2. ROCK MASS CLASSIFICATION SYSTEMS

2.1 Scope of the Analysis

The aim of the present study is to assess the usefulness and limitations of a number of published classification systems.

Table I lists the rock mass classification systems included in the present assessment.

Table I

	Classification	Source
(i)	Rock Quality Designation (RQD)	Deere et al. (1966)
(ii)	Fissuration Factor (C)	Hansagi (1965)
(iii)	Rock Mass Rating (RMR)	Bieniawski (1973, 1976)
(iv)	Rock Mass Quality (Q)	Barton et al. (1974)
(v)	Modified Rock Mass Rating (Mod.RMR)	Laubscher and Taylor (1976)

2.2 Required Input Parameters

A detailed description of each system is outside the scope of this paper. However, to maintain clarity, the required input parameters are briefly listed in Table II.

Table II

System	Input Parameters
RQD-Index	Cumulative proportion of diamond drill core segments greater than 0.1 m within a selected depth of borehole.
C-Factor	Various parameters based on core diameter and lengths of recovered segments.
RMR	Unconfined compressive strength, RQD, spacing, orientation and condition of fractures, groundwater and limited number of excavation types.
Q	RQD, number of fracture sets, roughness and degree of alteration along weakest fractures, groundwater, rock stresses, excavation type.
Mod.RMR	A more detailed knowledge of parameters listed for RMR (with an associated different classification rating), plus adjustments for the effect of weathering field and mining induced stresses, and mining technique.

3. GEOLOGICAL INPUT FOR MOUNT ISA

The lead-zinc orebodies at Mount Isa Mine are essentially tabular and trend parallel to bedding. The average dip of bedding is 65° from horizontal. The ore is currently being mined by cut-and-fill and sub-level open stoping methods. The hanging-wall and footwall of stopes are defined by moderately to highly jointed and bedded shales.

The analysis is based on Orebodies 5, 7 and 11 within the dolomitic shales at the Mount Isa Mine. These are purposely selected to embrace the full range of ground conditions encountered in the lead-zinc orebodies.

3.1 Model for Fracture Orientation

Four principal fracture sets and several other locally common sets were differentiated for the dolomitic shales at the mine (Baczynski, 1974). The range of orientations for each set is represented on a lower hemisphere, equal area, stereographic projection plot of poles to fracture planes in Figure 1.

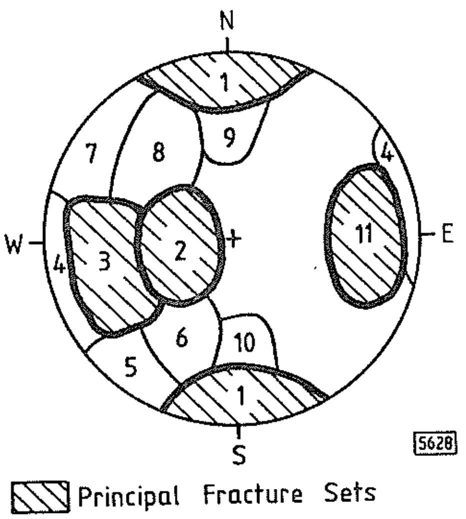

Figure 1 - Orientation of Fracture Sets at Mount Isa Mine.

3.2 Model for Fracture Spacing

Model for the variability in the intensity of fractures within the mine shales is based on the "zonal" concept for the spatial distribution of fractures in rock. The writer describes the basis for this model elsewhere (Baczynski, 1980). The mean intensity for each fracture set is indicated below.

Table III

Mean in situ Intensity and Corresponding Spacing

Set No.	Intensity (m/m^2)	Spacing (m)
1	2.17	0.46
2	2.17	0.46
3	1.12	0.89
4	0.24	4.2
5	0.12	8.3
6	0.28	3.6
7	0.05	20.0
8	0.23	4.3
9	0.15	6.7
10	0.12	8.3
11 (5 Orebody)	6.0	0.17
11 (7 Orebody)	5.2	0.19
11 (11 Orebody)	15.6	0.06

Field investigations suggest that there is no correlation between the intensity of bedding plane partings (Set No. 11) and other fracture sets within the shales.

3.3 Model for RQD-Index

As this parameter was not determined during field mapping, it was necessary to establish a correlation between fracture frequency and RQD-index rating on basis of diamond drill core data.

A literature survey on the topic indicates marked differences between the various published correlations. The mean trends adapted from Deere et al (1966) for a metamorphic rock type and proposed by Barton et al (1975) for essentially igneous rock types, by Priest and Hudson (1976) for sedimentary rocks, and by Kulhawy (1978) from theoretical considerations, are illustrated in Figure 2.

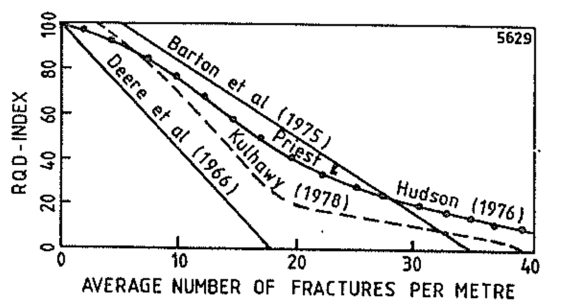

Figure 2 - Summary of Published RQD-Fracture Frequency Correlations.

It is apparent from these results that no single method can be considered to have universal application.

Figure 3 illustrates the correlation established for the dolomitic shales at the mine. This relationship is in extremely good accord with the results of Priest and Hudson (1976), especially for fracture frequencies less than 20 per metre. The trend at higher fracture frequencies is poorly defined because of lack of appropriate data.

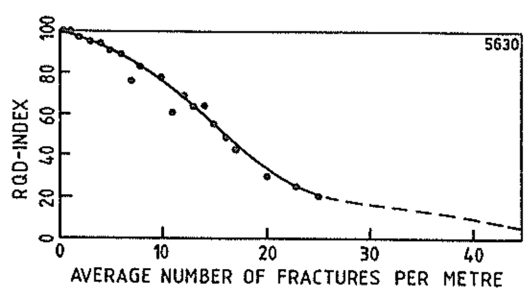

Figure 3 - Relationship Between Fracture Frequency and RQD for Dolomitic Shales at Mount Isa Mine.

It is interesting to note that both the Mount Isa and Priest and Hudson (1976) trends were established for sedimentary strata. These results suggest that one of the governing factors in the observed relationships is rock type. However, more evidence is necessary to confirm this suggestion.

3.4 Model for C-Factor Index

This index was not determined from diamond drill cores, but was derived on the basis of transformations between RQD and C-Factor published by Granstrom (1969) and later by Roberts (1977). The relationship between fracture frequency, RQD and C-Factor for the present study is summarized in Table IV. Non-tabulated values may be approximated by linear interpolation.

Table IV

Relationship Between RQD and C-Factor for Mount Isa

Fracture Frequency/m	RQD	C-Factor
0.0	100	1.00
3.0	95	0.79
5.5	90	0.65
7.0	85	0.56
8.5	80	0.50
9.5	75	0.45
24.0	22	0.13
56.0	0	0.00

3.5 Model for Strength and Modulus

The mean unconfined compressive and tensile strengths of the intact rock cores are assumed to be 180 MPa and 20 MPa, respectively.

The mean Young's modulus of the cores is 100 GPa.

3.6 Model for Condition of Fractures

The relative frequency per metre of core of bedding plane partings (Set No. 11) that may be classed as "planar fractures with slickensided, graphitic surfaces" may be described by means of a normal probability density function with mean of 0.42 and standard deviation of 0.26.

The remainder of the partings and all other fractures (i.e., Set Nos. 1-10) may be broadly classed as "discontinuous fractures with slightly rough surfaces which have a separation of less than 1 mm and hard wall rock" (Barton et al, 1974 and Bieniawski, 1973).

Although the broad classification cannot be considered to be universally applicable, it was necessary to characterize the fractures within a particular class for purposes of the analysis.

The analysis does not extend to mine areas where major, gouge-infilled faults are present.

3.7 Model for Stress Field

Three principal stresses are assumed to be 36 MPa, 26 MPa and 16 MPa, respectively; with the major principal stress acting normal to bedding.

3.8 Model for Groundwater and Weathering

Both parameters are assumed to be negligible for purposes of the analysis.

3.9 Mining Techniques

A classification of just below "good conventional blasting" as designated in Laubscher and Taylor (1976) is assumed for the mine.

4. METHOD OF ANALYSIS

Both the RQD-Index and C-Factor ratings were determined directly from the statistical model for local variability in the intensity of fracturing within the mine shales.

A simple computer program based on the "Monte Carlo" method (Hammersley and Handscomb, 1964) was written and used to statistically assess the ranges of RMR-, Q- and Mod.RMR-index ratings for the hangingwall shales of the orebodies investigated. Statistical probability density function for classification ratings was derived on the basis of a sample of 1000 randomly generated test blocks with respect to each selected block dimension.

The aim of the analyses was to evaluate the local variability in ground conditions within single stopes as well as the overall variability in mean ground conditions between stopes within particular orebodies.

All results are expressed in terms of means and ranges of values within 2 standard deviations about the mean. This range accounts for 95 per cent of values that may be anticipated within the hangingwall shales. The probability that poorer conditions exist is 0.025.

5. PRESENTATION AND DISCUSSION OF RESULTS

5.1 Rock Mass Strength

The ranges of unconfined compressive and tensile rock mass strengths deduced for the three orebody hangingwalls on the basis of the strength reduction factor proposed by Hansagi (1965) are summarized in Table V. Estimates of rock mass friction angles based on Bieniawski (1976) are also indicated in this table.

The estimates appear to be in reasonable accord with the values commonly assumed at the mine for design purposes.

The estimate of the mean pillar unconfined compressive strength for Orebody No.7 on the basis of the C-Factor is 87 MPa. This compares well with the 90 MPa suggested by Brady (1977) from back-analysis of experimental stoping in that orebody.

Although the results permit the construction of simple Mohr-envelopes for the rock mass, it must be emphasized that the shape of the resulting envelopes is directly related to the magnitude of the values assumed for the mean strengths of intact rock cores.

The use of the C-Factor method should be restricted to rock masses with similar ground conditions to those studied by Hansagi (1965).

5.2 Rock Mass Modulus

Rock mass modulus estimates based on RQD, as derived by Coon and Merritt (1970) and Cording et al. (1971), as well as estimates on basis of RMR-rating proposed by Bieniawski (1975) are also summarized in Table V.

Both methods yield similar modulus values. However, the results based on RQD display a greater range of values for local variability. Similar ranges may also be achieved by the use of the RMR-

Table V

Estimates of Rock Mass Properties

Rock Mass Property	Orebody	Local Variability Within Stope		Variability Between Stopes	
		Mean	Range	Mean	Range
Compressive Strength (in MPa) on basis of Hansagi (1965).	5	68	30-131	68	54-83
	7	74	37-135	74	61-93
	11	35	11-130	35	19-74
Tensile Strength (in MPa) on basis of Hansagi (1965).	5	8	3-15	8	6-10
	7	8	5-15	8	7-11
	11	4	1-15	4	2-8
Friction Angles on basis of Bieniawski (1976).	5	40	36-44	40	38-42
	7	40	36-44	40	38-42
	11	36	32-41	36	34-40
Modulus (in GPa) on basis of RQD-Index Rating.	5	19	14-80	19	17-35
	7	20	15-80	20	18-40
	11	14	11-70	14	12-19
Modulus (in GPa) on basis of RMR-rating, Bieniawski (1975).	5	22	18-39	22	19-26
	7	23	19-39	23	20-28
	11	18	15-29	18	15-24

Table VI

Estimate of Hangingwall Spans (in Metres) on Basis of Various Rock Classifications

Orebody	Rock Mass Classification System					
	Bieniawski		Laubscher and Taylor		Barton et al.	
	Mean	Range	Mean	Range	Mean	Range
5	11	7-16	25	17-33	28	16-48
7	11	7-16	25	18-34	28	16-48
11	6	3-15	15	7-32	11	4-26

relationship published in Bieniawski (1978b). The latter values are not tabulated in this paper.

Although Bieniawski (1978a) indicates that the RMR-method yields a lower degree of scatter of values about the mean, there is no conclusive evidence to suggest that this method is more reliable. The similarities between both sets of results indicate that either method may be used to estimate the mean rock mass modulus.

Moreover, both indices are, to varying extents, an indirect estimate of the total intensity of fracturing within the mass.

The RQD rating is not only governed by the total fracture intensity, but is also a function of the spatial relationship between fractures. Where fracture clustering occurs, a higher RQD rating is achieved and hence a higher modulus is estimated. For example, the same fracture frequencies per metre of core at Mount Isa yield a scatter of 30 per cent in RQD estimates.

On the other hand, estimates of the RMR-index incorporate parameters that have little or no effect on modulus.

This problem is best illustrated by means of a simple example. If the "unconfined compressive strength" and "spacing of fractures" parameters of the RMR-classification are considered, then similar rating reductions could be achieved for two different rock mass conditions. In the first instance, a mass with no fractures and strength of 3-10 MPa would contribute 31 points out of a possible 45 towards the total rating. In the second case, a mass with fractures spaced 0.3-1.0 m and an unconfined compressive strength in the range 100-200 MPa would contribute 32 points. In brief, both masses contribute a similar point score towards the cumulative RMR rating. However, both masses should have different modulus reduction factors. In the first case, this factor should be close to unity since there are no fractures in the mass and the modulus of intact cores should reflect the modulus of the mass. In the second example, the reduction factor will be governed by the stiffness of the fractures and its value will be less than unity, possibly 0.7 or lower.

It is apparent from the above discussion that there are real difficulties associated with each method. Neither method can be expected to yield anything more than an approximate estimate of rock mass modulus.

However, as the RQD-index is far easier to derive in the field, the writer would recommend its use over the more complicated RMR geomechanics classification rating for modulus determinations.

5.3 Stable Spans for Hangingwall of Stopes

Stable hangingwall spans have been estimated on the basis of the RMR-, Q- and Mod.RMR-index ratings. The results are summarized in Table VI.

The results indicate that Bieniawski's RMR classification system yields conservative estimates for unsupported spans, especially since stopes with hangingwall spans in excess of 30 metres have been mined in 5 and 7 Orebodies at the mine.

However, it must be appreciated that the RMR system was basically designed for the evaluation of near surface structures and was never intended to embrace mining situations. Its principal applications are to permanent engineering structures within rock masses that are subjected to relatively low stresses. With respect to these structures, the classification provides an excellent system which is no more conservative than any of the others.

For example, on the basis of Barton's ESR value of 1.0 for "major road and rail tunnels", the mean and range of unsupported spans determined for the 5 Orebody structural environment are 5.5 and 2.0-10.0m respectively. These values are even more conservative than those derived by the RMR-system for the upper limit of applicability.

The following three main factors confound the application of Bieniawski's RMR-system to mining situations:

(i) The system does not provide for the incorporation of stress effects on stability.

(ii) Although the system attempts to determine stand-up time which could then be indirectly related to stability in mining situations, the proposed times appear to be conservative with respect to past experience at the mine.

(iii) There is an upper limit of 20 metres for the maximum permissible span dimension. This value is extremely conservative.

It is considered by the writer that none of the above factors can be resolved without considerable redesigning of the existing system. This prospect makes the RMR-classification unacceptable to open stoping situations.

Both Laubscher and Taylor's Mod.RMR-system and Barton's Q-index yield similar estimates for stable unsupported spans. The values again appear to be conservative. However, the results are considerably better than those derived on the basis of Bieniawski's RMR-classification. Moreover, the derived spans for 5 and 7 Orebodies are probably within 30 per cent of the average values suggested by past mining experience.

It is apparent from the input parameters in Table II that both systems were proposed for or extended to embrace mining situations. In fact, Laubscher and Taylor's classification was designed specifically for mine assessments.

Each of the two systems permits stress effects to be incorporated into the analysis. This provides an opportunity for assessment of stope stability at various stress levels expected in the mine workings.

Unfortunately, practical difficulties are encountered in application of stress factor adjustments to ratings.

The basis for Laubscher and Taylor's stress criterion is poorly defined. Only a range of permissible adjustment ratios is indicated without any discussion or formula by which the appropriate ratio may be ascertained. This limits the usefulness of their system.

Barton's stress reduction factor (SRF) appears to offer considerable scope. However, a degree of personal judgement is permitted, especially in the case of extreme ground conditions. Thus, a likelihood exists that personal bias may enter and distort an analysis. It should be noted that small differences in the SRF-value will yield markedly different ratings and span estimates. This occurs because the Q-index is extremely stress sensitive.

The main disadvantage of the Q-system is its failure to include the effect of fracture orientation in the assessment procedure. All engineering structures are presumed to be already orientated in the most favourable direction with respect to geological structure. This situation does not commonly exist in mining where orientation of stopes is basically governed by economic geology and not entirely by structural considerations.

It is considered by the writer that the effectiveness and sensitivity of Barton's classification would be improved by the incorporation of the following three parameters in the assessment procedure:

(i) Adjustment factor (GEO) for orientation of geological structures with respect to geometry of the excavation.

(ii) Use of a "blockiness reduction factor (BRF)". The blockiness of a rock mass is a function of the number of fracture sets, as well as their intensity and continuity. As the intensity of these fractures increases, the same relative degree of blockiness or complete block isolation will exist, even with lower mean fracture continuity. Thus for a given rock mass, the value of the BRF-parameter is largely governed by the total intensity and mean continuity of fractures. The overall rock mass rating could be reduced by some ratio proportional to the BRF-value.

(iii) Use of an "orthogonal fracture factor (OFF)". In situations where fractures are essentially orthogonal with respect to the effective stress field, normal forces acting on the planes will be proportional to this field. These forces contribute towards interlock between fracture surfaces and thus act to stabilize the mass. Rock mass rating should be increased by some ratio which is directly, or possibly logarithmically, proportional to the relative frequency of othogonal fractures within the mass.

5.4 Correlation Between Classification Ratings

The following linear relationships were established between RMR-, Q- and Mod.RMR-ratings for the dolomitic shales at the mine. The trends are based on a SRF-value of 2.0 with respect to the Q-index.

(i) $RMR = 7.5 \operatorname{Log}_n Q + 42$

(ii) $Mod.RMR = 7.5 \operatorname{Log}_n Q + 19$

(iii) $RMR = 0.93\ Mod.RMR + 25$

The analysis is based on a sample of 2000, statistically generated rock mass blocks for 7 and 11 Orebodies. Correlation coefficients between RMR, Mod.RMR and $\operatorname{Log}_n Q$ are in the range of 0.8 - 0.9.

The first equation is in close agreement with the trend proposed by Bieniawski (1976):

$$RMR = 9 \operatorname{Log}_n Q + 44$$

However, it must be strongly emphasized that the correlations are stress dependent. The relationship will be significantly altered if, for example, different SRF-values are assumed in the determination of Barton's Q-rating. It is therefore important that any relationship for the transformation from one classification rating to another is not assumed to have universal application.

6. CONCLUSIONS

There are certain difficulties associated with the application of each rock mass classification system to unsupported openings such as the lead-zinc orebodies at the Mount Isa Mine. Moreover, none of the published systems appear to be completely satisfactory. However, a number are considered to be potentially useful classifications which could be modified to suit local mining requirements.

Aspects of the following rock mass classifications appear to be potentially useful with respect to underground mining:

Table VII

Rock Mass Parameter	Classification System
Unsupported Spans	(i) Barton's Q-index, or (ii) Laubscher and Taylor's Modified RMR-index.
Strength	(i) Hansagi's C-Factor in conjunction with Bieniawski's RMR-index.
Modulus	(i) Deere's RQD-index, or (ii) Bieniawski's RMR-index.

Overall, Barton's Q-index appears to be the most promising classification for the determination of stable spans within the dolomitic shales at Mount Isa Mine. However, the system needs to be modified to suit the structural environment at the mine.

Use of the "Monte Carlo" method for the generation of statistically valid input for geological structure and possibly some of the other input parameters, offers a technique by which it is possible to make a rapid assessment of the ranges of ground conditions that are likely to be encountered during mining.

7. ACKNOWLEDGEMENTS

The study was undertaken as part of a post graduate project which is financially sponsored by Mount Isa Mines Limited. The writer also gratefully acknowledges the generous assistance provided by CSIRO Division of Applied Geomechanics. The supervisory capacity of Mr. W.E. Bamford and Dr. J.R. Barrett during the course of this work are greatly appreciated.

8. REFERENCES

BACZYNSKI, N.R.P. (1974). Structure and Hangingwall Stability in Lead Orebodies at the Mount Isa Mine. Thesis (M.Sc.), James Cook University of North Queensland.

BACZYNSKI, N.R.P. (1980). Zonal Concept of Spatial Distribution of Fractures in Rock. Proc. Third Aust. N.Z. Conf. Geomech., Wellington, May 12-16.

BARTON, N.; LIEN, R. and LUNDE, J. (1974). Engineering Classification of Rock Masses for the Design of Tunnel Support. Rock Mech., Vol. 6, pp. 189-236.

BARTON, N.; LIEN, R. and LUNDE, J. (1975). Estimation of Support Requirements for Underground Excavations. Proc. 16th Symp. Rock Mech., University of Minnesota, Sept. 22-24, pp. 163-177.

BIENIAWSKI, Z.T. (1973). Engineering Classification of Jointed Rock Masses. Trans. S. Afr. Instn. Civil Engrs., Vol. 15, No. 12, pp. 335-343.

BIENIAWSKI, Z.T. (1975). Case Studies: Prediction of Rock Mass Behaviour by the Geomechanics Classification. Proc. Second Aust. N.Z. Conf. Geomech., Brisbane, July 21-25, pp. 36-41.

BIENIAWSKI, Z.T. (1976). Rock Mass Classification in Rock Engineering. Proc. Symp. Exploration for Rock Engineering, Johannesburg, Nov. 1-5, Vol. 1, pp. 97-106.

BIENIAWSKI, Z.T. (1978a). A Critical Assessment of Selected In Situ Tests for Rock Mass Deformability and Stress Measurements. Proc. 19th U.S. Symp. Rock Mech., Stateline, May 1-3, pp. 523-529.

BIENIAWSKI, Z.T. (1978b). Determining Rock Mass Deformability: Experience from Case Histories. Int. J. Rock Mech. Min. Sci. & Geomech. Abstr., Vol. 15, No. 5, pp. 237-247.

BRADY, B.H.G. (1977). An Analysis of Rock Behaviour in an Experimental Stoping Block at the Mount Isa Mine, Queensland, Australia. Int. J. Rock Mech. Min. Sci. & Geomech. Abstr., Vol. 14, pp. 59-66.

COON, R.F. and MERRITT, A.H. (1970). Predicting In situ Modulus of Deformation Using Rock Quality Indices. Determination of the In situ Modulus of Deformation of Rock, ASTM STP 477, pp. 154-173.

CORDING, E.J.; HENDRON, A.J. and DEERE, D.U. (1971). Rock Engineering for Underground Caverns. Proc. Symp. Underground Rock Chambers, Phoenix, January, pp. 567-600.

DEERE, D.U.; HENDRON, A.J.; PATTON, F.D. and CORDING, E.J. (1966). Design of Surface and Near-Surface Construction in Rock. Proc. 8th Symp. Rock Mech., University of Minnesota, pp. 237-302.

GRANSTROM, S.A. (1969). Special Discussion: Paper by K.S. Bawa on "Design and Instrumentation of Underground Strata for Washington Metro System". Proc. Int. Symp. Large Permanent Underground Openings, Oslo, Sept. 23-25, p.117.

HAMMERSLEY, J.M. and HANDSCOMB, D.C. (1964). Monte Carlo Methods. Methuen & Co. Ltd., London, 178p.

HANSAGI, H. (1965). Numerical Determination of Mechanical Properties of Rock and Rock Masses. Int. J. Rock Mech. Min. Sci., Vol. 2, No. 2, pp. 219-223.

KULHAWY, F.H. (1978). Geomechanical Model for Rock Foundation Settlement. ASCE J. Geotech. Engng. Div., Vol. 104, No. GT2, pp. 211-227.

LAUBSCHER, D.H. and TAYLOR, H.W. (1976). The importance of Geomechanics Classification of Jointed Rock Masses in Mining Operations. Proc. Symp. Exploration for Rock Engineering, Johannesburg, Nov. 1-5, Vol. 1, pp. 119-128.

PRIEST, S.D. and HUDSON, J.A. (1976). Discontinuity Spacing in Rock. Int. J. Rock Mech. Min. Sci. & Geomech. Abstr., Vol. 13, No. 5, pp. 135-148.

ROBERTS, A. (1977). Engineering in Earth Materials. Geotechnology: An Introductory Text for Students and Engineers, Chap. 1, Pergamon Press, pp. 1-16.

Numerical Analysis of Failed Cemented Fill at ZC/NBHC Mine, Broken Hill

M. A. COULTHARD
Senior Research Scientist, Division of Applied Geomechanics, CSIRO, Australia
P. M. DIGHT
Research Student, Monash University; Formerly Experimental Officer, Division of Applied Geomechanics, CSIRO, Australia

SUMMARY The behaviour of a stope of cemented fill at ZC/NBHC Mine, Broken Hill, which failed twice during excavation of adjacent ore, has been analysed. The fill as designed had a cement content ranging from 9% near the base to 3% at the top. The variations, with cement content and time, of the elastic and strength parameters of fill were estimated from laboratory tests. A series of plane strain finite element analyses, using an elasto-plastic limited tension material model for the fill, has been performed to simulate the sequential filling of the stope and the subsequent mining of ore at one side. The side boundary conditions at each stage of stope filling, and the material parameters used for each lift of fill, have been chosen to simulate the progressive curing of the fill. Arching in the fill is shown to significantly affect the calculated fill stresses. Adjacent mining is modelled by removing in two stages the support at one side of the fill. The predicted failure zones are examined as functions of fill strength and other variables, and compared with the failure surfaces actually observed.

1 INTRODUCTION

Cemented fill is placed in stopes in underground mines to provide support during subsequent operations to recover remnant pillars of ore. The success of the pillar recovery relies heavily on the stability of exposures of cemented fill, as fill failure may reduce the efficiency of ore recovery by diluting the ore. Economic considerations require that the cement content of the fill should be kept to a minimum. The object of fill design, therefore, is to determine the cement content that will just develop sufficient strength in the fill to ensure its stability.

The study of the behaviour of cemented fill at Mount Isa Mine has been one of the objects of a recent research project which was jointly sponsored by CSIRO (Commonwealth Scientific and Industrial Research Organization) and AMIRA (Australian Minerals Industry Research Association Limited). The use of cemented fill at ZC/NBHC Mine, Broken Hill, has been described by Askew *et al.* (1978). They discussed the properties of the hydraulically placed sand fill and the design methods employed for determining cement content, and reported a fill failure that occurred at the time of excavation of an adjacent ore pillar. This particular volume of fill is analysed here using the techniques developed in the CSIRO-AMIRA project (Barrett *et al.* 1978). It is shown that its failure can be understood if a suitable factor of safety is applied to the cohesive strength of fill to allow for the uncertainties and simplifications implicit in the analyses.

2 THE FAILED PILLAR

An attempt was made at NBHC in 1973 to expose cemented fill at Panel 8 South during mining of the remnant pillar between the fill and the open stope at Panel 8 Centre. The exposure, which was to have been 60 m wide and 49 m high, failed after the initial blast, causing some dilution of broken ore. Another failure followed the second blast, and ultimately resulted in the loss of about 15,000 tonnes of high grade ore. The stope and failure geometries are shown in Figure 1.

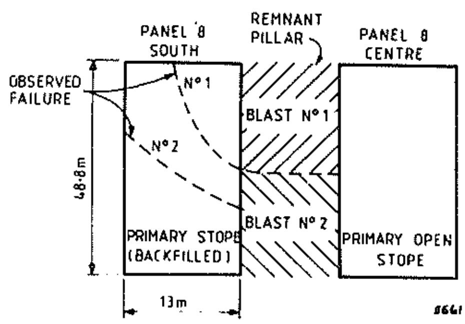

Fig. 1 Vertical section of exposed backfill failure (after Askew *et al.*) at mid-stope.

As discussed by Askew *et al.* (1978), the fill design was based upon a simple two-dimensional (2-d) finite element model which made no allowance for progressive curing of or development of arching in the backfill. The design resulted in the use of variable cement content, reducing from 9.1% at the toe to 3.2% at maximum height. Askew *et al.* found that their design procedure, which was based on Terzaghi's arching model, predicted failure of all but the 9.1% cement content fill.

The locations of the various zones within the fill, and the corresponding mean cement contents calculated from production records (ZC/NBHC, private communication), are shown in Figure 2. A polymer was added to the fill to reduce the loss of cement in decant water (Askew *et al.* 1978), but the actual cement contents may be somewhat less than those in the Figure. The records of stope filling also indicated that narrow, weakly cemented bands of fill were present at several horizons (Askew *et al.*)

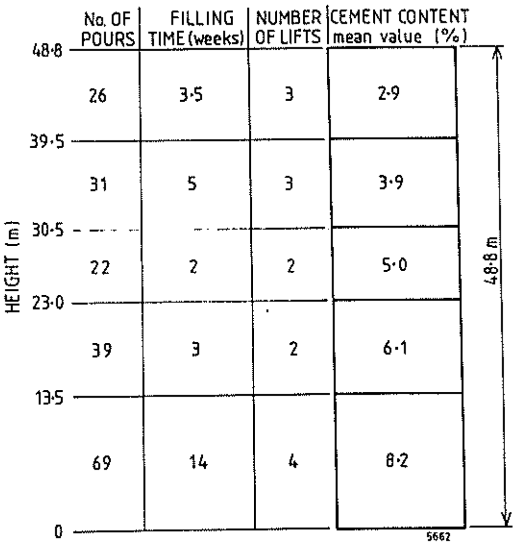

Fig. 2 Geometry and filling details of stope.

Details of the filling rates, which are required so that the development of curing of the fill can be adequately modelled, are also included in Figure 2.

Material parameters which describe the changing elastic and strength properties of curing cemented fill have been deduced from results provided by ZC/NBHC and from data reported by Askew *et al.* (1978).

Unconfined compressive strengths (UCS) for fill of varying cement contents have been plotted as a function of time in Figure 3 (ZC/NBHC, private communication). Intermediate results for different cement content have been obtained by interpolation. While the experimental points can be reasonably

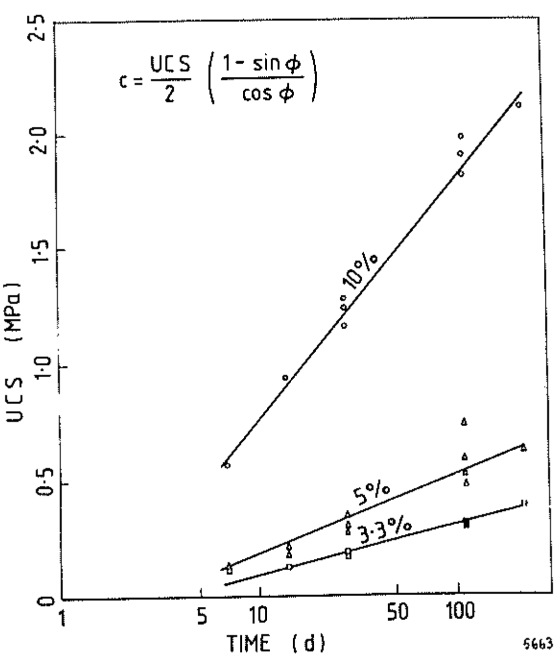

Fig. 3 Unconfined compressive strength of fill as function of time and cement content.

fitted by straight lines on this log-linear plot, it is unreasonable to extrapolate these fits to give UCS beyond 224 days (the oldest fill tested) as the fill cannot be expected to continue to increase in strength indefinitely.

Values of the friction angle of fill, deduced from triaxial tests, were given by Askew *et al.* Because the variation of their friction angles with both cement content and with time appear anomalous, constant values, arbitrarily obtained from Askew *et al.*'s curves at 50 days, have been used in this work. The variation of cohesion with time for each fill component has then been calculated from the UCS values in Figure 3 using

$$c = \frac{UCS}{2}\,\frac{(1-\sin\phi)}{\cos\phi}$$

Variation with cement content and time of the elastic modulus of fill is given in Figure 4 (ZC/NBHC, private communication). Values have been interpolated from these curves where required. Poisson's ratio for different stages of curing has been estimated, taking into account the relative incompressibility of newly poured, semi-liquid fill and the expected value for cured, drained fill.

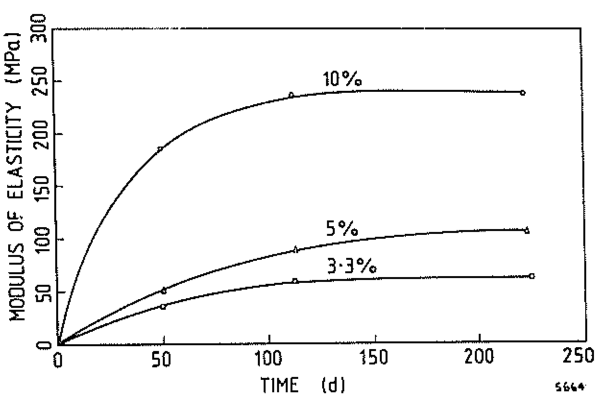

Fig. 4 Modulus of elasticity of fill as function of time and cement content.

The density of fill used (23 kN/m^3) represents an average from several core samples taken recently from fill remaining in the Panel 8 South primary stope. This value is significantly higher than the values of about 15 kN/m^3 and 20 kN/m^3 used in different analyses by Askew *et al.*, and reflects the best information currently available to the mine.

3 FINITE ELEMENT MODEL

The vertical section of the Panel 8S fill, as shown in Figure 2, is 13 m wide and 49 m high. The other horizontal dimension of the fill (the width of the exposure) is about 60 m. As the failure profiles were observed to be fairly constant across the exposed face, a 2-d, plane strain, approximation to the fill can be expected to be reasonable. The analyses of construction and exposure of the fill were therefore performed using a 2-d finite element program developed (Barrett *et al.*, 1978) from Chang and Nair's (1972) program TNJTEP. This allows consideration of material non-linearities arising from elasto-plastic behaviour and limited tensile strength.

As a stope is filled, shear stresses develop at the fill/stope wall interface and lead to arching within the fill. The vertical stresses generated within fill can thus be significantly less than those indicated by a simple overburden pressure calculation. It has been demonstrated by Barrett *et al.* (1978) that the inclusion in analyses of the sequential filling of a stope and the progressive curing of the fill both significantly affect the calculated stress distributions. The stresses calculated using their technique have been found to agree well with those measured in filled stopes at Mount Isa Mine (Cowling, 1978 private communication).

3.1 Pillar Construction

For a stope 200 m high and 40 m wide, Barrett *et al.* showed that a construction sequence of 10 (horizontal) lifts was sufficient; more lifts did not greatly alter the final calculated stresses. In their analyses, curing was considered to occur in three stages. At each stage of the construction calculation, the newly placed lift of semi-liquid fill was taken to have an elastic modulus of 1/10 the long term value, and a Poisson's ratio of 0.45. The relative lack of shear interaction between the fill and the stope walls was modelled by using vertical roller boundary conditions for the new lift. The full load from the weight of this lift was thus transferred to the top of the previous lift, which was taken to be partly cured - its modulus was ½ the long-term value, Poisson's ratio was 0.30, and the developing shear interaction was modelled by fixing the nodes at the fill/rock interface. Material in all lower lifts was described by the long-term material parameters, and the sides were also fixed.

Whilst it is recognized that this model is a gross simplification of the actual number of pours, of the time scale of the pour and of the material inhomogeneity caused by the filling geometry, segregation, degradation and variable cemention of the fill, it is a significantly better approximation than the "overburden" initial stresses used by Cundall *et al.* (1978). For a nonlinear material such as cemented fill it is important that the stress path be modelled realistically if confidence is to be placed upon results of analyses of the stability of subsequent fill exposures.

The same technique for modelling stope filling was used in this study, with the additional feature that the cohesion of fill was reduced almost to zero for new fill, and to half the long-term value for the penultimate lift at each stage. This should further improve the modelling of fill curing. A more detailed calculation, in which the material parameters used at each construction stage have been closely related to the actual pouring schedule, is discussed in section 4.1.

As with other cemented granular materials (e.g. Metcalf and Frydman, 1962), the tensile strength of fill is low. Therefore, in most of these analyses, a limited tensile strength of half the cohesion was assumed for the fill. The measured (long-term) density of fill was used in calculating the loads applied to the system by each newly placed lift. No account is therefore taken of the water which drains from the fill after placement, or of the consolidation of fill whilst filling proceeds, as these effects would cause compensating variations in density.

Additional approximations which are implicit in the treatment of boundary conditions at the fill/rock interface are :

(a) The rock walls are assumed to be rigid relative to the fill, so only the fill itself is included in the finite element mesh, and wall closure during subsequent adjacent mining is not allowed for. Three-dimensional calculations of wall closure during exposure of a square fill pillar are discussed by Coulthard (1979). For the exposure being considered here, hanging wall closure was about 75-100 mm (ZC/NBHC, private communication), which is unlikely to be important because of the essentially 2-d geometry of the fill.

(b) The fill is assumed to be in intimate contact with the rock walls, so that the full shear strength of the fill can be mobilised along the interface.

The finite element mesh used in the analyses is shown in Figure 5. The horizontal spacing of nodes is 1.5 m, except near the stope sides where previous experience indicates that stress gradients are greater. The average vertical nodal spacing is about 1.3 m, and has been chosen to allow at least two lifts of two or more layers of elements to be used in modelling the placement of each zone of fill shown in Figure 2. A finer vertical mesh was used in the lowest zone because this was poured more slowly and so may need more lifts to model it adequately.

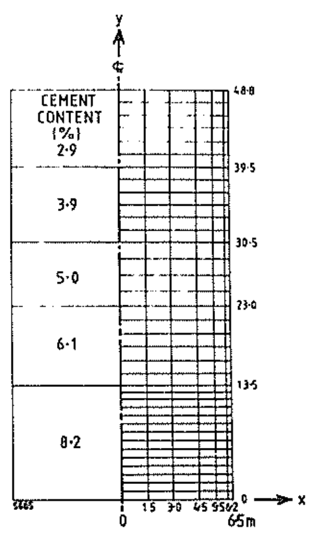

Fig. 5 Finite element mesh for analyses

The variations in calculated post-construction stresses which arise from changes in material parameters and from the use of different numbers of construction lifts, are reported in section 4.1.

3.2 Stability of Fill Exposures

In this particular case, the remnant ore was blasted into an adjacent open stope. As a result, the part of the side of the fill adjacent to the blast would be almost totally free, with no loading from broken ore. The effects of this removal of the lateral and shear support from the side of the fill are modelled by freeing the nodes along the exposure and applying to the nodes forces equivalent to the negative of the previous effective support. These unloading forces are calculated from the shear and horizontal stresses existing in the fill near the stope walls.

TABLE 1

STRENGTH PARAMETERS USED IN ANALYSES

cement content	E (MPa) long-term	ν long-term	c (kPa) 50 days	ϕ (deg.)	ρg (kN/m^3)	c (kPa) (224 days)
2.9%	25	0.15	60	37	23.0	80
3.9%	35	0.15	75	37	23.0	120
5.0%	50	0.15	110	36	23.0	160
6.1%	80	0.15	160	35	23.0	240
8.2%	120	0.15	270	33	23.0	400

As exposures were created more than 1 year after the completion of filling of the stope, the "long-term" material parameters used in the construction are inappropriate. Estimates of the subsequent increase in cohesion of fill have been made (see Table 1), and these properties used in some of the stability analyses.

It has been found (Barrett *et al.* 1978) that, if redistribution of excess stresses in the fill has not converged within 30 iterations, numerical instability has usually developed. This is arbitrarily taken to indicate failure of the fill material, and thus is used to estimate whether, and to what extent, exposures of fill will be unstable. Elements which have "failed" in the first stage of the exposure cannot readily be removed from the mesh, and so are included in the analysis of the second stage also.

The fill/rock contact at the sides of fill zones has sometimes been observed to be broken (Barrett, 1978, private communication). This may be due to shrinkage and consolidation of fill, but could also arise from blast vibration reflection. In these analyses, a variety of different boundary conditions have been applied along the opposite side of the fill from the exposure to investigate whether fill stability might be thereby affected. These include fixed and vertical roller boundaries, and a case where the cohesive bond between fill and rock wall is assumed to have broken so that only the frictional component of shear strength remains.

4 RESULTS AND DISCUSSION

4.1 Construction Sequence

The number of lifts used to model construction of each layer in the fill has been chosen so that each lift corresponds approximately to the same filling time - for 18-, 10- and 6-lift construction sequences, a lift is equivalent to about 1½, 3 and 4½ weeks of filling respectively.

A 10-lift construction has been performed in which the material parameters used for each lift at each construction stage have been obtained, from Figures 3 and 4, to correspond closely with the actual age of the fill. Contours of the stresses developed during this sequential construction of a pillar are shown in Figure 6 and the corresponding centreline vertical stress and side horizontal and shear stresses are plotted, as functions of height in the fill, in Figure 7. These results are typical of the calculated "initial" stresses within fill.

The development of arching is clear from the shape of the vertical stress (σ_v) curve in Figure 7. Near the top σ_v increases steadily with depth. In the body of the fill, side shear stresses are able to carry most of the weight of the fill, so σ_v remains at a fairly constant value until it increases again near the base as the side shear stress drops to near zero.

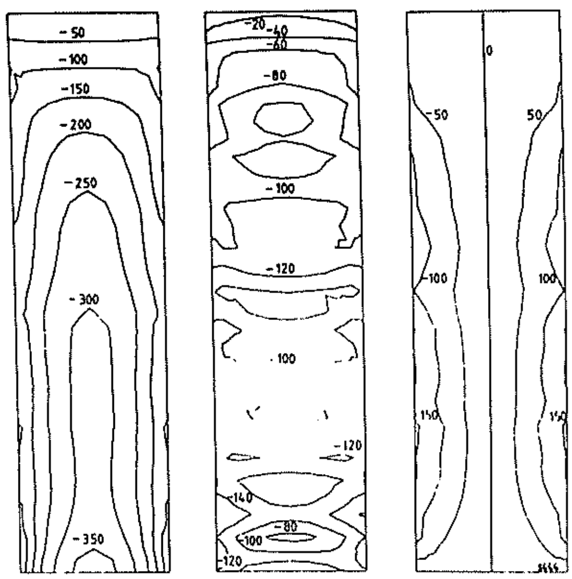

Fig. 6 Calculated stresses after sequential construction of fill pillar. Material properties as in Table 1; 10 lift construction. (a) vertical stress (b) horizontal stress (c) shear stress

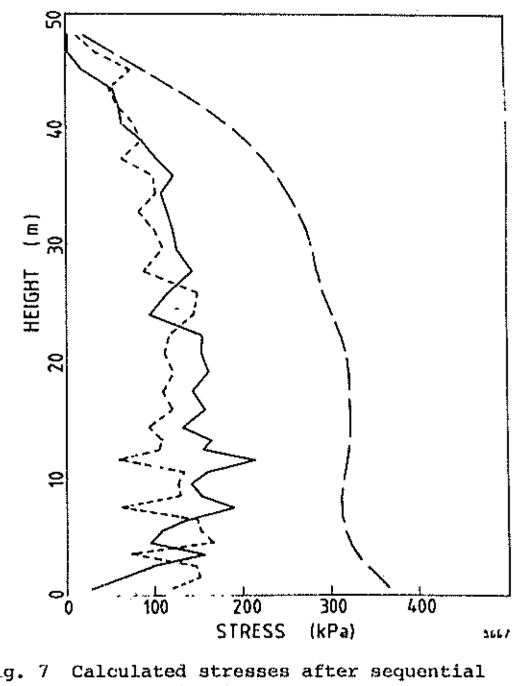

Fig. 7 Calculated stresses after sequential construction, as in Fig. 6: vertical stress near centreline (— —), horizontal stress near side (---), shear stress near side (———).

Because of the roller boundary conditions, the stresses within a new lift are almost uniform across the fill, with the vertical and horizontal stresses varying linearly with depth. The sides of the penultimate lift, however, have just been fixed, and the stiffness and strength of the fill increased. Application of the load from the new lift then results in a sharp increase in the shear stress near the top of that lift. The construction sequencing thus leads to an oscillation of the side horizontal and shear stresses between successive lifts, which may be reduced if the strength of the fill is such that some yielding and stress redistribution occurs at the sides.

It is generally not realistic to attempt to model fill property changes as in the above analysis. When curing is modelled in three stages, as done by Barrett *et al.* (1978), the calculated stresses are found to differ very little from those in Figures 6 and 7. This indicates that only broad details of the strengthening and stiffening of fill need to be accounted for in the analysis of construction. In a further analysis using a two-stage curing process, the stresses again changed little, except that the horizontal side stresses were somewhat lower because of the more rapid decrease of Poisson's ratio. All other analyses discussed below use a three-stage curing model, which has been shown to provide a reasonable compromise.

Variations in the initial stresses with the number of construction lifts are illustrated in Figure 8 for analyses in which a lower density of 16 kN/m^3 and zero tensile strength were used. The corresponding 10-lift curves differ little from those in Figure 7 apart from a scaling factor. With more lifts, (Figure 8(a)), the increase in vertical stress in a new lift is restricted to a shallower region and arching begins to develop sooner. The resulting stresses are thus generally smaller in magnitude and the oscillations of the side stresses are also decreased. The mid-stope vertical stress level for the 18-, 10- and 6-lift constructions are 192.6, 203.9 and 240.7 kPa respectively. These results suggest that a 10-lift approximation will be adequate for use here, as it was in the work of Barrett *et al.* (1978).

A number of other construction analyses were performed to determine the influence of tensile strength and elastic properties of the fill on the calculated stresses. Comparing results obtained with tensile strengths of c/2 and zero, vertical stresses in the former were generally about 3% higher and the oscillations in side stresses were enhanced because slightly less yielding occurred near the sides of the fill.

Increasing the long- and medium-term Poisson's ratios to 0.25 and 0.35 respectively increased the horizontal stresses by about 10%, but had little effect on the other components. The uncertainties in the values of Poisson's ratio as used are therefore unlikely to be of great significance. The calculated stresses were also affected little by halving the long- and medium-term Young's moduli.

Given the relative insensitivity of the initial stresses to these parametric variations, and the reasonable agreement obtained using this numerical technique with measured fill stresses at MIM, the three-stage curing results corresponding to those in Figures 6 and 7 should be adequate for use in calculations of the stability of exposures of this volume of fill.

4.2 Stability of Exposures

As discussed above, the upper half of one side of the fill was exposed after the initial blast of the remnant ore, and the exposure was completed following the second blast. After the first stage of the exposure, and the associated removal of shear and lateral support from the fill, the stresses typically change as shown in Figure 9. These can be compared with the corresponding pre-exposure stresses in Figure 7. The vertical stresses in most of the fill and the side stresses below the exposure all increase as the loads are redistributed. Stability of the exposure is estimated from the extent of unconverged plastic and/or tensile yield remaining after 30 stress redistribution iterations, whilst the shape of a potential failure can be deduced from the location of unconverged elements and/or from the contours of shear stress and shear strain. The results in Figure 10, which are from the same calculation as Figure 9, indicate the development of a curved shear band extending from the toe of the exposure up through the fill. The zones of unconverged yield indicate that a substantial failure of fill is likely. When the full exposure is completed, the corresponding results in Figure 11 suggest massive failure of the fill.

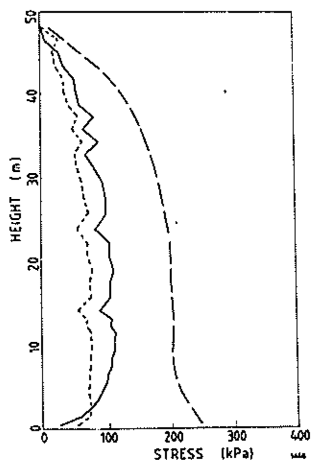

(a)

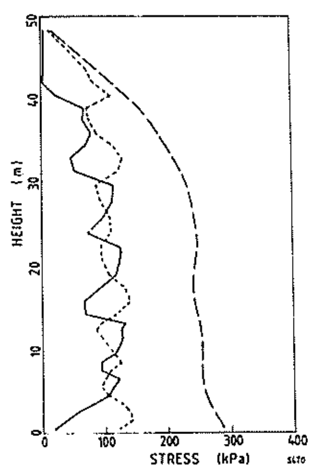

(b)

Fig. 8 Effects on calculated stresses of number of lifts used in construction. Material parameters as in Table 1, except γ = 16. Key as for Fig. 7. (a) 18 lifts, (b) 6 lifts.

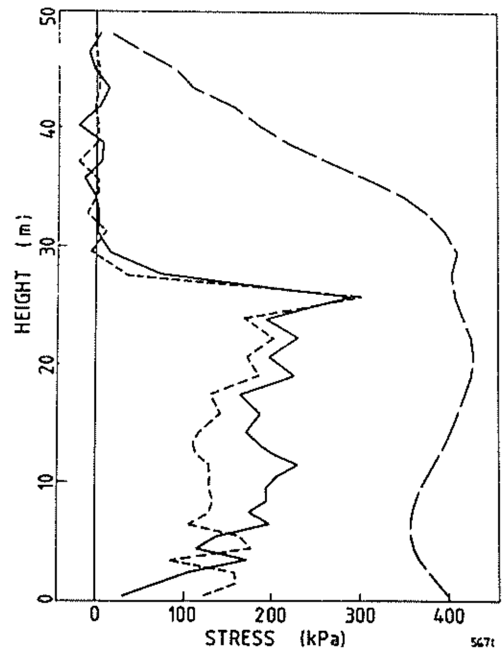

Fig. 9 Calculated stresses after exposure of upper half of pillar; initial stresses as in Fig. 7. Key as for Fig. 7, with horizontal and shear stresses from near the side on which exposure is created.

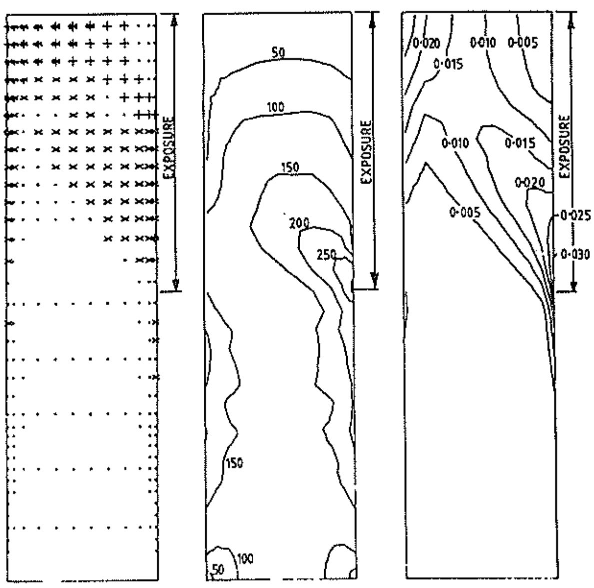

Fig. 10 Results of analysis of exposure on right hand side of upper half of pillar, as in Fig. 9.
(a) Plastic and tensile yield (x and + respectively) and failure (X and ✛ respectively) (b) Maximum shear stress (c) Maximum shear strain.

This procedure has been used to study the effects on calculated fill stability of variations in initial stress levels, of changes in the boundary conditions imposed on the face opposite the exposure, and of different fill strengths. The results of these calculations are now discussed and the "best" prediction of stability of these fill exposures is described and compared with the actual failures.

The results in Figure 9 and 10 were obtained using, in the exposure analyses, the 50-day fill strengths which had also been used in the final (third) stage of curing in the construction model. The areas of shear and tensile failure calculated, for the same post-construction stresses, but using 224-day fill strengths (the maximum available from the experimental curves in Figure 3) are given in Figure 12. These suggest that the first exposure would be stable, but that shear yield in the middle of the fill and non-convergence around the back face could lead to failure when the full face is exposed. The actual exposures were created more than one year after the completion of filling, so a further analysis was performed for strengths extrapolated approximately to 700 days. In this case, the fill appeared to remain stable for both exposure heights, with only a small amount of unconverged yield near the side of the pillar opposite the exposed face.

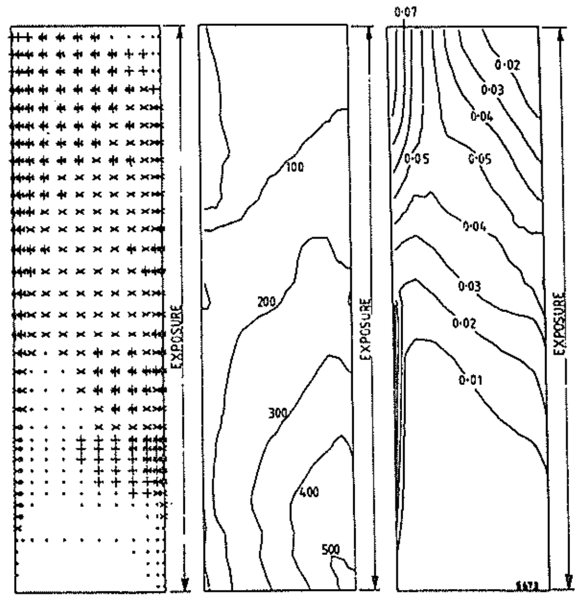

Fig. 11 Results of analysis of extension of exposure in Fig. 10 to full right hand side of pillar; (a), (b) and (c) as for Fig. 10.

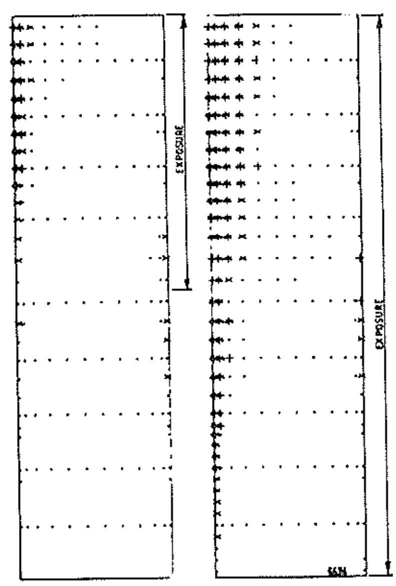

Fig. 12 Areas of plastic and tensile yield and failure using 224 day fill strengths. (a) upper exposure; (b) full exposure.

The greatest effect of initial stresses on stability might be expected to occur if arching was not allowed to develop in a sequential construction, and hydrostatic initial stresses were used instead (c.f. Cundall *et al.*, 1978). For analysis of this case, all the fill was considered to be placed instantaneously, with "uncured" properties and roller boundary conditions for the entire stope. Although the vertical and horizontal stress levels are then much higher than those in Figure 7 and 8, shear stresses are virtually zero. Exposures appeared to be slightly more stable than those in Figures 9 and 10, for the same long-term fill properties. This indicates that an unconservative design could result in this case if arching in the fill is not allowed for in exposure analyses.

As discussed in section 3.2, it is possible that blasting of the remnant ore may lead to a breaking of the bond between fill and rock along the side of the stope far from the exposure. This effect has been modelled by reducing to zero the cohesion and tensile strength of the left-most column of elements opposite the exposure, but retaining for them the long-term frictional strength and elastic properties of fill. The resulting stress fields and zones of yield/failure were found to be almost identical with those obtained when the fill/rock bond was assumed to remain at full strength. In each case several columns of fill elements near that side failed in tension and shear (see Figures 10 to 12, for which the bond-breaking model was used).

The strength of fill at the time of the exposures was likely to have been at least as great as that used in the analyses shown in Figure 12. Therefore, in spite of the movement away from the far wall which is implied by the areas of failure there, the first exposure would be expected to be stable. For the full exposure, the analysis indicates that extensive shear yield develops within the fill and may lead to failure. It is unlikely, though, that predicted failure would be nearly as extensive as that which occurred (see Figure 2).

In summary, analyses with 50-day fill cohesive strengths yield zones of failure which are consistent with those which actually occurred, whereas much greater stability of fill exposures is implied by analyses with the apparently more appropriate longer term strength. From Table 1, it can be seen that the two sets of cohesions differ by a factor of about 1.5. These results therefore suggest that the uncertainties and simplifications implicit in the analysis can be approximately allowed for by inclusion of a factor of safety of 1.5 on the cohesive component of fill strength. However, before such an approach could be used confidently for routine fill design, it would need to be checked further by comparison with other case histories of stable and failed fill exposures.

5 CONCLUSIONS

The finite element method has been used to simulate the sequential construction and curing of a volume of cemented mine fill, and to model the subsequent excavation of an adjacent remnant pillar of ore. The material parameters used for the fill were mainly obtained from conventional geomechanical tests, but some had to be estimated.

The finite element model necessarily neglected some factors which could affect fill behaviour, e.g.:

(i) inhomogeneities in the fill, apart from the variation of cement content, as designed - the narrow, weakly cemented bands of fill which are known to have been present (section 2 and Askew *et al.* 1978) were not included, but could have been critical in initiating failure;

(ii) Blast vibrations and/or drawdown pressures exerted by the broken ore, which could also affect fill stability;

(iii) the real stress-strain relationship for fill is more complex than the elasto-plastic limited-tension model used.

However, results of the numerical analysis of these particular failed fill exposures have suggested that these and other factors may be allowed for by way of a factor of safety of 1.5 applied to the measured cohesion of fill for the design cement content(s). As fill cohesion increases rapidly with increasing cement content (see Table 1), it follows that much less than 50% additional cement should have been sufficient to prevent these failures. Analyses of other case histories of fill exposures need to be performed to further test this approach.

6 ACKNOWLEDGEMENTS

The authors wish to express their appreciation for the cooperation received from ZC/NBHC in providing the essential data for these analyses and also wish to acknowledge the encouragement and continuing interest of Dr. J.R. Barrett.

7 REFERENCES

ASKEW, J.E., McCARTHY, P.L. and FITZGERALD, D.J. (1978). Backfill Research for Pillar Extraction at ZC/NBHC, Mining with Backfill, Proc. 12th Can. Rock Mech Symp., Sudbury, May 23-25, pp. 100-110.

BARRETT, J.R., COULTHARD, M.A. and DIGHT, P.M. (1978). Determination of Fill Stability, Mining with Backfill, Proc. 12th Can. Rock Mech. Symp., Sudbury, May 23-25, pp. 85-91.

CHANG, C.-Y., and NAIR, K., (1972). A Theoretical Method for Evaluating Stability of Openings in Rock, Final Report to U.S. Bureau of Mines on Contract No. HO210046.

COULTHARD, M.A. (1979). Numerical Analysis of Fill Pillar Stability - Three-dimensional Linearly Elastic Finite Element Calculations, CSIRO, Division of Applied Geomechanics Technical Report No. 97 (in preparation).

CUNDALL, P., SHILLABEER, J.H. and HERGET, G. (1978). Modelling to Predict Backfill Stability in Transverse Pillar Extraction, Mining with Backfill, Proc. 12th Can. Rock Mech. Symp., Sudbury, May 23-25, pp. 92-99.

DIGHT, P.M. and COWLING, R. (1979). Determination of Material Parameters in Cemented Fill, Proc. 4th ISRM Congress, Montreux, Sept.

METCALF, J.B. and FRYDMAN, S., (1962). A Preliminary Study of the Tensile Stresses in Stabilized Soil Pavements, Proc. Aust. Road Research Board Conf. 1 (2), 1048-57.

Three-Dimensional Analysis of Rock Failure Zones Around Rectangular Mine Openings in Room and Pillar Workings

B. N. WHITTAKER
Department of Mining Engineering, University of Nottingham, U.K.
A. S. GRANT
Department of Mining Engineering, University of Nottingham, U.K.

SUMMARY The stability of rectangular-shaped mining tunnels in stratified mineral deposits of sedimentary origin is discussed with reference to geological and mining factors. Design of support system is commented upon with specific reference to coal and ironstone mining conditions. Assessment of stability of such mining tunnels and associated intersections is also discussed. Successful designs of instrumentation used for stability assessment in difficult geological and mining conditions are compared. The application of a three dimensional rock fracture analysis program to assessing the stability of the roof strata overlying a four-way intersection (cross-cut) of rectangular mining tunnels is described and compared with field results. Computer derived results compare favourably with field observations and it is generally concluded that such analyses can provide valuable guidance to design of mine openings in this form of commonly encountered mining and geological situation.

1 INTRODUCTION

Stratified mineral deposits which are predominantly flat frequently offer conditions which permit extensive use of rectangular shaped mine openings within the mineral bed. The systematic removal of mineral by a pattern of intersecting rectangular mining drivages leaving regular pillars of mineral for support of the overburden between the mining horizon and the surface, is often known as room-and-pillar mining. It is used throughout the world for a range of different types of minerals especially coal and ironstone. Although the pillars are left to provide support for the surface, the mining rooms frequently require some form of support other than the natural bridging of the strata across the mining excavation. Roof bolting is the main form of support used although in some countries rectangular sets of steel girders and props are popular where the mining excavation height is less than 3 m. For wide and large scale mining operations the rectangular shape of mine opening has major economic attractions in terms of drivage when compared to other shapes within a mineral bed. The form of induced rock stress configuration which occurs with rectangular openings does not however possess the increased degree of natural stability inherent with arched profiles. The increased intensity of rock stress at the corners of the roof in room and pillar mining frequently governs the maximum permissible excavation width especially at the intersections of such drivages. Knowledge of such stresses and their likely effect on excavation stability forms a major objective of the research described in this paper.

2. STABILITY ASPECTS OF RECTANGULAR MINE OPENINGS

The minimum width of rectangular mine openings in predominantly horizontal bedded formations is generally 4-5 m for single drivages, whereas 6-8 m is common for coal and ironstone room and pillar workings owing to the need for adequate width to cater for mine vehicles of sufficient economic capacity. When the width of mining room is less than 6 m, significant problems arise for mine vehicles manoeuvring around pillared workings. Consequently, the minimum width of such mining rooms is often governed by what is acceptable to the mining operations for economic working.

The strata immediately overlying the mineral bed has a major influence on the stability of mining rooms, cross-cuts and junctions. Where competent sandstone is present as a massive bed immediately above the mineral horizon, stability of the rooms is rarely a problem and natural support with occasional roof bolting may be all that is required. However, the strata overlying coal and ironstone beds are more frequently fairly weak sedimentary rocks such as mudstone or clay and do not permit natural spanning unless supplemented with support by rock bolts or rectangular sets of girders and props. Coal mine rectangular drivages generally use the seam roof level because this often provides a good natural parting and is convenient for rock bolting or setting of rectangular sets. Ironstone beds do not normally have a well-defined parting at the top of the bed and often require a thickness of ironstone to be left to promote bridging of the strata across mining rooms. Depth of working and the percentage extraction (in plan) of mining in room and pillar layouts also present major stability factors which must be considered together with the pillar height to width ratio and the strengths of the associated rocks. Pillar design for long-term strength against ultimate collapse is well documented in the case of coal mine workings and much experience exists regarding choice of stable pillar designs in ironstone room and pillar workings. The most common form of instability in such workings is the occasional collapse of roof at junctions of the rooms; the largest expanse of exposed roof strata occurs here and is accompanied by high stress changes in the immediate roof strata, and special considerations must be given to support requirements.

3 ASSESSMENT OF ROOF STABILITY

Underground instrumentation schemes can make a considerable contribution to assessing roof stability in mining rooms and at junctions of rooms and cross-cuts. Such schemes are generally installed during normal mining operations which are then used to provide data on roof stability during subsequent operations, or even throughout the operational life of that part of the mine. Displacement measurements of roof sag and room convergence have proved the most reliable and convenient means of assessing stability. Instrumentation schemes developed at Nottingham University for room and pillar mine workings have been proved over a number of years of continuous operation by mine personnel and are referred to here. Room convergence is measured by a stainless steel tape suspended from the centre of the junction; a weight of 8 kgf is used to tension the tape. A micrometer, incorporated in a framework which is seated on a specially designed mine floor reference point (grouted rock bolt), is used to measure to the base of the weight; special guides eliminate any tendency for the tape to swing. An electrical circuit is used to indicate micrometer contact. The entire measuring assembly is conveniently set up and measurements can be made in a few minutes; the instrument is then taken to another observation station. The room convergence measuring equipment is used in room heights of up to 8 m and a measuring accuracy of 0.01 mm can be achieved.

Roof bed sag has been most conveniently observed (as continuous recording or as spot readings between mining operations) by means of steel rods suspended from different horizons in the same borehole drilled vertically in the immediate roof of the mining room. The Nottingham University type of scheme for measuring roof sag involves placing each measuring rod within a protective plastic tube and grouting the entire unit (between borehole wall and plastic tubes) throughout the full length of the borehole; the point of suspension of each rod has special wings which become embedded in the grout. Consequently, the borehole is effectively sealed and prevents water escaping from upper horizons which can interfere with roof sag measurements in addition to being a nuisance to mining operations. A surface ground platen located on the standpipe is used to seat a depth micrometer for making measurements to the stainless steel rods suspended in the borehole. The standard system involves suspending four rods at different heights in a 43 mm diameter borehole up to a maximum height of 10 m above the roof level of the mining room. This system has proved convenient for coupling to linear voltage displacement transducers and an ultra violet recording system for continuous monitoring of roof sag behaviour during rock blasting operations within the mining rooms. Accuracy of roof sag measurement is normally to 0.01 mm.

These methods of observing room convergence and roof sag have proved valuable bases from which roof stability can be assessed. Comparisons can be made of the influence of changing the roof support method and also the sequence of forming the mining rooms in addition to changes in layout. The influence of time on roof stability is readily assessed by these two instrumentation methods.

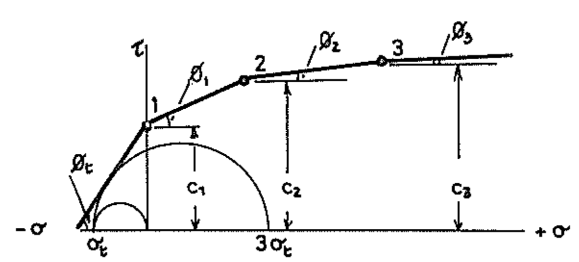

Figure 1 Multi-linear envelope

4 COMPUTER MODELLING OF MINE STABILITY AND ROCK FAILURE DETERMINATION

The Griffith and modified Griffith criteria of rock failure have been used here. The strength of intact rock at a given point is determined to a large extent by k (the ratio of minimum principal stress σ_3 to maximum principal stress σ_1). Failure at any point in the rock mass is predicted by selecting one of a series of related equations, the choice of which depends on the value of k at that particular point. The relevant rock parameters needed for this analysis are obtained from triaxial testing of prepared rock specimens, that is angle of internal friction acting over the negative part of the envelope (ϕ_t), and a series of values of cohesion (c) and angle of internal friction (ϕ) for each stratum to be included in the analysis;ϕ_t is determined by graphic analysis as shown in Figure 1. The Griffith criterion is a two dimensional model with cracks represented by randomly orientated flat ellipses. In order for the predicted strengths to agree as closely as possible with reality the applied stress field must be of the order $\sigma_3/\sigma_1 \leq -0.33$, i.e. there are tensile stress fields in the material. To clarify this point consider uniaxial tensile stress conditions, which under this type of stress field the fracture stress is known as the tensile strength ($-\sigma_t$). When these conditions exist the ratio of minor to major principal stresses is $(-\sigma_t/0) = -\infty$. When Griffiths criterion is applied to a biaxial state of stress with k = -0.33 the predicted fracture stress is also $-\sigma_t$. Thus the first condition for failure will apply when σ_3 equals $-\sigma_t$ if $-\infty \leq k \leq -0.33$.

Research by Morlier and Parate (1971) on the tensile strength of an isotropic fine grained granite under several different stressing conditions (Table 1) demonstrated that the criterion is valid under these conditions. Note that the intermediate principal stress has no influence on the strength. When k is greater than -0.33 failure determination is made by applying the modified Griffith criterion. The transition from Griffith to modified Griffith is made by utilising the multi-linear envelope, as shown in Figure 1.

The equation predicting failure over each linear section of the envelope is derived as follows:-

$$\sigma_{1_f} = \sigma_3 \tan^2(45+\phi/2) + 2c\tan(45+\phi/2) \qquad (1)$$

letting $k = \dfrac{\sigma_3}{\sigma_1}$

we obtain $$\sigma_{1_f} = \frac{2c\tan(45+\phi/2)}{1-k\tan^2(45+\phi/2)} \qquad (2)$$

In order to establish which values of ϕ and c are to be used to determine the failure stress a table is constructed of limiting values of k. These correspond to the maximum and minimum values of k at which failure can occur on that section of the envelope. If k is less than the minimum tolerable value failure occurs on a lower section, if greater it occurs on a higher section. There is a maximum value of k above which failure cannot occur, this is explained towards the end of the section.

These limiting values are determined for each section by finding the value of k at which σ_{1_f} is the same when either σ and c from the current section or σ and c from the previous section are substituted in equation (2). For example the limiting value of k between sections 1 and 2 (Figure 1) is found as follows:-

$$\sigma_{1_f} = \frac{2c_1\tan(45+\phi_1/2)}{1-k_{12}\tan^2(45+\phi_1/2)} = \frac{2c_2\tan(45+\phi_2/2)}{1-k_{12}\tan^2(45+\phi_2/2)}$$

rearranging gives

$$c_1\tan(45+\phi_1/2) - c_1k_{12}\tan(45+\phi_1/2).\tan^2(45+\phi_2/2)$$

$$= c_2\tan(45+\phi_2/2) - c_2k_{12}\tan^2(45+\phi_2/2)\tan^2(45+\phi_1/2)$$

resulting in

$$k_{12} = \frac{c_1\tan(45+\phi_1/2) - c_2\tan(45+\phi_2/2)}{c_1\tan(45+\phi_1/2)\tan^2(45+\phi_2/2) + A}$$

$$A = -c_2\tan(45+\phi_2/2)\tan^2(45+\phi_1/2) \qquad (3)$$

From equation (2) it is apparent that there exists an asymptotic value of k above which failure cannot occur. This is given by:-

$$k_{asy} = \frac{1}{\tan^2(45+\phi/2)} \qquad (4)$$

This value of ϕ belongs to the last section of the envelope.

Since we are dealing with an elastic case (see later) it follows that the magnitude of the principal stresses are directly proportional to the total load applied. Thus if the depth to the workings is doubled the cover load and the principal stresses in the rock mass would also be doubled. Hence a cover load factor or failure factor could be defined as

$\frac{\sigma_{1_f}}{\sigma_1}$ for the modified Griffith criterion and

$\frac{\sigma_t}{\sigma_3}$ for the Griffith criterion.

4.1 Description of Failure Program

A computer program was written utilising the theory described in the previous section.

4.1.1 Input to the Program

The input to the program was obtained from finite element analysis. Since most finite element programs use the convention that compressive stresses are negative, tensile positive, the input follows that convention. A subroutine in the program changes the signs of the principal stresses and values of the related angles to the convention used in rock mechanics, namely compressive stresses positive, tensile stresses negative.

Triaxial strength characteristics are also required as input data. Although a quad-linear envelope is shown in Figure 1 a strength envelope consisting of up to ten linear portions can be handled by the program.

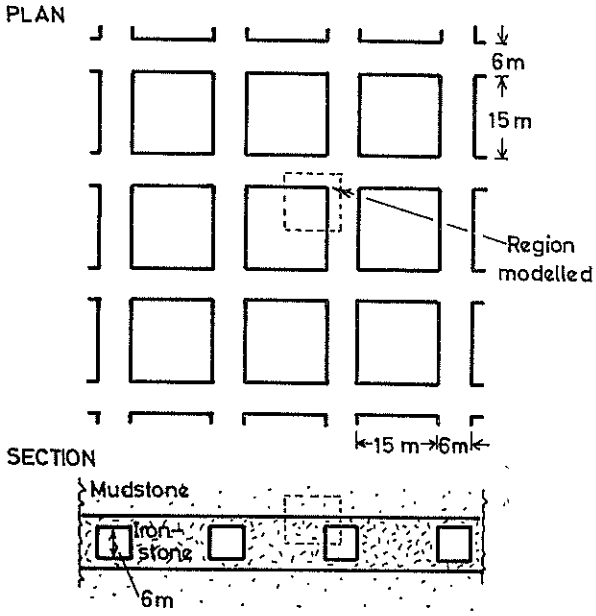

Figure 2 Modelled region of room and pillar mine workings

4.1.2 Output of the Program

The program gives as output a listing of node numbers, X,Y,Z co-ordinates, failure stress and failure factor. Also if desired a graphical plot can be drawn.

4.1.3 Two Dimensional and Three Dimensional Analyses

The program was written originally to deal only with two dimensional problems, however it has now been extended to deal with problems in three dimensions. This could be accomplished because the intermediate principal stress σ_2 has insignificant influence on the predicted failure stress according to the failure criterion employed.

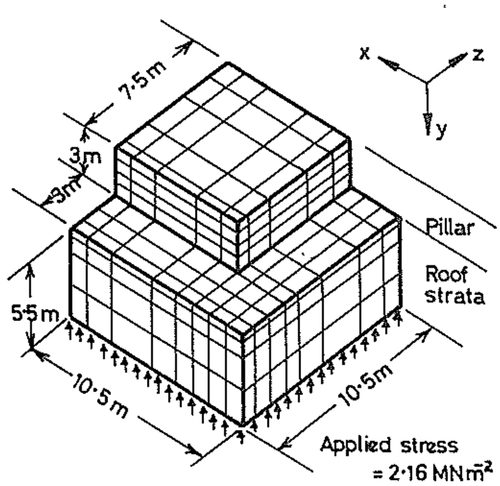

Figure 3 Finite Element Mesh

TABLE I (after Morlier and Parate, 1971)

	Loading conditions	$-\sigma_3$ at failure* MNm^{-2}
	$\sigma_3<0$, $\sigma_1 = \sigma_2 = 0$	8-14
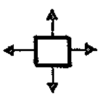	$\sigma_3 = \sigma_2<0$, $\sigma_1 = 0$	10
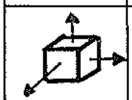	$\sigma_3 = \sigma_2 = \sigma_1<0$	10
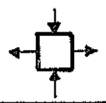	$\sigma_3<0$, $\sigma_2=0$, $\sigma_1>0$	10 for $0<\sigma_1<50$
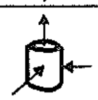	$\sigma_3<0$, $\sigma_1 = \sigma_2>0$	8-10 for $20<\sigma_1<100$
	$\sigma_3 = -\sigma_1$, $\sigma_2 = 0$	13

* Tests carried out on granite

When dealing with problems in three-dimensions the most suitable elements to be employed in the original finite element mesh are brick-shaped rather than prismatic or more complex shaped elements. This is due to the fact that the failure zones are observed in slices at user specified increments along the X, Y or Z axes. From these two dimensional views a three-dimensional picture of the failure zone can be built up. The assumptions made for finite element analysis and failure analysis are listed as follows:-

(i) Loading occurs in an elastic manner.
(ii) Static loading only is considered, with no redistribution of stress occurring after the rock has failed. Also connected with this point is the assumption that the rock is held in place after failure has occurred. If the rock were allowed to move appreciably stress redistribution would occur, with a consequential increase in the size of the failure zone.

5 STRESS AND FAILURE ANALYSIS APPLIED TO ROOM AND PILLAR WORKINGS

Since roof stability is of most concern at the junctions of rooms in a room and pillar mine layout this study has directed attention specifically towards this area and its influence on the stress patterns encountered within and around the pillars. The authors have chosen an ironstone mining system for the purposes of computer modelling, since the ironstone geological, and mining conditions proved a suitable test case for a realistic model. It was considered a valid assumption that the mining situation in this case could be represented by a linear elastic model.

The specific test case used here corresponds to a mining depth below surface of 100 m in a flat ironstone bed of 9-10 m thickness which is overlain by a mudstone. Mining experience at this depth has indicated that for room stability it is necessary to leave an ironstone roof beam of about 1.5 m for room and cross-cut widths and heights of 6 m and square pillars of 15 m side length. Experience has shown that when the thickness of ironstone roof beam is appreciably less than 1 m there is a significant possibility of roof failure resulting in possible collapse. The main requirements of the computer model in this particular test case were firstly to investigate the stress configuration associated with this particular room and pillar geometry and secondly to establish the validity of the failure criteria utilised in the rock failure analysis program described in this paper.

The stresses were obtained from a three dimensional finite element analysis program, (PAFEC 75) developed by the Department of Mechanical Engineering, Nottingham University.

The program was used initially for two test cases, firstly a known stable mining situation with an ironstone roof beam of 1.5 m thickness, and secondly a known unstable situation having an ironstone roof beam of 0.5 m thickness. Finally a third test case was considered where a much higher degree of stability was known to exist since the ironstone roof beam was 3.5 m thick.

5.1 Finite Element Mesh

Since two axes of symmetry exist, one halfway along the side of each pillar and one at the mid-point of the extracted room height only one quarter of a pillar and associated rooms were modelled (Figure 2). The finite element mesh used is shown in Figure 3. The same mesh was utilised in all three test runs. The mesh consisted of rows of elements arranged in the horizontal (X,Z) plane. In each individual run the rows of elements were assigned different properties to simulate either mudstone or ironstone. Thus the three different thicknesses of ironstone (0.5, 1.5 and 3.5 m) in the roof could be simulated.

An eight noded isoparametric brick element was used in the analysis. This type of element was specifically coded for use in large 3D problems in preference to the normal 21 noded brick elements due to the savings that can be achieved in both core requirements and run time. The choice of brick element as opposed to other shapes of elements has previously been discussed.

5.2 Loading Conditions and Strength Properties

The loading at the top of the block of elements (Y = 8.5 m) was assumed to be due to cover load generated by the weight of overburden. An average density value of 2200 kgm^{-3} was used to represent the strata between the ironstone bed and the surface. This produces a vertical component of geostatic stress of 2.16 MNm^{-2} at the upper horizon of the ironstone mine workings. In addition it was necessary to establish values for the elastic constants of the ironstone and mudstone strata. Young's modulus and Poisson's ratio values were determined from laboratory tests and the results are summarised in Table II.

5.3 Stress Output

The relevant information required for the second part of the analysis (σ_1, σ_3 and their nodal coordinates) was output to a computer file for each of the three separate test runs. The vertical stresses obtained from the finite element analysis for a stable case (ironstone roof beam = 1.5 m) are shown as contoured plots in Figures 4 and 5. Each of these plots represents the stresses along a constant horizontal (X,Z) plane through the mesh. The

Figure 4 Vertical Stresses in Pillar and Roof Strata

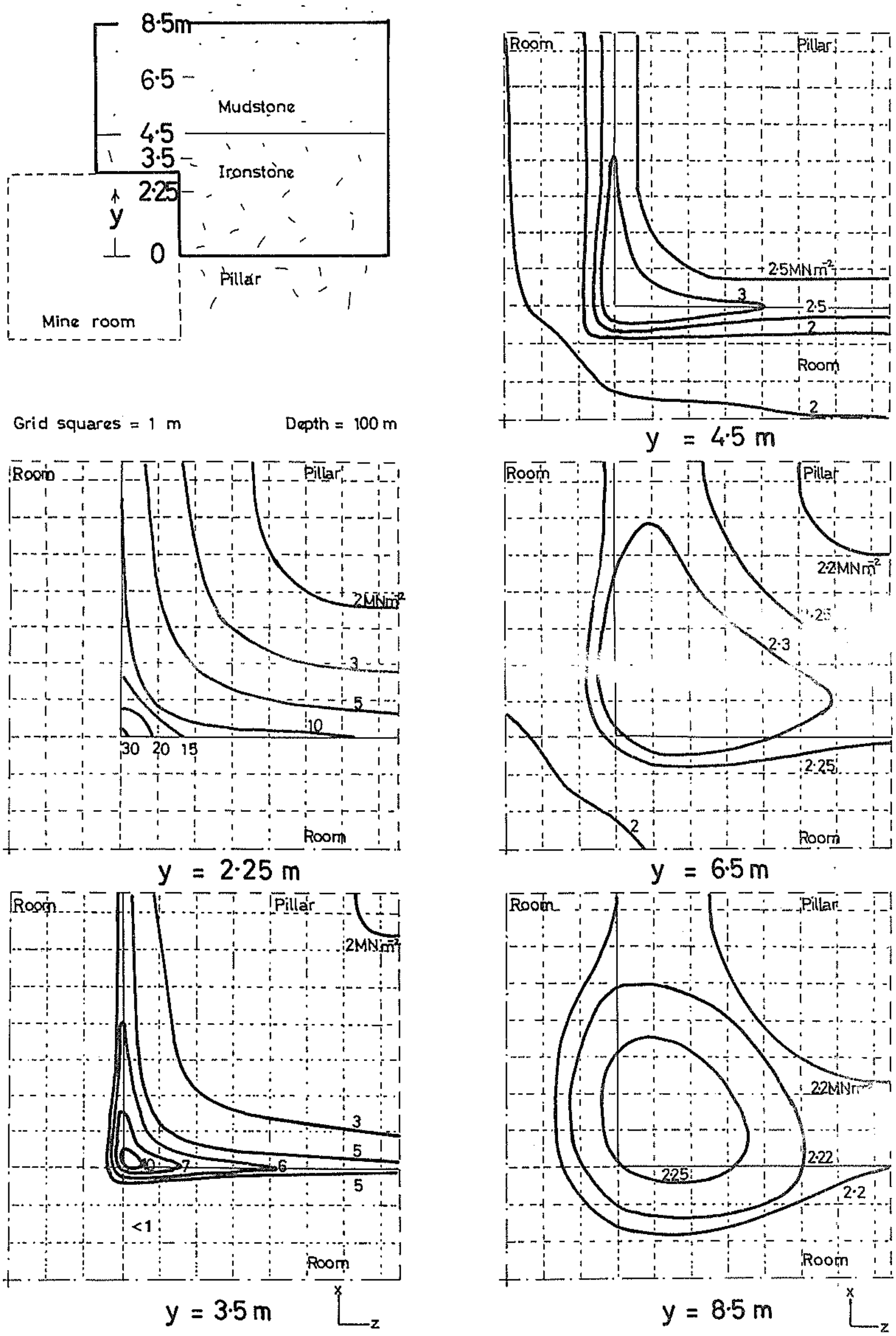

TABLE II
ROCK STRENGTH PARAMETERS

	Mudstone	Ironstone
Young's Modulus (GNm^{-2})	0.5	15
Poisson's Ratio	0.3	0.15
U.C.S (MNm^{-2})	3	36
Tensile strength (MNm^{-2})	N.A.	2.25

Cohesion (MNm^{-2})	Ironstone Triaxial Data
$c_1 = 4.5$	$\phi_1 = 47^\circ$
$c_2 = 9$	$\phi_2 = 40^\circ$
$c_3 = 20$	$\phi_3 = 26^\circ$
$c_4 = 42$	$\phi_4 = 17^\circ$

vertical stresses were selected so as to enable a direct comparison between the cover load of 2.16 MNm^{-2} and the distribution of stress throughout the pillar, roof and pillar intersection and in the roof. The stresses are shown in MNm^{-2}.

The highest stresses occur in the pillar below the level of the roof. This is to be expected since the pillars must support the load originally borne by the whole area prior to mineral extraction.

Figure 5 Vertical Stresses in Pillar and Roof-Pillar Intersection

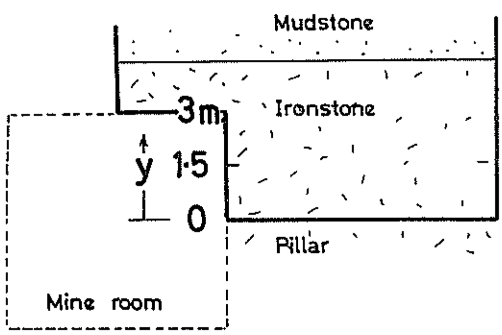

Grid squares = 1 m Depth = 100m

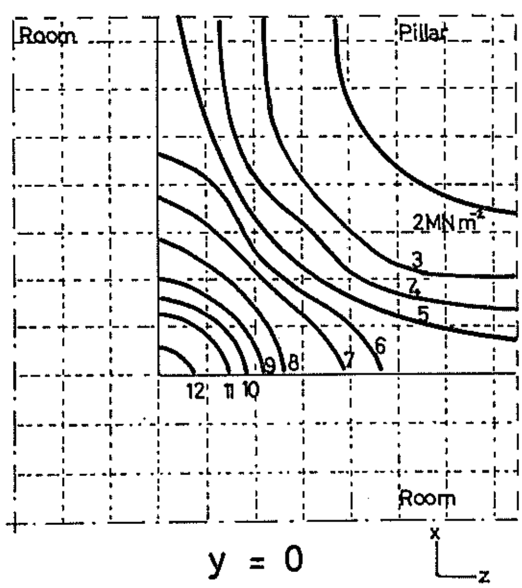

These plots illustrate how the stresses in the pillar and up to 1.5 m above the roof level slope away into the centre of the pillar area from the stress concentrations at the sides and the peak stress occurring at the corner. The lowest stresses occur in the strata directly above the roadway with the area of greatest stress relief occurring above the junction. At 3.5 m above roof level (Y = 6.5 m) the stress field is virtually uniform.

5.4 Failure Condition

The information obtained from the finite element analysis together with the triaxial strength characteristics of the ironstone were used as data for the failure prediction program. Since the overlying mudstone was a weak rock no triaxial data were assigned to it. The assumption being that if failure was predicted in the ironstone roof beam up to or very close to the intersection of the mudstone bed then significant failure of the roof will occur. The reason for this assumption becomes apparent when it is realised that at the mine concerned rock bolting is utilised as the only method of support within the mining rooms. One of the important design factors of rock bolting is a firm anchorage to enable the load to be carried, and this requirement

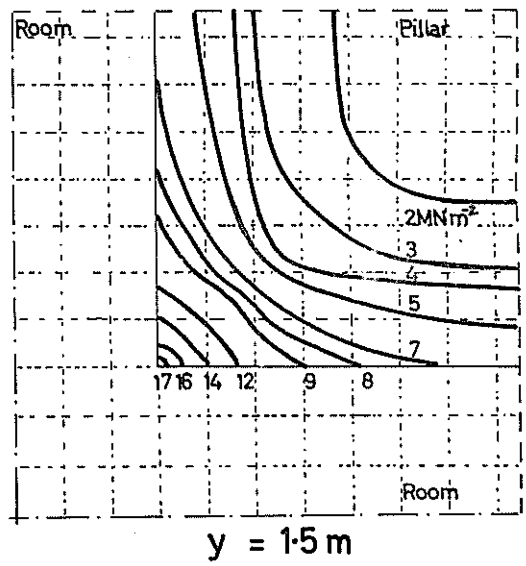

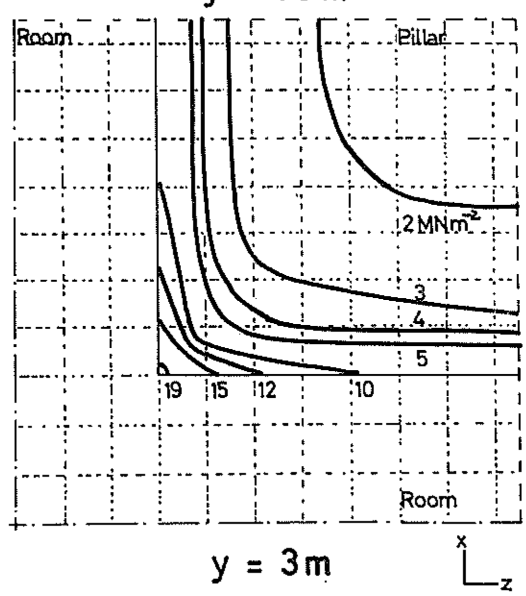

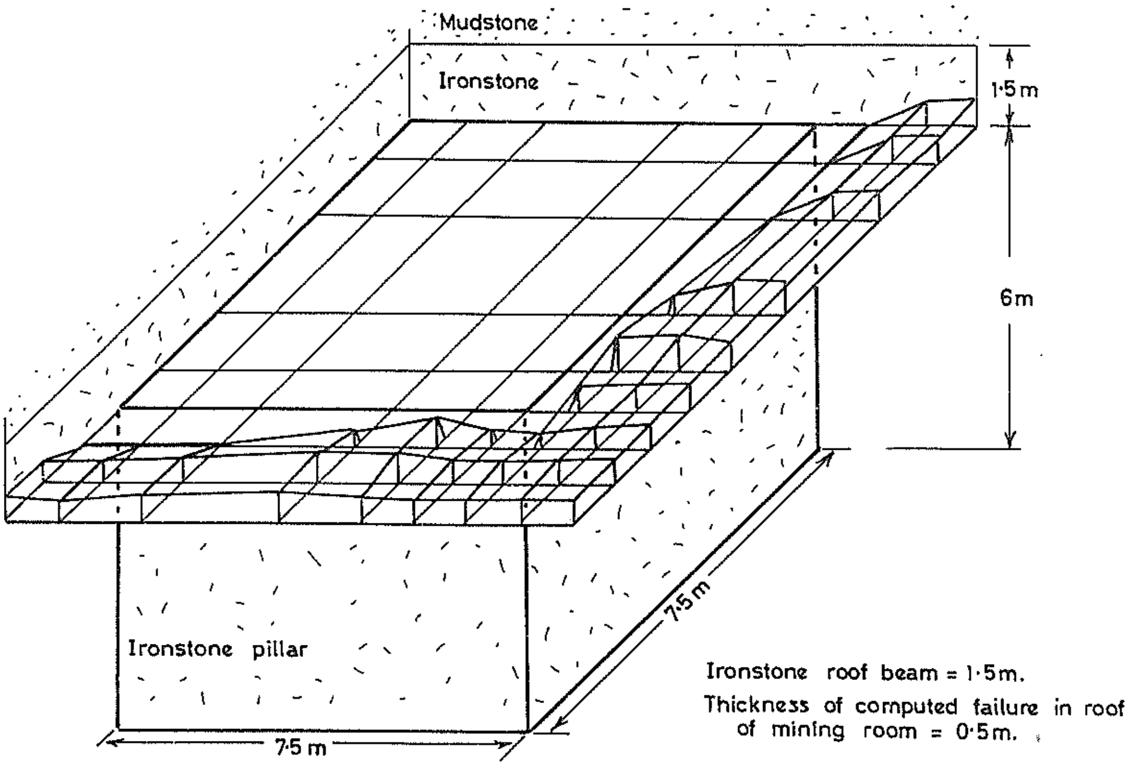

Figure 6 Computed Failure Surface for Depth of 100m and 1.5 m Thickness of Roof Beam

cannot be met effectively by a weak mudstone bed.

5.5 Results

Computer plots of depth to failure contours (failure factor multiplied by depth of initial analysis) were obtained for all three cases tested. Thus the failure surface (zones of instability) could be predicted for similar extraction methods at a variety of working depths. Due to limitations of space only two of these plots are shown in Figures 7 and 8. These are for the most stable cases where the ironstone roof beam was 3.5 m thick.

In one of the cases tested (roof beam = 0.5 m) failure was shown to occur up to the ironstone/mudstone intersection. Therefore according to the assumption previously made failure would occur if rock bolting was used as the only method of support (wire mesh and/or trusses with bolts inclined over the sides are used to supplement bolts in special circumstances). Since the failure zones can only be shown as roof slabs of up to 0.5 m thickness (failure zones in the mudstone being indeterminate) a plot of these has been omitted from this paper.

A three dimensional representation was constructed

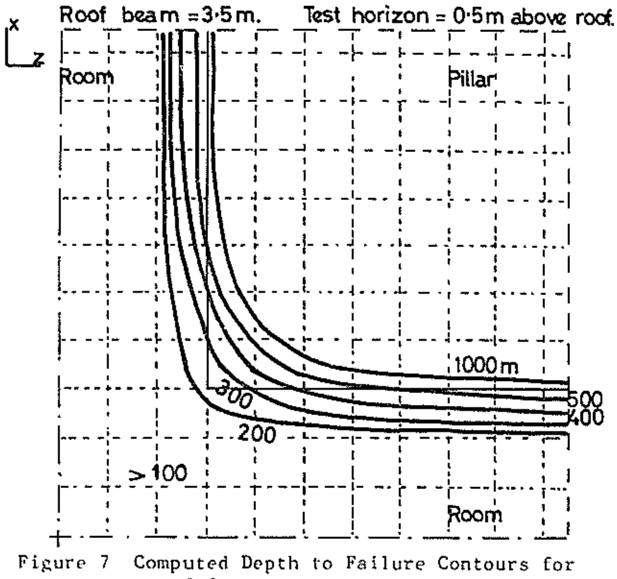

Figure 7 Computed Depth to Failure Contours for y = 3.5 m

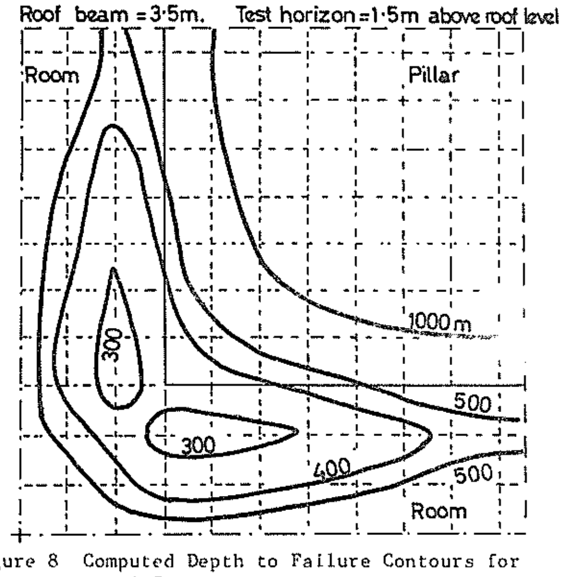

Figure 8 Computed Depth to Failure Contours for y = 4.5 m

showing the zones of instability existing at the working depth of 100 m for the case where the ironstone bed extended 1.5 m into the roof, see Figure 6. The failure surface extends up to 0.5 m above the level of the roof. It is limited in extent to the central portion of the roadway and junction area with no failure occurring within one metre of the pillar. Even though zones of instability are indicated there remains a sufficient thickness of intact ironstone to act as a firm anchorage for bolting. In the third case tested (ironstone beam = 3.5 m) a zone of instability was predicted extending 0.2 - 0.3 m above the workings for a depth below surface of 100 m. Contoured depth to failure plots given figures 7 and 8 show that if the workings were situated at a depth of 200 m then failure would extend approximately 0.7 m into the roof. For failure to occur up to a localised maximum of 1.5 m the corresponding depth to the mine workings would be 300 m. It should be noted that the distances stated for the failure zones are design guide lines for roof support by bolting. The three dimensional nature of the failure surface is shown in Figure 6.

6 CONCLUSION

The main conclusions drawn from this study are listed as follows:-

(i) Design of workings in room and pillar mining will always require underground instrumentation methods as a means of assessing stability. Displacement measurements of room convergence and roof sag have been found to be very useful parameters for investigating room stability.

(ii) Computed stress configurations in three-dimensions have allowed a better appreciation to be attained of the likely effects of making changes to the dimensions of room and pillar mine workings.

(iii). The three-dimensional stress analyses described here are particularly helpful in ascertaining the influence of making changes in the thickness of competent roof beam spanning room and pillar openings.

(iv) The computed extent of rock failure in the roof of a mining room compares favourably with field observations in an ironstone mining situation.

7 REFERENCE

MORLIER, P. & PARATE, N.S. (1971). Critere de Rupture des Roches Fragiles au Voisinage du Sommet de la courbe Intrinseque. International Symposium on Rock Mechanics, Nancy. Report II 2.

8 BIBLIOGRAPHY

HOEK, E. (1965). Rock fracture under static stress conditions. South African Council for Scientific and Industrial Research, Report MEG 383, Pretoria, South Africa.

Experience with the Monitoring of Crown Pillar Performance in Two Australian Mines

G. WOROTNICKI
CSIRO, Division of Applied Geomechanics
J. R. ENEVER
CSIRO, Division of Applied Geomechanics
B. McKAVANAGH
CSIRO, Division of Applied Geomechanics
A. SPATHIS
CSIRO, Division of Applied Geomechanics
R. WALTON
CSIRO, Division of Applied Geomechanics

SUMMARY: The optimisation of crown pillar dimensions is of concern to the metalliferous mining industry throughout the world. Excessively large pillars may sterilize valuable ore reserves whilst undersized pillars may be prone to failure, leading to hazardous situations and/or loss of reserves through premature interruption to mining operations. The work described in this paper was carried out at the Mt. Isa Mine of Mount Isa Mines Pty. Ltd. and at the New Broken Hill Consolidated Mine of Australian Mining and Smelting Pty. Ltd. and was concerned with monitoring to assess the status of crown pillars in relation to cut and fill and open stoping operations respectively. The work was part of a wider program concerned with the rational design of crown pillars and was undertaken to provide *in situ* information on the performance of crown pillars for comparison with the results of predictive models.

Monitoring techniques employed included static measurements of deformation and point stress changes as well as geophysical measurements (microseismic noise, transmitted wave velocity). An automatic data acquisition system was also developed. This paper describes the instrumentation and methods of application, and summarises and discusses the results obtained.

1 INTRODUCTION

The use of crown pillars to limit stope wall movements and reduce the possibility of large scale failure affecting surrounding development is a well established mining practice. The pillars left must be large enough to remain stable, often for extended periods of time. However, since crown pillars are often formed within an orebody, large pillars could represent a substantial loss of reserve or involve the need for costly pillar recovery techniques. Crown pillar dimensioning has to date relied largely on experience of past pillar behaviour. Increase in depth of mining and new mining practices coupled with depletion of valuable reserves is, however, highlighting the need for a more quantitative approach to crown pillar design.

To achieve this it is essential to gain an understanding of the bulk strength (including reinforcement) of crown pillars, as well as the nature of loadings generated as a result of mining. This is particularly true in the case of crown pillars associated with large open stopes where stoping limits and pillar dimensions are often decided prior to commencement of mining with little if any scope for modification of final pillar size once mining has started. In this situation, failure of crown pillars arising as a result of inadequate initial dimensioning may lead to excessive dilution as well as possibly endangering the regional stability of the mine.

In overhead cut and fill stoping there is often scope for deciding on "pillar" thickness during the mining operation, based on progressive assessment of the stability of the material remaining above the stope back. "Pillars" left at any stage may subsequently be reduced by further cut and fill lifts, if and when conditions permit, provided this is done cautiously by taking small lift heights. Refinement of this approach requires the development of practical monitoring techniques that can describe the relative stability of a "pillar". Such techniques will make more objective decisions on when to stop mining, and when further mining is possible.

The work described in this paper forms part of an ongoing project concerned with crown pillar design, being conducted by CSIRO Division of Applied Geomechanics in collaboration with Australian mining companies, with financial sponsorship through AMIRA Ltd. The work is being undertaken with the dual aims of gaining a quantitative understanding of crown pillar performance in general as well as attempting to develop procedures for predicting the onset of pillar failures. Experience gained during the monitoring of crown pillars in cut and fill mining (8 Orebody, Racecourse Orebodies, Mt. Isa Mine) and open stoping (B Lode Orebody, New Broken Hill Consolidated) situations is presented.

2 8 OREBODY, RACECOURSE AREA, MT. ISA

The Racecourse Orebodies consist of an *en echelon* series of thin, tabular, steeply dipping silver-lead-zinc deposits mined by an overhead, mechanised, cut and fill technique (Goddard and Bridges, 1977). The plan of the orebodies at 11 level is shown in Figure 1. The locations of the two sites selected for study in 8 Orebody are marked. Number 8 Orebody is one of the major orebodies occurring in the series, and at the time of the monitoring program was being mined between 13 and 11 levels, having been previously mined from 12 m above 11 level to 9 level (Figure 2). At the commencement of the monitoring program the total height of the 11 level crown "pillar" of 8 Orebody was approximately 30 m.

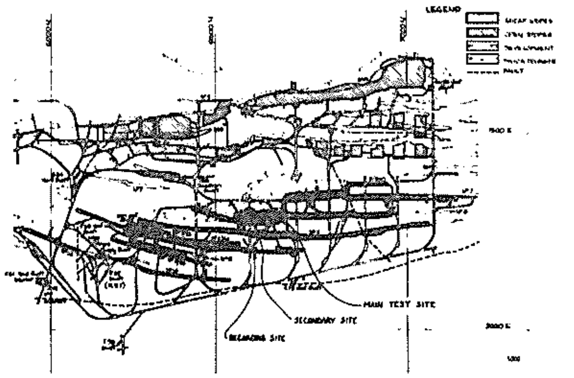

Fig. 1. Plan of 11 level Racecourse area Mount Isa Mine showing location of test sites in 8 Orebody.

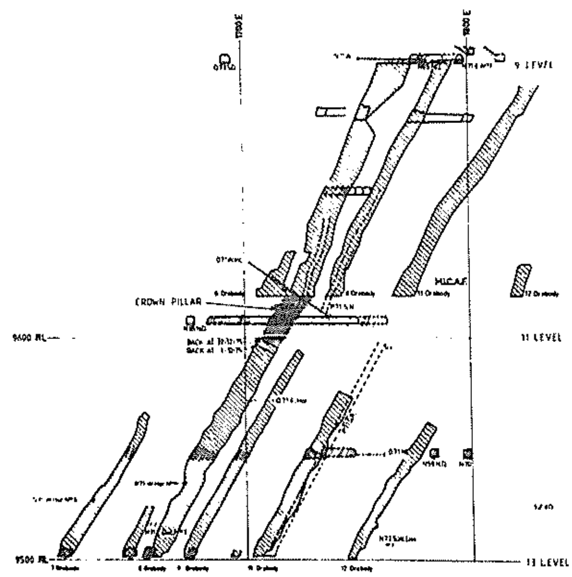

Fig. 2. Vertical cross section at northern test site (Fig. 1) showing mining development at the time of commencement of the monitoring program.

The monitoring period described extended from September 1975 to June 1976 during which a total of four lifts (each approximately 2.5 m high) were mined along the length of 8 Orebody, reducing the average thickness of the material remaining below 11 level from approximately 18 m to 8 m, at which time the pillar was noticeably cracking. Mining was discontinued shortly after. During the same period, the adjacent orebodies of the Racecourse series were being mined. Number 9 Orebody was of particular importance in this regard as it was in very close proximity to 8 Orebody and was being mined at approximately the same elevation. Mining was resumed in 8 Orebody approximately two years after completion of the monitoring program. During the intervening period, considerable mining activity had taken place in the parallel stopes of the Racecourse series. Upon resumption of mining, the remaining material in 8 Orebody up to 11 level was removed with little difficulty.

Absolute stress measurements were conducted at the approximate mid-height of the "pillar" using the stress relief overcoring technique, in conjunction with a USBM borehole deformation cell and the CSIRO hollow inclusion gauge (Worotnicki and Walton, 1976) in December 1975 (i.e. at the commencement of the monitoring program) and in December 1977 (i.e. well after its completion). The results for the northern most test site are given in Table No. 1. Severe core disking was encountered at both sites during the earlier measurements. This is consistent with the stress magnitude reported, in particular the very high cross-stope (approx. E-W) stress component which approached the measured uniaxial compressive strength of the rock forming the crown "pillar" (Miller, 1977). The reduced stress magnitude indicated by the latter measurements is consistent with the relative ease with which the "pillar" was mined subsequent to the monitoring program (see earlier). In fact it was partly on the basis of the latter stress measurements that mining was recommenced in 8 Orebody. The actual mechanism by which the stress relief took place is as yet uncertain, but a combination of bedding plane slip, stress shielding and cracking has been suggested. In this regard, significant subsidence and bedding plane movements have been observed by Mt. Isa personnel.

TABLE 1

RESULTS OF ABSOLUTE STRESS MEASUREMENT (STRESS COMPONENTS IN MPa), 8 OREBODY 11 LEVEL CROWN PILLAR

Date	σ_1 (approx) E-W	σ_2 (approx) N-S	σ_3 (approx) Vert.
Dec. 1975	95	46	27
Dec. 1977	19	13	7

Stress change monitoring was undertaken to provide a continuous record of the magnitude of cross-stope stress changes. A number of uniaxially sensitive rigid inclusion stress meters were installed at various locations between the stope back and 11 level at both sites. Although results were obtained from both sites, it was only from the northern-most site that a continuously reliable record resulted.

The National Coal Board (U.K.) instrument (Enever, 1977) was used for the monitoring. This device consists of a tapered steel plug (Fig. 3) fitted with electrical resistance strain gauges oriented to measure diametric strain changes. The device is forced into a matching tapered socket prepared at the bottom of a hole drilled to the required location. Increases in uniaxial compression occurring in the host rock, in the sensitive direction of the instrument, are transferred to the stressmeter and registered as strain changes. Calibration of the instrument/rock system enables electrical output to be related to changes in rock stress.

For the work in 8 Orebody, a number of holes were drilled from 11 level, parallel to dip, and one instrument inserted per hole, at the required depths, with the required orientation. Instrument cables emerging from the holes were terminated at secure locations on 11 level near to the respective test sites. Signals from the instruments were

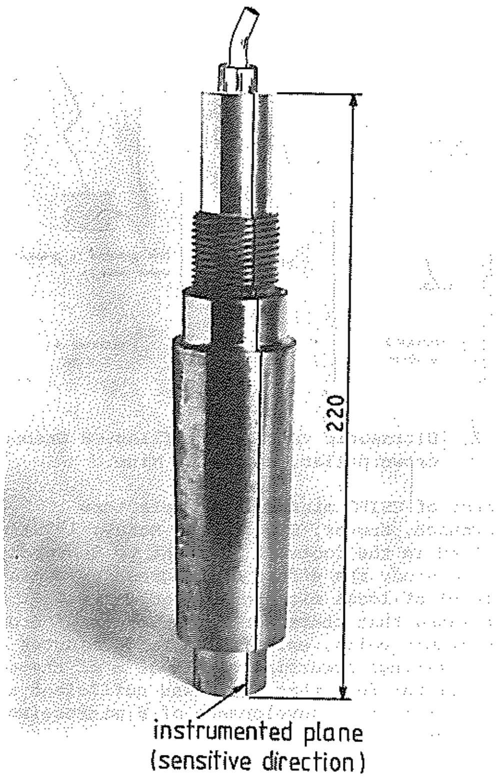

Fig. 3. National Coal Board (U.K.) Rigid Inclusion STressmeter.

transmitted up to 500 m to a central recording site (Fig. 1) where they were registered on a data logging system providing the capability for continuous monitoring. Results were provided both in hard copy format (for immediate inspection and manual reduction) and in the form of magnetic tape records permitting automatic data reduction. This system proved effective in providing essential data at critical times, but did present maintenance problems. These were largely overcome by providing strict environmental control for the logger (Spathis, 1978).

Figure 4 shows the results of monitoring of cross-stope stress in 8 Orebody at the northern site, for a period during which three lifts were mined in both 8 and 9 Orebodies. Incremental stress changes associated with specific events in the mining history for the period concerned are shown in respect to their relative location in the pillar as it existed at that particular time. A significant increase in cross-stope compression occurred up to approximately 5 metres above the new stope back formed by removing a lift in 8 Orebody. The peak stress change occured approximately 2 to 3 metres above the back. The displacement of the peak stress change away from the back can be explained in terms of the superpositioning of induced increments of compressive stress from previous lifts on the already high cross-stope stress (see above) leading to failure of the rock near the stope back. This condition would be aggravated by blast damage. This region is therefore unable to accept further stress increase.

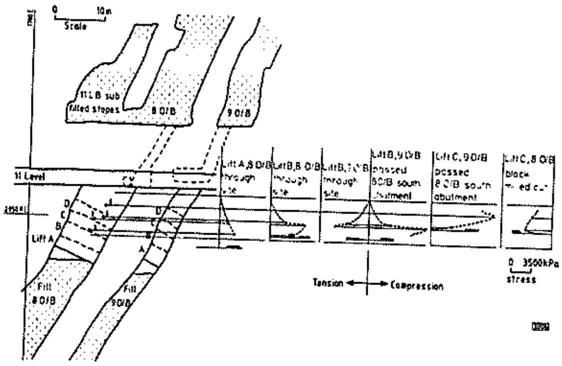

Fig. 4. Incremental cross-stope stress changes for various stages of mining sequence, 11 level crown pillar, 8 Orebody, Mount Isa Mine.

A number of interesting observations regarding the interactive effect of parallel mining in 8 and 9 Orebodies on the 8 Orebody crown pillar can be deduced from Figure 4. On one occasion, a reduction in cross-stope stress was measured when mining of lift B in 9 Orebody passed the test site. At this stage, the height of development of 9 Orebody, measured in the dip plane, exceeded that of 8 orebody at the test site. This partial destressing effect was attributed to stress "shielding" of the 8 Orebody crown pillar by 9 Orebody. On two separate occasions a large increase in compression was noticed at the test site when no mining was being conducted in the immediate vicinity. In both instances a "pendant" block had been left in 8 Orebody close to the test site, from the preceding lift, and mining of 9 Orebody was proceeding past the vicinity of the south "abutment" of 8 Orebody. The postulated explanation is shown diagramatically in Fig. 5. It was noticeable that when the "pendant" block was subsequently mined, a stress decrease was recorded at the test site. The effects observed demonstrate the need for attention to mine scheduling to avoid potentially troublesome situations and/or to take advantage of the benefits offered by the concept of "shielding".

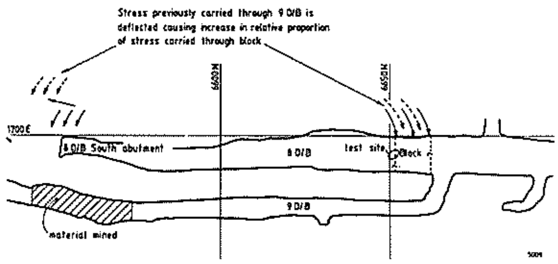

Fig. 5. Representation of proposed interaction in longtitudinal direction between 9 Orebody and 8 Orebody.

Incremental ultrasonic wave velocity and attenuation measurements were made along the centre-line of the crown pillar, in the dip direction. A piezoelectric crystal detector was lowered down a water-filled hole drilled from 11 level, at the northern site. Ultrasonic pulses were generated near the collar of the hole by means of a magneto-strictive transducer attached to a large pad of concrete. This system was arranged to produce pulses travelling nearly parallel to the direction of the hole (Fig. 6). The fastest travel path for the pulses was through the rock in the hole wall and then, via the water, directly to the detector. By recording the arrival time and the amplitude of the first peak of repeated pulses, at a series of s[illegible]ay points down the hole, it was possible to determine incremental transmission velocities and signal attenuations for waves travelling in the rock (McKavanagh and Lee, 1979). Periodic surveys of this type were made of the 8 Orebody crown pillar at various stages during the monitoring period and continuous profiles of velocity and attenuation produced, as shown in Fig. 7.

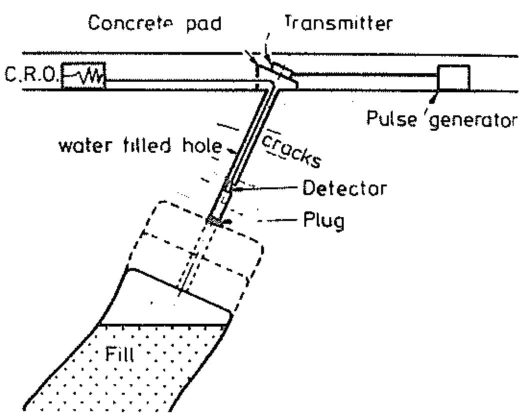

Fig. 6. Photo of ultrasonic set-up Mt. Isa.

The first survey (6/12/75) shows a marked decrease in incremental velocity from approximately 5 metres above the stope back to the back. This can be readily attributed to increasingly severe development of cracks approximately parallel to the stope back, causing increase in travel path length with commensurate apparent decrease in incremental velocity. This observation is generally consistent with the results of the stress change monitoring. The marked change in velocity approximately 7 metres above the back was attributed to a large single crack thought to exist at the location. Smaller scale variations in velocity were observed to be due to different rock types. The latter surveys (10/1/76 and 7/2/76) yielded substantially similar results, both indicating a tendency for reduction of incremental velocity in the region approximately 5 metres above the new stope back. The other interesting facet of the latter surveys was the relative reduction of velocity for the higher region of the pillar, which may be indicative of the development of ubiquitous cracking in the pillar.

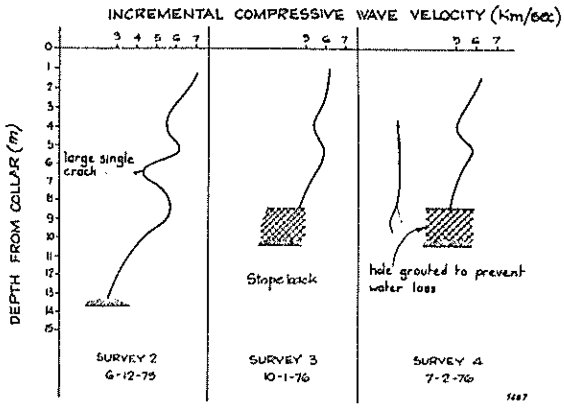

Fig. 7. Ultrasonic velocity profiles, 8 Orebody crown pillar, Mount Isa Mine.

A number of CSIRO microseismic detectors (McKavanagh, Enever, Siggins and McKay, 1978) were installed in the footwall adjacent to 8 Orebody, in order to study the effect of progressive mining on the level of local microseismic activity. It was established that there were high levels of broadband microseismic noise, existing up to 30 minutes after orebody firings occurring within 30 m of the test site. It was felt that there was sufficient activity to warrant further development of a microseismic warning system.

A number of rod and resistance wire extensometers (Enever, McKavanagh and Carson, 1977) were installed in holes drilled parallel to the dip of 8 Orebody to monitor "pillar" dilation. These instruments were connected to the automatic data acquisition system described previously. As a general comment it was found that dilation was of a negligible magnitude during the monitoring period.

3 PANEL 10, B LODE OREBODY, BROKEN HILL

Panel 10 is one of the series of large open stopes developed to extract the lower, northern, portions of the zinc rich B Lode Orebody. Figure 8 is a generalized longitudinal section through the major orebodies in the region, showing the location of

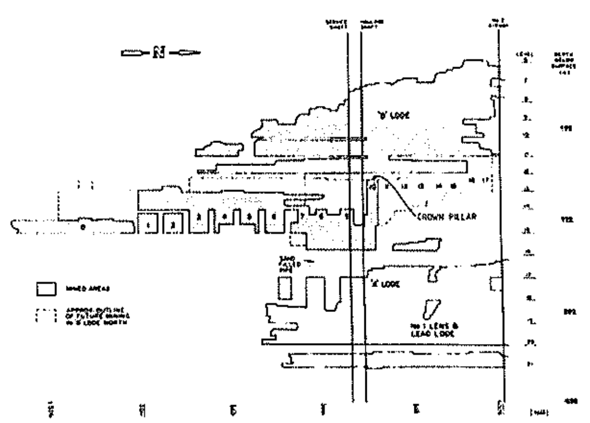

Fig. 8. Longtitudinal section of New Broken Hill Consolidated mine showing position of Panel 10 in "B" Lode sequence.

Panel 10. The designed height of the opening was 120 m and the maximum length at mid-height, 44 m. The stope was mined by developing a vertical cut-off slot at the southern end, progressing from east to west, followed by larger ring firings, extending to the full width of the stope, progressing towards the north. The crown pillar above the stope (below 12 level) was planned to be 12 metres thick. Due to overbreak, however, the actual height of the pillar was reduced over part of its length to approximately 6 metres. During extraction of the stope, the crown pillar began to "bump" and drives contained within the pillar suffered spalling and timber damage. The pillar was reinforced by installation of fully grouted cables at this time (approximately half way through the lift of the stope). It was concurrently decided to commence monitoring of the pillar. The detailed geometry of the crown pillar and the arrangement of instrumentation is shown in Figures 9(a & b). Between October 1976 (when mining was completed) and February 1977, sporadic signs of increased activity (large audible bumps) were reported from the crown pillar, one event being large enough to be recorded on a nearby seismic station (21/1/77). From shortly after this latter event, however, the pillar appeared to become stable with no further signs of significant activity.

Absolute stress measurements were made, using the stress relief overcoring method in conjunction with the CSIRO hollow inclusion gauge (see earlier) at three stages during the monitoring program; at the commencement of monitoring (August 1976), at the completion of excavation of the stope (October 1976) and after a further period of approximately four months (February, 1977).

The results of the absolute stress measurements conducted during the course of the monitoring program are given in Table No. 2. The first two measurements show essentially uniaxial E-W loading of the pillar with an increase in E-W stress between August and October that can be attributed to the mining that took place during that period. The difference between the results of October 1976 and February 1977 is particularly interesting. In general terms the stress field in the pillar during this period tended to become more isotropic, with an increase in the intermediate and minor stress component magnitudes without any substantial change in the E-W stress. It was during this period that the significant seismic activity mentioned earlier occurred, even though the size of the stope was not increased (the stope was in fact being filled with dry fill during this period). It may be postulated that during this period the pillar, which had been effectively overloaded due to mining, suffered an extended phase of instability. This was due, possibly to a combination of the effects of time dependent material and/or discontinuity behaviour and continuing stress readjustments resulting from sequential small scale failures near the stope back In this region the highly concentrated stress may have exceeded the uniaxial strength of the rock (McKavanagh, Tillman, Alexander and Enever, 1978). This could eventually lead to major failure of the pillar under the action of the predominant E-W stress. Yielding of the pillar in the E-W direction under approximately constant stress can be imagined to have caused a sympathetic increase in the vertical and N-S stress components, due to a "mutual confinement" effect. As such a process continued, a point was presumably reached when the net stress condition in the pillar resulted in the pillar becoming stable, due to the strength enhancing effect of the confinement provided by the vertical and N-S stress components.

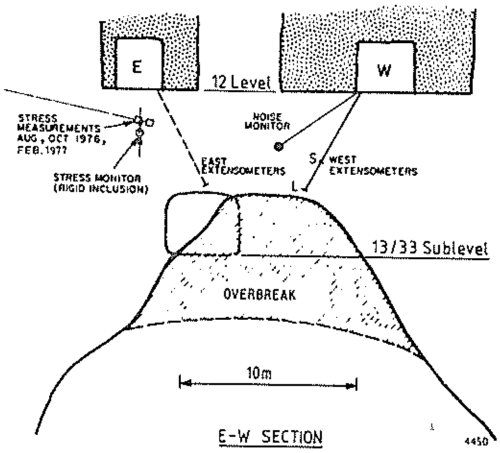

Fig. 9a. E-W section of Panel 10 crown pillar showing overbreak and monitoring installations.

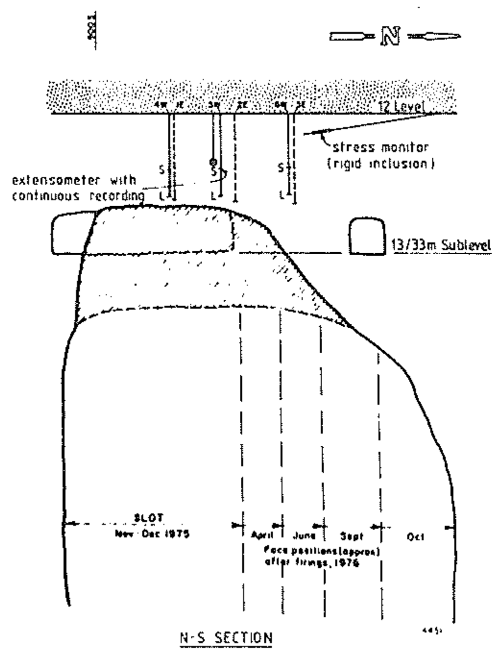

Fig. 9b. N-S section of Panel 10 crown pillar showing overbreak and monitoring installations.

TABLE 2

RESULTS OF ABSOLUTE STRESS MEASUREMENT (STRESS COMPONENTS IN MPa), PANEL 10 CROWN PILLAR.

Date	σ_1 (approx E-W)	σ_2 (approx VERT)	σ_3 (approx N-S)
30 August '76	33	5	3
21 October '76	58	6	-5
18 February '77	56	26	25

A number of rod extensometers were installed, in August 1976, to monitor dilation of the pillar. Most of these were read manually on a periodic basis by mine personnel. As such they provided a means of keeping track of the magnitude of deformations, but not necessarily of being able to locate precisely, in time, the point at which sudden movements occurred. For this specific purpose, one extensometer was fitted with a continuous deflection transducing and recording system (DC-LVDT attached to analogue chart recorder).

The overall history of pillar stability can be observed from the extensometer results (Fig. 10). For the period of active mining up until the end of October all extensometers revealed an approximately linear pillar dilation of modest mganitude, that can be attributed to the quasi-elastic response of the pillar to the increase in E-W compression generated in the pillar by mining. The period between the end of October 1976 and February 1977 is typified by two pronounced jumps in dilation, corresponding to episodes of violent pillar failure, with an intermediate phase of steadily increasing dilation occurring at an accelerated rate relative to the movements prior to October 1976. This mode of behaviour is consistent with the mechanism postulated previously, with two distinct large scale pillar failures occurring about the end of October 1976 and approximately mid January 1977. Soon after the event of January 1977, the pillar reached a stable condition with negligible further dilation. This implies that the event in January eventually resulted in the pillar reaching a stable condition.

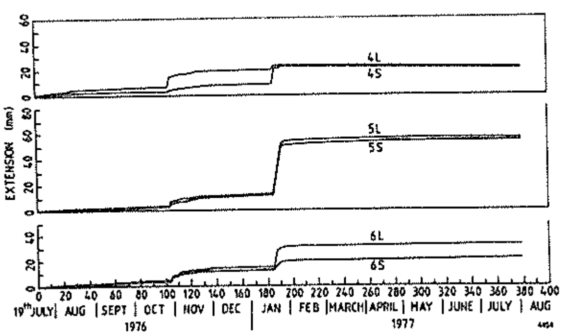

Fig. 10. Pillar dilation measured on the west side of the Panel 10 crown pillar. Two extensometers per hole S:shorter, L:longer.

In order to identify precisely when the pillar was displaying seismic activity, a CSIRO microseismic detector was installed in the pillar near to the anchor location of the extensometer fitted with the continuous recording system. Microseismic noises detected by the device were transmitted to a recording station located on 12 level, where a CSIRO "count rate converter" was used to filter out background noise below a frequency of 10 kHz and then to convert each remaining analogue signal to a digital count representative of the intensity of the signal. The principle of operation is illustrated in Fig. 11 for a microseismic noise recorded from the 10 Panel crown pillar. The total cumulative count for repeated noises detected in the crown pillar was displayed in

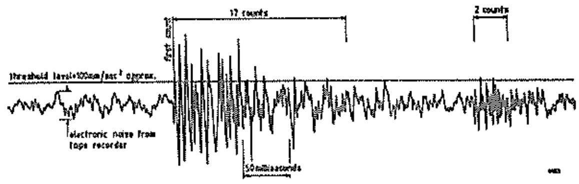

Fig. 11. Typical microseismic noise, recorded in Panel 10 crown pillar at 23.05 h 29 October, 1976 showing principle of noise counting.

analogue format on the same chart recorder that was used for the continuous record of deformation, on the same time base. This meant that periods of high activity in the pillars, which appeared as high count levels, could be directly compared with the occurrence of deformations.

A single National Coal Board rigid inclusion stressmeter was installed, in early November 1976, to monitor changes in the vertical stress component in the upper portion of the pillar. The aim of this was not so much to gain a complete understanding of the changes occurring in the total state of stress, but to be able to record, in time, for purposes of correlation, the occurrence of sudden changes in stress.

Figure 12 shows the combined results of the continuous monitoring for the period, November 1976 to February 1977, with displacement, change in vertical stress and cumulative noise count displayed on the same time scale. The pronounced changes in all quantities recorded early in the period of monitoring may be attributable to the after-effects of the activity known to have occurred around the end of October. The equipment had not been operating long enough, however, to get a reliable record of the complete behaviour. There was certainly some evidence of a specific event of pillar failure occurring on 15 November. This event was not nearly as significant, however, as the major event that occurred on 21 January, 1977 for which a complete record was obtained.

At this time all quantities showed a dramatic increase. Pillar dilation increased by approximately 50 mm, and at the same time a very large increase in vertical stress was observed. The interpreted magnitude of this latter change was considerably greater than the net change in the approximately corresponding stress component indicated by the absolute stress measurements. This discrepency was most likely the result of the application of an incorrect calibration factor for the interpretation of stress changes from the stressmeter strain changes. This discrepency in the magnitude of the stress change has not been satisfactorily resolved. The important aspect is, however, that an increase in vertical stress of significant magnitude was noted to occur contemporaneously with the pillar failure, after which, for the relatively short period of monitoring remaining, the stress appeared reasonably constant (as did displacement and noise count). This behaviour is consistent with the mechanism postulated previously in which it was the event of January 1977 which eventually marked the advent of pillar stability.

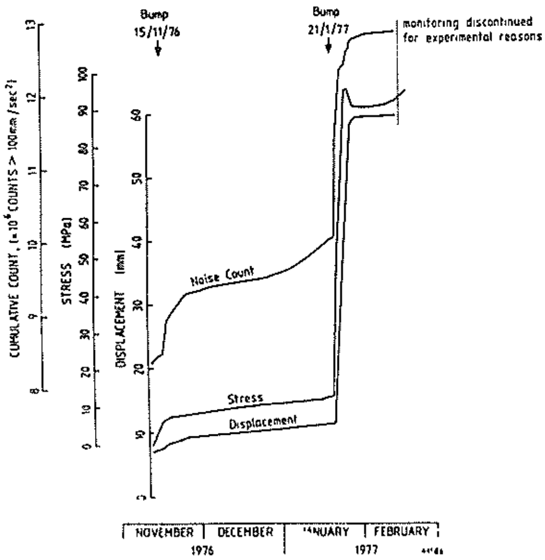

Fig. 12. Extensometer movement, vertical stress and noise measured in Panel 10 crown pillar.

Figure 12 shows clearly that the sudden jump in noise count that occurred as a result of the event of January 1977 was preceded by a significant period in which the background noise count rate noticeably increased (at least one week) without corresponding acceleration of stress and displacement. For approximately half an hour immediately prior to the event, the noise count was observed to drop to a negligible level. This form of behaviour has been previously observed in relation to microseismic monitoring overseas (Leighton and Steblay, 1975) and is currently being used as one of the bases for microseismic warning systems.

4 CONCLUSIONS

From the results of the two monitoring programs described, a number of specific observations were made in relation to the performance of crown pillars in the particular mining situations concerned. Such conclusions are, by their nature, of greatest significance in the context of the relevant mining situations and have already been discussed. There were, however, some aspects of general interest. In the broadest possible sense, the following points can be made:

(a) High compressive stresses, close to the relevant uniaxial compressive strength of the rocks involved, appeared to be the primary cause of instability at both mines. The situation was influenced in each case by local factors such as geology and mining practice.

(b) The major stress in both cases was the east-west component. Both in the Mt. Isa and Broken Hill areas the major tectonic stress is in the E-W direction (Worotnicki and Denham, 1976) and the orientation of the orebodies and/or stopes was such as to cause a further concentration of the E-W stresses in the pillars.

(c) Pillar stability appeared to be affected by pillar geometry. The squat pillar (normal to predominant loading) at Mt. Isa showed evidence of being relatively more stable (small dilation) than the approximately equidimensional pillar produced in Panel 10 (relatively large dilation).

(d) In both situations, the investigations helped to gain a more quantitative understanding of pillar behaviour and to judge their relative state of stability. For the range of instrumentation employed, the following comments can be made:

(i) Absolute stress measurements (particularly employing the CSIRO hollow inclusion cell) proved universally effective.

(ii) Stress change monitoring proved useful, but refined and more reliable instruments are required before the technique could be used on a routine basis.

(iii) Deformation monitoring techniques are well established and relatively reliable. As demonstrated, however, dilation cannot always be relied on as a precursor of failure. Pillars with squat geometries (e.g. Mt. Isa) may not exhibit significant dilation prior to reaching critical stress levels.

(iv) Microseismic monitoring showed positive indication of potential value as a practical tool for giving warnings of imminent violent failure (marked count rate decrease) and possibly as a means of giving long range forecasts (increase in count rate) enabling remedial action to be attempted (reinforcing, destressing). Considerably more work is required to develop the full potential of the technique. Variations including local and regional systems employing various frequency ranges are possible. The promise shown by this technique has led Mt. Isa Mines to install a comprehensive rock noise location system in the area of the Racecourse Orebodies (Godson, Bridges and McKavanagh, 1978) as the most cost-effective way of monitoring an extensive area.

(v) The ultrasonic wave propagation technique gave some evidence of being able to monitor pillar cracking, and may be able to be developed to a stage of becoming a practical tool. Operational complexity and the localised nature of the technique, however, means that even if developed it will probably only ever be useful for application in specific areas of great importance and would not be able to compete with the wider application possible with the microseismic technique.

5 ACKNOWLEDGEMENTS

The authors would like to thank Mt. Isa Mines Pty. Ltd. and Australian Mining and Smelting Pty. Ltd for their support of this work. Particular thanks go to the authors' colleagues in the CSIRO Division of Applied Geomechanics (especially L.G. Alexander and G.H. Carson), to the staff of Mining Research at Mt. Isa (especially M.F. Lee) and the staff of the Rock Mechanics Section at NBHC (especially V.H. Tillman and A. Simonsen).

6 REFERENCES

ENEVER, J.R. (1977). Stress change monitoring in the crown pillar beneath 11 Level, 8 Orebody cut-and-fill stope Racecourse area, Mount Isa. CSIRO Div. Appl. Geomech. Support and Stabilization of Stopes Project Report No. 17.

ENEVER, J.R, McKAVANAGH, B.M. and CARSON, G.H. (1977). Some applications of instrumentation in the Australian mining industry. Proc., Int. Symp. on Field Meas. in Rock Mechanics, Zurich, April, pp. 47 - 60.

GODDARD, I.A. and BRIDGES, M.C. (1977). Development in lead-zinc mining methods at Mount Isa, Australia. Proc., SME Conf. on lead-zinc Update, St. Louis, USA.

GODSON, R.A., BRIDGES, M.C. and McKAVANAGH, B.M (1978). A 32 channel rock noise location system. Proc., 2nd Conf. on Acoustic Emission/Microseismic Activity in Geological Structures and Materials, Univ. Pennsylvania, Nov.

LEIGHTON, F. and STEBLAY, B.J. (1975). Coal mine bounce and roof fall research. Proc., 1st Int. Conf. on Acoustic Emission/Microseismic Activity in Geological Structures and Materials, Univ. Pennyslvania, Nov. pp. 104 - 119.

McKAVANAGH, B.M., ENEVER, J.R., SIGGINS, A.F. and McKAY, J. (1978). Evaluation of the microseismic technique applied to outburst prediction at Westcliff Colliery, CSIRO Div. Appl. Geomech Geomechanics of Coal Mining Report No. 4.

McKAVANAGH, B.M. and LEE, M.F. (1979). Ultrasonic velocity measurements in the 8 Orebody crown pillar, 11 Level, Mount Isa Mine. CSIRO Div. Appl. Geomech. Technical Report No. 81.

McKAVANAGH, B.M., TILLMAN, V.H., ALEXANDER, L.G., and ENEVER, J.R. (1979). Stress, noise and displacement monitoring of Panel 10, Crown Pillar, NBHC. CSIRO Div. Appl. Geomech. Technical Report No. 101.

MILLER, D.R. (1977). Strength and deformability of rock materials from the crown pillar 11 Level, 8 Orebody, Mt. Isa Mine, Qld in triaxial compression. CSIRO Div. Appl. Geomech. Support and Stabilization of Stopes Project Report No. 24.

SPATHIS, A. (1978). Experience with a fast automatic data acquisition system in the 8 Orebody crown pillar on 11 Level, Mount Isa Mine. CSIRO Div. Appl. Geomech. Support and Stabilization of Stopes Project Report No. 36.

WOROTNICKI, G. and WALTON, R. (1976). Triaxial hollow inclusion gauges for determination of rock stresses *in situ*. Proc. ISRM Conference on Advance In Rock Stress Measurements, August, Sydney.

WOROTNICKI, G. and DENHAM, D. (1976). The state of stress in the upper part of the earth's crust in Australia according to measurements in mines and tunnels and from seismic observations. Proc. ISRM Symposium on Advances in Rock Stress Measurement, Sydney, August pp. 71 - 82.

WOROTNICKI, G. and WALTON, R.J. (1977). Rock stress measurements in a crown pillar - 11 level, 8 Orebody Racecourse area, Mt. Isa Mine. CSIRO Div. Appl. Geomech. Support and Stabilization of Stopes Project Report No. 19.

Geotechnical Measurements and Analyses of Open Stoping Operations at Warrego Mine

G. WOROTNICKI
CSIRO, Division of Applied Geomechanics
M. B. WOLD
CSIRO, Division of Applied Geomechanics
R. J. WALTON
CSIRO, Division of Applied Geomechanics

SUMMARY A geotechnical investigation was performed to assist in the problems of recovery of large pillars formed during open stoping at the Warrego mine, N.T., Australia.

The investigation included laboratory and *in situ* tests of rock properties; measurement of the primary rock stresses in the ore and in the country rock using the newly developed CSIRO triaxial stress gauge; and theoretical analysis of stresses and deformations around stopes and in pillars using photoelastic finite element and boundary integral equation methods. A program of monitoring mining-induced stresses and deformations was also begun, using newly developed instruments.

The pre-mining stress measurements showed the presence of high horizontal compressive stesses with the major stress conformant with past folding in the area. The influence of the three-dimensional geometry on the mining-induced stresses was assessed from comparative finite element and analytical studies of idealized two-dimensional and three-dimensional models. For the Warrego mine, estimates of stability from two-dimensional analyses were found to be generally conservative with respect to those from three-dimensional analyses. Monitoring of pillar stresses and deformations during progressive firing of the uppermost pillar has shown changes similar to those predicted from the theoretical analysis.

1 INTRODUCTION

As the cost of pillar recovery per tonne of ore is usually much higher than that of mining primary stopes, maximisation of the size of primary stopes and minimisation of the size of pillars, and the selection of the most economical and safe method of pillar recovery, are the cardinal aims in planning open-stoping operations.

However, the theoretical methods of design of stopes and pillars in metalliferous mines are still in an early stage of development and the relative complexity and variability of mining conditions hinder the establishment of empirical design rules and criteria. To develop these methods, observations are needed of the behaviour of stopes and pillars, particularly of "failure" behaviour, backed up by information about the rock properties, structure and stress conditions of the rock. These observations require improved methods of measurement of parameters which determine the rock behaviour, of prediction of the rock failure and the manner in which it will progress, and of monitoring rock behaviour *in situ*.

This paper presents a summary of a geotechnical investigation performed to assist the optimization of open stoping operations and pillar recovery at the Warrego mine, Tennant Creek, Northern Territory, Australia.

The study included the determination of premining rock stresses, rock structure and properties; a theoretical analysis for prediction of rock behaviour during mining using photoelastic, finite element and boundary integral equation methods; and the monitoring of stress changes and deformations during mining.

The paper is primarily concerned with aspects of the investigations which are of general interest regarding the methods used in, and observations obtained from the investigations. Details of the different stages of the investigations are presented by Worotnicki, et al. (1976, 1977, 1979) and Wold and Worotnicki (1979).

2 WARREGO MINE

2.1 Geology

The main orebody at Warrego is essentially a flattened pipe of magnetite and quartz-magnetite plunging approximately $40^{\circ} \rightarrow 155^{\circ}$ (mine bearing). A schematic north-south elevation is shown in Figure 1.

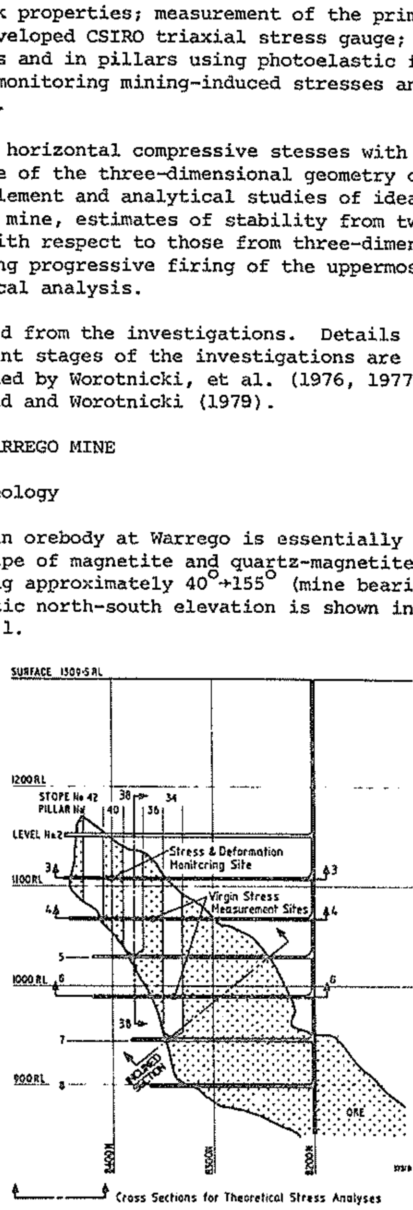

Fig. 1 Schematic N-S elevation of Warrego orebody indicating stress measurement sites and planes for theoretical analysis.

The pipe contains irregularly dispersed sulphides, chiefly chalcopyrite, pyrite, bismuthinite, and some gold. It is surrounded by quartz (-chlorite) porphyroid and chloritic slates to the east (hangingwall) with chloritic slates and chloritic spotted slates to the west (footwall). These footwall slates are separated by a major fault (the Footwall Fault) with an associated shear zone, from quartz-muscovite-haematite sediments further west.

Mining is generally confined within the magnetite orebody with the hangingwalls and footwalls of the stopes situated close to or at the contact of the magnetite with the quartz porphyroids and the chloritic slates. A geological plan showing the main rock units and the stope and pillar configuration at 3 level is given in Figure 2.

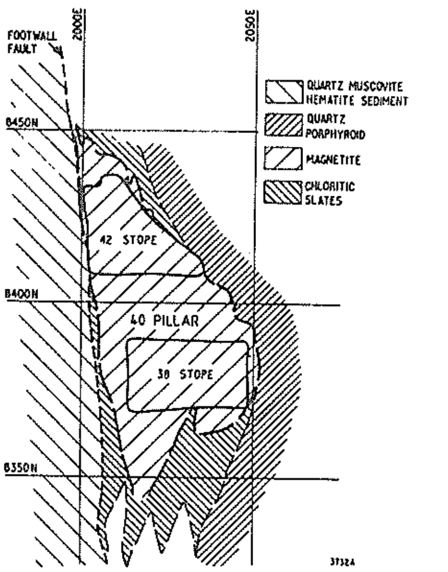

Fig. 2 Plan of 3 level, Warrego Mine, showing main rock types and 40 pillar

The main structural features in the country rock are the bedding, the slatey cleavage, and the joints associated with the fold pattern. The mean orientations of these structures are shown in Figure 3.

The joints in the magnetite orebody are tight and discontinuous, and structurally as well as strength-wise the orebody is a much more competent formation than the country sediments. However, no general patterns of joints have been identified in the orebody from the available information.

At the orebody-country rock contact the slates and porphyroids are intensely fractured, and irregularly jointed to a depth of a few metres, the footwall being more severely fractured than the hangingwall. The magnetite does not show this form of fracturing.

2.2 Rock Properties

Rock properties were determined from uniaxial and biaxial compression tests on cores obtained from exploration diamond drilling, flat-jack installation drilling, and stress-measurement overcoring.

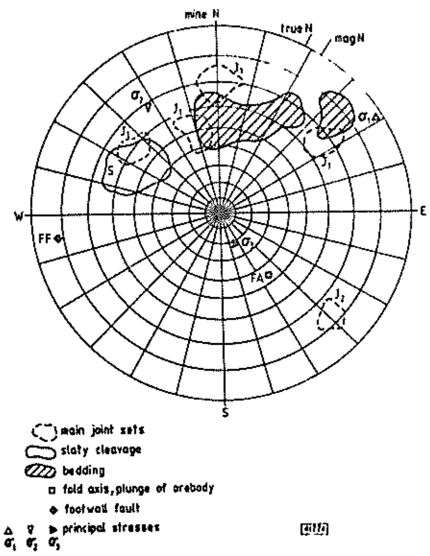

Fig.3 Lower hemisphere projection of principal stresses and geological features at Warrego

Mean values for the uniaxial compressive strength (U.C.S.), tangent modulus and specific gravity of the ore and country rocks are given in Table 1. The best estimate of the ratio of ore specimen strength to country rock specimen strength is 5.6 (range 2.5 - 12.0 with 80% probability). The best estimate of the ratio of ore specimen modulus to country rock specimen modulus is 2.0 (range 0.9 - 4.5 with 80% probability). The country rock specimens could not be subdivided into ock-type groups on the basis of strength, modulus or specific gravity, but this may have been due to the small sample tested.

TABLE 1

Rock group	Mean unconfined compressive strength (U.C.S.) (MPa)	Mean tangent modulus at 50% U.C.S. (GPa)	Mean specific gravity
Ore	305 (202-463 with 80% probability)	65 (48-79)	4.08
Country rock	55 (21-84)	36 (20-62)	2.76

2.3 Mining

During the period 1973-1975, primary open stopes 20m wide and 85-150m high wer excavated at the upper levels (42, 38 and 34 stopes in that order) with the stopes separated by pillars 20m thick (40 and 36 pillars) as illustrated schematically in Figure 1.

The following pillar recovery sequence was proposed by Peko Mines Ltd. engineers for the upper region of the orebody.

(i) Firing of the southern half of 40 pillar into 38 stope, in two 5m segments, followed by drawdown of the fragmented ore, and the filling of 38 stope with cemented fill.

(ii) Firing of the northern half of 40 pillar into 42 stope, followed by drawdown of the fragmented ore from 42 stope and the filling of 42 stope with uncemented gravel fill.

(iii) Extraction of 36 pillar by firing segments into 34 stope, or alternatively mining a 5m wide expansion slot along the mid-plane of the pillar and mass firing the outer shell of the pillar into the slot.

Following the firing of the first 5m thick segment of 40 pillar, mining has been temporarily suspended in this region, with mining and development proceeding at lower levels. Theoretical analyses of stoping operations at lower levels, performed as part of the overall geotechnical investigations (Wold and Worotnicki, 1979), are not presented in this paper.

3 STRESS MEASUREMENTS

3.1 Test Procedure

Virgin rock stresses were measured at three sites in the upper levels of the mine. Two sites were within the orebody at 4 level and at 6 level, and one in the country rock at 4 level (see Figure 1). The borehole overcoring technique was employed, utilising two types of borehole deformation measuring devices.

One was the well known USBM borehole deformation gauge which permits the calculation of the secondary principal stresses in the plane perpendicular to the axis of the borehole. To determine the three dimensional stress tensor, separate tests needed to be carried out in at least three non-coplanar boreholes.

The other was the newly developed CSIRO hollow inclusion stress cell. This cell measures nine components of the strain on the pilot hole surface due to overcoring and thus permits the full determination of the stress tensor in one overcoring operation. Figure 4 shows the type of the CSIRO stress cell used in the Warrego tests. The cell basically consisted of an epoxy resin shell containing strain gauges which was mounted on a steel pipe which served as a cement container. All electrical connections were encapsulated with the cable emerging through the steel rear end. A modified design is given by Worotnicki and Walton (1976).

In both the original and modified designs, three $45^{\circ}/90^{\circ}$ strain gauge rosettes spaced at 120° along the circumference are embedded in the epoxy pipe. The arrangement of strain gauges gives three circumferential and two axial gauges and four gauges at $\pm 45^{\circ}$ to the axis of the hole. This layout allows approximately evenly balanced sensitivity to different components of the stress tensor, and provides for some duplication of gauges so that in the event of a malfunction of one strain gauge of any of these three groups, it would still be possible to obtain the full stress tensor with reasonable accuracy. The strain gauge circuit is of three wires quarter-bridge type, and utilises the internal dummy of the strain indicator. Correction factors are applied to allow for the fact that the strain gauges are not situated on the surface of the pilot hole.

The rock stresses were computed from the overcoring and biaxial compression test results using a computer program based on the work of Panek (1966). In the program the least squares method is used to compute the most probable values of the rock stresses and the standard errors of the six stress components in a chosen coordinate system (in this case the vertical, and the mine -north and -west directions).

A total of 53 overcoring tests were performed, of which 35 were successful. Of the 18 unsuccessful tests, 11 were caused by core breakage problems. Results from the USBM type gauges were similar to those from the CSIRO stress cell. Further work has confirmed that the two techniques give similar results when rock conditions are suitable.

3.2 Stresses

The average stresses obtained for the different sites are shown in Table 2. At all three sites the vertical stress is approximately consistent with the depth of overburden above the site (taking into account the magnetite above the sites 1 and 3). The horizontal stresses are 2.0 to 2.5 times the vertical stress, with the east-west stress generally greater than the north-south stress.

The similarity of the major principal stress σ_1 at the sites in magnetite (sites 1 and 3) is notable. However, at site 2 it is the intermediate principal stress σ_2 which is directed similarly to σ_1 at sites 1 and 3.

Because of the scatter of the stress observations (both of an experimental nature and due to the stress variations *in situ*) and the relative closeness of test sites, no conclusion can be made about the manner in which stresses in the Warrego orebody vary with depth (except for the vertical stress which seems to be proportional to overburden).

Pooling the results from all sites (1, 2 and 3) together shows that all observed strains appeared to belong to the same statistical population. The average stresses for all three sites are very similar to those for sites 1 and 3 analysed together. (Table 2.)

The major principal stress σ_1 is apparently directed perpendicular to the fold axis and approximately parallel to the mean planes of joint sets J1 and J2 and the slatey cleavage S, as described by Goulevitch (1975) and shown in Figure 3. It is directed at about 60° - 75° angle to the footwall fault. It would appear that at the time of folding which produced the girdles of J1 and S, the major pressure was in a direction close to that of the present σ_1 with J1 and J2 extension joints caused by this pressure. This would support the hypothesis that at the lower levels in Warrego Mine the major stress acts in a direction similar to that at levels 4 and 6.

4. THEORETICAL STRESS ANALYSIS

4.1 Approach

The theoretical analysis was performed with the following objectives:

(i) to estimate the stress levels in the stope walls and pillars after mining of the primary stopes;

(ii) to study the effect of pillar recovery methods on the stresses and deformations in the stope walls and pillars, in conjunction with the *in situ* measurements and observations.

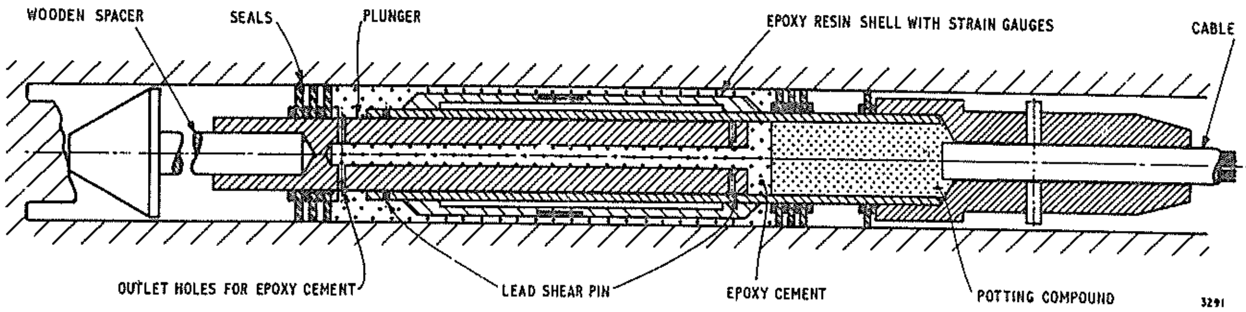

Fig. 4 Hollow inclusion stress cell used at Warrego

TABLE 2

VIRGIN ROCK STRESSES AT THE UPPER LEVELS OF THE WARREGO MINE USING MEAN VALUES OF E = 69 GPa, ν = 0.25

	Depth (m)	Stress Components (MPa) σ_{NS}	σ_{EW}	σ_V	τ_{NW}	τ_{HV}	τ_{VN}	Principal Stresses (MPa) & Directions σ_1	BRG_1 (°)	EL_1 (°)	σ_2	BRG_2 (°)	EL_2 (°)	σ_3	BRG_3 (°)	EL_3 (°)
Site 1	245	17.6 (2.1)	17.5 (1.4)	7.6 (1.3)	-2.7 (1.0)	0.4 (0.9)	0.2 (1.0)	20.2	224	1	14.9	314	3	7.6	120	87
Site 2	245	13.2 (1.9)	15.6 (2.5)	8.2 (1.5)	0.6 (1.6)	-3.7 (1.3)	-3.2 (1.1)	18.0	116	26	13.4	211	9	5.6	319	62
Site 3	320	11.3 (4.2)	19.6 (1.7)	12.3 (2.2)	-5.3 (1.6)	2.2 (1.2)	-2.6 (1.6)	23.1	243	16	12.0	119	63	8.2	339	21
Site 1 & 3 Ore sites	see above	16.0 (2.0)	18.2 (1.1)	9.4 (1.2)	-4.1 (0.9)	0.8 (0.7)	-1.2 (0.9)	21.6	232	6	12.9	142	7	9.2	4	81
Site 1,2 & 3	see above	14.0 (1.4)	16.4 (1.0)	9.0 (1.0)	-2.3 (0.8)	-0.6 (0.6)	-1.7 (0.7)	17.9	238	3	13.3	147	22	8.3	334	68
Stresses at Site 1 by Different Techniques																
USBM Tests		13.7 (4.4)	16.3 (2.1)	7.1 (1.8)	-0.6 (1.7)	-0.8 (1.3)	3.0 (1.5)	16.7	67	11	14.4	334	18	5.9	188	69
Hollow Inclusion Gauge		15.4 (0.8)	20.6 (0.5)	11.3 (0.8)	-1.4 (0.4)	-2.0 (0.4)	0.3 (0.5)	21.3	76	11	15.0	347	-2	10.9	267	79

N.B. (i) Values in parenthesis are standard errors.
(ii) BRG = bearing, east of mine north.
(iii) EL = Elevation, upwards from the horizontal.

The modelling methods used were the photoelastic method, the finite element method and the boundary integral equation method. The complex three-dimensional geometry of the mine could not be practically simulated, and it was necessary to make significant assumptions when trying to represent the problems theoretically. The approach adopted was to select two-dimensional planes through the region of interest, in which it was assumed that the geometry and rock structure did not vary significantly in directions perpendicular to the chosen planes and that no deformations could occur in these directions (i.e. plane strain conditions).

Five planes were chosen in which these conditions were thought to be most closely approximated. These were three horizontal planes though 3,4 and 6 levels of the mine; a vertical plane through the mid-section of a primary stope (38 stope); and an inclined section, dipping 60°N, which intersected the pipe-shaped orebody nearly perpendicularly, between 5 and 7 levels. These planes are indicated on Figure 1. (It was assumed for the inclined plane model that both the primary stopes and the pillars had been excavated.)

The general approach in interpreting the results from the two-dimensional analyses with respect to the three-dimensional prototype was to endeavour to represent the general geometry of the prototype in a simple three-dimensional model which could be analysed theoretically, then to consider two-dimensional sections of the simplified three-dimensional model; and finally to apply the results of comparisons between the simplified two-dimensional and three-dimensional models to the more complex two-dimensional model of the prototype.

In the case of the Warrego mine, to estimate the effect of pillar and stope wall stresses of the three-dimensionality of the stope geometry, an analysis of stresses around a spheroidal opening (ellipsoid of rotation) was performed using the finite element method, and the results compared with the results for infinitely long tunnels with circular and elliptical cross sections, similar to the cross sections of the spheroid normal to its minor and major axes respectively. Pillars were included in some of the analyses.

4.2 Analysis

4.2.1 Two-dimensional

In brief summary, the two-dimensional models showed that after excavation of the pillars, the convex footwall was likely to develop semi-vertical tensile stresses to a considerable depth (up to 15m) over a height of up to 100m (Figure 5). The horizontal stresses in the wall were predicted to be compressive while the pillars separating the stopes were still intact. However it was found that progressive mining of the pillars would tend to relieve the horizontal compression of the stope walls (Figure 6(a), (b), (c)) with a state of biaxial tensile stress indicated in the footwalls of the models after removal of the pillars.

Pillar stresses at the higher levels in the mine were indicated by the models to be up to 40 MPa, and at lower levels, in pillars with a considerably greater height to width ratio, up to 50 MPa *in situ*.

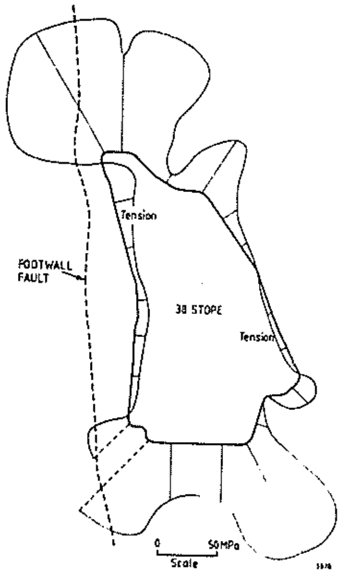

Fig. 5 Boundary stresses around vertical section through 38 stope, adjacent pillars, assumed excavated. Stress plotted normal to boundary, boundary as origin

With regard to leaving a skin of magnetite ore for the purposes of ground control, the analysis indicated that this would concentrate stresses in the relatively stiff magnetite by a factor of between 1.3 to 1.9 depending on stope geometry and the thickness of the skin. However the higher strength and structural integrity of the magnetite would be expected to adequately compensate for the increase in stress level.

4.2.2 Three-dimensional

The coordinate system for the analysis of the spheroidal, elliptical, and cylindrical openings is shown in Figure 7(a). Normalized stresses at five points of interest, as indicated in Figure 7(b) are given in Table 3 for uniaxial and biaxial loading cases of the FEM model, and from the analytical solution for the cylinder. Typical principal stress vector patterns for the case of uniaxial loading of the spheroid and the elliptical tunnel with pillars are given in Figures 8(a) and 8(b).

There is a strong similarity between the two-dimensional and three-dimensional stress distributions, with a general reduction in stress levels both in the pillars and stope walls of the three-dimensional model, compared to the two-dimensional model.

The distribution of stresses with increasing distance from the stope walls, as given in Figures 9(a), 9(b), 9(c) for the spheroid with and without pillars, and for the cylindrical tunnel without pillars, shows a marked decrease in the volume of rock which is affected by the spheroidal opening with pillars, compared to that without pillars and to that which is affected by the cylindrical tunnel.

With respect to the two-dimensional models of sections through the Warrego mine, results of the three-dimensional analysis suggest that the tensile stress zones in stope walls would be shallower and the stresses of lower magnitude, than those predicted from the two-dimensional models.

Estimates of the effect of the finite length of the orebody on the stresses in the stope walls and the pillars were also obtained by comparison of the results for the spheroid with those for the infinitely long cylindrical tunnel without pillars, and with transverse pillars. The results showed that the load carried around the ends of the

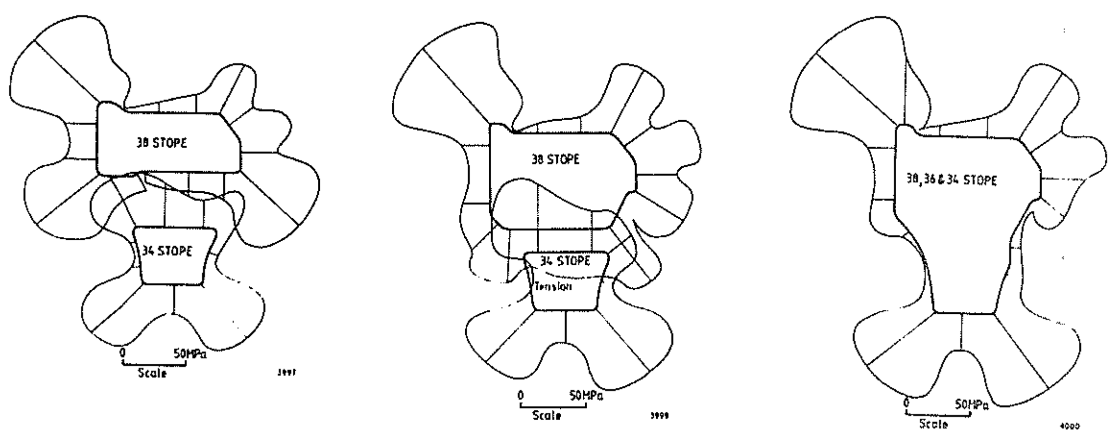

Fig. 6 Boundary stresses around plan section of 4 level, for three stages of excavation. Stresses plotted normal to boundary, boundary as origin - (a) stage 1, (b) stage 2, (c) stage 3

TABLE 3

Applied Stress			$P_x = P_y = 0$; $P_z = 1$		$P_x = P_y = 1$; $P_z = 0$		$P_x = P_y = P_z = 1$	
$E_{\text{"pillar"}}$: $E_{\text{"country rock"}}$			1:1	2:1	1:1	2:1	1:1	2:1
Spheroidal opening a:b:c = 1:1:2 Pillars normal to z axis	Radial stress at pts. A,B in pillars	σ_A	-0.17	-0.24	1.31	1.89	1.14	1.65
		σ_B	-0.20	-0.29	1.30	1.87	1.10	1.57
	Tangential stress at pts. C,D,E in "stope" wall	σ_C	-0.13	-0.13	1.57	1.51	1.44	1.39
		σ_D	0.97	1.02	-0.10	-0.20	1.09	1.01
		σ_E	1.54	1.64	-0.21	0.21	1.44	1.64
Elliptical tunnel a:b:c = 1:∞:2 Pillars normal to z axis	x direction stress at pts. A,B in pillars	σ_A	-0.34	-0.40	1.75	2.06	1.41	1.67
		σ_B	-0.37	-0.46	1.76	2.08	1.38	1.62
	Tangential stress at pts. C,D,E in "stope" wall	σ_C	-0.35	-0.29	2.41	2.05	2.06	1.78
		σ_D	1.32	1.39	-0.26	-0.36	1.27	1.18
		σ_E	2.12	2.23	-0.38	-0.26	1.91	2.22
Circular tunnel a:b:c = 1:1:∞ Pillars normal to z axis	x direction stress in pillars				1.41	1.87		

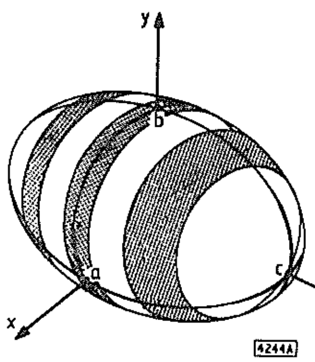

Fig. 7a) Coordinate system for analysis of spheroidal, elliptical and cylindrical openings; showing e.g. spheroidal opening with pillars

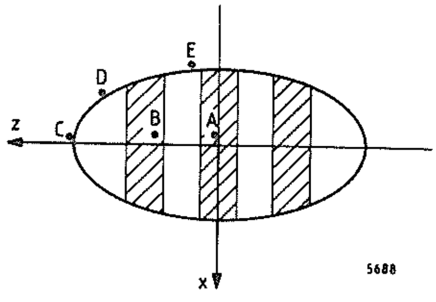

Fig. 7b) Section through x-z plane showing points chosen for comparison of stresses (Table 2)

spheroid reduced the stresses in the central region of the spheroid by up to 15% compared with those around the cylindrical tunnel.

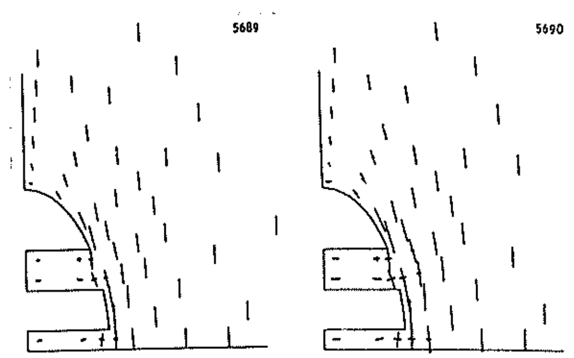

Fig. 8 Principal stress vectors in x-z plane of opening with pillars; $E_p:E_c = 2:1$; $P_x = P_y = 0$, $P_2 = 1$ (see Table 2). Note use of symmetry. a) spheroid, a:b:c = 1:1:2; b) ellipse, a:b:c = 1:∞:2

5. MONITORING OF ROCK BEHAVIOUR

5.1 General

The first pillar to be formed at the Warrego mine was 40 pillar (Figures 1 and 2). A programme of instrumentation was developed to study the behaviour of this pillar during the excavation of its southern face in 5m segments. This consisted of:

(i) Monitoring the stress changes in the pillar from a selected area in the drive at 3 Level using plastic borehole strain measuring cells.

(ii) Monitoring the deformations of the pillar and in the hangingwall and footwall abutments using wire extensometers.

(iii) Visual observation of the condition of the pillar from a drive through it.

In addition, an investigation was undertaken into using changes in the magnetic susceptibility of rock to monitor stresses in the pillars.

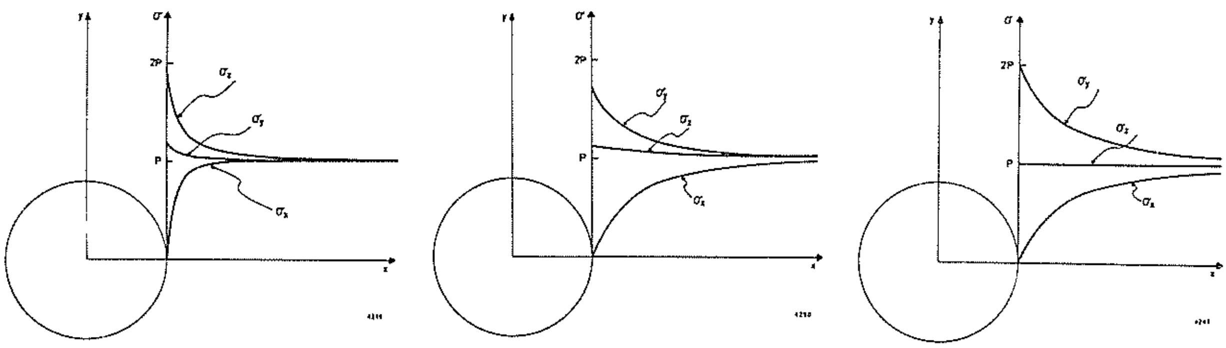

Fig. 9 Distribution of stresses with distance from 'stope' wall - a) spheroid with pillars, $E_p:E_c$ = 2:1, b) spheroid without pillars, c) cylindrical tunnel

5.2 Borehole Strain Measuring Cell

The cell is a miniaturized version of the LNEC solid inclusion cell (Rocha and Silverio, 1969) used for the determination of the absolute values of stresses by overcoring. It is basically a solid epoxy (Araldite B) cylinder in which there are embedded nine active electrical strain gauges at $45^{\circ}/90^{\circ}$ rosettes in three perpendicular planes and one dummy gauge. In the CSIRO version, the length of the strain gauged section is 5cm, and the total length of the cell is 20cm, compared with 20cm and 56cm, respectively in the LNEC cell.

Four cells were installed in four, 38mm diameter, 45° dipping boreholes located in the central area of the pillar. The cells were monitored approximately once per day for a week before and for a week after the pillar firing.

The average observed stress changes are given in Table 4.

TABLE 4

Virgin stresses in the Warrego orebody				Stress changes in 40 pillar due to removal of 5M segment			
	MPa	BRG	EL		MPa	BRG	EL
σ_1	21.6	232°	6°	$\Delta\sigma_1$	1.8	243°	9°
σ_2	12.9	142°	7°	$\Delta\sigma_2$	1.2	5°	73°
σ_3	9.2	4°	81°	$\Delta\sigma_3$	-0.4	150°	14°

The observed stress changes were of similar type but smaller in magnitude to those obtained from the theoretical analysis. The theoretical values were calculated taking into account the three-dimensionality of the orebody as previously discussed and also utilizing the results of a similar and independent analysis (Hocking, 1978) concerning stresses in pillars in an ellipsoidal opening. The observed and theoretical changes in pillar stress are given in Table 5.

TABLE 5

	$\Delta\sigma_{\text{east-west}}$ (MPa)	$\Delta\sigma_{\text{vertical}}$ (MPa)
observed	1.7	1.3
theoretical	2.8	1.1

The differences between observed and theoretical values could be caused by experimental factors, by variations in *in situ* stresses, by the proximity of pillar 40 to the northern end of the orebody, and by the assumptions and approximations inherent in the theoretical analysis.

Another possible cause is that the modulus of rock mass in the pillars was lower than was assumed in the computations. A reduction of the pillar modulus to less than half of that of the country rock could account for the differences in observed and theoretical values.

5.3 Extensometer Observations

Rock deformations in the east-west direction within 40 pillar and in the eastern and western abutments of the pillar were measured using Potts Mark II extensometers.

Stainless steel wires of 1.1mm diameter were spanned between target points located in an east-west drive through the pillar and in the western abutment of the pillar.

The largest movements were observed in the western abutment of the pillar across the footwall fault. During the firing an extension of approximately 3mm - 5mm occurred across the fault. The movements between pairs of reference points in the drive in the pillar itself were in most cases too small to be measured accurately.

The movements within 40 pillar and in the pillar abutments which could be expected theoretically as a result of firing of the 5m segment, were analysed using the boundary integral equation method (Ricardella, 1973). The rock was assumed to be a continuous, linearly elastic, isotropic material. The deformation modulus of the pillar was taken to be about one half of the modulus value of intact magnetite specimens.

The analysis confirmed that under the assumed conditions, mining of a 5m segment would cause only very small compressive deformations in the pillar and small tensile deformations in the western abutment of the pillar. There was much smaller compression on the northern side of the pillar than on the southern side. Visual observations in the drive containing the extensometers showed the formation of cracks in several places, particularly on the northern side. It appears that the condition of the pillar during and after firing of the 5m segment was considerably worse than indicated in the theoretical analysis.

5.4 Magnetic Susceptibility Measurements

Attempts to monitor changes in the magnetic susceptibility of 40 pillar during excavation, based on the results of laboratory experiments were inconclusive due to field instrumentation problems.

6. CONCLUSIONS

The investigation has produced benefits in two main areas: the development of more reliable and advanced methods of obtaining geomechnical data; and a better understanding of the behaviour of the stopes and pillars at Warrego, and of methods of modelling this behaviour.

The premining stress measurements showed the presence of high horizontal compressive stresses at Warrego conformant with the past folding in the area. The major rock stress at the upper levels of the Warrego mine acts approximately horizontally at 60° east of mine north and is approximately 2.0 to 2.5 times the overburden stress. From the mine design point of view this is unfavourable as it leads to higher stress in the pillars (directed east-west) and to a greater possibility of tensile stresses in the stope walls.

With respect to methods of stress measurement, the newly developed CSIRO hollow inclusion stress cell was found to be a practicable instrument for use under mining conditions.

Comparison of the two- and three-dimensional stress solutions showed that the two-dimensional models would give reasonable analyses of stresses, even near the ends of an orebody such as at the upper levels of the Warrego mine. The two-dimensional analyses would err on the "safe" side both in the compressive and tensile zones around the stopes and in the pillars.

Observations during mining of 40 pillar showed stress changes similar to those predicted but somewhat smaller. Both the observed and predicted deformations were small except for deformations across the footwall fault. The deterioration within the northern side of the pillar which has occurred at moderate stress levels suggests that the pillar has passed its peak strength, which may be attributed partly to the slenderness of the pillar.

The solid inclusion triaxial cell of LNEC type used to monitor stress changes during the mining of 40 pillar, gave reasonable results but showed drift with time and needs to be improved to permit the monitoring of stress changes which occur over a period of time as for example, in cut-and-fill mining operations.

The monitoring of the magnetic susceptibility of the Warrego pillars to observe the changes in the rock stresses has been confirmed in the laboratory as theoretically possible, but would require extensive further development work under *in situ* conditions. The use of wire extensometers for monitoring of rock deformations gave useful results, but rod extensometers would have been superior, particularly for monitoring pillars where even small deformations can be significant.

7 ACKNOWLEDGEMENTS

The authors wish to thank Peko Mines Ltd., in particular Dr. E. Miller, and their colleagues at CSIRO, especially Messrs. J.R. Enever and D.R. Miller for their valuable contributions to the study.

8 REFERENCES

GOULEVITCH, J., 1975. Warrego Copper-Gold Orebody. Economic Geology of Australia and New Zealand. AIMM Monograph 5:Metals.

HOCKING, G., 1978. Stress Analyses of the 1100 Orebody at Mt. Isa. Proc. 19th U.S. Symp. on Rock Mechanics Stateline Nevada, May, 1978 Uni. of Nevada.

PANEK, L.A., 1966. Calculation of the Average Ground Stress Components from Measurements of Diametral Deformation of a Drill Hole. Testing Techniques for Rock Mechanics, A.S.T.M. STP No.402, 1966, pp.106-132.

RICCARDELLA, P.C., 1973. An Implementation of the Boundary - Integral Technique for Planar Problems of Elasticity and Elasto-Plasticity. Carnegie - Mellon University, Ph.D., Engineering Mechanics.

ROCHA, M. and SILVERIO, A., 1969. A New Method for the Complete Determination of the State of Stress in Rock Masses. Geotechnique 19, No.1, pp.116-132.

WOLD, M.B. and WOROTNICKI, G., 1979. Stress Analysis of the 27 Pillar Region of the Warrego Mine CSIRO Div. Appl. Geomech. Technical Report No.88.

WOROTNICKI, G. and WALTON, R.J., 1976. "Triaxial "Hollow Inclusion" Gauges for Determination of Rock Stresses In Situ. Proc. ISRM Symposium on Investigations of Stresses in Rock - Advances in Stress Measurement, Institution of Engineers, Aust. National Conference Publication No.76/4.

WOROTNICKI, G. and WALTON, R.J., 1979. Virgin Rock Stress Measurements at the Warrego Mine. CSIRO Div. Appl. Geomech., Technical Report No.93.

WOROTNICKI, G., WALTON, R.J. and ENEVER, J.R., 1977. Stress and Deformation Monitoring of 40 Pillar at the Warrego Mine. CSIRO Div. Appl. Geomech., Geomechanics of Filled High Rise Stopes Project Report No.5.

WOROTNICKI, G. and WOLD, M.B., 1977. Stress Analysis of the 38 Stope Region at the Warrego Mine. CSIRO Div. Appl. Geomech. Geomechanics of Filled High Rise Stopes, Project Report No.4.

WOROTNICKI, G., WOLD, M.B. and MILLER, D.R., 1976. Strength and Deformation Properties of Small Rock Cores from the Warrego Mine. CSIRO Div. Appl. Geomech. Geomechanics of Filled High Rise Stopes Project Report No.2.

The Performance of Disc Cutters in Simulated Jointed Rock

D. F. HOWARTH
Research Associate, School of Mining Engineering, The University of New South Wales

SUMMARY A series of controlled laboratory experiments has been undertaken to assess the performance of disc cutters in simulated jointed rock. The disc cutters used (similar to those found on full face tunnelling machines) were mounted on a linear rock cutting rig capable of cutting at speeds up to 300 mm/s and sustaining thrust forces of up to 100 kN. The simulated jointed rock test samples consisted of rectangular blocks of sandstone clamped together. The parameters measured to assess disc performance were thrust, rolling and lateral forces on the cutting tool together with a quantitative assessment of the size and mass of debris produced. Several types of experiment were undertaken in order to ascertain both fundamental and practical aspects of cutting in jointed rock. These experiments involved varying joint width, joint spacing, overburden pressure, tool spacing and the angle of attack of the cutting tool relative to the joint planes. The results show the effects of jointed rock masses on cutting tool forces, energy involved in cutting and the size of debris produced. In addition a mechanism is proposed to explain the low strength characteristics of jointed rock.

NOTATION

D	disc diameter	mm
C	confining load	t
C.I.	coarseness index	-
F_L	mean lateral force	kN
F_R	mean rolling force	kN
F_T	mean thrust force	kN
P	penetration	mm
Q	yield	m^3/km
S.E.	specific energy	MJ/m^3
T	joint width/thickness	mm
V	velocity	mm/s
X	block width or spacing between joints	mm
σ_c	uniaxial compressive strength	MPa
θ	breakout angle	degrees
ϕ	disc edge angle	degrees
ψ	angle of attack (angle of joint plane relative to line of action of disc cutter)	degrees

1 INTRODUCTION

The performance of disc cutters of varying geometries in continuous rock has been well established (Roxborough and Phillips, 1975a) and (Ozdemir, Miller and Wang, 1977). However, little or no work has been undertaken to assess the performance of disc cutters in jointed rock. (It should be stated here that for the purposes of this paper jointed rock is defined as a series of regular blocks of rock, artificially separated to give open joints or fissures of known regular dimensions.)

It is generally accepted that under most circumstances jointed rock is weaker than a comparable block of solid rock. However, no quantitative assessment of the forces and energy required to excavate jointed rock has been made. This information may have a practical application when designing disc arrays for a tunnelling machine head when cutting in areas with preferred joint directions.

Mathematical models that have been proposed to predict the disc forces required to penetrate continuous rock are not applicable for a comparable situation in jointed rock. The mechanism of failure of jointed rock under the action of a disc cutter is complex and difficult to quantify.

2 ROCK CUTTING RIG AND INSTRUMENTATION

2.1 Cutting Rig

The cutting rig used in these experiments was an extensively modified planing machine shown in Figure 1. This machine is capable of accepting large blocks of rock, has variable cutting speed and is robust enough to sustain static and dynamic thrust forces (vertical) up to 100 kN.

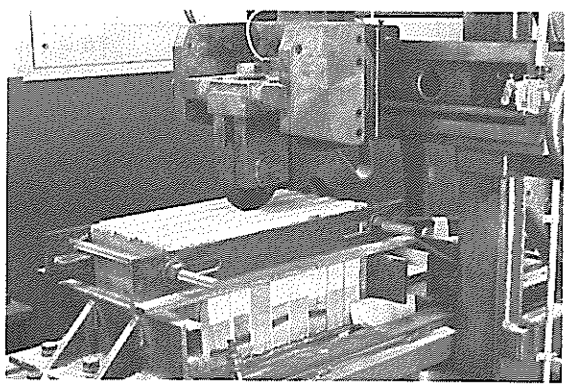

Figure 1 Rock cutting rig

In this system the cutting tool remains stationary while the rock sample is passed beneath it. The table is driven by a 7.5 kW induction motor which in turn is controlled by an AC variable frequency inverter which allows the speed of the table to be continuously varied from 50-300 $mm.s^{-1}$. Rock samples of approximately 450mm x 450mm x 350mm are mounted on the table and clamped firmly prior to cutting. The individual blocks of rock comprising the jointed rock mass were cut from large samples using a diamond saw, blocks were separated using a low strength material such as paper, care being taken when assembling the units to ensure that the media used for separating the blocks was below the penetration level of the cutting tool. This ensured that the disc cut through open joints. A confining load was provided in a line parallel to the direction of motion of the table by a hydraulic power pack capable of providing loads up to 10t. A tensioned framework, also shown in Figure 1, was provided to give a degree of lateral constraint. The rig also has the facility to dress rock samples prior to cutting.

2.2 Mode of Operation and Instrumentation

The experimental procedure involved setting the experimental variables such as confining load and penetration then passing the block beneath the cutting tool. Thrust, rolling and lateral forces were continually monitored during the experiment. At the end of each cut, the length of cut was recorded, debris collected and a screen analysis undertaken.

Instrumentation included a triaxial dynamometer, shown in Figure 1, (O'Dogherty and Whittaker, 1965) capable of resolving the force acting on the disc into three othogonal components. Signals are sent from the dynamometer via dynamic strain amplifiers to a microprocessor based data acquisition and mini computer facility described in detail by Howarth (1978). Data is stored in digital form on flexible magnetic discs for future analysis.

3 TEST MATERIAL

The experimental programme was conducted in Gosford Summersby Sandstone and has the measured properties detailed in Table 1.

TABLE 1

PROPERTIES OF GOSFORD SUMMERSBY SANDSTONE

Grain size mm	0.7
Quartz content %	34
Unconfined compressive strength MPa	42.3±2.56(A)*
Unconfined tensile strength MPa	2.84±0.36(B)*
Unconfined shear strength MPa	14.5±1.62(C)*
Static Young's Modulus GPa	9.62±2.47(D)*
Schmidt rebound number	47.4±6.43(E)*
Dry mass density kg/m^3	2200±61

*Mean value of property in two directions, one at right angles to the other

A.20 samples, cylinders 54.2mm dia.x 108.3mm long
B.10 samples, discs 40.6mm dia.x 19.8mm long
C.10 samples, cylinders 40.7mm dia.x 78.5mm long
D.Tangent modulus, 10 samples dimensions as A.
E.125 values

4 EXPERIMENTAL PROGRAMME & DESIGN OF EXPERIMENTS

4.1 Experimental Programme

Six major experiments were undertaken to establish the effect of jointed rock masses on the performance of disc cutters, each variable having five levels in arithmetic progression and each individual test within an experiment repeated four times to obtain mean values (Roxborough and Phillips, 1975b). A series of preliminary experiments was undertaken to assess the levels of variables to be used in the main experimental programme. It was found that as disc diameter increased the damage to the jointed blocks also increased. Therefore in an effort to minimise damage and preserve the integrity of the jointed blocks the smallest diameter disc, namely 100mm, was chosen for the entire series of experiments. The experiments are detailed in Table II.

TABLE II

EXPERIMENTAL PROGRAMME

Exp* No.	Parameters under Investigation	Constants	Variables	Level of Variables	Type of Exp.
1	F_T, F_R, Q, SE (1.For validation of rock cutting system 2.For comparison with jointed rock experiments.)	D = 100mm V = 50mm/s	P ϕ	2, 4, 6, 8, 10mm 30, 45, 60, 75, 90°	a
2	F_T, F_R, Q, SE	D = 100mm X = 60mm V = 50mm/s ψ = 90°	P ϕ C T	2, 4, 6, 8, 10mm 30, 45, 60, 75, 90° 2, 4, 6, 8, 10 t 0,0.75,1.5,2.25,3.0mm	b
3	F_T, F_R, Q, SE	D = 100mm C = 6 t V = 50mm/s ψ = 90° P = 6mm ϕ = 60°	X T	20, 40, 60, 80, 100mm 0,0.75,1.5,2.25,3.0mm	a
4	F_T, F_R, Q, SE	D = 100mm C = 6 t V = 50mm/s X = 60mm P = 6mm	ψ ϕ	30, 45, 60, 75, 90° 30, 45, 60, 75, 90°	a
5	Q, SE, CI	X = 60mm C = 6 t V = 50mm/s ψ = 90° T = 1.50mm P = 6mm D = 100mm ϕ = 60°	S/P	2,4,6,8,10,15,20	c
6	Q, SE, CI (For comparison with Exp. 5)	ϕ = 60° P = 6mm D = 100 mm V = 50mm/s	S/P	2,4,6,8,10,15,20	c

* Experiment 1 and 6 in solid rock
Experiments 2 to 5 in jointed rock

a - two variable, full factorial
b - partial factorial
c - one variable, full factorial

4.2 Design of Experiments

Experiment 2 was a partial factorial experiment based on a method proposed by Protodyakanov and Teder (1970) whereby experiments are chosen systematically from an experimental matrix based on orthogonal Latin squares. Essentially the method allows a comparison of a parameter with a variable at mean values of the other variables in the experiment. The remaining experiments are either single or two variable experiments as indicated in Table II.

4.3 Disc Cutting Parameters

The parameters of disc performance are defined as follows :-

1) Thrust force F_T - the average force required to be applied vertically to effect a prescribed penetration.

2) Rolling force F_R - the average force required to be applied in the direction of motion of the cutting tool to effect a prescribed penetration.

3) Yield Q - the volume of rock excavated per unit distance cut.

4) Specific energy SE - the work done per unit volume of rock excavated.

5) Coarseness index CI - a measure of the debris size from an excavated cut. This is a dimensionless number, being the sum of the cumulative mass percentages recorded in the screen analyses (Barker, 1964).

The mean lateral force F_L was monitored for all experiments and was found to be sensibly zero, and hence no further reference is made to this parameter.

5 VALIDITY OF ROCK CUTTING SYSTEM

5.1 Experimental Results

It was deemed necessary to carry out rock cutting experiments similar to those undertaken elsewhere (Roxborough and Phillips, 1975a) in order to establish the validity of the rock cutting system. The results of this experiment (Experiment 1, Table II) are shown in Figure 2.

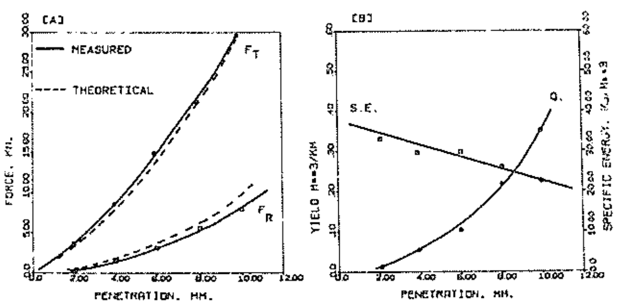

Figure 2 Comparison of measured and theoretical values in unjointed rock (Exp. 1)

$\phi = 60^\circ$

The results show the same trends as reported elsewhere. Furthermore, Figure 2A shows that the measured and theoretical values of F_T and F_R are in close agreement. The theoretical values are calculated from the equations proposed by Roxborough and Phillips (1975a).

$$F_T = 4\,\sigma_c \tan\frac{\phi}{2} \sqrt{DP^3 - P^4} \qquad (1)$$

$$F_R = 4\,\sigma_c\, P^2 \tan\frac{\phi}{2} \qquad (2)$$

Figure 2B shows the yield to increase as the square of the penetration and is described by the equation

$$Q = P^2 \tan\theta \text{ (per unit distance cut)} \qquad (3)$$

where θ is the breakout angle of the rock and is equal to 72°. Again this is in accordance with work undertaken elsewhere.

6 EXPERIMENTAL RESULTS IN JOINTED ROCK

6.1 Effect of Penetration

The effect of penetration on F_T and F_R is shown in Figure 3A.

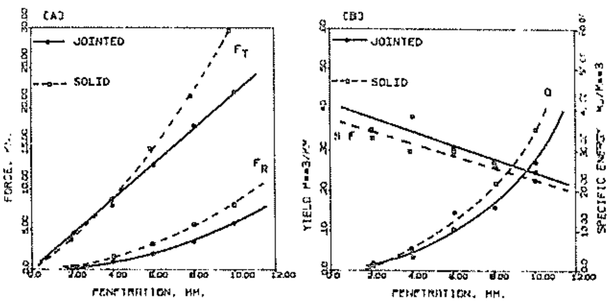

Figure 3 Effect of penetration (Exp. 2)

$\phi = 60^\circ$, T = 1.5mm, C = 6t

Both F_T and F_R increase with increasing penetration and follow similar trends as shown by an identical disc in solid rock. There is close agreement in solid and jointed rock forces at low penetration however, as penetration increases so does the discrepancy between the forces. At a penetration of 10mm the difference between F_T (solid) and F_T (jointed) is approximately 25 percent.

Figure 3B, shows the curves for solid and jointed rock for both yield and specific energy to be in close agreement in both trend and magnitude. These results appear to be anomalous; it was reasonable to expect that the yield would be higher in the case of jointed rock as a result of end chips being formed at the air/rock interfaces. The specific energy appears to be anomalously high, this is a direct consequence of the lower yield. These apparently anomalous results are being investigated further.

6.2 Effect of Edge Angle

Thrust and rolling forces increase with increasing edge angle as shown in Figure 4A.

The trends for jointed and solid rock are similar. At small edge angles the discrepancy between jointed and solid rock forces is negligible, however, as edge angle increases the discrepancy increases and in the case of F_T, at $\phi = 90^\circ$, this discrepancy is approximately 36%. These results together with the similar result reported in 6.1 suggests that jointed rocks should be excavated with high edge angle discs at high penetrations to obtain maximum cutting efficiency.

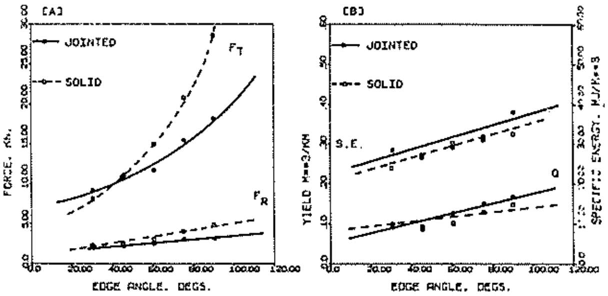

Figure 4 Effect of edge angle (Exp. 2)

P = 6mm, T = 1.50mm, C = 6t

Figure 4B, shows both yield and specific energy increasing with increasing edge angle. The results do not indicate any significant difference between the magnitudes of yield and specific energy when compared to an identical situation in solid rock.

6.3 Effect of Confining Load

The confining load was applied in a direction normal to that of the joint planes. The effect of confining load on F_T and F_R is shown in Figure 5A.

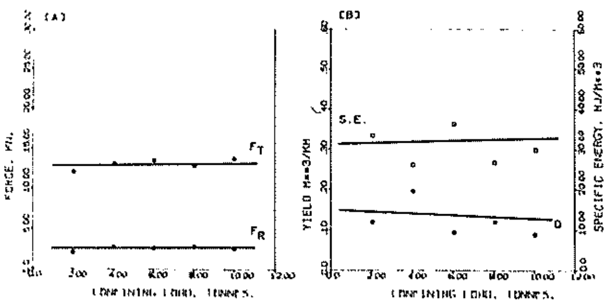

Figure 5 Effect of confining load (Exp. 2)

P = 6mm, T = 1.50mm, $\phi = 60^o$

Thrust and rolling force are marginally affected by confining load.

Figure 5B, shows a reduction in yield and corresponding increase in specific energy with increasing confining load. However, as the data is scattered it is suggested that in actual fact yield and specific energy are only marginally affected by confining load. The maximum load (10 tonnes) that could be applied to the jointed mass represents a confining stress of less than 5% of the ultimate compressive strength, however it was not technically possible to increase the load further. It is possible that loads in excess of 10 tonnes may have an effect on the parameters shown in 5A and 5B.

6.4 Effect of Joint Width

Joint width is the distance between two adjacent blocks of rock and was created by inserting low strength media between the blocks. The effect of joint width on F_T and F_R is shown in Figure 6A. Rolling force is unaffected by joint width however, thrust force decreases with increasing joint width. This is partially due to the increasing reduction in disc area in contact with the rock as joint width increases. A further mechanism to explain this reduction in force is discussed in detail in section 7.

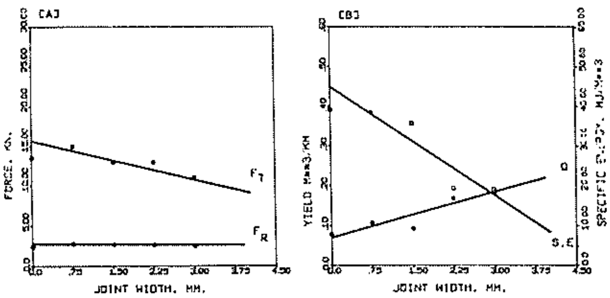

Figure 6 Effect of joint width (Exp. 2)

P = 6mm, $\phi = 60^o$, c = 6t

Figure 6B, shows the yield increasing the increasing joint width. This is a result of larger end chips being formed as the joint width increases. The specific energy shows a significant decrease with increasing joint width. Thus cutting efficiency increases with increasing joint width.

6.5 Effect of Block Width

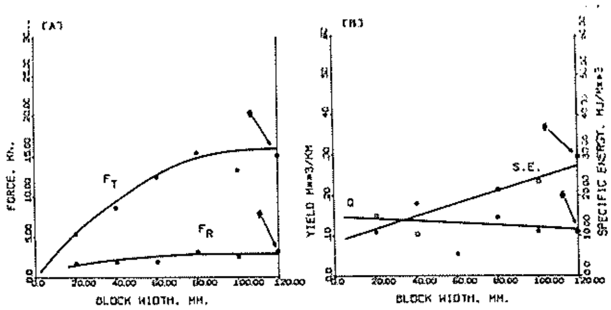

Figure 7 Effect of block width (Exp. 3)

T = 1.50 mm # These points extracted from Exp. 1, i.e. Block width → ∞ (solid rock)

Figure 7A, shows F_T and F_R increasing with increasing block width to a point where both force curves become parallel with the X axis. This occurs at a block width of 100-120mm, at which point the jointed rock can be regarded as a continuous mass. Furthermore, the values of F_T and F_R at this point are in close agreement with those obtained in solid rock.

Yield decreases with increasing block width as shown in Figure 7B. This is due to the smaller weaker blocks producing larger end chips. Specific energy increases with increasing block width, implying that excavation is more efficient in ground comprising of small blocks. Both curves tend towards values obtained in solid rock, however, due to the scatter of the data, the point at which the jointed rock approximates the behaviour of a solid rock cannot be defined.

6.6 Effect of Block to Joint Width Ratio

Further analysis of the data obtained in Experiment 3 yields the graphs shown in Figure 8. The points on the graph represent the ratio, block width divided by joint width plotted against the relevant parameter for all tests conducted.

These results confirm those reported in Section 6.5. The limiting value of X/T (where the parameter becomes parallel with the X axis) is approximately 80. At this point the value of the parameter approximates the value obtained in solid rock.

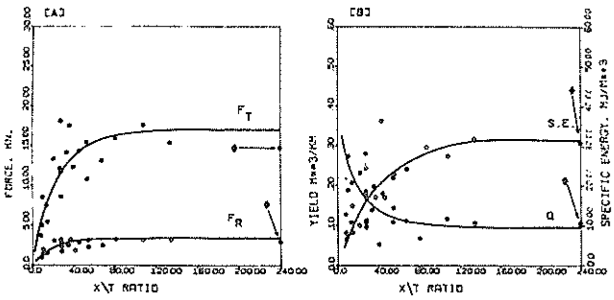

Figure 8 Effect of block width to joint width ratio (Exp. 3)

\# These points extracted from Exp. 1, i.e. Block width → ∞ (solid rock)

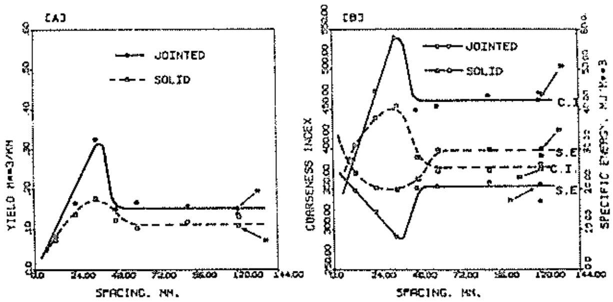

Figure 10 Effect of tool spacing (Exp. 5 and 6)

$P = 6$ mm, $\phi = 60^{o}$

* data points taken from unrelieved cutting experiments 1 and 2

6.7 Effect of Angle of Attack

Angle of attack is defined as the angle of the joint plane relative to the line of action of the disc cutter. An angle of attack of 90^{o} is defined as the disc is cutting normal to the direction of the joint planes. The effect of angle of attack is shown in Figure 9.

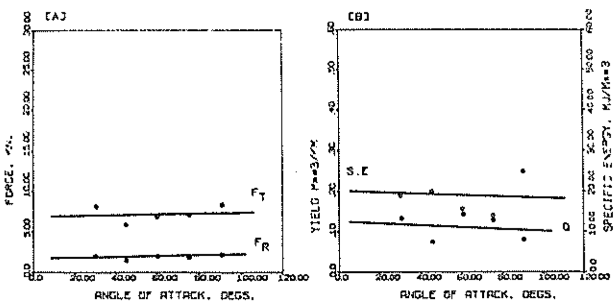

Figure 9 Effect of angle of attack (Exp. 4)

$\phi = 45^{o}$

The effect of angle of attack on thrust and rolling force, yield and specific energy is negligible. For practical purposes it may be stated that the parameters are only marginally affected by angle of attack.

6.8 Effect of Tool Spacing

Disc cutters do not generally operate in isolation, normally they are disposed in an array on the cutting head of the tunnelling machine. It is, therefore, useful to know at what distance to space cutting tools in the array. In this experiment discs were spaced at set distances from previously excavated grooves.

The most useful parameters available when assessing the effect of spacing, are those which involve the mass of rock created by cutting. These are namely yield, specific energy and coarseness index. The effect of spacing on these parameters for both solid and jointed rock are shown in Figure 10. The trends of these curves are in close agreement with other published experimental data (Roxborough and Phillips, 1975a).

Figure 10A, shows jointed rock yield to rise rapidly as tool spacing increases. The yield reaches a maximum at a spacing of approximately 40mm, this corresponds to a S/P (spacing to penetration) ratio of 6.6, a sharp decrease follows and the curve levels off at a S/P ratio of approximately 9.0. At this point the cutter is operating in isolation, or in the unrelieved situation.

Figure 10B, shows coarseness index to have a maximum value (coarse debris-large chips) at a S/P ratio of 6.4 and levelling out at a S/P ratio of 9.0. The specific energy curve indicates that the cutter reaches peak efficiency at an S/P ratio of 6.4 and levels out at an S/P ratio of 9.0.

Maximum disc interaction is indicated at a S/P ratio of approximately 6.5. This was observed during the experimental work, when the disc spacing was set close to a value corresponding to an S/P ratio of 6.5 relatively large slabs of rock were observed to break out between adjacent disc grooves. Interaction between discs was observed to stop at a S/P ratio of 9-10, at this ratio and higher ratios the cutters operate in isolation.

The differences between the optimum and 'cut-off' S/P ratios for solid and jointed rock are marginal as shown in Table III.

TABLE III

OPTIMUM AND 'CUT-OFF' S/P RATIOS IN SOLID AND JOINTED ROCK

Rock Type	S/P Ratio	
	Optimum	'Cut-off'
Jointed Rock (Exp. 5)	6.5	9.0
Solid Rock (Exp. 6)	5.9	11.0

$P = 6$mm, $\phi = 60^{o}$

It is apparent that in relieved cutting in jointed rock shear failure between adjacent grooves is the predominant mechanism of failure and the formation of end chips has very little effect.

7 A POSSIBLE MECHANISM TO EXPLAIN THE LOW STRENGTH CHARACTERISTICS OF JOINTED ROCK

Figure 3A shows that at a penetration of 10mm the difference in F_T (solid) and F_T (jointed) is approximately 25%. Equation (1) can be used to calculate the thrust force required to penetrate solid rock, the reduction in thrust force due to the decrease in projected disc surface area contact can be found by using the equation

$$F_T = \sigma_c\ ([4\tan\frac{\phi}{2}\ \sqrt{DP^3-P^4}]-[2PT\tan\frac{\phi}{2}]) \qquad (4)$$

The function 2PT $\tan\frac{\phi}{2}$ is the projected area of disc contact over one open joint. For the purposes of the following calculation the disc is assumed to cut one open joint and to have its centre lie over the centre of the joint.

If values of ϕ, D and T are extracted the experimental conditions (P = 10mm) shown in Figure 3A and substituted in equation (4) the reduction in thrust force as a result of the reduction in projected disc surface area in contact with the rock can be shown to be 2.5%.

It is evident that the reduction in thrust force required to excavate the rock is not wholly attributable to the reduction in projected area of disc contact area with the rock. Equations (1) and (4) assume that the rock is broken under the action of compressive forces, it is suggested that some other mode or modes of failure operate when discs cut jointed rock. Furthermore, it is suggested that when a disc penetrates a jointed block the block expands or dilates at right angles to the direction of application of the applied stress (the Poisson effect). Consequently interparticle tensile stresses are set up and therefore the rock under the disc may fail partly in tension. Taking this concept one step further is is possible to explain the decreasing strength of rock with decreasing block width as shown in Figure 7A. When a disc penetrates a block the block is deformed and strained. It is suggested that if the deformation remains constant, as block width increases the degree of strain decreases, therefore decreasing the tendency of the rock to fail in tension and hence increasing the force required to excavate the rock. Investigations are presently being undertaken to investigate this mechanism further.

8 CONCLUSIONS

The following conclusions relate to the experimental conditions discussed in this paper.

1. The rock cutting system described produces data from cutting continuous rock that is in close agreement with other published experimental data.

2. To achieve maximum effectiveness when cutting in jointed rock disc cutters should have large edge angles and cut at high penetrations.

3. Cutting efficiency increases with increasing joint width.

4. Cutting efficiency decreases with increasing block width.

5. When the block width to joint width ratio exceeds 80 the jointed rock behaves as a continuous mass.

6. Angle of attack and confining load have little or no measurable effect on the performance of disc cutters in jointed rock.

7. The optimum and 'cut-off' S/P ratios are in close agreement to those of solid rock.

9 ACKNOWLEDGEMENTS

The equipment used in this work was provided by a grant from the Australian Research Grants Committee.

The author wishes to thank Dr. H.R. Phillips, Lecturer in the School of Mining Engineering, The University of New South Wales, for his assistance in the preparation of this paper.

10 REFERENCES

BARKER, J.S. (1964). A laboratory investigation of rock cutting using large picks. Int. J. Rock Mech. Mining Sci. Vol. 1, pp519-534.

HOWARTH, D.F. (1978). Tunnelling machine research at The University of New South Wales. Symp. Rock Breaking Equipment and Techniques, Melbourne, pp43-49.

O'DOGHERTY, M.J. and WHITTAKER, D. (1965). An examination of the characteristics of a solid plate dynamometer designed for triaxial force measurements. N.C.B./M.R.E. Technical Memorandum, U.K., No. 197.

OZDEMIR, L., MILLER, R. and WANG, F.D. (1977). Mechanical tunnel boring, prediction and machine design. Annual Report, Colorado School of Mines.

PROTODYAKANOV, M.M. and TEDER, R.I. (1970). Rational methods of planning experiments. Dynamic Rock Mechanics (Ed. G.B. Clark) Twelfth Symp. on Rock Mech.: Univ. Missouri, Rolla, pp129-149.

ROXBOROUGH, F.F. and PHILLIPS, H.R. (1975a). Rock excavation by disc cutter. Int. J. Rock Mech. Min. Sci. and Geomech. Abstr. Vol. 12, pp361-366.

ROXBOROUGH, F.F. and PHILLIPS, H.R. (1975b). The mechanical properties and cutting characteristics of the Bunter Sandstone. Report to T.R.R.L., Univ. of Newcastle upon Tyne, U.K., 292 pp.

Geometric Design of Underground Openings for High Horizontal Stress Fields

P. J. N. PELLS
Department of Civil Engineering, University of Sydney

SUMMARY Tunnels and hydro-power stations are frequently excavated in layered rock within 500 metres of the surface where the horizontal virgin stress can be expected to be greater than the vertical. The selection of the most suitable shape for such excavations is an important part of the design process and is usually based on stress analyses using elastic theory. This paper uses cross-anisotropic elastic theory to investigate the problem of the stress in the crown areas of common tunnel shapes in layered rocks with high horizontal stress fields. The paper also shows how consideration of the three dimensional aspect of hydro-power stations leads to an unusual chamber shape when high horizontal virgin stresses exist.

1. INTRODUCTION

A major aspect to the design of an underground structure is the selection of the shape of the opening. Within the constraints of the function of the opening the shape must be optimised in terms of the rock mass properties and the virgin stress field. The many measurements of these stresses made throughout the world have shown, (Herget 1974, Orr 1974, Blackwood 1978, Brown and Hoek 1978) that for depths of less than 1000m the major and intermediate principal stresses are likely to act horizontally or sub-horizontally. Such relatively high horizontal stresses have an important bearing on opening shape selection. In particular when combined with sub-horizontally bedded material, these virgin stresses can lead to unexpectedly high compressive stress concentrations. For homogenous, isotropic rock, optimum tunnel shapes are known for certain virgin stress fields provided body forces are excluded. These are :

(i) circular tunnel for a hydrostatic stress field,

(ii) elliptical tunnel with axis ratio equal to K (σ_h/σ_v) for a biaxial stress field,

(iii) deloid (Richards and Bjorkman, 1978) for a biaxial stress field with the horizontal component increasing linearly with depth.

For anisotropic rock, optimum tunnel shapes are not known even for a hydrostatic stress field. However, this paper does not attempt to solve this general problem but is rather directed to the practical problem of the stresses in the crown areas of common tunnel shapes in layered rock with K>1.0. The paper also presents an important practical consequence of considering the three dimensional aspect of excavations for hydro-power stations.

2 PATTERN OF HORIZONTAL STRESS

The measurement of virgin rock stress is difficult and thus while very many measurements have been conducted throughout the world, the accuracy of many results is suspect. However, it is quite clear that the general relationship between average horizontal stress and overburden pressure is as shown in Figure 1. It appears that this pattern of stress reflects primarily the effect of surface

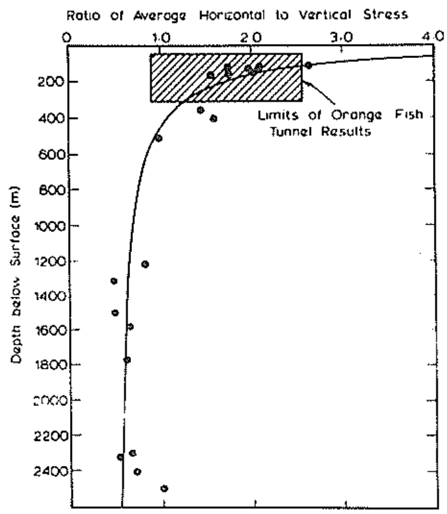

Figure 1 Variation of horizontal to vertical stress ratio with depth in Southern Africa (Van Heerden, 1976)

denudation (unloading) of virtually all continental crust. The process whereby such load removal (overconsolidation) generates values of K ($\sigma_{h\ ave}/\sigma_v$) greater than 1.0 is well established in soil mechanics theory. The linking of this theory to virgin rock stress in sedimentary rocks is given by Voight (1967). In the case of igneous and probably certain metamorphic rocks Goodman (1970) has shown how denudation will lead to very high horizontal stresses.

Imprinted over this high horizontal near surface stress pattern are the stresses associated with tectonic forces and also topographical variations. In certain areas e.g. Broken Hill, Australia the pattern of major and secondary horizontal stress can be closely linked with the tectonic features. However, there also appear to exist overall continental patterns; although to what extent these very near surface stresses can be linked to continental movements is at present uncertain. While it would be valuable in a predictive sense to understand what has led to the observed patterns of horizontal stress, it is more important to realise that most civil engineering underground openings must be designed for K values greater than 1.0.

3 CONSEQUENCES OF HIGH HORIZONTAL STRESSES ON TUNNEL DESIGN

In essence high horizontal virgin stresses lead to high compressive stresses in the roof (crown) of an underground excavation and usually tensile stresses in the sidewalls. Sometimes the compressive stress levels are not high enough to cause compressional failure in the form of slabbing or shear. In such cases the opening shape is selected on the basis of rock mass discontinuities so that critical wedges can be properly supported (Cording and Mahar, 1978). However, particularly in horizontally bedded sedimentary strata, compressional failure may well be a potential problem in the roof and also large zones of tension in the sidewalls may cause difficulties. The question is whether the selection of a suitable shape for the tunnel or power station chamber may minimise these problems. Certainly significant failures have occurred in conventionally shaped tunnels due to high horizontal stresses. For example certain sections of the 80 km long Orange-Fish tunnel (constructed in mudstone) showed major longitudinal compressional cracks in the roof shotcrete associated with shearing along bedding planes. This shearing reached such a magnitude that rock bolt holes closed up sufficiently rapidly to make redrilling necessary. A programme of rock stress measurement was instigated as a result of these problems and showed values of K ranging from 1.0 to 2.6 (Van Heerden, 1972). Similar problems were encountered in two tunnels in shale in Toronto where again high horizontal stresses were measured (Lo and Morton, 1976).

At least one case is recorded in the literature where an underground opening in sedimentary rock was designed specifically to reduce the effects of high horizontal virgin stresses on roof instability. This was the Poatina power station in Tasmania (Endersbee and Hofto 1963) which was successfully constructed with the shape shown in Figure 2. Some of the ideas adopted at Poatina were successfully incorporated in the shape design for the Drakensberg pumped-storage station (Bieniawski, Orr and Pells, 1974). The remainder of this paper shows how these ideas are of general validity and suggest tunnel and power station shapes somewhat different from the basic circle or horseshoe shape usually adopted.

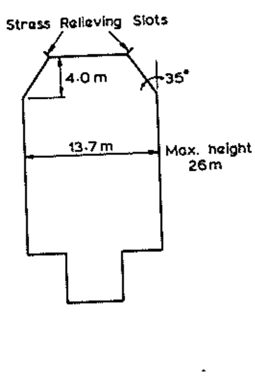

Figure 2 Poatina power station final design cross section

4 TUNNEL SHAPES IN HORIZONTALLY BEDDED OR LAMINATED ROCK

Because of their length, tunnels can be analysed in two dimensions and usually tunnel shapes are evaluated on the basis of solutions for isotropic elasticity. While the finite element method has been developed to the stage that virtually any discontinuous, non-linear rock mass can be modelled (Pells, 1974) it remains true that most opening shape selection is based on isotropic elasticity. This is usually satisfactory as comparisons of elastic solutions for different shapes enable one to select the optimum shape on the basis of :

(i) the minimum volume of rock subject to high compressive stresses,

(ii) the magnitude of the maximum compressive stress on the opening surface,

(iii) the location and magnitude of tensile stress zones,

(iv) the length of planar surfaces parallel to the direction of maximum compressive stress (Cording and Mahar, 1978).

In the case of openings in horizontally bedded rock subject to high horizontal stress fields, isotropic elasticity is unsatisfactory in indicating the magnitude and size of zones of compressive stress in the crown area. Where the rock layers are massive but separated by clearly defined bedding discontinuities, it is possible to use joint elements in numerical analysis of particular openings. However, for shales and closely bedded siltstones, mudstones and sandstones this approach is not feasible. It is suggested that these latter materials can be modelled using cross-anisotropic elasticity (Salomon, 1968). This involves five independent elastic parameters, namely :

E_v = Young's modulus in the vertical direction

E_h = Young's modulus in the horizontal direction (parallel to bedding)

ν_{vh} = Poisson's ratio for effect of vertical stress on horizontal strain

ν_{hh} = Poisson's ratio for effect of horizontal stress on horizontal strain

G = Independent shear modulus in a vertical plane.

It is postulated that the behaviour of closely layered rock around a tunnel can be modelled by assuming $E_h=E_v$, $\nu_{hh}=\nu_{vh}$ but with G being low so that $E_h/G >> 2(1+\nu)$. This model is analogous to a stack of playing cards with the cards being held together with extremely thin layers with very low shear stiffness. In reality, for bedded sedimentary rocks E_h is usually 1.5 to 3 times E_v (Gerrard, Davis and Wardle, 1972) but if all other parameters remain the same then such small differences between E_h and E_v have little effect on the overall stress pattern around a tunnel, although the maximum stress concentration at the periphery is increased.

Lo and Morton (1976) have analysed the stress concentrations around the periphery of a circular tunnel in cross-antisotropic rock and show (see Figure 3) how the stress concentration in the crown increases rapidly with increasing values of E_h/G. A similar increase in stress concentration was obtained by Goodman (unpublished) by considering a single horizontal bedding discontinuity at different distances above the crown of a circular tunnel. Both

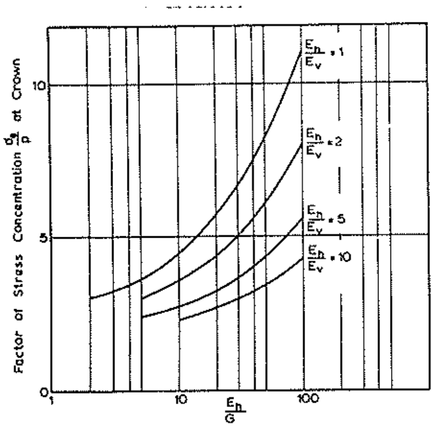

Figure 3 The effect of the ratio E_h/G on the stress concentration factor

these approaches show quite clearly that compressional failure may occur in the crown area of openings with circular roofs in bedded rock when conventional isotropic stress concentration factors would indicate stability.

In the light of the experience at Poatina it was decided to investigate the stresses around flat topped tunnels with bevelled corners using the anisotropic rock mass model described above. The analyses were conducted using 8 node isoparametric finite elements and it was assumed that the tunnels were sufficiently deep that the unit weight of the rock could be ignored. Two, square, flat-topped tunnels were considered with bevelled corners of 0.1 and 0.2 times the tunnel height respectively. For comparison purposes the circular tunnel was also analysed.

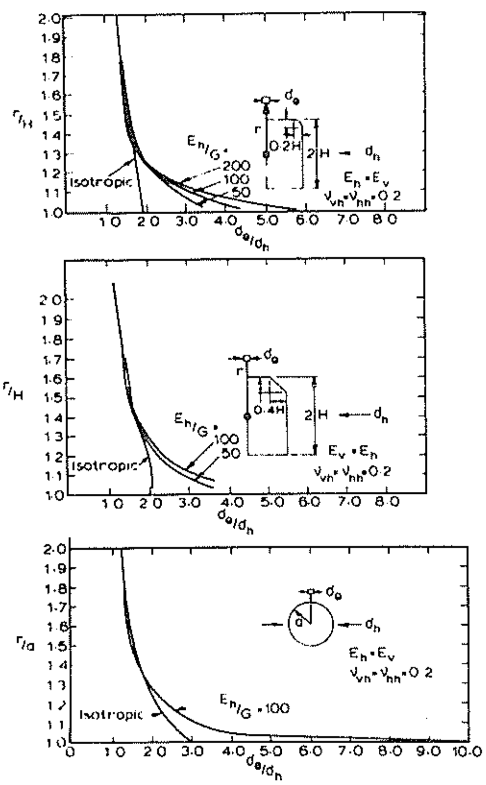

Figure 4 Stress concentration in tunnel crowns

Figure 4 shows the horizontal stress concentration for a purely horizontal virgin stress along the vertical axis at the centre of the roof, for each of the three tunnel shapes, for different values of E_h/G. Also shown are the values for isotropic rock. For this purely horizontal stress field and for E_h/G = 100 the contours of horizontal stress for the three shapes are given in Figure 5. Finally for a purely vertical virgin stress field the horizontal stresses above the crown centreline are shown in Figure 6.

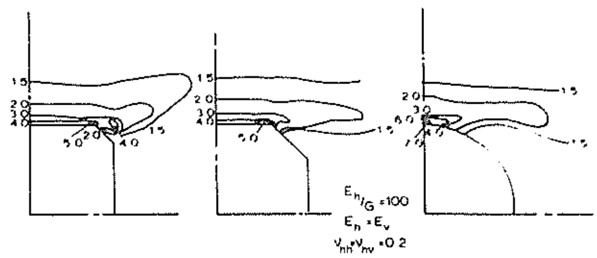

Figure 5 Contours of horizontal stress as a function of the virgin horizontal stress field

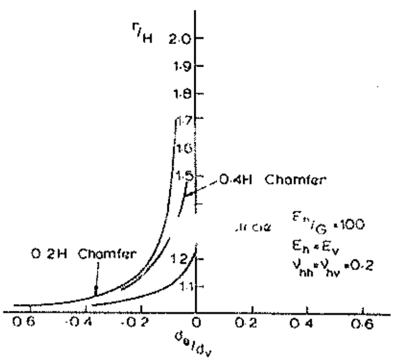

Figure 6 Horizontal stress concentration in crown for vertical virgin stress field

Examination of the results presented in Figure 4 to 6 reveals the following points :

(i) The greatest value of the horizontal stress concentration is in the crown of the circular tunnel. This value is greater than the stress concentration above the haunches in the square tunnels. This is similar to the situation for square tunnels with rounded corners in isotropic rock (Obert and Duval 1967).

(ii) The horizontal stresses above the flat roof are similar for both square tunnels with the stress being equal to about 4 times the virgin horizontal stress for a distance of 0.04H into the rock. The maximum stress is thus directed parallel to the bedding which is a situation that Cording and [illegible] (1978) suggest should be avoided. However, the present author considers this preferable to the situation in the circular tunnel where, in the centre of the roof, for a distance of 0.04D into the rock, the horizontal stresses exceed 6x the horizontal virgin stress field. Furthermore Figure 6 shows that the vertical stress field will reduce the crown stresses to a greater extent in the flat topped tunnels than in the circular tunnel.

(iii) The horizontal stress concentration above the flat topped tunnels decays more slowly with depth than above the circular tunnel. Thus the shear stresses on the bedding planes are greater above the circular tunnel.

(iv) The stresses above both square tunnels are very similar and thus the use of a large haunch is indicated as this reduces the flat roof span.

It would thus appear that the roof shape adopted at Poatina is valid for reducing compressive roof stresses in all situations where high horizontal virgin stresses occur, particularly where these are associated with horizontally bedded strata. However, it should be noted that where compressive failure will not occur but where the rock mass is blocky, this flat topped shape is probably undesirable.

5 UNDERGROUND POWER STATION SHAPES FOR HIGH HORIZONTAL STRESS FIELDS

5.1 The Drakensberg Pumped Storage Power Station

The author's comments on the subject of shape selection for underground power stations dates from his involvement in the design of the 1000 MW Drakensberg pumped storage scheme (Bieniawski, Orr and Pells, 1974). This power station has recently been completed and is excavated in horizontally bedded Triassic mudstones and sandstones. At the early design stage it was suspected that the horizontal virgin stress would be greater than the vertical but because stress measurements had not yet been performed, all analyses were carried out for K = 0.4, 1.0 and 2.0. The initial shape selection was based on the results for K = 2.0. Subsequent measurements indicated that the horizontal stress varied from 1.2 to 2.6 times the vertical stress with an average value of 2.1.

In the initial design three shapes were considered. The first, shown in Figure 7a, is the classic shape for an underground power station. The second, shown in Figure 7b, is based on the Waldeck II power station in West Germany. The third shape was based on the Foyers pump storage scheme in Scotland. This involved placing the machines in shafts and not in a massive machine hall. At Foyer's the shafts were excavated from the surface and the control building is a surface structure. At Drakensberg, proposal 3 was for two 36m diameter shafts for the 4 x 250 MW machines but excavated underground with the control system being housed in an underground chamber passing over the two shafts. Figure 7c shows a cross-section of this proposal.

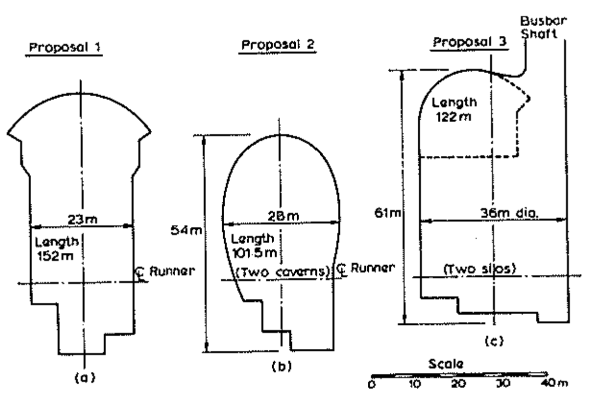

Figure 7 Three alternative shapes for the power station

5.2 Stress Analyses

Isotropic elastic analyses were used in all cases. Shape proposals 1 and 2 could be analysed in two dimensions but proposal 3 involved a 3D finite element analysis. Figure 8 shows the outline of the block that was divided (by hand) into 1522 eight node brick elements.

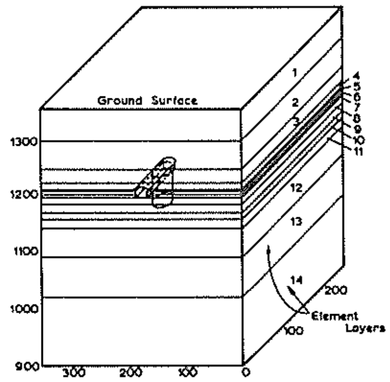

Figure 8 Three dimensional finite element model of shape proposal 3

Figures 9 and 10 show the contours of major and minor principal stress for a virgin stress field ratio K = 2.0, for shapes 1 and 2. In both cases there are large zones of tensile minor principal stress in the sidewall with small regions of tensile major principal stress. Also in both cases the crown compressive stresses exceed 20 MPa which was greater than the unconfined strength of certain of the mudstones.

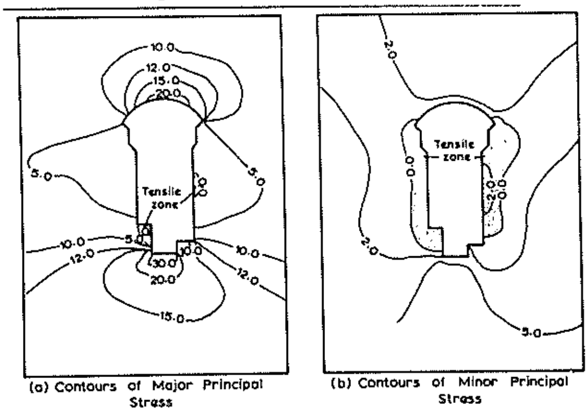

Figure 9 Shape proposal 1: horizontal stress = 2 x overburden pressure

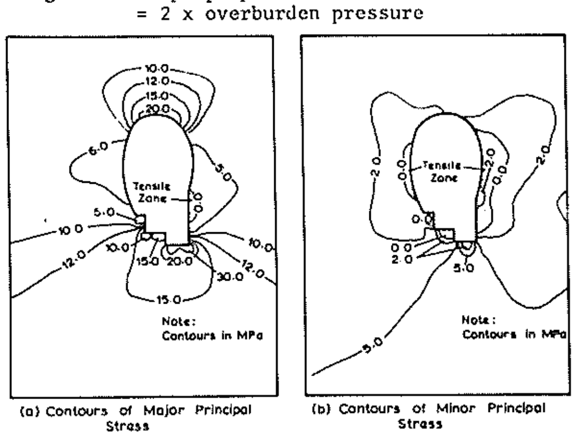

Figure 10 Shape proposal 2: horizontal stress = 2 x overburden pressure

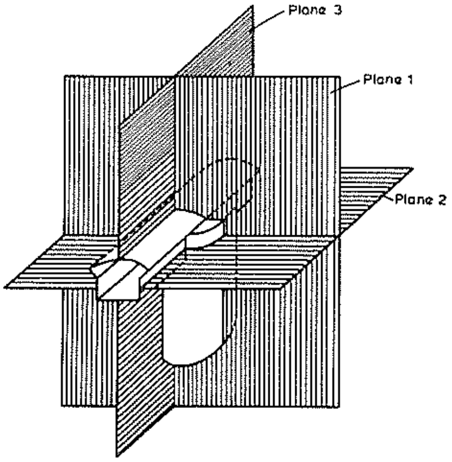

Figure 11 Shape proposal 3 planes on which stress contours are given in Figures 12,13 & 14

Figure 11 shows the three planes in which stress contours were produced from the 3D analysis of proposal 3. The contours are given in Figures 12, 13 and 14. In considering those contours, two particular points arise. The first is that, as opposed to shapes 1 and 2, very limited zones of tensile stress occur in the sidewalls of the machine chamber. This is because this shape offers a circular "ring" to the high horizontal stresses and not a long and high, flat or slightly curved wall. The second point is that the stresses induced in the roof are less than those in shapes 1 and 2.

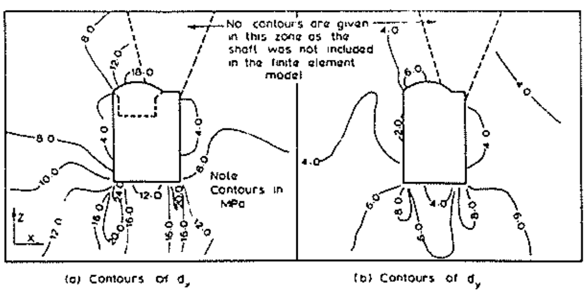

Figure 12 Shape proposal 3
Contours of stress in plane 1

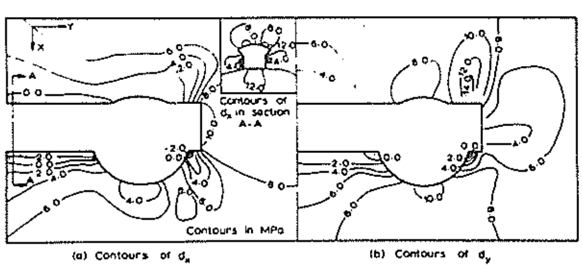

Figure 13 Shape proposal 3
Stresses in plane 2

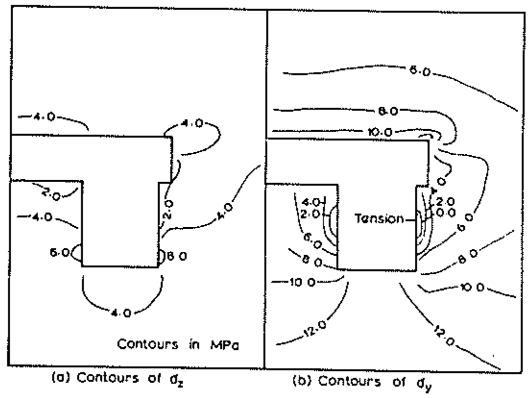

Figure 14 Shape proposal 3
Stresses in plane 3

As a result of these analyses and certain other practical considerations it was proposed that the final power station shape be based on a combination of the shaft feature of proposal 3 with the roof shape used at Poatina. This is shown in Figure 15. As described by Bowcock, Boyd, Hock and Sharp (1977) the final power station shape did incorporate the features suggested in Figure 1 and has been successfully completed. It is suggested that these features could be incorporated in any underground power station constructed in similar rock and virgin stress conditions.

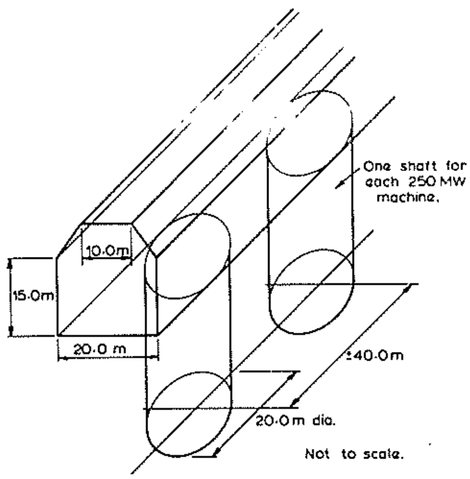

Figure 15 Suggested optimum shape for power house

CONCLUSIONS

1. The use of cross-anisotropic elasticity with high values for the ratio E_H/G appears to provide a good model for the evaluation of tun shapes in layered rock.

2. Openings constructed in layered rock and subject to relatively high horizontal stress fields may be subject to very high crown compressive stresses.

3. In horizontally bedded strata with high horizontal stresses it appears that flat topped openings with large corner haunches are more suitable from the point of view of compressive roof stresses that openings with circular roofs.

4. The most suitable shape for large underground hydro power stations in layered rock subject to high horizontal stresses involves the machines being housed in individual shafts with a relatively low height control chamber passing over the shafts. The roof of this control chamber should be flat topped with large corner haunches.

REFERENCES

BIENIAWSKI, Z.T., ORR, C.M. and PELLS, P.J.N. (1974) Drakensberg pumped storage scheme: Rock mechanics feasibility study of the underground power station. CSIR. Report ME 1325, Pretoria.

BLACKWOOD, R.L. (1978). Stress field considerations in tunnel location and design. Inst. of Eng. Australia, Pub. 78/10, Proc. 3rd Australian Tunnelling Conf., Sydney, pp. 36-41.

BOWCOCK, J.B., BOYD, J., HOEK, E. and SHARP, J. (1977). Drakensberg pumped storage scheme - rock mechanics aspects. Proc. Symp. Exploration in Rock Engineering ed. Z.T. Bieniawski, A.A. Balkema, Vol. 2, pp. 149-158.

BROWN, E.T. and HOEK, E. (1978). Trends in relationships between measured in-situ stresses and depth. Int. Jnl. Rock Mech. and Min. Sci. Vol. 15, pp. 211-215.

ENDERSBEE, L. and HOFTO, E.O. (1963). Civil engineering design and studies in rock mechanics for Poatina Underground Power Station, Tasmania, J. Australian Inst. Eng. Vol. 35, pp. 187-206.

CORDING, E.J. AND MAHAR, J.W. (1978). Index properties and observations for design of chambers in rock. Engineering Geology Vol. 12, pp. 113-142.

GERRARD, C.M., DAVIS, E.H. and WARDLE, L.J. (1972). Estimation of the settlements of cross-anisotropic deposit using isotropic theory. Australian Geomechanics Journal Vol. G2, No. 1, pp, 1-10.

GOODMAN, R.E. (1970). In-situ stresses in granites. Proc. 2nd Congress ISRM Vol. 4, p.210.

HERGET, G. (1974). Ground stress determinations in Canada. Rock Mechanics Vol. 6, pp. 53-64.

LO, K.Y. and MORTON J.D. (1975). Tunnels in bedded rock with high horizontal stresses. Canadian Geot. Jnl. Vol. 13, No. 3, pp. 216-242.

OBERT, L. and DUVALL, W.I. (1967). Rock mechanics and the design of structures in rock. Wiley, New York.

PELLS, P.J.N. (1974). The finite element method in tunnel design. Chapt. 12 in Tunnelling in Rock ed. Z.T. Bieniawski, S.A. Inst. of Civil Engineers, pp. 187-231.

RICHARDS, B. and BJORKMAN, G.S. (1978). Optimum shapes for unlined tunnels and cavaties. Engineering Geology Vol. 12, pp. 171-179.

ORR, C.M. (1975). High Horizontal stresses in near surface rock masses. Proc. 6th Reg. Conf. Africa Soil Mech., Durban, Balkema, pp. 201-206.

SALAMON, M.D.G. (1968). Elastic moduli of a stratified rock mass. Int. Jnl. Rock Mech. and Min. Sci. Vol. 3, pp. 611-645.

VAN HEERDEN, W.L. (1972). Determination of the complete state of stress in the rock surrounding the Orange Fish Tunnel. CSIR Report ME 1129, Pretoria.

VOIGHT, B. (1967). Interpretation of in-situ stress measurements. Proc. 1st Congress ISRM Vol. 3, pp. 332-347.

Some Aspects of the Behaviour of Tunnels That Cross Active Faults

I. BROWN
Post Graduate Student, University of California, Berkeley
T. L. BREKKE
Professor of Geological Engineering, University of California, Berkeley

1 INTRODUCTION

Active faults have been recognized in many parts of the earth's crust. They are mapped as nearly linear features, and are often crossed by civil engineering structures. The classification of a fault as active implies a probability that fault slippage will cause damage to structures that cross it.

Design philosophies in lifeline earthquake engineering have been developed for structures on the ground surface. Underground structures that cross an active fault are less common and such a situation is usually avoided if at all possible. This paper describes the problems that arise when a tunnel is located across an active fault, and some design solutions are suggested.

The Bay Area Rapid Transit (BART) Berkeley Hills tunnels that cross the active Hayward Fault in California are used as a case study. The behaviour of these tunnels has been monitored since they were constructed in 1967.

2 ACTIVE FAULT PHENOMENA THAT CAN AFFECT A TUNNEL

2.1 Squeezing Ground

Fault zones encountered during tunnelling usually consist of unfavourable ground from a tunnelling point of view. The material found may range from fractured yet unweathered rock, to a low strength clay gouge that requires special tunnelling techniques.

Squeezing ground is commonly associated with a fault zone. This phenomenon occurs when the stress state within the vicinity of the excavation is high relative to the strength of the material. The high stress to strength ratio results in a slow, time dependent displacement of the ground around the tunnel toward the tunnel opening. Squeezing ground causes tunnelling difficulties due to heading instabilities, excessive overbreak, and in shallow tunnels, ground surface settlement may be a problem.

2.2 Ground Vibration

When an earthquake occurs along a fault, vibrations at the ground surface will be strongest close to the fault plane, attenuating with distance. Empirical attenuation laws have been developed by a number of investigators; however, it is not clear whether these relationships can be applied at some depth below the ground surface. Japanese experience (Nasu, 1931) indicated that underground velocities may be four times less than at ground surface.

The effects of ground vibration on tunnel performance have been reviewed by Dowding and Rozen (1978). They surveyed the behaviour of 71 tunnels during earthquakes and compared accelerations at ground surface with tunnel damage. For each site, ground surface acceleration was calculated based on attenuation relations developed for earthquake magnitude and epicentral distance, however, no allowance was made for possible attenuation with depth. This work showed that tunnels are less susceptible to damage than surface structures or facilities. A correlation of damage and peak ground motion showed that no damage occurred in tunnels where the peak ground velocity was less than 20 cm/sec. Minor damage was observed for values of peak acceleration and velocity up to 0.5 g and 94 cm/sec respectively. "No damage" means there were no reports of rock falls in an unlined tunnel, or of new cracking in a lined tunnel. "Minor damage" included rock falls and minor cracking of lin[illegible] did not include partial collapse. Above an acceleration of 0.5 g, "damage" included major rock falls, severe cracking, and collapse.

2.3 Fault Displacement

The historical record of large magnitude earthquakes with epicentres near the ground surface suggest they are intimately associated with displacement along a fault. Further, the record of fault activity suggests that it is very likely that displacements along a given fault will occur on or near the most recently active fault trace. The sense of displacement will most likely follow that of previous events, responding to a tectonic stress field that changes only slowly with time.

The effect of fault displacement on a tunnel that crosses it is dependent on the sense of movement of the fault (normal, reverse, strike-slip), amount of displacement, and width of the zone over which displacement takes place. The sense of displacement determines whether a section of tunnel in an active fault zone undergoes compression or extension, as well as shear.

2.4 Fault Creep

Fault creep has been defined by Burford et al. (1978) as the "gradual, aseismic slip that is apparently produced by viscous yielding within a relatively weak fault gouge." Fault creep is considered to be an aseismic rupture process because the associated accelerations are so low that no detectable seismic waves are generated.

In California, data from small scale geodetic arrays, and continuous monitoring by surface creep-meters across active faults has shown that creep is a common behaviour of active faults. Both discrete creep events, and steady-state creep have been observed, typically with occasional discrete creep events superimposed on a background of steady slip at low rates. Creep events usually have displacements of a few millimeters and durations of several hours.

To the best of our knowledge, fault creep has not been detected in New Zealand, and it is usually assumed that creep does not occur along the various active faults (Suggate, 1979). This may be due to a lack of sensitive structures that cross active faults; also, no systematic monitoring programme has been undertaken that might detect fault creep. Gravels with a low elastic modulus commonly overlie bedrock along many of the major faults, and creep at depth may not produce time dependent displacements at the ground surface.

3 TUNNEL DAMAGE RELATED TO FAULT DISPLACEMENT

In Izu, Japan, faulting accompanied by a magnitude 7.1* earthquake in 1930 caused about 2.4 m of horizontal displacement and about 0.6 m of vertical displacement (Bonilla, 1979) in a railway tunnel with 160 m of cover. At ground surface above the tunnel, horizontal and vertical displacements were less, about 1 m and 0.5 m respectively. Bonilla discussed reports of variation in strike of the fault between the ground surface and in the tunnel, suggesting that rupture in the tunnel was en echelon with respect to the surface trace.

In 1906, a magnitude 8.25 earthquake occurred near San Francisco, California; there was relative displacement along about 430 km of the San Andreas Fault, with a maximum offset of about 5 m horizontally (Lawson, 1908). A Southern Pacific Railroad tunnel crossed the San Andreas Fault near Wright Station in Santa Clara County. As a result of the earthquake, there was lateral displacement of 1.4 m along a shear zone about 120 m from the northeast portal. Within this part of the timber supported tunnel, there was considerable crushing of the timbers and heaving upward of rails.

Other shear zones with small offsets were found at a distance of between 400 m and 700 m from the portal. These shear zones had a similar orientation to the main fault break. When the tunnel was surveyed during reconstruction, it was found that there was progressively increasing horizontal displacement from a point about 1,500 m from the main fault break until the shear zone where 1.4 m offset was measured. Immediately above the tunnel, larger displacements were found along the fault trace at ground surface than had been observed underground.

In 1952, a magnitude 7.7 earthquake occurred in Kern County, California, with displacement measured along the White Wolf Fault. Three Southern Pacific Railroad tunnels were intersected by a fault zone, presumably an extension of the White Wolf Fault (Kupfer et al. 1955). Each tunnel was damaged over a length of about 150 m near the fault zone, but at ground surface there were only a few minor fractures with small displacements. The tunnels were lined with concrete 300 mm to 600 mm thick, with minimal reinforcing concentrated on the inner face. The tunnel walls do not appear to have been tied to the invert, and much of the damage that occurred was due to varying response of the walls and invert.

The San Fernando (California) earthquake of 1971, with a magnitude of 6.5, affected the Balboa Inlet Tunnel of the Metropolitan Water District of Southern California (Dowd, 1974). The Santa Susana Thrust Fault, along which 300 mm of left lateral displacement occurred during the earthquake, crossed the tunnel about 300 m from a portal. The reinforced concrete lining was cracked and there was some spalling in a 90 m long section at the fault crossing. There was also longitudinal cracking in the tunnel lining for some 300 m on each side of the fault. The Santa Susana Fault had been inactive since the middle Pleistocene, and was not related to the faults that were active during the earthquake. Movement was probably due to the response of a pre-existing fault to stress originating in another fault system (Saul, 1975).

4 THE EFFECT OF FAULT CREEP ON TUNNELS IN THE BERKELEY HILLS, CALIFORNIA

4.1 The Hayward Fault

The Berkeley Hills are bounded to the west by the Hayward Fault, a right lateral strike-slip fault which is at least 72 km long (Figure 1), and believed to be actively creeping along much of its length. Three tunnels in the Berkeley area cross the Hayward Fault more or less at right angles; two water supply tunnels owned by the East Bay Municipal Utility District (EBMUD), the Claremont and the San Pablo tunnels, and the BART twin tunnels. All four tunnels have been affected by fault creep.

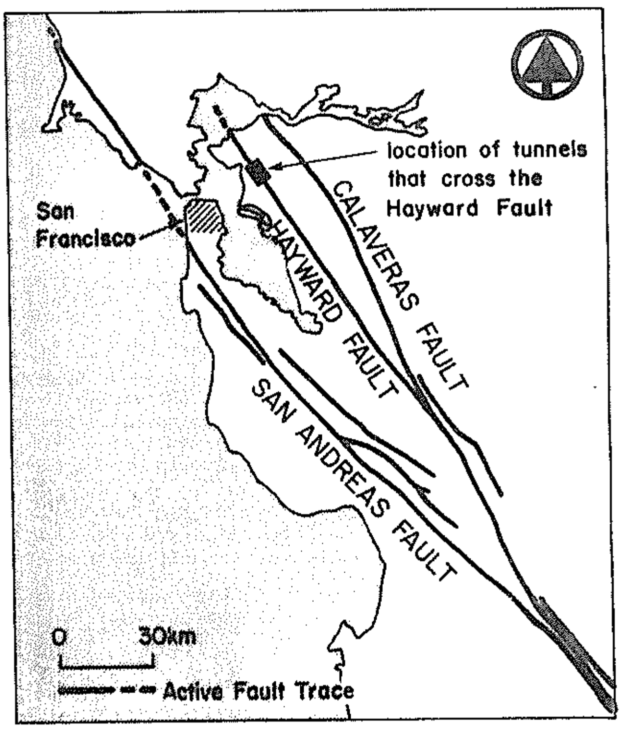

Figure 1 Active fault traces in the Bay Area, California

*Earthquake magnitudes are in terms of the Richter scale (Gutenberg and Richter, 1956).

Fault creep measurements at various locations have been undertaken by the U.S. Geological Survey (Schultz et al. 1976). The amount of fault creep has also been estimated by indirect methods. For example, in built-up areas fault slippage breaks or offsets streets, curbs, sidewalks, culverts (Radbruch and Lennert, 1966; Bolt and Marion, 1966) and other structures. Rates of creep in the order of 5 to 8 mm per year are believed to occur along the Hayward Fault.

Seismicity on the Hayward Fault has been relatively low in the past 45 years, with only four earthquakes of magnitude 4 or greater. Surface ruptures have occurred during earthquakes, over an unknown length in 1836, and over a length of about 30 km in 1868 (estimated magnitude 6.5 ± 0.5).

4.2 Water Supply Tunnels

The San Pablo tunnel was built in the early part of this century. As the tunnel lining is now in a poor condition, it is difficult to ascertain whether there is any concentrated area of damage across the Hayward Fault zone. During construction, the Hayward Fault was encountered between 70 m and 100 m below ground surface. Louderback (1942) described the material in the fault zone: "...the serpentine is so sheared that it flowed under its own weight into the tunnel like a viscous liquid and presented a serious problem of control. Parts of the Franciscan Formation there were thoroughly sheared and traversed by innumerable slickensided surfaces, and again with harder residuals, such as masses of crystalline schists, floating in the midst of the sheared weaker material."

The Claremont water tunnel was lined with unreinforced concrete except for short sections in squeezing ground where some reinforcing steel was incorporated. Following completion of the lining, longitudinal cracking in sidewalls of part of the unreinforced lining was noted. During a routine inspection of the tunnel in 1964, a 2.5 m section in the Hayward Fault zone was found to be cracked, and the invert was also buckled. The tunnel alignment was surveyed and 168 mm of right lateral offset was considered to have occurred since construction in 1929 (Blanchard and Laverty, 1966). This displacement corresponds to a rate of creep of 5 mm per year. A further survey in 1973 showed that this rate of creep has continued in the period 1964 to 1973. Survey results also indicated that a shortening or compression of the tunnel of 40 mm had occurred across the Hayward Fault in the period from 1935 to 1973.

4.3 Bay Area Rapid Transit Tunnels

The BART tunnels are 4,950 m in length, they are 30 m apart and cross the Hayward Fault about 300 m south of the EBMUD Claremont tunnel. At this location the Hayward Fault is a zone at least 215 m wide, with several surface traces indicating recent movement. The tunnels have about 70 m of cover where they cross the Hayward Fault zone (Figure 2). The fault zone was characterized by fragments of sheared rock (sandstone, shale, rhyolite, and serpentine) in a matrix of fault gouge. Fault gouge varied from a granular material to low strength squeezing clays, and gave considerable problems during tunnel construction (Ayres, 1969). The materials encountered were not particularly difficult to excavate, although crown bars, breast boards and spiling were commonly used. Following excavation, squeezing ground broke timbers and distorted sets, although invert struts were used and steel sets were spaced at 610 mm centres. In places the ground squeeze between the sets was 200 to 250 mm. The squeeze decreased over a period of one to two months, however, squeeze was further observed when retimbering and realigning sets in preparation for placing the concrete lining.

Uncertainties of rock loading conditions led to a circular section for the tunnel lining, although the tunnel was excavated with a horseshoe shaped section. To reduce possible long term loading, an elaborate drainage system was included. It was also considered desirable to have a flexible lining;

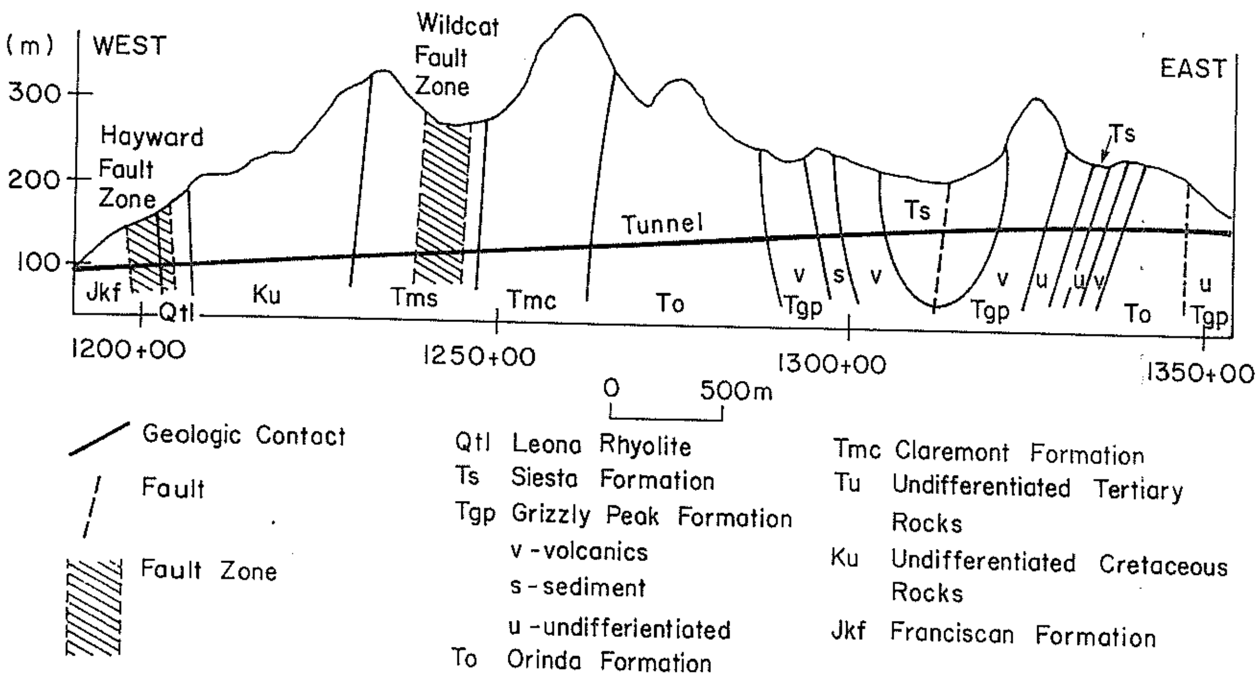

Figure 2 Geological section along BART tunnels, Berkeley Hills (after Ayres, 1969)

consequently, the final lining was kept as thin as practicable (460 mm) and longitudinal reinforcement steel was added. To accommodate possible movement along the Hayward Fault during an earthquake, a tunnel section larger than required for the operation of BART trains was constructed.

Tectonic creep along the Hayward Fault was not considered in design. During construction, this aspect of fault behaviour was brought to the attention of the designers with the result that track was laid on wooden ties to allow future realignment. At the same time it was decided to instrument the section of the northern tunnel where it crosses the Hayward Fault. Six load cells and twenty single position rod extensometers were installed to monitor deformations and changes in loading following tunnel construction, due to continued ground squeeze and tectonic activity.

A typical instrumentation station is shown in Figure 3. These instruments have been monitored from time to time over a period of 13 years. Typical load cell and extensometer curves are given in Figure 4. The extensometer readings show a common trend; maximum positive deflection (corresponding to extension of the extensometer rod) after a period of 1 to 2 years followed by a change in direction of movement and a slow rate of contraction. Load cells have indicated a slow increase in pressure with time. Apart from two instruments, the measurements appear to be consistent with each other and it is considered that the instruments are providing reliable results. When instrumentation results are plotted at a large scale to exaggerate the small fluctuations, there appears to be a correlation between extensometer contraction, load cell increase, and an increase in microseismic activity along the section of Hayward Fault adjacent to the tunnels.

Since 1971, the BART Berkeley Hills tunnels have been surveyed to detect relative changes in alignment. Unfortunately, these surveys have not been referenced to a point outside the tunnels. A laser is used for producing a survey line, and offsets are read at regular intervals along the south wall of each tunnel. As an example, the change in alignment that occurred between December 1971 and May 1973 is shown in Figure 5. To enable

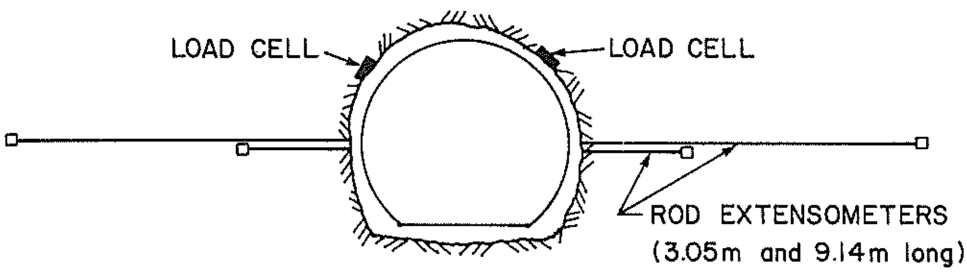

Figure 3 Typical instrumentation station in Hayward Fault zone

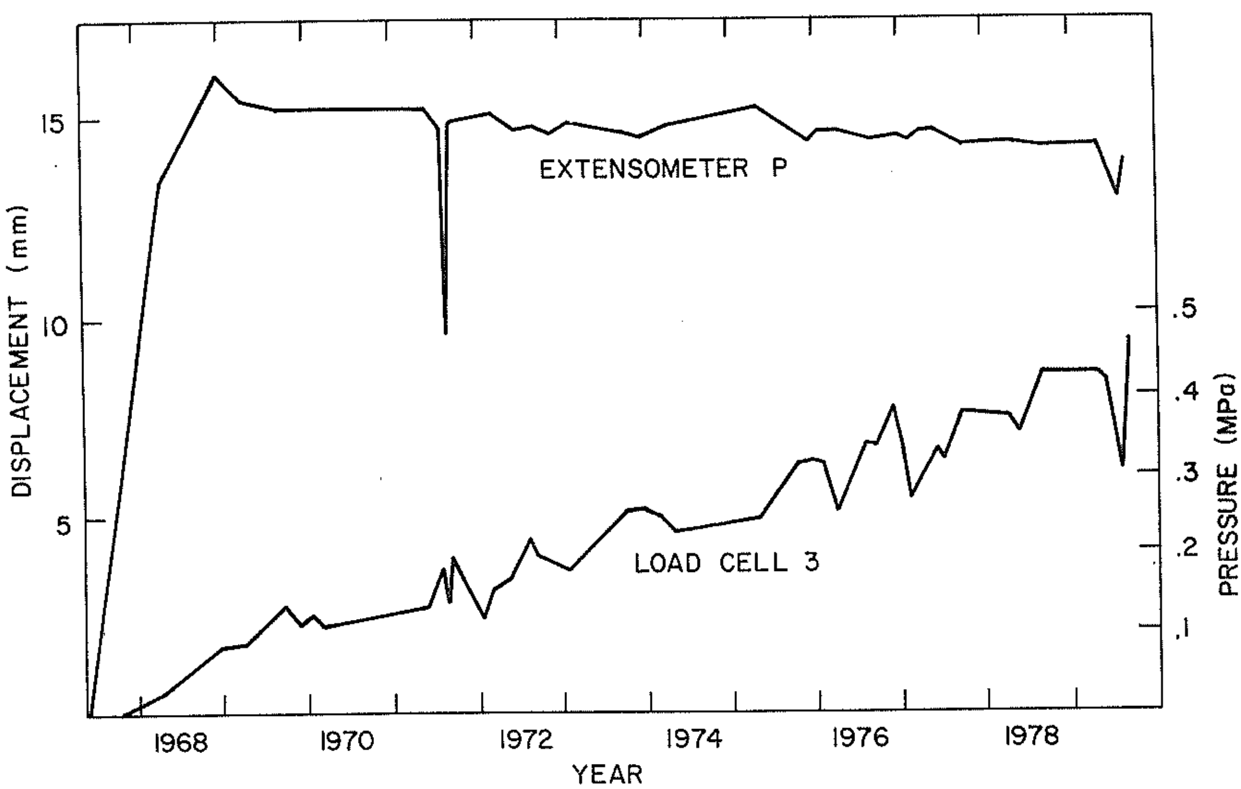

Figure 4 Load cell and extensometer curves from section of tunnel in Hayward Fault zone

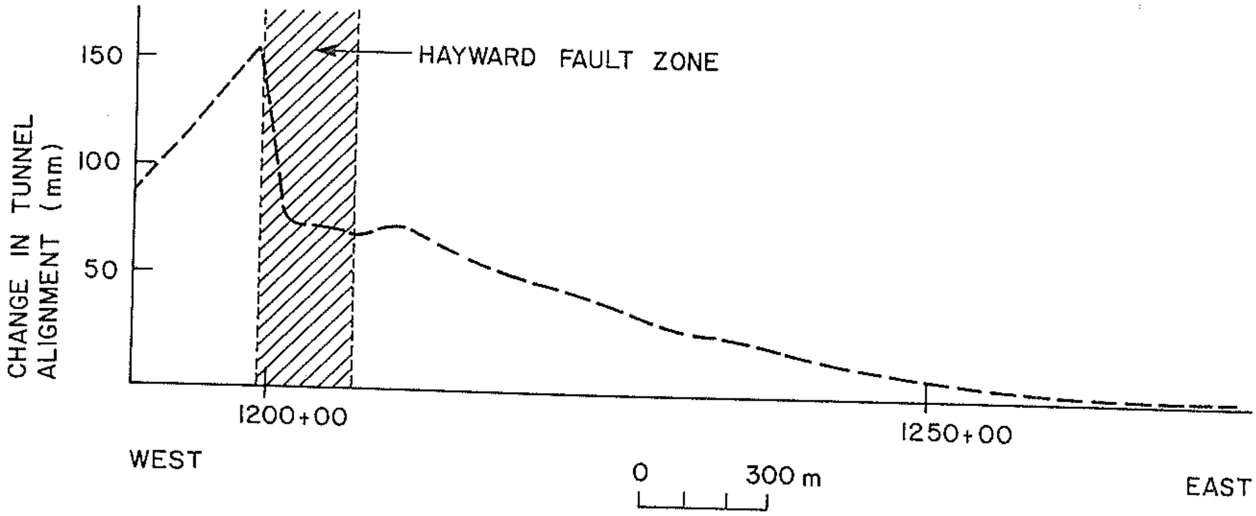

Figure 5 Tunnel alignment change, December 1971--May 1973

the reduction of the survey data, it was necessary to assume that the two points at the eastern end of the array have not displaced relative to each other. This had the effect of rotating the fixed reference line in an anticlockwise direction, thereby exaggerating the calculated offsets. We believe, however, that the offset pattern is valid even though the magnitude of offsets may be in error. The offset pattern shows that shear strain increases as the Hayward Fault is approached, and that much of the creep along the Hayward Fault takes place along a narrow zone, perhaps along one active trace.

Mapping of fractures in the concrete lining also suggested that most of the creep takes place along a narrow zone. The cracks logged were generally vertical, apparently due to concrete shrinkage. In some parts of the Hayward Fault zone, there are numerous longitudinal cracks in the tunnel crown, the result of high bending stresses from excessive horizontal ground pressure. At about station 1200+65 there is a change in the attitude of cracks, many of which have a low angle. The location of these low angle cracks coincides with a specific shear zone within the Hayward Fault zone, and it appears that most of the creep takes place at this location. For the pattern of low angle cracks to be consistent with those produced when loading a beam, it is necessary that components of either compression or vertical movement, as well as strike-slip movement, occur along the Hayward Fault.

5 DESIGN CONSIDERATIONS FOR TUNNELS THAT CROSS AN ACTIVE FAULT

Design decisions for structures that cross an active fault depend on the predicted magnitude and sense of displacement that could occur during the life of the structure, as well as the ability of the structure to survive deformations, and the consequences of failure including the cost of repair or replacement.

The magnitude and sense of displacement due to an earthquake with an epicentre on the fault can be estimated using geological methods. For California, empirical relationships have been developed for fault displacement and earthquake magnitude; these might be used when the geological evidence is incomplete. The amount and sense of displacement along a fault at depth may not be the same as that observed at the ground surface. Consequently, there is a danger that surface studies may be misleading. If the fault is subjected to tectonic creep, rates of creep may be determined from indirect evidence of offsets of structures, or from careful measurements during site investigations. It is likely that fault creep is a more common phenomenon than is generally recognized.

Deformation of a tunnel may not be restricted to the narrow zone along an active fault. The surrounding rock mass responds to the same tectonic stresses that cause movement along the fault. Small displacements may take place along adjacent shear zones resulting in incremental straining of the tunnel lining. Where the strain gradient is high, damage to the tunnel lining may result. If such behaviour is anticipated, a thin flexible lining is necessary with adequate longitudinal reinforcing.

The level of vibrations and the response of a tunnel to strong earthquakes are not well known. The interaction between the tunnel and the surrounding rock is complex, and an analytical solution has yet to be derived. One design measure that has been suggested is where the space between the tunnel lining and the surrounding rock is filled with a material with a low density (Owen, 1979). This material would provide a mismatch of acoustic impedence so that reflection could take place at the rock interface rather than at the surface of the lining.

The nature of the ground in an active fault zone makes implementation of these design measures difficult. Squeezing ground during construction may require increased temporary support (closer spacing of sets, the use of heavier sets, and invert struts) which when incorporated into the final concrete lining gives a stiffer lining than might be desired.

6 CONCLUSIONS

There appears to be no way to avoid damage to a tunnel if displacement along an intersecting fault occurs either during an earthquake, or due to fault creep. However, it may be possible to detect where damage might occur if careful geological studies during investigation and construction are undertaken to identify high risk areas. These parts of the tunnel should then be instrumented with extensometers and load cells such that potentially damaging changes in loading and deformation can be detected. Alignment surveys should also be carried out. Furthermore, a monitoring system to detect impending structural failure should be considered.

7 ACKNOWLEDGMENTS

The assistance of engineering staff at BART is gratefully acknowledged. The study of the BART tunnels is continuing, and is funded by a grant from Urban Mass Transit Authority. Ian Brown has been supported by an NRAC Fellowship while on leave from the Department of Scientific and Industrial Research, Wellington.

8 REFERENCES

AYRES, M. O. (1969). Case history--Berkeley Hills twin transit tunnels. Proc. Second Symposium on Rapid Excavation, Sacramento, CA, pp 10-26--10-37.

BLANCHARD, F. B. and LAVERTY, G. L. (1966). Displacements in the Claremont water tunnel at the intersection with the Hayward Fault. Bulletin of the Seismological Society of America, Vol. 56, pp 291-293.

BOLT, B. A. and MARION, W. C. (1966). Instrumental measurement of slippage on the Hayward Fault. Bulletin of the Seismological Society of America, Vol. 56, pp 305-316.

BONILLA, M. G. (1966). Deformation of railroad tracks by slippage on the Hayward Fault in the Niles district of Fremont, California. Bulletin of the Seismological Society of America, Vol. 56, pp 281-289.

BONILLA, M. G. (1979). Historic surface faulting--map patterns, relation to subsurface faulting, and relation to pre-existing faults. U.S. Geological Survey Open File Report 79-1239.

BURFORD, R. O., NASON, R. D., and HARSH, P. W. (1978). Studies of fault creep in Central California. U.S. Geological Survey Earthquake Information Bulletin, Vol. 10, pp 174-181.

DOWD, M. W. (1974). Earthquakes and underground structures. Proc. Conference on Earthquake Engineering for Water Projects, Sacramento, CA, pp 99-107.

DOWDING, C. H. and ROZEN, A. (1978). Damage to rock tunnels from earthquake shaking. Proc. Geotechnical Division, American Society of Civil Engineers, Vol. 104, pp 175-191.

GUTENBERG, B. and RICHTER, C. F. (1956). Earthquake magnitude, intensity, energy and acceleration. Bulletin of the Seismological Society of America, Vol. 46, pp 105-195.

KUPFER, D. H., MUESSIG, S., SMITH, G. I., and WHITE, G. N. (1955). Arvin-Tehachapi earthquake damage along the Southern Pacific Railroad near Bealville, California. California Division of Mines Bulletin, Vol. 171, pp 67-74.

LAWSON, A. C. (1908). The California earthquake of April 18, 1906. Carnegie Institute of Washington Publication 87.

LOUDERBACK, G. D. (1942). Faults and earthquakes. Bulletin of the Seismological Society of America, Vol. 32, pp 305-330.

NASON, R. D. (1971). Investigations of fault creep slippage in northern and central California. University of California, San Diego, Ph.D. Dissertation.

NASU, N. (1931). Comparative studies of earthquake motions above-ground and in a tunnel. Tokyo University Earthquake Research Institute Bulletin, Vol. 9, pp 454-472.

OWEN, G. N. (1979). Earthquake and blast effects on large underground structures. URS/Blume Engineers, San Francisco, Draft report for National Science Foundation.

RADBRUCK, D. H. and LENNERT, B. J. (1966). Damage to culvert under Memorial Stadium, University of California, Berkeley, caused by slippage in the Hayward Fault zone. Bulletin of the Seismological Society of America, Vol. 56, pp 295-304.

SAUL, R. B. (1975). Geology of the southest slope of the Santa Susana Mountains and geologic effects of the San Fernando earthquake. California Division of Mines and Geology Bulletin 196, pp 53-70.

SCHULZ, S. S., BURFORD, R. O., and NASON, R. D. (1976). Catalog of creepmeter measurements in Central California from 1973 through 1975. U.S. Geological Survey Open File Report 77-31.

SUGGATE, R. P. (1979). Seismotectonics and earthquake risk macrozoning in New Zealand. Bulletin of the New Zealand National Society for Earthquake Engineering, Vol. 12, pp 3-6.

Engineering Geological Investigations in Soft Rock Terrain, Poro-o-tarao Tunnel, New Zealand

G. W. BORRIE

Engineering Geologist, Mandeno, Chitty & Bell Ltd, Lower Hutt.

B. W. RIDDOLLS

Engineering Geology Section, New Zealand Geological Survey, Lower Hutt

1. INTRODUCTION

Construction of tunnels in soft sedimentary rocks and colluvium derived from them can pose problems that are not normally encountered in hard rocks or soils (Prebble, 1977). This was illustrated recently during investigations for the construction of a new 1.3 km, 6 m diameter tunnel at Poro-o-tarao for the North Island Main Trunk Railway. The tunnel replaces an adjacent existing brick-lined structure built in the late 19th century which had become increasingly unreliable due to deterioration of the lining (Webley, 1970). The various investigations undertaken are reviewed, and the effects on construction of the geomechanical characteristics of the materials encountered are described.

2. ENGINEERING GEOLOGY OF PORO-O-TARAO AREA

2.1 General Geology

The tunnel was constructed through a ridge which divides the Puputaha Stream, a north flowing tributary of the Mokau River, from the Ohinemoa Stream, a south flowing tributary of the Wanganui River (Fig. 1). The ridge rises to 457 m above sea level, giving a maximum cover above the new tunnel of 115 m. To the north the ground slopes away from the ridge at 15° while to the south the slope is about 25°; further away from the ridge the slope-angles average about 10° and the surfaces are commonly hummocky, indicating that widespread land-sliding has occurred in the past. Some ridges in the vicinity are capped by ignimbrite which typically forms distinctive cliffs and steep bluffs.

On the 1:250 000 Geological Map of New Zealand, Sheet 8 (Hay, 1967), the area around the site is included within the "Mahoenui Mudstone" formation of the Mahoenui Group. This group is assigned to the Upper Landon - Lower Pareora Series (Miocene). The rocks have recently been included in the Taumarunui Formation, a new unit established by Nelson & Hume (1977). For the purposes of this paper Mahoenui Group is adequate as a stratigraphic name. Bedding dips from 4° - 18° to the north or northwest. The area is mantled extensively by colluvium, which generally makes bedrock mapping difficult.

2.2 Lithology

The Mahoenui Group lithology is typically fine-grained, consisting predominantly of mudstone (as defined by Folk et al. 1970), with sporadic thinly laminated sandstone beds. Colour banding is a characteristic feature, dark grey bands alternating with light grey green bands up to 10 cm thick. The rock is commonly calcareous and ranges in hardness

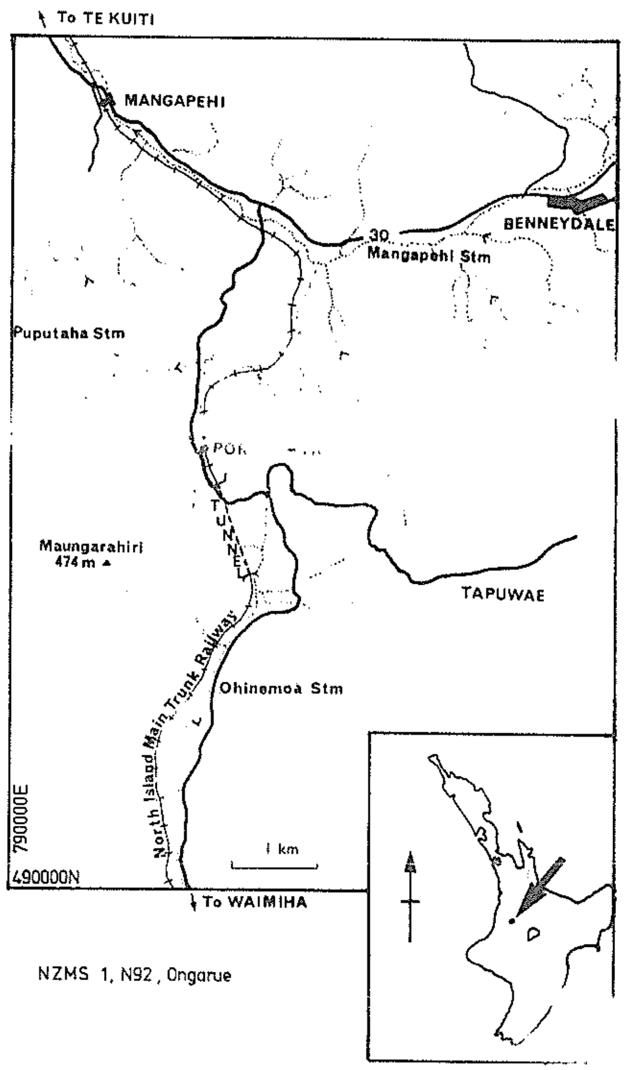

Figure 1 Location of the Poro-o-tarao Tunnel

from soft to moderately hard. Particle size analyses commonly indicate that the mudstone is composed mainly of silt, but thin section and scanning electron microscope studies suggest that the "silt" particles may actually be aggregates of clay, thus petrographically much of the mudstone might be described as claystone.

Typical whole-rock mineralogical determinations by infra-red spectrophotometry are given in Table I.

The overlying colluvium consists mostly of fragments of bedrock in a silt-clay matrix with local organic debris. It varies in grading, water content and thickness over short distances.

2.3 Investigations

Deformation of the lining of the old tunnel, thought to be possibly due to deep-seated landsliding, together with widespread topographic evidence of slope instability, indicated that careful evaluation was required to determine the influence that landsliding could have on the proposed tunnel project. Engineering geological investigations to select a suitable tunnel alignment began with aerial photograph inspection and surface mapping, and was followed by the drilling of 35 N-size cored drillholes which were concentrated around the portals and southern approaches. Diamond tipped drill bits tended to clog in both the mudstone and colluvium. The most successful core recovery was achieved using tungsten-carbide tipped bits with double or triple, split-inner core barrels (NMS or NMLC). The core retrieved contained many fine crushed and/or thin soft gouge-like zones which at first appeared to confirm the theory that the bedrock had been affected by deep-seated landsliding.

The next stage in the investigations was the excavation of a 50 m-long drive in the north portal area, to experiment with lining systems and to permit comparison of core data with in situ conditions. It became evident that the crushed zones were much less common than previously thought and that unsuitable drilling techniques were responsible for most of the defects visible in the cores. From these observations it was concluded that landsliding within bedrock was unlikely to cause problems in the construction and long term maintenance of the new tunnel. Furthermore, at Poro-o-tarao local flat areas were thought to possibly represent slumped blocks but studies beyond the site show that this is a typical geomorphic feature of Mahoenui terrain (Marwick 1946, Chandler 1978), marking changes in lithology.

Investigations then concentrated on delineating the thickness, extent and geomechanical properties of the overlying colluvium in the portal areas, especially at the south end of the tunnel. The difficulty in obtaining small diameter core representative of in situ conditions was a particular problem in this phase of the investigations. Seismic refraction surveys and penetrometer soundings to locate the bedrock-colluvium transition zone were also inconclusive. The most successful investigative tool proved to be 1 metre diameter Caldweld shafts which allowed in situ inspection of subsurface conditions. At the south portal shaft inspection identified the heterogeneous nature of the colluvium and enabled sampling for laboratory testing. The degree of weathering, water content, clay fraction, rock fragment size, interface contact and depth to mudstone-colluvium interface all varied considerably. It was shown that the thickness of colluvium was as great as 20 m, and that the colluvium-mudstone contact was either abrupt, or transitional through a zone of blocky bedrock.

However the site investigations at the north portal did not detect a colluvium-filled channel that intersected the tunnel between construction distances 98 m and 112 m. This feature was identified during installation of the north portal settlement gauges after tunnel construction had commenced thus emphasising the necessity for continual site assessment throughout construction.

2.4 Geomechanical Characteristics

A summary of selected properties of Mahoenui Group rocks and its colluvium is given in Table II.

3. CONSTRUCTION CHARACTERISTICS OF COLLUVIUM AND BEDROCK

3.1 Colluvium

The extent and marginal stability of the colluvium at the southern portal lead to the design of stabilization measures consisting of a contiguous piled concrete retaining structure founded into bedrock and a series of vertical sand drains linked to a 300 m drainage drive to lower piezometric levels upslope (Parton 1974). As excavations proceeded bedrock profiles inferred from interpolation between borehole and shaft data required modification. This changed the input data for slope stability analyses and hence cut slope design was continually reassessed and modified as further geologic information became available (Ramsay 1980). A combination of wet weather and local overstressing at the toe of a cut slope initiated some progressive slope failures which resulted in careful control of the rate and method of subsequent excavation of this inherently unstable material.

Due to the variability of the colluvium in situ, the long term effectiveness of the sand drains in dewatering the south portal slopes is as yet uncertain. However short-term observations of Geonor and standpipe piezometers indicate that, allowing for seasonal fluctuations, overall groundwater levels are being lowered (Fig.2). Significant

TABLE I

WHOLE-ROCK MINERALOGY
(Analyst: Mr C.W.R. Soong)

Tunnel Distance (m)	Qtz	Plag.	Calcite	Illite	Montmorillonite	Kaolinite
670	20	8	7	14	42	3
1350	20	6	9	15	44	2

TABLE II
SUMMARY OF ENGINEERING GEOLOGICAL PROPERTIES

	Mahoenui Group	Colluvium	Base of the Colluvium
Lithology	Mudstone with minor sandstone beds	Mudstone fragments in a silt-clay matrix	Clay with rare mudstone fragments
Colour	Dark grey/grey green	Blue-grey to yellow-brown	Light grey
Weathering	Unweathered	Moderately to highly weathered	Moderately weathered
Hardness	Soft - mod. hard (calcareous bands hard)	Very soft	Very soft
Consistency		Firm to stiff with medium plasticity	Very soft to firm
Bedding (i) Bedding Plane separation	< 0.1 mm	-	-
(ii) Dip	Between 4^{o} - 18^{o} N to NW	-	-
Defects (i) Sets	2 plus random	-	-
(ii) Spacing	0.3 to 1.0 m	-	-
(iii) Continuity	2.0 to 3.0 m	-	-
(iv) Amplitude of Waviness	2 - 4 cm	-	-
(v) Surface Roughness	Slightly rough	-	-
(vi) Fracture separation	Mainly < 0.1 mm Always < 1 mm	-	-
(vii) Water conditions	Generally dry	Dry to moist	Moist to wet
Uniaxial Compressive Strength	Average: 6 MPa	-	-
Point-Load Index	0.1 - 0.3 MPa	-	-
Schmidt Hammer Rebound No.	Average ⊥ Bedding = 38 Average II Bedding = 23	- -	 -
NCB Cone Indenter No.	0.63 - 0.88	-	-
Angle of Shearing Resistance and Apparent Cohesion			
Triaxial ⊥ Bedding	27 - 58^{o}, 300 - 2000 kPa	-	31^{o} - 37^{o}, 10 - 20 kPa
Direct Shear ⊥ Bedding	58^{o}, 1200 kPa	-	-
II Bedding	45^{o}, 1000 kPa	-	-
Remoulded Residual Strength	-	-	$\phi' = 16^{o}$
Remoulded Cohesion	-	-	C' = 0 kPa
Slake Durability (2nd cycle %)	Hard sandstone bands: 84 - 96 Mod. hard mudstone: 16 - 25	-	-
Bulk Density	1.92 - 2.22 tonnes/m^3	1.65 tonnes/m^3	1.75 tonnes/m^3
Particle Size (Average values) Clay %	22 - 38 (35)	17 - 37 (26)	
Silt %	55 - 78 (60)	48 - 70 (65)	
Sand %	0 - 10 (5)	0 - 20 (9)	
Clay Mineralogy	See Table I		
Moisture Content % (Average Values)	8 - 12 (11)	21 (29)	-
Plasticity Index (Average)	22	28	-
Mean Plastic Limit (No. samples)	22 (57)	27 (16)	-
Mean Liquid Limit (No. samples)	44 (57)	55 (16)	-

reductions of localised water-table levels were achieved by well point pumps during the excavation and concreting of piles for the south portal retaining structure (Fig. 2).

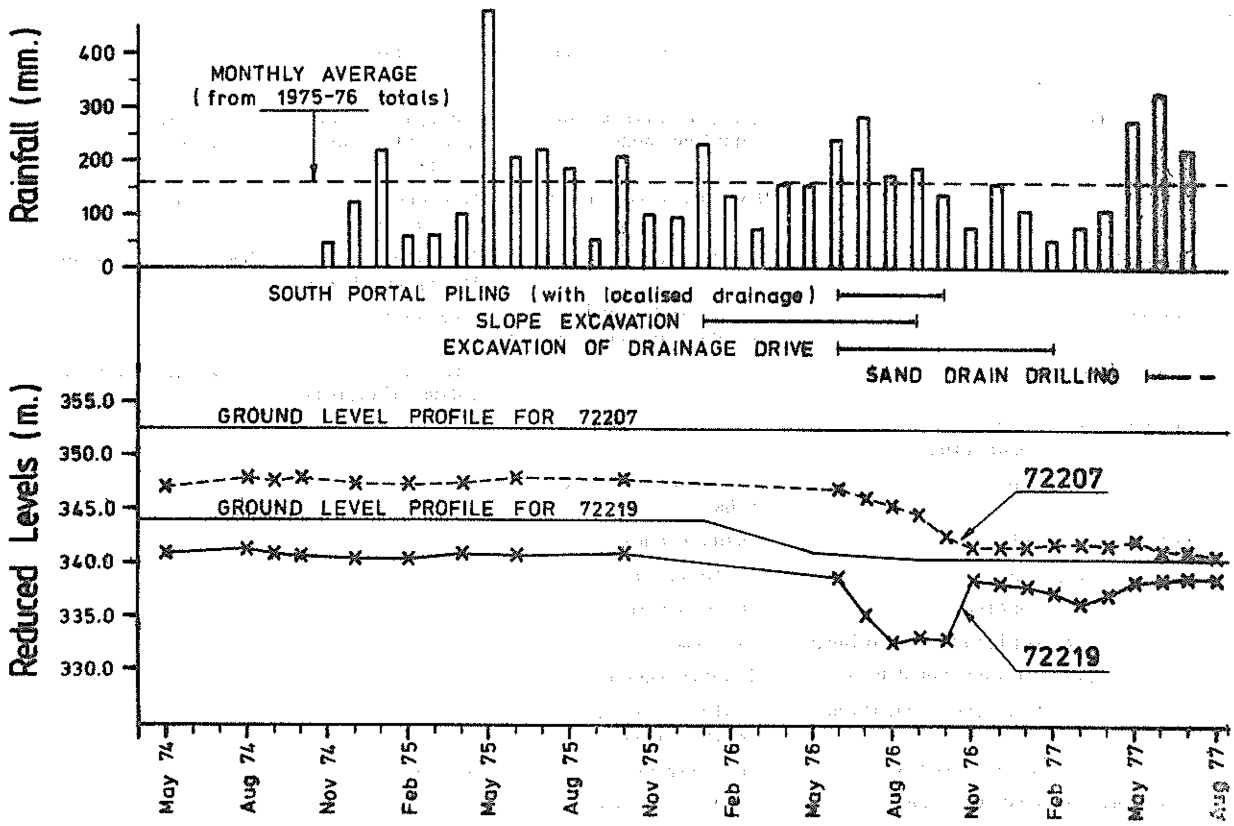

Figure 2 Groundwater levels as recorded in south portal geonor piezometers

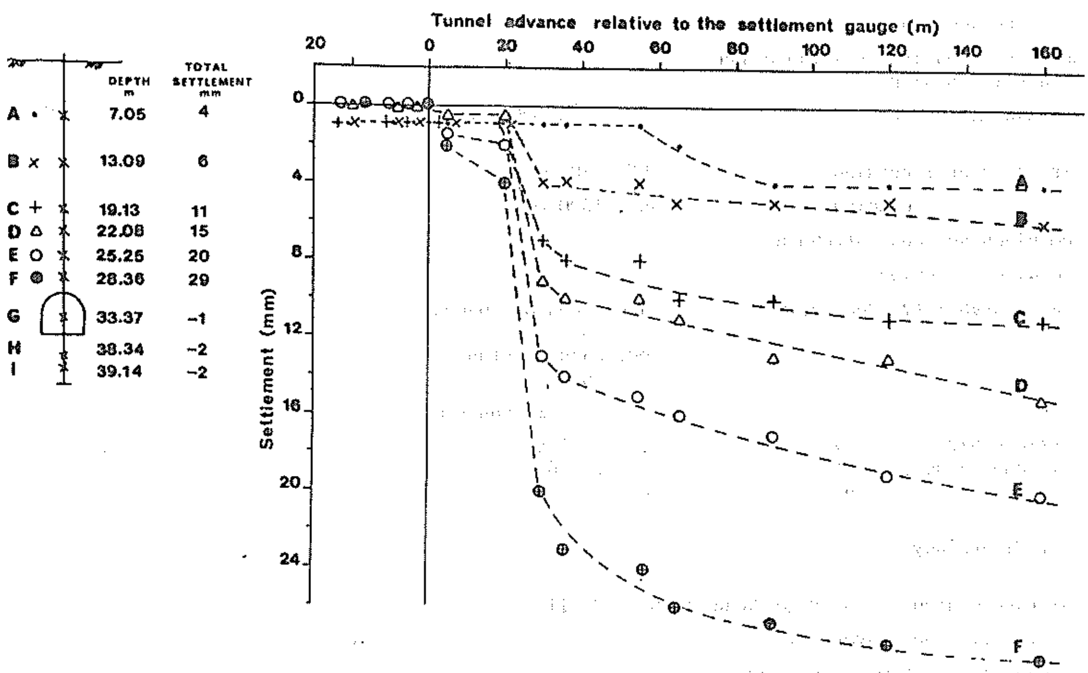

Figure 3 North portal borehole settlement gauge at tunnel construction distance of 191 m

Near the north portal the tunnel intersected the base of a trough of colluvium which reduced full face excavation to heading and benching. Prelining and spilling support ahead of the excavation face were required (Borrie, 1977).

3.2 Bedrock

The response to excavation of soft rock may be controlled both by the intact material properties and rock mass defects. The influence that rock mass defects had on excavation was minimised by the use of a Dosco Roadheader rather than using drill and blast techniques. The rock was noticeably harder towards the middle of the tunnel but this did not affect construction.

Overbreak was low compared to the conventionally excavated drainage drive, due to less peripheral rock mass disturbance. The overbreak that did develop was caused by randomly orientated joint sets intersecting subhorizontal bedding defects resulting in slabbing in the crown and the occasional large wedge failure at the face. The former required extensive use of steel mesh installed between the sets to stop slabbing of small blocks.

Settlements of up to 30 mm occurred in the crown with perceptible movements being detected 2 - 3 tunnel diameters away. The most significant settlements occurred at tunnel construction distance of 191 metres when the tunnel face had been advanced a further 3 - 4 tunnel diameters past the multi-position magnetic borehole settlement gauge (Fig. 3). The movements are attributed to downward movement of bedding slabs, resulting in a zone of loosened material developing above the tunnel crown. Heavy rain may have accentuated the process.

Predictions of support requirements using rock mass classification schemes (Wickham, Tiedmann and Skinner, 1974, Bieniawski, 1975, Barton, Lien and Lund, 1975) proved to be reasonably reliable (Rutledge, 1977, Borrie, 1977). Limitations are evident when predicting support requirements for smaller openings and for tunnels in softer sedimentary rocks where rock mass breakdown occurs. However the use of an active, rock mass sealing, support system such as shotcrete applied immediately after excavation rather than the conventional passive steel sets, would have eliminated much of the fretting and bedding plane slabbing that occurred in the tunnel crown.

A factor that was not anticipated during the investigations was the large quantity of dust generated by roadheader excavation. Initially dust caused industrial problems due to the health risk that it imposed. The tungsten carbide cutters liberated dust particles of which about 10% were quartz fragments within the respiratory range (< 5 μm). Formation of dust size particles depends on two main factors; grain size of the rock, and its mineralogy. The dust problem with Mahoenui Group rocks is probably the result of very fine grain size coupled with relatively high quartz-feldspar content (Dr G.A. Challis, personal communication). The problem was alleviated using steam and/or water dust suppression units and extraction fans near the face.

Little water was encountered in the tunnel but the combination of water resulting from dust suppression and rolling stock caused the invert to disintegrate to a muddy slurry. When tunnel advance was slower the problem compounded as construction machinery was more concentrated within the affected area. The Mahoenui Group rocks are prone to shrinkage and fretting on drying. Simple experiments show that a block of mudstone will break down to chips and friable particles when left outside for a few days. The effect underground is to cause unlined tunnel walls to fret and hence, with time, leading to increased overbreak. A sealing primary support system would have eliminated this problem.

4. CONCLUSIONS

Various difficulties with subsurface investigations in Mahoenui Group rocks and its overlying colluvial weathering products and related engineering problems encountered during the construction of the new Poro-o-tarao tunnel included:

- Recovery of small diameter drill core representative of subsurface <u>in situ</u> conditions was difficult. Core drilling in soft rock terrain should therefore be interpreted with caution, at least until the technique is proved reliable.

- The more meaningful investigative methods were those which allowed <u>in situ</u> inspection, such as large diameter bucket auger holes.

- Extension of field studies beyond the site which has limited outcrop proved worthwhile.

- Because of the variable nature of the colluvium care was needed in selection of geomechanical design parameters and excavation techniques.

- Bedding plane failures migrated above the tunnel crown to cause settlement when active support systems were not installed soon after excavation.

- Machine excavation resulted in neater excavation profiles but excessive dust was liberated by the cutter header action.

- Invert breakdown due to rolling stock and wet conditions often caused construction difficulties. Concrete lined drains and sump holes would have been necessary to channel water away from the face and invert effectively.

- Shrinkage on drying causes fretting, leading to overbreak in unlined tunnel walls. Sealing primary support systems can eliminate this problem.

These factors will not necessarily be relevant to other Tertiary soft rocks but provide guidelines as to the kinds of investigations which may be appropriate for civil engineering projects in similar materials.

5. ACKNOWLEDGEMENTS

The authors thank Mr S.A.L. Read for comments and Mr N.D. Perrin for results of recent geomechanical testing of Mahoenui Group rocks.

6. REFERENCES

BARTON, N.; LIEN, R. and LUNDE, J. (1975). Estimation of support requirements for underground excavations. <u>Proc. Symp. Design Methods in Rock Mechanics, ISRM</u>, Minneapolis, pp 99-113.

BIENIAWSKI, Z.T. (1975). Case studies: Prediction of rock mass behaviour by the geomechanics classification. <u>Proc. 2nd Aust - N.Z. Conf. on Geomech.</u>, Brisbane, pp 36-41.

BORRIE, G.W. (1977). Engineering geology studies at the Poro-o-tarao tunnel, King Country, New Zealand. MSc Thesis, University of Canterbury.

CHANDLER, M.P. (1978). Some causes and effects of shallow landsliding on mudrocks, King Country, New Zealand. MSc Thesis, University of Waikato.

FOLK, R.L.; ANDREWS, P.B. and LEWIS, D.W. (1970). Detrital sedimentary rock classification and nomenclature for use in New Zealand. N.Z. Jl Geol. Geophys, Vol. 13(4), pp 937 - 968.

HAY, R.F. (1967). Sheet 7, Taranaki (1st Ed.) Geological Map of New Zealand, 1:250 000. Department of Scientific and Industrial Research, Wellington, New Zealand.

MARWICK, J. (1946). The geology of the Te Kuiti subdivision. N.Z. Geological Survey Bull. n.s. 41.

NELSON, C.S. and HUME, T.M. (1977). Relative intensity of tectonic events revealed by the Tertiary sedimentary record in the North Wanganui Basin and adjacent areas, New Zealand. N.Z. Jl Geol. Geophys, Vol. 20(2), pp 369-392.

PARTON, I.M. (1974). Assessment of slope stability at Poro-o-tarao tunnel south portal. Proc. Symp. on Stability of Slope in Natural Ground. The N.Z. Geomechanics Society, Nelson.

PREBBLE, W.M. (1977). Engineering geological investigations for tunnel location and design. Proc. Symp. on Tunnelling in New Zealand. The N.Z. Geomechanics Society, Hamilton.

RAMSAY, G. (1980). Stabilisation of a colluvium slope. Proc. 3rd Aust. - N.Z. Conf. on Geomech., Wellington.

RUTLEDGE, J.C. (1977). Engineering classifications for rock for the determination of tunnel support. Proc. Symp. on Tunnelling in New Zealand. The N.Z. Geomechanics Society, Hamilton.

WEBLEY, J.F. (1970). Repairs to a main trunk railway tunnel. N.Z. Engineering, Vol. 25, pp 186-189.

WICKHAM, G.E.; TIEDEMANN, H.R. and SKINNER, E.H. (1974). Ground support prediction model, RSR concept. Proc. RETC, AIME, San Francisco, pp 691-707.

In Situ Rock Stress Measurement at Rangipo

M. J. PENDER
Senior Lecturer in Civil Engineering, University of Auckland
M. E. DUNCAN FAMA
Mines Division, N.Z. Ministry of Energy

SUMMARY The results of in situ rock stress measurements at the site of the Rangipo underground powerhouse are presented. The Rangipo project is part of the Tongariro Power Development in the central North Island of New Zealand. The rock at the site is greywacke and argillite, mostly unweathered and closely jointed. The measurement technique used was the hollow inclusion triaxial stress gauge, (Rocha et al. 1974 and, Worotnicki and Walton 1976). The results of the five successful tests show that the stress magnitudes are not large and that normal stresses in horizontal directions are slightly greater than those in the vertical direction.

1 INTRODUCTION

In this paper the results of tests to measure the in situ state-of-stress at the site of the Rangipo underground powerhouse are presented. The Rangipo powerhouse, 120 MW generating capacity, is part of the Tongariro Power Development in the central North Island of New Zealand. The powerhouse will be excavated from a deposit of greywacke and argillite, mostly unweathered but closely jointed. The approximate dimensions of the powerhouse excavation are: length 60 m, height 40 m and width 20 m. A downstream serge chamber of similar dimensions is to be excavated 40 m downstream from the powerhouse cavern.

Many techniques have been developed for the measurement of in situ stresses in rock. Most have been applied to rock conditions rather better than those at Rangipo. Considerable difficulty was experienced in adapting existing techniques to the conditions at the Rangipo site. Despite these problems knowledge of the in situ stresses remains an important facet of the input data for underground powerhouse design. In effect these stresses determine the loading on the structure.

The investigation work was a joint effort between the New Zealand Ministry of Works and Development Central Laboratories and the Ministry of Works and Development investigation staff at the powerhouse site. Central Laboratories directed the investigation, developed instruments and techniques. The site staff provided drilling crews and back-up services. The results are also presented in an M.W.D. Central Laboratories Report (Pender 1977).

2 STRESS MEASUREMENT TECHNIQUE

The technique adopted for the measurements was the hollow inclusion triaxial stress gauge, (Rocha et al. 1974 and, Worotnicki and Walton 1976). A number of electrical resistance strain gauges are embedded in a hollow epoxy cylinder. The details of the probe used are shown in Figure 1. The probe is very similar to that developed by Worotnicki and Walton (1976). The thickness of the epoxy cylinder was a few millimetres greater, and air pressure (200 kPa) was used to expel the epoxy from the reservoir at the end of the probe. This probe is cemented into a predrilled Ex hole. The whole assembly is then overcored with a drilling barrel producing a 150 mm diameter core. The overcoring releases the strain in the rock due to the in situ stresses. An elastic analysis of the strain readings gives the in situ stresses, Duncan Fama and Pender (1980).

The above description belies the difficulties experienced in achieving successful measurements. The difficulties were all associated with the jointed nature of the rock. The technique used would certainly not have been appropriate in the most intensely

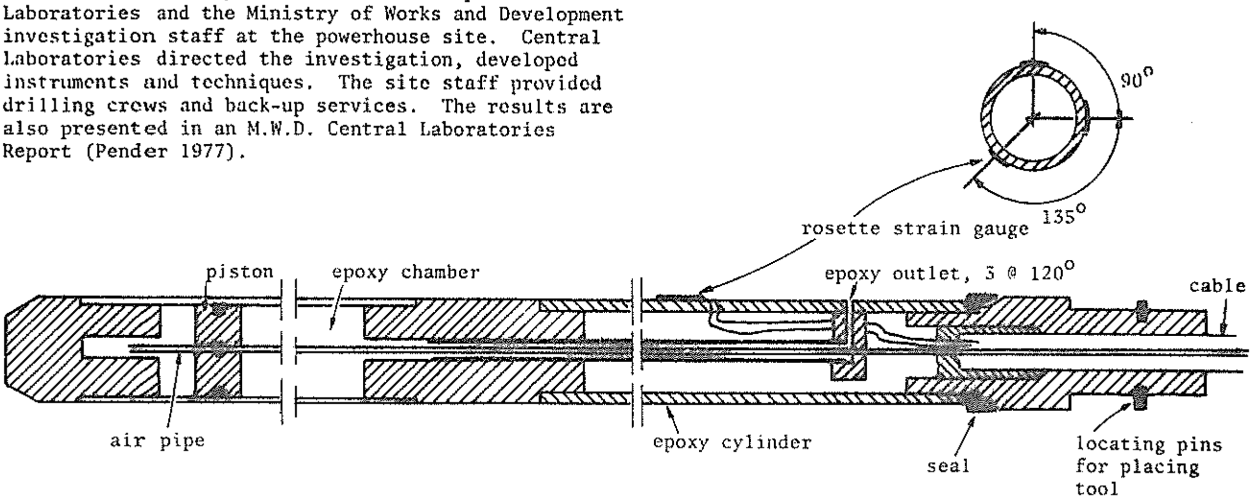

Figure 1 Hollow inclusion triaxial stress gauge

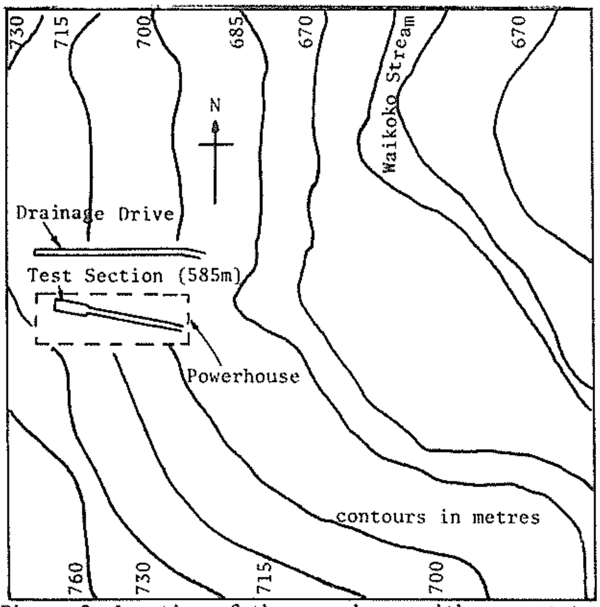

Figure 2 Location of the powerhouse with respect to the surrounding topography

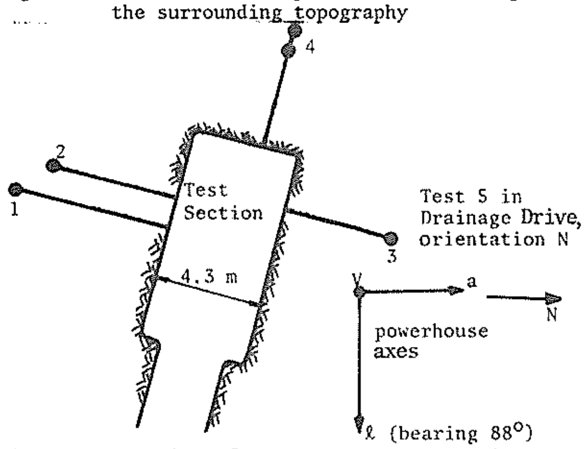

Figure 3 Location of stress measurement points

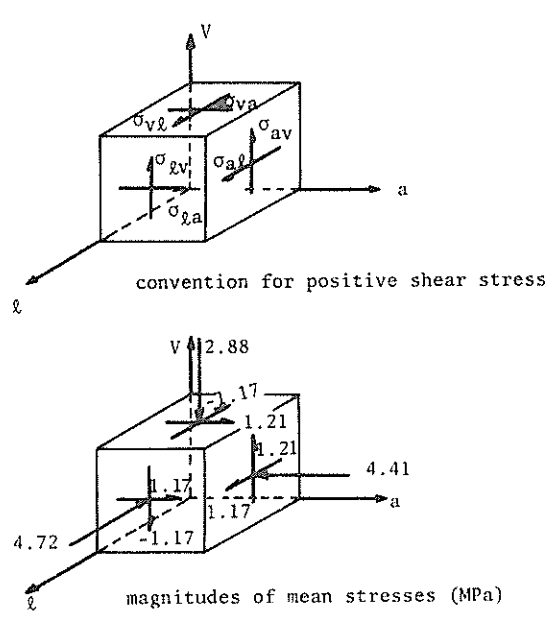

Figure 4 Stress components acting on planes orthogonal to the powerhouse coordinate axes

jointed rock at the site. Also the jointing pattern was not regular. Although the analysis of joint data, (Hegan 1977), showed that three dominant joint directions were indicated the spread of joint directions was very large. A considerable amount of investigation drilling with an NMLC core barrel was done in an attempt to locate suitable blocks of rock for the measurements. Cores in excess of 400-500 mm long were regarded as indicative of suitable rock for the stress measurements. Two localities were found: the test section at the west end of the powerhouse and in the drainage drive near the east end of the powerhouse. The final selection of the stress measurement position was chosen by considering the jointing pattern revealed in the NMLC cores from holes nearby. In principle the core from the Ex pilot hole in which the stress measurement probe was to be cemented should indicate if the rock is satisfactory. However it was found that because of the small diameter of Ex core this is often broken in the drilling process.

The presence of joints also lead to problems during the overcoring. The standard procedure of using a diatube did not work at all well. The cause of trouble was the unexpected presence of a joint near the front of the core during the overcoring process. The drilling action of the diatube tended to twist and vibrate the core and eventually break the stress measurement probe. For this reason a double tube coring barrel was constructed, the inner tube of which was mounted on bearings so that the core was not twisted. This greatly increased the success rate of the measurements which involved overcoring runs of 500 to 750 mm.

The main indication that an overcoring run had been successful was the variation of the strain readings with the penetration of the drilling barrel. The type of plot shown by Worotnicki and Walton (1976), in which some of the strain components rise to a peak and then settle down to a steady value, is required. Some of the pieces of overcore were cut through with a diamond saw to check that the bond between the rock and epoxy had not failed. Generally this was not a problem as the relatively low levels of the in situ stresses meant that the tensile stress set up at the epoxy/rock interface during the release of the strain in the rock was small.

3 RESULTS

The topography of the ground surface above the site and position of the powerhouse are shown in Figure 2. In Figure 3 the positions of the stress measurements are shown. The results of the five measurements are given in Table I. Presented are the calculated principal stresses and also the normal and shear stresses which act on three orthogonal planes relative to the powerhouse axes, Figure 4. The measured strains were reduced to stresses using the analysis of Duncan Fama and Pender (1980). The properties of the rock were taken as E 67.0 GPa and ν = 0.25. These figures were indicated by the extensive testing done by Bryant (1977) on NMLC cores from the site. The properties of the epoxy were taken as E 3.45 GPa and ν = 0.40. The six stress components were then reduced to principal stresses and principal stress directions.

The principal stress results are rather variable. The mean and standard deviation have been calculated. It is seen that the level of confidence decreases as the magnitude of the stresses decreases. The results for test three have the unlikely result that the minor principal stress is close to zero. This is reflected in the fact that the standard deviation for σ_3 is nearly the same magnitude as the mean value

TABLE I

RESULTS OF STRESS MEASUREMENTS (units MPa)

Test	σ_1	σ_2	σ_3	σ_{aa}	σ_{vv}	$\sigma_{\ell\ell}$	σ_{av}	$\sigma_{v\ell}$	$\sigma_{\ell a}$
1	8.76	5.79	0.75	5.30	2.58	7.52	1.37	-2.67	1.20
2	7.90	2.81	1.51	7.90	1.60	2.78	0.48	0.28	0.09
3	5.96	3.45	-0.07	3.28	3.11	2.77	2.27	-0.52	1.82
4	6.46	3.59	2.35	3.43	2.21	6.46	-0.08	0.30	-0.05
5	8.33	1.52	0.77	2.12	4.90	4.06	2.01	-3.25	2.80
Mean	7.48	3.43	1.06	4.41	2.88	4.72	1.21	-1.17	1.17
Standard Deviation	1.21	1.55	0.91	2.26	1.26	2.17	1.00	1.68	1.20

for σ_3. The principal stress directions are plotted with respect to the powerhouse axes, Figure 4a, in Figure 5. Once again a large amount of scatter is evident.

This scatter of results is also present when the principal stresses are reduced to normal and shear stresses acting on planes orthogonal to the powerhouse axes. As with the principal stresses the relative magnitude of the uncertainty rises as the average value of the stresses decreases. The average value of the vertical stress, 2.88 MPa, correlates reasonably well with the depth of overburden at the site, although the complexity of the overlying topography, Figure 2, makes it difficult to decide exactly what is the equivalent overburden depth. These calculations suggest that the normal stress levels in the horizontal directions are a little greater than those in the vertical direction. The level of the scatter from one result set to another precludes any more definite statement. The ground surface above the site contains the stream valley shown in Figure 2. Such a valley configuration would be expected to give a gravitational stress field beneath the bottom of the valley which had the horizontal stresses slightly higher than the vertical stresses. Thus it is unlikely that the stresses measured are of tectonic origin.

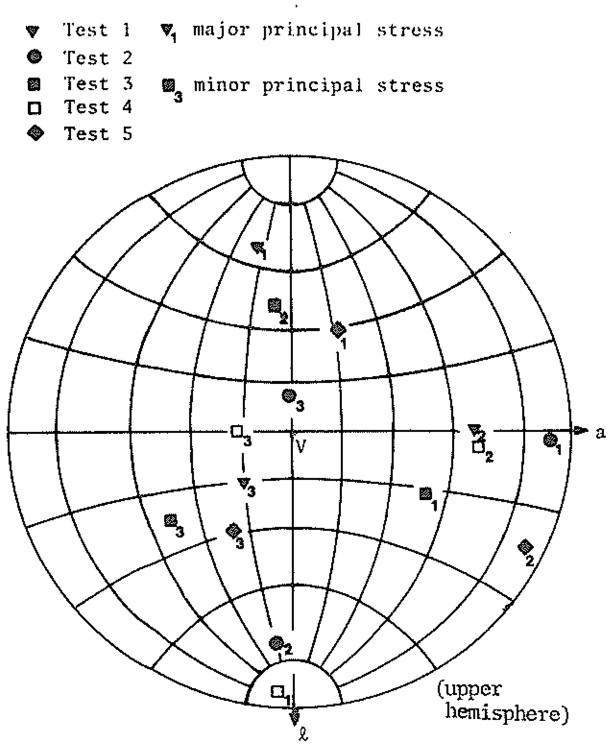

Figure 5 Orientation of the major principal stress directions with respect to the powerhouse

The variability of stress results could be a consequence of difficulties in the measurement technique, variability in the rock properties or true variations in the rock stress from point to point. It is not clear what the explanation is, although the consistent results obtained by Bryant (1977) suggests that the rock properties are unlikely to be the cause. The rock in which the measurements were made was the best rock at the site. The properties of the more intensely jointed rock from which the bulk of the powerhouse had to be excavated are clearly inferior to those of the rock on which the measurements were made. Thus the variability evident in Table I has another dimension not explored with these measurements. It is assumed that this better quality rock is stiffer and would be better capable of supporting differences in principal stress than the more intensely jointed material. The principal stress magnitudes elsewhere in the rock would thus tend to be more equal.

4 CONCLUSIONS

Existing rock stress measurement techniques have been applied to the difficult rock conditions at the site of the Rangipo powerhouse. The use of a double tube drilling barrel increased the success rate of the overcoring.

Five measurements were obtained. The results from these indicated much scatter both in the magnitude of the principal stresses and the principal stress directions. The results indicate that the normal stress in the horizontal direction is slightly greater than that in the vertical direction. Because of the topography of the ground surface above the site this stress condition is probably of gravitational rather than tectonic origin.

5 ACKNOWLEDGEMENTS

These stress measurements would not have been possible without the painstaking work of the drilling

crews at the site. In particular Mr J. Chapman exhibited much insight into the nature of the overcoring operation and suggested the use of the double tube overcoring barrel.

The permission of the Commissioner of Works to publish the paper is acknowledged.

6 REFERENCES

BRYANT, J.M. (1977). Some properties of Kaimanawa greywacke. M.W.D. Central Laboratories Report No.2-76/4.

DUNCAN FAMA, M.E. and PENDER, M.J. (1980). Analysis of the hollow inclusion technique for measuring in situ rock stress. Int. Jnl. Rock Mech. & Min. Sciences. To Appear.

HEGAN, B.D. (1977). Engineering geological aspects of Rangipo underground powerhouse. Proc. of the Symposium Tunnelling in New Zealand, Hamilton, pp. 6.23-6.32.

PENDER, M.J. (1977). In situ stresses at the site of the Rangipo underground powerhouse. M.W.D. Central Laboratories Report No. 2-77/3.

ROCHA, M., SILVERIO, A., PEDRO, J.O. and DELGADO, J.S. (1974). A 'new' development of the LNEC stress tensor gauge. Proc. 3rd Congress ISRM, Denver.

WOROTNICKI, G. and WALTON, R.J. (1976). Triaxial hollow inclusion gauges for the determination of rock stress in situ. Proc. ISRM Symposium on Investigations of Stresses in Rock - Advances in Stress Measurement. Institution of Engineers Australia, Conference Publication No. 76/4.

The Effects of Some Structural Properties of Rock on the Design and Results of Blasting

T. N. HAGAN
Senior Mining Engineer, ICI Australia Operations Pty Ltd, Melbourne

SUMMARY. This paper describes the effects of porosity, joints, bedding planes and rock type combinations on the design and results of blasting. It also examines means of minimising explosives' energy losses which such discontinuities encourage. Rocks with closely-spaced discontinuities and/or high intergranular porosities should be blasted with well stemmed charges which generate high heave energy:strain wave energy ratios. Best fragmentation is usually obtained where the face is parallel to and on the dip side of principal joints; as the dip flattens however, inclined blastholes may become necessary to maintain front-row toe burdens at their design distance. Where a sub-vertical fault forms the contact between ore and waste within a blast block, initiation should proceed from the stronger into the weaker rock; if a different blasthole pattern is required beyond the contact, only the spacing should be changed, the burden remaining constant. Where softer overburden strata sandwich a hard band, fully-coupled centre-primed charges should be located within the band, the charge being efficiently stemmed at both ends. Band thickness restricts the dimensions of the blasthole pattern. Good fragmentation of thin bands necessitates the use of small patterns which, in turn, encourage the drilling of small diameter blastholes.

1 INTRODUCTION

Shortcomings in our understanding of the effects of rock properties are the major obstacle to progress towards optimum blasting. If rocks were homogenous isotropic media, one could confidently expect more rapid advances towards this goal. But such an assumption, even as a first approximation, is rarely valid. Almost invariably, rocks exhibit numerous natural discontinuities (e.g. joints, bedding planes, faults, soft seams, vughs, pores, etc.) and cracks created by previous detonations. Some of these discontinuities may be extensive and wide; others will be localised and narrow.

Both experiments and practice have indicated that blasting results are influenced by rock properties more than by explosives' properties. But the nature and degree of heterogeneity of the rock affect not only fragmentation, displacement, muck-pile looseness and toe conditions; they also exert a considerable influence upon

1. the selected blast design and
2. the intensities of undesirable side effects such as blast-induced overbreak and slope instability.

Because of its heterogeneity, rock may exhibit planes of preferential fracture oriented in any one of an infinite number of directions. In some cases, the rock's structural features allow the explosive's energy to be wastefully dissipated rather than perform the work intended.

Despite the problems associated with heterogeneity and anisotropy (and contrary to one's prima facie expectations), rock properties are not always an uncontrollable blast parameter. Although there are factors over which the blasting engineer has a much higher degree of control, one should recognise the fact that rock properties can often be controlled to a limited extent. This control may be achieved for example, by designing the blast such that the initial free face and/or the effective free faces (which are created progressively during the blast) are at the desired angle to dominant joints or bedding planes. This selective ability may enable the operator to improve blasting results.

2 EFFECTS OF POROSITY

2.1 Intermediate Porosity

The vughs which result from dissolution of the primary rock structure by groundwater are much larger and less uniformly distributed than the intergranular pores which are present in rocks such as sandstones. Vughs up to 150mm across can be found in many sulphide ores. Some limestones and iron ores contain vughs which are at least an order of magnitude larger than this.

Vughs tend to reduce blasting efficiency. When intersected, vughs can cause drill steels to jam. Vughs can also cause the following charging problems, especially where bulk ANFO or pumped water gel blasting agents are used.

1. Where a standard weight of explosive is charged into each blasthole, large vughs can result in

(a) an excessive charge concentration within the vugh, and
(b) a corresponding lack of explosive's energy in the upper part of the blasthole.

When it is possible to obtain stemming rise within that part of the blasthole immediately above the vugh, a separate column charge should be used. If stemming difficulties prevent this procedure, efforts should be made to increase the energy yields of upper parts of charges in surrounding blastholes. Such measures are most easily carried out with bulk water gel mix trucks or with bulk ANFO trucks having an aluminised ANFO capability.

2. When all blastholes are charged to give a constant stemming length, large vughs may allow very heavy charge weights per blasthole with consequent risks of cut-offs, flyrock and/or overbreak.

If the charged section of the blasthole lies near a sizeable vugh, blasting effectiveness is reduced as a result of

1. the premature termination of outward-propagating cracks at the wall of the vugh (see Fig. 1) and
2. the more rapid drop in blasthole pressure as explosion gases jet into the vugh via discontinuities and strain-wave generated cracks (see Fig. 2).

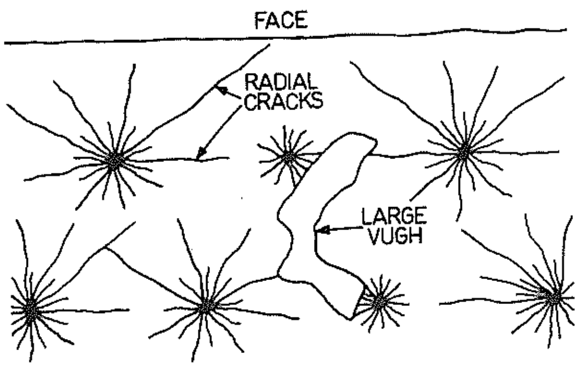

Fig 1 - Premature termination of outward-propagating radial cracks by a vugh

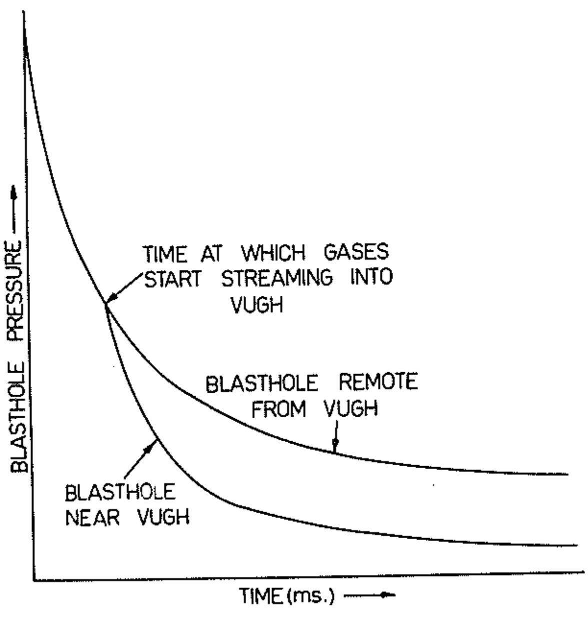

Fig 2 - Effect of nearby vugh on rate of decay of blasthole pressure

Once the explosion gases start to stream through a radial crack or a combination of discontinuities into a nearby vugh, they cease to fully pressurise other radial cracks. For this reason, radial cracks in directions other than towards the vugh then tend to stop propagating (see Fig. 1).

Currently, there is no practical technique to determine whether or not a blasthole is close to a sizeable vugh. As soon as suitable instrumentation for this purpose becomes available (Anon., 1978), the energies of charges in blastholes surrounding a vugh can be suitably increased either throughout their length or at the appropriate horizon.

2.2 Intergranular Porosity

Increases in intergranular porosity cause

1. greater dissipation of strain wave energy and
2. reductions in dynamic compressive strength and hence, increases in both the amount of crushing and the percentage of fines produced.

The work of fragmenting highly-porous rocks, therefore, is performed almost entirely by the heave energy component of an explosive's total energy output. Consequently, it is important to retain the explosion gases at high pressures until they have completed all the work of which they are capable. This situation is best realised where stemming lengths and burden distances prevent the premature release of energetic explosion gases.

3 EFFECTS OF MACROFISSURES

All rocks contain in-situ macrofissures, the influence of which often outweighs that of the intact rock's mechanical and physical properties. Discontinuities such as joints and weak bedding planes tend to dominate both the nature and extent of the fracture pattern. Indeed, the spacing of discontinuities was found to be the blasting variable having greatest influence on degree of fragmentation and, hence, working cost per cubic metre of rock (Kaufman, 1971).

Blasting can extend discontinuities to great lengths. The longer a discontinuity, the easier it is extended. The formation of new cracks (by explosion-generated strains) in the immediate vicinity of propagating discontinuities is suppressed.

Joints and bedding planes can be tight, open or filled. For this reason, they can exhibit different energy-transmitting abilities. The walls of such discontinuities represent surfaces from which strain waves may be reflected. A strain wave in a heavily jointed or densely bedded rock mass, therefore, suffers greater attenuation and dispersion. The spacing, orientation, persistence, aperture and filler material of the discontinuity all affect the attenuation and continued propagation of the strain wave.

Blast-induced overbreak and overdigging are usually strong functions of the type and number of macrofissures. The degree of success of overbreak-control blasting techniques depends primarily on the structural geology. In strong massive rocks, such techniques are usually successful, but in unconsolidated or highly-fissured strata, consistently good results may not be possible.

The frequency, width, distribution and direction of discontinuities in a face are usually so variable that is quite impossible to drill two or more blastholes that have identical burdens and degrees of confinement. Hence it is rarely possible to carry out a single test that clearly demonstrates just how much one explosive, initiation system or blasthole pattern is better than another. For this and other reasons, then, one blast does not constitute a trial. Except when there is some drastic difference in results, one usually needs to fire several blasts before the influence of a change in blast design can be accurately assessed.

In many cases, cut-offs are not strongly time-dependent, but are caused by low-friction sliding along joints or bedding planes, especially in the upper bench alongside the stemming column.

3.1 Joints

Provided a joint is closed or well cemented, blast-induced fractures can propagate across it. Fractures will not propagate over an open joint until the joint is closed. Whether new fractures are created beyond the joint depends on the strain in the rock beyond the joint and on the presence of a discontinuity which is long enough to propagate under the reduced strain.

At tight air-filled cracks, water-filled cracks and moderate density changes in the rock, some strain energy is reflected and some refracted. Tight joints parallel to the blasthole may not cause any appreciable reflection of the wave. Because of their inability to transmit tensile stress, however, even tight joints separate under the influence of the tensile wave which returns from an effective free face further out from the blasthole. This may reduce interaction between the reflected wave and the radial cracks, and may even prevent the degree of fragmentation required for satisfactory displacement.

Where a wide air-filled joint is parallel (or nearly so) to the blasthole's axis, the joint is not completely closed by the incident compressive strain wave. Therefore, it introduces an acoustic impedance mismatch and reflects the wave. If the reflected tensile wave is sufficiently strong, internal spalling occurs (see Fig. 3). Radial cracks which the strain wave would have formed in a massive rock are (prematurely) interrupted by the joint. This gives better fragmentation between the blasthole and the joint, but reduces breakage beyond the joint.

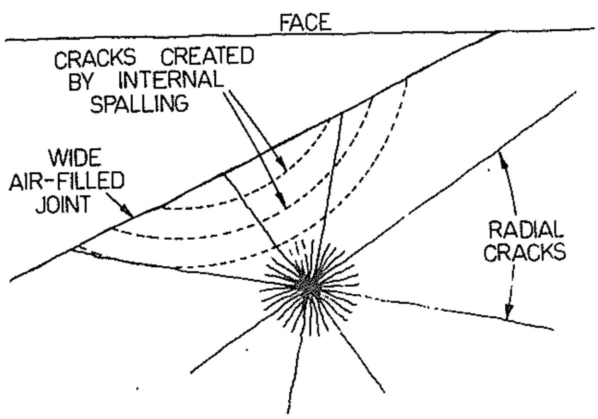

Fig 3 - Termination of radial cracks and creation of internal spalling cracks at wide air-filled joint.

A similar effect is observed where the joint is filled with a material which has an acoustic impedance much less than that of the rock; the percentage of strain energy refracted increases as the filler impedance:rock impedance ratio approaches unity. Experiments have indicated (Seinov and Chevkin, 1968) that fragmentation varies considerably with both the aperture and filling of the discontinuity.

Whenever an open discontinuity is crossed by a blasthole, explosion gases escape through the discontinuity without performing all the work expected of them. If an open joint intersects the charged section of the blasthole, it allows high gas flows which cause this joint to expand preferentially due to the wedge effect. Loss of gas into the joint causes a rapid drop in blasthole pressure and a consequent reduction in rock breakage by heavy energy. The reduced effectiveness of heave energy is most critical, of course, where persistent open joints extend from the blasthole to the face and/or top of the bench and allow gases to be vented directly to atmosphere. Premature venting through such discontinuities leads not only to poor overall fragmentation and displacement; it is also often responsible for airblast and/or flyrock problems. Where persistent open joints running normal to the face pass through the blasthole, high pressure gases also tend to open up the joints behind back-row blastholes; breakage often extends beyond the intended excavation boundary, and the newly-formed face can be quite ragged.

Best fragmentation is usually obtained where the face is parallel to and on the dip side of principal joint planes (Belland, 1966). The newly-formed face is then often a joint face, and blasthole spacings appreciably greater than the burden can be used satisfactorily. Where joints are subvertical, this configuration also gives minimum toe problems and a relatively high probability of diggable (bonus) overbreak. As the dip flattens, however, the slope of the face tends to follow the dip, and inclined blastholes may become necessary where the horizontal distance between the toe and crest of the bench becomes large. In such situations, vertical blastholes cause considerable variation in the front-row burden from top to bottom of the face.

The major disadvantage of blasting down-dip is usually that of surface overbreak (see Fig. 4). Where this, together with vertical drilling, gives excessive toe burdens on front-row blastholes, better results may well be achieved where the face lies at 45° and 135° to the strike. But when the angle between dominant joint planes and the face lies in the 30°-60° range, the development of long wide cracks behind back-row blastholes can give an irregular and shattered new face. These cracks are joints which have been opened up

1. by invading explosion gases, and
2. by the levering action associated with forward motion of the burden.

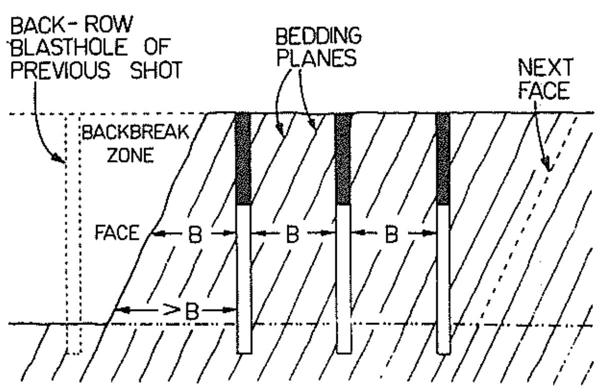

Fig 4 - Excessive toe burden caused by structurally-controlled backbreak zone and face angle

This problem is minimised

1. by initiating V-type patterns from that end of the blast block for which most of the rock moves in the down-dip direction (see Fig. 5) and
2. by using a staggered 'VI' (see Fig. 5) or square 'VI' rather than square 'V' pattern, so that explosion gases from simultaneously-initiated charges cannot act in unison in streaming into, widening and extending backward facing joints (Duffy, 1979).

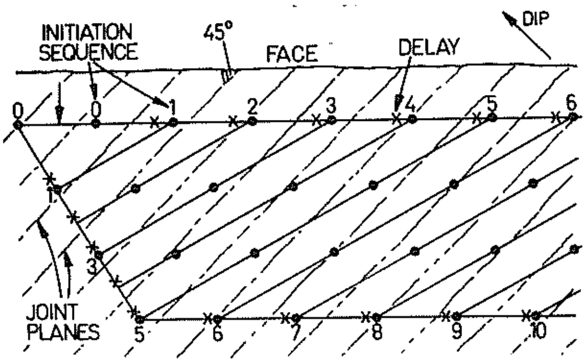

Fig 5 - Shooting down dip with a staggered 'VI' pattern

Blasts in which the strike was normal to the face produced large slabby muck (Belland, 1966).

Joints often have the effect of determining the actual boundaries of the blast block. In vertical crater retreat mining, craters tend to terminate at joints and/or weak bedding planes.

3.2 Bedding Planes

Where a vertical blasthole intercepts weak horizontal bedding planes, the widening and extension of these discontinuities is not assisted by the strain wave. Radial and release-of-load fractures (both of these being in vertical planes) are supplemented by the opening up of these bedding planes by heave energy.

Weak horizontal bedding in bench blasting is often responsible for extensive horizontal displacement of the rock. Where a well-defined bedding plane exists at floor level, very little, if any, subdrilling is necessary (cf. subdrilling of about 8 times the blasthole diameter for strong massive rocks). If the sub-drilling in densely bedded/ fissured rock is greater than that required, the floor of the bench is highly disrupted by the blast, and drilling of the next lift may become very difficult. If some of the blastholes on the lower bench have to be abandoned, the actual blasthole pattern will then be quite different from the design pattern, and inferior blasting results will be obtained.

4 'FLOATERS'

Mixtures of elastic and plastic-acting rocks can cause formidable blasting problems. Where 'floaters' (i.e. boulders of a relatively elastic rock embedded in a much softer plastic-acting matrix) are encountered, the strain wave propagates with little attenuation in the boulders, but its energy is rapidly dissipated in the matrix. Floaters which do not contain part of the explosive charge receive very little strain energy and, often, are simply pushed out intact into the muckpile. When floaters contain some of the charge, the degree of breakage can range from inadequate to excessive depending on the size of the floater, charge location and matrix characteristics.

If the floater is large, the charge located only within the floaters outer shell (as in A3 in Fig. 6) and the matrix highly compressible, breakage will be poor. Where a small floater contains a comparatively long charge (as in A6 in Fig. 6) and the overlying stemming material is relatively efficient, on the other hand, high degrees of breakage result.

The combination of inefficient stemming and a highly compressible matrix reduces the contribution of heave energy to breakage, since rapid "bulling" of the blasthole in the matrix allows an impulsive drop in blasthole pressure. In these conditions, the charge within the floater should be fully-coupled and, preferably, should exhibit a high detonation velocity and high strain energy:heave energy ratio.

5 BEDS OF DIVERSE MATERIALS

5.1 Ore/Waste Blasts in Open Pits

Consider a blast block which contains both ore and waste, the contact being a sub-vertical fault. Where the simplicity of a standard drilling pattern is required, burdens and spacings are usually such that continuous column charges give good blasting results in the stronger rock. Lighter (perhaps decked) charges are used in the weaker rock.

It is usually more difficult to standardise charge weight and then select different blasthole patterns for the ore and waste. If the pattern is altered at the contact, it is advisable to keep the burden constant and change the spacing (see Fig. 7). Where charges are fired in a V-type sequence, this introduces bends in the detonating cord trunkline network (see points A, B, C in Fig. 7) and, therefore, necessitates increased supervision and care in tying in the trunklines. Where both burden and spacing are changed

1. the complexity of drilling and connecting trunklines can become unacceptable, and
2. the newly-created face may be stepped (see Fig. 8), thereby increasing blast design problems in the block immediately behind.

In blasts which include both ore and waste, it is preferable to shoot from the stronger into the weaker rock. If the reverse order is chosen, explosion gases from a charge which lies within that part of the stronger rock alongside the contact can jet through radial cracks and/or natural discontinuities and expand with relative ease into the weaker rock, because this has been already disrupted by charges on an earlier delay (Mathieson, 1979). This causes a higher rate of decay of blasthole pressure which is manifested as reduced breakage and displacement of the harder rock around that particular charge.

The presence of such contacts within a blast tends to increase the probability of cut-offs, especially where the the contact can be mobilised by water or clay-like fillers.

These problems would seem to suggest that operators should blast up to rather than through the contact. But there can be difficulties associated with this alternative approach. In some cases, discrete

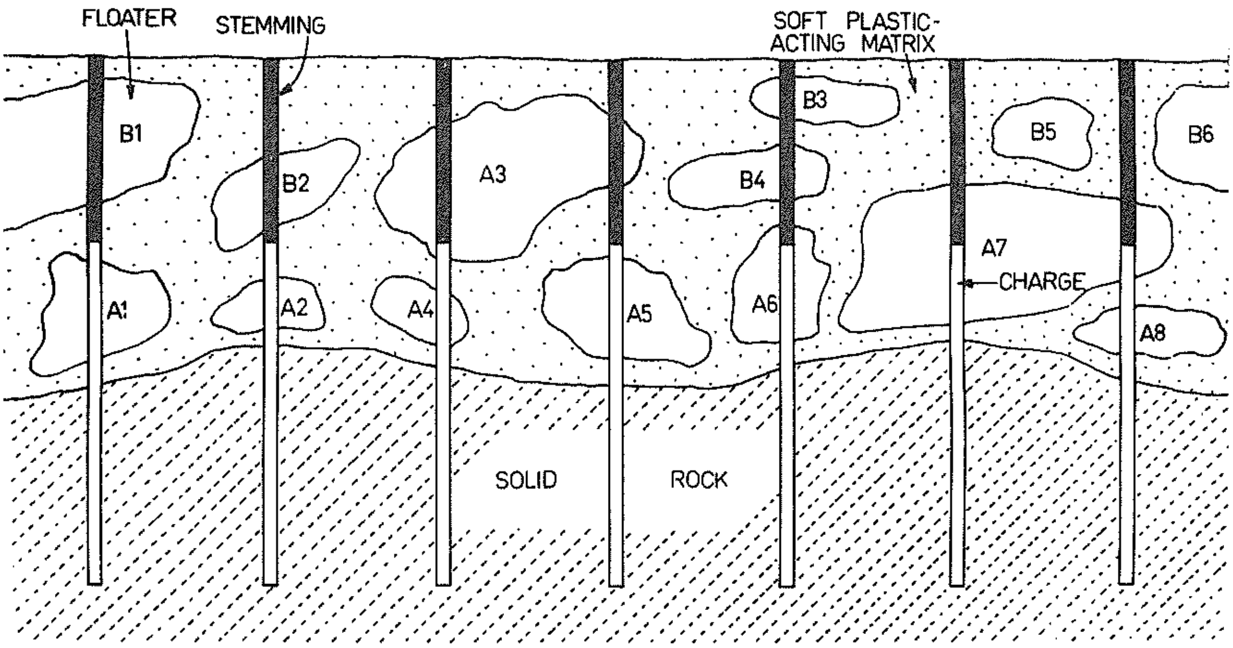

Fig 6 - Blasting of hard boulders embedded in softer plastic-acting matrix

beds or rock types extend over only short distances, and to blast within a single rock type would lead to shots which are too small and/or of unacceptable shape. In cases where ore/waste contacts are shallow-dipping, it is preferable to blast through these contacts in order to avoid

1. overbreak to the contacts and, as a consequence, large boulders, and
2. shallow-dipping faces for subsequent blasts.

Considerable secondary drilling may well be required to correct each of these effects.

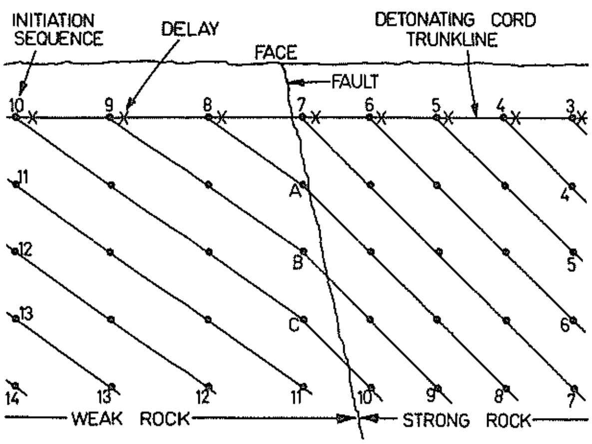

Fig 7 - Recommended change in blasthole pattern of 'V'-type blast at contact between weak and strong rock (or waste and ore)

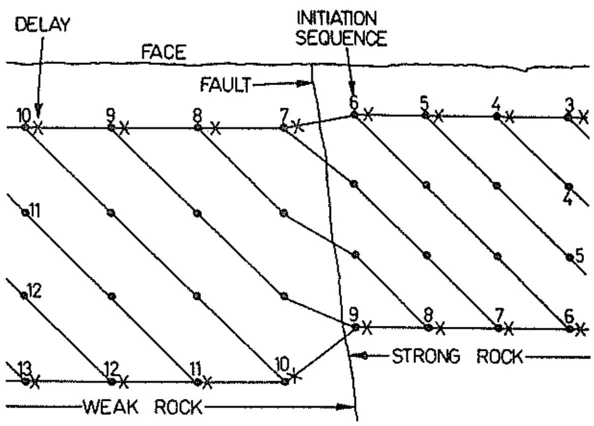

Fig 8 - The type of blasthole pattern change (at contact) which should be avoided

5.2 Overburden Blasts in Surface Coal Mines

Where overburden characteristics are relatively constant from top to bottom of the face, blastholes are usually stopped at or just above the overburden /coal contact, and continuous column charges are normally employed. If soft beds lie immediately above the coal, blastholes can sometimes be bottomed at the base of the lowest hard bed.

Where hard strata occur only at the base of the bench, a single column charge in the bottom of the blasthole is generally used. As the thickness of such hard strata becomes a smaller percentage of face height, however, horizontal blastholes become increasingly attractive.

Where the only hard band lies between softer beds, most effective blasting results are obtained by locating the charge

1. totally within the hard band or
2. within and just below the band.

These charges should be initiated at the points shown in Figs. 9 and 10. This priming geometry ensures that the resultant strain wave intensity in the band is maximised through superposition of waves from those charge elements which are equidistant from the primer. In large diameter blastholes, where standard 450g cast primers cause relatively long run-up velocity regimes in ANFO, it may well be cost effective to increase the strain energy concentration in the band by locating high-energy, fully slumpable water gel booster charges both below and above the primer. The selected water gel

1. should not be side-initiated by the downline (as this method of initiation increases heave energy at the expense of strain energy) and

2. should attain its steady-state velocity within the shortest possible distance from the primer.

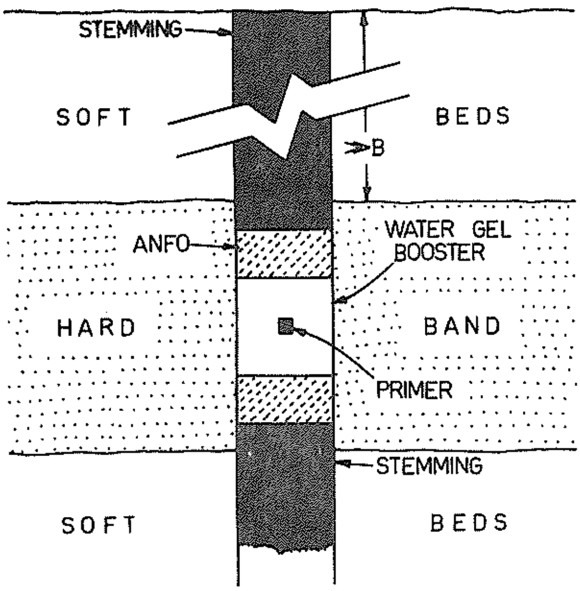

Fig 9 - Charge/priming geometry for thick hard band or thin hard band at depth

Because explosion gases should be retained at their initially high pressures within the hard band for the longest possible time, it is important to increase the efficiency of stemming material both above and below the charge. If the type and/or length of stemming is unsuitable, gases will rapidly escape into the weaker adjacent beds, thereby causing a relatively rapid reduction in blasthole pressure. But even where correctly-positioned charges are <u>well</u> stemmed, the spacing of such charges will be restricted by the thickness of the hard bed. This being the case, it is prudent to select the most efficient type of blasthole pattern (viz. a staggered pattern based on an equilateral triangular grid).

5.2.1 Thick hard bands

Totally enclosed charges (see Fig. 9) are most suitable where the hard band is thick and especially where this is a considerable distance from the top of the bench. Thick beds also allow the

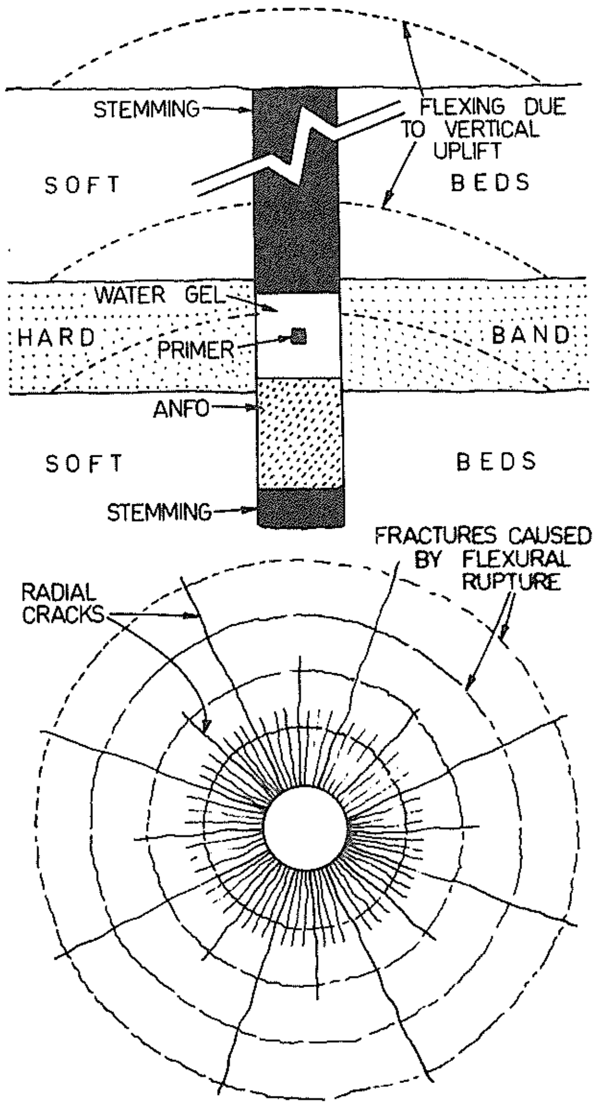

Fig 10 - Recommended charge/priming geometry for thin hard band close to top of bench

effective use of relatively wide blasthole patterns and, hence, larger blasthole diameters.

5.2.2 Thin hard beds at depth

5.2.2.1 Using vertical blastholes

Where a thin hard band lies well below the top of the bench, totally enclosed charges should be used (see Fig. 9). Whatever improvements are incorporated into blast design, such bands can be finely broken only by drilling a relatively close pattern of blastholes. For this reason, large diameter blastholes should be employed

1. only when small diameter blastholes cannot be drilled or are more expensive to drill or
2. where large bucket dimensions reduce the need for a high degree of fragmentation.

Where the distance between blastholes increases beyond about twice the thickness of the band, the upper size range of the fragmented band is relatively insensitive to variations in the diameter or weight of each charge; further increases in blasthole diameter and, hence, charge weight tend to cause greater deformation and disruption of the softer beds alongside rather than reduce the dimensions of the largest fragment in the band. This effect is important where it is necessary to break up a massive band which lies in softer matrices being worked by bucket wheel excavators. Where a 2m thick band of massive sandstone is to be blasted to produce fragments no longer than 1m, for example, patterns larger than 4m x 4m cannot be expected to give satisfactory results. Such a 4m x 4m pattern would be quite adequately drilled out with blastholes having a diameter of 125mm or less. Larger diameter blastholes would have no technical (or, in most cases, economic) advantage.

5.2.2.2 Using horizontal blastholes

Because they overcome the need to drill through softer strata in order to penetrate the hard band, horizontal blastholes may well be more efficient than vertical blastholes. But even where it is possible to drill horizontal blastholes, the charging of these is considerably more difficult than for vertical blastholes. If long horizontal blastholes are attempted, the drill bit may sag or "wander"; the base of the charge would then be nearer to the bottom than the top of the band. This, of course, would result in less uniform breakage and a greater proportion of larger rock fragments.

Where blasthole length is restricted to prevent such deviations, it may not be possible to keep drilling and blasting operations sufficiently far ahead of the digging equipment. Even where drilling and digging can be well co-ordinated, the diameter of horizontal blastholes is restricted by the thickness of the band. In the ideal case shown in Fig. 11, for example, propagation of radial cracks A,B,C, and D will be retarded as soon as cracks E,F,G, and H intersect contacts WX and YZ and allow high-pressure gases to stream into the weaker strata. Where these softer beds are highly compressible, propagation of cracks A,B,C and D may well be arrested abruptly.

If depth below the horizontal free face prevents upward flexing of the band, charges should be initiated in a delayed sequence so that additional breakage (in vertical planes) is encouraged by flexing in a horizontal plane (see Fig. 12).

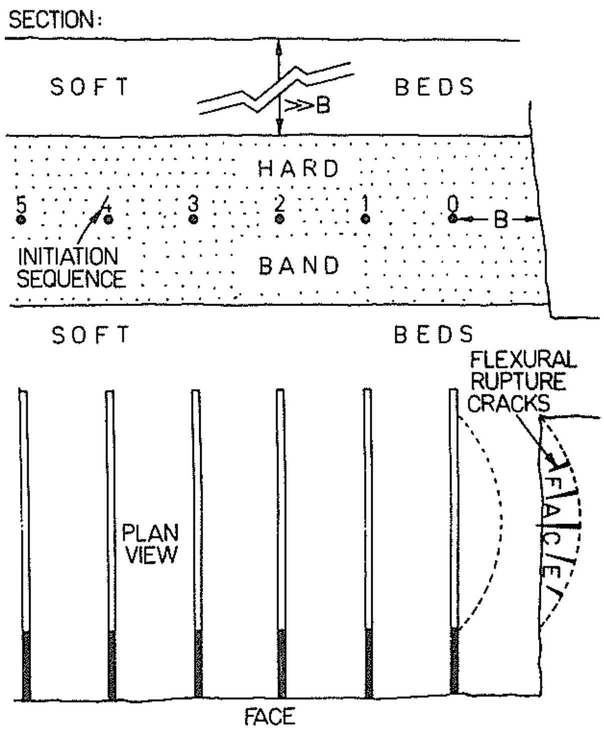

Fig 12 - Breakage of thin hard band at depth by flexural rupture using horizontal blastholes

5.2.3 Thin hard bands near the surface

Where a thin hard band lies relatively close to the top of the bench, the charge should be located both within and immediately below the band (see Fig. 10). The enclosed section of the charge creates a radial crack pattern within the band. These cracks are supplemented by cracks created by flexing of the band due to vertical uplift (see Fig. 10). The amount of flexural breakage increases with the weight of charge beneath the band.

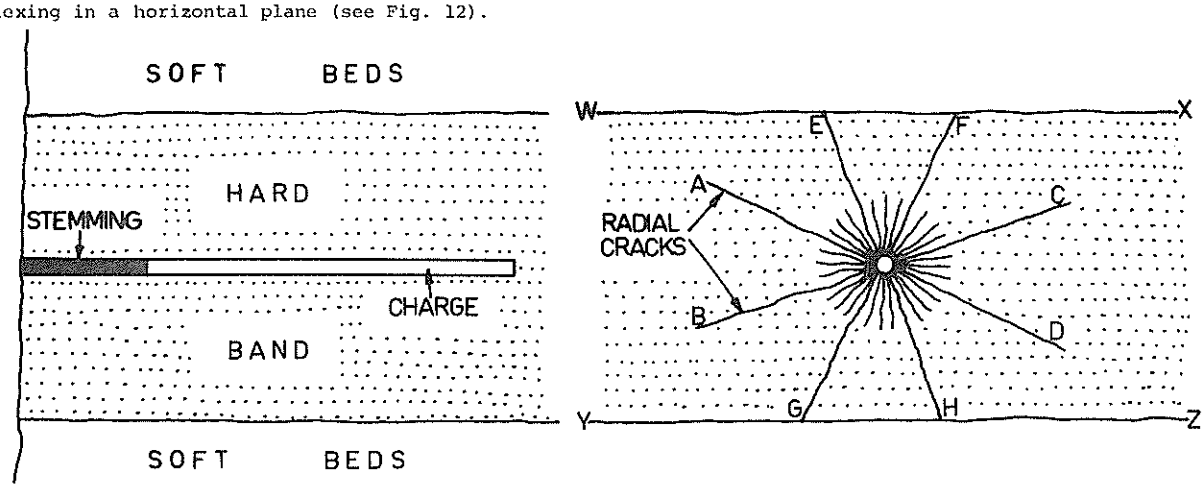

Fig 11 - Premature termination of radially-propagating cracks at contact planes above and below a horizontal blasthole

5.3 Quarry Blasts

In some quarries, hard basalt flows overlie relatively soft clays. If blastholes are drilled completely through the basalt and then charged such that the base of the explosive column is at the basalt/clay contact, explosion gases stream into a rapidly expanding cavity in the clay (see Fig. 13a). The rate of expansion is encouraged by bottom priming and by increases in both the plasticity and porosity (up to 50%) of the clay. Because blasthole pressure falls at an unacceptably high rate, fragmentation and displacement of the basalt are usually far from satisfactory.

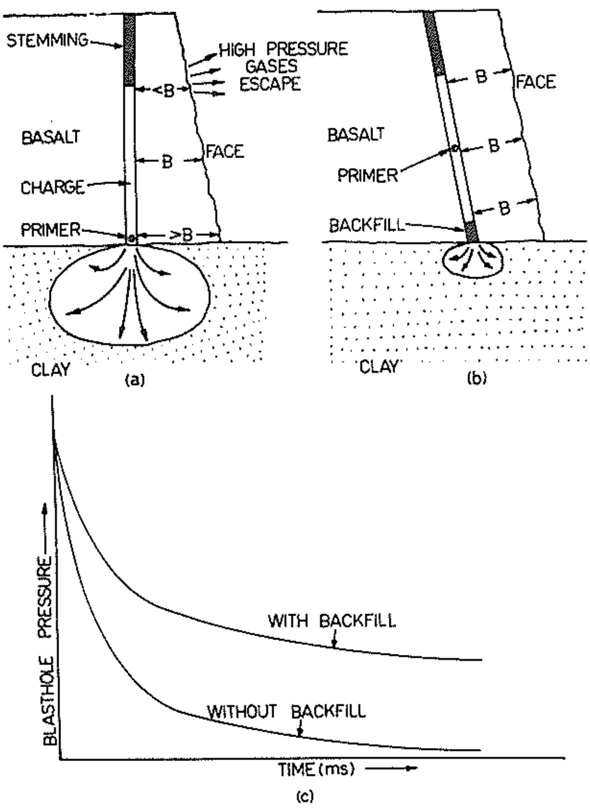

Fig 13 - Plastic deformation of clay beneath basalt flow and associated blasthole pressure-time curves

Improved blasting results are achieved

1. by bottoming blastholes a nominal selected distance above the basalt/clay contact or
2. by drilling to the contact and then backfilling a suitable length of the blasthole with an efficient stemming material (e.g. graded angular crushed rock) before charging (see Fig. 13b).

This will maintain high pressures within the blasthole for a longer period of time (see Fig. 13c) and will reduce energy losses associated with plastic deformation of the clay. Energy losses can be further reduced and muckpile characteristics enhanced by taking the following action.

1. Use a fully-coupled explosive having high detonation velocity and a high strain energy: heave energy ratio.

2. Initiate the charge at its centre (see Fig. 13b), so that the upper and lower halves undergo simultaneous axial detonation (thereby increasing the resultant strain wave intensity through superposition).

3. Prevent premature escape of explosion gases to atmosphere by ensuring that the length of stemming column and the upper burden distance have satisfactory values. Wherever possible, graded angular crushed rock should be used as stemming, the length of the column being at least 20 blasthole diameters. In high and/or shallow-dipping faces, angled blastholes are often necessary if inadequate upper burden distances are to be avoided (see Fig. 13b).

Similarly, where a charge is located totally within a soft seam, the soft material

1. causes considerable attenuation of the explosion-generated strain wave, and
2. is rapidly compressed thereby allowing the blasthole pressure to fall at an excessive rate.

This tends to result in expanding the blasthole to a much larger effective diameter, but with little breakage taking place beyond the soft seam (see Fig. 14).

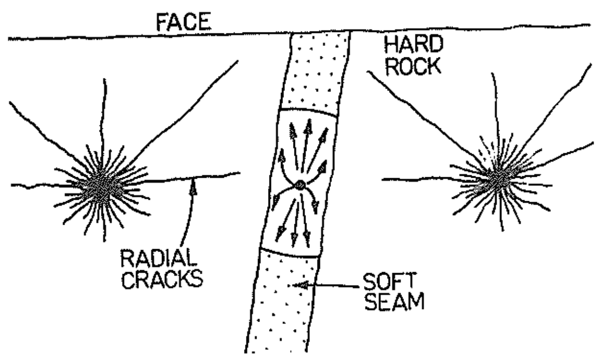

Fig 14 - Poor blasting performance of a charge located within a soft seam

6 CONCLUSIONS

The heterogeneity of rock has a major influence on both the design and results of blasting. Unless the effects of the many structural features of rock are understood and considered when selecting blast parameters, much of the explosive's energy will fail to contribute to the desired muckpile characteristics.

When intersected by blastholes, large vughs can cause charging problems and/or inadequate energy distribution. Whether they are adjacent to or intersected by a blasthole, vughs encourage excessive rates of decay of explosion gas pressures. These are manifested as poor fragmentation and displacement of the rock around the vugh. Although the influence of vughs cannot always be overcome, problems are often minimised by adjusting the amount and distribution of energy liberated by surrounding charges.

Rocks with high intergranular porosity should be blasted with well-stemmed charges which generate high heave energies. The cost effectiveness of explosives with high detonation velocities and high strain wave energies is usually low, an excessive percentage of energy being dissipated in creating fines.

Open joints and bedding planes arrest the propagation of strain wave-generated fractures. In blocky strata, this usually gives good fragmentation between the blasthole and the discontinuity but inadequate breakage beyond the discontinuity. In highly fissured strata, the suppression of strain wave effects rarely causes a problem, the network of discontinuities being opened up and extended by invading explosion gases.

Best fragmentation is usually obtained where the face is parallel to and on the dip side of principal joints or bedding planes. As the dip flattens, however, the slope of the face tends to follow the dip, and inclined blastholes may become necessary if the toe burdens of front-row blastholes are not to exceed their design distances.

In general, closer wider and more persistent discontinuities cause

1. a decrease in the effectiveness of overbreak control blasting techniques and
2. an increase in the probability of cut-offs.

Where hard massive boulders are embedded in softer, plastic-acting strata, fragmentation of boulders increases with the percentage of boulders within which detonation occurs. Satisfactory breakage may necessitate the reduced blasthole patterns and shorter stemming columns associated with the drilling of smaller diameter blastholes.

Where a sub-vertical fault forms the contact between ore and waste within a blast block, efforts should be made to shoot from the stronger into the weaker rock. If a different blasthole pattern is required beyond the contact, only the spacing should be changed, the burden remaining constant.

When softer overburden strata sandwich a thick hard band or thin hard band at depth, fully coupled charges should be located within the band. These should be initiated at their centres and efficiently stemmed both below and above. In cases where good fragmentation is essential, ANFO charges may need to be boosted by a fully-slumped, high-energy water gel. Thin hard bands near the surface are best broken by extending the charge below the bottom of the band; this allows rupture by upward flexing (i.e. doming) to supplement radial cracking. The spacing of blastholes is always restricted by the thickness of the band. Good fragmentation of thin bands necessitates the use of small blasthole patterns which, in turn, encourage the drilling of small diameter blastholes.

7 ACKNOWLEDGEMENT

The author extends his thanks to ICI Australia Operations Pty Ltd for permission to publish this paper.

8 REFERENCES

ANON., 1978, Hi-Fi Probe in Bore Holes Spots Voids, Coal Age, March, p. 121.

BELLAND, J.M., 1966. Structure as a Control in Rock Fragmentation. Can. Min. Metall, Bull., Montreal, March, p.323.

DUFFY, S., 1979. Savage River Mines Ltd., Personal Communication.

KAUFMAN, I.A., 1971. Simulation of the Structure of a Rock Mass for Investigating the Effect of an Explosion with the Aid of Models Made From Equivalent Materials, Sov. Min. Sci., July-August., p.462.

MATHIESON, R.J., 1979. Hamersley Iron Pty Ltd. (Tom Price Mine), Personal Communication.

The Behaviour of Circular Tanks on Deep Elastic Foundations

J. C. SMALL
Lecturer, School of Civil Engineering, University of Newcastle
J. R. BOOKER
Reader, School of Civil Engineering, University of Sydney
P. G. REDMAN
Research Student, School of Civil Engineering, University of Sydney

1 INTRODUCTION

Cylindrical tanks are widely used for storage purposes. Often they are sufficiently large that they exert considerable pressure on the soil and so induce significant settlement. While the behaviour of circular rafts has been investigated extensively, Borowicka (1963), Habel (1937), Holmberg (1946), Brown (1969), there has been surprisingly little research into the modifications of the raft behaviour induced by interaction with the tank walls. In this paper the behaviour of a cylindrical tank resting on a deep elastic soil is investigated, the important features of the problem are identified by examination of a realistic example. A study of the behaviour, of a uniform tank with equal wall and base thickness, is then presented, for a range of geometric and stiffness parameters.

2 THEORY

It might perhaps be thought that, with the existence of high speed computers and the extensive development of finite element methods, the analysis of cylindrical tanks would be a straightforward matter which could be accomplished using standard finite element codes Smith, (1970). Unfortunately this is not the case, experience with circular rafts, Brown (1969), indicate that considerable care is necessary to obtain reasonably accurate solutions. To illustrate this point a rigid raft has been analysed using a conventional finite element approach. The reaction pressure q_s obtained using the finite element method is compared with the analytic solution in Figure 1 and it is clear that the finite element results, calculated from the nodal forces are inaccurate and oscillate about the correct solution. To overcome this difficulty the semi-analytic technique presented below has been developed. It is essentially a substructure approach, the equations governing the behaviour of the soil, the circular base plate and the cylindrical walls are developed and then combined to obtain the complete response.

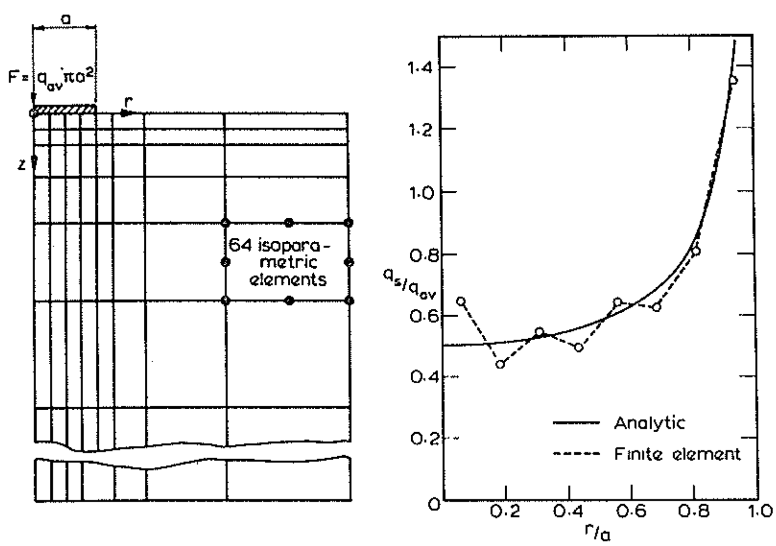

Figure 1 Comparison of finite element and analytic solutions for a rigid raft

2.1 Analysis of Soil

Suppose that a tank of radius, a, rests on a deep (semi-infinite) layer of a homogeneous soil with Young's Modulus E_s and Poisson's ratio ν_s, suppose also that the normal traction, q_s, exerted by the base plate on the soil can be expressed in the form:

$$q_s = \sum_{n=1}^{m} F_n \phi_n(r) \qquad (1)$$

where the coefficients F_n can be considered as generalised forces.

It is convenient to introduce the generalised deflections δ_n defined by

$$\delta_n = \int_0^a r\,\omega(r)\,\phi_n(r)\,dr \qquad (2)$$

where $\omega(r)$ is the deflection of the soil surface.

It may be shown using the theory of elasticity, that the relation between generalised forces and deflections may be expressed in the form

$$\underset{\sim}{\delta} = C\underset{\sim}{F}$$

where $\underset{\sim}{\delta} = (\delta_1, \ldots, \delta_m)^T$

$\underset{\sim}{F} = (F_1, \ldots, F_m)^T$

and C is the generalised flexibility matrix with coefficients

$$C_{mn} = \frac{2(1-\nu_s^2)}{E_s} \int_0^\infty \Phi_m(\alpha)\,\Phi_n(\alpha)\,d\alpha \qquad (4)$$

where $\Phi_m(\alpha) = \int_0^\infty r\,J_o(\alpha r)\,\phi_m(r)\,dr$

Brown (1969) has shown that a suitable set of functions $\{\phi_n\}$ is $\{(a^2-r^2)^{\frac{1}{2}}, 1, (a^2-r^2), (a^2-r^2)^2 \ldots\}$. In this investigation it was only found necessary to use the first six terms of this sequence.

2.2 Analysis of Tank Base

The tank base is assumed to be a circular plate of radius a and rigidity D_p which is subjected to an applied normal traction q_A. The tank will be acted on by a pressure $q_p = q_A - q_s$ and a moment, M_e, induced by the presence of the tank walls (it will be assumed that radial deflections of the base plate may be neglected). It may be shown that the deflected shape the plate $\omega(r)$ is given by

$$\omega(r) = \omega_o + \int_0^a r_o G(r,r_o)\,q_p(r_o)/D_p\,dr_o$$
$$+ M_e r^2/(2D_p(1+\nu_p)) \qquad (5)$$

where ω_o is the central deflection and ν_p is Poisson's ratio of the plate and

$$G(r,r_o) = \frac{r_o^2}{4}\left(1+\log\frac{r}{r_o}\right) + \left(\frac{1-\nu_p}{1+\nu_p}\right)\frac{r^2 r_o^2}{8a^2} \qquad r \leq r_o$$
$$G(r,r_o) = \frac{r^2}{4}\left(1+\log\frac{r_o}{r}\right) + \left(\frac{1-\nu_p}{1+\nu_p}\right)\frac{r^2 r_o^2}{8a^2} \qquad r_o \leq r \qquad (6)$$

Equations (1,2,5) lead to the flexibility relation

$$\underset{\sim}{\delta} = -H\underset{\sim}{F} - \underset{\sim}{\beta}M_e + \underset{\sim}{\alpha}\omega_o + \underset{\sim}{\gamma}$$
$$a\theta_e = -\underset{\sim}{\beta}^T\underset{\sim}{F} - \frac{a^2}{D_p(1+\nu_p)}M_e + S \qquad (7)$$
$$0 = \underset{\sim}{\alpha}^T\underset{\sim}{F} + \frac{P_A}{2\pi}$$

where θ_e is the edge rotation and

$$H_{mn} = \frac{1}{D_p}\int_0^a\int_0^a r r_o\,G(r,r_o)\,\phi_m(r_o)\,\phi_n(r)\,dr\,dr_o$$

$$\gamma_m = \frac{1}{D_p}\int_0^a\int_0^a r r_o\,G(r,r_o)\,\phi_m(r)\,q_A(r_o)\,dr\,dr_o$$

$$\left(\frac{P_A}{2\pi}, S\right) = \int_0^a \left(r_o\,,\ \frac{r_o^3}{2D_p(1+\nu_p)}\right) q_A(r_o)\,dr_o$$

$$(\alpha_m, \beta_m) = \int_0^a \left(r_o\,,\ \frac{r_o^3}{D_p(1+\nu_p)}\right)\phi_m(r_o)\,dr_o$$

2.3 Analysis of Tank Wall

The tank wall is assumed to be a cylindrical shell of height d, thickness t_w and radius a, with a Young's modulus E_w and rigidity D_w, which is subjected to a pressure which increases linearly from zero at the top of the tank to γd at the base. Integration of the governing differential equations (Timoshenko Woinowsky-Krieger (1959)) can then be used to establish that for shells of practical properties

$$\theta_e = \frac{M_e}{2D_w\zeta} + \frac{\gamma d^2}{E_w t_w}(1-\zeta d) \qquad (8)$$

where $\zeta^4 = \dfrac{t_w E_w}{4a^2 D_w}$

2.4 Analysis of the Soil-Base-Wall System

Assuming that compression of the base plate can be neglected and that the wall-plate joint is rigid, the behaviour of the soil, base, and tank wall (equations (3,7,8)) may now be combined to obtain the following equations governing the combined system

$$\begin{bmatrix} \underset{\sim}{A}, & \underset{\sim}{\beta}, & -\underset{\sim}{\alpha} \\ \underset{\sim}{\beta}^T, & b, & 0 \\ -\underset{\sim}{\alpha}^T, & 0, & 0 \end{bmatrix} \begin{bmatrix} \underset{\sim}{F} \\ M_e \\ \omega_o \end{bmatrix} = \begin{bmatrix} \underset{\sim}{\gamma} \\ c \\ -\frac{P_A}{2\pi} \end{bmatrix} \qquad (9)$$

where $A = H + C$

$$b = \frac{a^2}{D_p(1+\nu_p)} + \frac{a}{2D_w\zeta}$$

$$c = S - \frac{\gamma a^3(1-\zeta d)}{E_w t_w}$$

EXAMPLES:

The first example is of a water storage tank constructed with walls of constant thickness, and founded on a deep uniform clay layer. The following properties, and dimensions were chosen for the tank-soil system:-

Unit weight of fluid	γ	=	9.81 kN/m^3
Depth of tank	d	=	7.5 m
Radius of tank	a	=	9.0 m
Thickness of walls	t	=	360 mm

Elastic modulus of tank E_p = 1.4×10^4 MPa
Elastic modulus of soil E_s = 20 MPa
Poisson's ratio of tank ν_p = 0.3
Poisson's ratio of soil ν_s = 0.4

Results of the analysis are plotted in Figures 2-5 which show the radial moment resultant M_R (Figure 2), the thrust resultant N_θ (Figure 3) the reaction distribution (Figure 4) and the base deflection w (Figure 5) for the tank walls and base. This analysis shows that the most important quantities are the radial moments which occur at the centre and edge of the tank base, these moments having opposite signs. Also of importance is the maximum tensile force resultant in the wall, N_θ, which occurs at some distance from the base of the wall.

In order to allow rapid determination of some of the important quantities required in the design of reinforced concrete water tanks, non-dimensional plots are presented for a range of geometric and stiffness parameters. In all cases it is assumed that $\nu_p = \nu_w = 0.3$ and that the top of the tank wall is pinned. It is found that for a tank with uniform wall and base (i.e. same thickness and elastic modulus) that the results depend upon three parameters, K, $\frac{d}{a}$, $\frac{a}{t}$ where

$$K = \frac{E_p}{E_s}(1 - \nu_s^2)\left(\frac{t}{a}\right)^3$$

(E_p, E_s, t, a, ν_s have been defined previously).

Figure 6 shows the edge moment resultant, M_e (i.e. moment/unit length) for various radius to thickness ratios a/t, and values of K. The edge moment is not very sensitive to the d/a ratio, values of d/a = 1, 2 giving coincident values in this figure. A similar plot may be made for the central moment resultant M_c (see Figure 7). Differential deflections in the base of the tank are shown in Figures 8-10, for various values of K. Ratios of d/a again have little influence on results for differential deflections. The central or maximum deflection of the tank base ω_0 is given in Figure 11 for various a/t ratios, and values of K.

Finally values of the maximum tensile force resultant N_θ in the walls is presented in Figure 12 for various value of K, and a/t ratio. Curves are presented for d/a values of 1, 2.

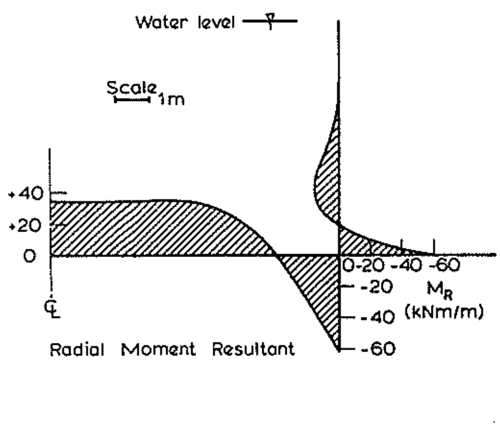

Figure 2 Radial moment resultant

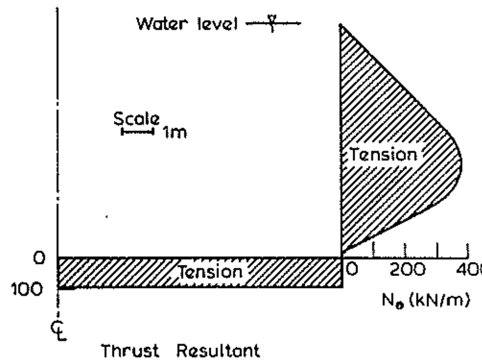

Figure 3 Thrust resultant

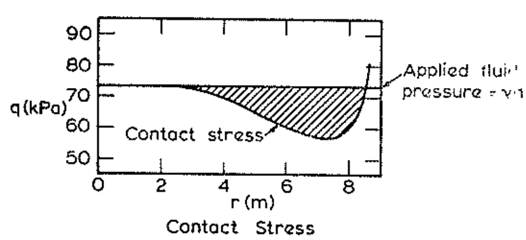

Figure 4 Contact stress

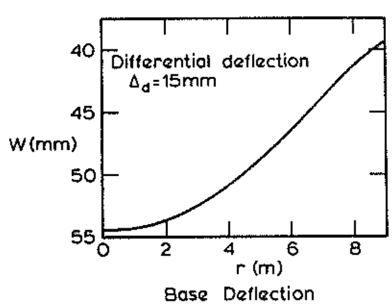

Figure 5 Base deflection

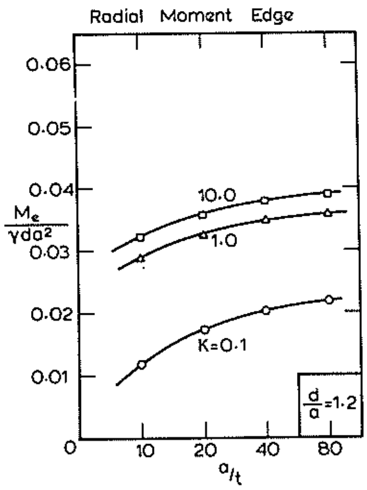

Figure 6 Radial moment - edge

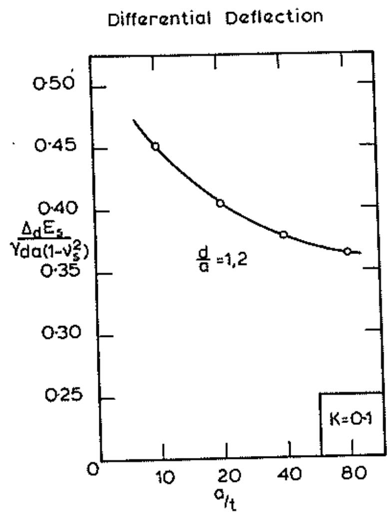

Figure 8 Differential deflection K=0.1

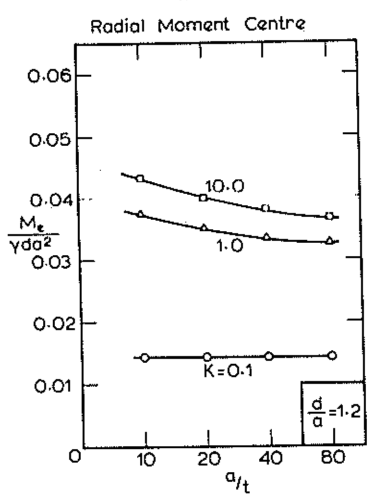

Figure 7 Radial moment - centre

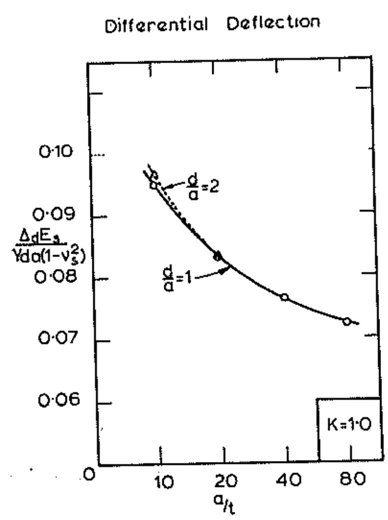

Figure 9 Differential deflection K=1.0

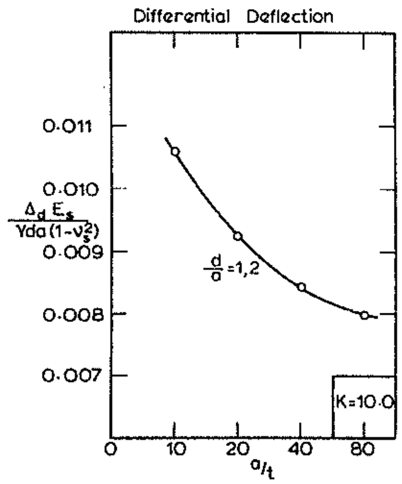

Figure 10 Differential deflection K=10.0

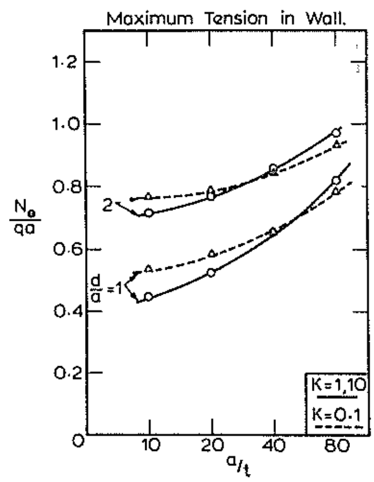

Figure 12 Maximum wall tension

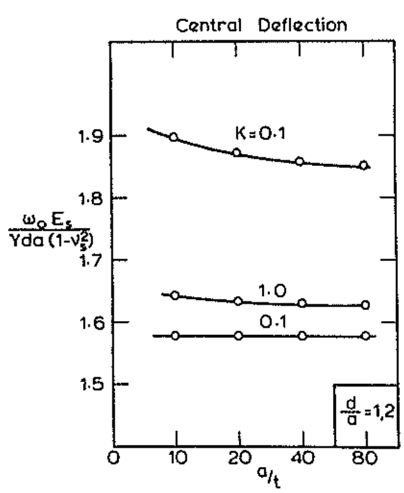

Figure 11 Central deflection

4 CONCLUSIONS

A semi-analytic technique for the analysis of the behaviour of a cylindrical tank resting on a deep clay layer has been presented. The method has been used to analyse a realistic problem and to perform a parametric study of a homogeneous tank having base and walls having equal thickness.

The method can easily be extended to include situations in which the tank wall is tapered or stepped and the effects of only partial filling of the tank.

5 REFERENCES

BOROWICKA, H. (1936). Influence of rigidity of a circular foundation slab on the distribution of pressures over the contact surface. Proc. First Int. Conf. Soil Mech. and Found. Engineering, p. 144.

BROWN, P.T. (1969). Numerical analyses of uniformly loaded circular rafts on deep elastic foundations. Geotechnique, Vol. 19, pp. 301-306.

HABEL, A. (1937). Die auf dem elastisch-isotropen Halbraum aufruhende zentral-symmetrische belastete elastische Kreisplatte. Der Bauingenieur, Vol. 18, No. 15/16, p. 188.

HOLMBERG, A. (1946). Cirkulära plattor med, fördelad last pa elastiskt underlag. Betong, No. 1, p. 7.

SMITH, I.M. (1979). A finite element approach to elastic soil-structure interaction. Canadian Geotech. Jl., Vol. 7, No. 2.

TIMOSHENKO, S.P. and WOINOWSKY-KRIEGER, S. (1959). Theory of plates and shells, McGraw-Hill Book Company, New York.

Prediction of Structure-Foundation Interaction Behaviour

S. J. HAIN
Lecturer in Civil Engineering, The University of New South Wales
I. K. LEE
Professor of Civil Engineering, The University of New South Wales

SUMMARY. An examination of the influence of interaction between a three dimensional frame structure and a raft foundation. The effect on column loads, raft differential settlement and maximum positive and negative bending moments is considered for 3 bay and 5 bay multistorey structures. The supporting soil is considered to be an isotropic perfectly elastic continuum with either a constant modulus or a modulus which increases linearly with depth.

Results of the analyses are presented in terms of two relative stiffness parameters in such a way that predictions of interaction behaviour for a wide range of structure and raft conditions can be made. The graphs show under what conditions interaction can reasonably be ignored or when a full interaction analysis will be required.

1. INTRODUCTION

The designer has two basic problems to consider in the design of a raft foundation for a framed structure. Firstly the total and differential settlements of the foundation must be predicted and compared to the allowable settlements that the structure can withstand. Secondly the distribution of bending moment within the raft must be predicted so that the detailed structural design can be completed.

Traditional methods (Teng, 1962) for calculating settlements and bending moments of raft foundations ignore the influence of the structure thus implying that the forces transmitted to the raft are independent of the differential settlements of the system. Recent studies have shown that for certain situations this is not the case and structure-foundation interaction should be considered (Lee and Brown, 1972) and (Hain and Lee, 1974). The extent to which interaction causes a redistribution of forces will depend on the stiffness characteristics of the frame structure, the raft and the supporting soil. Thus it is essential that the designer have at his disposal a means of readily assessing the stiffness characteristics of these three components and thus predicting the interaction behaviour.

Meyerhof (1953) suggested a means of evaluating the combined stiffness of the structure and the raft which he then compared to the stiffness of the supporting soil to give one relative stiffness parameter. The influence of structure foundation interaction could then be assessed using behaviour of a uniformly loaded raft of stiffness equal to the combined structure and raft. This approach was subsequently adopted by the A.C.I. Committee 436 (1966) for their recommendations regarding raft foundation design and the influence of structure-foundation interaction. However, this simplified approach can be shown to lead to an overprediction of differential settlement and raft bending moments.

Brown (1975) examined the behaviour of a multibay plane frame on a strip foundation in terms of three relative stiffness parameters. The results enable an assessment of the likely influence of interaction for a two dimensional situation; however they may not always be reliable for the three dimensional situation involving a raft foundation. Hain (1977) has shown that a two dimensional analysis which neglects twisting moments in the raft and the redistribution of load that occurs between frames can lead to significantly different results to a three dimensional analysis which considers these aspects.

The present paper presents the results of a series of three dimensional analyses of a multibay multistorey space frame supported on a raft foundation. The system is described by two relative stiffness parameters and the results are presented in such a way that the designer can readily follow the trends in behaviour and therefore predict the likely effects of structure foundation interaction.

2. NOTATION

a = thickness of shear wall

B_R = width of the raft foundation

E' = Young's modulus of the materials used in the structure

E_L = Young's modulus of the supporting soil layer at a depth of $L_R/2$

E_o = Young's modulus of the supporting soil layer at the surface

E_o^* = $E_o/(1 - \nu_s^2)$

E_s = Young's modulus of the supporting soil layer at depth

h = height of shear wall

h_ℓ = storey height of lower columns at sto[illegible] j

h_u = storey height of upper collumns at st[illegible]

i = frame number

I_b = moment of inertia of the beam at storey j

I_b' = effective moment of inertia of the beam at storey j

I_ℓ = moment of inertia of lower columns at storey j

I_u = moment of inertia of upper columns at storey j

j = storey number

K_b = I_b/ℓ = stiffness of the beam at storey j

$(K_f)_i$ = effective stiffness of frame i

K_ℓ = I_ℓ/h_ℓ = stiffness of the lower columns of storey j

K_R = stiffness of the raft foundation per unit width compared to the stiffness of the supporting soil

K_S = stiffness of the structure per unit width compared to the stiffness of the supporting soil

K_T = $K_S + K_R$ = total stiffness of the structure and raft compared to the supporting soil

K_u = I_u/h_u = stiffness of the upper columns of storey j

ℓ = bay length of frame i

L_f = total length of frame i

L_R = length of the raft foundation

n_f = number of structural frames spaced across the foundation width B_R

n_s = number of storeys in the structure

t_R = thickness of the raft foundations

ν_s = Poisson's ratio of the supporting soil

3. INTERACTION ANALYSIS

The interaction analysis used in this analysis is based on the substructuring method and has been presented by Hain (1977). The components of the system have been modelled as follows:-

(i) the supporting soil is represented by an isotropic perfectly elastic continuum of infinite extent with either a constant modulus or a modulus which increases linearly with depth.

(ii) the raft foundation is represented by an assemblage of thin plate bending finite elements (Zienkiewicz, 1971).

(iii) the structure is represented by a three dimensional assemblage of beam elements according to traditional methods of structural analysis.

Figure 1 shows a simplified two dimension representation of the problem considered. Two multistorey structures, 3 bays and 5 bays in both directions, were considered for uniformly distributed floor loadings on every storey. Two supporting soil conditions, homogeneous and linearly increasing modulus with depth such that $E_L/E_o = 2$, were also considered. For these cases analyses covering the practical range of structure, raft and supporting soil stiffnesses were performed.

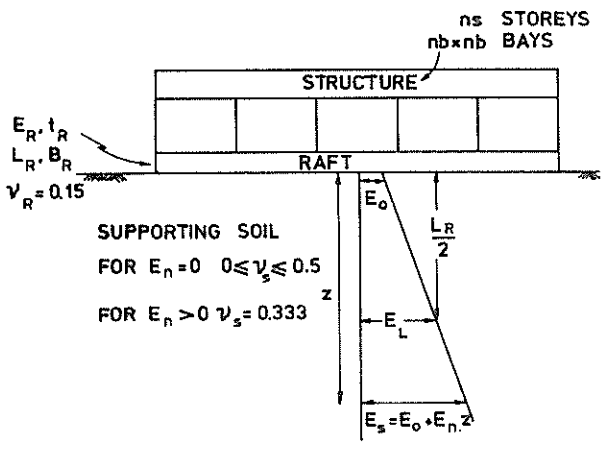

Figure 1. The problem analysed

4. RELATIVE STIFFNESS PARAMETERS

The problem can be described by three independent parameters - the structure stiffness, the raft stiffness and the supporting soil stiffness. From these two independent relative stiffness parameters were selected as follows:-

$$K_R = \frac{\text{stiffness of the raft foundation per unit width}}{\text{stiffness of the supporting soil}} \tag{1}$$

$$K_S = \frac{\text{stiffness of the structure per unit width}}{\text{stiffness of the supporting soil}} \tag{2}$$

A third parameter, the combined stiffness of the structure and raft compared to the supporting soil, was given by:-

$$K_T = K_S + K_R \tag{3}$$

The parameters K_R and K_S, can be calculated from:-

$$K_R = \frac{4\ E_R\ B_R\ t_R^3\ (1 - \nu_S^2)}{3\ .\ \pi\ .\ E_o\ .\ L_R^4} \tag{4}$$

$$K_S = \frac{\sum_{i=1}^{i=nf} \frac{(K_f)_i}{B_R}}{E_o^*\ .\ L_R^3} \tag{5}$$

Meyerhof (1953) suggests the following approximate expression for the stiffness of a f[illegible] subjected to differential settlement of the colum[illegible]s.-

$$(K_f)_i = \sum_{j=1}^{j=ns} \left(E'I_b' + \frac{E'.ah}{12}\right)_j \tag{6}$$

$$\text{where } I_b' = I_b\ .\ \left[1 + \frac{K_\ell + K_u}{K_b + K_\ell + K_u}\ .\left(\frac{L_f}{\ell}\right)^2\right]$$

5. DISCUSSION OF RESULTS

The relative stiffness parameters defined in equations (1) and (2) allow the examination of the total system stiffness as well as the distribution of stiff -ness between the structure and the raft. Analyses were performed for K_T = 10.0, 1.0, 0.1, and 0.01 for K_S/K_R values covering the range 0.01 to 100.0.

5.1 Column Loads

Figures 2 and 3 show the results in terms of the column loads for various ratios of K_S/K_R when K_T = 1.0. Actual column loads have been normalized with respect to the average column load and curves are shown for the corner column, the average of all the edge columns and the average of all the interior columns. When K_S/K_R tends towards 0.01, the distribution of column loads approaches the rigid raft (zero differential settlement) conditions. As K_S/K_P increases, interaction leads to a transfer of load from interior columns to edge and corner columns and the perfectly flexible raft condition is approached. Most of the redistribution of column loads occurs within the region $0.1 < K_S/K_R < 10.0$ and thus this would appear to be the area where an interaction analysis may be necessary. For values of K_T within the range 0.1 to 10.0 the interaction results were found to be virtually identical to results shown in Figures 2 and 3. For $K_T = 0.01$ there was significantly less redistribution of column load as this

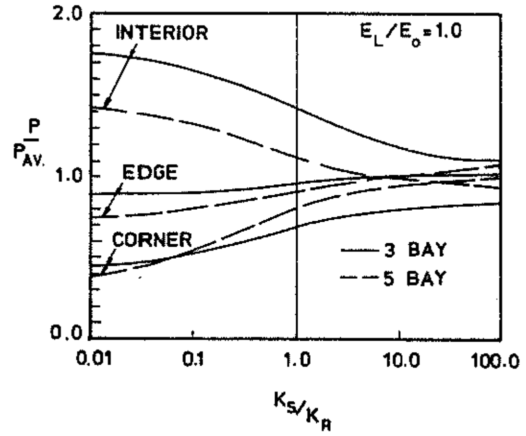

Figure 2. Column Loads for $K_T = 1.0$ when $E_L/E_o = 1$

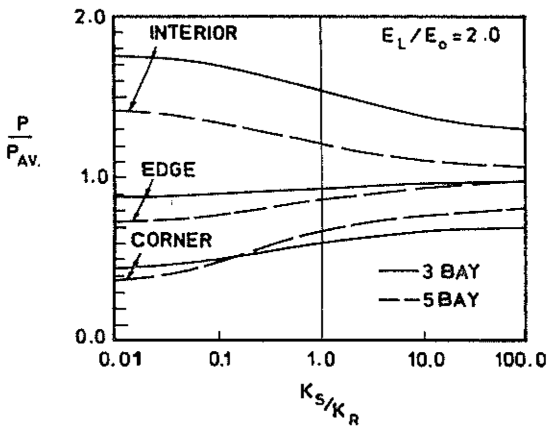

Figure 3. Column Loads for $K_T = 1.0$ when $E_L/E_o = 2$

situation represents a very stiff supporting soil. As could be expected the stiffer non-homogeneous supporting soil leads to a reduction in column load redistribution compared to the homogeneous case.

5.2 Differential Settlement

The differential settlement presented is the maximum differential settlement which occurs between the corner column and the interior column closest to the centre of the raft. Figures 4 and 5 show the variation of raft differential settlement for $K_T = 1.0$ and various K_R values.

The maximum differential settlement obtained when only the raft is analysed is shown as the CCL (constant column load) result. The constant column loads applied to the raft were determined from a zero differential settlement analysis of the structure. The importance of the CCL result is that all interaction results will converge to this result as K_S tends to zero.

The results indicate that providing the structure is at least as stiff as the raft, i.e. $K_S > K_R$, then the maximum differential settlement is determined by the total system relative stiffness, K_T, independent of the raft relative stiffness, K_R. This differential settlement is always of the order of 50% of

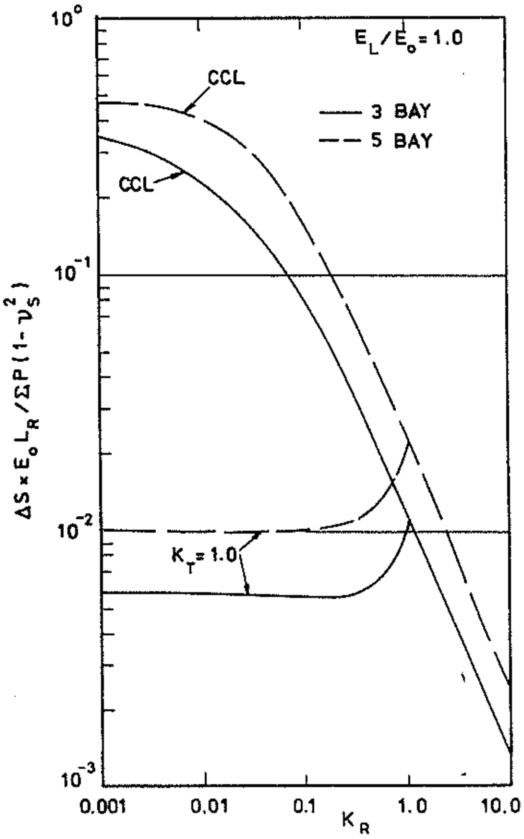

Figure 4. Raft differential settlement for $K_T = 1.0$ when $E_L/E_o = 1$

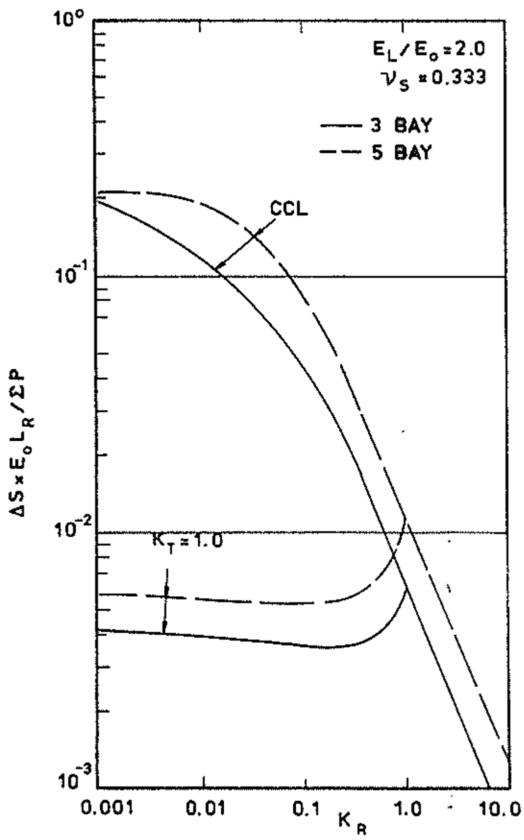

Figure 5. Raft differential settlement for $K_T = 1.0$ when $E_L/E_o = 2$

the maximum differential settlement of a raft without a structure of the same stiffness as the actual structure and raft. Indicating the effectiveness of the structure in reducing differential settlements because it reinforces the raft between those points where the maximum loads, and hence settlements, occur. If the raft is stiffer than the structure, i.e. $K_R > K_S$, then the differential settlement is very sensitive to the ratio K_R/K_T and there is considerable increase in values as this ratio tends towards one. The present value for $K_T = 1.0$ can be used to indicate results for values K_T in the range 0.1 to 10.0. Within this range K_T contours are practically identical in shape and will intersect the CCL curve at the point where $K_T = K_R$.

5.3 Raft Bending Moments

Figures 6 and 7 show the maximum positive raft bending moments for $K_T = 1.0$ as a function of K_R. For the frames considered the maximum positive bending moment occurs at the interior column closest to the centre of the raft. Interaction which redistributes some of this load to the peripheral columns

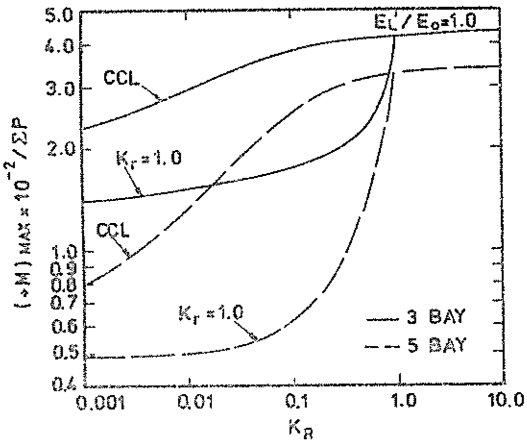

Figure 6. Maximum positive bending moments for $K_T = 1.0$ when $E_L/E_o = 1$

produces a significant reduction in bending moment most of which occurs over the range $0.1 < K_R/K_T < 1.0$. Results for other values of K_T in the range 0.1 to 10.0 can be predicted using the present results. For $0.01 < K_R/K_T < 1.0$ all K_T contours have a similar shape while for $K_R/K_T < 0.01$ all contours asymptote to the same value of maximum bending moment for a given frame and E_L/E_o value. Again the CCL result is shown and it is noted that K_T contours converge onto this result as K_R/K_T tends towards 1. A better appreciation of the reduction in bending moment that occurs when interaction is considered can be obtained from a study of Table 1 which compares interaction bending moments with those obtained from the conventional CCL analysis.

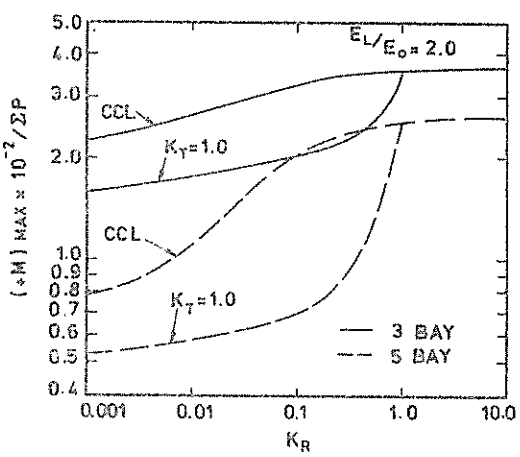

Figure 7. Maximum positive bending moments for $K_T = 1.0$ when $E_L/E_o = 2$

TABLE I

COMPARISON OF RAFT BENDING MOMENTS FOR $K_T = 1.0$ AND $K_R = 0.1$

	3 Bay Frame		5 Bay Frame	
	$\frac{E_L}{E_o} = 1$	$\frac{E_L}{E_o} = 2$	$\frac{E_L}{E_o} = 1$	$\frac{E_L}{E_o} = 2$
No interaction considered (CCL)	100	85	100	78
Interaction considered	46	52	24	27

Figures 8 and 9 show the variation of the maximum negative bending moments for $K_T = 1.0$ as a function of K_R. The maximum negative bending moment occurs

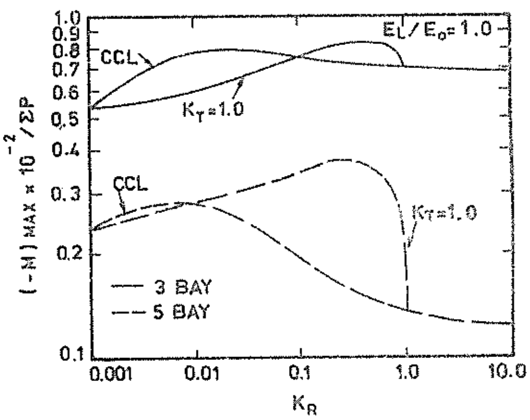

Figure 8. Maximum negative bending moments for $K_T = 1.0$ when $E_L/E_o = 1$

along the line between an edge column and an interior column and is influenced by the size of the edge column load as well as the raft relative stiffness. Interaction between the structure and the raft redistributes load from interior columns to edge columns and hence negative bending moments will increase. For a given K_T value the maximum negative bending moment occurs when the structure and raft relative stiffnesses are equal (i.e. $K_R = K_S$). If K_S is then increased and K_R appropriately reduced, then little additional change in column loads occurs and hence negative bending moments reduce as K_R reduces.

Comparing the curves for the 3 bay and the 5 bay structures in Figures 8 and 9 indicates that although the values are greater for the 3 bay structure, there is a greater range of values for the 5 bay structure. Comparison with Figures 6 and 7 shows that negative bending moments are generally of a similar size to the positive bending moments when interaction is considered.

Results for values of K_T in the range 0.1 to 10.0 can be estimated from the $K_T = 1.0$ curves shown in Figures 8 and 9 by observing the following characteristics. All K_T contours have a similar shape in the range $0.1 < K_R/K_T < 1.0$ with a maximum value when $K_R = K_S$.

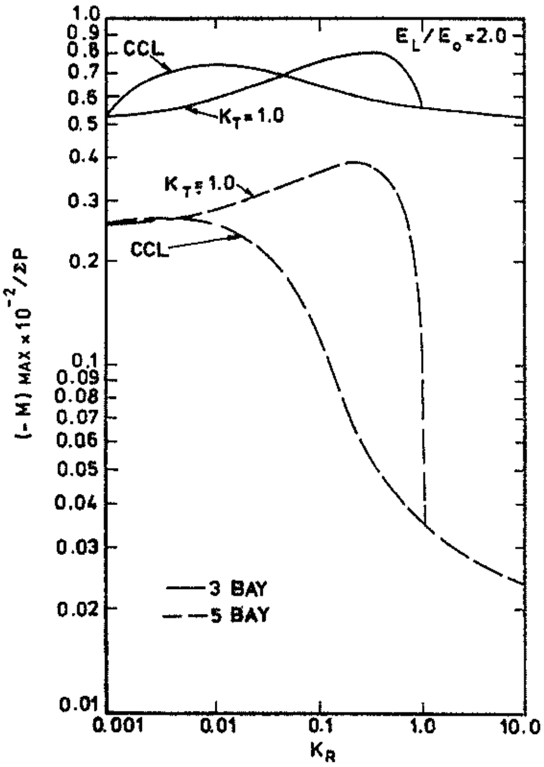

Figure 9. Maximum negative bending moments for $K_T = 1.0$ when $E_L/E_o = 2$

This maximum value is essentially constant regardless of K_T. As K_R tends towards 0.001 the K_T contour asymptotes to the CCL curve.

6. CONCLUSIONS

The interaction behaviour of a three dimensional frame and a raft foundation can be predicted if the relative stiffness of the components is expressed by the parameters presented herein. Consideration of a large number of analyses of 3 and 5 bay frames indicates the following trends:-

(i) most redistribution of column loads occur for $0.1 < K_S/K_R < 10.0$.

(ii) differential settlements of a structure raft system are always less than those for a raft with K_R equal to K_T.

(iii) for a given K_T the larger the value of K_S, then the smaller the maximum positive raft bending moments.

(iv) for a given K_T the largest negative bending moments occur when $K_R \approx K_S$.

(v) differential settlements increase with the number of bays in the structure and reduce as the rate of increase of the soil modulus with depth increases.

(vi) the reduction in maximum positive bending moment that occurs because of interaction increases with the number of bays in the structure and reduces slightly as the rate of increase of soil modulus with depth increases.

(vii) the increase in maximum negative bending moment that occurs because of interaction increases with the number of bays in the structure and reduces as the rate of increase of soil modulus with depth increases.

7. REFERENCES

AMERICAN CONCRETE INSTITUTE (1966). Suggested design procedures for combined footings and mats. Journal of the American Concrete Institute, Vol. 63, No. 10, p. 1041.

BROWN, P.T. (1975). The significance of structure-foundation interaction. 2nd Australia-New Zealand Conference on Geomechanics, Brisbane, pp. 79-82.

HAIN, S.J. and LEE, I.K. (1974). Rational analysis of raft foundation. Journal of the Geotechnical Engineering Division, ASCE, Vol. 100, No. GT7, pp. 843-860.

HAIN, S.J. (1977). A rational analysis for raft and raft-pile foundations. Ph.D. Thesis, The University of New South Wales, Australia.

LEE, I.K. and BROWN, P.T. (1972). Structure foundation interaction analysis. Journal of the Structural Engineering Division, ASCE, Vol. 98, No. ST11, pp. 2413-31.

MEYERHOFF, G.G. (1953). Some recent foundation research and its application to design. Structural Engineer, Vol. 31, part 1, pp. 151-167.

TENG, W.C. (1962). Foundation Design. New Jersey, Prentice-Hall.

ZIENKIEWICZ, O.C. (1971). The Finite Element Method in Engineering Science. London, McGraw-Hill.

Ultimate Load Foundation Design Using Statistically Based Factors

P. A. McANALLY
Lecturer in Civil Engineering, Queensland Institute of Technology

SUMMARY. The results of pile load tests are presented from various sites in stiff fissured clays, with a statistical model of soil response to foundation load. The significance of some deviations in observed pile performance from conditions commonly assumed in design is tested by means of this model. It is shown that the model allows the evaluation of a material response factor for ultimate load design of foundations, and a design example is given.

1 INTRODUCTION

The uncertainties in the bearing capacity performance of foundations lie in the loads which they must carry, the strength response of the founding stratum and the adequacy of the design modelling and analysis.

For foundation loads, the uncertainties in extreme values are the same as those for the design of the supported structure.

There will be uncertainty with respect to the mean value and variability of the strength of a founding stratum, arising from limited sampling in a variable material. There will also be uncertainty with respect to the magnitude of any possible bias between the strength response of the soil at the test specimen and prototype scales. In clays, for example, such bias is often attributed to sampling disturbance or the presence of fissures or other macro-structure.

Estimates of the bearing capacity response of a soil stratum are generally based on an approximate analysis of the performance of a simplified model (eg. a homogeneous, isotropic, semi-infinite medium) and the results of these estimates may be biased with respect to the actual mean response of the stratum.

The uncertainties in bearing capacity are conventionally allowed for in foundation design by dividing the estimated nett ultimate soil resistance by a safety factor to give the maximum safe soil resistance, and hence the maximum safe working load. This procedure lumps all formal uncertainty allowance into the loading. A more rational approach would be provided by ultimate load design, in which uncertainty in loads is allowed for by a load factor and uncertainty in strength properties and due to bias is allowed for by a material response factor.

2 NOTATION

The following are the main symbols used.

c_a ultimate shaft adhesion
c_u undrained cohesion
D base diameter of pile
d shaft diameter of pile
L length of pile
N bearing capacity factor
n,p number of test results
Q load
R soil resistance force
s^2 variance of log property values from test results
t Student's t value
x log value of soil response
y value of soil response
α bias factor
β material response factor
γ load factor
ν degrees of freedom

Subscript notation is defined as it is used in the text.

3 THE STATISTICAL MODEL

The Author has described a statistical model for the undrained strength behaviour of soils which allows the evaluation of a material response factor on the basis of the probability of satisfactory soil behaviour (McAnally, 1977). An outline of the principles of this model are given here.

- The soil zones influenced by individual foundations (referred to as significant units of influence, or sui's) are considered to be composed of a number of smaller units, within each of which strength can be considered to be homogeneous (referred to as equivalent homogeneous units, or ehu's).
- The strength properties of the ehu's are considered to have a log-normal distribution and to vary randomly spatially.
- The strength response of an sui is considered to be related to the strengths of the ehu's within it by

$$y_s = \alpha \, \bar{y}_e \tag{1}$$

where y_s = sui strength response
$\bar{y}_e$ = geometric mean of the strength values of the ehu's in the sui

Conventional strength tests (eg. unconfined or triaxial compression tests) may be considered to be samples from the ehu population, and observations of the bearing capacity response of prototype foundations may be considered as samples from the sui population.

If a set of n_1 conventional strength test results, (log property values having mean $\bar{x}_{e1}$ and variance, s_{e1}^2)+ and a set of p_1 prototype test results, (log property values having mean $\bar{x}_{s1}$ and variance s_{s1}^2) are available, then confident limits for prototype response, y_{s1}, can be found.

$$\alpha\bar{y}_{e1}\exp(-t\phi) < y_{s1} < \alpha\bar{y}_{e1}\exp(t\phi) \qquad (2)$$

where $\phi^2 = s_{s1}^2 + s_{e1}^2/n_1$

$\bar{y}_{e1}$ = geometric mean of the conventional (ehu) test results

t = Student's t value for the confidence coefficient chosen and degrees of freedom, ν_ϕ, given by

+ The variances are computed as the unbiased estimates of the population variances, ie.
$s^2 = \Sigma \dfrac{(x - \bar{x})^2}{n - 1}$

$$\frac{\phi^4}{\nu_\phi} = \frac{(s^2_{s1})^2}{p_1 - 1} + \frac{(s^2_{e1}/n_1)^2}{n_1 - 1} \qquad (3)$$

If a set of n_2 conventional strength test results (log property values having mean $\bar{x}_{e2}$ and variance s_{e2}^2) and a set of p_2 prototype response results (log property values having mean $\bar{x}_{s2}$ and variance s_{s2}^2) are available, then confidence limits for α can be found.

$$a_2\exp(-t\psi) < \alpha < a_2\exp(t\psi) \qquad (4)$$

where $\psi^2 = s_{s2}^2/p_2 + s_{e2}^2/n_2$

$\bar{y}_{s2}$ = geometric mean of prototype response (sui) results

$a_2 = \bar{y}_{s2}/\bar{y}_{e2}$

t = Student's t value for the confidence coefficient chosen and degrees of freedom, ν_ψ, given by

$$\frac{\psi^4}{\nu_\psi} + \frac{(s^2_{s2}/p_2)^2}{p_2 - 1} + \frac{(s^2_{e2}/n_2)^2}{n_2 - 1} \qquad (5)$$

If the bias factor, α, is the same for both pairs of samples, then(2) and (4) may be combined to give confidence limits for y_{s1}, independant of α.

$$a_2\bar{y}_{e1}\exp(-t\omega) < y_{s1} < a_2\bar{y}_{e1}\exp(t\omega) \qquad (6)$$

where $\omega^2 = \phi^2 + \psi^2$

t = Student's t value for the confidence coefficient chosen and degrees of freedom, ν_ω, given by

$$\frac{\omega^4}{\nu_\omega} = \frac{\phi^4}{\nu_\phi} + \frac{\psi^4}{\nu_\psi} \qquad (7)$$

If the geometric mean of the results of a set of conventional strength measurements, $\bar{y}_{e1}$, is chosen as the shear strength design parameter, then a material response factor, β, can be estimated from (6) to cover uncertainties in soil properties and bias in prototype response.

$$\beta = a_2\exp(-t\omega) \qquad (8)$$

Comparison of design on this basis with conventional design on the basis of a safety factor indicates that a confidence coefficient of 0.99 on the lower confidence limit will give a similar probability of failure as a safety factor of 3. (The probability of failure will be much less than 0.01, as both the material response factor and the load factor must be concurrently exhausted for failure to occur).

4 PILE LOAD TEST RESULTS

The results of load tests on a number of cast-in-situ piers and piles in fissured clays have been collected to illustrate the use of this model and provide data for design. The results of site investigation work on these sites are summarised in Table 1. Sites A to F were located in south-eastern Queensland. Sites G and H are the results of deep plate load tests and cast-in-situ pier performance in London Clays reported by Marsland (1971) and Whitaker and Cooke (1965) respectively, which have been included for comparison purposes.

Values of ultimate shaft resistance, R_{u_s}, and nett ultimate base resistance, R_{nu_b}, were determined from the load-deflection plots for the piles from sites A to F, by the method outlined by Whitaker (1970). An example of this determination is shown in Fig. 1.

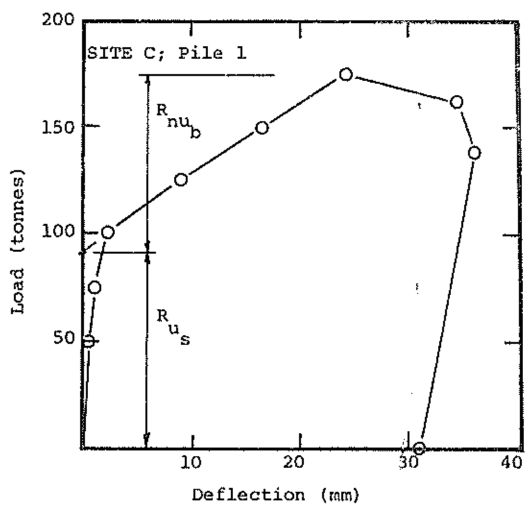

Fig. 1. Typical Pile Load-Deflection Plot Showing Estimation of R_{u_s} and R_{nu_b}

The soil response values for ultimate shaft resistance and nett ultimate base resistance were estimated, for sites A to F, from the common design expressions

$$c_a = R_{u_s}/(\pi dL) \qquad (9)$$

$$c_u = R_{nu_b}/(\frac{9\pi D^2}{4}) \qquad (10)$$

Details of the pile dimensions, and the estimated values of soil response are given in Table 2, for sites A to F. The estimated values of soil res-

TABLE 1

SUMMARY OF SITE INVESTIGATION RESULTS						
SITE	SOIL DESCRIPTION	CLASSIFICATION			STRENGTH	
		w %	L.L. %	P.I. %	Type of Test	Shear Strength (kPa)
A	Stiff mottled grey & brown fissured CLAY (Shaft Zone)	29 - 61	-	-	U(48)	34 - 99+
	Stiff mottled grey & brown fissured CLAY (Base Zone)	43 - 57	-	-	U(48)	46 - 125
B	Stiff to very stiff mottled red, grey & brown fissured CLAY	28 - 49	88 - 91	47 - 48	UC(48)	29 - 99
C	Stiff to very stiff mottled red grey & brown fissured CLAY (Shaft Zone)	21 - 34	80 - 96	59 - 72	UC(48)	35 - 265
	Stiff to very stiff mottled red grey & brown fissured CLAY (Base Zone)				UC(48)	45 - 195
D	Stiff mottled grey & brown fissured CLAY	32 - 43	-	-	UC(48)	25 - 103
E	Stiff mottled grey & brown fissured CLAY	15 - 31	-	-	U (48)	34 - 105
F	Very stiff to hard grey brown fissured CLAY	14 - 27	42 - 80	26 - 63	U(48)	150 - 335
G	Very stiff grey fissured CLAY	-	-	-	U(38)	104 - 240
H	Stiff to very stiff grey to brown fissured CLAY (Shaft Zone)	-	-	-	U(38)	58 - 149
	Stiff to very stiff grey fissured CLAY (Base Zone)	-	-	-	U(38)	75 - 150

* U( ) denotes undrained triaxial test on ( ) mm dia. specimen

UC( ) denotes unconfined compression test on ( ) mm dia. specimen

\+ Residual strengths in sensitive clay

ponse, determined by the methods of 9 and 10, were taken directly from the references for sites G and H.

The statistics for the ehu and sui sample sets for each site are given in Table 3.

5 ANALYSIS OF VARIANCE

Valid use of data from more than one site, in (6), depends upon the condition that the same bias factor applies for all the sites from which the data is drawn. An analysis of variance expression may be developed, as described in Appendix I, to test this hypothesis.

Analysis of variance was made on the ehu and sui statistics from various combinations of sites. The results of this analysis is given in Fig. 2 for shaft adhesion, and in Fig. 3 for nett end bearing resistance.

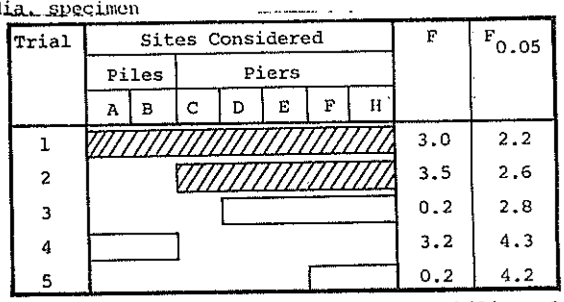

Shaded trials indicate estimated probability of less than 0.05 that α is the same for all sites considered.

Fig. 2. Results of Analysis of Variance for Shaft Adhesion Bias.

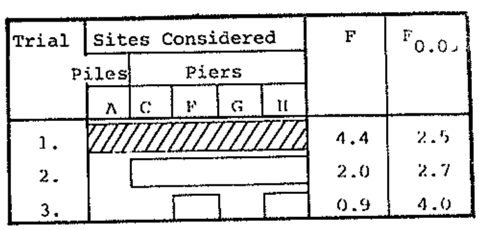

Fig. 3. Results of Analysis of Variance for Nett Base Resistance Bias.

TABLE 2

DETAILS OF PILES AND LOAD TEST RESULTS

Site	Pile No.	Length (m)	Shaft Diam. (m)	Base Diam.* (m)	Soil Response c_a (kPa)	c_u (kPa)
Cast-in-situ Piles (Hammered base and shaft)						
A	1	9.0	0.55	0.75	41.5	108.6
	2	9.0	0.40	0.75	49.4	108.3
	3	7.3	0.40	0.75	53.4	147.9
	4	9.0	0.40	0.86	52.9	110.6
	5	7.0	0.40	0.75	40.0	160.2
B	1	10.0	0.50	0.64	62.4	-
	2	8.7	0.50	0.64	71.7	-
	3	7.0	0.40	0.75	85.3	193.4
Cast-in-situ Piers						
C	1	4.0	0.75	1.0	89.3	123.4
	2	4.0	0.75	1.0	112.3	92.9
D	1	9.0	0.50	0.50	46.1	-
	2	9.0	0.50	0.50	41.6	-
E	1	10.0	0.60	0.60	39.0	115.5
	2	8.4	0.40	0.47	65.0	-
F	1	5.0	0.64	0.64	66.7	114.0
	2	5.0	0.64	0.64	65.7	152.0
	3	5.0	0.64	0.64	60.4	-

* Base diameter of cast-in-situ piles estimated from volume of concrete displaced and assumed spherical shape.

\- Indicates ultimate end bearing resistance not fully developed.

In the design of cast-in-situ piers or piles, the design value of c_a is generally obtained by multiplying the average measured value of undrained shear strength by a factor (less than or equal to one) according to the magnitude of that average value (SAA Piling Code - 1978). The values of $\bar{y}_e$ (=c_a) for shaft adhesion were obtained by reducing the mean of the measured values of c_u by the recommended factors from the SAA Piling Code (Fig. 4). Hence, the bias factor, α, for shaft adhesion will represent bias with respect to the design value of c_a which would be chosen on the basis of this code recommendation. The values of $\bar{y}_e$ (= c_u) for end bearing have been obtained from the actual measured values of undrained cohesion, and hence the bias factor, α, for base resistance will represent bias with respect to the bearing capacity factor of 9 from (10).

A number of observations may be made, in passing, on the results of these analyses.

- The ultimate shaft adhesion developed on bored piers can be significantly higher than the design values which would be chosen from the SAA Piling Code (Fig. 2; Tials 2 and 3, and Fig. 4, with respect to Site C). This is of particular significance in the design of piers in expansive soil, where the development of high values of shaft adhesion can result in high tension stresses in the pier shafts.

- The ultimate shaft adhesion developed on cast-in-situ piles, in which the shaft concrete is compacted by hammering, can be significantly greater than that predicted by the SAA Piling Code and developed on bored pier shafts in many instances (Fig. 2; Trials 1 and 3, and Fig. 4: Site B).

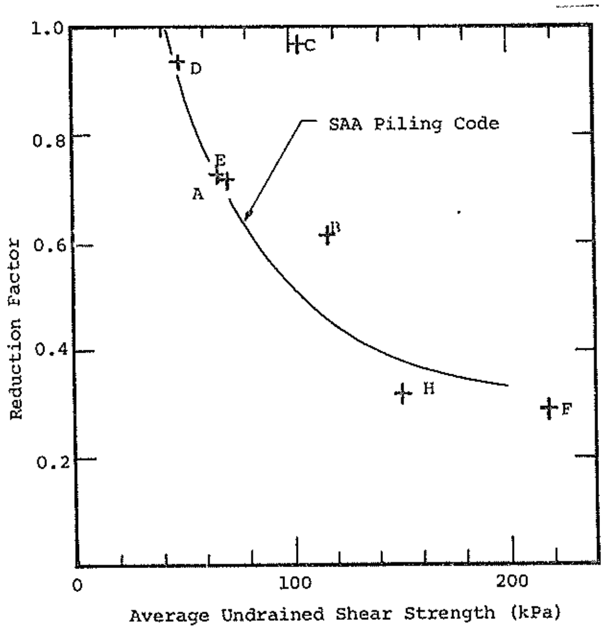

Fig. 4. Adhesion Reduction Factor for Piles in Clays

- The estimated nett ultimate bearing pressure for enlarged base cast-in-situ piles, for which the bases have been formed by hammering the concrete to displace the soil, can be significantly higher than the nett ultimate bearing pressure for bored piers (Fig. 3; Trials 1 and 2, and Fig. 4: Site A).

TABLE 3

STATISTICS FROM PILE LOAD TEST SITES

Site	Investigation (ehu) Statistics n	$\bar{y}_e$ (kPa)	s_e	Load Test (sui) Statistics p	$\bar{y}_s$ (kPa)	s_s
Shaft Adhesion						
A	13	65.7$^+$	0.368$^+$	5	47.1	0.136
B	17	117.9	0.341	3	72.5	0.157
C	21	104.1	0.549	2	100.1	0.162
D	5	47.2	0.605	2	43.8	0.073
E	18	70.9	0.339	2	50.3	0.361
F	7	219.1	0.307	3	64.2	0.053
H	18	148.2	0.278	10	47.7	0.202
Base Resistance						
A	13	95.3	0.224	5	125.3	0.191
C	6	99.2	0.621	2	107.1	0.201
G	18	148.3	0.290	6	98.6	0.063
H	18	138.7	0.356	10	110.4	0.186
F	7	219.1	0.307	2	131.6	0.203

$^+$ Residual strengths in sensitive clay

6 EXAMPLE OF ULTIMATE LOAD DESIGN

The form of the ultimate load design equation for cast-in-situ piers or piles in clays will be

$$\gamma Q + Q_F = N_a\beta_a y_{da} A_a + (N_b\beta_b y_{db} + p_o)A_b \qquad (11)$$

where Q = working load
γ = load factor
Q_F = gravity load of the foundation
N_a = adhesion factor ($c_a/c_{u_{av}}$ from SAA Piling Code in this instance)
β_a = material response factor for shaft adhesion
y_{da} = design value of shear strength of soil around shaft ($\bar{y}_e$: geometric mean of shear strength measurements in this instance)
A_a = area of soil contact on shaft
N_b = bearing capacity factor (9 in this instance)
β_b = material response factor for end bearing capacity
y_{db} = design value of shear strength for soil at base ($\bar{y}_e$: geometric mean of shear strength measurements in this instance)
A_b = area of base

A method for the estimation of material response factors for shaft adhesion and end bearing, where the two act concurrently, is developed in Appendix II.

Suppose that the following shear strength measurements have been obtained by triaxial testing from a Site, J, in the same soil type as Site F.

Shaft Zone: 220 kPa, 110 kPa, 145 kPa, 180 kPa, 130 kPa
Base Zone: 135 kPa, 155 kPa, 230 kPa, 190 kPa

This data, together with the sui data from Site F, can be used to estimate the effect of soil variability on foundation performance. If the ehu and sui data from Site H is available, this can be used to estimate the effect of bias on foundation performance. (The probability that the bias factors for these two soils are different has been shown to be very low). The statistics for these tests are summarised in Table 4.

TABLE 4

SUMMARY OF STATISTICS FOR EXAMPLE

SITE INPUT	Investigation (ehu) Statistics			Load Test (sui) Statistics		
	n	$\bar{y}_e$ (kPa)	s_e	p	$\bar{y}_s$ (kPa)	s_s
Shaft Adhesion						
F & J Variability	5	152.4	0.272	3	64.2	0.053
H Bias	18	148.2	0.278	10	47.7	0.202
Base Resistance						
F & J Variability	4	173.9	0.233	2	131.6	0.203
H Bias	18	138.7	0.356	10	110.4	0.186

This data will be used to estimate the acceptable working load on a 500mm diameter bored pier, with 6m shaft length and base enlargement to 850mm diameter (founding depth 6.3m), for a load factor of 1.6 and a material response factor calculated for a lower confidence limit with confidence coefficient of 0.99. The average bulk density of the soil is 2.0 t/m^3.

$A_a = 9.42\ m^2 \qquad A_b = 0.567\ m^2$

$N_a = 0.38$ for $y_{da} = 152.4$ kPa (SAA Piling Code)

$N_b = 9$

$a_{2a} = y_{s2a}/y_{e2a} = 47.7/(0.38 \times 148.2) = 0.847$ (Eqn. II.2)

$a_{2b} = y_{s2b}/y_{e2b} = 110.4/138.7 = 0.796$ (Eqn. II.2)

$$\omega_a^2 + \omega_b^2 = 0.053^2 + 0.272^2/5 + 0.202^2/10 + 0.278^2/18 + 0.203^2 + 0.233^2/4 + 0.186^2/10 + 0.356^2/18 = 0.0914 \qquad \text{(Eqn. II.2)}$$

$$\frac{(\omega_a^2 + \omega_b^2)^2}{\nu} = \frac{(0.053^2)^2}{2} + \frac{(0.272^2/5)^2}{4} + \frac{(0.202^2/10)^2}{9} + \frac{(0.278^2/18)^2}{17} + \frac{(0.203^2)^2}{1} + \frac{(0.233^2/4)^2}{3} + \frac{(0.186^2/10)^2}{9} + \frac{(0.356^2/18)^2}{17}$$

giving $\nu = 4.6$ (Eqn. II.3)

From tables of Student's t for P = 0.01; t = 3.52

$\beta = 0.847 \times 0.796 \exp(-3.52\sqrt{0.0914}) = 0.233$ (Eqn. II.4)

$\beta_a = \sqrt{\frac{9 \times 173.9 \times 0.567}{0.38 \times 152.4 \times 9.42}} \times 0.233 = 0.616$ (Eqn. II.7

$\beta_b = \beta/\beta_a = 0.233/0.62 = 0.378$ (Eqn. II.7)

$Q_F = 9.8 \times 2.4 \times \frac{\pi}{4} \times 0.5^2 \times 6.3 = 29.1$ kN

$1.6Q + 29.1 = (0.38 \times 0.616 \times 152.4 \times 9.42) + (9 \times 0.378 \times 173.9 + 9.8 \times 2.0 \times 6.3)\ 0.567$ (Eqn. 11)

giving $Q = 445$ kN

7 CONCLUSIONS

Foundation design is carried out using limited information and inexact methods. A bias will often exist between the predicted and the actual foundation performance. The designer must steer a course between undue and costly conservatism and an unacceptably high probability of failure.

Conventional design requires judgement to be exercised in the sensitive and subjective area of choice of design strength and safety factors, to select this course. In the proposed method, the designer's judgement decisions are removed from this area to the less sensitive and more objective decision on the compatibility of his concept of the soil properties on the site with his experience of similar soils. In addition, he is able to make quantitative use of data from previous experience in his judgement decisions and design.

The collection, correlation and dissemination of data from engineering experience (eg. the results of investigation and prototype tests) is of advantage to the profession, whatever design method is used. The prototype tests which yield information on the ultimate soil resistance are often those which have failed to meet the designer's expectations, and there is an understandable reluctance to publish this information. However, the value of such information lies in the comparison of actual and predicted performance, and provided that this is presented in a manner similar to the sites in this paper, sensitive information, such as the actual site location and the design loads, would not be relevant. Therefore, it would seem both feasible and advantageous to the profession to have such information processed by reliable, independant bodies on this basis.

8 ACKNOWLEDGEMENTS

The assistance of the Queensland Department of Works, Frankipile Aust. Pty. Ltd., Ground Test Pty. Ltd. and Soil Surveys Pty. Ltd. is gratefully acknowledged, in making available the investigation and pile load test results used.

9 REFERENCES

AS2159 (1978) "SAA Piling Code", Standards Association of Australia.

MARSLAND, A., (1971) "The Use of In-situ Tests in a Study of the Effects of Fissures on the Properties of Stiff Clays", Proc. First A.N.Z. Geomech. Conf., Melbourne, Australia.

McANALLY, P.A., (1977) "A Method for the Application of Soil Mechanics to Non-Homogeneous Soils", M.E. Thesis, University of Sydney.

WHITAKER, T., (1970) "The Design of Pile Foundations", Pergamon Press.

WHITAKER, T., & COOKE, R.W., (1965) "Bored Piles with Enlarged Bases in London Clay", Proc. Sixth Int. Conf. Soil Mech. & Found. Eng., Montreal Canada

10 APPENDIX I - ANALYSIS OF VARIANCE FORMULAE

Equation 4 is derived from its logarithmic form

$$T = \frac{\ln.a - \ln.\alpha}{\psi} \qquad \text{I.1}$$

where $\ln.a$ is a normal variable

T is an approximate Student's t variable with degrees of freedom, given by (5).

Equation I.1 is of the form

$$T = \frac{\ln.a - \ln.\alpha}{s/\sqrt{\nu + 1}} \qquad \text{I.2}$$

where s = the unbiased estimate of the variance, σ^2, of $\ln.a$

$\nu s^2/\sigma^2$ will be χ^2 variable with ν degrees of freedom, and hence $\nu(\nu + 1)\ \psi^2/\sigma^2$ will be an approximate χ^2 variable with ν degrees of freedom. Thus, the sum of k such variables from independant samples.

$\Sigma_1^k\ \nu_j(\nu_j + 1)\ \psi_j^2/\sigma^2$ will be a χ^2 variable with $\Sigma_1^k\ \nu_j$ degrees of freedom.

Also, $\sqrt{\nu_j + 1}\ (\ln.a_j - \ln.a)/\sigma$ will be a standard normal variable, where $\ln.a = \Sigma_1^k\ (\nu_j + 1)\ln.a_j / \Sigma_1^k(\nu_j + 1)$.

Therefore, $\Sigma_1^k\ (\nu_j + 1)\ (\ln.a_j - \ln.a)^2/\sigma^2$

$$= \{\Sigma_1^k\ (\nu_j + 1)(\ln.a_j)^2 - (\ln.a)^2\ \Sigma_1^k\ (\nu_j + 1)\}/\sigma^2\ .$$

will be a χ^2 variable with (k-1) degrees of freedom if α is the same for all the populations from which the k sample sets have been selected.

Under the hypothesis $H_o : \alpha_1 = \alpha_2 = \ldots$ the ratio of the two χ^2 variables, divided by their respective degrees of freedom

$$F = \frac{\Sigma_1^k\ \nu_j\{\Sigma_1^k\ (\nu_j+1)(\ln.a_j)^2 - (\ln.a)^2\Sigma_1^k\ (\nu_j + 1)\}}{(k-1)\Sigma_1^k\ \nu_j(\nu_j + 1)\ \psi_j^2}$$

will have an f distribution and provides a form of the conventional one way analysis of variance expression.

11 APPENDIX II - MATERIAL RESPONSE FACTORS FOR JOINT ACTION OF BASE AND SHAFT RESISTANCE

The ultimate soil resistance of a deep foundation will be given by

$$R_u = N_a y_{sa} A_a + (N_b y_{sb} + p_o)A_b \qquad \text{II.1}$$

It can be shown from the statistical model that

$$a_{2a}a_{2b}\exp\ (-t\sqrt{\omega_a^2 + \omega_b^2}) < y_{sa}y_{sb}/\bar{y}_{ela}\bar{y}_{elb}\ \ldots \qquad \text{II.2}$$

where a_{2a}, a_{2b} are values of $\bar{y}_{s2}/\bar{y}_{e2}$ from (6) for shaft and base respectively

ω_a^2, ω_b^2 are values of ω from (6) for shaft and base respectively

y_{sa}, y_{sb} are values of sui response for shaft and base respectively

$\bar{y}_{ela}$, $\bar{y}_{elb}$ are values of $\bar{y}_{el}$ for shaft and base respectively

t is the Student's t value for the confidence level chosen and degrees of freedom, ν, given by

$$\frac{(\omega_a^2 + \omega_b^2)^2}{\nu} = \frac{\omega_a^4}{\nu_a} + \frac{\omega_b^4}{\nu_b} \qquad \text{II.3}$$

$$\text{If}\ \beta = a_{2a}\ a_{2b}\ \exp\ (-t\sqrt{\omega_a^2 + \omega_b^2}) = y_{sa}y_{sb}/\bar{y}_{ela}\bar{y}_{elb} \qquad \text{II.4}$$

Also, the values of y_{sa} and y_{sb} giving the minimum value of R_u can be found from

$$\partial R_u/\partial y_{sa} = 0 \qquad \partial R_u/\partial y_{sb} = 0 \qquad \text{II.5}$$

The values of y_{sa} and y_{sb} giving the minimum value of R_u at the chosen lower confidence limit can be found from II.1, II.4 and II.5

$$y_{sa}^2 = \frac{N_b A_b}{N_a A_a}\ \bar{y}_{ela}\bar{y}_{elb}\beta \quad y_{sb}^2 = \frac{N_a A_a}{N_b A_b}\ \bar{y}_{ela}\bar{y}_{elb}\beta \qquad \text{II.6}$$

If the material response factors for shaft and base response are defined in terms of the values of y_{sa} and y_{sb} from 6 as $y_{sa} = \beta_a\bar{y}_{ela}$ and $y_{sb} = \beta_b\bar{y}_{elb}$ respectively, then from II.6 where $\beta = \beta_a\beta_b$

$$\beta_a = \sqrt{\frac{N_b\bar{y}_{elb}A_b\ \beta}{N_a y_{ela}A_a}} \quad \beta_b = \sqrt{\frac{N_a\bar{y}_{ela}A_a\ \beta}{N_b y_{elb}A_b}} \qquad \text{II.7}$$

Automatic Joint Element Generation to Simulate Strain Softening Yield Behaviour in Earthern Materials

B. G. RICHARDS
Principal Research Scientist, Division of Soils, CSIRO

SUMMARY This paper describes a model incorporating automatically generated joint elements to simulate the observed behaviour of strain softening materials, including the post-yield behaviour. Good agreement was obtained when this model was used to back analyse triaxial and direct shear tests of such a material. The collapse load of strip footings as predicted by this model was also compared with previously published results, giving excellent agreement. This model, therefore has a useful capability of analysing the complete stress-strain behaviour of soils, including the prediction of the collapse load and the post-yield behaviour. At the same time, it maintains the advantages of non-linear elastic models in that it incorporates directly the constitutive relationships and the yield criteria based on experimental evidence, in this case, the results of conventional triaxial and direct shear tests.

1 INTRODUCTION

The stress-strain behaviour of naturally occurring soils is very complex and therefore difficult to simulate using mathematical models. Excellent summaries of such mathematical modelling techniques applicable to wide range of soil mechanics problems have already been given by numerous authors (e.g. Zienkiewicz et al., 1978). It is obvious that in the present state of understanding of soil behaviour and the definition of the relevent soil properties, accurate predictions of soil behaviour cannot be achieved. What is required for practical purposes, is to model as accurately as possible, those properties which are essential in the solution of a given problem. For this purpose, the finite element method has invariably been used with appropriate constituitive relationships for the stress-strain behaviour.

For pre-failure deformation states, non-linear elastic models have been developed to the point where they are the most suitable for the prediction of the stress-strain behaviour of soils so long as zones of near failure stress are limited. These models represent the soil as non-dilatant (i.e. shear stresses cause no volume change) with a non-associated behaviour (i.e. maximum shear strain occurs in the direction of the maximum shear stress). They also give poor simulation of the behaviour of soils which exhibit ideal plasticity or strain softening, but may prove adequate for those soils such as loose sands or normally consolidated clays, which exhibit continual strain hardening. Their main advantage is that they incorporate directly constituitive relationships based on experimental evidence e.g. the results of conventional triaxial compression tests with volume change measurements. This permits considerable flexibility in the use of the constituitive material relationships and for example permits the use of stress and/or strain dependent properties.

One such non-linear elastic model, which has been found to be simple to use in practical problems, is the hyperbolic stress-strain model, developed for clays by Konder (1963) and for sands by Konder and Zelasko (1963). Various forms of this model have subsequently been developed, but a modification of the Variable Moduli Model II (first proposed by Nelson, 1970) was used by the author (Richards, 1978) to model experimental stress-strain relationships for a range of soils in both field or laboratory applications. This model was shown to be able to describe the non-linear stress dependent properties of the soils based on the entire experimentally determined stress-strain curves at least, up to failure conditions.

For deformation states at or post-failure, most soil mechanics workers have extended the concepts of the classical plasticity theory to simulate the soil behaviour (Wroth, 1973). Whilst this theory applied only to ideal materials it had the advantage that the classical bounding theorems for collapse loads applied ensuring the uniqueness of the results. However, to obtain reasonable results with real soils, much of the classical theory had to be abandoned or considerably modified (Zienkiewicz et al., 1975).

The main problem with the classical plasticity theory was the assumption that the plasticity behaviour is "associated". It is now accepted (Davis, 1968a, 1968b; Davis and Booker, 1973; Zienkiewicz et al., 1975) that associated behaviour using Mohr-Coulomb yield criteria contradicted experimental observations and gave excessive rates of dilation. Attempts to extend plasticity ideas to a "non-associated" form have become necessary, but no useful bounds can be placed on the collapse loads and this creates doubts on the uniqueness of the results. Consequently, one of the main advantages of the plasticity theory no longer applies.

This paper looks at the possibility of extending the hyperbolic stress-strain model to simulate the failure and post-failure behaviour of strain softening soils. In one application (Richards, 1979) viz. the back-analyses of spoil pile failures at a strip coal mine in the Bowen Basin, Queensland, strain softening of the spoil pile was the significant factor. As no other method of analysis was found to be suitable, the finite element program using the hyperbolic stress-strain model was modified to include fixed joint elements (Ghaboussi et al., 1973) along the previously surveyed location of the failure planes. These joint elements had non-linear hyperbolic shear stress-displacement relationships with a shear stress release and redistribution technique to simulate strain softening (Zienkiewicz et al., 1968; Lo and Lee, 1973). Using the elastic properties from triaxial tests and joint properties from direct shear tests, it was possible to closely model both the triaxial and shear box tests themselves as well as the slope behaviour in the field.

One interesting point arising out of the analyses of the spoil piles was the fact that the maximum shear strain contours given by the non-linear elastic analyses predicted the location of the observed failure planes very closely as suggested by Resendiz and Romo (1972). This led to the possibility of inserting joint elements automatically into the finite element mesh when yield occurs, at the location and orientation determined by the yield criteria adopted.

2 MATERIAL MODEL

2.1 Basic Continuum Model

The hyperbolic model used to describe the continuum material up to yield can be summarized by the simplified relationships (Richards, 1978) as:

$$K = K_1 \sigma_m{}^n + K_o \tag{1}$$

and

$$G = G_1 \sigma_m{}^m \left(1 - \left(\frac{\tau}{\tau_f}\right)^p\right) + G_o \tag{2}$$

where K = bulk modulus
G = shear modulus
σ_m = maximum value of the mean stress
$= 1/3\ (\sigma_1 + \sigma_2 + \sigma_3)$
σ = shear stress) according to yield criteria
σ_f = yield stress) adopted

K_1, K_o, G_1, G_o, n, m and p are material constants.

These equations can readily be programmed into non-linear elastic finite element programs using continuum elements and incremental loading. Typical results using such a program have already been published elsewhere (Richards, 1978).

2.2 Joint Elements

The joint element used in the finite was based on that proposed by Ghaboussi et al., (1973). The finite element formulations for constant strain joint elements are:

$$\{F_n\} = [k]\ \{\sigma_n\} \tag{3}$$

where $[k]$ = stiffness matrix
$k_{ns} = \int vol\ B^T C\ Bdvol.$
$[C]$ = stress matrix
$[B]$ = strain matrix
$\{F_n\}$ = nodal forces
$\{\sigma_n\}$ = nodal displacements

The strain matrix $[B]$ as used by Ghoboussi et al., (1973) is similar in form to that for the simple constant strain continuum elements. However, the stress matrix $[C]$ is different and has the form for two dimensional problems:

$$\begin{matrix} \sigma_n \\ \sigma_t \\ \sigma_s \end{matrix} \quad \begin{matrix} C_{nn} & 0 & C_{ns} \\ 0 & 0 & 0 \\ C_{sn} & 0 & C_{ss} \end{matrix} \quad \begin{matrix} \varepsilon_n \\ \varepsilon_t \\ \varepsilon_s \end{matrix} \tag{4}$$

where σ_n = stress normal to joint
σ_t = stress transverse to joint
σ_s = shear stress in joint direction
ε_n = strain normal to joint
ε_t = strain transverse to joint
ε_s = shear strain in joint direction

C_{nn}, C_{ns}, C_{sn} and C_{ss} are the joint parameters
C_{nn} = joint stiffness normal to joint
C_{ss} = shear stiffness of joint
$C_{ns} = C_{sn}$ is the coupling between normal displacement and shear force and vice-versa (i.e. are zero for non-dilatant joints).

Thus it can be seen that any continuum element can be converted to an effective joint element by changing the stress matrix $[D]$ for a continuum element to the $[C]$ matrix for a joint element at any time when yield occurs during the incremental loading process. This technique has been checked by comparing analyses with those using the specially designated joint elements as defined by Ghaboussi et al., (1973). The joint parameters differ from the elastic parameters, but in the following examples, C_{nn} has been equated with 3K and C_{ss} with G with C_{ns} and C_{sn} equal to zero (i.e. equivalent to putting $\nu = 0$).

The main difficulty in changing to the joint element is the determination of the joint angle, α, i.e. the angle between the n-s co-ordinate system of the joint and the x-y co-ordinate system used in the analysis. Morgenstern and Tchalenko (1967) have investigated the microscopic structures in kaolin subjected to direct shear and considered two component viz. original fabric (e.g. pre-existing joints) and shear-induced fabric (e.g. joints formed during the loading stages). Up to failure i.e. the creation of a discontinuity or a joint, the deformations are assumed to be strain controlled, but the formation of the joint is due to a displacement discontinuity and the deformations are the result of principle displacement shear (Skempton, 1966). Hence the best estimate of the angle α, at least for a non dilatant material, is given by the maximum or principal shear strain direction corresponding to the incremental nodal displacements during yield i.e. joint formation.

The stiffness matrix for the joint element in the general x-y co-ordinate system is:

$$[k]_{xy} = [T]^T [k]_{ns}\ [T] \tag{5}$$

where $[T]$ is the transformation matrix containing the direction cosines of the joint angle, α.

2.3 Strain Softening

The model used in this paper assumes that strain softening occurs only in the joint elements. At yield, the actual shear stresses are equal to or exceed the yield stresses for peak strength and the shear stiffness from equation (2) has been reduced to near zero values. The yield stresses for residual strength are then calculated and the difference is redistributed until the shear stresses in the yielded elements are at the residual values.

The excess shear stress along the joint at angle, α, is given by:

$$\Delta\tau_\alpha = \tau_\alpha - \tau_{\alpha R} \tag{6}$$

where τ_α = actual shear stress along the joint
$\tau_{\alpha R}$ = residual shear strength

The excess stresses to be redistributed in the x-y co-ordinate system are given by:

$$\{\Delta\sigma\} = \begin{Bmatrix} \Delta\sigma_x \\ \Delta\sigma_y \\ \Delta\tau_{xy} \end{Bmatrix} = \begin{Bmatrix} -\Delta\tau_\alpha \sin 2_\alpha \\ \Delta\tau_\alpha \sin 2_\alpha \\ -\Delta\tau_\alpha \cos 2_\alpha \end{Bmatrix} \qquad (7)$$

where α is the inclination of the joint to the horizontal.

Using the "initial stress" method (Zienkiewicz et al., 1968), the excess stresses are redistributed by generating a new set of nodal forces.

$$\{F\} = \int [B]^T \{-\Delta\sigma\} \, dvol \qquad (8)$$

where $[B]^T$ is the transpose of the strain matrix

$\{-\Delta\sigma\}$ is the negative value of the excess stresses

As the shear modulus of the yielded elements is near zero, the iterative method used by Lo and Lee (1973) was not required for the reduction of the stresses in the yielded elements, but was required to ensure redistribution of these stresses to the elements not yet yielded.

2.4 Tensile Failure

The model used for tensile failure in some of the applications described in the following sections was simply to reduce any tensile stresses exceeding the tensile strength of the material to zero and redistribute them by the "initial stress" method discussed above.

3 ANALYSES OF LABORATORY TESTS

The mud stone underlying the coal and forming the floor of a strip coal mine in the Bowen Basin, Queensland has already been extensively investigated (Richards, 1979). This material exhibited brittle failure with strain softening and little or no volume change or dilatancy. It was therefore an ideal material for the application of the model described above. This material also formed the base of the spoil piles, standing over 70 metres high at their natural angle of repose (up to 35°) and which have had a history of failures (Boyd et al., 1978).

FIG. 1

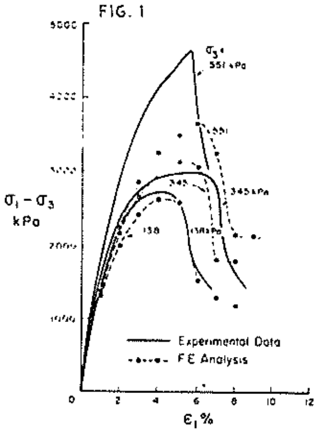

FIG. 2

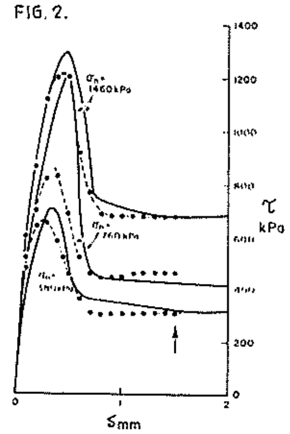

Figure 1. Triaxial test results for mud-stone, Bowen Basin, Queensland.

Figure 2. Direct shear test results for mud-stone, Bowen Basin, Queensland: Shear stress versus shear displacement.

Undrained triaxial tests without volume change measurement were carried out on 200 mm dia. sealed 'intact' cores of the material sampled at its natural water content. Typical results of the deviatoric stress versus vertical strain curves for various cell pressures are shown in Fig. 1. Direct shear tests were also carried out on the same material and typical shear stress versus displacement curves for various normal stresses are shown in Fig. 2. The normal displacement versus shear displacement curves for the same samples is shown in Fig. 3.

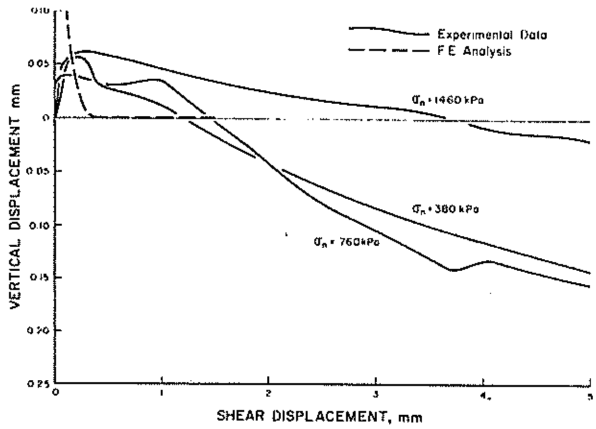

Figure 3. Direct shear test results for mud-stone, Bowen Basin, Queensland: Normal displacement versus shear displacement.

The hyperbolic parameters including the peak strength parameters as defined in equations (1) and (2) were determined using the triaxial data in Fig. 1. The residual strength parameters were determined using the direct shear box data in Fig. 2. These parameters can be summarized in the following expressions:

$K = 154{,}000$ kPa

$G = 71{,}000 \left(1-\left(\frac{\tau}{\tau_f}\right)^{1.0}\right) + 150$ kPa

$C_{nn} = 462{,}000$ kPa

$C_{ss} = G$

$C_{ns} = C_{sn} = 0$

τ_{fp} = peak yield stress, $(\sigma_1-\sigma_3)_p/2$

$= 625 \cos 34° + (\sigma_1+\sigma_3) \sin 34°$ kPa

τ_{fr} = residual yield stress

$= 170 + \sigma_n \tan 16°$ kPa

It should be noted that the triaxial test using Mohr-Coulomb yield criteria and the direct shear test using the Coulomb criteria on the failure plane give different results for non-associated materials (Davis, 1968b and Morgenstern et al., 1967). This difference is taken into account in the model described above as the shear strength on the actual failure plane is predicted not assumed in each analysis.

The laboratory tests showed that the material exhibited little or no dependency on the mean stress and soil suction. For example, the effect of soil suction on the residual shear strength is shown in Fig. 4.

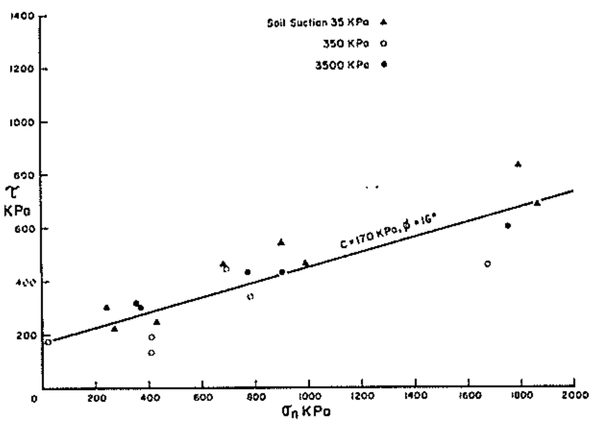

Figure 4. Direct shear test results for mud-stone, Bowen Basin, Queensland: Residual shear strength versus soil suction.

Using these parameters, the laboratory tests themselves were back-analysed. The triaxial tests could not be exactly modelled as the applied stresses were axi-symmetric, but the observed failure planes were distinct planar surfaces at angles of 50° to 55° to the horizontal. As a compromise, the triaxial tests were modelled as plane strain tests as these give planar failure surfaces similar to those observed and the intermediate stress, σ_2, does not affect the Mohr-Coulomb yield criteria. The results of these plane strain analyses are summarized in Figs. 1, 5, 6 and 7 and gave excellent agreement with the test data.

Similar plane strain analyses of the direct shear tests were carried out assuming a shear plane 2 mm thick. The results of these analyses are summarised in Figs. 2, 8 and 9. It is interesting that the directions of the maximum shear strains varied from 25° to the horizontal initially to approximately 0° at yield. Therefore, any shear induced sub-structures could be similar to those reported by Morgenstern and Tchalenko (1967).

One obvious question, which could be raised concerning these analyses, is the influence of the finite element mesh, particularly the orientation of the nodes in the simulated triaxial tests as shown in Fig. 10. Analyses were repeated of these tests with no strain softening (i.e. $\tau_{fp} = \tau_{fr}$), but with the orientation of the nodes varied. Fig. 10 also shows the stress-strain results for a 45° orientation and Fig. 11 shows the variation of predicted peak strength with node orientation. In each case, the joint angles, α at yield were predicted to be approximately 52° in the vicinity of the failure surface, which corresponded with the angle for minimum strength shown in Fig. 11. The failure surfaces predicted by the maximum shear strain contours were stepped except in the case of the nodes orientated at 52°, but in each case, the average slope approximated 52°. At an orientation greater than 63°, every diagonal line of nodes was impeded by the end caps and this apparently impeded failure as shown in Fig. 11.

4 ANALYSES OF THE YIELDING OF STRIP FOOTINGS

The first example analysed was that of a rigid frictionless strip footing being pushed into weightless frictionless soil at a constant strain rate. Fig. 12 shows the geometry of the problem and Fig. 13 the displacement (i.e. flow) patterns at peak load. Fig. 12 also shows the load-settlement curve, which compares favourable with the Prandtl solution. Results for a similar analysis with strain softening such that $\tau_{fr} = 0.5\tau_{fp}$ is also shown in Fig. 12.

Attempts at analysing a cohesionless soil were not so successful as convergence could only be achieved after a very large number of iterations per increment of loading. While the initial stress method used ultimately gives the correct result, intermediate results can give temporary peak strengths much higher than the true peak strength.

As a further check on the model, the plane strain analysis of a uniformly loaded flexible and frictionless strip footing by Zienkiewicz et al., (1975) was repeated. The load settlement curve is shown in Fig. 17 compared with their curve for non-associated flow (θ=0) and the Prandtl collapse load. The differences between the load-settlement

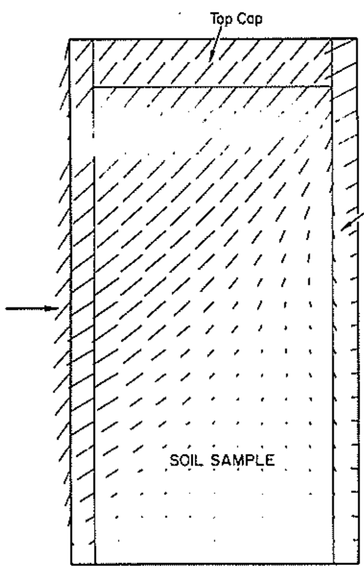

FIG.5

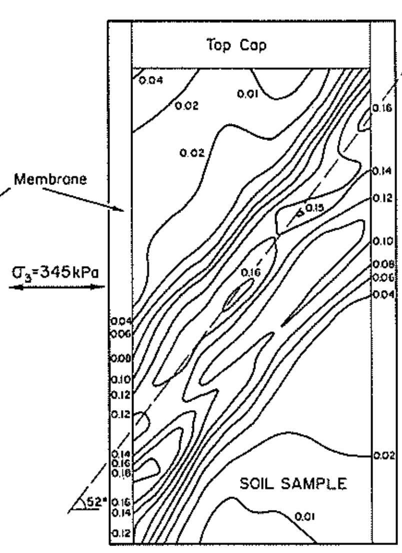

FIG.6

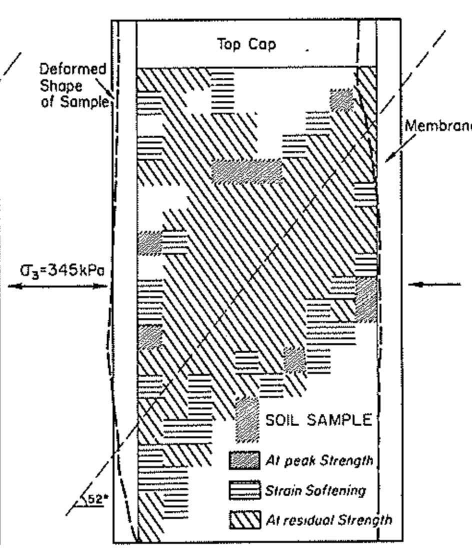

FIG.7

Figure 5. Results of finite element analysis of triaxial test: displacement vectors.
Figure 6. Results of finite element analysis of triaxial test: max. shear strain contours.
Figure 7. Results of finite element analysis of triaxial test: zones of failure.

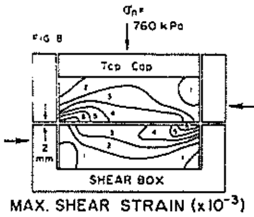

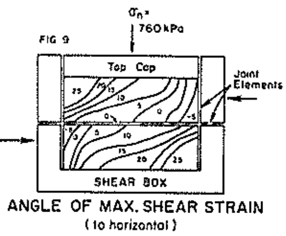

Figure 8. Results of finite element analysis of direct shear test: max. shear strain contours.
Figure 9. Results of finite element analysis of direct shear test: orientation of joint angles.

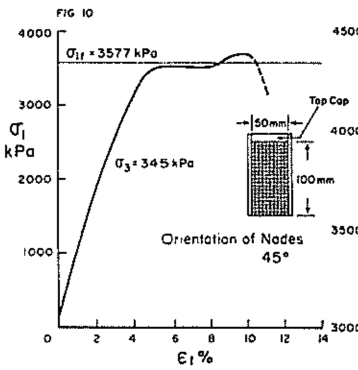

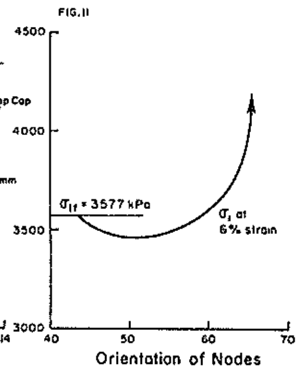

Figure 10. Results of finite element analysis of plane strain test with elements at 45° orientation.
Figure 11. Variation of predicted shear strength with element orientation.

curves in Fig. 17 are due to the differences between the linear elasticity used by Zienkiewicz et al. and the non-linear elasticity used in this paper. The displacement patterns post-yield are shown in Fig. 15. Figs. 16 and 17 show the maximum shear strain contours and the spread of yielded zones at peak load.

5 ANALYSES OF SLOPE FAILURES

Space does not permit a detailed description of the analyses of slope stability problems. However, the analyses of a spoil failure at the Goonyella mine, Queensland, previously reported by the author (Richards, 1979) were repeated using the model described above with very similar results. Using the construction sequence shown by stages 1 to 6 and the final rise in the groundwater level, i.e. stage 7 shown in Fig. 18 together with the actual material parameters previously determined, the analyses indicated that the slope was near failure. The displacement pattern shown in Fig. 19 and yielded zones shown in Fig. 20 indicate that the predicted failure planes

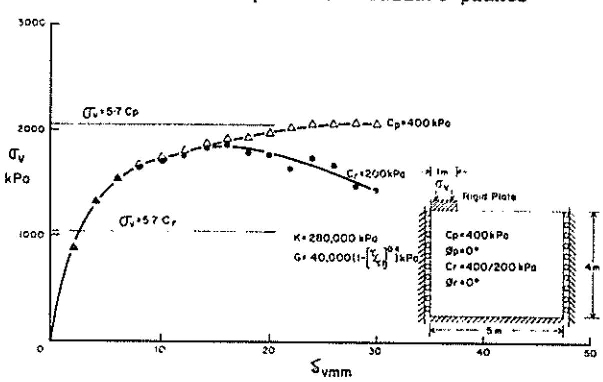

Figure 12. Load-settlement curve for rigid frictionless strip footing.

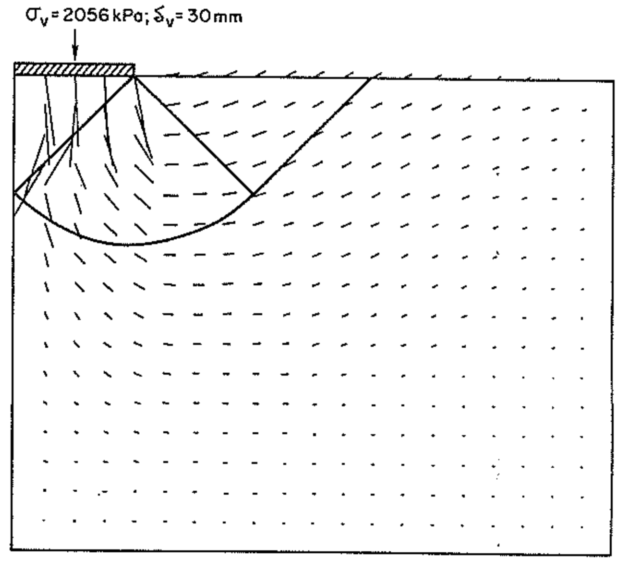

Figure 13. Displacement vectors for rigid frictionless strip footing at yield.

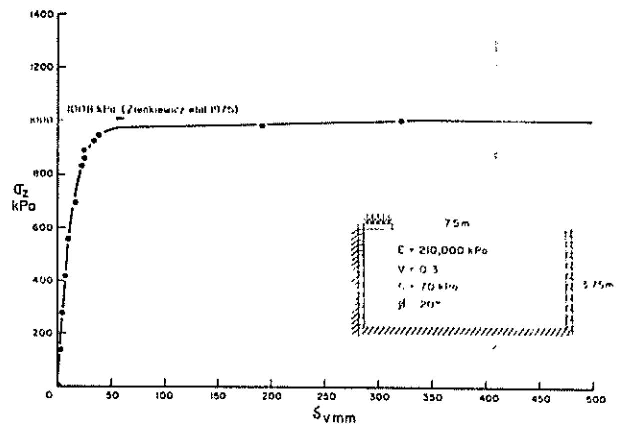

Figure 14. Load-settlement curve for flexible frictionless strip footing.

would be similar to those observed and used in the previously reported analyses.

6 CONCLUSIONS

The model incorporating automatically generated joint elements as described in this paper has been used to closely simulate the observed behaviour of a strain softening material including the post-yield behaviour in laboratory tests. Results for the collapse load of strip footings also compare favourably with those obtained previously using visco-plasticity models and the Prandtl collapse loads. Attempts at modelling the strain softening effects in a spoil pile at a strip coal mine were successful and predicted the sequential failure a manner similar to that observed in an actual failure.

This model therefore has a useful capability of analysing the complete stress-strain behaviour of soils including the prediction of the collapse load and the post-yield behaviour. At the same time, it maintains the advantages of non-linear elastic models in that it incorporates directly the constitutive relationships and yield criteria based on experimental evidence, in this case, the results of conventional triaxial and direct shear tests.

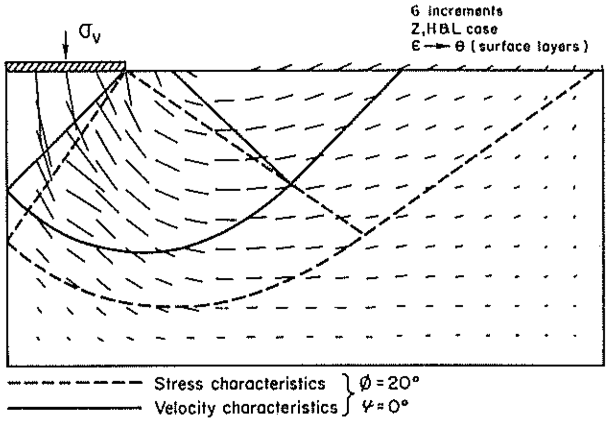

Figure 15. Displacement vectors for flexible frictionless strip footing.

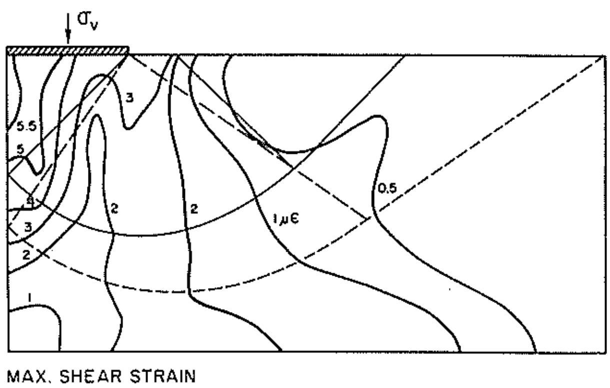

Figure 16. Contours of max. shear strain for flexible frictionless strip footing.

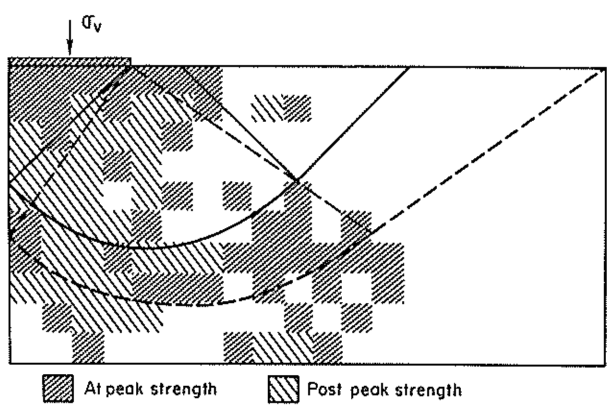

Figure 17. Zones of failure for flexible frictionless strip footing.

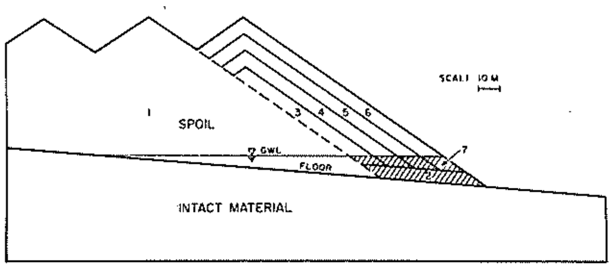

Figure 18. Construction sequence for spoil pile.

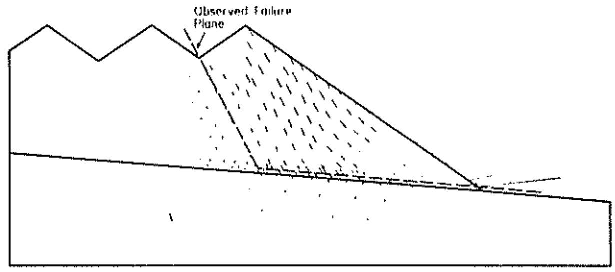

Figure 19. Displacement vectors for completed spoil pile.

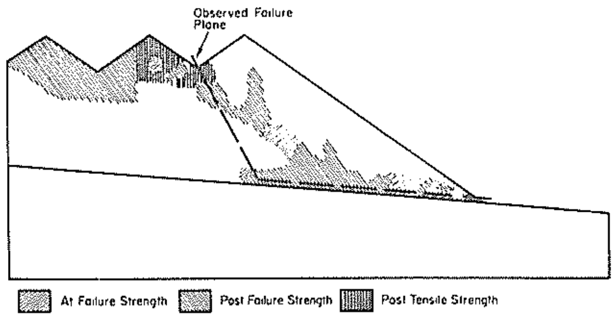

Figure 20. Zones of failure for completed spoil pile.

7 REFERENCES

ZIENKIEWICZ, O.C., NORRIS, V.A., WINNICKI, L.A., NAYLOR, D.J. and LEWIS, R.W. (1978). A Unified Approach to the Soil Mechanics Problems of Offshore Foundations, in "Numerical Methods in Offshore Engineering" ed. by O.C. Zienkiewicz, R.W. Lewis and K.G. Stagg, Chicester, Wiley, 1978.

KONDER, R.L. (1963). Hyperbolic Stress-Strain Response: Cohesive Soils, J. Soil Mech. and Foundations, Div., A.S.C.E., Vol. 89 No. SMI, pp 115-143.

KONDER, R.L. and ZELASKO, J.S. (1963). A Hyperbolic Stress-Strain Formulation for Sand. Proc. 2nd Pan-American Conf. on Soil Mech. and Fndn. Engng., Vol. 1, pp 289-333.

NELSON, I. (1970). Investigation of Ground Shock Effects in Non-linear Hysteretic Media. Report 2, Modelling the Behaviour of a Real Soil, Report S-68-1, Contract DACA 39-67-C-0048, Paul Weidlinger Consulting Engineer, U.S. Army Waterways Experiment Station.

RICHARDS, B.G. (1978). Application of an Experimentally Based Non-linear Constitutive Model of Soils in Laboratory and Field Tests. Aust. Geomechanics Journal, Vol. G8, pp 20-30.

WROTH, C.P. (1973). A Brief Review of the Application of Plasticity to Soil Mechanics Proc. Symp. Role Plasticity in Soil Mech., Cambridge, 1-11 (ed. A.C. Palmer).

ZIENKIEWICZ, O.C., HUMPHESON, C. and LEWIS, R.W. (1975). Associated and Non-associated Visco-plasticity and Plasticity in Soil Mechanics, Geotechnique, 25(4):671-689.

DAVIS, E.H. (1968a). A Discussion of Theories of Plasticity and Limit Analysis in relation to the failure of soil masses. Proc. 5th Aust. N.Z. Conf. Soil Mech. and Fndn. Engng. 175-182.

DAVIS, E.H. (1968b). Theories of Plasticity and the Failure of Soil Masses. In "Soil Mechanics: Selected Topics" (Ed. I.K. Lee): 341-380, London, Butterworths.

DAVIS, E.H. and BOOKER, J.R. (1973). Some Applications of Classical Plasticity Theory for Soil Stability Preblems. Plasticity and Soil Mechanics, Cambridge, 24-43.

RICHARDS, B.G. (1979). Finite Element Analyses of Spoil Pile Failures at the Goonyella Mine, CSIRO, Div. of Appl. Geomech., Tech. Report No. 96.

GHABOUSSI, J., WILSON, E.L., and ISENBERG, J. (1973). Finite Element for Rock Joints and Interfaces, Proc. ASCE, Jn. Soil Mech. and Fndn. Div., 99 (SMIO):833-848.

ZIENKIEWICZ, O.C., VALLIAPAN, S. and KING, I.P., (1968). Stress Analysis of Rock, as a "No-tension" material, Geotechnique, 18(1):56-66.

LO, K.Y. and LEE, C.F. (1973). Stress Analysis and Slope Stability in Strain-softening Materials, Geotechnique, 23(1):1-11.

RESENDIZ, D. and ROMO, M.P. (1972). Analysis of Embankment Deformations Proc. ASCE, Specialty Conf. on Performance of Earth and Earth Supported Structures, Purdue University, Vol. 1, Part 1:817-836.

MORGENSTERN, N.R. and TCHALENKO, J.S. (1967). Microscopic Structures in Kaolin Subjected to Direct Shear, Geotechnique, 17(4):309-382.

SKEMPTON, A.W. (1966). Some Observations on Tectonic Shear Zones, Proc.
BOYD, G.L., KOMDEUR, W. and RICHARDS, B.G. (1978). Open Strip Pitwall Instability at Goonyella Mine - Causes and Effects, Aust. I.M.M. Conf., North Queensland, :139-157.

Finite Element Analysis of a Slope At Illawarra Escarpment

S. VALLIAPPAN
Associate Professor, School of Civil Engineering, The University of New South Wales
R. S. EVANS
Materials Research Division, Country Research Board, Victoria

SUMMARY The results of the investigation into the stability of slope at Illawarra Escarpment using finite element method are discussed. The numerical modelling of the slope include both jointed and intact rock mass assumptions. For the continuum modelling, isoparametric quadrilateral elements have been used whereas for the jointed rock mass, in addition to the quadrilateral elements, Goodman type joint elements have been used. The material nonlinearities of the rock mass include elasto-plastic, no-tension and creep behaviour. The results for the models representing both a typical section and a steeper section of the slope indicate that no large scale failure is possible at the escarpment.

1. INTRODUCTION

The analyses of rock slopes are, in general, carried out on the basis of phenomenological approach or on the basis of design approach. A phenomenological approach is aimed at a study of the general behavioural pattern and mechanism of failure, whereas a design approach is intended to provide quantitative information on the stability of a particular slope. In this paper, a phenomenological approach has been primarily adopted.

The three major methods for rock slope stability analyses are - model studies, limit equilibrium methods and analytical or numerical techniques. Physical scale models are concerned with the behaviour patterns of rock slopes and, as such, aim at modelling the failure mechanisms and fabric effects. In limit equilibrium methods, a failure mode is often assumed and then the stability of a particular slope is determined on the basis of that particular mode. Numerical techniques are used to determine not only the stress distribution within the rock mass but to evaluate the deformation characteristics of the slope itself. These techniques are capable of including the discontinuities in the rock mass for evaluating the stability of the slopes. The physical models, although sometimes invaluable, provide limited quantitative information and moreover the time involved in the construction of models preclude them as efficient tools. The main drawback of the limit equilibrium methods is the assumption of a particular mode of failure before any analysis is carried out. The behaviour of rock mass adjacent to the failure surface is not accounted for. In addition, the progressive failure which actually happens due to the break-up of rock mass and the associated stress redistribution cannot be considered. Moreover the time dependent behaviour due to creep or weathering cannot be directly incorporated in limit equilibrium methods. Among the analytical and numerical techniques, one of the most widely used technique for slope stability analysis is the well established finite element method. The finite element method has been popular because of its capability to include the nonlinear behaviour,(both time dependent (creep) and time independent (plasticity)) of the rock mass, the influence of discontinuities such as joints, the progressive failure and the associated stress redistribution, the influence of initial tectonic stress system, and above all, it is not necessary to assume any particular mode of failure for determining the stability of the slope.

However, in all finite element analyses, the accuracy of the results depends on the accuracy of the material properties adopted for the analysis. Since there may be a large variation in mechanical properties assumed for the analysis, the actual values obtained for displacements and stresses may not be as accurate as it should be for design purposes. However, for phenomenological approach as adopted in the present paper, the tendency of movement and deformation of rock mass will provide more significant information than actual values.

The aim of the present paper is to illustrate the use of finite element nonlinear analysis for a particular slope at Illawarra Escarpment. In fact, two sections of the escarpment have been modelled, one being a typical section encountered and the other being a steep one where rock failures are most common. The results for both sections indicate that eventhough there may be some local failures, it is not likely for a large scale failure to occur at the escarpment.

2. FINITE ELEMENT MODEL

The finite element analysis has been based on two dimensional plane strain assumption. The material nonlinearities include plastic yielding, tensile cracking and creep. In order to account for these nonlinearities two separate analyses have been carried out. In one, both elastic-plastic behaviour and 'no-tension' have been combined together whereas in the other, only creep has been included. The rock mass was modelled both as in tact and jointed. For the jointed medium, Goodman type joint elements have been used to model the discontinuities. For the elasto-plastic analysis, the 'initial stress method' has been used as the iterative technique and for the creep analysis, the 'initial strain process' has been used. For the elasto-plastic analysis, Drucker's modified von Mises yield criterion has been used whereas for the creep analysis, a power law has been adopted in the following form.

$$d\varepsilon_e{}^c = K\sigma^n$$

where $d\varepsilon_e{}^c$ is the incremental effective creep strain
σ_e is the effective stress
K and n are material constants

The selection of proper time increment for the creep analysis is quite important. The choice of small time increment demands more computer time while a very large increment may cause divergence of the solution. With the creep law adopted for this investigation, various time increments were tried and it was found that the optimum increment is 500 days, considering economy in computation and satisfactory results. It can be generally postulated that the results will diverge if the incremental creep strain exceeds the elastic strain.

The material properties used for the elasto-plastic and creep analyses have been tabulated in Table I.

The finite element meshes for a typical section and a steeper section of the escarpment are shown in Fig. 1 and 10 respectively. The numbers given in the various layers of the mesh indicate the appropriate material properties corresponding to those given in Table I.

The initial tectonic stress system was included in the analysis by means of applying gravity loading to simulate vertical stress and loads at both vertical sides of the mesh to simulate horizontal stresses. The importance of tectonic stresses in any rock mechanics problems is well established. With particular reference to rock slopes, high horizontal stresses may be important in deep seated large scale failures where the stresses are not relieved. On the other hand, the relief of high horizontal stresses over time may have an effect on the stability of the slope causing the opening of the joints in the vicinity of the free face. Therefore, in the present analyses, the influence of horizontal stresses has been studied by assuming two values for k values ($\sigma_H = k\sigma_V$), that is, 1/3 and 3, corresponding to low and high horizontal stresses respectively.

3. DISCUSSION OF RESULTS

3.1 Brokers Nose Section

Brokers Nose Section is immediately west of Bellambi between Bulli and Wollongong and is considered to represent the typical slope at Illawarra Escarpment. The finite element division of this section is shown in Fig. 1. The joints are considered to extend to the base of the Wombarra claystone because this is the maximum depth to which any large scale failure is likely to progress. Due to the limitation of the finite element division, only those outer elements of the claystones in the Narrabean Group are considered to be slightly weathered.

The contours of the maximum principal stress, σ_1 for the elasto-plastic, no-tension analysis of the slope are plotted in Fig. 2 to 5. Fig. 2 and 3 refer to the in-tact rock model for low and high horizontal stresses whereas Fig. 4 and 5 refer to the jointed model for low and high horizontal stresses. There is practically no difference in the stress distribution between the jointed and unjointed models for low horizontal stresses. On the other hand for the case of high horizontal stresses, there seems to be less cracking in the jointed model. This is expected since the joints are likely to relieve the stresses by allowing sliding. The stresses determined are not sufficient enough to produce any plastic yielding.

Comparing the displacements, there was not any significant difference between the results of jointed and unjointed models. However, the ratio of maximum horizontal displacement occuring at the top outermost node between the cases of high and low horizontal stresses was nearly 14.

The principal stress (σ_1) contours for the creep analysis are shown in Fig. 6 to 9. For the unjointed model, the high horizontal stresses (Fig. 7) produce a larger tensile region than the low stress (Fig. 6), especially at the crest of the slope. The stresses in claystones near the crest are so low that little creep displacements occur. However, near the toe of the slope, the stresses are higher and much larger cracked regions occur. Irrespective of this, in these relatively flat regions, rock failures are less likely to occur. As would be expected, the jointed model results in a slightly reduced tensile region. The softer rocks such as claystones and shales show larger tensile areas and this could influence the breaking of rock and aid weathering and erosion.

3.2 Clifton Section

This section of the Illawarra Escarpment between Coalcliff and Clifton is one of the most critical regions since there are localised steeper sections caused by the presence of some benches. The finite element mesh for this section is shown in Fig.10. The vertical joints are assumed to extend to the base of the Illawarra coal measures. In addition to gravity and tectonic loading, the water loads as shown in Fig.10 have also been applied in this case because the base of the slope where the Coal-cliff Sandstone crops out represents the high tide shore line.

As in the case of Brokers Nose section, for Clifton section, the difference in the stress distribution between the unjointed and jointed cases is negligible. Hence, only the results for the jointed model are presented since this model is a better representation of the escarpment.

The principal stress contour, σ_1 for low and high horizontal stresses has been plotted in Fig. 11 and 12. Compared to the case of low stresses, the cracked zone for high stresses is extensive. It is worth noting that the joints tend to slide for the case of high stress which did not happen for the other case. Moreover, there is a region of plastic yielding near the toe of the slope. From Fig.12, it can be seen that significant cracking has occured further back in the Newport Formation and Bald Hill claystone. Extensive cracking has also occured in the upper part of Bulgo Sandstone and Scarborough Sandstone. The plastic zone occurs in the vicinity of the coastal road and this could be due to the high compressive stresses caused by the rock mass above this zone. Deep seated joint movements have also been observed. The ratio of the maximum horizontal displacement between the cases of high and low horizontal stresses is about 13.

The creep results are presented in Fig. 13 and 14. As can be seen from these stress plots, the case of high stresses produce an extensive tensile region near the toe compared to the case of low stresses. However, the tensile region at the top of the slope for both cases are similar since the creep strains in that region are low. For the case of high stresses, the vertical displacement is reduced by 40% after creeping for 2000 days, compared to elastic displacement. A similar trend was noted for the case of low stresses also. This 'settling' of the rock slope over time, is dependent on the rate of weathering and the creep behaviour of softer claystones and shales. Due to creeping, there is also a tendency for a decrease in the normal compressive stresses across the joint elements in the Hawkesbury Sandstone. This probably indicates tensile cracking of the sandstone beds overlying claystones.

4. CONCLUSIONS

Nonlinear finite element analyses incorporating plasticity, tension cut-off and creep behaviour of rock mass as well as joint elements to model the discontinuities in the rock medium, have been carried out to assess the overall stability of the slopes at Illawarra Escarpment. As practical as possible, the finite element analyses have used the actual geological properties of the region modelled. Nevertheless, it must be realized that this investigation is only phenomenological and not design oriented. The study includes the results of two tectonic situations - one with a low horizontal stress (k = 1/3) and another with a high horizontal stress (k = 3).

The results indicate that there is some difference as far as eroding and yielding zones are concerned as well as to the sliding of joints, between the cases of in-tact rock mass and jointed medium. Eventhough this difference is not significant, the use of joint elements is a more appropriate model for this region. Between the cases of low and high horizontal stress, the results clearly indicate that the latter is more critical due to the extensive development of tensile regions.

In the case of Brokers Nose, there are a few cracked regions near the top of the cliff whereas in the case of Clifton, there are three major localised regions of cracking. Nevertheless, it is very unlikely that a large scale failure will occur even in the case of high horizontal tectonic stress.

The displacements of the outer nodes of Clifton section were often approximately double those observed for Brokers Nose section, indicating the possibility of some failure.

The finite element analyses of the escarpment as carried out in this investigation indicate where preventive measures can be carried out. The rapid alternation of tensile and compressive regions which would contribute to the general breaking of rock mass, can also be avoided by rock bolts or anchors.

5. ACKNOWLEDGEMENTS

The authors wish to acknowledge the help provided by Dr. P. Boonlualohr and Dr. K. Matzusaki in the investigation of this project.

TABLE I. MATERIAL PROPERTIES

Material Property Number		Rock Type and/or Formation Name	Degree of weathering	Modulus of Elasticity GPa	Poisson's Ratio	Elastic Plastic Analysis		Creep Analysis	
Brokers Nose	Clifton					Yield Stress MPa	Tangent Modulus GPa	K	n
1	1	Sandstone & Claystone at depth	Fresh	14.0	0.26	45.0	10.0	0	0
2	2	Sandstone & Claystone	Fresh	7.0	0.26	20.0	4.6	0	0
3	5	Claystone	Slightly weathered	3.0	0.34	11.0	1.7	8.2×10^{-10}	1.07
4	3	Sandstone	Fresh	9.6	0.22	29.0	5.8	0	0
5	4	Claystone	Fresh	6.8	0.30	17.0	3.8	0	0
6	6	Shale & Claystone	Fresh	6.4	0.25	23.0	5.8	0	0
7	8	Hawkesbury Sandstone	Fresh	8.6	0.29	26.0	7.0	0	0
8	7	Shale & Claystone	Slightly weathered	2.7	0.34	14.0	2.5	8.2×10^{-10}	1.07
				Shear Stiffness GPa/m	Normal Stiffness GPa/m	Residual Shear GPa/m	Cohesion MPa	Friction Angle degrees	
9	9	Joint in Sandstone	Slightly weathered	1.0	2.6	0.5	0.27	29°	
10	10	Joint in Claystone	Slightly weathered	0.8	1.5	0.3	0.75	21°	

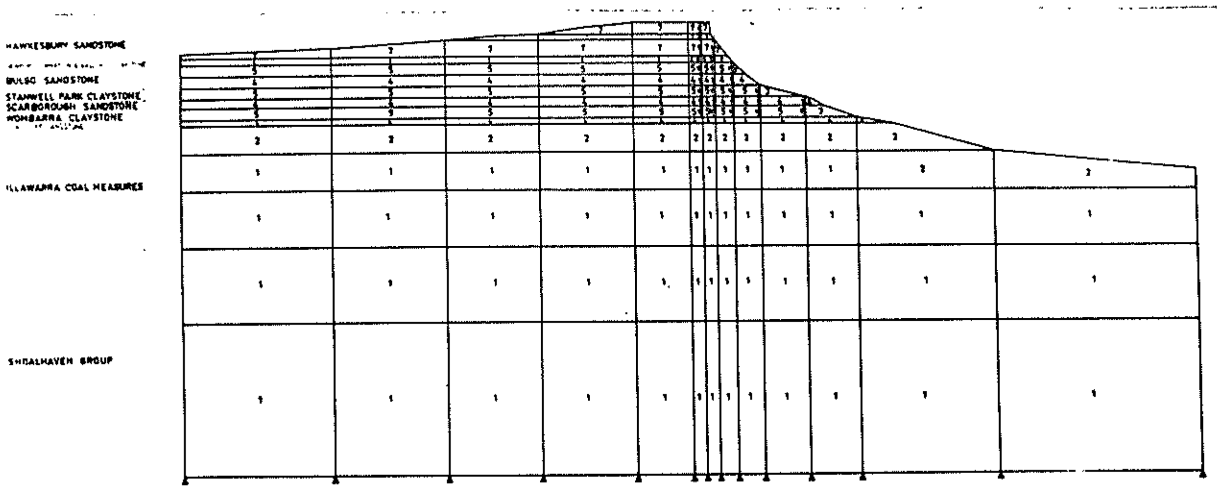

FIGURE 1 BROKERS NOSE SECTION
Finite Element Mesh

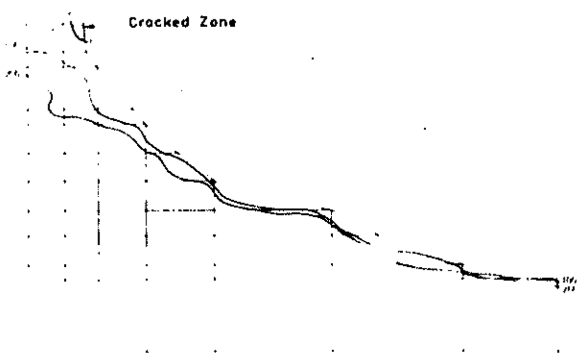

FIGURE 2 CONTOURS OF σ_1 - ELASTIC-PLASTIC ANALYSIS
No Joints k = 1/3

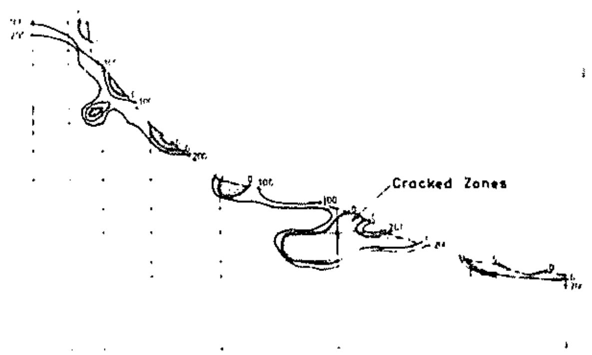

FIGURE 3 CONTOURS OF σ_1 - ELASTIC-PLASTIC ANALYSIS
No Joints k = 3

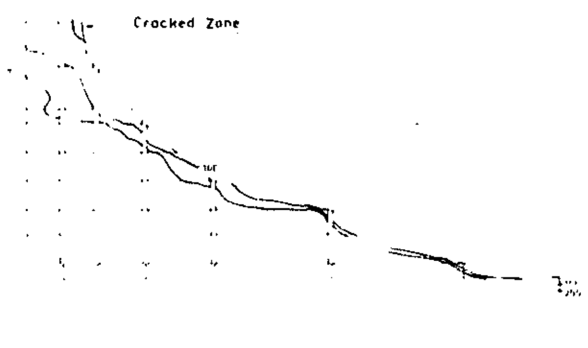

FIGURE 4 CONTOURS OF σ_1 - ELASTIC-PLASTIC ANALYSIS
Joints k = 1/3

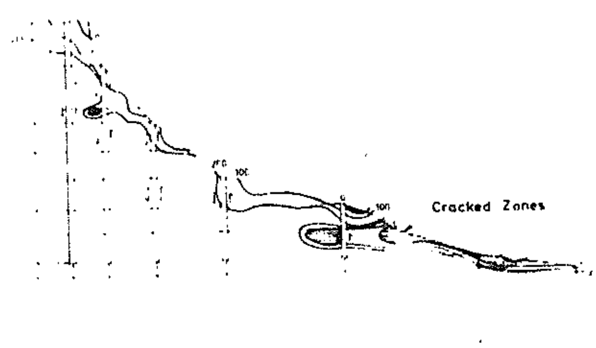

FIGURE 5 CONTOURS OF σ_1 - ELASTIC PLASTIC ANALYSIS
Joints k = 3

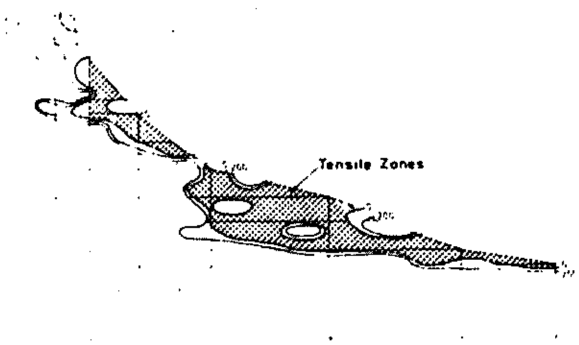

FIGURE 6 CONTOURS OF σ_1 - CREEP ANALYSIS
No Joints k = 1/3

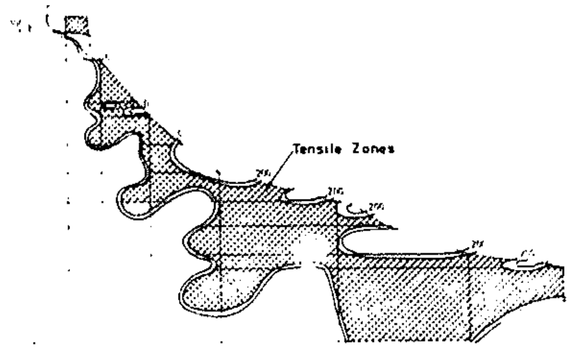

FIGURE 7 CONTOURS OF σ_1 - CREEP ANALYSIS
No Joints k = 3

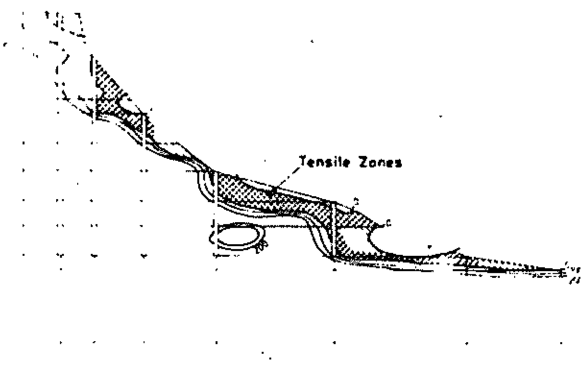

FIGURE 8 CONTOURS OF σ_1 - CREEP ANALYSIS
Joints k = 1/3

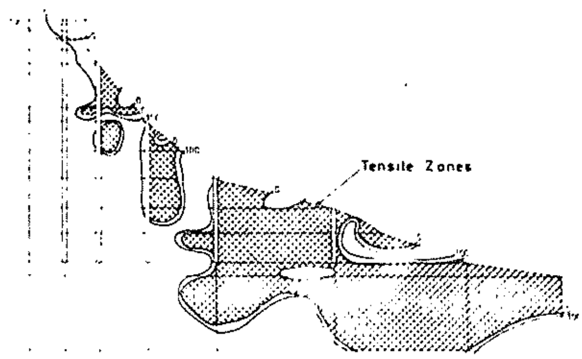

FIGURE 9 CONTOURS OF σ_1 - CREEP ANALYSIS
Joints k = 3

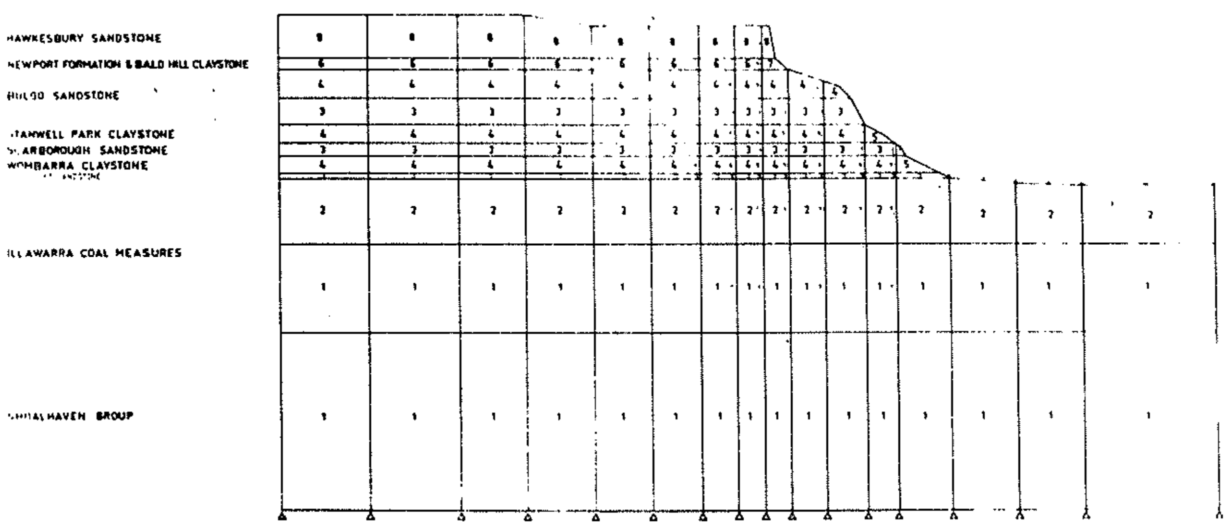

FIGURE 10 CLIFTON SECTION
Finite Element Mesh

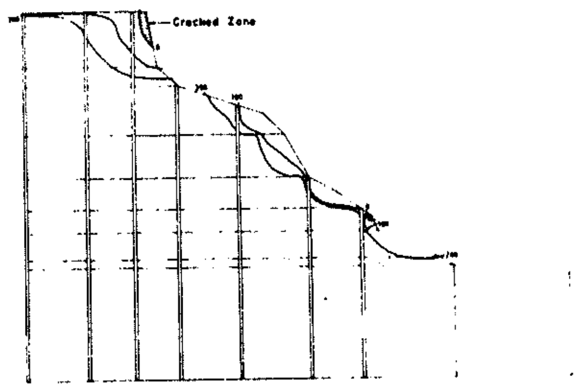

FIGURE 11 CONTOURS OF σ_1 - ELASTIC-PLASTIC ANALYSIS
Joints k = 1/3

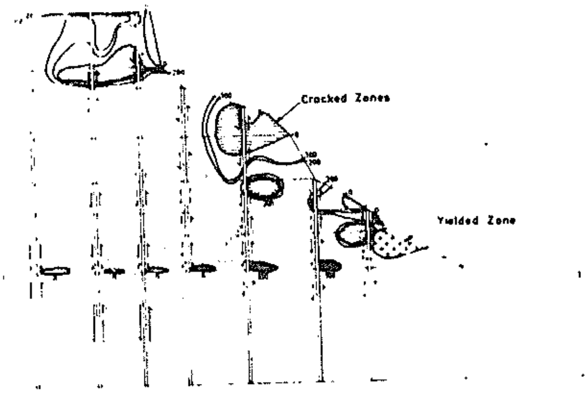

FIGURE 12 CONTOURS OF σ_1 - ELASTIC-PLASTIC ANALYSIS
Joints k = 3

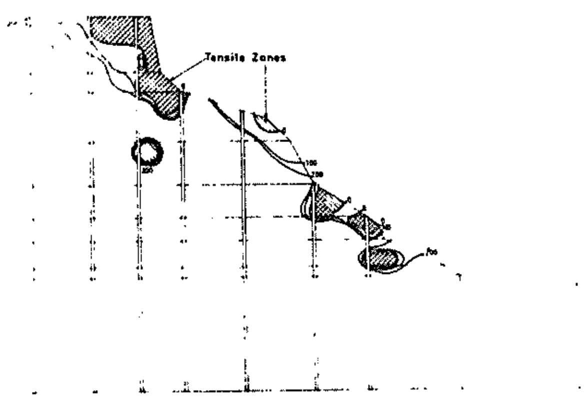

FIGURE 13 CONTOURS OF σ_1 - CREEP ANALYSIS
Joints k = 1/3

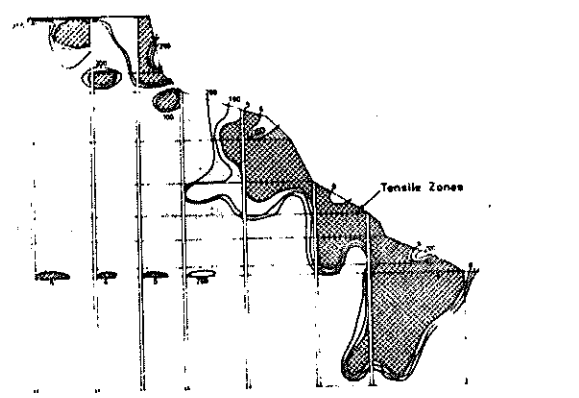

FIGURE 14 CONTOURS OF σ_1 - CREEP ANALYSIS
Joints k = 3

The Analysis of Multiple Underream Anchors

R. K. ROWE
Assistant Professor, Faculty of Engineering Science, The University of Western Ontario
J. R. BOOKER
Reader, School of Civil Engineering, University of Sydney

1 INTRODUCTION

In recent years, there has been an increasing acceptance of the use of multiple underream anchor systems for the support of both temporary and permanent structures. This acceptance has been facilitated by the development of construction techniques which allow convenient and economical installation of multiple underreams, and has been accompanied by the formulation of empirical rules for use in design. Some experimental research has been undertaken into the performance of multiple underream anchors (e.g. Swain, 1976) however there has been relatively little theoretical research into the factors influencing the behaviour of these anchors.

In this paper, an analytical technique for calculating the elastic response of multiple underream anchors is outlined and is then used to investigate the effects of the number and spacing of underreams upon the behaviour of anchor systems resting in an elastic half-space. In this study, consideration is given to the influence of the anchor's proximity to the free surface and its inclination upon the elastic response.

The results of this study into multiple underream anchor behaviour are summarised in the form of influence charts which may be used in hand calculations for estimating the elastic response of anchor systems for a wide range of anchor depths, inclinations, number and spacing of underreams.

It is considered that the elastic solutions presented in this paper for multiple underream anchors, may be used for designing anchor systems in the same manner that elastic solutions are currently used for designing surface footings and pile foundations.

2 THEORY

Figure 1 shows a series of anchors $A_1, \ldots A_n$ in an elastic soil. Each anchor A_i is subdivided into a number of subregions or elements $D_{i1}, \ldots, D_{im}$ and it is assumed that the forces $\tilde{F}_{ij} = (X, Y, Z)^T_{ij}$ acting on each element are uniformly distributed over that element. The theory of elasticity may then be used to establish the relation

$$\tilde{W} = J \tilde{F} \qquad (1)$$

where $\tilde{W}^T = (\bar{\tilde{W}}^T_{11}, \bar{\tilde{W}}^T_{12}, \ldots, \tilde{W}^T_{nm})$

is the vector of element displacements

$\tilde{F}^T = (\tilde{F}^T_{11}, \tilde{F}^T_{12}, \ldots, \tilde{F}^T_{nm})$

is the vector of element forces

and $\bar{W}_{ij}$ is the average deflection of "jth" element of the "ith" plate

and J is a (3nm) x (3nm) matrix of influence coefficients.

Details regarding the calculation of these influence coefficients are given by Rowe and Booker (1979b).

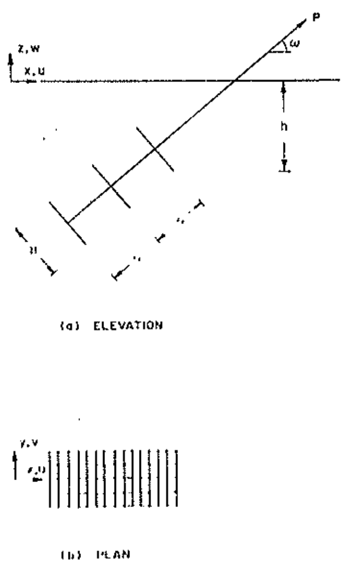

FIG. 1 TYPICAL PROBLEM CONFIGURATION

If the anchors are rigid, then each anchor will only undergo rigid body movement. In this paper attention will be restricted to the case of inextensible anchor rods and it will be assumed that each anchor undergoes a translation δ parallel to the anchor shafts. Clearly this assumption is only correct if the anchor rod is rigidly attached to the anchor shaft, however previous results obtained by Rowe and Booker (1979b, 1979c) indicate that in general very little rotation or deviation of the translation from the direction of the anchor shaft occurs. Thus in the majority of cases, and particularly for cases of practical interest, this assumption is quite accurate.

Equation (1) may therefore be written

$$J \underset{\sim}{F} = \delta \underset{\sim}{a} \quad (2)$$

where $\underset{\sim}{a}$ is a vector of length (3nm) as defined below

$$\underset{\sim}{a}^T = (l_x, l_y, l_z, l_x, l_y, l_z \ldots)$$

and $(l_x, l_y, l_z)^T$ is a unit vector parallel to the anchor rods.

Suppose that equation 2 is solved for $\delta = \hat{\delta}$ (conveniently taken to be unity) and that in this case $\underset{\sim}{F} = \hat{\underset{\sim}{F}}$

so that $$\hat{\underset{\sim}{F}} = \hat{\delta} \; J^{-1} \underset{\sim}{a} \quad (3)$$

The tension $T_k = \hat{T}_k$ in the "kth" rod may now be found from equilibrium since

$$\hat{T}_k = \sum_{i=k}^{n} \sum_{j=1}^{m} (l_x \hat{X}_{ij} + l_y \hat{Y}_{ij} + l_z \hat{Z}_{ij}) \quad (4)$$

and thus the applied load $P = \hat{P}$ is given by

$$\hat{P} = \sum_{k=1}^{n} \sum_{j=1}^{m} (l_x \hat{X}_{ij} + l_y \hat{Y}_{ij} + l_z \hat{Z}_{ij})$$

It now follows from linearity that in the general situation

$$\delta = \frac{P}{\hat{P}} \hat{\delta}$$

$$\underset{\sim}{F}_{ij} = \frac{P}{\hat{P}} \hat{\underset{\sim}{F}}_{ij} \quad (5)$$

$$\underset{\sim}{T}_k = \frac{P}{\hat{P}} \hat{\underset{\sim}{T}}_k$$

3 THE BEHAVIOUR OF MULTIPLE ANCHORS

The theory outlined in section 2 may be used to analyse the general case involving arbitrary anchor inclination, number of underreams and spacing between underreams. In this paper, consideration will be restricted to a number of typical cases involving no more than five underreams which are positioned at equal spacings. The solutions were obtained for underreams which are square in section, however a comparison between the elastic response of square and circular anchors (Rowe and Booker, 1979a) indicates that the solutions for a square anchor may be used for circular anchors of equal area. Provision for the effect of anchor shape can be made by modifying Selvadurai's (1976) analytical solution for a rigid circular anchor at infinite depth; viz

$$\delta_\infty = \frac{c_\infty}{BE} \cdot P \quad (6a)$$

where δ_∞ is the displacement of an anchor at infinite depth, of diameter (or width B), subjected to an applied load P.

E is the Young's modulus of the soil;

$$c_\infty \text{ (circular)} = \frac{(1+\nu)(3-4\nu)}{8(1-\nu)} \quad (6b)$$

$$c_\infty \text{(square)} = \sqrt{\pi} \; \frac{(1+\nu)(3-4\nu)}{16(1-\nu)} \quad (6c)$$

and ν is Poisson's ratio of the soil.

If it is assumed that the anchor rod connecting the underreams is relatively inextensible, then the deflection of the anchor system may be given in terms of the results for a single anchor at infinite depth multiplied by a correction factor M_G; i.e.

$$\delta = \delta_\infty \cdot M_G = \frac{c_\infty}{BE} \cdot M_G \cdot P \quad (7)$$

where the correction factor M_G incorporates the effects of:

- anchor inclination angle ω (see Figure 1);
- the distance h between the soil surface and the bottom of the leading underream;
- the number of underreams;
- the spacing s between underreams.

Although the theory can be generalised to consider a number of different boundary conditions at the interface, attention will be restricted here to the rigid displacement of an underream system with rough anchor plates which are fully bonded to the soil. The case of a fully bonded anchor is considered to be the most practical limiting case for the application of elastic solutions since it has been shown by Rowe (1978) that separation of an anchor plate from the underlying soil is often associated with significant plastic failure within the soil mass; this usually occurs at loads well above the working load.

If interaction effects were neglected, then superposition of the elastic results for a single underream (Rowe and Booker, 1979b) could be used to estimate the displacement of multiple anchor systems. However, one might expect that this approach would lead to an unconservative estimate of anchor displacement since interaction between anchors will reduce the efficiency of the anchor system. To illustrate the magnitude of the interaction between underreams, consider an anchor system with n underreams at very great depth and subjected to a load P. If the displacement of an isolated underream subjected to unit load is δ_o, then the displacement of the anchor system (neglecting interaction) would be $\delta_s = \delta_o P/n$. Now if the actual displacement of the anchor system (allowing for interaction) is δ_G then the increase in displacement of the anchor system due to interaction between underreams is given by the ratio δ_G/δ_s ; this ratio is shown in Figure 2 for a number of cases. In the case of a 2 underream system, the actual displacement of the anchor system exceeds the value that would be determined from a simple analysis, neglecting interaction, by more than 10% for anchor spacings less than 6 anchor widths (diameters). The degree of interaction increases with the number of underreams; thus, with a 5 underream system an unpractical spacing of almost 20 anchor plate widths is required between each adjacent pair of underreams, to achieve negligible interaction.

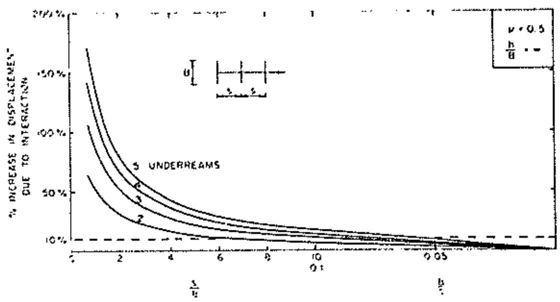

FIG. 2 EFFECT OF INTERACTION UPON THE DISPLACEMENT OF A MULTIPLE UNDERREAM ANCHOR AT INFINITE DEPTH

Figure 2 could be used to modify the displacement obtained by superposition of single underream results to give the correct elastic response for a particular deep anchor system. However it is more convenient to express the displacement of the anchor system in terms of the solution for a single deep underream, multiplied by a correction factor M_G as indicated in Equation 7. The correction factor M_G for an anchor system at great depth ($h/_B \to \infty$) is given in Figure 3 for $\nu = 0.5$. From consideration of the results given in Figure 3 it may be concluded that increasing the number of underreams leads to an appreciable decrease in anchor system displacement, although the magnitude of this reduction is dependent upon the spacing between underreams. Indeed the results indicate that it is more beneficial (in terms of reduced anchor displacement for a given load) to increase the number of underreams at the expense of reducing the spacing, provided that the spacing is not reduced to less than 1.5 anchor widths. For example, the deflection of an anchor system with two underreams at a spacing of 8 anchor widths (for a given total load P) is more than 50% greater than the displacement of an anchor system with five underreams at a spacing of two anchor widths; there is a monotonic variation in displacement with the number of underreams between these two cases.

It may be anticipated that the response of a multiple underream anchor will be influenced by the depth h of the anchor system beneath the soil surface and the inclination ω of the anchor system to the horizontal. The variation in anchor performance with anchor inclination and the number and spacing of underreams is quite complex. In part, this apparent complexity arises from the manner in which the results are compared in non-dimensional form. For example, the embedment ratio is defined as the depth to the bottom of the leading underream and so altering the inclination of the anchor system changes the minimum distance between the underream and the soil surface while the maximum distance remains constant (for given $h/_B$). It is found that the elastic response (displacement for a given load) of a very shallow (e.g. $h/_B = 1$) single underream does not not necessarily vary monotonically with inclination angle ω, however for most single anchors (i.e. $h/_B > 1.5$) the elastic response does increase with the inclination angle. For second and subsequent underreams in the anchor system, both the maximum and minimum distance between the underreams and the surface increase with the inclination angle ω (for given $h/_B$ to the leading underream). Consequently, the elastic response of the latter underreams decreases as the anchor system is rotated from $\omega = 0^o$ through to $\omega = 90^o$. The combination of these two effects results in the trend shown in Figure 4 for $h/_B = 1$, where the displacement of an anchor system for a particular number and spacing of underreams is greatest when $\omega = 0^o$ and is least for $\omega = 45^o$. The displacement for a system with $\omega = 90^o$ is slightly greater than that for $\omega = 45^o$.

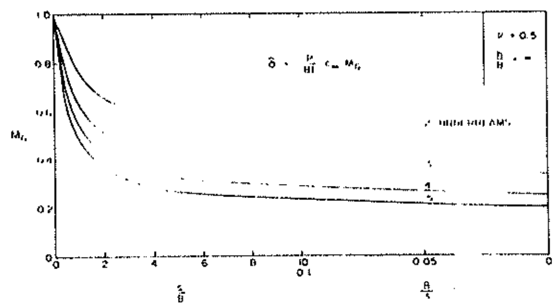

FIG. 3 DISPLACEMENT REDUCTION FACTOR M_G FOR AN ANCHOR SYSTEM AT INFINITE DEPTH $\nu = 0.5$

The solution where the anchor system is horizontal $\omega = 0^o$ may be regarded as a special case since the depth of each underream is independent of spacing s. For all other cases the depth of second and subsequent underreams increases with increasing spacing between underreams and it is found that for $\omega > 15^o$ the variation in the displacement of a given multiple anchor system with changing inclination angle ω is less than 7%. Thus for $\omega > 15^o$ the variation in the elastic response of shallow anchors for different inclinations ω decreases with increasing spacing s between underreams, however because of the special nature of the case where $\omega = 0^o$, the difference between solutions for $\omega = 0^o$ and those for $\omega > 0^o$ becomes more pronounced at large spacings.

Anchor inclination becomes less important as the embedment ratio becomes larger. This trend may be appreciated by comparing the results given in Figures 4, 5, 6 and 7 for a range of embedment ratios. These results indicate a relatively complex interaction between the effects of inclination, embedment ratio and the number and spacings of underreams. However in practical terms, for anchor systems with $h/_B > 3$ the effect of inclination upon anchor response can be largely neglected since there is less than a 7% variation in anchor system response over the entire range of inclination $0^o < \omega < 90^o$.

The proximity of an anchor system to the free surface has a noticeable effect upon the anchor system response although, in general, this effect is not as significant as the interaction due to the spacing between underreams. Figure 3 to 7 indicate the variation in displacement of multiple

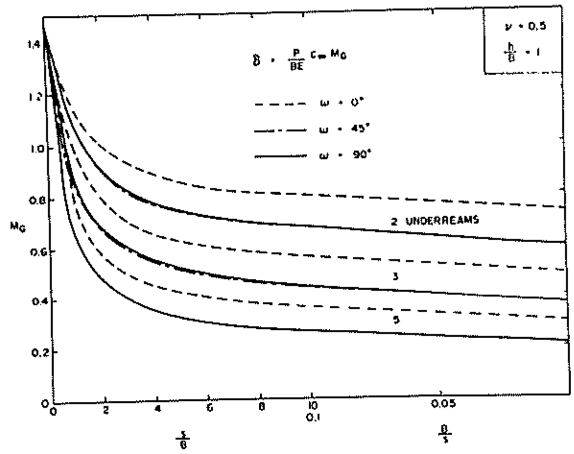

FIG. 4 VARIATION IN M_G WITH SPACING $s/_B$ AND INCLINATION: $\frac{h}{B} = 1$, $\nu = 0.5$

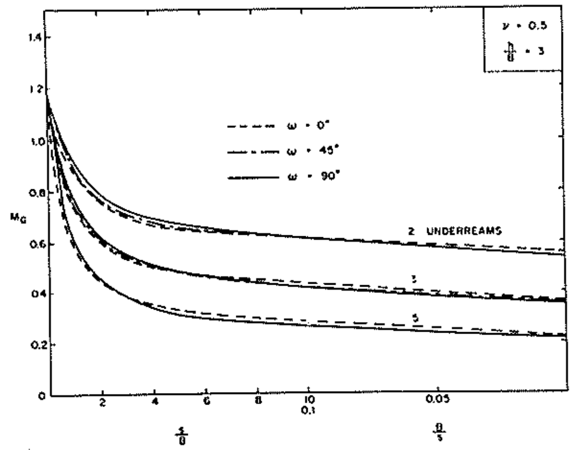

FIG. 5 VARIATION IN M_G WITH SPACING AND INCLINATION: $\frac{h}{B} = 3$, $\nu = 0.5$

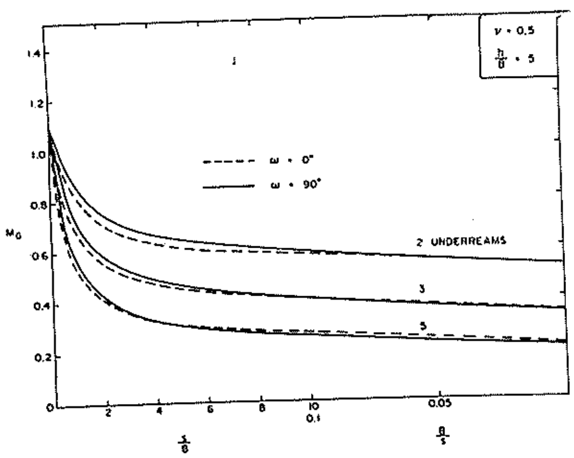

FIG. 6 VARIATION IN M_G WITH SPACING AND INCLINATION: $\frac{h}{B} = 5$, $\nu = 0.5$

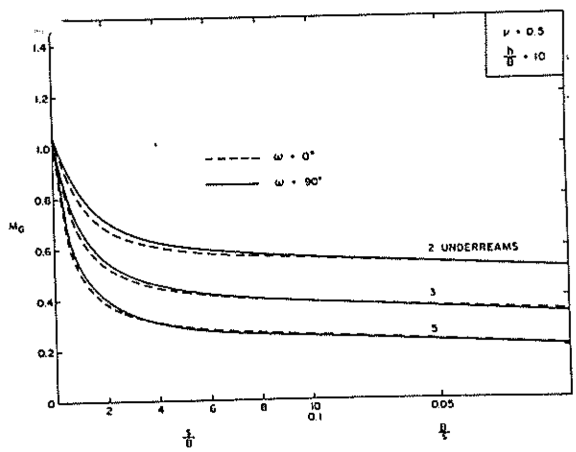

FIG. 7 VARIATION IN M_G WITH SPACING AND INCLINATION: $\frac{h}{B} = 10$, $\nu = 0.5$

anchor systems as a function of underream spacing for a range of embedment ratios. A comparison of the results for an anchor system at infinite depth (Figure 3) with anchor systems at finite depth shows two types of behaviour. For anchor systems with inclination $\omega > 0^o$, the embedment ratio $h/_B$ becomes less important as either the number or spacing of the underreams is increased. This trend is to be expected since increasing either parameter leads to an increase in the distance between the bottom of the anchor system and the soil surface. However for the special case of anchors with inclination $\omega = 0^o$, there is no change in depth associated with altering the number and spacing of underreams and in this case, the depth of embedment has a more pronounced influence upon anchor performance than is observed when $\omega > 0^o$.

The effect of proximity to the soil surface decays rapidly with increasing embedment and the displacement of anchor systems with an embedment ratio of 10 is generally within 10% of that for similar systems at infinite depth. Thus for practical purposes, an anchor system may be considered to be "deep" at an embedment ratio of 10. Under some circumstances, notably for systems with $\omega = 0^o$ and only a few underreams, the critical embedment ratio (i.e. the embedment ratio at which the displacement is within 10% of the value for an infinitely deep anchor) may be as low as 4.

The influence of Poisson's ratio upon anchor response depends upon anchor depth and inclination as well as the number and spacing of underreams. To indicate the effect of Poisson's ratio upon anchor displacements, the ratio of the anchor displacement for a given ν, denoted by $\delta(\nu)$, to the displacement for $\nu = 0.5$, denoted by $\delta(\nu = 0.5)$, is shown in

Figures 8 and 9 as a function of ν for a number of specific cases. These results raise a number of interesting points. Firstly it will be noted (see Figure 8) that for an isolated anchor at infinite depth the displacement for ν = 0 is equal to that for ν = 0.5 and the maximum displacement at ν = 0.3 is only 11% above that for ν = 0.5 (this result follows directly from Equation 6.) This situation is markedly different from that encountered with a surface footing where the increase in displacement for ν = 0.3 is 21% and this rises to 33% for ν = 0. The important practical implication of this result for anchors (or footings) in clay is that increasing the embedment of an anchor decreases the amount of "consolidation settlement" that would be obtained, particularly for soils with a low drained Poisson's ratio. Furthermore, with respect to the effect of Poisson's ratio upon anchor behaviour, the transition from surface footing behaviour to deep anchor behaviour is very rapid. All single anchors with an embedment ratio greater than or equal to three show a very similar variation in displacement with Poisson's ratio as that indicated for an infinitely deep anchor. This allows convenient, and relatively accurate, determination of the displacement for an anchor in a soil with any Poisson's ratio ν by interpolation of the results given in this paper.

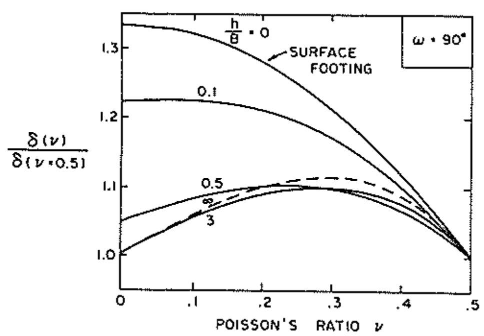

FIG. 8 EFFECT OF POISSON'S RATIO UPON DISPLACEMENT OF A SINGLE ANCHOR PLATE

A similar trend in the effect of Poisson's ratio upon anchor displacement is observed for multiple underream anchors (see Figure 9) although in this case the influence of Poisson's ratio depends not only on anchor depth and inclination, but also upon the number and spacing of underreams. The interaction between underreams is greatest for an incompressible material and decreases with Poisson's ratio; since interaction has its greatest effect upon anchor systems with a large number of closely spaced underreams, it might then be expected that the influence of Poisson's ratio upon the anchor displacement would be greatest for these cases. Indeed Figure 9 demonstrates that under certain circumstances the displacement of a multiple anchor system in an incompressible soil will be larger than the displacement for ν < 0.5 (assuming the same elastic modulus). Of greater practical importance however is the fact that for a wide range of conditions the displacement of a multiple anchor system is relatively insensitive to the value of Poisson's ratio, generally varying by less than 10% over the entire range of values of ν.

The solutions presented in this paper are for an anchor system embedded in an elastic half-space. Provision could be made in the analysis for the case where there is a rigid stratum at finite depth beneath the anchor system, however results obtained by Rowe and Booker (1979a) for a single, horizontally embedded, circular anchor plate indicate that the depth to the rigid stratum has relatively little effect (i.e. less than 10%) upon single anchor response provided the rigid stratum is at least 10 anchor plate diameters below the anchor. Accordingly it is considered that solutions obtained for a half-space are sufficiently accurate for practical cases where the soil mass extends at least 10 anchor diameters below the deepest underream; the displacement obtained using half-space theory will be conservative.

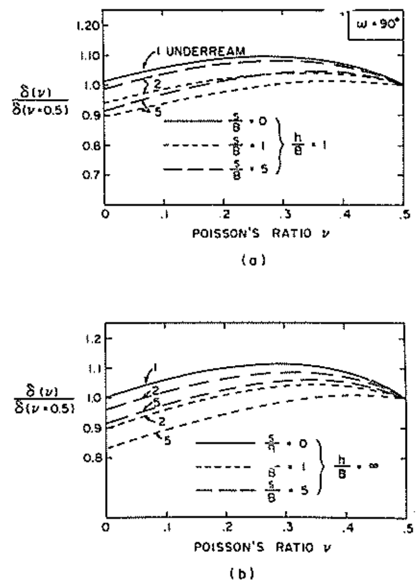

FIG. 9 EFFECT OF POISSON'S RATIO UPON ANCHOR DISPLACEMENT

4 CONCLUSIONS

The behaviour of multiple underream anchor systems, resting in a homogeneous elastic half-space has been examined using an analytical technique which is outlined in the paper. The study has shown that in general, the elastic performance of an anchor system is significantly enhanced by increasing the number of underreams, even at the expense of a reduction in spacing between the underreams.

Consideration of anchor systems with a given number of underreams indicated that anchor spacing was the dominant parameter influencing the anchor system response. The effect of interaction between underreams upon anchor behaviour increased with the number of underreams, however even for small anchor systems, significant interaction may occur at relatively large spacings. Consequently, it is usually necessary to take account of interaction effects when predicting anchor behaviour.

The depth of anchor system embedment noticeably influenced the response of shallow anchor systems, however the influence of the free surface decayed rapidly with increasing embedment and for practical purposes may be neglected when the depth of soil above the anchor system is greater than ten underream diameters.

Anchor inclination was generally found to have very little effect upon anchor system response and in particular it was found that it is usually sufficient to restrict attention to the limiting cases of anchor systems with vertical and horizontal axes.

Finally, it was shown that the elastic response of a multiple anchor system was relatively insensitive to the value of Poisson's ratio and it is suggested that anchor systems in clay would exhibit relatively little consolidation displacement.

Parametric solutions are presented in the form of influence charts which may be used directly in hand calculations to predict the elastic load deflection behaviour of multiple underream anchors for a wide range of parameters; the use of the influence charts is illustrated by a worked example in the appendix.

5 ACKNOWLEDGEMENT

The work described in this paper was supported by grant No. A1007 from the Natural Science and Engineering Research Council of Canada.

6. REFERENCES

ROWE, R.K., (1978). Soil structure interaction analysis and its application to the prediction of anchor plate behaviour. Ph.D Thesis, University of Sydney, Australia.

ROWE, R.K. and BOOKER, J.R. (1979a). A Method of Analysis for Horizontally Embedded Anchors in an Elastic Soil. International Journal for Numerical and Analytical Methods in Geomechanics, Vol. 3, No. 2, pp. 187-203. For additional details see also Research Report 316, School of Civil Engineering, University of Sydney (1978).

ROWE, R.K. and BOOKER, J.R. (1979b). Analysis of Inclined Anchor Plates, Proceedings of the 3rd International Conference on Numerical Methods in Geomechanics, Aachen, April 2-6, 1979, pp. 1227-1236.

ROWE, R.K. and BOOKER, J.R. (1979c). The Elastic Response of Multiple Underream Anchors. Research Report GEOT-1-79, Faculty of Engineering Science, University of Western Ontario.

SELVADURAI, A.P.S., (1976). The load-deflection characteristics of a deep rigid anchor in an elastic medium, Geotechnique 26, No. 4, pp. 603-612.

SWAIN, A. (1976). Model Ground Anchors in Clay, Ph.D Thesis, University of Cambridge.

7 APPENDIX ILLUSTRATIVE EXAMPLE

Estimate the elastic displacement of the anchor system shown in Figure 10 for a soil with E' = 3000 kPa, $\nu = 0.4$ where the anchor system is subjected to a working load of 1000 kN.

The non-dimensional parameters are

$$h/_B = \frac{3}{0.54} = 5.5 \quad ; \quad s/_B = \frac{1.15}{0.54} = 2.1$$

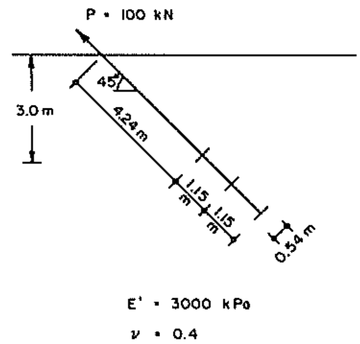

FIG. 10 EXAMPLE

From Equation 7

$$\delta = \frac{c_\infty}{BE} M_G P$$

where

$$c_\infty = \frac{(1+\nu)(3-4\nu)}{8(1-\nu)} \quad = 0.408 \text{ for } \nu = 0.4$$
$$= 0.375 \quad \nu = 0.5$$

since the curves for $\nu = 0.4$ are not given, use M_G results for $\nu = 0.5$ and correct by interpolation from Figure 9.

(1) From Figure 6 for a 3 underream system,

$$h/_B = 5, \quad s/_B = 2.1, \quad M_G = 0.565$$

Now determine

$$\delta(\nu = 0.5) = \frac{c_\infty(\nu = 0.5) \cdot M_G (\nu = 0.5) P}{B.E.}$$

$$= \frac{0.375 \times .565 \times 100}{.54 \times 3000}$$

$$= 0.0130$$

(2) Estimate $\frac{\delta(\nu)}{\delta(\nu = 0.5)}$ by interpolation from Figure 9

Thus $\frac{\delta(\nu)}{\delta(\nu = 0.5)}$ 1.04 for $s/_B = 2$, 3 underreams

(3) $(\nu = 0.4) = 1.04 \times 0.0130 = 0.0136$m

i.e. 13.6 mm

This is 6.6% above the displacement of 12.8 mm obtained from a full analysis. Note that the approximate answer was determined using the results for $h/_B = 5$; an additional refinement would be to interpolate between the results for $h/_B = 5$, $h/_B = 10$ to obtain M_G for $h/_B = 5.5$.